

CR 114615
AVAILABLE TO
THE PUBLIC

FINAL REPORT

V/STOL TILT ROTOR STUDY - VOLUME VI HOVER, LOW SPEED AND CONVERSION TESTS OF A TILT ROTOR AEROELASTIC MODEL

MODEL 300

REPORT 301-099-002

NASA CONTRACT NAS 2-6599



NASA-CR-114615) V/STOL TILT ROTOR STUDY.
VOLUME 6: HOVER, LOW SPEED AND
CONVERSION TESTS OF A TILT ROTOR
AEROELASTIC MODEL (MODEL (Bell Helicopter
Co.) 326 p HC \$18.50
CSCL 01C

N73-30950

G3/02 Unclas
14159

 **BELL**
HELICOPTER COMPANY
POST OFFICE BOX 482 • FORT WORTH, TEXAS 76101 • A  COMPANY

CR 114615

V/STOL TILT ROTOR STUDY - VOLUME VI
HOVER, LOW SPEED AND CONVERSION TESTS OF A
TILT ROTOR AEROELASTIC MODEL

by

R. L. Marr
K. W. Sambell
G. T. Neal

Bell Helicopter Company Report No. 301-099-002
May 15, 1973

Prepared Under Contract No. NAS 2-6599 by
Bell Helicopter Company, A Textren Company
Fort Worth, Texas

for

National Aeronautics and Space Administration
Ames Research Center
and

United States Army Air Mobility Research and
Development Laboratory, Ames Directorate

This data is furnished in accordance with the
provisions of Contract NAS 2-6599

Foreword

This report is one of a series prepared by the Bell Helicopter Company, Fort Worth, Texas, for the National Aeronautics and Space Administration, Ames Research Center, Moffett Field, California, under Contract NAS2-6599. These Tilt Rotor Research Aircraft studies were jointly funded by NASA and the U. S. Army Air Mobility Research and Development Laboratory, Ames Directorate.

The Administrative Contracting Officer was Mr. Richard J. Abbott. The Technical Monitor was Mr. Martin D. Maisel, Tilt Rotor Research Aircraft Project Office. Mr. Gary B. Churchill, Tilt Rotor Research Aircraft Project provided technical support to the effort reported in Volume V.

- Volume I -- V/STOL Tilt Rotor Study - Conceptual Design -- CR114441
- Volume II -- V/STOL Tilt Rotor Study - Research Aircraft Design -- CR114442
- Volume III -- V/STOL Tilt Rotor Study - Research Aircraft Project Plan -- CR114443
- Volume IV -- V/STOL Tilt Rotor Study - Wind Tunnel Investigation Plan - CR114444
- Volume V -- V/STOL Tilt Rotor Study - A Mathematical Model for Real Time Flight Simulation of the Bell Model 301 Tilt Rotor Research Aircraft -- CR114614
- Volume VI -- V/STOL Tilt Rotor Study - Hover, Low Speed and Conversion Tests of a Tilt Rotor Aeroelastic Model -- CR114615

TABLE OF CONTENTS

	<u>Page</u>
LIST OF ILLUSTRATIONS	iii
LIST OF TABLES	xi
LIST OF SYMBOLS	xii
I. SUMMARY	I-1
II. INTRODUCTION	II-1
A. PREVIOUS TESTS	II-1
B. TECHNICAL BACKGROUND	II-1
C. SCOPE OF THE PROGRAM	II-2
D. OBJECTIVES OF THE PROGRAM	II-3
III. DESCRIPTION OF THE MODEL	III-1
A. MODEL SCALING	III-1
B. CONSTRUCTION AND DESIGN PARAMETERS	III-1
C. MODEL CONTROLS	III-4
D. NATURAL FREQUENCIES	III-4
E. INSTRUMENTATION	III-5
IV. DESCRIPTION OF THE TESTS	IV-1
A. HOVER TEST	IV-1
B. SEMI-FREE FLIGHT, ROD MOUNT TEST	IV-2
C. STING MOUNT TEST	IV-3
D. DATA REDUCTION	IV-4
V. RESULTS OF TESTS	V-1
A. HOVER TEST	V-1
B. SEMI-FREE FLIGHT, ROD MOUNT TEST	V-4
C. STING MOUNT TEST	V-14
VI. ANALYSIS OF TEST RESULTS	VI-1
A. ANALYSIS OF ROTOR WAKE TUFT GRID PATTERNS AND SMOKE OBSERVATIONS	VI-1
B. DETERMINATION OF NET EFFECT OF ROTOR WAKE AT EMPENNAGE	VI-2
C. ANALYSIS OF DISCREPANCY BETWEEN MEASURED AND CALCULATED LATERAL FLAPPING	VI-8
VII. CONCLUSIONS	VII-1
VIII. REFERENCES	VIII-1

TABLE OF CONTENTS (CONT'D)

	<u>Page</u>
APPENDIX	
A. RUN SCHEDULE SUMMARY	A-1
B. STING TEST BALANCE DATA	A-13
C. TUFT GRID PHOTOGRAPHS	A-84

LIST OF ILLUSTRATIONS

<u>Number</u>		<u>Page</u>
I-1	Powered Aeroelastic Model on Vertical Rod Mount, LTV LSWT Test 418, January 1973	I-4
I-2	Powered Aeroelastic Model on Sting Mount LTV LSWT Test 421, March 1973	I-4
I-3	Summary of Roll Stability Characteristics in IGE Hover	I-5
I-4	Level Flight Trim Attitude and Control Positions Versus Airspeed, Mast Angle 90° and 75°.	I-6
I-5	Level Flight Trim Longitudinal Cyclic Versus Yaw Angle, Mast Angles 90° and 75°.	I-7
I-6	Correlation Between Calculated and Measured Flapping, Mast Angles 90° and 75°	I-8
III-1	Fuselage Spar, Wing, and Rotors Sting Test	III-15
III-2	Fuselage Fairings	III-15
III-3	Empennage Balance and Variables Incidence Adjustment	III-16
III-4	Rotor-Hub	III-16
III-5	Model Motors, Couplings, and Interconnect Shaft (Following Coupling Failure).	III-17
III-6	Schematic of Offsite Data Acquisition Package	III-18
III-7	Instrumentation, Discriminator Panel and Magnetic Tape	III-19
III-8	Instrumentation. Model Pilot Controls Panel Meters and Closed Circuit TV	III-20
III-9	Instrumentation, Oscillographs	III-20
III-10	Instrumentation, Power Supply and Motor Temperature	III-21
IV-1	Roll Test Rig Schematic	IV-5
IV-2	Hover Test, Wing Fairings On	IV-6

LIST OF ILLUSTRATIONS (Cont'd)

<u>Number</u>		<u>Page</u>
IV-3	Hover Test, Wing Fairings Removed	IV-7
IV-4	Free Flight Test Rig Schematic	IV-8
IV-5	Rod Test, Mast 90 Degrees	IV-9
IV-6	Rod Test, Mast 75 Degrees	IV-9
IV-7	Rod Test, Mast 60 Degrees	IV-10
IV-8	Rod Test, Mast 30 Degrees	IV-10
IV-9	Rod Test, Sideward Flight Mast 90 Degrees	IV-11
IV-10	Rod Test, Rearward Flight Mast 90 Degrees	IV-11
IV-11	Rod Test, IGE, Mast 90 Degrees	IV-12
IV-12	Sting Test, Mast 60 Degrees Rotors-On	IV-13
IV-13	Sting Test, Mast 60 Degrees Rotor-Off	IV-13
IV-14	Sting Test, Tuft Grid	IV-14
IV-15	Force and Moment Sign Convention	IV-15
V-1	Weight Required to Maintain a Given Roll Angle versus Roll Angle, h/D = 0.5, Wing Fairings On	V-23
V-2	Weight Required to Maintain a Given Roll Angle versus Roll Angle, h/D = 0.75, Wing Fairings On	V-24
V-3	Summary of Roll Stability Characteristics in IGE Hover	V-25
V-4	Hover Performance, h/D = 1.0	V-26
V-5	Hover Performance, h/D = .75	V-27
V-6	Hover Performance, h/D = 0.5	V-28
V-7	Wing Down Load Summary, IGE	V-29
V-8	Drag Coefficient of Wing at $\alpha = 90^\circ$ versus Reynolds Number	V-30

LIST OF ILLUSTRATIONS (Cont'd)

<u>Number</u>		<u>Page</u>
V-9	Power Reduction in Ground Effect	V-31
V-10	Vertical "Spring" in Ground Effect	V-32
V-11	Level Flight Trim Parameters, Mast Angle 90°	V-33
V-12	Effect of Horizontal Stabilizer Incidence on Level Flight Trim Parameters, Mast Angle 90°	V-36
V-13	Effect of Gross Weight on Level Flight Trim Parameters, Mast Angle 90°	V-39
V-14	Effect of Wing Lift on Level Flight Trim Parameters, Mast Angle 90°	V-42
V-15	Method of Determining Simulated Rate of Descent or Climb from Rod Thrust or Drag	V-45
V-16	Trim Parameters versus Rate of Descent in Descents and Autorotation, Mast Angle 90°	V-46
V-17	Trim Parameters for Level Flight IGE, Mast Angle 90°	V-49
V-18	Sideward Flight Trim Parameters	V-51
V-19	Rearward Flight Trim Parameters	V-53
V-20	Level Flight Trim Parameters, Mast Angle 75°	V-55
V-21	Effect of Gross Weight on Level Flight Trim Parameters, Mast Angle 75°	V-58
V-22	Effect of Flaps on Level Flight Trim Para- meters, Mast Angle 75°	V-61
V-23	Level Flight Trim Parameters, Mast Angle 60°	V-64
V-24	Level Flight Trim Parameters, Mast Angle 30°	V-67
V-25	Variation of Trim Parameters with Fuselage Angle of Attack, Mast Angle 90°	V-70
V-26	Variation of Trim Parameters with Fuselage Angle of Attack, Mast Angle 75°	V-71

LIST OF ILLUSTRATIONS (Cont'd)

<u>Number</u>		<u>Page</u>
V-27	Variation of Trim Parameters with Fuselage Yaw Angle, Mast Angle 90°	V-72
V-28	Variation of Trim Parameters With Fuselage Yaw Angle, Mast Angle 75°	V-73
V-29	Blade and Control System Load Waveforms at Mast Angles 90° and 75°	V-74
V-30	Blade Station 52.5 Beamwise Oscillatory Bending Moment versus Airspeed	V-75
V-31	Blade Station 52.5 Chordwise Oscillatory Bending Moment versus Airspeed	V-76
V-32	Pitch Link Oscillatory Load versus Airspeed	V-77
V-33	Blade and Control System Loads versus Gross Weight	V-78
V-34	Frequency Spectrum of Airframe Vibration for Several Accelerometer Locations	V-79
V-35	Two-Per-Rev Vibration Level versus Airspeed	V-80
V-36	Three-Per-Rev Vibration Level versus Airspeed	V-81
V-37	Two-Per-Rev Vibration Level versus Conversion Angle	V-82
V-38	Three-Per-Rev Vibration Level versus Conversion Angle	V-83
V-39	Airframe Lift and Pitching Moment versus Angle of Attack, Rotors Removed	V-84
V-40	Airframe Yaw Moment versus Yaw Angle, Rotors Removed	V-85
V-41	Comparison of Rod Test with Sting Test Level Flight Trim Parameters, Mast 90°	V-86
V-42	Lift Coefficient versus Fuselage Angle of Attack, Mast Angle 90°, Airspeed 40 knots	V-88
V-43	Lift Coefficient versus Fuselage Angle of Attack, Mast Angle 90°, Airspeed 60 knots	V-89

LIST OF ILLUSTRATIONS (Cont'd)

<u>Number</u>		<u>Page</u>
V-44	Lift Coefficient versus Fuselage Angle of Attack, Mast Angle 90°, Airspeed 80 knots	V-90
V-45	Pitching Moment versus Fuselage Angle of Attack, Mast Angle 90°, Airspeed 40 knots	V-91
V-46	Pitching Moment versus Fuselage Angle of Attack, Mast Angle 90°, Airspeed 60 knots	V-92
V-47	Pitching Moment versus Fuselage Angle of Attack, Mast Angle 90°, Airspeed 80 knots	V-93
V-48	Yaw Moment Coefficient versus Yaw Angle, Mast Angle 90°, Airspeed 40 knots	V-94
V-49	Yaw Moment Coefficient versus Yaw Angle, Mast Angle 90°, Airspeed 60 knots	V-95
V-50	Yaw Moment Coefficient versus Yaw Angle, Mast Angle 90°, Airspeed 80 knots	V-96
V-51	Lift Coefficient versus Fuselage Angle of Attack, Mast Angle 75°, Airspeed 40 knots	V-97
V-52	Lift Coefficient versus Fuselage Angle of Attack, Mast Angle 75°, Airspeed 60 knots	V-98
V-53	Lift Coefficient versus Angle of Attack, Mast Angle 75°, Airspeed 80 knots	V-99
V-54	Pitching Moment versus Fuselage Angle of Attack, Mast Angle 75°, Airspeed 40 knots	V-100
V-55	Pitching Moment versus Fuselage Angle of Attack, Mast Angle 75°, Airspeed 60 knots	V-101
V-56	Pitching Moment versus Fuselage Angle of Attack, Mast Angle 75°, Airspeed 80 knots	V-102
V-57	Yawing Moment Coefficient versus Yaw Angle, Mast Angle 75°, Airspeed 40 knots	V-103
V-58	Yawing Moment versus Yaw Angle, Mast Angle 75° Airspeed 60 knots	V-104
V-59	Yawing Moment Coefficient versus Yaw Angle, Mast Angle 75°, Airspeed 80 knots	V-105

LIST OF ILLUSTRATIONS (Cont'd)

<u>Number</u>		<u>Page</u>
V-60	Lift Coefficient versus Fuselage Angle of Attack, Mast Angle 60°	V-106
V-61	Lift Coefficient versus Fuselage Angle of Attack, Mast Angle 30°	V-107
V-62	Pitching Moment versus Fuselage Angle of Attack, Mast Angle 60°	V-108
V-63	Pitching Moment versus Fuselage Angle of Attack, Mast Angle 30°	V-109
V-64	Yawing Moment Coefficient versus Yaw Angle, Mast Angle 60°	V-110
V-65	Yawing Moment versus Yaw Angle, Mast Angle 30°	V-111
VI-1	Flow Patterns in the Vicinity of the Empennage in Level Flight, Mast Angle 90°	VI-12
VI-2	Effect of Yaw Angle on Flow Pattern, Mast Angle 90°, Airspeed 40 Knots	VI-13
VI-3	Horizontal Stabilizer Aerodynamic Characteristics, Mast Angle 90°, Rotors Off	VI-14
VI-4	Horizontal Stabilizer Aerodynamic Characteristics, Mast Angle 75°, Rotors Off	VI-16
VI-5	Horizontal Stabilizer Aerodynamic Characteristics, Mast Angle 60°, Rotors Off	VI-18
VI-6	Horizontal Stabilizer Aerodynamic Characteristics, Mast Angle 30°, Rotors Off	VI-20
VI-7	Horizontal Stabilizer Aerodynamic Characteristics, Mast Angle 90°, Rotors On	VI-22
VI-8	Horizontal Stabilizer Aerodynamic Characteristics, Mast Angle 75°, Rotors On	VI-24
VI-9	Horizontal Stabilizer Aerodynamic Characteristics, Mast Angle 60°, Rotors On	VI-26
VI-10	Horizontal Stabilizer Aerodynamic Characteristics, Mast Angle 30°, Rotors On	VI-27

LIST OF ILLUSTRATIONS (Cont'd)

<u>Number</u>		<u>Page</u>
VI-11	Rotor Upwash at the Horizontal Stabilizer versus Angle of Attack for Several Air-speeds, Mast Angle 90°	VI-28
VI-12	Rotor Upwash at Horizontal Stabilizer in Climb and Descent Compared to Level Flight, Mast Angle 90°	VI-29
VI-13	Rotor Upwash at Horizontal Stabilizer versus Fuselage Angle of Attack, Mast Angle 75°	VI-30
VI-14	Rotor Upwash at Horizontal Stabilizer versus Fuselage Angle of Attack, Mast Angle 60°	VI-31
VI-15	Rotor Upwash at Horizontal Stabilizer versus Fuselage Angle of Attack, Mast Angle 30°	VI-32
VI-16	Comparison of Measured Upwash at Horizontal Stabilizer with Upwash Used in Phase I Study	VI-33
VI-17	Effect of Yaw Angle on Rotor Wake Upwash at Horizontal Stabilizer, Mast Angle 90°	VI-34
VI-18	Effect of Yaw Angle on Rotor Wake Upwash at Horizontal Stabilizer, Mast Angle 75°	VI-35
VI-19	Effect of Yaw Angle on Rotor Wake Upwash at Horizontal Stabilizer, Mast Angles 60° and 30°	VI-36
VI-20	Effect of Rotor Wake on Directional Stability, Mast Angle 90°	VI-37
VI-21	Effect of Rotor Wake on Directional Stability, Mast Angle 75°	VI-38
VI-22	Effect of Rotor Wake on Directional Stability, Mast Angles 60° and 30°	VI-39
VI-23	Comparison of Empennage Lift Rotors On and Rotors Off, Mast Angle 90°	VI-40
VI-24	Comparison of Rotor Lift Rotors On and Rotors Off, Mast Angle 75°	VI-41
VI-25	Comparison of Empennage Lift Rotors On and Rotors Off, Mast Angle 60°	VI-42

LIST OF ILLUSTRATIONS (Cont'd)

<u>Number</u>		<u>Page</u>
VI-26	Comparison of Empennage Lift Rotors On and Rotors Off, Mast Angle 30°	VI-43
VI-27	Comparison of Pretest Predicted Flapping with Measured Flapping, Mast Angle 90°	VI-44
VI-28	Comparison of Calculated and Observed Longitudinal Distribution of Rotor Induced Velocity	VI-45
VI-29	Comparison of Post Test Predicted Flapping With Measured Flapping, Mast Angle 90°	VI-46
VI-30	Correlation of Post Test Predicted Flapping with Measured Flapping, Mast Angle 75°	VI-47
VI-31	Comparison of Post Test Predicted Flapping with Measured Flapping, Mast Angle 60°	VI-48
VI-32	Comparison of Post Test Predicted Flapping with Measured Flapping, Mast Angle 30°	VI-49

LIST OF TABLES

<u>Number</u>		<u>Page</u>
II-1	XV-3 FLYING QUALITIES PROBLEMS	II-5
III-1	SCALE FACTORS FOR ONE-FIFTH SCALE MODEL IN AIR	III-7
III-2	MODEL DESIGN PARAMETERS	III-8
III-3	HELICOPTER MODE NATURAL FREQUENCIES	III-11
III-4	MODEL INSTRUMENTED ITEMS	III-12
V-1	CORRELATION BETWEEN CALCULATED AND MEASURED DYNAMIC STABILITY CHARACTERISTICS	V-20
V-2	EVALUATION OF MODEL CONTROLLABILITY	V-21
VI-1	COMPARISON OF LATERAL FLAPPING CALCULATED USING SEVERAL THEORIES WITH MEASURED LATERAL FLAPPING	VI-11

List of Symbols

<u>Symbol</u>	<u>Description</u>	<u>Units</u>
a_1	F/A Flapping	deg
a_H	Horizontal Stabilizer Lift Curve Slope	1/deg
b	Wing span	ft
b_1	Lateral Mapping	deg
B_{1S}	F/A Cyclic, ref. to shaft	deg
c	Wing chord	ft
D	Rotor diameter	ft
GW	Gross Weight	lb
FS	Fuselage Station	in
h	height of rotor disc above the ground	ft
h/D	height to diameter ratio	-
I_{XX}	Aircraft rolling inertia	slug-ft ²
I_{XZ}	Aircraft product of inertia	slug-ft ²
I_{YY}	Aircraft pitching inertia	slug-ft ²
I_{ZZ}	Aircraft yawing inertia	slug-ft ²
I_{GE}	In-ground-effect	-
i_H	Horizontal Stabilizer Incidence, +L. E. up	deg
$K_{R/W}$	Induced velocity constant at wing due to rotor	-
$K_{R/H}$	Induced velocity constant at hor. stab. due to rotor	-
L_H	Lift of horizontal stabilizer	lb
PM	Pitching Moment	ft-lb
q	Free stream dynamic pressure	lb/ft ²
Q	Rotor Torque (per rotor)	in-lb
RM	Rolling Moment	ft-lb
R_N	Reynolds Number	-
RPM	Rotor RPM	RPM
S	Area, W-wing, H-horizontal	ft ²
SF	Side Force	lb
T	Rotor Thrust	lb

List of Symbols

<u>Symbol</u>	<u>Description</u>	<u>Units</u>
V	Full scale aircraft airspeed	kt
V_{iR}	Induced velocity at rotor disk	ft/sec
YM	Yawing Moment	ft-lb
WL	Waterline location	in
α_F	Fuselage angle of attack	deg
α_H	Angle of attack at horizontal stab.	deg
α_m	Mast angle (ref. from airplane mode)	deg
α_{TRIM}	Fuselage angle of attack for trimmed flight	deg
β	Sideslip angle	deg
β_m	Mast angle ($90 - \alpha_m$)	deg
δ_e	Elevator deflection angle, + dn	deg
δ_F	Flapperon deflection angle, + dn	deg
$\epsilon_{W/H}$	Wing wake deflection at horiz. stab.	deg
$\epsilon_{R/H}$	Rotor wake deflection at horiz. stab.	deg
ϵ_T	Wing + Rotor wake deflection at horiz. stab.	deg
$\theta_{3/4r}$	Rotor blade collective pitch setting at three quarter radius	deg
ψ	Fuselage yaw angle, + nose right	deg
r_e	Elevator effectiveness	
η_{HWB}	Dynamic pressure ratio at the horizontal stabilizer due to wing-body interference	
η_{HT}	Dynamic pressure ratio at the horizontal stabilizer due to wing-body-rotor interference	
$\partial \alpha / \partial \beta$	Sidewash factor	
C_L	Aircraft Lift Coefficient, L/qS	
C_m	Aircraft Pitching Moment Coefficient, PM/qSc	
$C_{m_{iH}}$	Aircraft Pitching Moment Coefficient, due to horizontal stabilizer incidence	
C_{m_H}	Aircraft Pitching Moment Coefficient, due to horizontal stabilizer	

List of Symbols

<u>Symbol</u>	<u>Description</u>	<u>Units</u>
$C_{m\delta_e}$	Aircraft Pitching Moment Coefficient, due to elevator	
C_l	Aircraft Rolling Moment Coefficient, RM/qSb	
C_n	Aircraft Yawing Moment Coefficient, YM/qSb	
C_y	Aircraft Side Force Coefficient, SF/qS	

Subscripts

e	elevator
F	Fuselage
H	Horizontal Stabilizer
R	Rotor
R/H	Due to rotor at horizontal stabilizer
T	Total, includes wing wake and rotor wake
V	Vertical stabilizer
WB	Wing-Fuselage
W/H	Due to wing at horizontal stabilizer

I. SUMMARY

Two series of tests evaluated the stability and control characteristics of a one-fifth scale powered aeroelastic model of the Model 300 Tilt Rotor Research Aircraft in hover, low speed helicopter, and conversion flight. Hover tests took place in the Bell Helicopter Company rotor whirl cage from September 13, 1972 to December 22, 1972. Helicopter and conversion mode tests took place in the Vought low speed wind tunnel from January 15, 1973 to March 30, 1973. This testing was performed under NASA Contract NAS 2-6599.¹

The hover testing was directed at measuring hover performance and roll static stability characteristics. During part of this testing, the model was secured to a mount which simulated free flight to investigate stability characteristics and control response.

The helicopter and conversion mode testing was in two phases, with a different mount for each. The first phase had the model mounted on the vertical rod shown in Figure I-1. This mount gave the model freedom to pitch, roll, and yaw and to translate vertically. Model "pilots" could adjust cyclic pitch, collective pitch, and elevator position to make the model fly in a trimmed flight condition. Trimmed flight conditions tested included level flight (OGE and IGE), climbs, descents, autorotation, and rearward and sideward flight. At selected flight conditions the model was disturbed from trim to investigate dynamic stability characteristics.

The second phase had the model mounted on a sting support, as shown in Figure I-2. Forces and moments were recorded with the model in the trim attitudes and its controls in the positions established during the first phase. Pitch and yaw sweeps about the trim condition determined the static stability characteristics. Tail-on, tail-off, rotors-on, and rotors-off configurations were tested to determine the influence of the rotor wake on the empennage.

The principal results of the tests are as follows:

- (1) The hover test confirmed the presence of a static roll instability in an IGE hover. Figure I-3 shows the roll instability in terms of inches of lateral stick required to balance the unstable rolling moment. The roll instability vanishes at airspeeds above approximately 20 knots.
- (2) The hover test showed the wing download to be greater than that estimated from previous test results. The measured download was 11.4 percent, compared to the 7

(2) Continued

percent estimated for the full-scale aircraft. Analysis indicates this discrepancy may be caused by the model's very low Reynolds number.

- (3) Flow visualization techniques confirmed that the wakes from the two rotors do not merge in the flight conditions tested, and an analysis of empennage balance data indicates that the wakes produce a net upwash at the horizontal stabilizer. The upwash is greater IGE than OGE. Vortex lift produced by the rolled up rotor wakes is a significant factor in the effect of the rotor wake on the empennage.
- (4) At mast angles of 90 and 75 degrees, the longitudinal stick gradient is shallow between hover and 60 knots with a slight stick reversal occurring between 20 and 40 knots (see Figure I-4). The shallow gradient and reversal are caused by the rotor wake upwash on the horizontal stabilizer.
- (5) The interaction between the rotor wake and the horizontal stabilizer causes a nose-up pitching moment when the aircraft is yawed. The longitudinal cyclic required to compensate for the pitching moment, shown in Figure I-5, is easily within a pilot's ability. On the Model 301 aircraft, with the SCAS on, the attitude-hold loop will make the longitudinal cyclic input.
- (6) At mast angles 90, 75 and 60 degrees, the rotor wake acts on the vertical fins in such a manner as to reduce directional stability for sideslip angles less than about 12 degrees and to increase it for larger sideslip angles. At mast angles 90 and 75 degrees and at speed less than 60 knots, the rotor wake causes this aircraft to be directionally unstable between ± 4 degrees of sideslip.
- (7) In autorotation at the speeds tested (80 and 90 knots), the model was very stable but had a rate of descent in excess of 4000 fpm, compared to the 2200 fpm predicted for the Model 301. Analysis indicates that the model's low Reynolds number is responsible for its higher rates of descent. The rate of descent predicted for the Model 301 is still considered to be correct.
- (8) On the rod the model was difficult to fly at speeds below 30 knots, but was controllable. Above 30 knots, the model was relatively easy to fly. Controllability was adequate for rearward and sideward flight at speeds up to 35 knots. It was not possible to fly the

(8) Continued

model in a sustained controlled hover in the hover test rig. Failure to accomplish this task is attributed to the faster response characteristics of the model (2.24 times full scale) and because of the lack of many of the normal pilot cues. It should be noted that the model was not equipped with a stability augmentation system (SAS).

- (9) Correlation between theory² and measured trim attitudes and control positions is generally good when Reynolds numbers effects on the model are accounted for.
- (10) Lateral flapping in helicopter mode was approximately 50 percent higher than predicted, as shown in Figure I-6, but was within flapping limits for all conditions tested. Analysis shows that the computer representation of the longitudinal distribution of rotor induced velocity was not representative of the actual longitudinal distribution. By modifying the computer representation good correlation with the measured flapping was obtained. The modified method is satisfactory for design purposes.
- (11) There was no evidence of rotor or rotor-pylon-wing instability during the tests.
- (12) Scaled rotor and control system loads were significantly lower than those predicted for the full-scale aircraft.
- (13) Airframe vibration levels were higher than predicted but within design limits.

Note: In referring to the Model 301 throughout the report, the Model 301 is of similar configuration as the Model 300. The Model 300 data is therefore considered applicable to the Model 301.

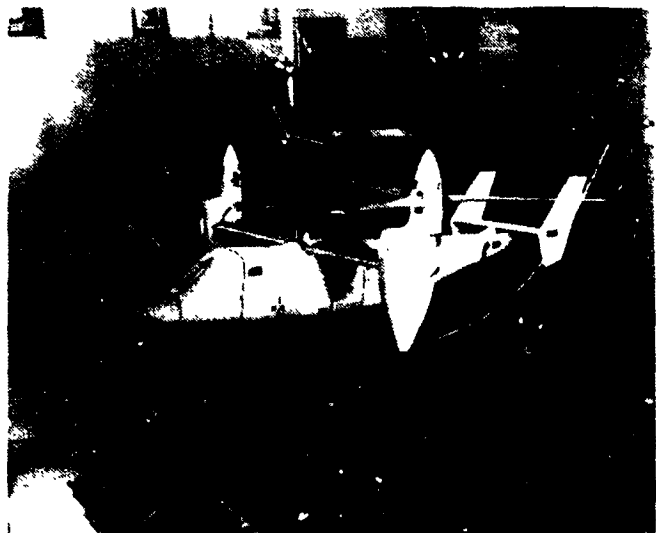


Figure I-1. Powered Aeroelastic Model on Vertical Rod Mount, LTV LSWT Test 418, January 1973.

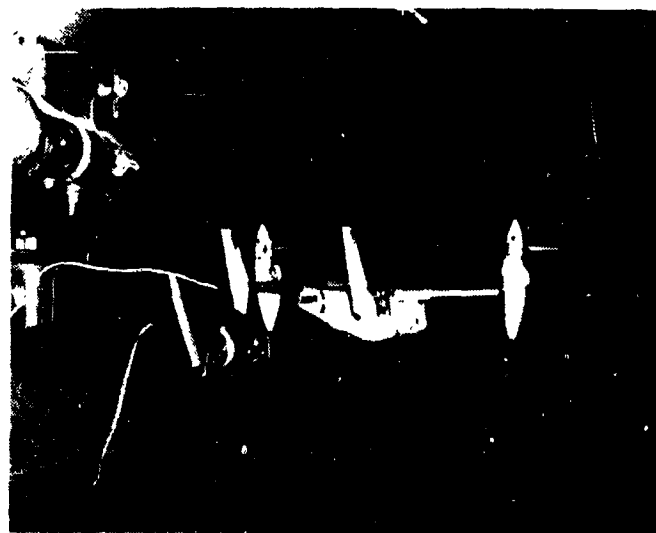


Figure I-2. Powered Aeroelastic Model on Sting Mount, LTV LSWT Test 421 March 1973.

HOVER TEST
MAST ANGLE = 90°

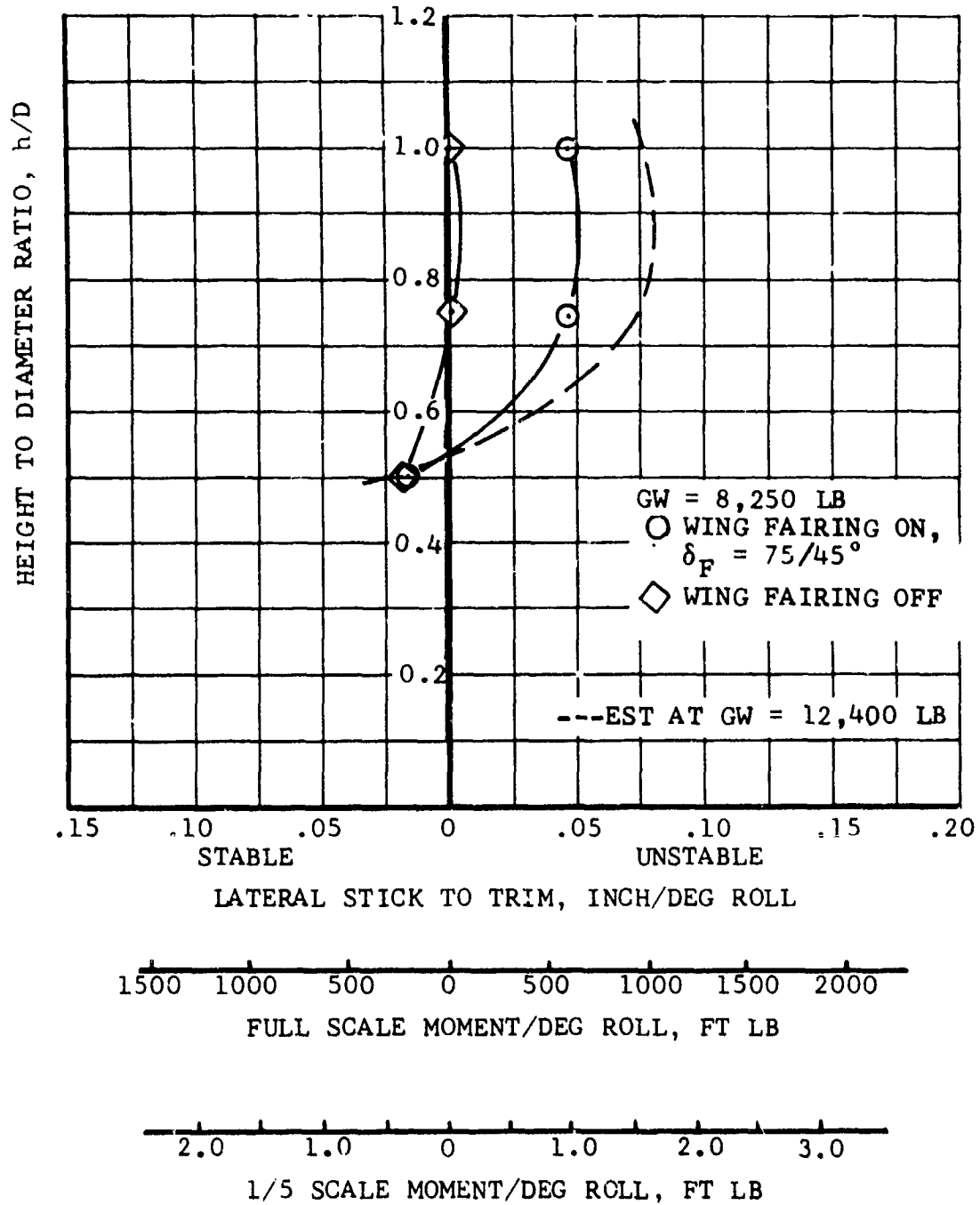


Figure I-3. Summary of Roll Stability Characteristics in IGE Hover.

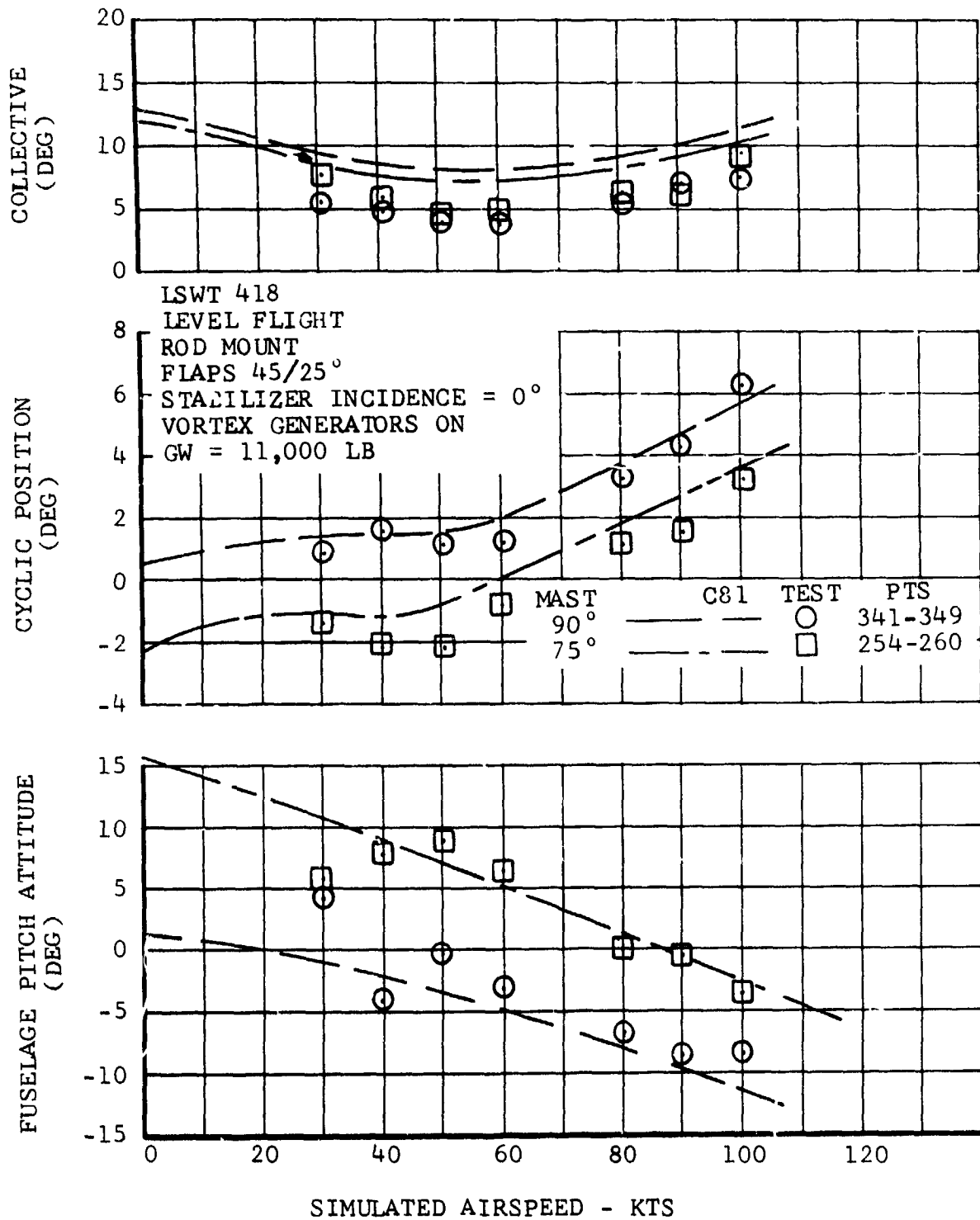


Figure I-4. Level Flight Trim Attitude and Control Positions Versus Airspeed, Mast Angles 90° and 75°.

LSWT 418
YAW SWEEP
ROD MOUNT
FLAPS = 45/25°
STABILIZER INCIDENCE = 0°
VORTEX GENERATORS ON
GW = 11,000 LB

	MAST	PTS
○	90°	370-372
□	75°	268-273

AIRSPEED 40 KTS

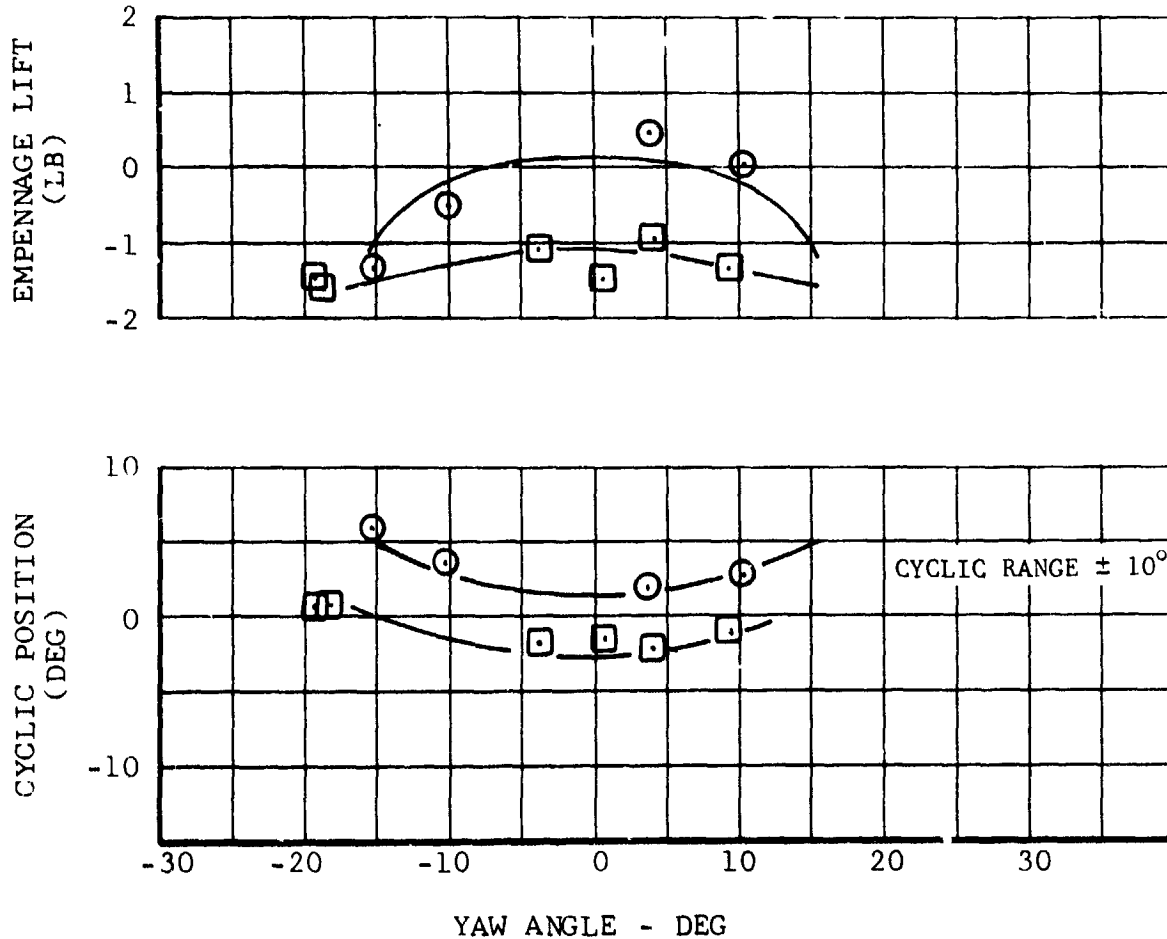


Figure I-5. Level Flight Trim Longitudinal Cyclic Versus Yaw Angle, Mast Angles 90° and 75°.

LSWT 418
LEVEL FLIGHT
ROD MOUNT
FLAPS 45/25°
STABILIZER INCIDENCE = 0°
VORTEX GENERATORS ON
GW = 11,000 LB

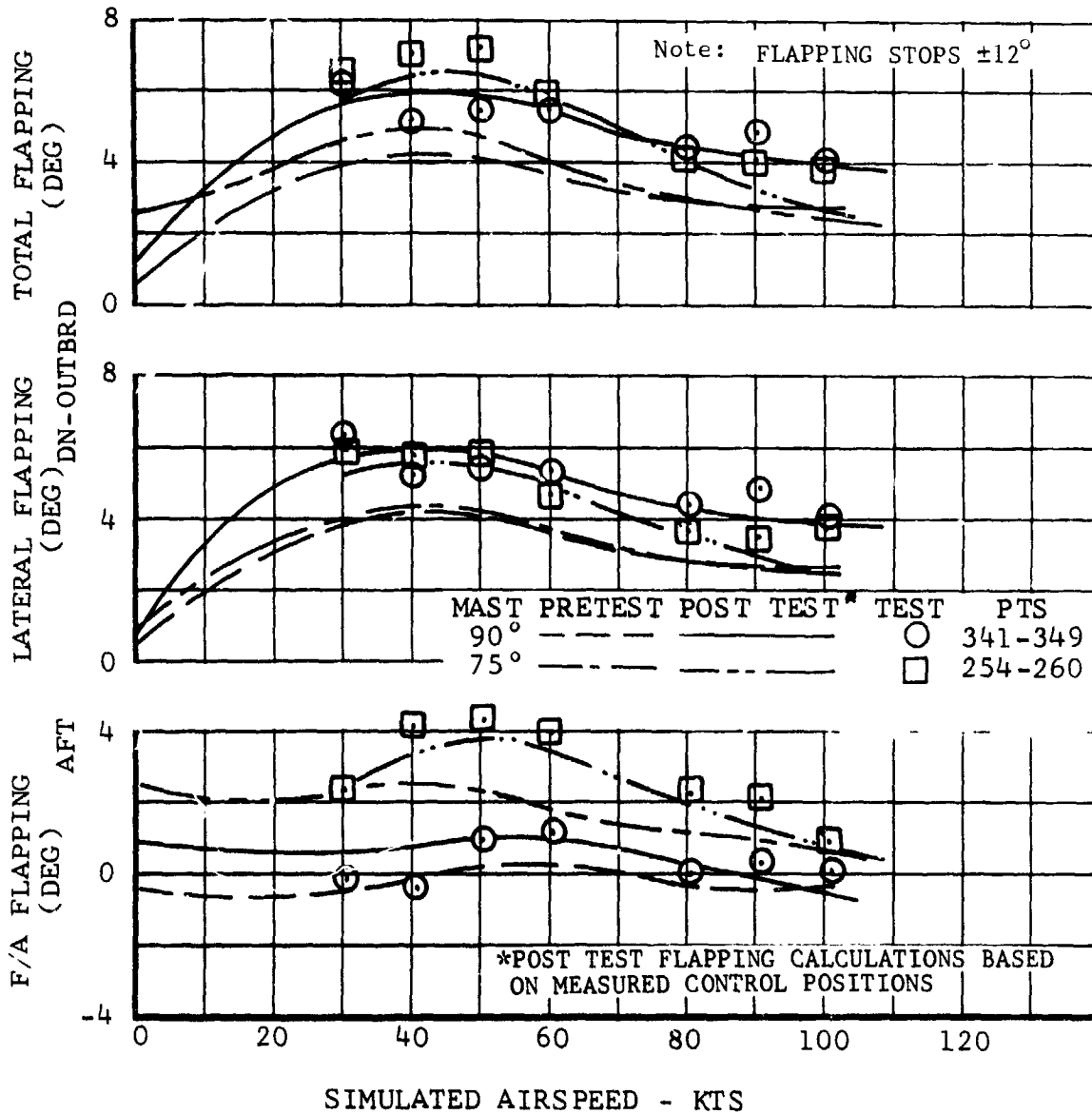


Figure I-6. Correlation Between Calculated and Measured Flapping, Mast Angles 90° and 75°.

II. INTRODUCTION

This report presents the results of an investigation into the hover, low speed helicopter and conversion flight characteristics of the Model 301 Tilt Rotor Research Aircraft. A one-fifth scale, powered aeroelastic model of the Bell Model 300 tilt rotor aircraft was tested to determine performance, stability and control, and aeroelastic characteristics. The Model 300 and 301 are nearly identical designs differing primarily in the power plant installations; therefore, the results of the tests are readily applicable to the Model 301. The principle objectives were to identify if any significant problems existed and to obtain data on rotor wake/airframe aerodynamic interference for use in the Model 301 real-time flight simulation mathematical model. The investigation was conducted under NASA Contract NAS 2-6599.

A. Previous Tests

Scale model testing of the Model 300, under way since 1968, has been directed at verifying that the aircraft met design requirements. These tests were a part of Bell Helicopter Company's tilt rotor IR & D program. One-fifth scale aerodynamic and aeroelastic models were designed and fabricated to confirm airframe performance, stability characteristics, dynamic design criteria, and demonstrate the aircraft to be free from flutter or other aeroelastic instability.³⁻¹¹ Airplane configuration tests of the aeroelastic model (unpowered) in the NASA Langley 16-foot Transonic Dynamic Tunnel were successfully completed in April 1972. This test confirmed the Model 300 to be free of rotor-pylon-wing instability and other forms of aeroelastic instability at all speeds up to 1.2 times limit dive airspeed, that the aircraft short period and Dutch Roll modes are adequately damped beyond the limit dive airspeed of the aircraft, and that loads and vibration levels are within design limits. The results of the airplane test program are discussed in Reference 12.

B. Technical Background

The results of the XV-3 convertiplane tests¹³, recent tests of a powered force model¹⁴, and analysis of the Model 301 stability and control characteristics were the basis for planning the current series of investigations. During the XV-3 flight test program several stability and control problems were noted in hover and low speed helicopter flights. No serious flying problems were encountered when operating at intermediate conversion angles or when converting. In airplane flight the only significant problems were light damping of the Dutch Roll and longitudinal short period modes and excessive transient flapping during maneuvers. A full scale wind tunnel test later indicated the potential of rotor-pylon-wing aeroelastic instability. The model tests, discussed above, have verified that the airplane flight problems have

B. (Continued)

been solved in the Model 300 and 301 designs. Problems encountered in hover and low speed helicopter flight during the XV-3 program, some of which have been addressed during this test program, are summarized in Table II-1.

Items 6 and 7 in Table II-1 have been corrected in the Model 301 design by providing adequate control power about all three axes. The pitch control power is 4.5 times, and the yaw control 2.74 times that of the XV-3. Item 3, likewise has been corrected in that the Model 301 has considerable excess power, whereas the XV-3 had insufficient power to hover. A blade-pitch governor, rather than pilot coordination, will automatically maintain rotor speed. As a result, the pilot effort required in the Model 301 to cope with the power rise is reduced to a level comparable to typical turbine-powered helicopters. The other items listed are inherent in the tilt rotor concept and are expected to occur to some degree in the Model 301 as discussed in the section noted. The subject investigation was directed at evaluating the magnitude of these problems and in obtaining data for use in real time flight simulation of the Model 301. The latter objective is significant since the real time flight simulation will be used to guide the design of the Model 301's Stability and Control Augmentation System which provides a substantial improvement in the flight characteristics in hover and in low speed helicopter flight. (The XV-3 did not have a stability and control augmentation system.)

C. Scope of the Program

The test program was accomplished in four tasks.

1. Task I Pretest Activities

Modifications were made to the model to meet the test requirements as follows:

- Addition of rotor drive system and motors
- Remote controlled rotor cyclic, differential cyclic, collective, and differential collective. Controls were designed with frequency response characteristics required to "fly" the model in semifree flight.
- Install a strain gage balance in the empennage to measure horizontal stabilizer normal force and rolling moment.

A hover test rig was designed for the semifree flight hover tests.

2. Task II Hover Test

The hover test was accomplished in two phases:

Phase I - Obtain performance and static stability data

Phase II - Obtain controllability data

3. Task III Wind Tunnel Test

Wind tunnel testing was in the low speed helicopter and conversion flight configurations. The model was tested in the Vought Aeronautics Low Speed Wind Tunnel located in Grand Prairie, Texas.¹⁵ The Vought tunnel has a 15 by 20-foot test section that can operate through a speed range of 9 to 77 feet per second and was ideal for this test program. Two types of mounting systems were used during this testing.

Phase I - Rod mount test which allowed the model to pitch, roll, yaw, and translate vertically. During this test trim flight data was obtained, dynamic stability characteristics were determined, and controllability was evaluated.

Phase II - Sting mount test with a six-component internal balance. This testing provided necessary data to define rotor wake/airframe aerodynamic interference.

4. Task IV Documentation

This task consisted of technical reports on program progress and analysis of test results.

D. Objectives of the Program

The investigation had the following specific objectives:

1. Measure roll static stability in hover as a function of hovering height (h/D).
2. Examine controllability in hover by "flying" the model in near free flight conditions.
3. Determine control settings for trimmed level flight, climbs, descents, rearward, and sideward flight, both in and out of ground effect.
4. Measure dynamic stability characteristics in low speed helicopter and conversion flight.

5. Investigate controllability in low speed helicopter and conversion flight.
6. Measure autorotational rate of descent and control positions.
7. Measure rotor wake effects on the empennage in sufficient detail to develop a mathematical model for real-time flight simulation.
8. Measure rotor and control system loads, airframe vibration, and aeroelastic stability during hover, low speed helicopter, and conversion flight.

All of these objectives were accomplished and the results are reported and discussed in the following sections.

TABLE II-1. XV-3 FLYING QUALITIES PROBLEMS

Problem Encountered During the XV-3 Test Program ¹³	Action Taken During The Test Program and Resolution of Problem in M301 Design
<p>1. <u>Roll Instability, IGE</u></p> <p>"When hovering within 5 feet of the ground the XV-3 exhibited an erratic tendency to dart laterally. These characteristics were considered unacceptable. Above a 5 foot skid height, these characteristics disappeared and a stabilized hover over a spot was accomplished without difficulty. ... When approaching the power required for hovering lift-off the aircraft reacted with a lateral oscillation that was disturbing to the pilot."</p>	<p>Action: Hover test to measure roll stability, Section V-A</p> <p>Resolution: Improved control power and addition of SCAS which provides additional roll damping</p>
<p>2. <u>Low Speed Stick Reversal</u></p> <p>"At low forward speeds (15 to 20 knots CAS) and small conversion angles ($\alpha_m = 90^\circ$ to 75°), there was a longitudinal stick position reversal. This characteristic had to be anticipated for each take-off."</p>	<p>Action: Rod test, cyclic stick position for level flight, Section V-B</p> <p>Resolution: Improved control power with small stick reversal (within MIL-SPEC Requirements)</p>
<p>3. <u>Increase in Power Required as Hovering Flight is Approached</u></p> <p>"At speeds between hover and best climb speed there was a large reduction in power required, which provided good forward acceleration and STOL capability. ... When approaching for a zero speed landing the change in power was even more pronounced. As hovering flight was approached (approximately 10 knots CAS) there was a sudden requirement for an additional 9 to 10 inches Hg manifold pressure. Even though</p>	<p>Action: Rod test demonstrates the effect of power (torque) change with airspeed, Section V-B</p> <p>Resolution: Increased power available and blade-pitch governor to give pilot effort</p>

TABLE II-1. (Continued)

Problem Encountered During the XV-3 Test Program ¹³	Action Taken During The Test Program and Resolution of Problem in M301 Design
<p>3. (Continued)</p> <p>anticipating this condition, it was nearly impossible to prevent the aircraft from suddenly losing 2 or 3 feet of altitude before sufficient power for stabilized hover could be obtained. This characteristic was undesirable and was considered a safety of flight item."</p>	<p>comparable to typical turbine-powered helicopter.</p>
<p>4. <u>Dynamic Directional Stability and Pitch With Yaw</u></p> <p>"In general, the stability and controllability characteristics in the helicopter level flight regime were satisfactory except at speeds below 35 knots CAS. At low speeds a divergent long-period (6 seconds per cycle) directional oscillation was apparent. The amplitude of this oscillation increased to the point where the tail swung into the proprotor wash, promptly inducing nose up pitch."</p>	<p>Action: Dynamic stability check during rod test, Section V-B, static directional stability, sting test, Section V-C, and analysis of rotor wake during sideslip, Section VI-A</p> <p>Resolution: Addition of SCAS</p>
<p>5. <u>Dynamic Longitudinal Stability</u></p> <p>"Longitudinal dynamic stability in configuration H and C15 was excellent above 40 knots CAS. Response to a pulse input of the longitudinal control was essentially deadbeat. At 25 knots or lower an unacceptable pitching oscillation was present. It was virtually impossible to stabilize the aircraft longitudinally in this low speed regime."</p>	<p>Action: Dynamic stability check during rod test, Section V-B</p> <p>Resolution: Addition of SCAS</p>
<p>6. <u>Longitudinal Controllability</u></p> <p>"The longitudinal maneuverability was unacceptable in the low speed (30 knots CAS or less), small conversion angle (C15 or Less) regime.</p>	<p>No testing of control power, Model 301 control power higher than XV-3</p>

TABLE II-1. (Continued)

Problem Encountered During the XV-3 Test Program ¹³	Action Taken During The Test Program
6. (Continued)	
The primary problem was in the poor response to control inputs. For example, in C15 at 30 knots CAS, after 0.4 inch aft control pulse, 2.3 seconds were required to obtain the maximum pitch rate of 3 degrees per second. ... At a higher speed, 42 knots, 1.9 degrees per second was recorded after 0.7 seconds after a similar stick displacement. The 0.7 second response time was acceptable."	
7. <u>Directional Controllability</u>	
"The directional maneuverability was unacceptable primarily because of poor response characteristics. At 30 knots CAS in configuration H, a maximum rate of yaw per inch pedal displacement of 12.4 degrees per second was recorded. However, more than 3 seconds were required to reach this maximum rate of yaw. ... The excessive delay time is especially irritating in the XV-3 because of the poor lateral directional stability characteristics in the low speed regime."	No testing of control power. Model 301 control power higher than XV-3

III. DESCRIPTION OF THE MODEL

The model tested is a one-fifth length scale, dynamically and aerodynamically similar model of the Bell Model 300 Tilt Rotor Research Aircraft. The model was designed and fabricated under Bell's Tilt Rotor research program and prior to this test program had been used for tests involving over 900 hours of test section occupancy. As noted earlier in Section II the purpose of previous testing was to investigate aeroelastic and flight stability characteristics in airplane mode. The tests were conducted with the model unpowered, since the windmilling thrust condition is the most critical from the standpoint of rotor-pylon-wing stability. These tests were made using remote trim type collective pitch and elevator controls. For the hover, low speed helicopter, and conversion tests the model was powered and had proportional type controls.

A. Model Scaling

Scale factors for the aeroelastic model are given in Table III-1. All components of the model have been weighed and swung to determine inertia properties and, where possible, stiffness properties have been measured. Vibration surveys have been conducted to verify dynamic similitude (see Reference 12). A force and moment wind tunnel test of the airframe less rotors has verified that the aerodynamic characteristics are the same as the Model 300 force and moment model.

B. Construction and Design Parameters

The basic dimensional parameters for the aeroelastic model are given in Table III-2 along with the corresponding full scale design parameters. A description of the model components are as follows:

1. Fuselage

The fuselage is an aluminum box spar, partially foam filled, which represents the fuselage stiffness both in bending and torsion. Figure III-1 shows the fuselage spar during buildup for the sting mount test. Non-structural fiberglass fairings, shown partially installed in Figure III-2, form the fuselage contour. The fuselage houses the instrumentation package, the motors, as well as balance weights used to simulate gross weight and center of gravity configurations.

2. Empennage

The horizontal stabilizer is composed of an aluminum spar which provides the required beam, chord, and torsional stiffness, and nonstructural segmented balsa and fiberglass fairings which give the aerodynamic shape. The elevator is remotely controlled. The mass balance of the elevator is duplicated. The vertical stabilizers, made entirely of balsa, were not designed to give the correct stiffness properties but have the correct mass, center of gravity and inertia. The rudders are not provided on the model.

A two component empennage balance was designed and fabricated for the helicopter and conversion portions of this program. The balance measures empennage lift and rolling moment. Figure III-3 shows a close up of the empennage balance. Empennage incidence is ground adjustable.

3. Wing

The bending and torsional stiffness characteristics of the wing are scaled by an aluminum spar filled with aluminum honeycomb. Aluminum-covered, nonstructural, segmented fairings provide the aerodynamic contour. Lead weights attached to the spar simulate fuel weight.

The wing spar is made in three parts: left and right sections (with 6.5 degrees forward sweep) and a carry-through center section with zero sweep. This arrangement maintains the chordwise location of the wing elastic axis. The attachments of the outer segments to the center section are at buttline 5.6 (model scale). This is also the location of the wing fuselage attachment, simulating to some degree the full scale wing-to-fuselage load paths.

The wing-pylon attachment is at buttline 35.85 (model scale). The full scale load paths are maintained through the ribs which carry the conversion spindle hanger bearings.

4. Nacelles

The distributed stiffness properties of the nacelle structure is not scaled, but mass, center of gravity, inertias, and mounting stiffnesses are matched to give the correct frequencies. Non-structural fiberglass fairings house the transmission drive system, collective drive system and dummy engine mounts. The engine mounts are designed to give the correct engine pitch and yaw natural frequencies. The transmissions have full-scale

4. (Continued)

gear ratios, therefore, the interconnect torque characteristics are scaled. (However, the torsional stiffness of the interconnect shafting is not scaled. It is several times the full-scale equivalent stiffness.)

Conversion struts with scaled axial stiffness provide the correct wing torsion (pylon pitch) natural frequencies in helicopter and conversion modes. The struts allow for manual adjustment of the pylon conversion angle from 95° (helicopter mode) to 0° (airplane mode) in fifteen degree increments.

5. Rotors

The blades are constructed to scale the appropriate material modulus, beamwise, chordwise, and torsional stiffness. Both the blade spar and the outer shell are fiberglass. The aluminum blade grips, which carry the pitch-change bearings, are bonded to the blade structure at the blade root. The aluminum hub yoke rings are machined to represent the yoke inplane and out-of-plane stiffness. Stainless steel spindles are assembled with a thermal fit to the hub. The retention system for attaching the blades to the hub duplicates the full scale design. The rotor system is shown in Figure III-4.

6. Drive System

Power for the rotors is provided by two task motors (3.4 horsepower each) mounted aft of the center wing section in the fuselage as shown in Figure III-5. The motors drive forward to individual right angle gearboxes which in turn power the rotor interconnect drive shaft. A two layer fiberglass coupling to relieve misalignment is located between each motor and gearbox. At the beginning of the test a coupling between the motor gearbox and the interconnect shafting was also used. Following failures of this coupling during testing, the drive system was redesigned to eliminate misalignment between the gearboxes and the interconnect shaft and couplings were added between the left and right gearboxes. Figure III-5 shows motors and gearboxes following a coupling failure prior to the redesign of the drive system. Additional couplings are used along the interconnect shaft outboard of the motors and at the outboard section of the wing to relieve misalignment. The interconnect shaft connects to 90 degree gearboxes mounted on the pylons. The pylon shaft is mounted to the pylon axis and drives two stage planetary gearboxes. The output shaft of the planetary gearboxes has a

6. (Continued)

coupling which enables the rotors to be readily disconnected from the drive system. The gear ratio of the transmission is 17.6 to 1; thus with the rotors at 1260 rpm, the normal operating speed, the interconnect shaft is turning at 22170 rpm.

C. Model Controls

A dc servo feedback system was used for the rotor controls because of the advantages of simplicity and reliability offered by the dc system. To determine design requirements for the rotor controls a mathematical model of the IGE hover dynamics, including the roll static instability, was derived and programmed on an analog computer. Several of the model "pilots" flew the math model using a control stick similar to that used with the aeroelastic model. Each pilot evaluated control systems having varying amounts of hysteresis, various time constants and values of rate limiting. The following design parameters were established: (1) hysteresis of two percent maximum, (2) time constant of 0.15 seconds maximum, and (3) rate limit of 3.5 degrees per second minimum. These are applicable to the model-pilot system and cannot be directly related to full-scale. A dc servo system which met these requirements was designed and fabricated. The system provided collective pitch, differential collective (for roll control), longitudinal cyclic, and differential cyclic (for yaw control).

The elevator and ailerons were controlled using "beep" type controls. Flaps and empennage incidence were ground adjustable.

D. Natural Frequencies

Prior to wind tunnel testing of the model in airplane mode a complete shake test was performed to verify placement of natural frequencies¹². Comparison of the frequencies obtained at that time with those calculated for the full-scale design indicated a good dynamic similitude. Therefore, prior to testing the model in helicopter mode it was only necessary to confirm the location of modes affected by nacelle conversion.

As noted earlier, conversion struts having scaled axial stiffness were used to provide the correct pitching mode frequency of the pylons. As shown in Table III-3 the measured pitching mode frequency is slightly above the full-scale equivalent frequency. However, this provided adequate margin with respect to one-per-rev resonance which was a major concern. The other important frequencies which were affected by the change to helicopter mode are also summarized.

E. Instrumentation

1. General

The model was instrumented to provide 61 channels of data as shown in Table III-4. The locations of the transducers were chosen to provide the required information on loads and stability.

A maximum of 39 of the 61 available channels was multiplexed from the model to the Bell Offsite Data Acquisition Package (ODAP). From the ODAP the data was recorded on magnetic tape and on direct write oscillographs, with selected data monitored on panel meters.

A schematic of the ODAP system as used on the model is shown in Figure III-6. The components of the system are identified as follows:

- Model Patch Panel - This panel, in the model, allows various transducers to be selected for signal conditioning and read out.
- Signal Conditioners - These amplify the transducer outputs to an analog output of ± 2.5 volts full scale. There are 39 signal conditioners available in the model.
- Voltage Controlled Oscillator - The VCO uses the conditioned analog output of each transducer to modulate the output frequency of an oscillator. These outputs are mixed in a linear mixer amplifier to create a composite signal containing up to 13 channels of data. There are 39 VCO's in the model which provide two channels of multiplexed data. This minimizes model umbilical cross-section requirements for carrying instrumentation data.
- Discriminators - Twenty-six (26) discriminators are available to return the multiplexed signal to an analog form. These are mounted in the portion of the equipment located in the model control room (Figure III-7). Selected data may be enlarged or reduced in amplitude at this point for display on panel meters (Figure III-8) or oscillograph recorders (Figure III-9). All composite signals are also recorded on magnetic tape, also shown in Figure III-7.

1. (Continued)

As shown in Figure III-8 a closed circuit TV was used to monitor the test so that problems during a run could be reviewed. The equipment used to monitor temperatures and the power supply to the motors is shown in Figure III-10.

2. Model Rotating System

One blade on the right hand rotor was fully instrumented with beam, chord, and torsion gages. In addition the hub, rotating controls, and shaft were gaged for pitch link loads, blade flapping and shaft torque. Both rotors were gaged for cyclic and collective pitch. The right rotor was fitted with a 28-ring slipring.

An encoder wheel was mounted on each rotor shaft to generate rpm and azimuth signals.

3. Non-Rotating System

Each wing spar was gaged for beam, chord and torsion. Accelerometers were mounted on each pylon as well as along the fuselage to obtain dynamic data. The gimbal-ring mount to the vertical rod was instrumented to provide fuselage pitch, roll, yaw and vertical position data. In addition a three axis gyro was used to obtain pitch, roll and yaw rates. The horizontal tail was gaged for beam and torsion bending loads and the vertical tail had provisions for mounting two accelerometers.

4. Balance Systems

On the rod mount a strain gage balance was placed in the model gimbal slider to measure the drag or thrust of the model. During the sting mount test, six component internal balance data referenced to the aircraft center of gravity was recorded. The empennage was mounted on a balance (Figure III-3) which measured empennage lift and rolling moment.

TABLE III-1 SCALE FACTORS FOR ONE-FIFTH SCALE MODEL IN AIR

Parameter	Scale Factor (Model/Full Scale)
Froude Number	1.0
Locke Number	1.0
Mach Number	0.447
Reynolds Number	0.0894
Length	0.2
Density	1.0
Velocity	0.447
Time	0.447
Mass	0.008
Frequency	2.24
Force	0.008
Power	0.00358
Bending Moment	0.0016
Stiffness	0.00032
Bending Spring Rate	0.04
Torsional Spring Rate	0.0016

TABLE III-2. MODEL DESIGN PARAMETERS

	Full Scale	Model
Aircraft:		
Overall Length	505 IN.	101.0
Overall Width (Rotor Turning)	686 IN.	137.2
Overall Height	300 IN.	60.0
Design Gross Weight	13000 LB	104
Model Flying Weight	11125 LB	89
Rotors:		
Blades Per Rotor	3	3
Diameter	25 FT	5
Blade Chord (Basic)	14 IN.	2.8
Hub Precone Angle	2.5 DEG	2.5
δ_3 (Minimum)	-15 DEG	-15
Flapping Clearance	± 12 DEG	± 12
Wing:		
Span (Pylon Edge to Pylon Edge)	412.80 IN.	82.56
Span (Pylon Centerline to Pylon Centerline)	386 IN.	77.2
Area (Total)	181 SQ FT	7.25
Mean Aerodynamic Chord	5.255 FT	1.045
Airfoil Section (Constant)	NACA 64A223 Modified	NACA 64A223 Modified

TABLE III-2. MODEL DESIGN PARAMETERS CONT'D.

	Full Scale	Model
Wing Cont'd:		
Aspect Ratio	6.6	6.6
Forward Sweep Angle	DEG	6.5
Dihedral	2.0	2.167
Aileron:		
Span (Along Hingeline)	94.32	19.0
Chord/Wing Chord	.25	.25
Flap:		
Span (Along Hingeline)	51.0	10.5
Chord/Wing Chord	.25	.25
Fuselage:		
Length	492	98.45
Maximum Breadth	66	13.2
Maximum Depth	74	14.8
Vertical Stabilizer:		
Span	92.16	18.44
Total Area Per Side	SQ FT	2.00
Aspect Ratio	1.18	1.18
Root Chord	49.04	9.808

TABLE III-2. MODEL DESIGN PARAMETERS CONT'D.

	Full Scale	Model
Vertical Stabilizer Cont'd:		
Tip Chord (Both Ends)	IN. 28.75	5.75
Mean Aerodynamic Chord	IN. 44.7	8.94
1/4 Chord at F.S. (Total)	570.015	114.003
1/4 Chord at W.L. (Total)	115.69	23.13
Sweep of 1/4 Chordline (Upper)	DEG 31.6	31.5
Horizontal Stabilizer:		
Span	IN. 153.96	30.8
Total Area	SQ FT 50.25	2.0
Aspect Ratio	3.28	3.28
Angle of Incidence	DEG +20 to -10	+25 to -25
Sweep of 1/4 Chordline	DEG 0.0	0.0
Root Chord	IN. 47.04	9.40
Tip Chord	IN. 47.04	9.40
Mean Aerodynamic Chord	IN. 47.04	9.40
1/4 Chord at F.S.	560.0	112.0
1/4 Chord at W.L.	103.0	20.6
Elevator:		
Area	SQ FT 13.0	.52
Chord/Stabilizer Chord	.30	.30

TABLE III-3. HELICOPTER MODE NATURAL FREQUENCIES

Mode	Frequencies - cps	
	Full-Scale Equivalent	Model Measured
Wing Symmetric Beam	7.17	6.8
Wing Chord	11.20	12.0
Wing Torsion (Pylon Pitching)	15.90	17.0
Horizontal Tail Beam	24.0	26.0
Pylon Yaw	25.0	26.0
Horizontal Tail Torsion	37.63	38.0

TABLE III-4. MODEL INSTRUMENTED ITEMS

Right-Hand Rotor Blade	Beam 31.7 Percent
Right-Hand Rotor Blade	Chord 31.7 Percent
Right-Hand Rotor Blade	Torsion 31.7 Percent
Right-Hand Rotor Blade	Beam 50 Percent
Right-Hand Rotor Blade	Chord 50 Percent
Right-Hand Rotor Blade	Beam 50 Percent
Right-Hand Rotor Blade	Chord 50 Percent
Right-Hand Yoke Chord	
Right-Hand Pitch Link	
Right-Hand Rotor Shaft	Torque
Right-Hand Rotor Flapping	
Right-Hand Rotor Tachometer	
Left-Hand Rotor Tachometer	
Right-Hand Rotor Collective Position	
Right-Hand Rotor Cyclic Position	
Left-Hand Rotor Collective Position	
Left-Hand Rotor Cyclic Position	
Right-Hand Wing Pod Conversion Strut	
Right-Hand Wing Pod Accelerometer	Longitudinal (Conv. Axis)

TABLE III-4. MODEL INSTRUMENTED ITEMS CONT'D.

Right-Hand Wing Pod Accelerometer	Axial (Conv. Axis)
Right-Hand Wing Pod Accelerometer	Longitudinal (Xmsn Case)
Right-Hand Wing Pod Accelerometer	Lateral (Xmsn Case)
Right-Hand Wing Spar	Beam 27.2 Percent
Right-Hand Wing Spar	Chord 27.2 Percent
Right-Hand Wing Spar	Torsion 27.2 Percent
Right-Hand Wing Spar	Beam 52 Percent
Right-Hand Wing Spar	Chord 52 Percent
Right-Hand Wing Spar	Torsion 52 Percent
Left-Hand Wing Pod Conversion Strut	Longitudinal (Xmsn Case)
Left-Hand Wing Pod Accelerometer	Beam 27.2 Percent
Left-Hand Wing Spar	Chord 27.2 Percent
Left-Hand Wing Spar	Torsion 27.2 Percent
Left-Hand Wing Spar	Beam 52 Percent
Left-Hand Wing Spar	Chord 52 Percent
Left-Hand Wing Spar	Torsion 52 Percent
Aft Fuselage Spar Vertical	Beam Station 71.79
Aft Fuselage Spar Horizontal	Beam Station 71.79
Aft Fuselage Spar	Torsion Station 71.79
Fuselage Crew Station Accelerometer	Vertical

TABLE III-4. MODEL INSTRUMENTED ITEMS CONT'D.

Fuselage Center of Gravity Accelerometer	Vertical
Aircraft Drag	
Aircraft Position	Pitch Rate
Aircraft Position	Roll Rate
Aircraft Position	Yaw Rate
Aircraft Position	Pitch Attitude
Aircraft Position	Roll Attitude
Aircraft Position	Yaw Attitude
Elevator Position	
Aileron Position	
Right-Hand Empennage Horizontal Spar	Inboard Beam
Right-Hand Empennage Horizontal Spar	Inboard Chord
Right-Hand Empennage Horizontal Spar	Inboard Torsion
Left-Hand Empennage Horizontal Spar	Inboard Beam
Left-Hand Empennage Horizontal Spar	Inboard Chord
Left-Hand Empennage Horizontal Spar	Inboard Torsion
Right-Hand Vertical Stabilizer Accelerometer	Fore and Aft
Left-Hand Vertical Stabilizer Accelerometer	Fore and Aft
Empennage Balance	Lift
Empennage Balance	Rolling Moment

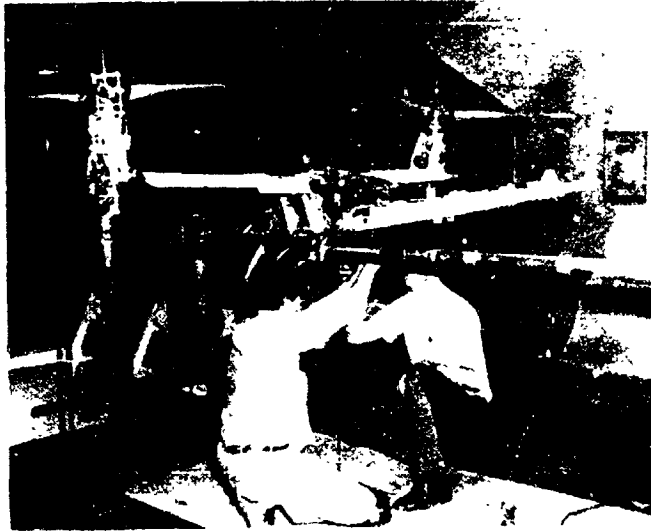


Figure III-1. Fuselage, Rotor Hub, and Rotor Shaft Assembly.

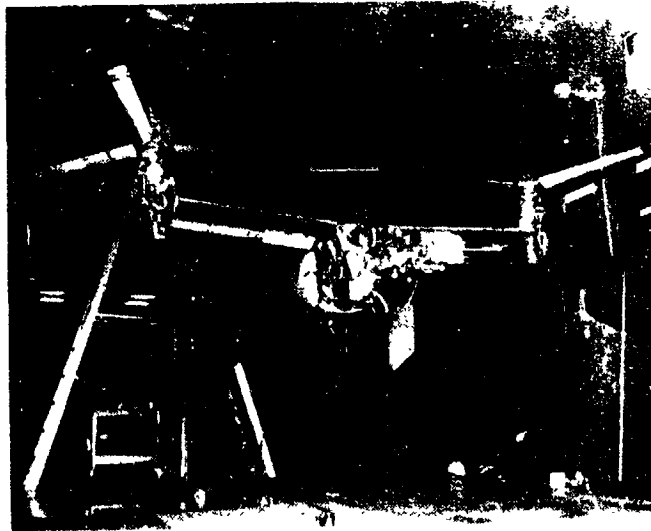


Figure III-2. Fuselage Fairings.

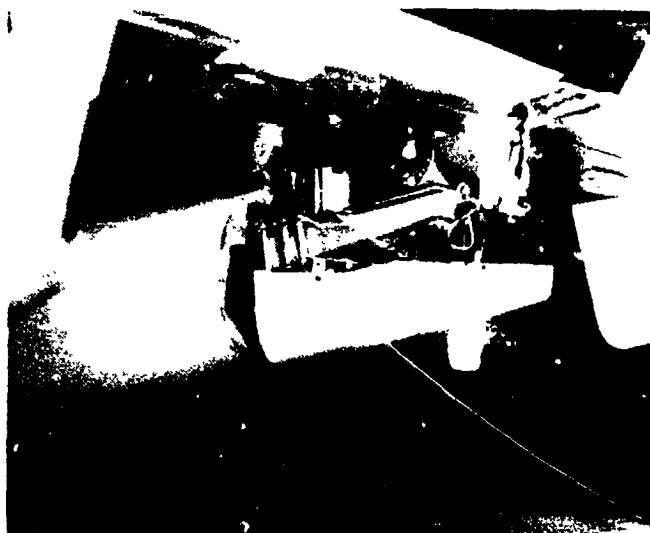


Figure III-3. Empennage Balance and Variable Incidence Adjustment.



Figure III-4. Rotor-Hub.

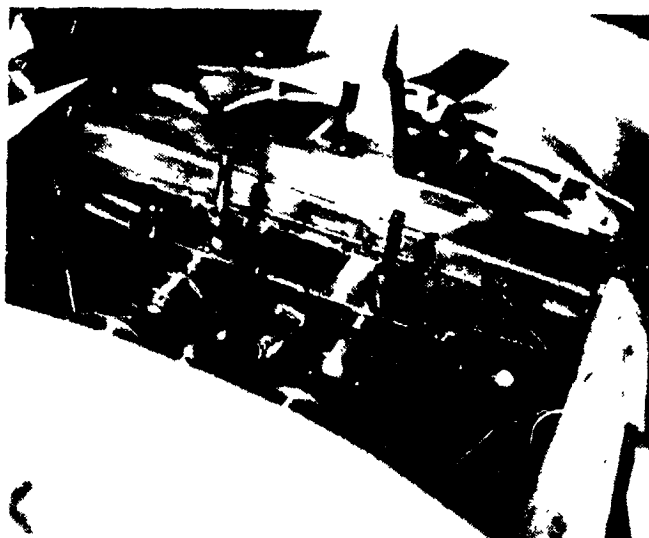


Figure III-5. Model Motors, Couplings, and
Interconnect Shaft (Following
Coupling Failure).

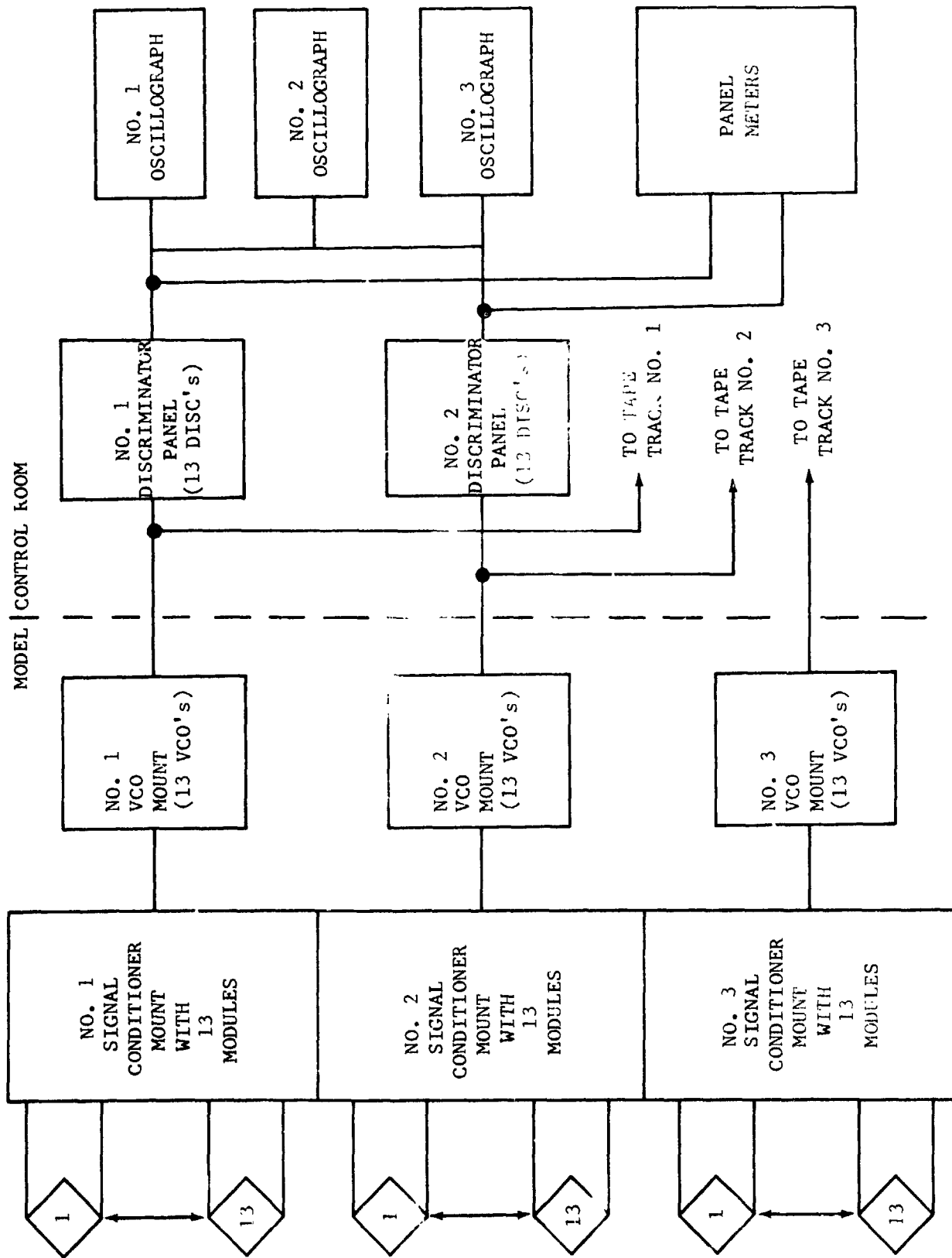


Figure III-6. Schematic of Offsite Data Acquisition Package.

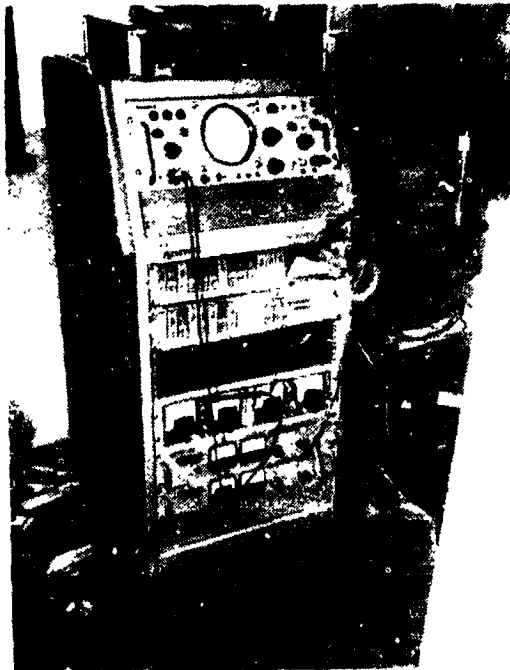


Figure III-7. Instrumentation, Discriminator
Panel and Magnetic Tape.

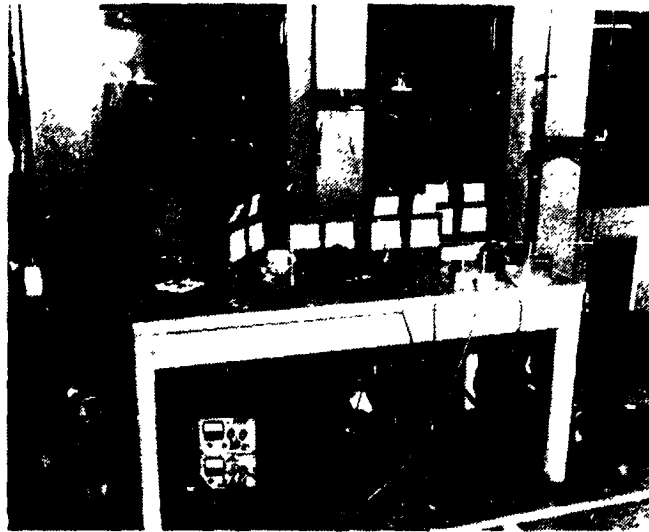


Figure III-8. Instrumentation, Model Pilot Controls Panel Meters and Closed Circuit TV.

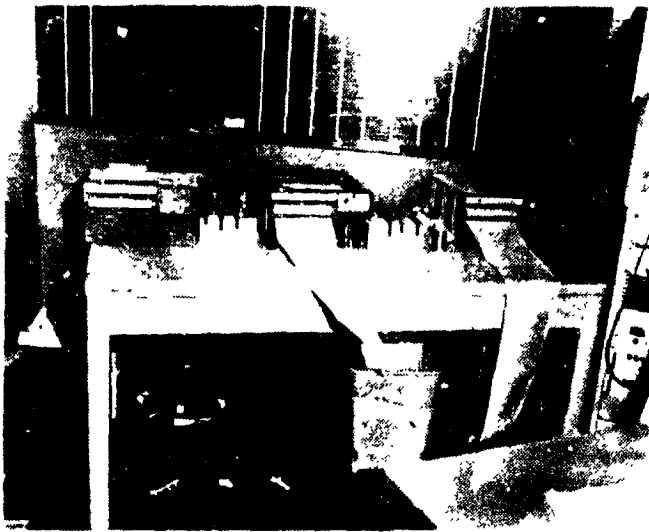


Figure III-9. Instrumentation, Oscillographs.



Figure III-10. Instrumentation, Power Supply and
Motor Temperature.

IV. DESCRIPTION OF TESTS

Tests of the Bell 301 one-fifth scale powered aeroelastic model were conducted during the period September 13, 1972 through March 30, 1973 in four phases:

Phase I, Hover Test, September 13 - October 3, 1972 (19 hours rotors turning) - This test was conducted in the Bell Helicopter Company whirl cage, on a rod-mount, to investigate hover performance and stability.

Phase II, Hover Test, December 18-22, 1972 (7 hours rotors turning) - This test was conducted in the Bell Helicopter Company whirl cage, in semi-free flight, to investigate stability and control response.

Phase III, Rod Test, January 15 - March 9, 1973 (220 hours occupancy, 34.5 hours rotors-turning) - This test was conducted in the Vought Aeronautics low speed wind tunnel, on a rod mount, to investigate trimmed flight control position, performance, and evaluate overall flying qualities.

Phase IV, Sting Test, March 15-30, 1973 (107 hours occupancy, 16.7 hours rotors-turning, 11.0 hours rotors-off testing) - This test was conducted in the Vought Aeronautics low speed wind tunnel, with an internal balance and mounted on a sting, to investigate static stability in yaw and pitch and measure rotor wake/airframe interference effects.

A. Hover Test

1. Phase I Hover Test

a. Roll Stability Investigation

A vertical rod mounting system was used which provided the model with ± 6 degrees of roll freedom at height/diameter (h/D) ratios from 0.5 to 1.0. The model control was with rotor cyclic pitch, collective-pitch and differential collective-pitch. The test rig shown in Figure IV-1, permitted the rolling moment required to hold the model at a given roll angle to be measured at any roll angle. The required moment was measured with the rotors stopped and with the rotors thrusting. The model was tested with the wing panels on and with the panels removed (Figures IV-2 and IV-3) at h/D ratios of 0.5, 0.75 and 1.0 to determine the influence of the wing/rotor interactions.

b. Wing Download Investigation

The wing download due to rotor downwash was investigated at h/D ratios from 0.5 thru 1.0 with the wing panels on and with the panels removed. The model was counterbalanced so that hover performance could be investigated at net-thrust values of 50 pounds to 100 pounds (6250 pounds to 12500 pounds full-scale).

c. Optimum Flap Setting to Minimize Hover Download

Various flap settings were tested at h/D = 1.0 to investigate hover download. The flap/aileron setting tested were 0/0°, 45/25°, 60/45°, 75/45°, and 75/75°.

2. Phase II Hover Test

a. Stability and Control Response

The model was mounted on a translational hover test rig such that free flight was nearly simulated. The model was free in pitch ($\pm 12^\circ$), roll ($\pm 8^\circ$), yaw ($\pm 30^\circ$), vertical translation (h/D = .5 to 1.5) and horizontal translational within a five foot diameter circle. The model could be restrained in yaw and in vertical and horizontal translation by tensioning snubber cables. The test rig is shown in Figure IV-4.

Three "pilots" were used to control the model. Pilot A controlled vertical height and roll, Pilot B controlled pitch, and Pilot C controlled yaw. The dc servo feedback control system discussed in Section III C was used for this portion of the test. The model pilots were stationed at the most convenient azimuth with respect to the pilots control (i.e., the roll and yaw pilots were behind the model and the pitch pilot to the side).

B. Semi-Free-Flight, Rod Mount Test

The model was mounted on a vertical rod and was free in pitch (-12° to $+10^\circ$), roll ($\pm 6^\circ$), yaw (generally $\pm 15^\circ$) and vertical translation (± 18 inches). The model control system was the same as for the Phase II hover test.

Realistic "flight" data was obtained at each level flight trim point by flying the model clear of the vertical restraint limits and by nulling the horizontal drag on the rod to zero, such that thrust equalled drag. Climb

B. (Continued)

and descent conditions were simulated by trimming the axial force on the rod to the value of thrust or drag required to simulate the gravity component acting parallel to the flight path. At selected data points the model was disturbed in pitch and yaw, separately, to obtain frequency and damping data.

Data was obtained in helicopter, conversion and auto-rotative flight to evaluate aircraft characteristics in the performance, dynamics, stability and control areas. Testing covered forward flight from hover to 100 knots full-scale at mast angles of 90 degrees (Figure IV-5), 75 degrees (Figure IV-6), 60 degrees (Figure IV-7), and 30 degrees (Figure IV-8). Sideward flight testing with a mast angle of 90 degrees was investigated from hover to 30 knots (Figure IV-9). Rearward flight was tested from hover to 35 knots (Figure IV-10) at yaw angles up to 45 degrees. IGE testing was at $h/D = .5$ to $.75$ from 16 to 60 knots using the moving belt ground plane (Figure IV-11).

C. Sting Mount Test

The model was mounted on a sting support system with an internal, six component strain gage balance to measure force and moment data. Fuselage pitch attitude was generally varied from -18 to +20 degrees and yaw angle varied from -2 to +20 degrees. Only forward flight was investigated.

Control position determined at the trim points during the rod test were used to set fuselage attitude, rotor control positions and elevator position. Static stability data were obtained during pitch and yaw sweeps from the trim condition. Control settings were held constant during the sweeps. Horizontal stabilizer incidence was varied to obtain stabilizer effectiveness and elevator sweeps were made for elevator effectiveness. Tests were also conducted with the empennage and/or the rotors removed (Figures IV-12 and IV-13).

A tuft grid (3 ft x 4 ft) was mounted on the sting and placed directly behind the empennage (Figure IV-14) to visually determine flow patterns in the vicinity of the empennage during low speed helicopter flight (airspeed from 16 to 40 knots). Photographs were taken with the rotors stopped and at trimmed level flight conditions for yaw angle of 0 and 10 degrees.

D. Data Reduction

Corrections for Reynolds number effects must be made to make the model data representative of the full-scale aircraft characteristics. Trends and rotor wake effects on the airframe are believed representative of what might be expected on the full-scale aircraft. Rotor and airframe aerodynamic parameters used in the correlation study have been modified to account for the model Reynolds numbers. Reynolds number during the test ranged from 80,000 to 500,000 referenced to the wing chord of 1.045 feet. Airspeed used in this report is the equivalent full-scale airspeed. Vortex generators were placed on the wing quarter-chord to better simulate full scale lift characteristics at high angles of attack. The data reference center for all data obtained during the sting test is stationline 60.0, waterline 16.7 and butto line 0.0 of the model. This corresponds to an equivalent full scale stationline 300.0 and waterline 83.5. Center of gravity positions tested during the rod test were equivalent to an aft cg for mast angles of 90 and 75 degrees. As the nacelles were tilted forward the weight of the model rotor gear box caused a forward shift in cg, more than for the full scale aircraft. This resulted in mast angles 60 and 30 degrees being tested at forward cg. Center of gravity locations for the rod test at the mast angles tested are as follows:

<u>Mast Angle</u>	<u>Fuselage* Station</u>	<u>Waterline</u>	
90	60.0	16.7	
75	59.4	16.6	
60	59.0	16.5	
30	58.2	16.2	*Model Scale

Force and moment data obtained during the sting test was measured on the wind tunnel six-component internal balance and data reduction was by a Vought Aeronautics Wind Tunnel data reduction program. Dynamic and static model data (control position, rotor parameters, and empennage lift) obtained during all phases of testing were recorded on magnetic tape and three oscillographs. Calibration of all strain gages were completed prior to testing with additional calibration made frequently during the tests. Magnetic tape data was put in digitized form at Bell Helicopter's Data Reduction Center. Comparisons and verification have been made with hand-reduced data from the oscillographs. The force and moment sign convention used for the rotor and airframe is shown in Figure IV-15.

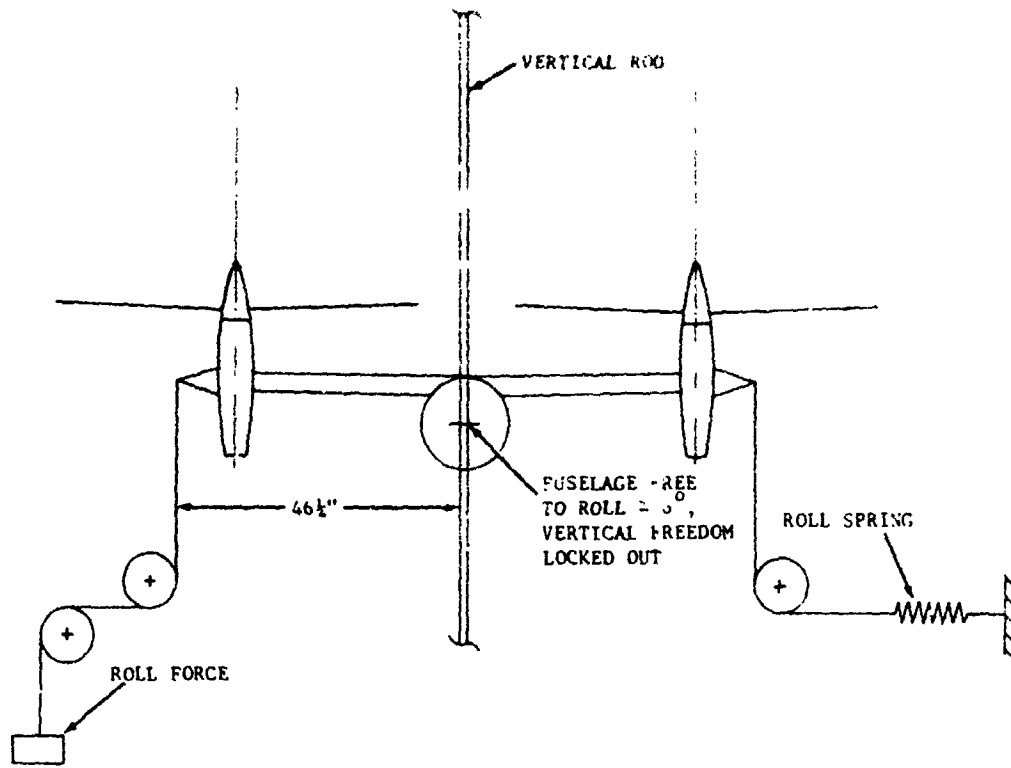


Figure IV-1. Roll Test Rig Schematic.

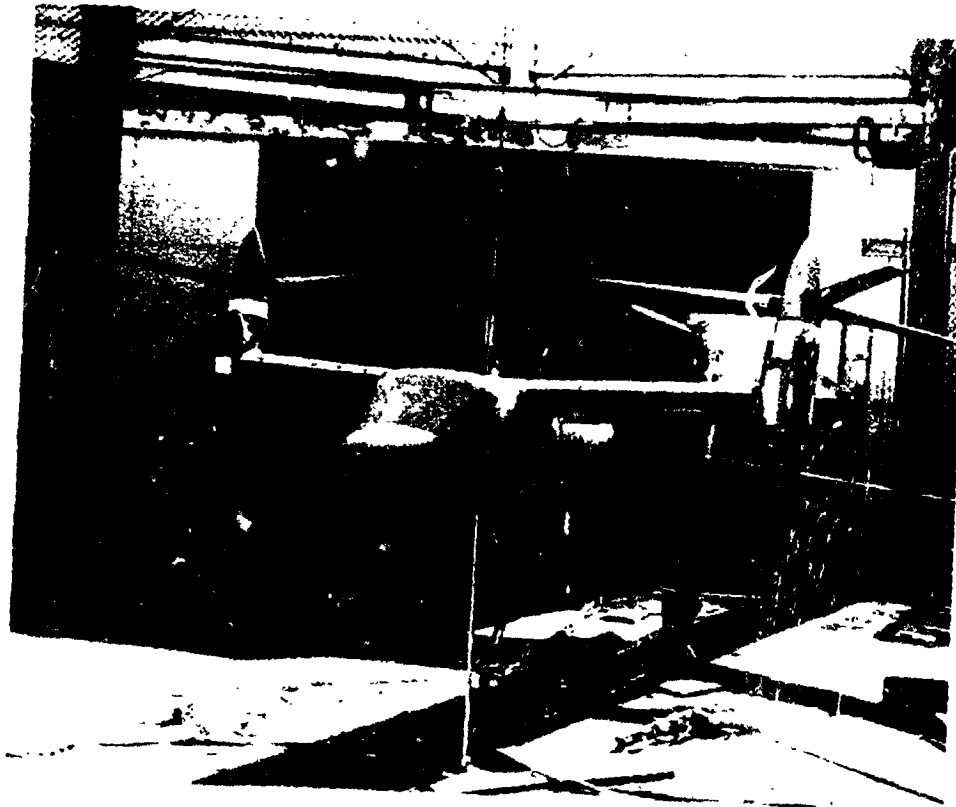


Figure IV-2. Hover Test, Wing Fairings On.



Figure IV-3. Hover Test, Wing Fairings Removed.

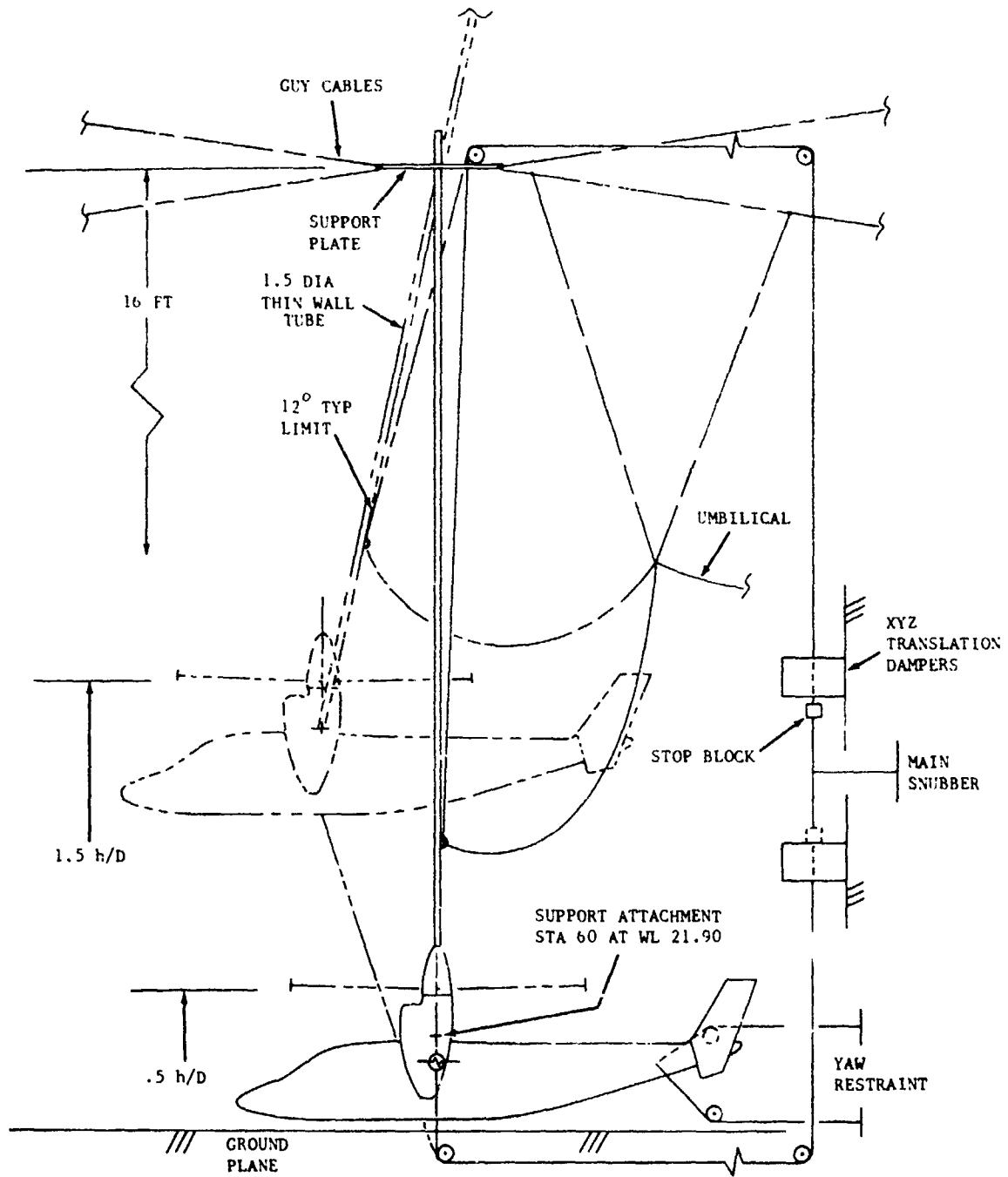


Figure IV-4. Free Flight Test Rig Schematic.

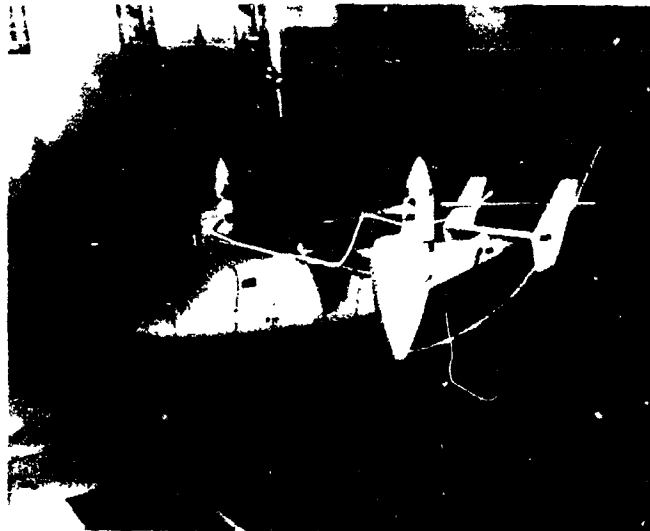


Figure IV-5. Rod Test, Mast 90 Degrees.

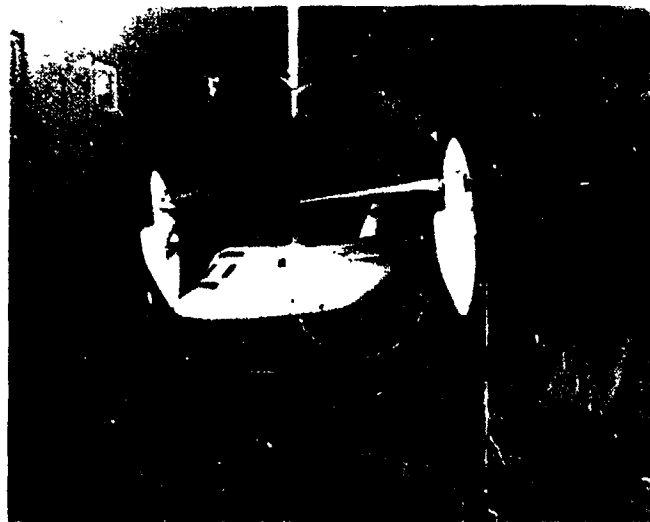


Figure IV-6. Rod Test, Mast 75 Degrees.

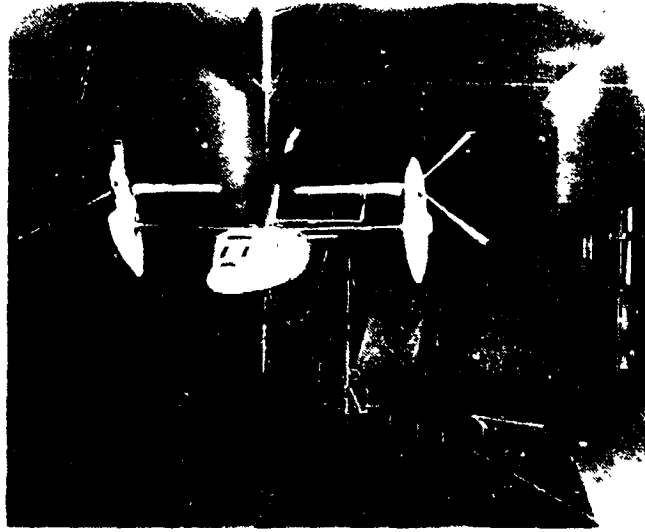


Figure IV-7. Rod Test, Mast 60 Degrees.

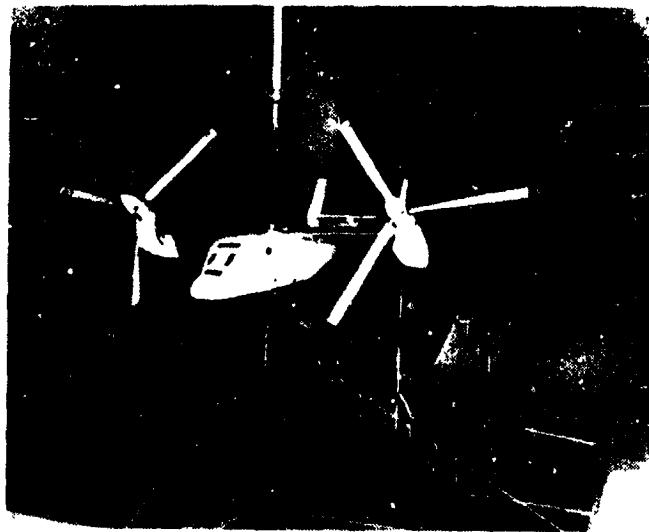


Figure IV-8. Rod Test, Mast 30 Degrees.

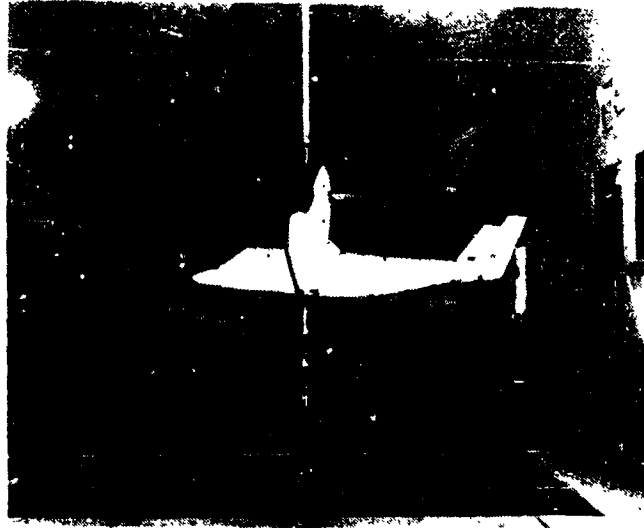


Figure IV-9. Rod Test, Sideward Flight
Mast 90 Degrees.

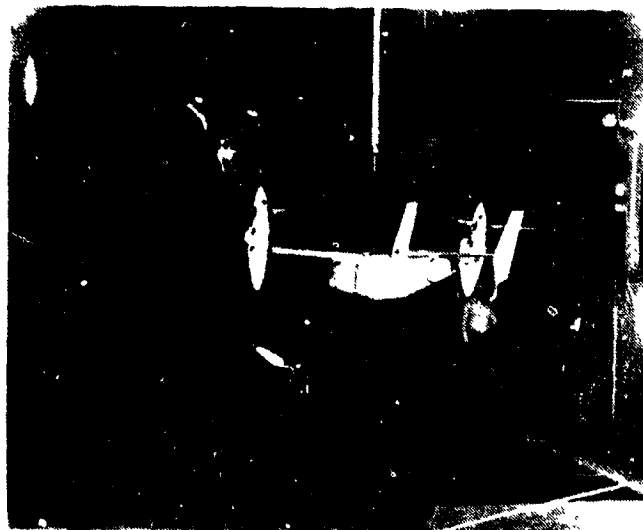


Figure IV-10. Rod Test, Rearward Flight
Mast 90 Degrees.

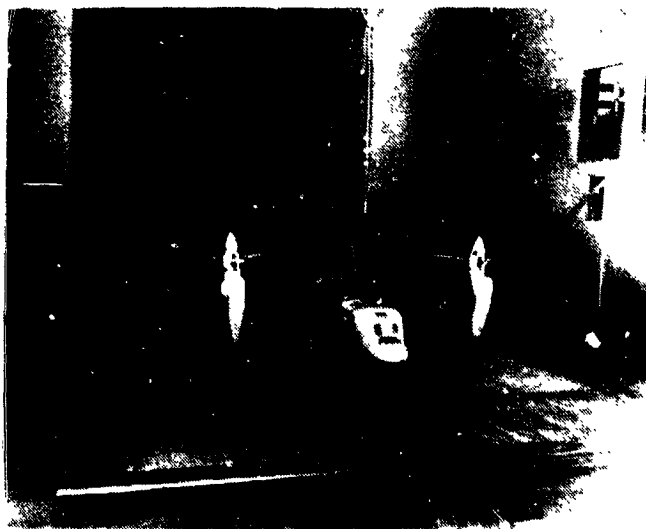


Figure IV-11. Rod Test, IGE, Mast 90 Degrees.

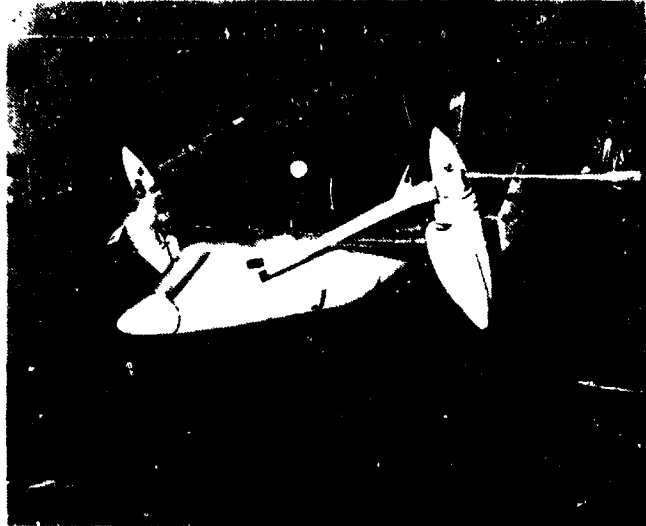


Figure IV-12. Sting Test, Mast 60 Degrees
Rotors-On.



Figure IV-13. Sting Test, Mast 60 Degrees
Rotors-Off.

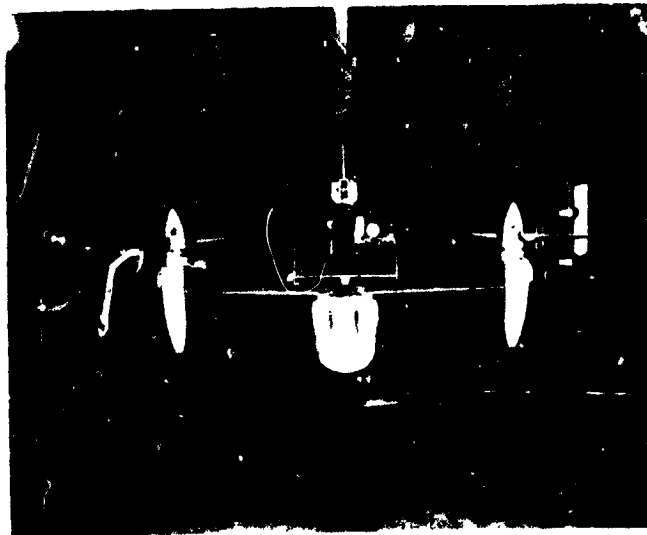


Figure IV-14. Sting Test, Tuft Grid.

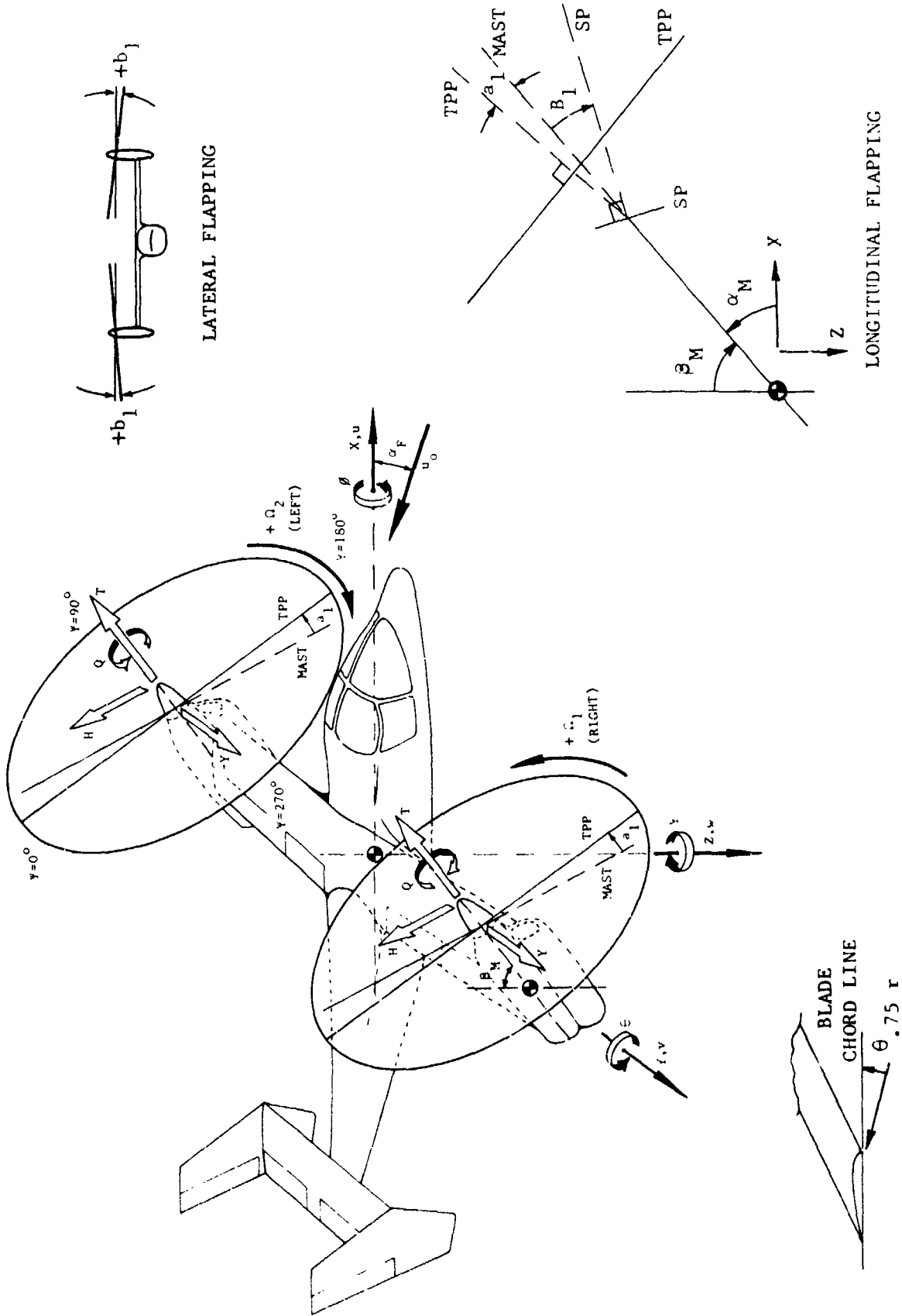


Figure IV-15. Force and Moment Sign Convention.

V. RESULTS OF TESTS

A. Hover Test

1. Roll Static Stability

The model was tested at h/D ratios of 0.5, 0.75, and 1.0. The moment required to hold the model at a given roll angle was measured first with the rotors stopped and then with the rotors turning and at lg thrust. The difference between the recorded moments is the contribution of the rotor wake-wing-ground aerodynamic interference. Data recorded in terms of weight at the wing tip required to maintain a given roll angle is given in Figure V-1 for h/D = 0.50. At h/D = 0.5 the roll moment is stabilizing. Figure V-2 shows the weight versus roll angle for h/D = 1.0 where the roll moment is destabilizing. Tests were also made with the wing aerodynamic fairings removed.

Figure V-3 summarizes the roll static stability data. As indicated, the model was found to have positive roll stability at touchdown, h/D = 0.50. Above an h/D = 0.54 the model showed negative roll stability which was linear with roll angle, over ± 6 degrees. The maximum instability was found to occur at h/D = 0.85. The full-scale control input required to trim this instability was found to be 0.051 inches of lateral stick per degree of roll at an equivalent full-scale gross weight of 8,250 pounds. The lateral control requirement is expected to increase linearly with the rotor downwash dynamic pressure. Thus at the maximum VTOL gross weight of the Model 301 (15,000 pounds) the maximum lateral control requirement is predicted to be 0.093 inches of stick per degree of roll. For a ten-degree wing drop in-ground-effect the lateral stick for trim would be 0.93 inches. Maximum lateral stick travel available is ± 4.8 inches.

2. Performance

The model was tested with wing panels on and off, at h/D ratios from 0.5 through 1.0. The model had vertical freedom, $\pm 4^\circ$ roll freedom and $\pm 20^\circ$ yaw freedom. Pitch freedom was locked out. The model was counterbalanced by weights so that hover performance could be investigated at net-thrust values of 50 pounds through 100 pounds (6250 pounds through 12,500 pounds full-scale).

2. (Continued)

The optimum flap setting to minimize wing download was investigated at $h/D = 1.0$. The baseline data point was the model hovering at a net thrust of 75 pounds (9375 pounds full-scale), flaps/ailerons at zero settings. Resetting the flaps/ailerons to 45/25°, 60/45° and 75/45° showed in each case an increase of 6.0 percent in net thrust compared to the baseline case. A setting of 75/75° showed only a 4.7 percent increase compared to the baseline case. The 75/45° setting was selected for further performance testing since it was apparently near optimum. This setting was also used for the roll stability testing. The wing panels were also removed to determine the difference in power required. (The exposed wing spar is a rectangular section so wing download was not completely eliminated.) Results at $h/D = 1.0$ are shown in coefficient form in Figure V-4.

The model rotor hovering performance was predicted by correcting the full scale blade aerodynamic characteristics for Reynolds number and Mach number effects. The blade profile drag coefficient at zero lift was increased and the section lift curve slope and maximum lift decreased. The computed model performance is compared to full scale and to the model data in Figure V-4. The calculated model performance compares reasonably well with the performance measured with the wing aerodynamic fairings removed, which approximates a zero download/upload condition. The model power coefficient is calculated to be about 12 percent higher than the full scale power coefficient at the same weight coefficient.

Model performance data at $h/D = 0.75$ and 0.50 are shown in Figures V-5 and V-6.

3. Wing Download

The wing download was measured by comparing wing-fairings on and off data. At thrust/sigma prime = 84.5 pounds (10,600 pounds full-scale) the wing-panel download was 11.4 percent of thrust at $h/D = 1.0$, as shown in Figure V-7. This is higher than the 7 percent predicted for full-scale and it is believed that a Reynolds number effect may explain the difference. Hoerner shows that the drag of cross-sectional shapes with rounded edges and flat sides are strongly dependent on Reynolds number as shown in Figure V-8. The sections tested by Hoerner are considered to be comparable to a wing, with flaps deflected, at an angle of attack of -90 degrees. The drag coefficients of Figure V-8 drop by at least 50 percent as Reynolds number is increased from that of the model (2×10^5) to that of full-scale (2×10^6). Thus the model download of 11.4 percent thrust can be predicted to reduce to 5-7 percent of full-scale thrust.

3. (Continued)

Also shown on Figure V-7 are the results of a recent test of the one-tenth-scale Bell C100 F1B tilt rotor model. This test was conducted at Reynolds numbers around 4×10^5 and showed a wing download under 7 percent. This Reynolds number is close to the "drag-bucket" of Figure V-8 and may be more representative of full-scale values. The reduction in power required in-ground-effect is shown in Figure V-9. The reduction is 12 percent at high model weights, increasing to over 19 percent at low model weights.

The vertical "spring" in ground effect is shown in Figure V-10. Collective pitch was not instrumented on this test so the thrust change is shown at constant torque. The vertical "spring" is virtually the same with wing-panels on or off. At medium model weights, the net thrust increased by 19 percent as h/D reduced from 1.0 to 0.5.

4. Controllability in Semi-Free Flight

The model was tested in a transitional hover test rig ($h/D = 1.0$) to investigate free flight stability and control response. Control of the model was found to be so difficult that most of the test period was spent developing piloting skill. The pilot's skill level at the end of the test period was much higher than at the beginning but was still less than that required for precision control of the model. Hover over a spot could generally be achieved until a wind gust or an input caused a roll disturbance. The model then translated rapidly until the transitional limits were reached. The tendency was aggravated by the horizontal translational restraint system causing a rolling moment with horizontal displacement.

Yaw control proved to be easy once the pilot recognized the need to lead yaw rate in order to stop on the desired heading. Pitch control was not difficult except where roll and lateral translation motion became large, then pitch could not be controlled.

The wing panels were removed from the model to see if rotor-wing aerodynamic interference contributed to the roll-lateral translation control problem. However, no significant change was observed. The model was also flown at $h/D = 0.75$. At that height it was not controllable. When the snubber was released, the model would translate laterally so quickly that the pilots did not have time to regain control over the model before it reached the stops.

4. (Continued)

It was apparent from the hover controllability test that given sufficient time to develop piloting proficiency, the model could be successfully hovered. However, this task was felt to be of low priority and was terminated in order to prepare for the wind tunnel tests.

B. Semi-Free Flight, Rod Mount Test

Tests on the vertical rod mount covered the mast angle range from 95 degrees to 30 degrees and airspeeds from hover to 100 knots. (Airspeeds and gross weights given in this report are equivalent full scale values. All other parameters shown are in model scale.) Tests were performed to determine control positions for trimmed flight and to evaluate stability and flying qualities about trim.

Airframe and rotor parameters monitored during the test included fuselage pitch attitude, elevator position, empennage lift, cyclic position, collective setting at 0.75 radius of the blade, rotor torque, and rotor flapping. Rotor loads and vibration levels were also monitored to prevent exceeding limits. There is some scatter in the test data which must be attributed to the model not being in trim flight. A trimmed level flight condition on the rod was obtained when the thrust/drag indicator on the rod indicated zero. Accuracy of the indicator and its reading, and the low dynamic pressure at the low airspeeds tested made it difficult to determine the precise trim point. Any off-trim thrust or drag is equivalent to flying in a climb or descent. Also, small roll and yaw angles were difficult to detect. Every attempt was made to maintain correct rigging between cyclic and elevator through the test, but some data points were taken with improper elevator settings. Combinations of these factors resulted in off-trim conditions for some recorded test points. Therefore, general trends should receive more emphasis than studying each individual data point.

Comparison between test data and parameters calculated using BHC computer program C81 is shown in each figure. Airframe and rotor aerodynamic inputs to program C81 were corrected to reflect Reynolds number effects. Reynolds number effects are significant and must be kept in mind when using the test data to predict full-scale characteristics. The recommended approach is to validate the computer program using test data and then scale up to predict full-scale characteristics using aerodynamic data appropriate to the full-scale Reynolds numbers.

1. Trimmed Flight Conditions

a. Mast angle 90°

(1) Level flight

Figure V-11 shows the model parameters for trimmed level flight versus airspeed. Vortex generators have been used during low Reynolds number scaled model testing of the Model 300 to obtain lift characteristics that approximate full scale¹². As shown in Figure V-11, vortex generators do not have a significant effect on the trim parameters. The largest difference occurred in the rotor torque. In analyzing the data for points 80 through 89 with the vortex generators off, it was noted that a small amount of drag was indicated on the rod which is equivalent to having a rate of descent. This may explain why the vortex generators off data required less power.

Cyclic position and empennage lift are a primary indicator of rotor wake effects on the horizontal stabilizer. The shallow stick gradient between 20 and 50 knots is the result of the rotor wake having the net effect of an upwash; positive empennage lift tends to confirm that the rotor wake acts as an upwash. As speed increases above 50 knots wing downwash becomes more effective, providing a stable stick gradient with airspeed. The shallow gradient between 20 and 50 knots is within the MIL-SPEC requirements and should not present a problem. During recent simulator studies of the Model 301 the shallow gradient did not present a problem for the pilots.

Calculated rotor torque (power) was found to be in very good agreement with test. Torque readings remained consistent throughout the test and were later used as a trim indicator during the sting test.

In general, calculated empennage lift is in close agreement with test data although the empennage lift data had the largest amount of scatter of all the parameters measured. Several items that affect empennage lift which contribute to this variation are fuselage pitch attitude, elevator position, and rotor power. The

(1) (Continued)

trend generally remained the same and shows a variation initially from a download to an upload. As speed increases, the upwash from the rotor decreases and the downwash from the wing increases. Another reason for the difference between theory and test is the present inadequate representation of the rotor wake in program C81. This will be discussed later in Section VI.

Rotor flapping was found to be up to 40 percent higher than calculated. This difference is primarily due to lateral flapping. Measured fore-and-aft flapping is in good agreement with that estimated. By refining the original theory, analysis shows that better agreement can be made with the measured flapping as discussed in detail in Section VI. Although flapping was higher than calculated, flapping does not appear to restrict any flight condition.

During the initial portion of the rod test the roll degree of freedom was locked out to reduce the model pilots work load and to allow a preliminary evaluation of flying qualities. Once the model was checked out and found to be easy to control the roll restraint was removed. No significant difference was observed in trim characteristics between having the roll fixed or free.

(2) Effect of Horizontal Stabilizer Incidence on Level Flight Trim

Figure V-12 illustrates the effect of horizontal incidence ($\pm 4^\circ$) on level flight trim parameters. The trends and agreement between theory and test data are similar to those discussed above. The main effect of changing stabilizer incidence is in the longitudinal cyclic stick trim position. Positive incidence (leading edge up) tends to reduce the gradient with airspeed between 20 and 60 knots. For the four degrees tested, the cyclic stick position showed a stick reversal. With negative incidence, the cyclic stick gradient with airspeed improves.

Changing incidence in either direction has advantages and disadvantages. Positive incidence produces a stick reversal between 20 and

(2) (Continued)

60 knots, but does not require as much forward stick at high speeds. High speed helicopter would then be limited by power instead of stick travel. Positive incidence also tends to pitch the aircraft more nose down which would be undesirable from a pilot's point of view (fuselage angle of attack with +4 degrees incidence is -15 degrees at 100 knots) and may also result in increased blade loads. Negative incidence on the other hand, although steepening the stick gradient, requires more cyclic for high speed helicopter flight and thereby restricts the speed in this mode.

(3) Effect of Gross Weight on Level Flight Trim

The effect of gross weight on level flight trim parameters is shown in Figure V-13. The parameters which are significantly affected by gross weight are collective pitch, mast torque, and blade flapping. Computed collective pitch and mast torque are in close agreement with test data. A significant difference was again found in computed lateral flapping due to the simplified math model used for the induced velocity distribution.

(4) Effect of Wing Lift on Trim Parameters

The aerodynamic fairings were removed from the wing spar to investigate the effect of wing lift on the level flight trim parameters. Figure V-14 shows the trim parameters versus airspeed, with the fairings removed. Comparison of the wing fairings off and fairings on data, Figure V-11, does not indicate a significant influence.

Early in the test program wing aerodynamic interference was suspected to be one of the reasons for the higher than calculated lateral flapping. However, flapping with the fairings removed was the same as with the fairings on.

(5) Descent and Autorotation Trim Parameters

Rate of descent or climb was determined from the magnitude of the model's drag or thrust on the vertical rods. The method is illustrated in Figure V-15.

(5) (Continued)

Descent and autorotation trim parameters were determined over a range of airspeed (50 to 90 knots), for flap settings of 0° and 45°, and mast angles of 90° and 95°. Descent and autorotation trim data is summarized in Figure V-16. Autorotation was achieved at an equivalent full-scale rate of descent of 4000 feet per minute at 80 knots airspeed. The calculated full-scale autorotation rate of descent at 80 knots is 2400 feet per minute. Reynolds number effects are considered to be responsible for this difference between the model and full-scale rates of descent.

Airframe and rotor characteristics were corrected to test Reynolds numbers and used to compute the rate of descent. Reasonable agreement with regard to fuselage attitude, rotor power and control positions was obtained for rates of descent up to about 2500 feet per minute. However, at higher rates of descent the calculated fuselage attitude was significantly higher than measured. Investigation showed that the wing was not stalled in the computer program whereas during the test tufts on the wing indicated flow over the wing was separated at the higher rates of descent. The inputs to the program were modified to reflect the model's wing stall characteristics, including the wing downwash above stall. Once this was done the calculated and measured rates of descent were in good agreement.

(6) Climb Trim Parameters

Structural interference limited the nose down pitch attitude with respect to the rod to -10 degrees. Consequently, very little data on climb trim parameters was obtained for mast angle 90°. What data was obtained is presented with the static stability data in section V.B.2.

(7) Forward Flight IGE, Sideward and Rearward Flight OGE

Tests were made in ground effect (IGE) at $h/D = .75$ and $.50$ with a moving ground plane and boundary layer suction. The moving ground plane was operated at speeds corresponding to the tunnel's

(7) (Continued)

air velocity. The test data for forward flight shown in Figure V-17 indicates the model to have a more nose down fuselage pitch attitude IGE than OGE. The cyclic stick position is more aft than OGE indicating a significant upload on the horizontal stabilizer. Torque was lower during hover IGE, but was about the same as OGE between 16 and 30 knots. More torque was required at 40 and 60 knots IGE than OGE.

Sideward flight was accomplished at airspeeds up to 30 knots. As shown in Figure V-18, approximately 4.6 degrees of differential cyclic pitch was required to hold heading at 30 knots. This is higher than the design value of 4.0. However, the model did not have rudders, which will tend to relieve the differential cyclic requirement. One significant factor observed during sideward flight was the increase in power required resulting from the tandem rotor effect. (The trailing rotor is in the downwash of the leading rotor and therefore has a higher induced power loss.)

Rearward flight was accomplished at speeds up to 35 knots at both forward and aft cg positions. Figure V-19 shows the trim parameters versus airspeed. Eight degrees of aft cyclic was required at 35 knots, forward cg. (Elevator settings were not set at the proper value for the cyclic position because of a physical limit on up-elevator. The proper value would tend to reduce the cyclic requirement slightly.) Blade flapping at forward cg was high because of the aft cyclic required to trim out the weight moment.

b. Mast angle 75°

Figure V-20 shows the level flight trim parameters for mast angle 75 degrees. Comparison between theory (C81) and measured parameters is similar to that discussed for mast angle 90 degrees.

The longitudinal cyclic gradient with airspeed shows a reversal between 30 knots and 60 knots that is more pronounced than the reversal at mast angle 90 degrees. The lateral flapping trend with airspeed is similar to that for mast angle 90 degrees.

b. (Continued)

Several gross weights were tested at mast angle 75 degrees; trim positions are shown in Figure V-21. The most significant variation with gross weight was in power and flapping.

Figure V-22 shows the effect of flap setting on trim parameters. During runs at 75 degrees (and at 90 degrees) it was noticed that the tufts on the flaps indicated separation and spanwise flow. This was considered as a possible unrealistic representation of the wing wake. Vortex generators were added to the wing at the flap hinge line, but did not change the appearance of the tufts. The flaps were then raised to eliminate the separation. However, little difference was noted in the trim attitude or cyclic stick position, as is shown in Figure V-22.

c. Mast angles 60° and 30°

Figures V-23 and V-24 show trim parameters for mast angle 60 degrees and 30 degrees respectively. Only a limited amount of data was taken at these mast angles since analysis and test (the XV-3) indicate the significant handling qualities problems are at mast angle 90 and 75 degrees.

In comparing computed and test for mast angles of 60 and 30 degrees, caution should be exercised in using these as realistic trimmed flight conditions. Incorrect cyclic/elevator gearing used for these mast angles caused large differences in empennage lift. Proper elevator settings at aft cyclic positions were not obtained because of limits on up elevator deflections. In addition are the model scale effects (low $C_{L_{max}}$ and low test airspeeds) as discussed earlier, which make these trim conditions unrepresentative of the full scale aircraft trim.

2. Static Stability Characteristics

a. Longitudinal

Longitudinal static stability at mast angles 90 and 75 degrees was investigated by trimming the model over a range of fuselage trim attitudes. Figures V-25 and V-26 show the trim parameters versus fuselage pitch attitude for mast angles 90 and 75 degrees respectively. These trim points correspond to climbing or descending flight.

a. (Continued)

At mast angle 90 degrees the longitudinal cyclic stick position gradient with fuselage pitch attitude indicates positive static stability. However, at mast angle 75 degrees and 30 knots, the stick gradient shows approximately neutral static stability. The model pilot found it very difficult to trim the model in this condition. Positive static stability was indicated at the higher speeds tested for mast angle 75 degrees.

b. Lateral directional

Lateral directional static stability was investigated at mast angles 90 and 75 degrees by yawing the model with differential cyclic and trimming roll and pitch with differential collective and longitudinal cyclic respectively. Figures V-27 and V-28 show the trim parameters versus yaw angle for mast angles 90 and 75 degrees respectively.

The differential cyclic required to maintain a given yaw angle was essentially linear over the range of speed and yaw angle tested. There was a significant variation in the longitudinal cyclic required for trim with yaw angle. This variation reflects the change in upload to download on the horizontal stabilizer due to the rotor wake with yaw angle.

3. Dynamic Stability Characteristics

At each trim point the model was disturbed in pitch and yaw to obtain dynamic stability data. The frequency and damping of the pitching and yawing modes were extracted from the time history of the model response.

Table V-1 compares calculated frequency and damping with that measured in the test. In general, agreement is good. Note that at the lower speeds the measured frequency and damping are not given because the model response was so sluggish that the frequency and damping could not be accurately calculated from the time history.

4. Controllability

The evaluation given in Table V-2 with regard to model controllability on the rod mount was recorded by the model pilots: (all comments pertain to the 11,000 pound gross weight configuration).

5. Aeroelastic Stability, Oscillatory Loads, and Vibration

a. Aeroelastic stability

The aeroelastic stability characteristics were investigated by exciting the coupled rotor-pylon-wing modes and observing the decay of the motion. The model was excited by plucking wires attached to the left hand nacelle and by bouncing the model on the vertical restraint cable. The damping was monitored visually and on an oscillograph.

Rotor-pylon-wing motions were well damped with no evidence of instability at any conversion angle or speed. It was not possible to accurately reduce the damping using conventional decay analysis because the steady-state forced vibration partially obscured the decay. Since aeroelastic stability has not been identified as a problem in helicopter and conversion mode, no attempt was made to reduce the data using other methods.

b. Oscillatory loads

Rotor and control system oscillatory loads were monitored during the test to avoid exceeding limits. Figure V-29 shows typical waveforms of the rotor loads and flapping. Loads were predominantly one-per-rev at all mast angles and airspeeds. One-per-rev loads were also predominant in the 25-foot prop-rotor test in the 40- by 80-foot wind tunnel.

Figures V-30 through 32 show measured beamwise and chordwise bending at blade station 52.5, and the pitch link load versus airspeed, for the four conversion angles tested. Blade and control loads were well below the equivalent full scale endurance limit and show a reduction in magnitude as the nacelles convert from helicopter to airplane mode. Figure V-33 shows the variation in blade and control loads with gross weight at constant airspeed. The load trend does not indicate the occurrence of stall flutter or other aeroelastic instability.

It should be noted that blade and control loads are well below the loads predicted for the Model 301¹⁷. This is caused by (1) the model rotor not being Mach scaled when tested in air (scale factor is 0.447) so that drag rise at high lift coefficients is not correct, and (2) the model blade first inplane natural frequency ratio is slightly higher than that for the full-scale blade.

c. Airframe vibration

Vibration levels were measured at seven locations: three on the right hand nacelle, one on the left hand nacelle, one on each of the vertical fins and one at the aircraft center of gravity. The nacelle accelerometers could be moved to monitor vibrations in either the fore-and-aft or the lateral sense. The vertical fin accelerometers measured in the fore-and-aft sense and the accelerometer at the aircraft center of gravity measured in the vertical sense.

Figure V-34 shows the frequency content of the vibration of four stations. The dominant frequency is one-per-rev (21 cps) and is caused by rotor out of balance and/or out of track. The operating tolerance on out of balance and out of track is much greater for the model than full-scale. Hence, the one-per-rev vibration is not considered representative of full-scale.

The two-per-rev vibration is caused by the Hooke's joint effects of the rotor gimbals in combination with rotor flapping. With a gimballed rotor, flapping induces a two-per-rev torque and moment at the hub which are proportional to the square of the flapping angle. Figure V-35 shows that the maximum two-per-rev vibration occurs at approximately 40 knots which is the airspeed at which flapping was the maximum.

The three-per-rev vibration results from two-per-rev and three-per-rev airloads. The three-per-rev vibration level, shown in Figure V-36 has a peak near 40 knots where the rotor near wake has the most significant effect and then begins to increase again about 80 knots as the rotor advance ratio becomes significant. The variation in vibration level with conversion angle is shown in Figures V-37 and V-38 for two-per-rev and three-per-rev respectively. In general the level of vibration decreases as the nacelles are converted forward.

Both the two-per-rev and three-per-rev vibration are representative of the full-scale aircraft. The levels are within design limits. Analysis of the airframe oscillatory load level corresponding to the measured vibration levels, indicate the loads are low with respect to structural allowables.

c. (Continued)

Empennage vibration levels were monitored to determine if the rotor wake excited empennage natural frequencies. While some natural frequency excitation was evident it was very low in magnitude. The dominant vibration frequency was one-per-rev but as noted earlier the one-per-rev level is not representative of full-scale.

C. Sting Mount Test

The sting mount test covered the same ranges of mast angle and airspeed covered in the rod mount test. Control positions and pitch attitude were based on the trim values determined during the rod mount test. The strain gage balance was used to verify that lift and pitching moment were in trim; when indicated, collective pitch and/or longitudinal cyclic was adjusted to improve the trim condition. In some cases climb and descent trim were estimated by extrapolating trim data from the rod test since only a limited amount of data for these conditions had been obtained.

A tuft grid was placed in the vicinity of the empennage in order to observe the rotor wake. Photographs of the tuft grid patterns are given in Appendix C. An analysis of the rotor wake observations is presented in Section VI-A.

1. Comparison of Airframe Characteristics with Previous Test Data

At the low Reynolds number tested, the stall characteristics are significantly different than estimated for the full scale aircraft. Stall occurred at 12 degrees which is 4 degrees lower than that obtained on the force model at a higher Reynolds number. The maximum lift coefficient for the aeroelastic model was 0.44 less than the force model. A comparison of the aeroelastic model with the force model showing the effect of Reynolds number is presented in Figure V-39. The reduction in maximum lift coefficient had a significant effect on simulation of autorotation as discussed in Section V-B.

There was very little difference in the lateral-directional characteristics as shown in Figure V-40.

2. Comparison of Rod and Sting Mount Trim Parameters

Figure V-41 shows comparison of typical trimmed level flight attitudes and control positions used during the rod and sting tests. Fuselage pitch attitude, cyclic position, and torque settings used during the sting

2. (Continued)

test were preset based on trim settings determined during the rod test. During the sting test torque was found to be the quickest and best indicator of the model being in trim. Higher collective pitch settings were required during the sting test than the rod test for the same torque readings. Checks made of model lift on the tunnel balance verified the model to be in trim and that the torque to be indicating properly. A difference in collective pitch calibration is suspected to be the reason for the difference between the tests. Collective pitch settings obtained during the sting test are in better agreement with the theoretically computed values. Empennage lift and rotor flapping, the two independent parameters in the two tests, are in close agreement.

3. Static Stability Characteristics

Force and moment data was obtained for rotors and/or empennage on and off to evaluate rotor wake effects. Pitch and yaw sweeps were made about the trim attitude for level, climb, and descent flight configurations. Lift, pitching moment, and yawing moment data are summarized in this section for level flight from 40 to 100 knots. A complete set of force and moment data at lower airspeeds, and climb and descent are given in Appendix B.

a. Lift coefficient, mast angle 90 degrees

A comparison between rotors-off and rotors-on lift coefficients at 40, 60, and 80 knots is shown in Figures V-42, V-43, and V-44. (Lift coefficient is based on wing area and freestream dynamic pressure.)

b. Pitching moment coefficient, mast 90 degrees

Pitching moment characteristics for the same speed range are shown in Figures V-45, V-46, and V-47. The change in pitching moment with angle of attack ($C_{m\alpha}$), rotors-off, does not change with airspeed.

Wing downwash and pitching moment at zero pitch ($C_{m\alpha=0}$), empennage off, changes due to Reynolds

number effects. These effects combine causing the shift in $C_{m\alpha=0}$, empennage on. At the low Reynolds numbers, the lift curve slope of the horizontal tail

b. (Continued)

($C_{L\alpha_H}$) is reduced and results in lower static longitudinal stability ($C_{m\alpha}$) than for the full scale airframe. The comparison of the aeroelastic model with the force model, given in Figure V-39 shows the effect of Reynolds number on $C_{m\alpha}$. The break in the pitching moment curve at 12 degrees is due to wing stall.

The effect of the rotor wake on the pitching moment is apparent when the rotors-on and rotors-off pitching moments are compared. At 40 knots the model is unstable for negative angles of attack and stable at positive angles. At 60 and 80 knots the model is stable on either side of trim. The change in pitching moment due to the empennage indicates that the wake changes from a downwash with rotors-off to an upwash with rotors-on (see Section VI for a more detailed discussion of rotor wake effects).

The pitching moment characteristics may be explained as follows: at 40 knots and at negative angles of attack, the rate of change of the upwash at the horizontal stabilizer with angle of attack ($d\epsilon_T/d\alpha$) is greater than 1.0, which cancels the stabilizing effect of the horizontal stabilizer. At positive angle of attack, $d\epsilon_T/d\alpha$ is nearly zero so the slope of the pitching moment is about the same as rotors-off. At 60 and 80 knots, $d\epsilon_T/d\alpha$ is lower than $d\epsilon_{W/H}/d\alpha$ (rotors-off wing downwash) making the aircraft more stable rotors-on than rotors-off. The unstable bump in the pitching moment coefficient around 8 degrees angle of attack at 60 and 80 knots is not understood. However, it may be due to the rotor vortices impinging on the horizontal stabilizer and causing the flow to separate.

c. Yawing moment coefficient, mast 90 degrees

Directional stability with rotors-on and -off at 40, 60, and 80 knots is shown in Figures V-49 through V-50 for up to 20 degrees of yaw. Again, the rotor wake effect on the empennage is significant at 40 knots and decreases with increasing airspeed.

c. (Continued)

Very little change in rotors-off directional stability is noted with airspeed for either empennage-off or on. A change in slope occurs at about 6 degrees yaw which appears to be a Reynolds number effect on the vertical fins.

At 40 knots, rotors-on, directional stability is neutral for yaw angles less than 4 degrees and increases in stability between 4 and 20 degrees yaw. As speed increases, stability improved between ± 4 and decreases between 4 and 20 degrees. For the airspeeds tested, directional stability above 12 degrees yaw is greater rotors-on than rotors-off.

d. Lift coefficient, Mast angle 75 degrees

Lift characteristics at mast angle 75 degrees are very similar to those for mast angle 90 degrees and are shown in Figures V-51, V-52, and V-53 respectively.

e. Pitching Moment Coefficient, Mast angle 75 degrees

Pitching moment characteristics are shown in Figures V-54, V-55, and V-56. Rotors-off characteristics with airspeed and angle of attack are similar to mast angle 90 degrees.

At 40 knots, rotors-on, empennage-on, the aircraft pitching moment shows a stable slope below trim, changing to an unstable slope above trim and then returns to a stable slope after wing stall. The pitch up which is also present at 60 knots, makes the aircraft unstable about level flight trim. The pitch up tendency disappears at 80 knots, when the pitching moment becomes slightly stable. This trend is different than at mast angle 90 degrees. At mast angle 90 degrees, rotors-on stability was better than rotors off (except at 40 knots). At mast angle 75 degrees the pitching moment varies with angle of attack and airspeed, and is less stable at the higher airspeed.

The unstable region in the pitching moment curve also exists at mast angle 90 degrees, but does not occur near the level flight trim attitude. Level flight trim for mast angle 90 degrees ranges from 0 to -8 degrees, several degrees below the pitch-up, whereas trim for mast 75 degrees is at angles of attack ranging from 8 to 2 degrees, right in the

e. (Continued)

middle of the pitch up. Referring to climb and descent data presented in Appendix B, it is seen that the pitch up occurs near these trim attitudes and would also have an effect on stability for these configurations. This change in stability with pitch attitude is caused by the relationship of the rotors tip vortices to the horizontal stabilizer. At small and negative angles of attack the horizontal stabilizer moves closer to the core of the vortices. The rate of change of the tail angle of attack with change in pitch attitude ($\partial\alpha_H/\partial\alpha_F$) is generally less in this region because of the strength of the rotor wake relative to the freestream. At positive angles of attack the horizontal stabilizer moves farther away from the vortices. In this region the total wake changes more rapidly with angle of attack, in some cases at nearly the same rate as the change aircraft pitch attitude eliminating the stabilizing contribution of the horizontal stabilizer ($\partial\alpha_H/\partial\alpha_F = 0$). It should be noted that this pitch up is dependent on the relationship of mast angle and airspeed and will not occur at the same angle of attack for all cases. The strength of the rotor wake, wing wake, and freestream must all be included. As speed increases this trend continues but the rotor wake weakens until the main influence on stability is the wing downwash. The rotors give an upwash in the 40 to 80 knots speed range.

f. Yawing Moment Coefficient, Mast angle 75 degrees

Directional stability for mast angle 75 degrees at 40, 60, and 80 knots is shown in Figures V-57, V-58, and V-59 respectively. Rotors-off, the yawing moment is very similar in magnitude and characteristics as for mast angle 90 degrees.

Rotors-on tests showed increased directional stability at yaw angles greater than six degrees. As airspeed increases directional stability rotors-on reduces at high yaw angles to nearly the level of rotors-off. At 40 knots, rotors-on, the rotor wake effects are more severe than for mast angle 90 degrees. Between yaw angles of ± 2.0 degrees the model was directionally unstable. As airspeed increased the model becomes more stable.

g. Lift Coefficient, Mast Angles 60 and 30 degrees

Lift coefficients at 80 and 100 knots for mast angles of 60 and 30 degrees are shown in Figures V-60 and V-61.

h. Pitching Moment Coefficient, Mast Angle 60 and 30 degrees

Pitching moment coefficient versus angle of attack for the same speeds are shown in Figures V-62 and V-63. The rotors-off pitching moment is similar to that at the other mast angles. The rotors-on pitching moment has a pitch up region at 80 knots, mast 60, as it did at mast angles 90 and 75 degrees at lower airspeeds. The pitch up does not occur at 100 knots or at mast angle of 30 degrees.

Rotors-on, empennage off data, shows very little destabilizing effect due to the rotor. Empennage on, the rotor wake effect is stabilizing in that the rotors-on pitching moment is more stable than the rotors-off.

i. Yawing Moment Coefficient, Mast angle 60 and 30 degrees

Directional stability for 80 and 100 knots is very good as shown in Figures V-64 and V-65. Rotor wake effects on the vertical fins' aerodynamics are still indicated to be destabilizing but do not reduce the directional stability between ± 4 degrees as much as at mast angles 90 and 75 degrees. Directional stability is still increased, rotors-on, at yaw angles greater than 4 degrees.

TABLE V-1. CORRELATION BETWEEN CALCULATED AND MEASURED
DYNAMIC STABILITY CHARACTERISTICS

<u>Pitch</u>			
<u>Mast Angle</u>	<u>Airspeed Knots</u>	<u>Measured¹ Period/Damping</u>	<u>Calculated¹ Period/Damping</u>
90°	80	3.6 sec/ζ = .41	3.2 sec/ζ = .66 (3.62 sec/ζ = .41) ²
	90	2.7 sec/ζ = .45	2.98 sec/ζ = .64
	100	2.34 sec/ζ = .35	2.7/ζ = .62
75°	60	3.42 sec/ζ = .33	4.4 sec/ζ = .67
60°	—	(Data At This Mast) (Angle Not Usable)	—
30°	100	3.03 sec/ζ = .42	2.0 sec/ζ = .47
<u>Yaw</u>			
<u>Mast Angle</u>	<u>Airspeed Knots</u>	<u>Measured Period/Damping</u>	<u>Calculated Period/Damping</u>
90°	100	5.6 sec/ζ = .190	4.6 sec/ζ = .14
75°	100	5.6 sec/ζ = .17	4.3 sec/ζ = .17
60°	80	7.05 sec/ζ = .25	5.6 sec/ζ = .24
30°	—	(Data At This Mast) (Angle Not Usable)	—
<p>1. Full-scale equivalent</p> <p>2. Calculated used measured static derivatives and with dynamic derivatives corrected for Reynolds number</p>			

TABLE V-2 EVALUATION OF MODEL CONTROLLABILITY

<u>Conversion Angle</u>	<u>Airspeed</u>	<u>Evaluation</u>
90°	Hover (IGE and OGE)	Very difficult to control and impossible to stabilize on trim. (Recirculation was evident in the test section.)
90°	16 to 20 Knots	Roll and pitch control very difficult but could be stabilized on trim. Directional control fairly easy. Height control easy.
90°	20 to 30 Knots	Roll control difficult but pitch control much easier. Directional and height control easy.
90°	35 Knots	All axes fairly solid at this speed. Easy to obtain trim condition.
90°	50 to 100 Knots	Model handles very well, trim flight is easy to obtain and can be maintained hands off.
90°	Sideward Flight	Roll control difficult. Pitch control easy and directional control fairly easy. Difficult to control height.
90°	Rearward Flight	Roll control difficult up to 20 knots, the less difficult up to 35 knots. Pitch control fairly easy. Yaw control power adequate to maintain directional control.

TABLE V-2 EVALUATION OF MODEL CONTROLLABILITY (CONT)

<u>Conversion Angle</u>	<u>Airspeed</u>	<u>Evaluation</u>
90°	Descent and Auto-rotation (50 to 80 Knots)	Easy to control up to the point where wing stall occurs, then porpoising in pitch was present.
75°	All Speeds	*Comments are essentially the same as for mast angle 90°.
60° and 30°	80 to 100 Knots	Easy to control about all axes.

*Except for trim at 30 knots where the model was difficult to hold in trim.

SEE FIGURE IV-1 FOR
TEST RIG SCHEMATIC

HOVER TEST
MAST ANGLE = 90°
FLAPS = $75/45^\circ$
WING FAIRING ON
 $h/D = 0.5$

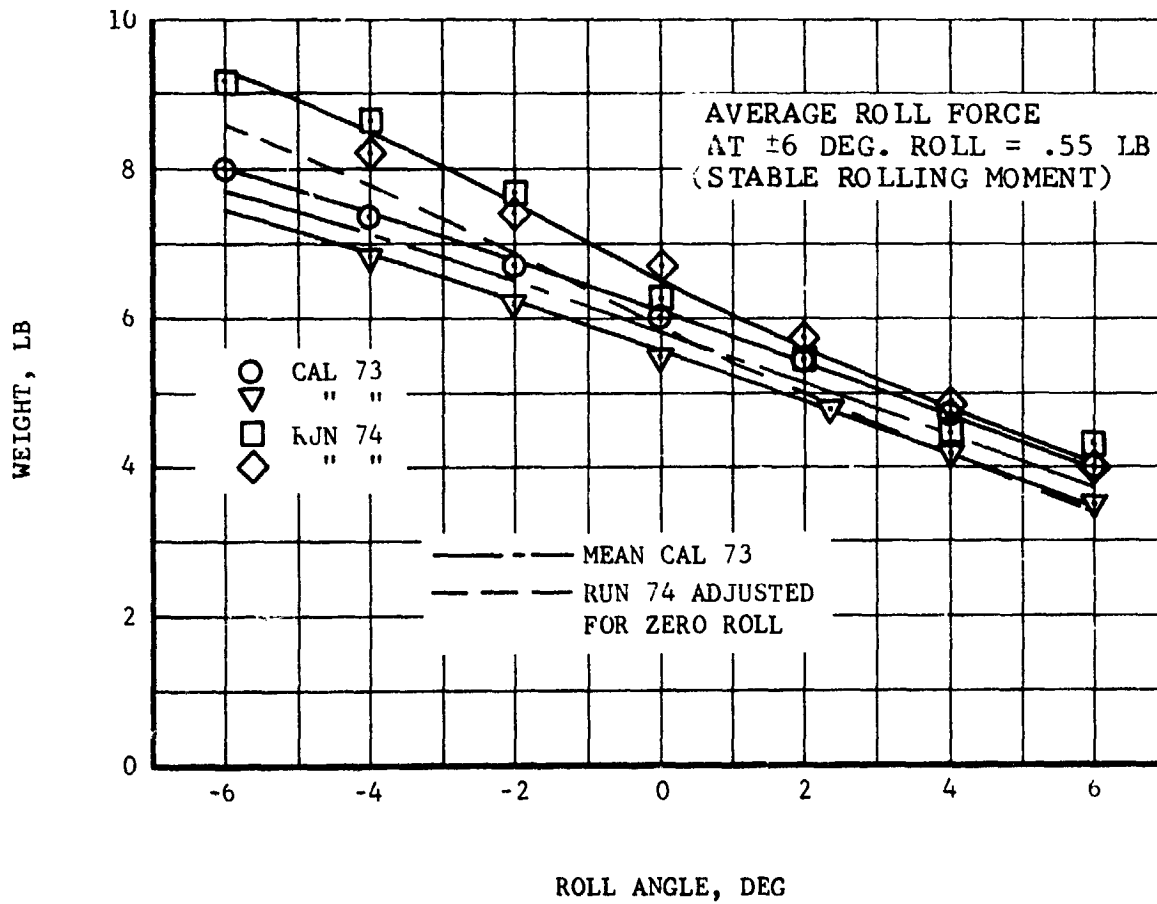


Figure V-1. Weight Required to Maintain a Given
Roll Angle versus Roll Angle, $h/D = 0.5$,
Wing Fairings On.

HOVER TEST
 MAST ANGLE = 90°
 FLAPS = $75/45^{\circ}$
 WING FAIRING ON
 h/D = 1.0

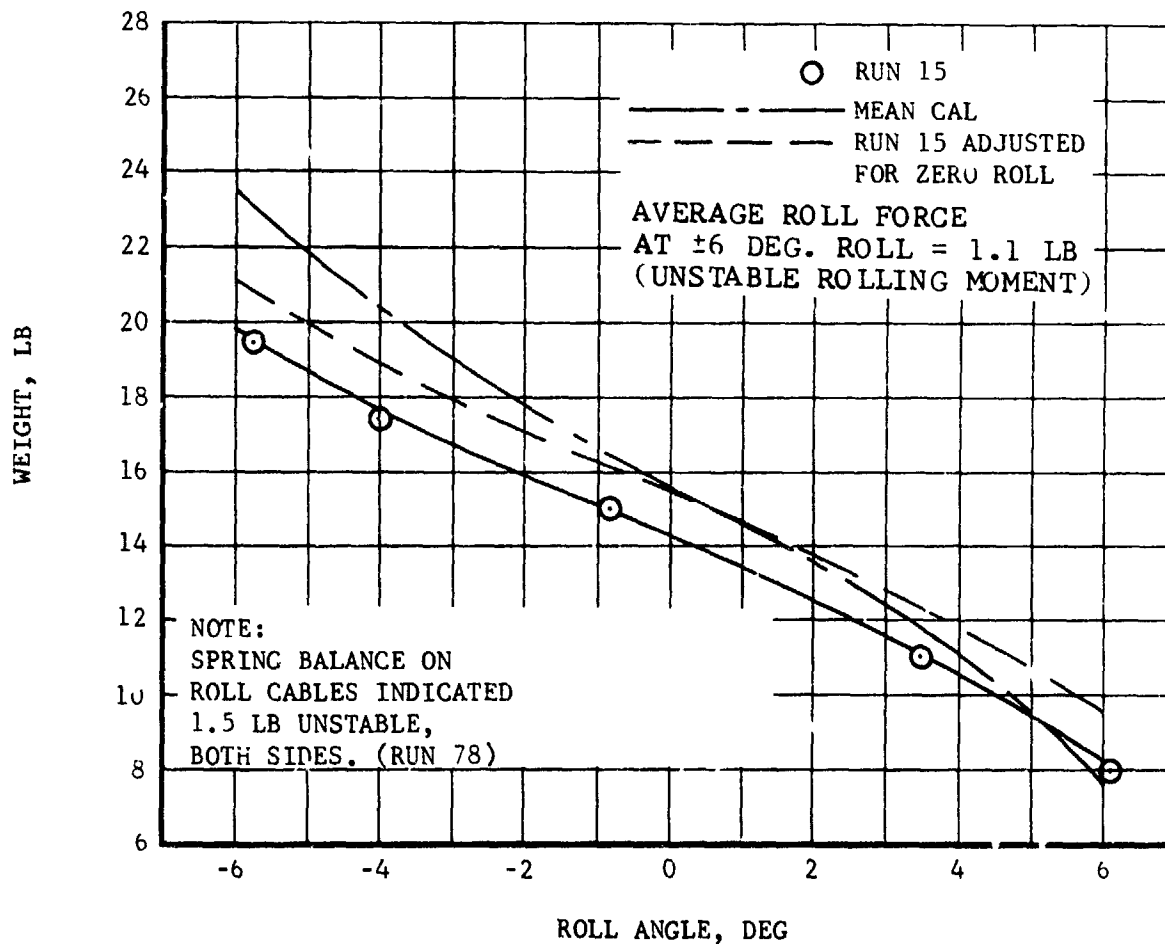


Figure V-2. Weight Required to Maintain a Given Roll Angle versus Roll Angle, h/D = 0.75, Wing Fairings On.

HOVER TEST
MAST ANGLE = 90°

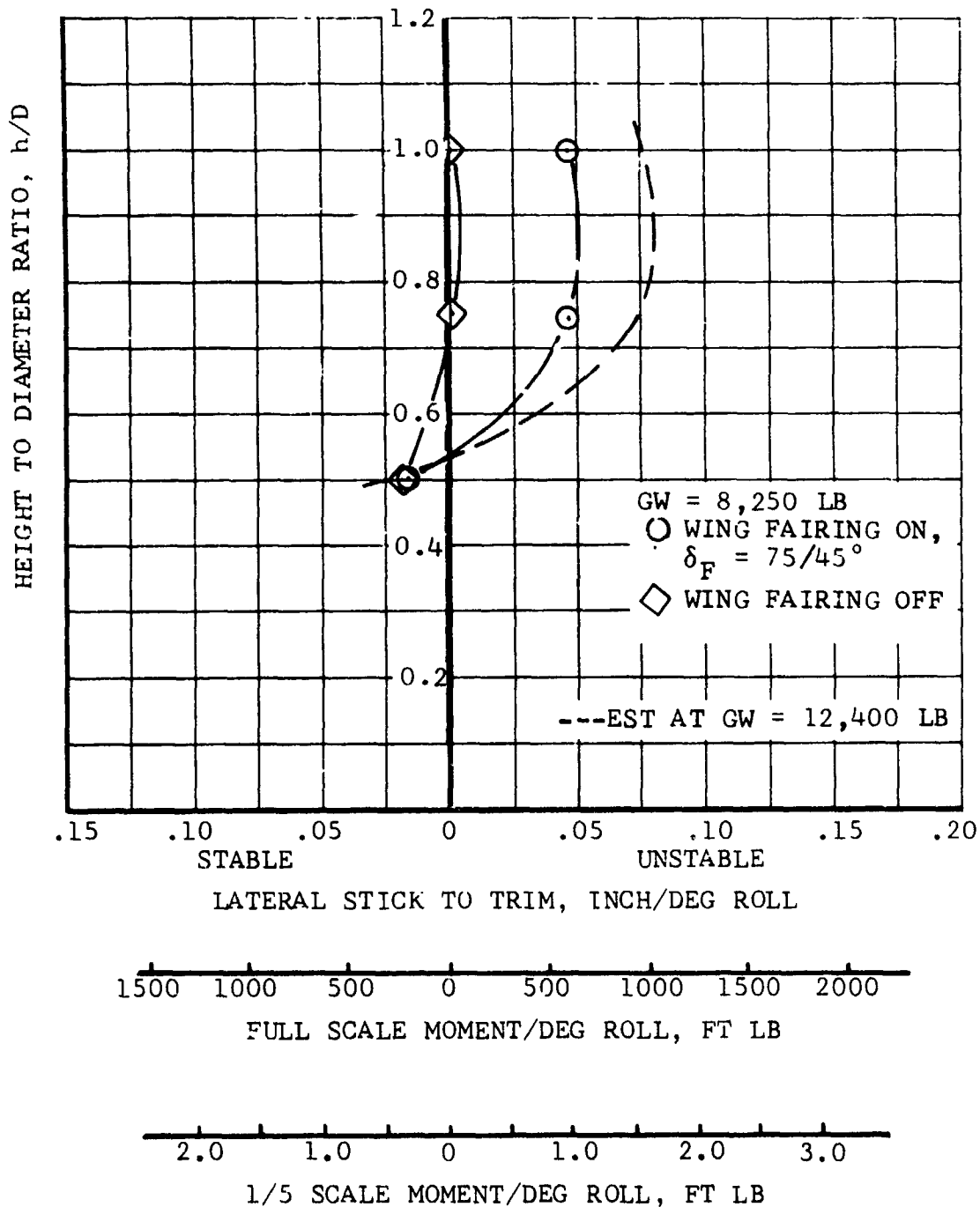


Figure V-3. Summary of Roll Stability Characteristics in IGE Hover.

HOVER TEST
MAST ANGLE = 90°
 $h/D = 1.0$

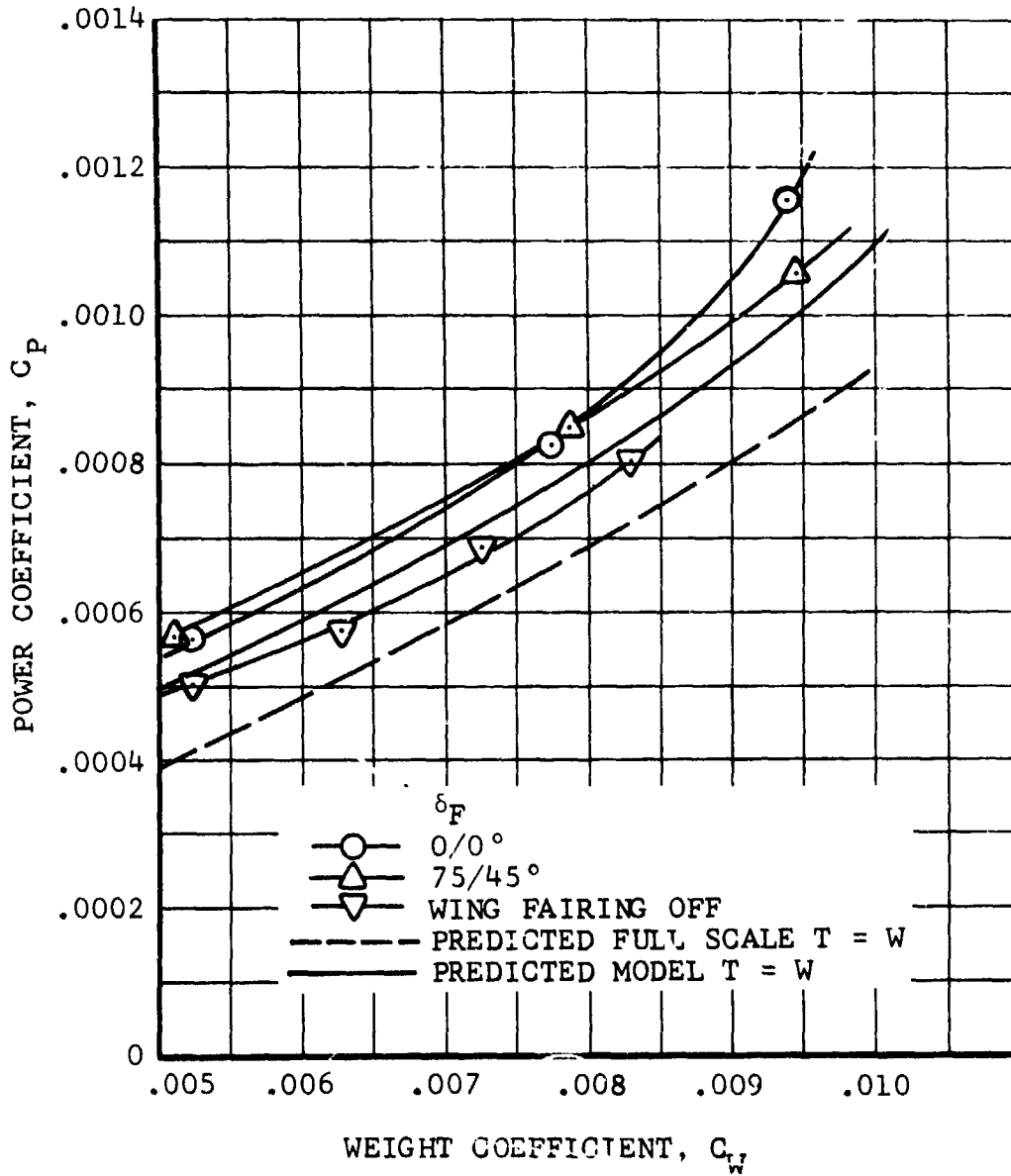


Figure V-4. Hover Performance, $h/D = 1.0$.

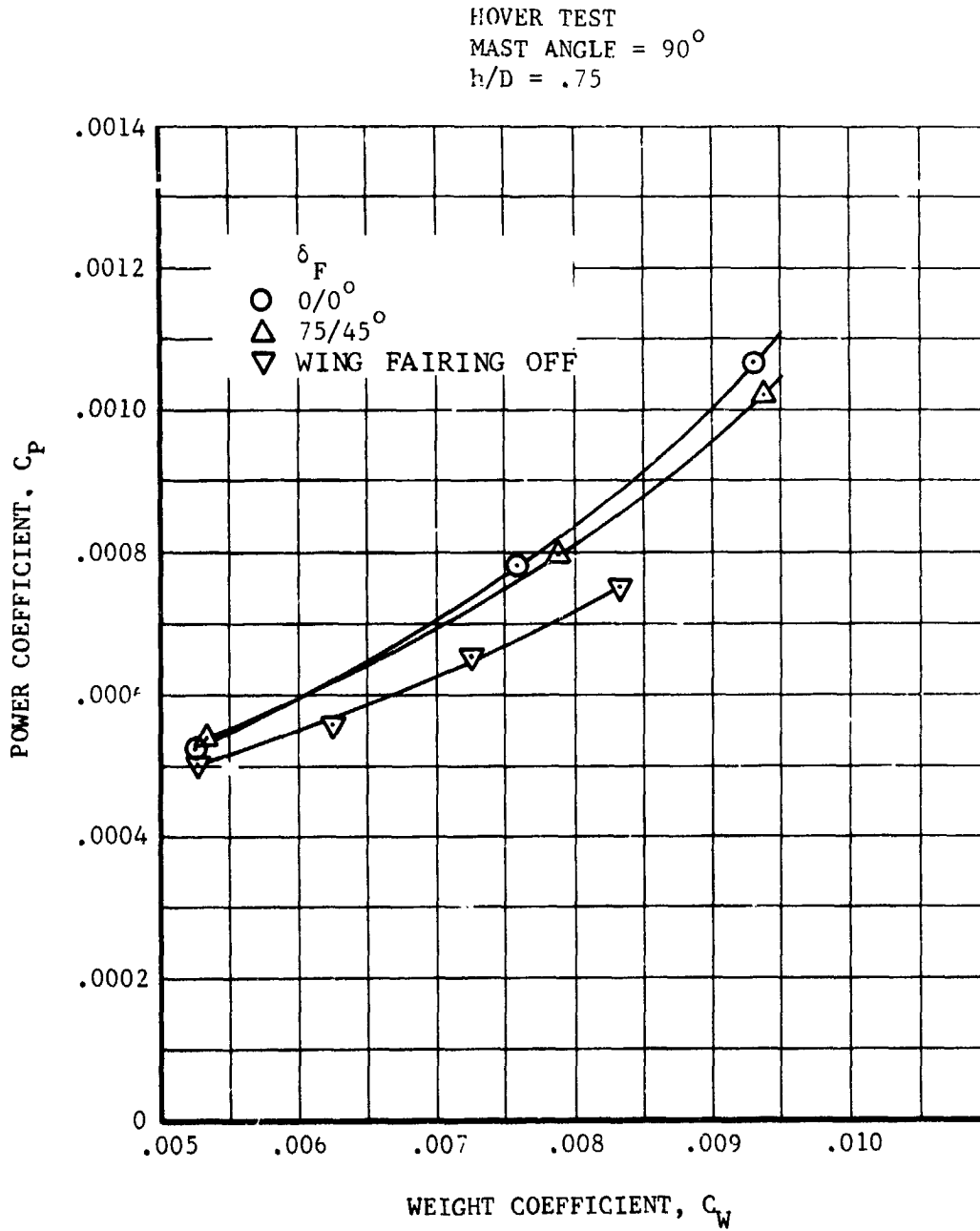


Figure V-5. Hover Performance, $h/D = .75$.

HOVER TEST
MAST ANGLE = 90°
 $h/D = .50$

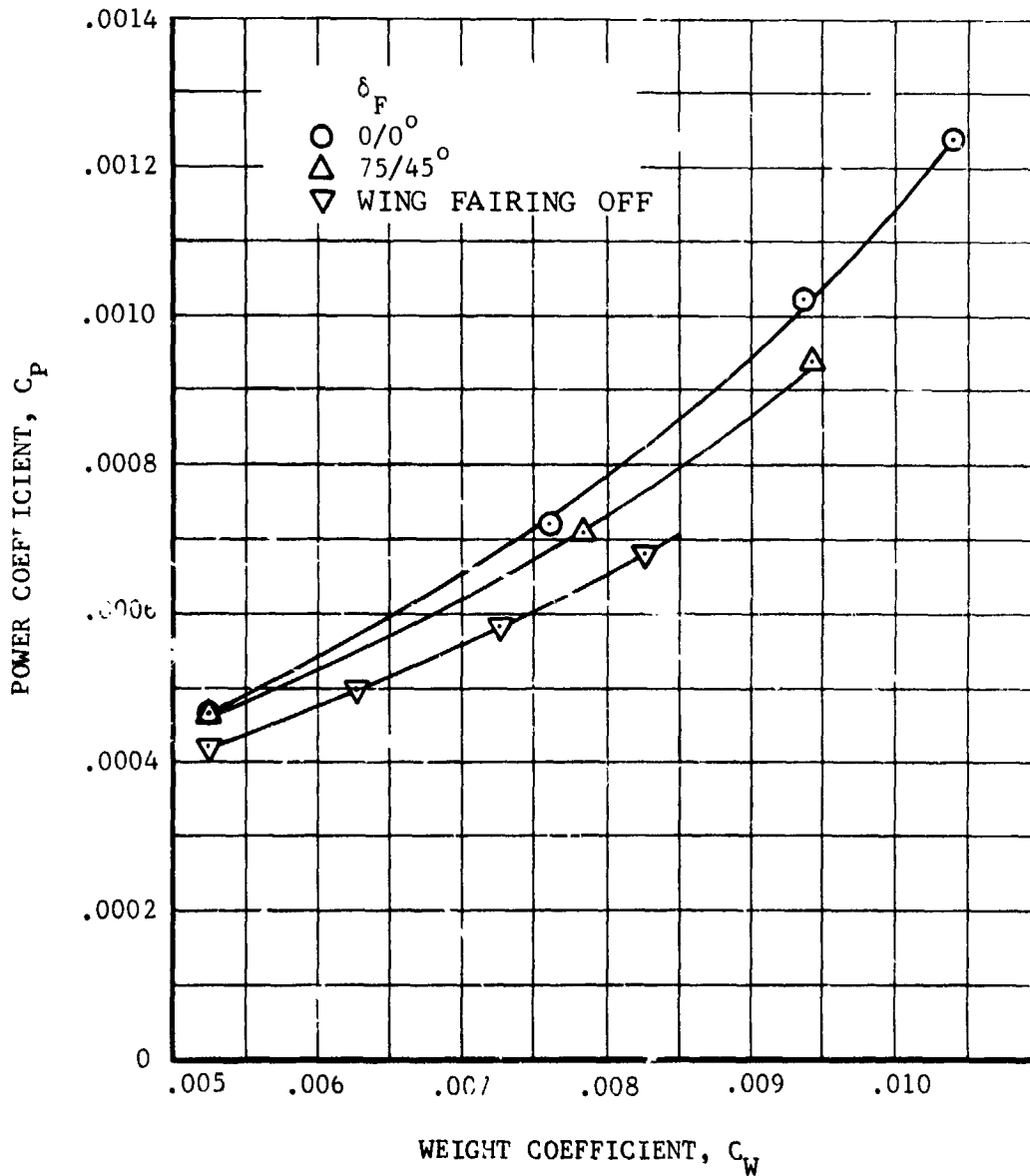


Figure V-6. Hover Performance, $h/D = 0.5$

○ 1/5 SCALE MODEL, $RN < 2 \times 10^5$
 ▼ 1/10 SCALE C100F1B, $RN = 4 \times 10^5$
 ▨ MODEL 301 FULL SCALE, $RN > 2 \times 10^6$

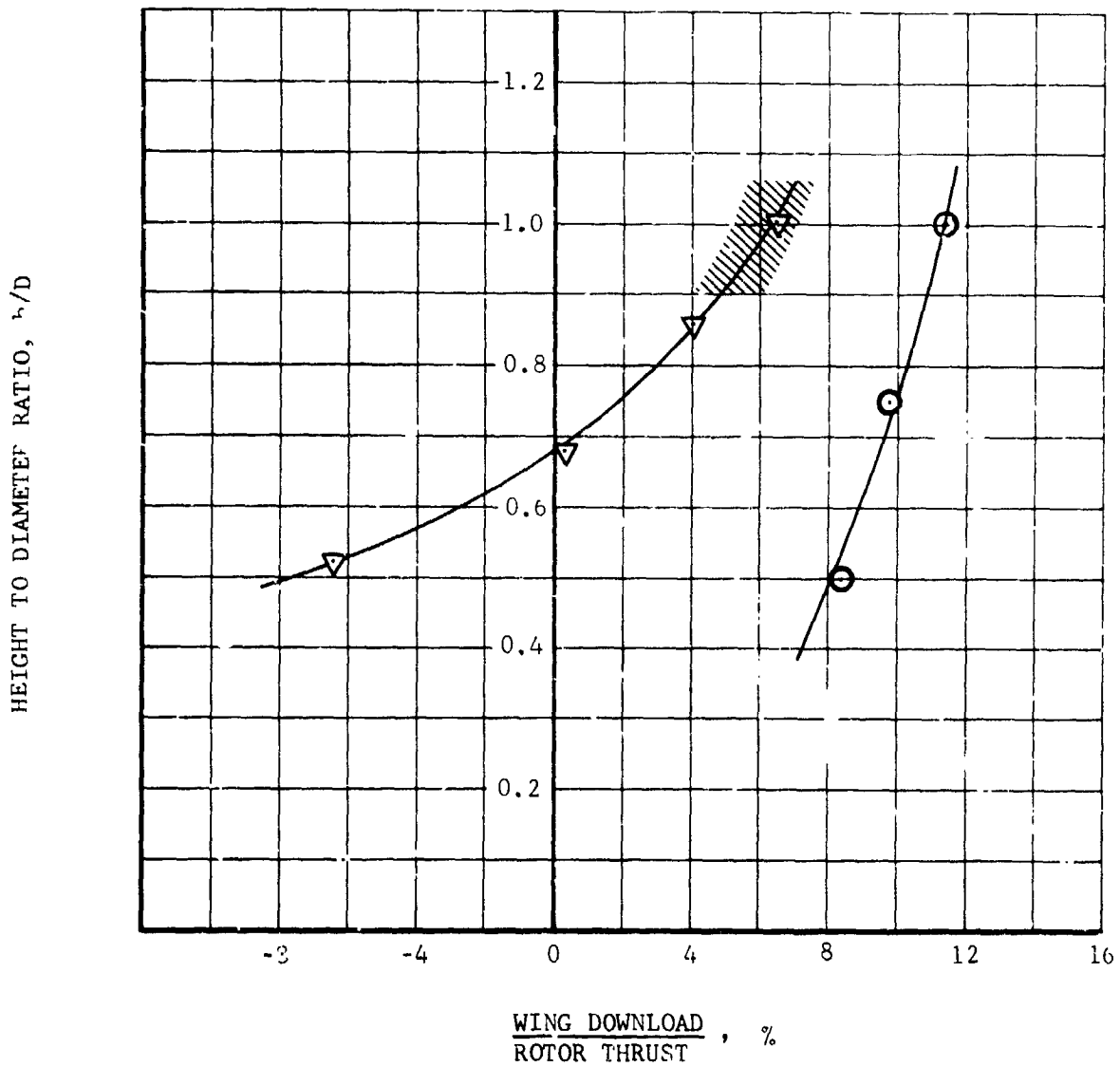


Figure V-7. Wing Down Load Summary, IGE.

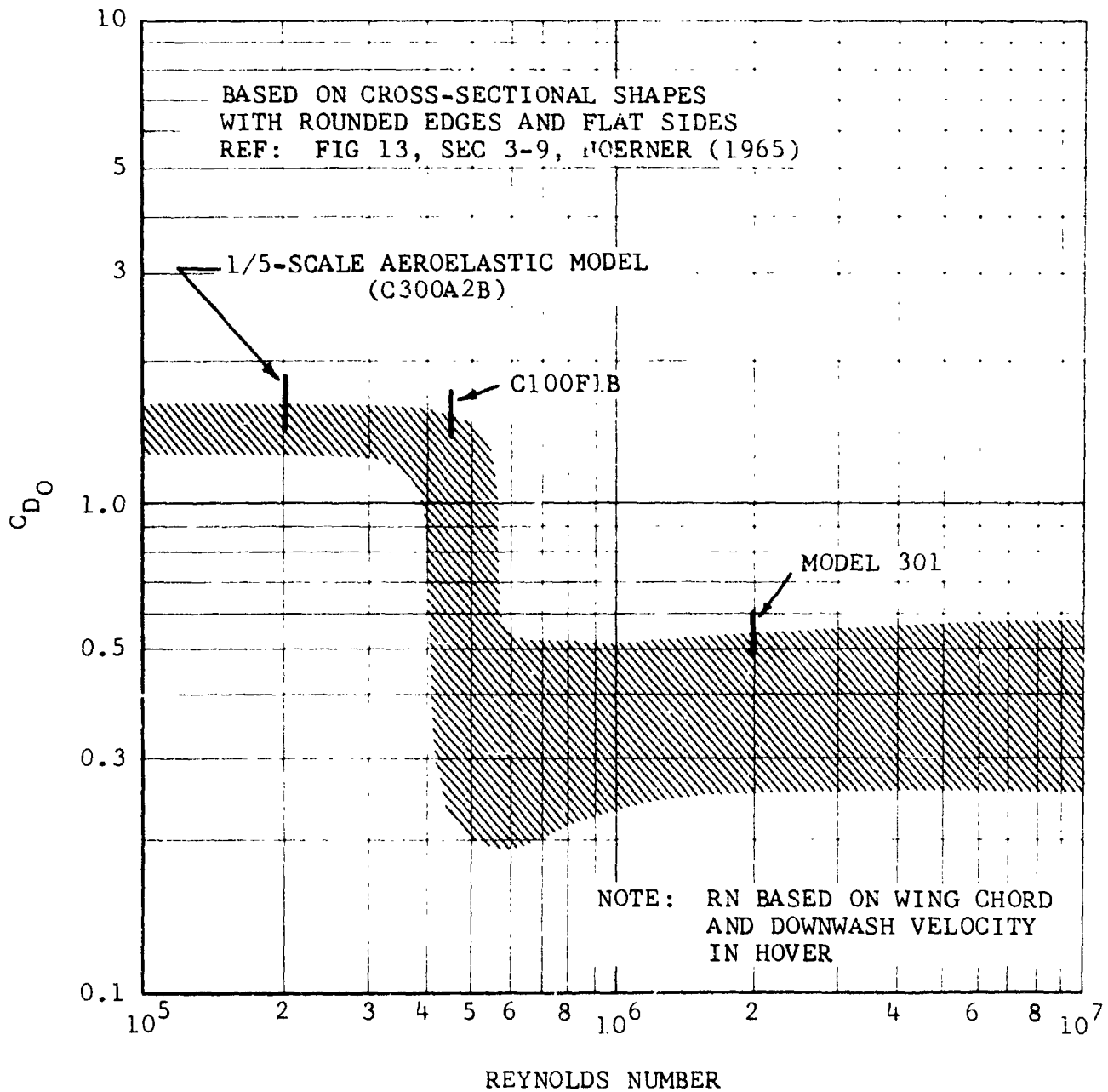


Figure V-8. Drag Coefficient of Wing at $\alpha_w = -90^\circ$ versus Reynolds Number.

HOVER TEST
MAST ANGLE = 90°
FLAPS = 75/45°
WING FAIRING ON

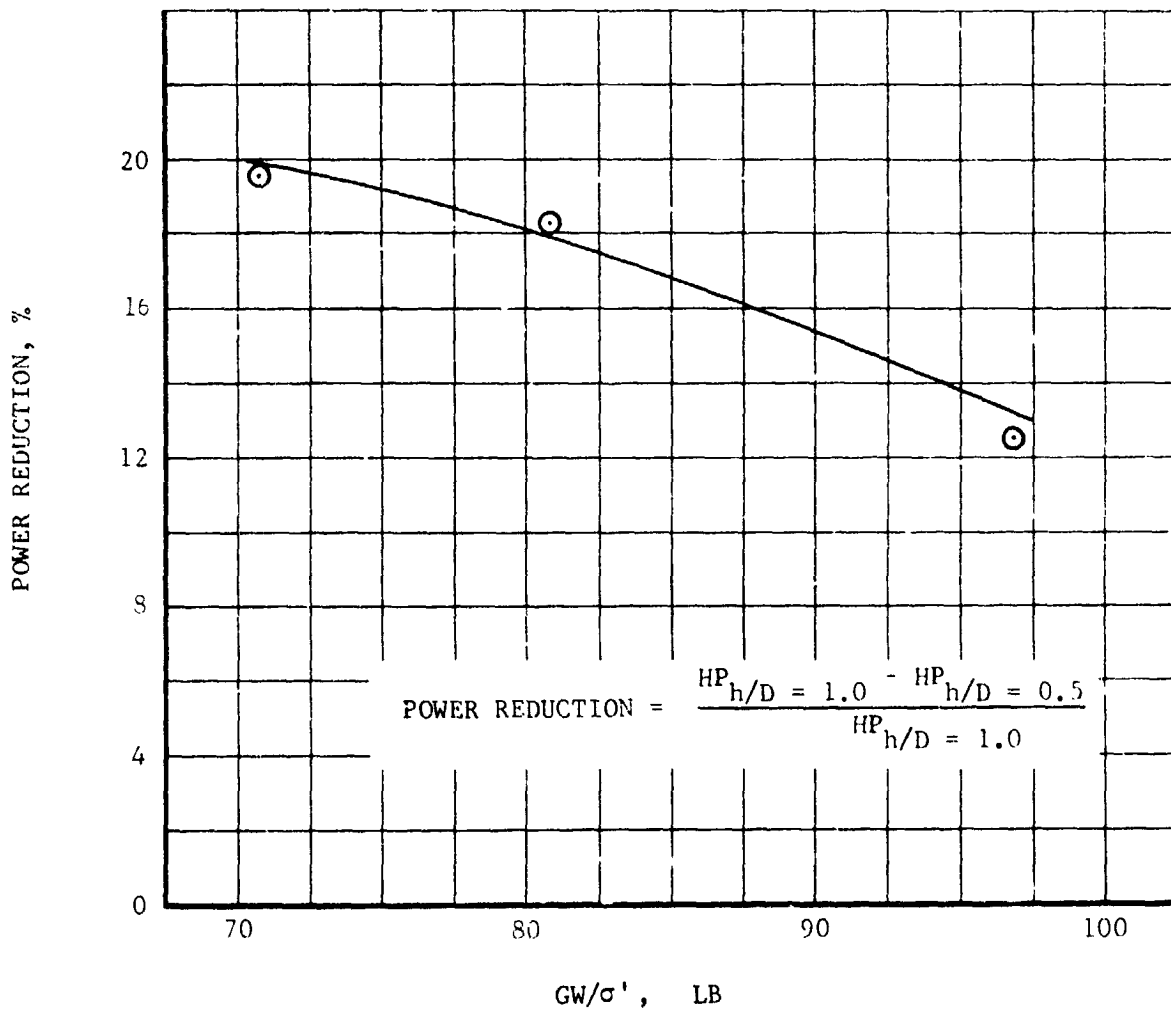


Figure V-9. Power Reduction in Ground Effect.

HOVER TEST
MAST ANGLE = 90°
GW/σ' = 69.8 LB

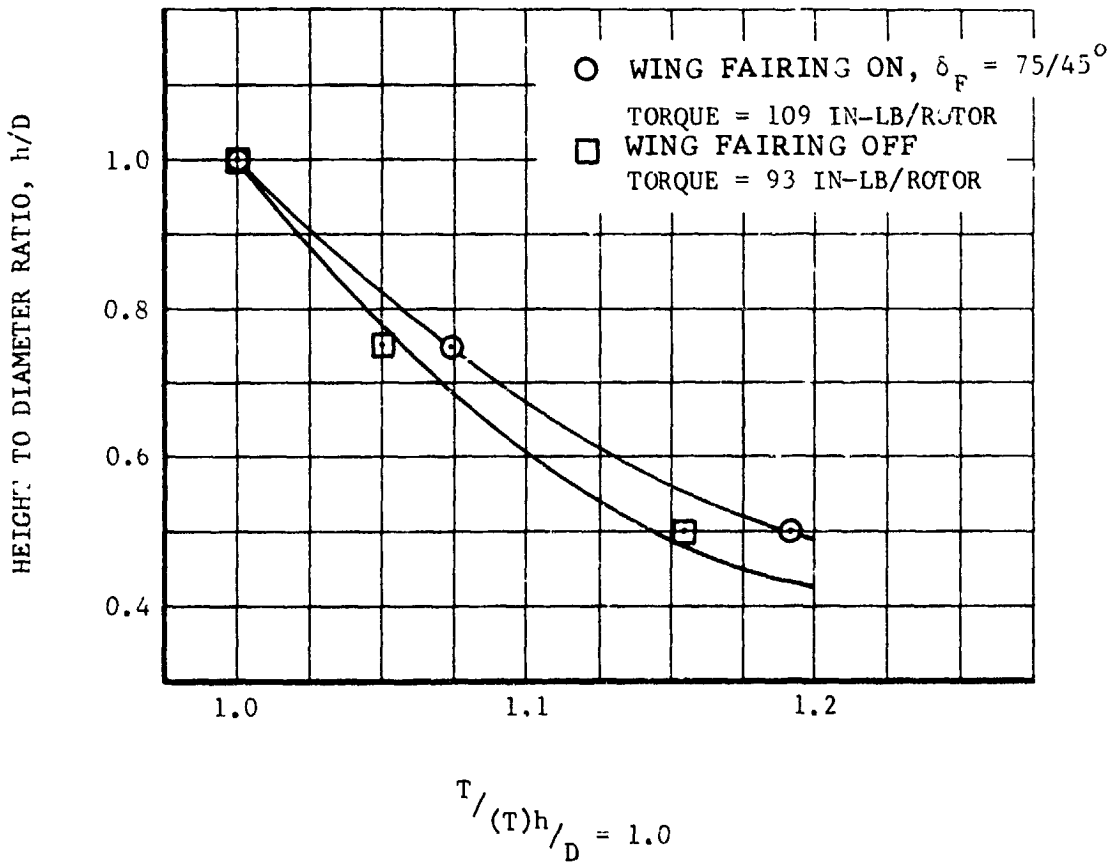


Figure V-10. Vertical "Spring" in Ground Effect.

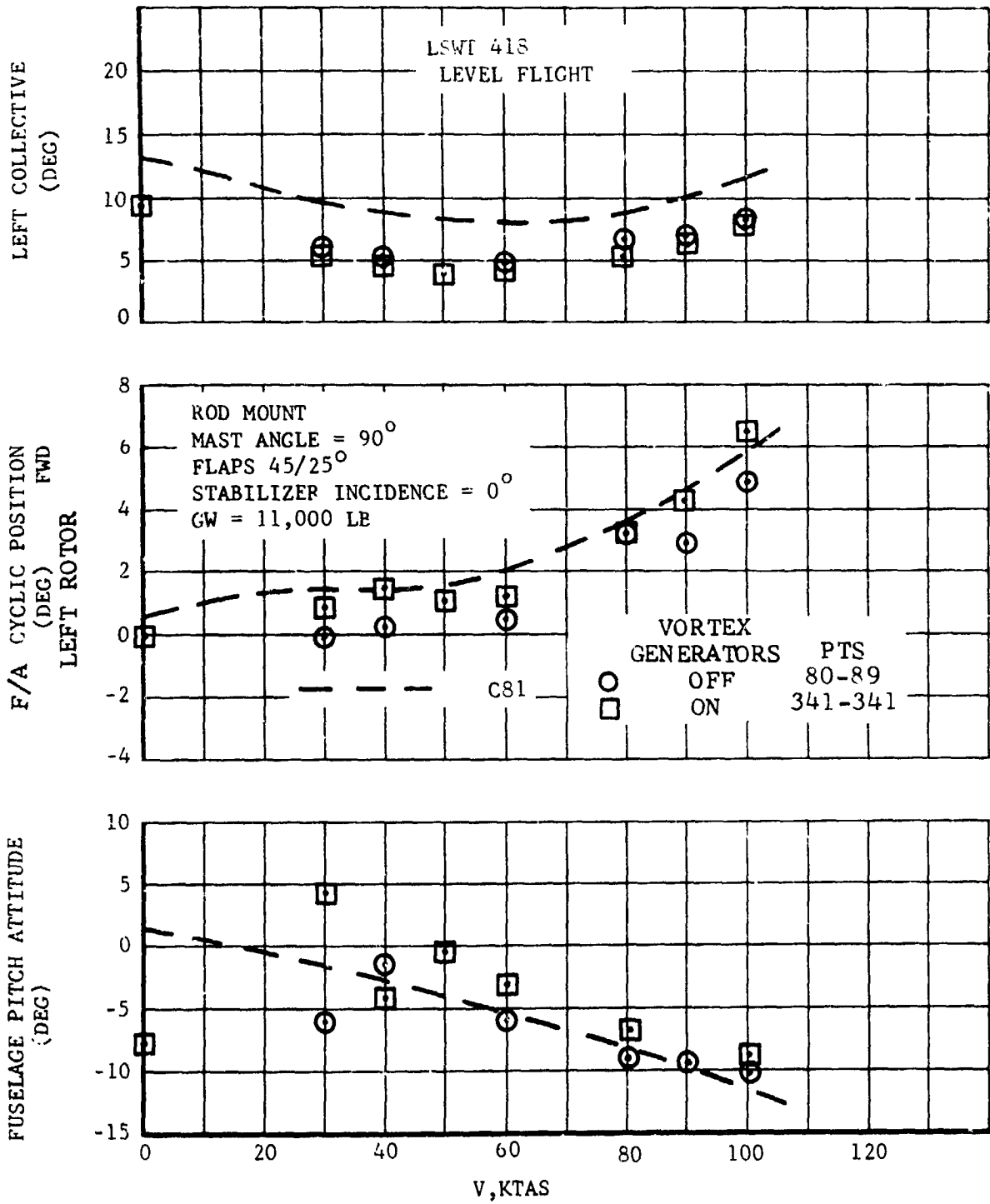


Figure V-11. Level Flight Trim Parameters, Mast Angle 90°.

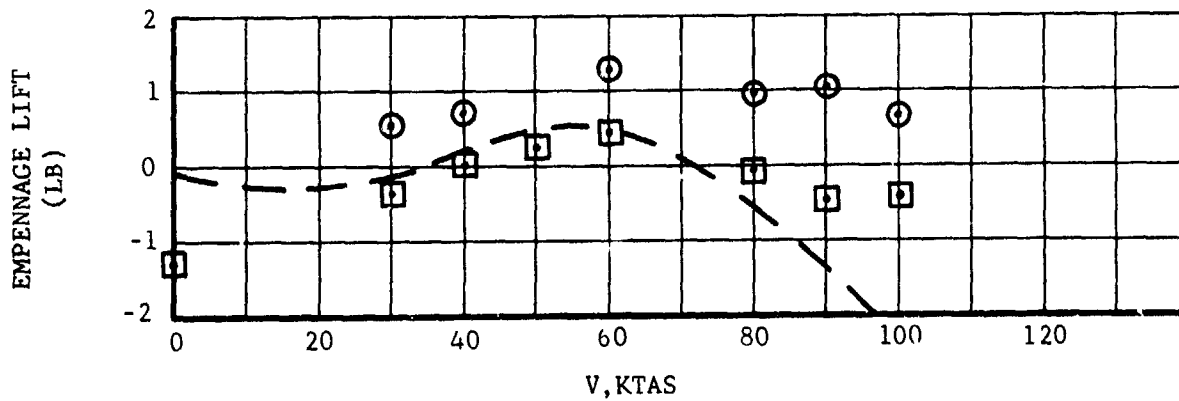
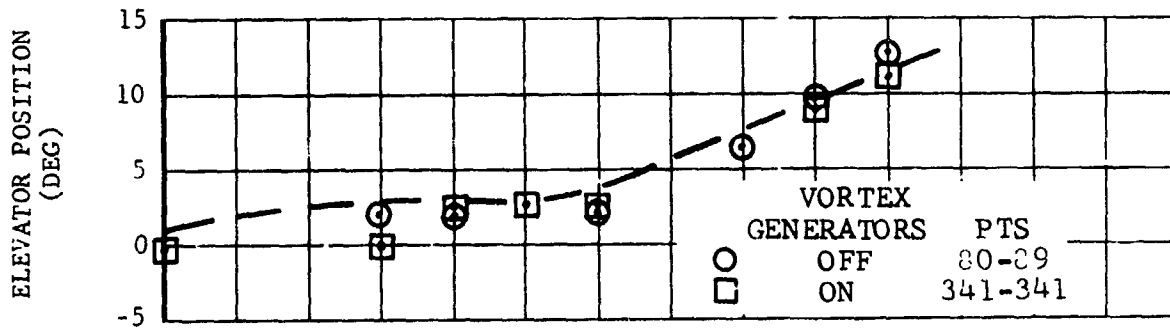
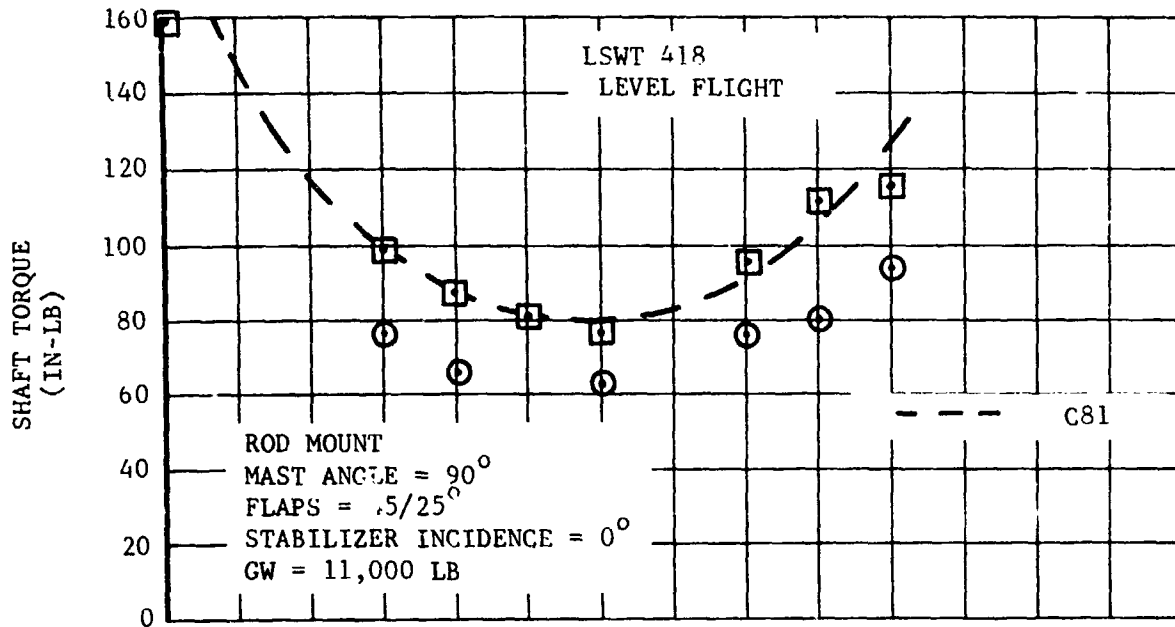


Figure V-11. Continued

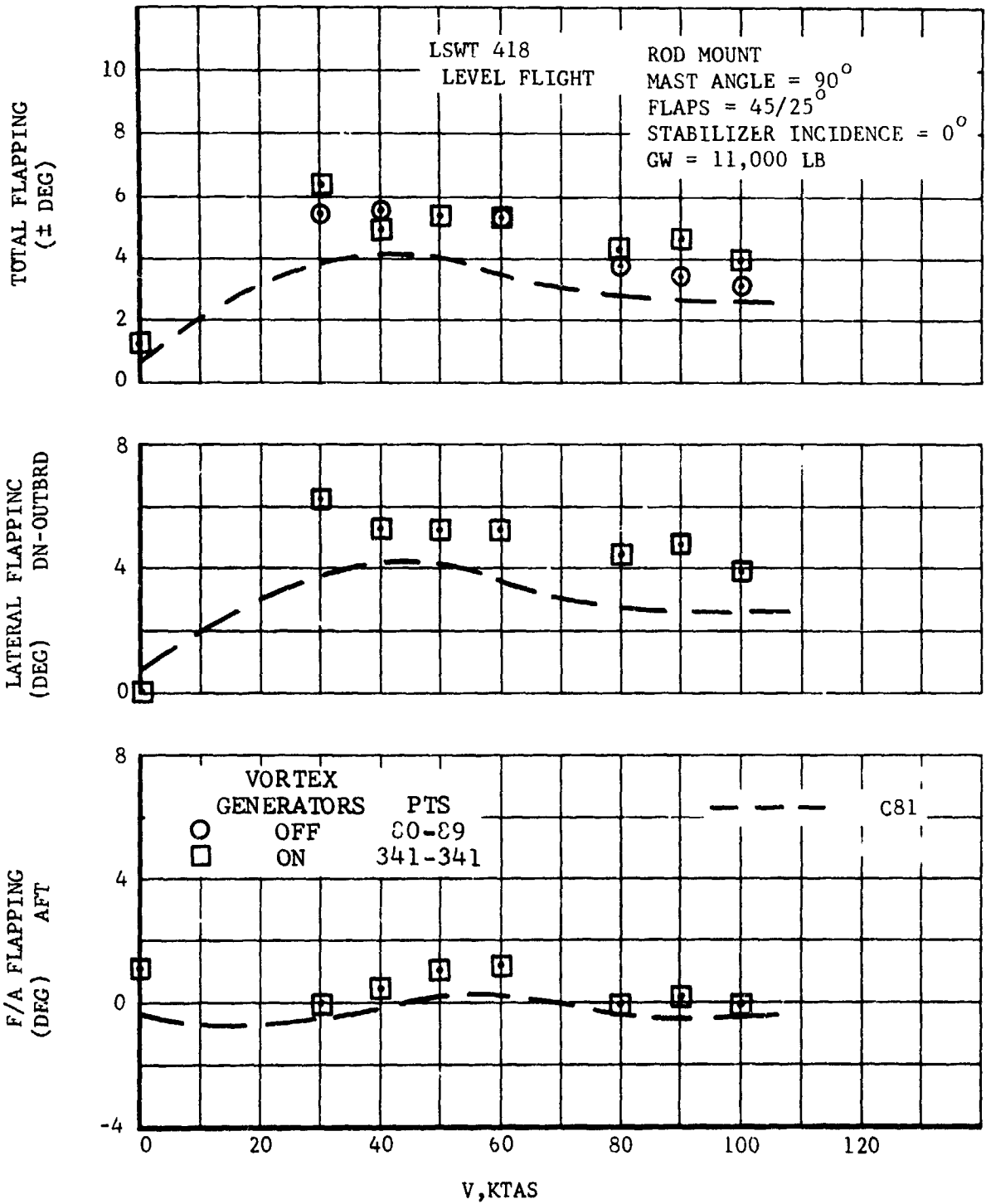


Figure V-11. Concluded

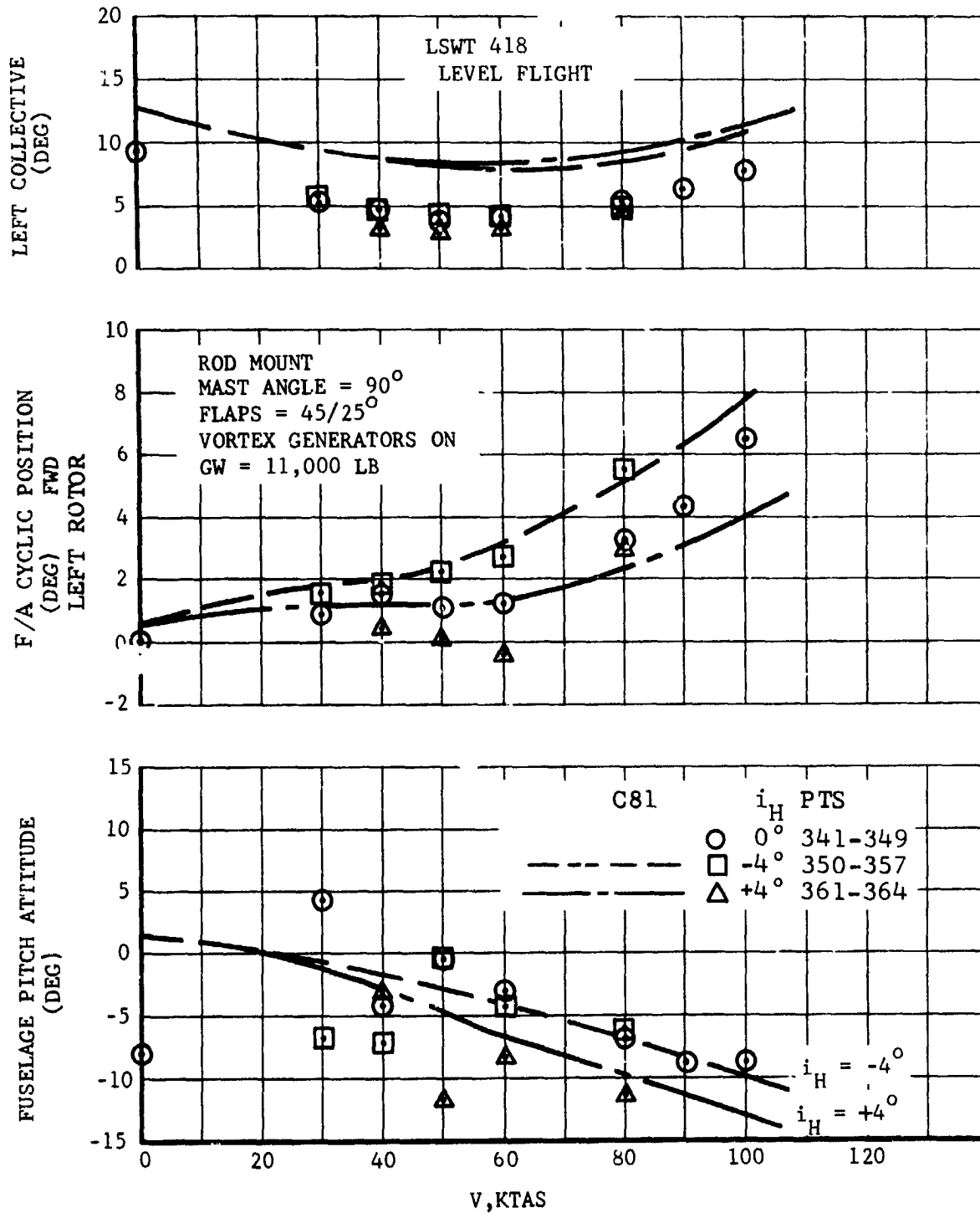


Figure V-12. Effect of Horizontal Stabilizer Incidence on Level Flight Trim Parameters, Mast Angle 90°.

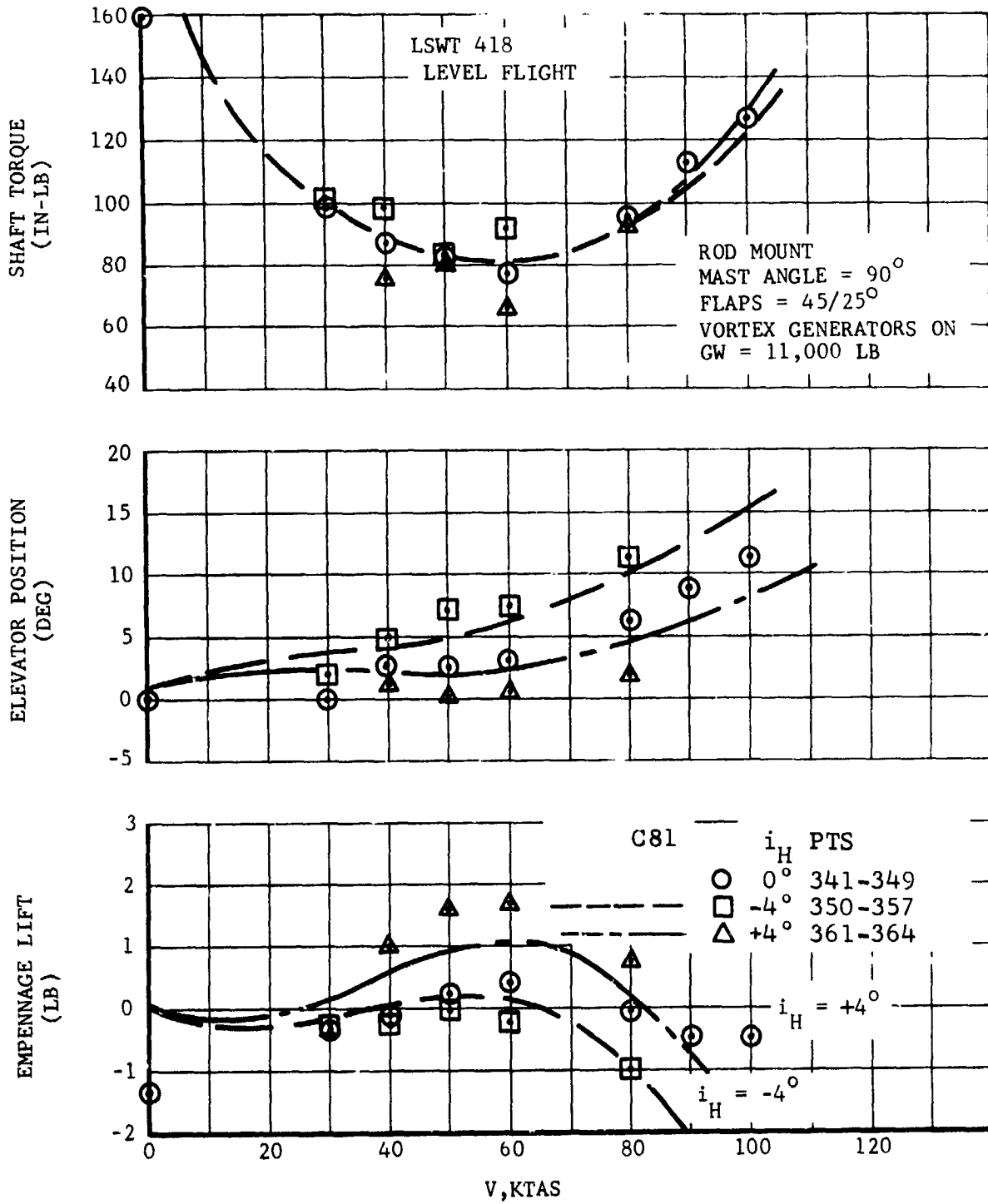


Figure V-12. Continued

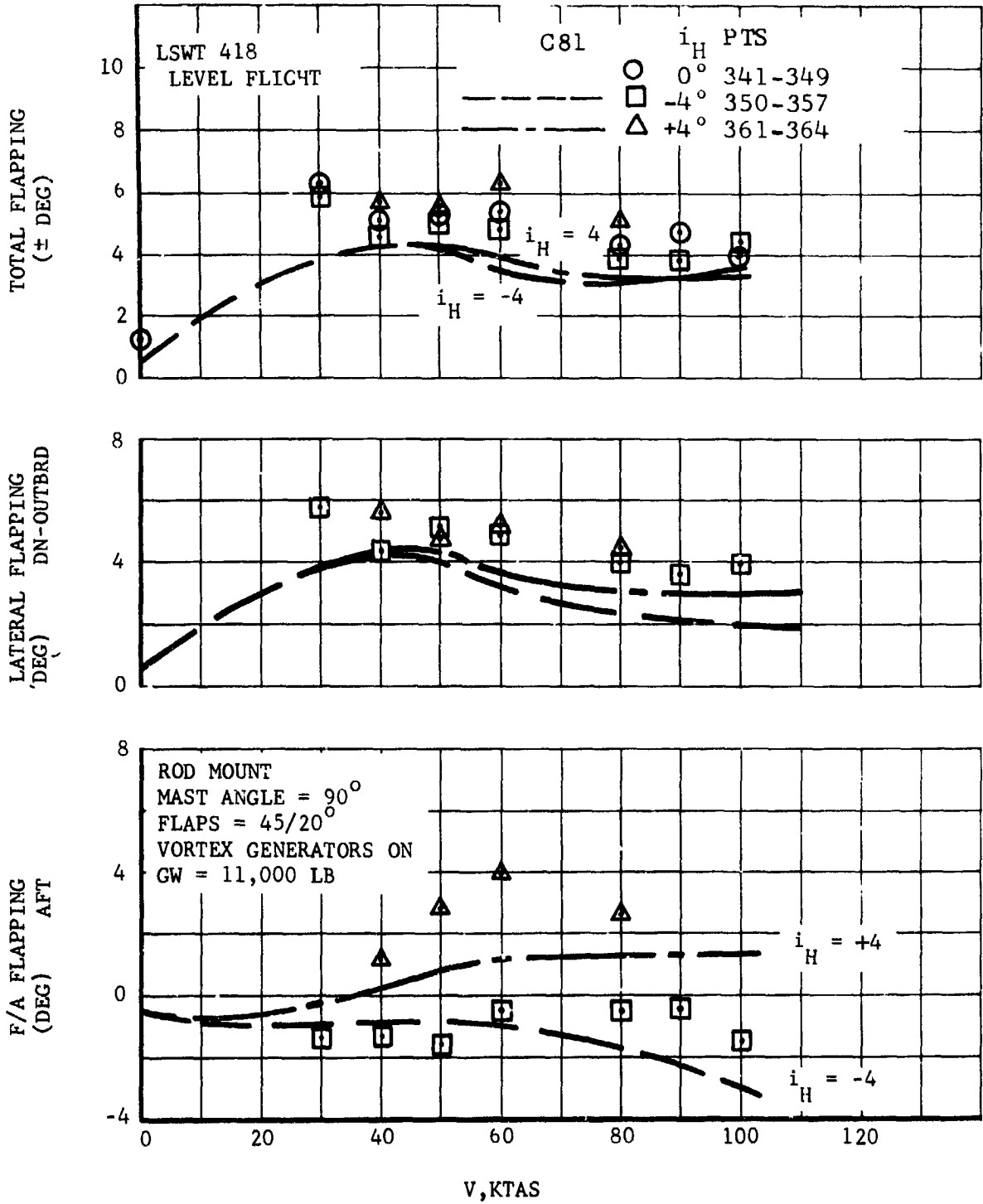


Figure V-12. Concluded

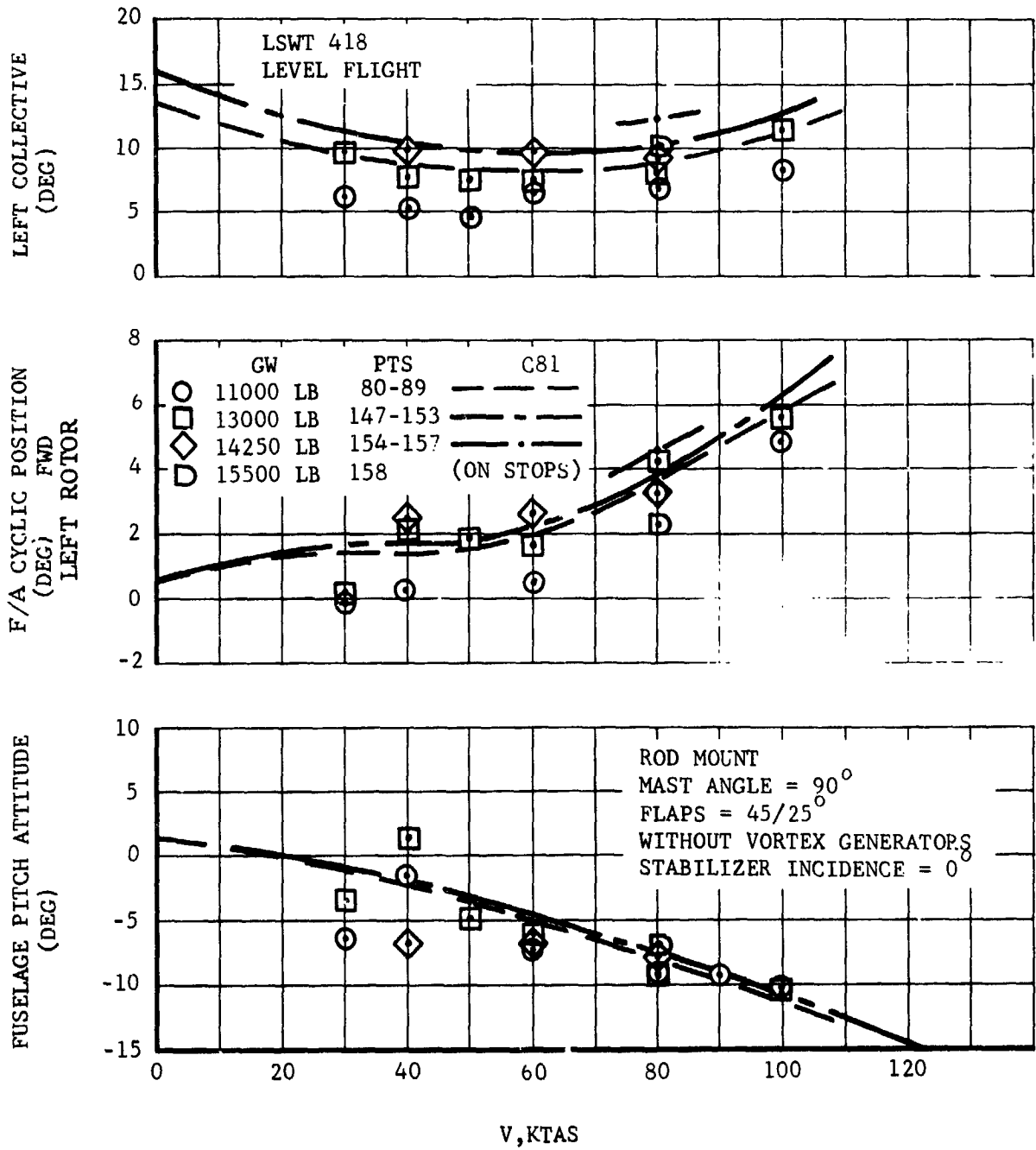


Figure V-13. Effect of Gross Weight on Level Flight Trim Parameters, Mast Angle 90°.

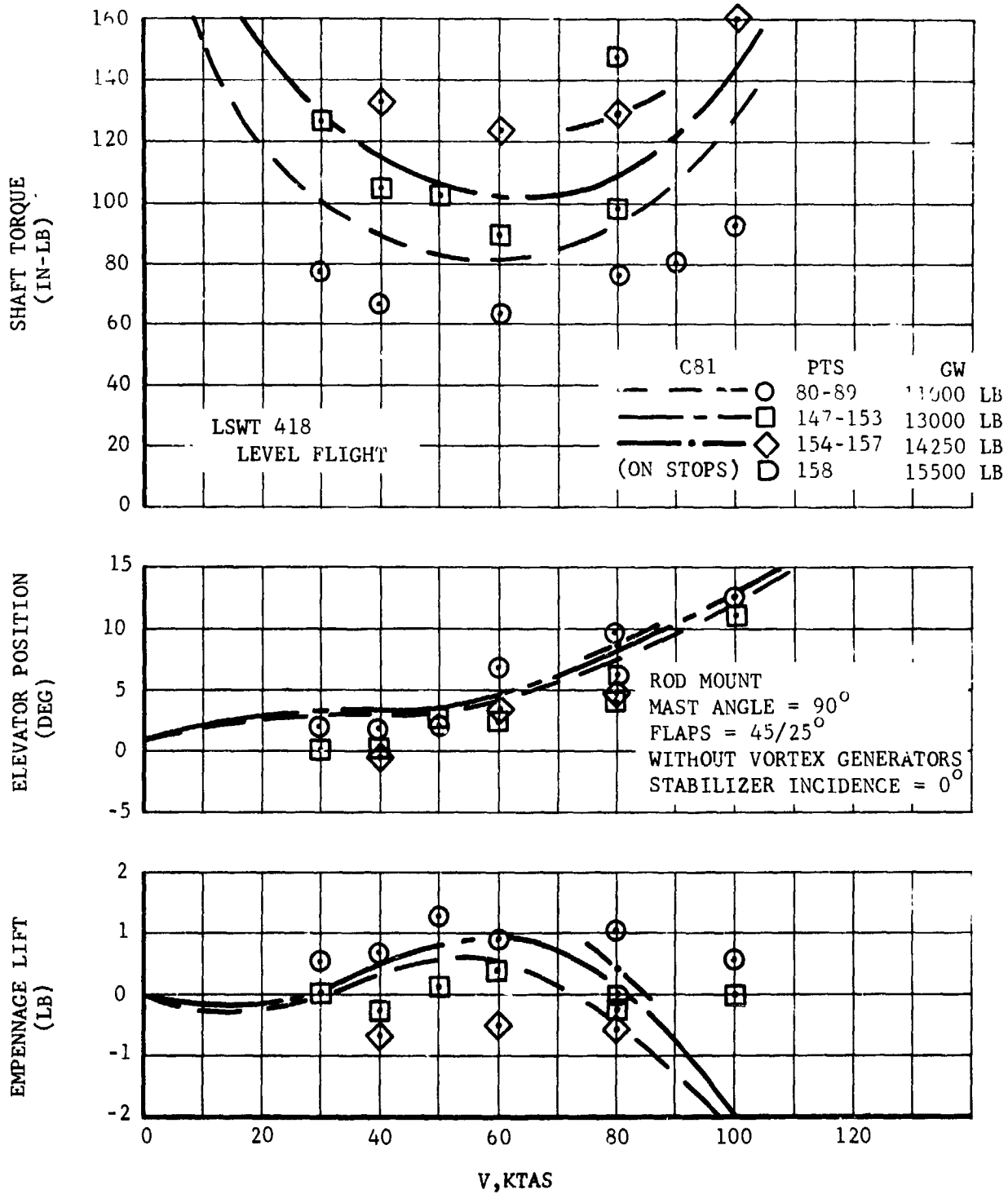


Figure V-13. Continued

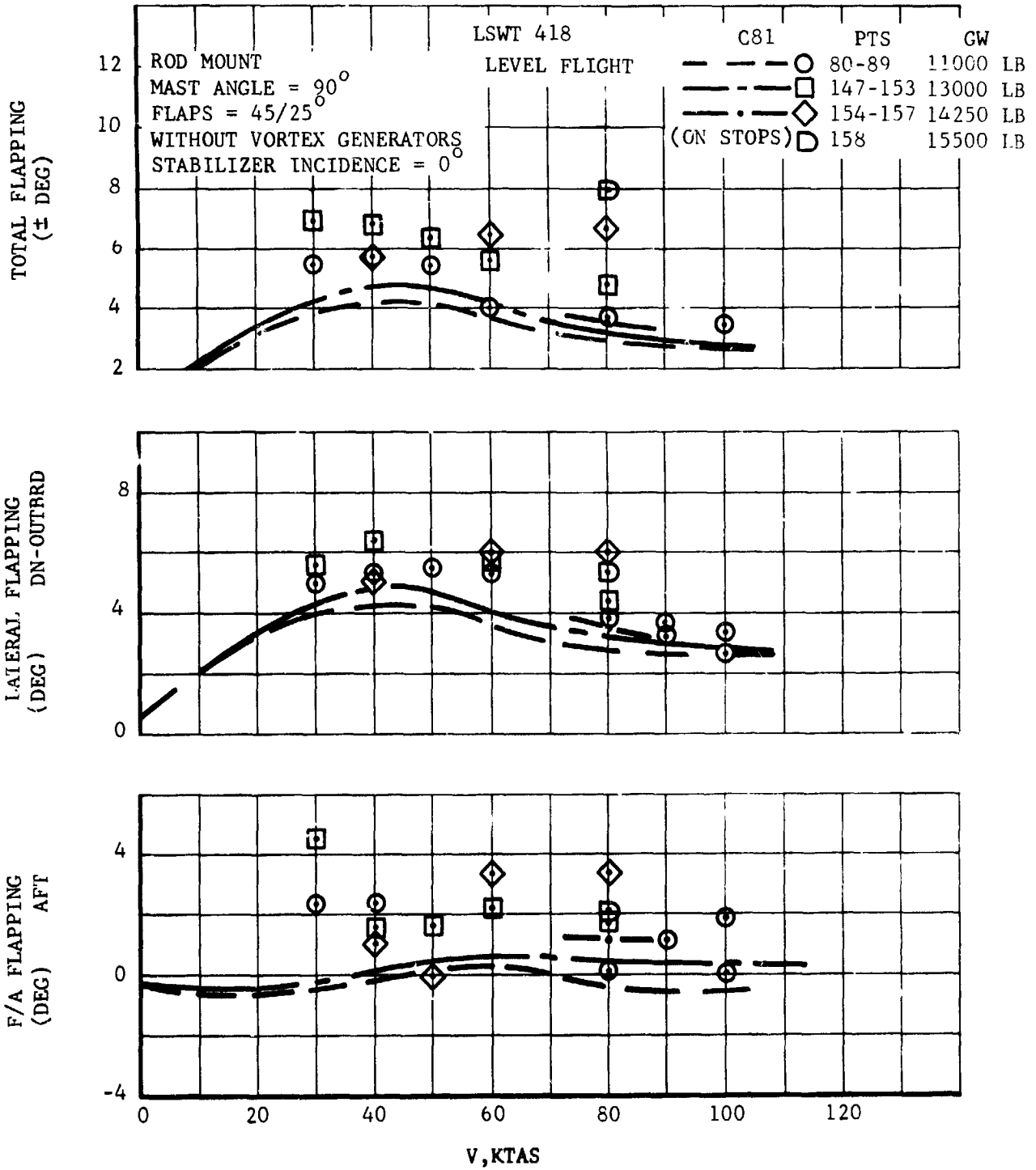


Figure V-13. Concluded

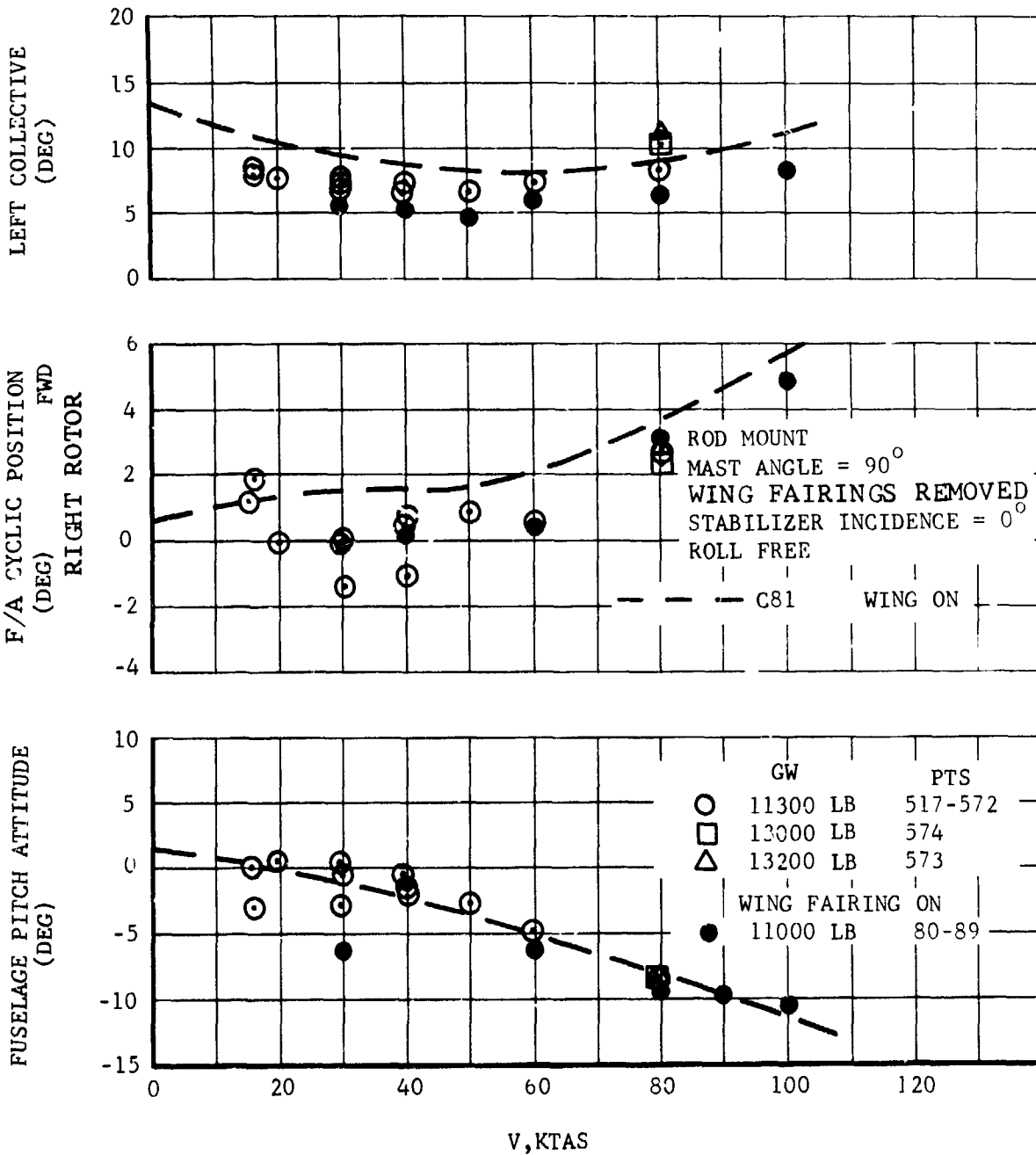


Figure V-14. Effect of Wing Lift on Level Flight Trim Parameters, Mast Angle 90°.

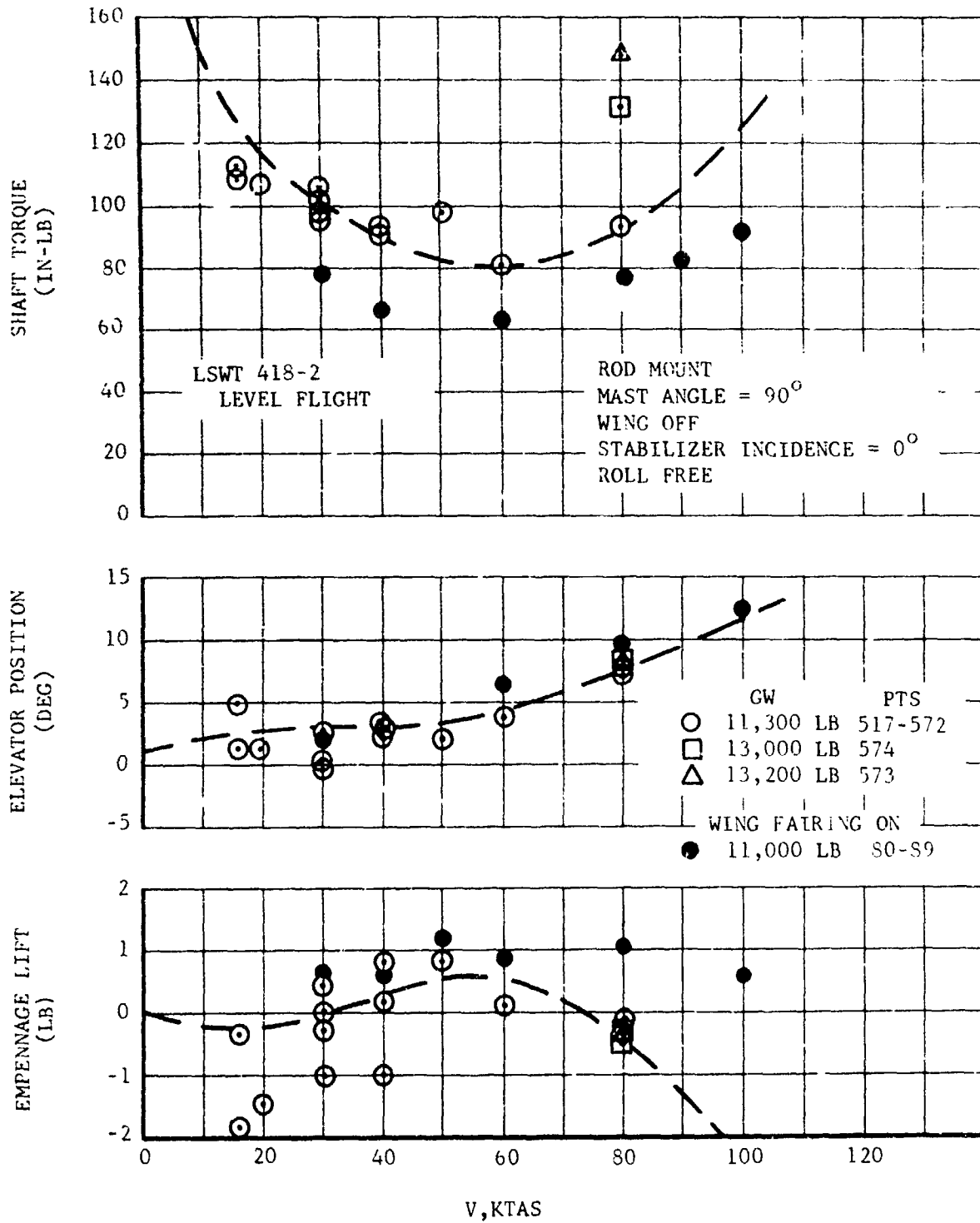


Figure V-14 Continued

ROD MOUNT
MAST ANGLE = 90°
WING FAIRINGS OFF
STABILIZER INCIDENCE = 0°
ROLL FREE

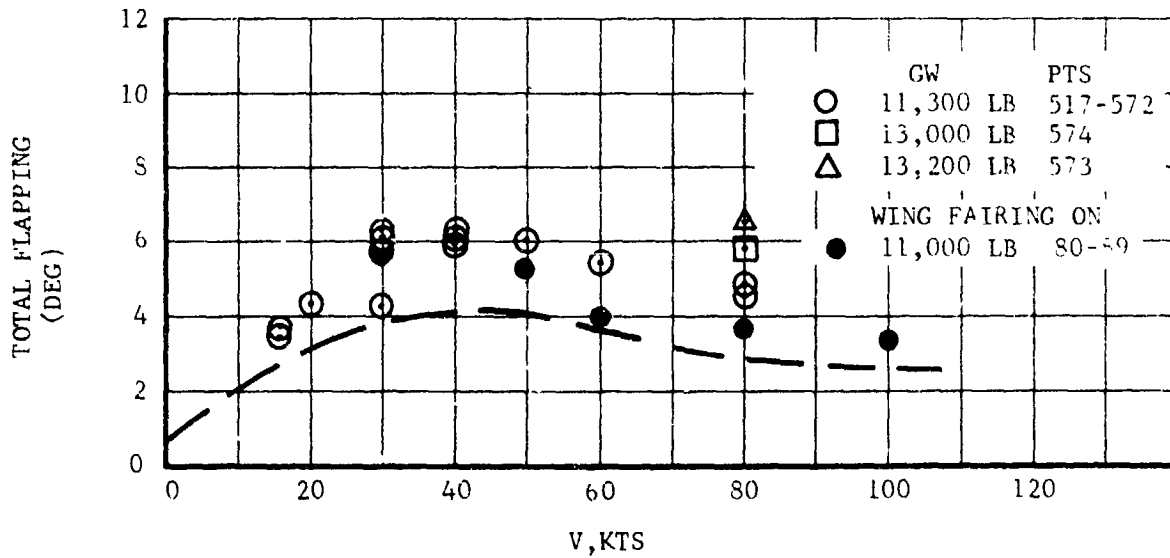
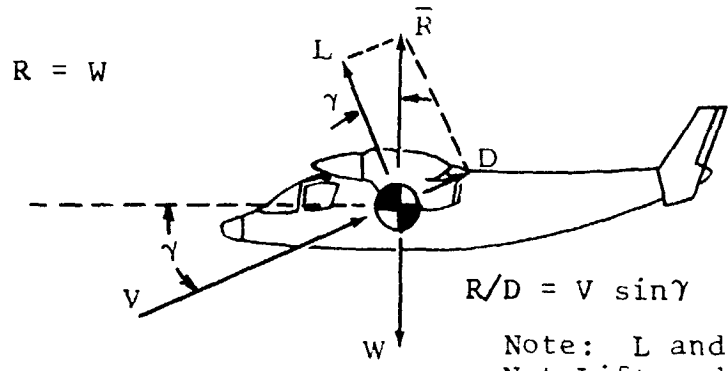


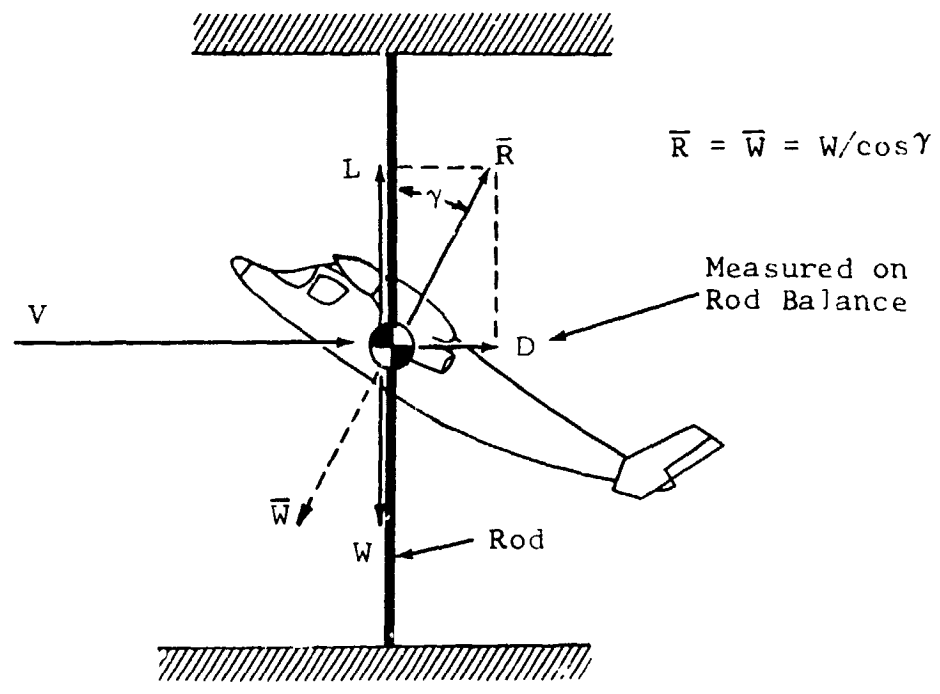
Figure V-14. Concluded

Flight



Note: L and D represent Net Lift and Drag With Respect to Relative Wind V.

Wind Tunnel



$$R/D = V \sin \gamma = V \tan^{-1} \left(\frac{D}{L} \right) = V \tan^{-1} \left(\frac{D}{\bar{W}} \right)$$

Simulated Weight $\bar{W} = W/\cos \gamma$

Figure V-15. Method of Determining Simulated Rate of Descent or Climb from Rod Thrust or Drag.

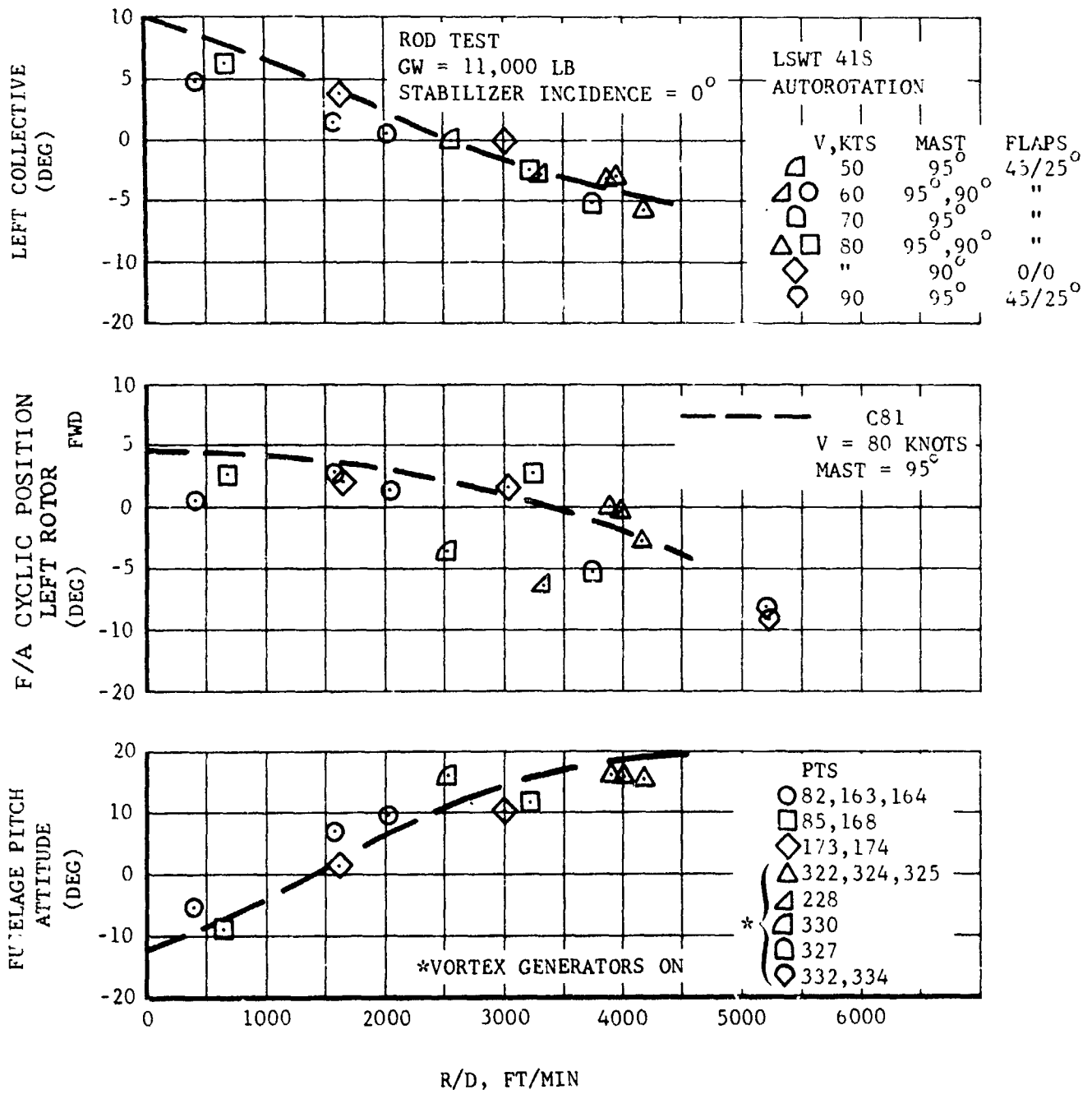


Figure V-16. Trim Parameters versus Rate of Descent in Descents and Autorotation, Mast Angle 90°.

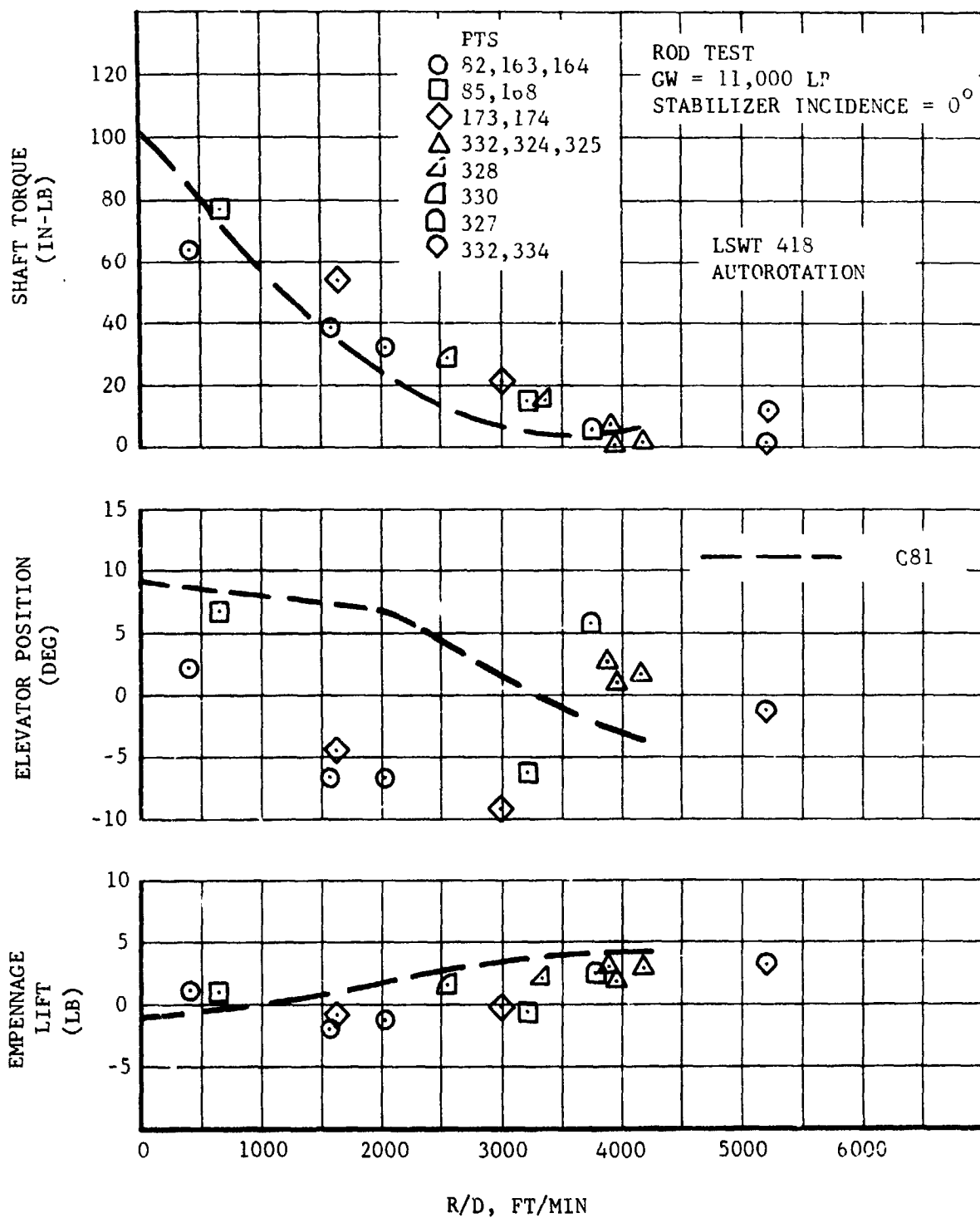


Figure V-16. Continued

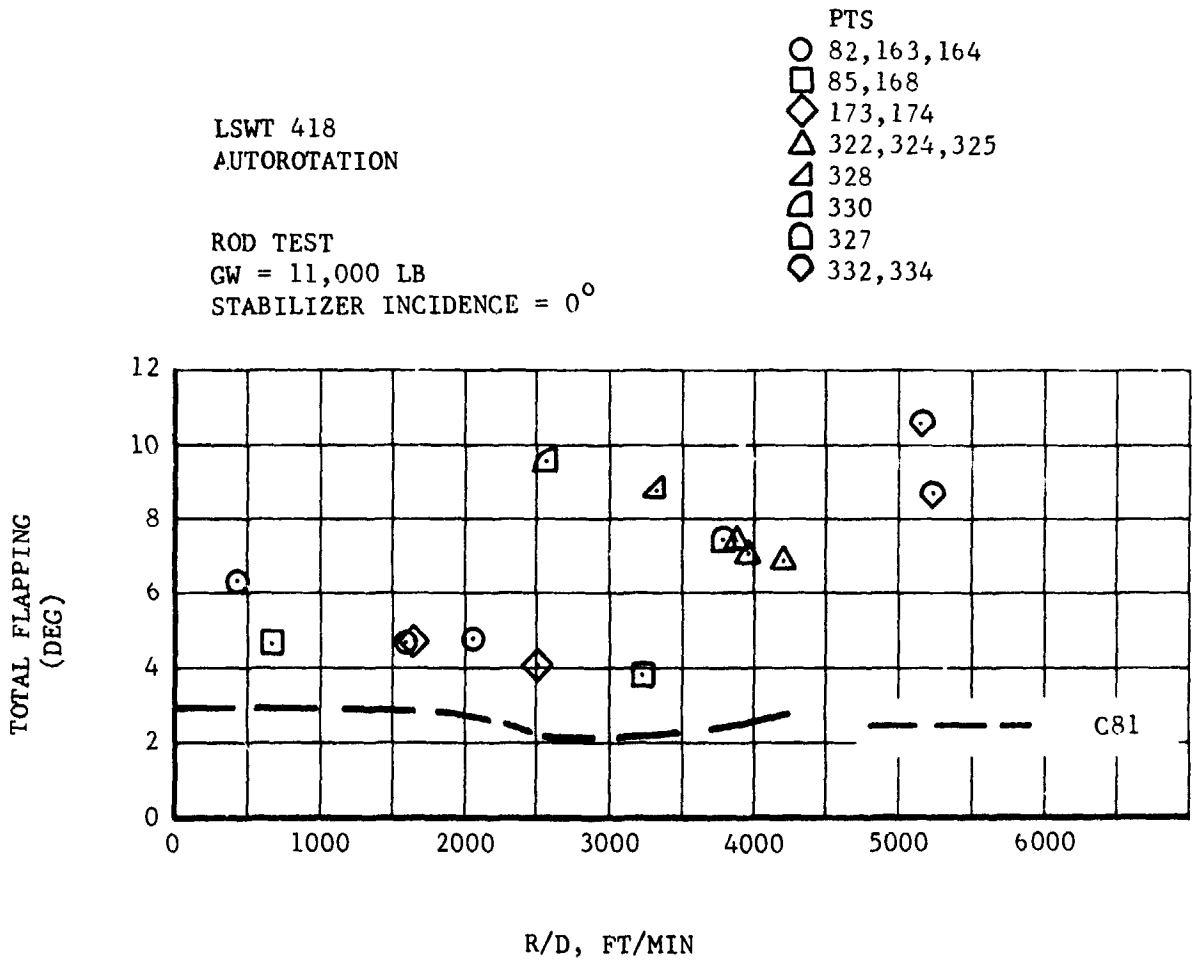


Figure V-16. Concluded

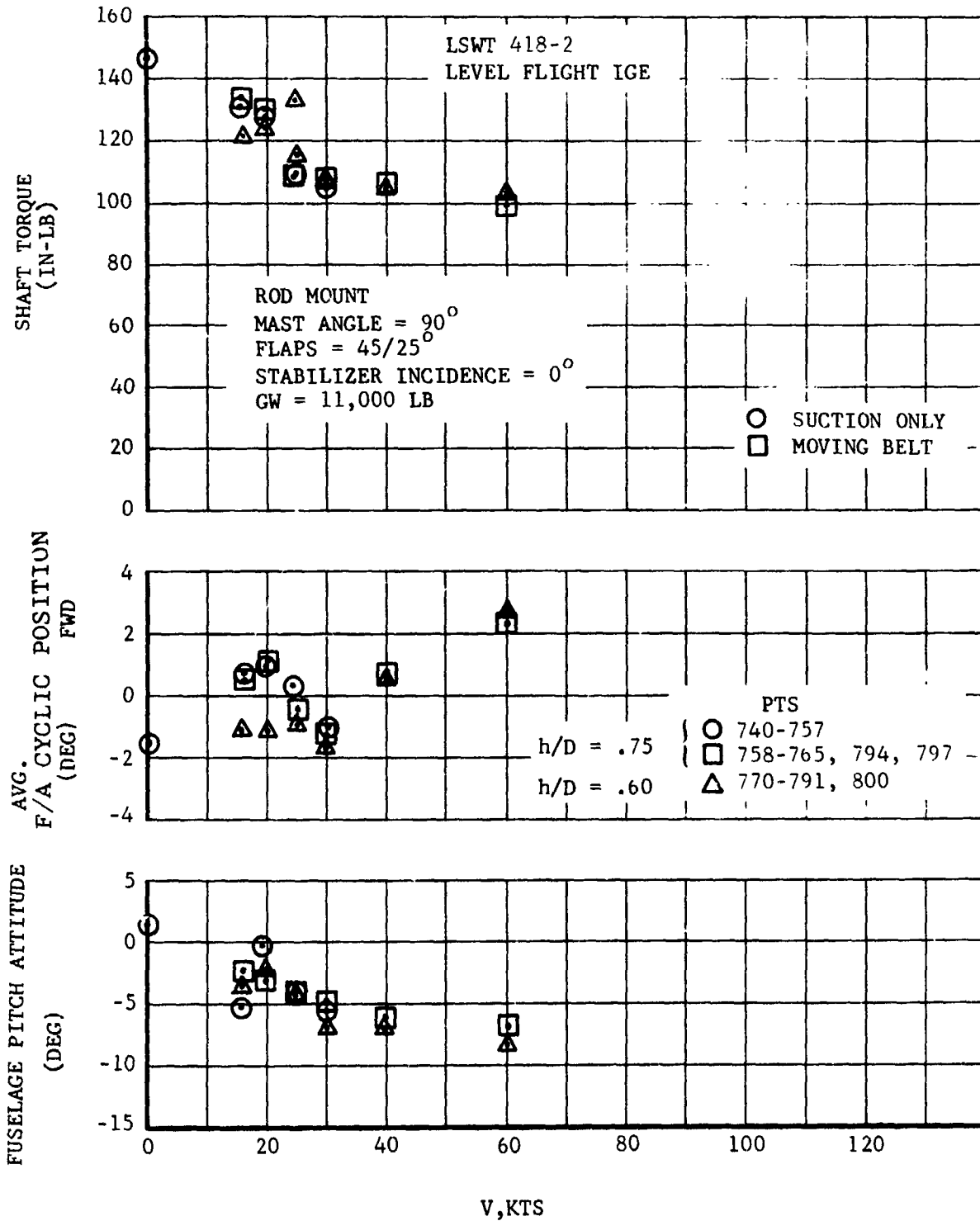


Figure V-17. Trim Parameters for Level Flight IGE,
Mast Angle 90° .

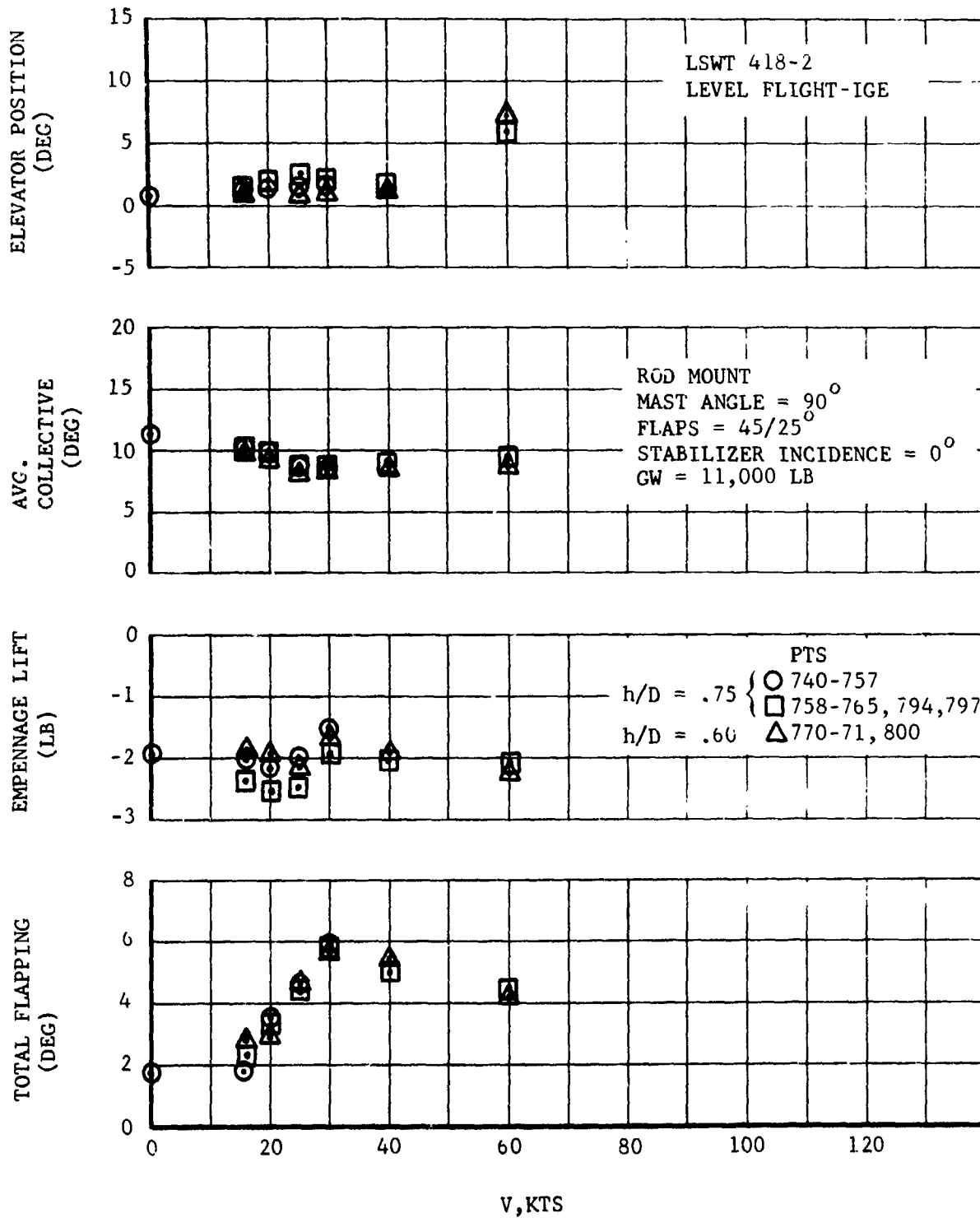


Figure V-17. Concluded

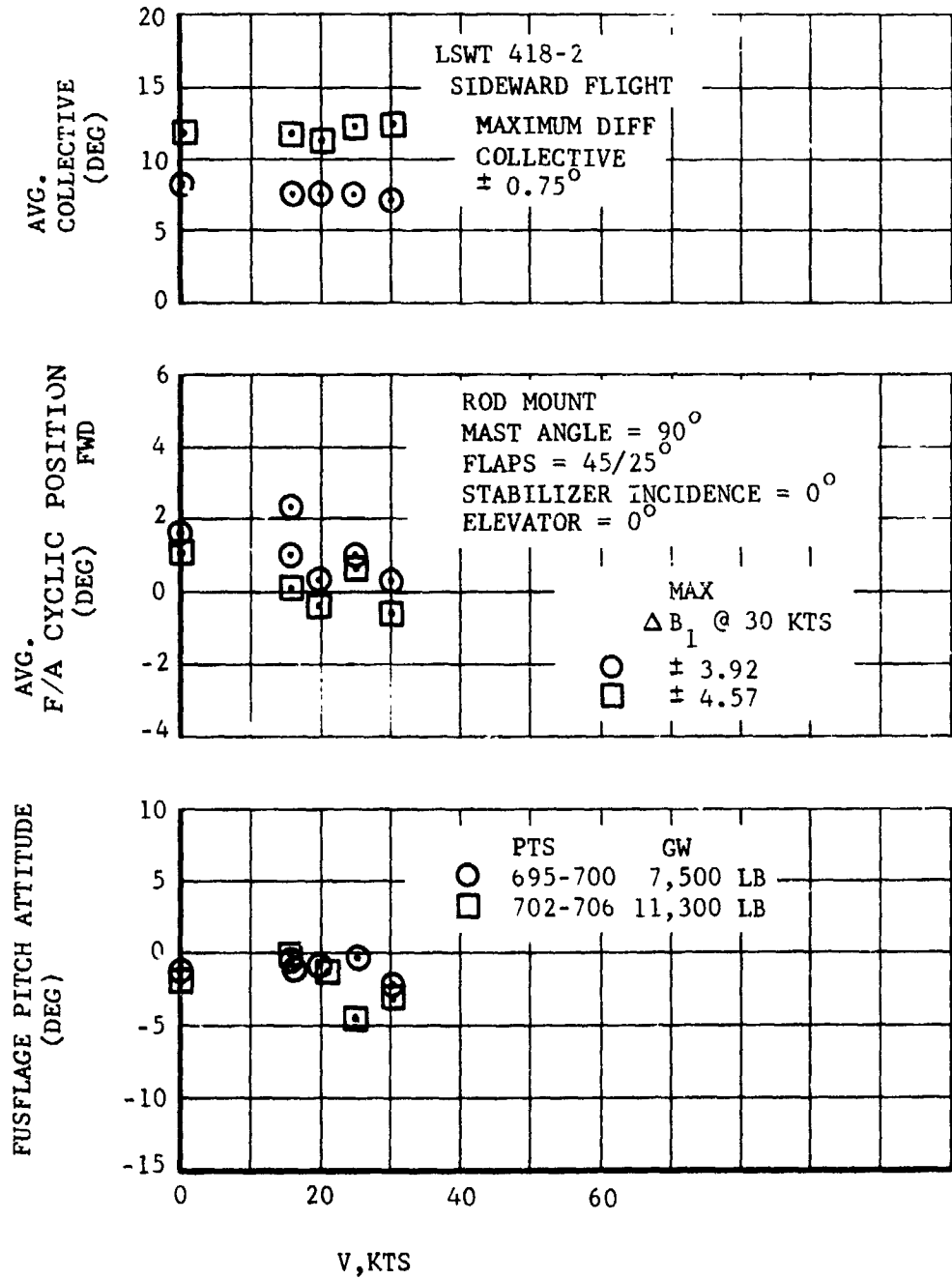


Figure V-18 Sideward Flight Trim Parameters

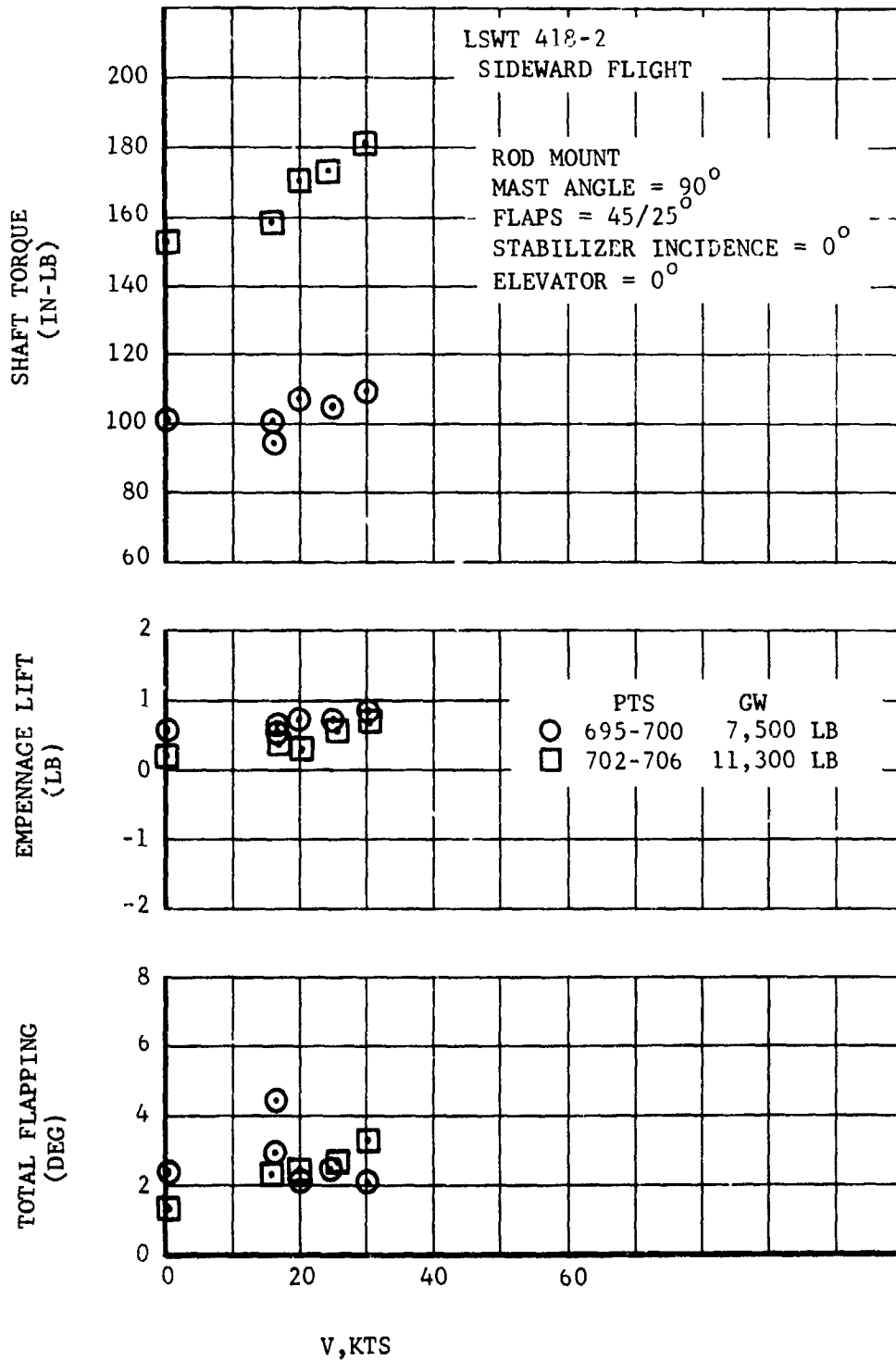


Figure V-18. Concluded

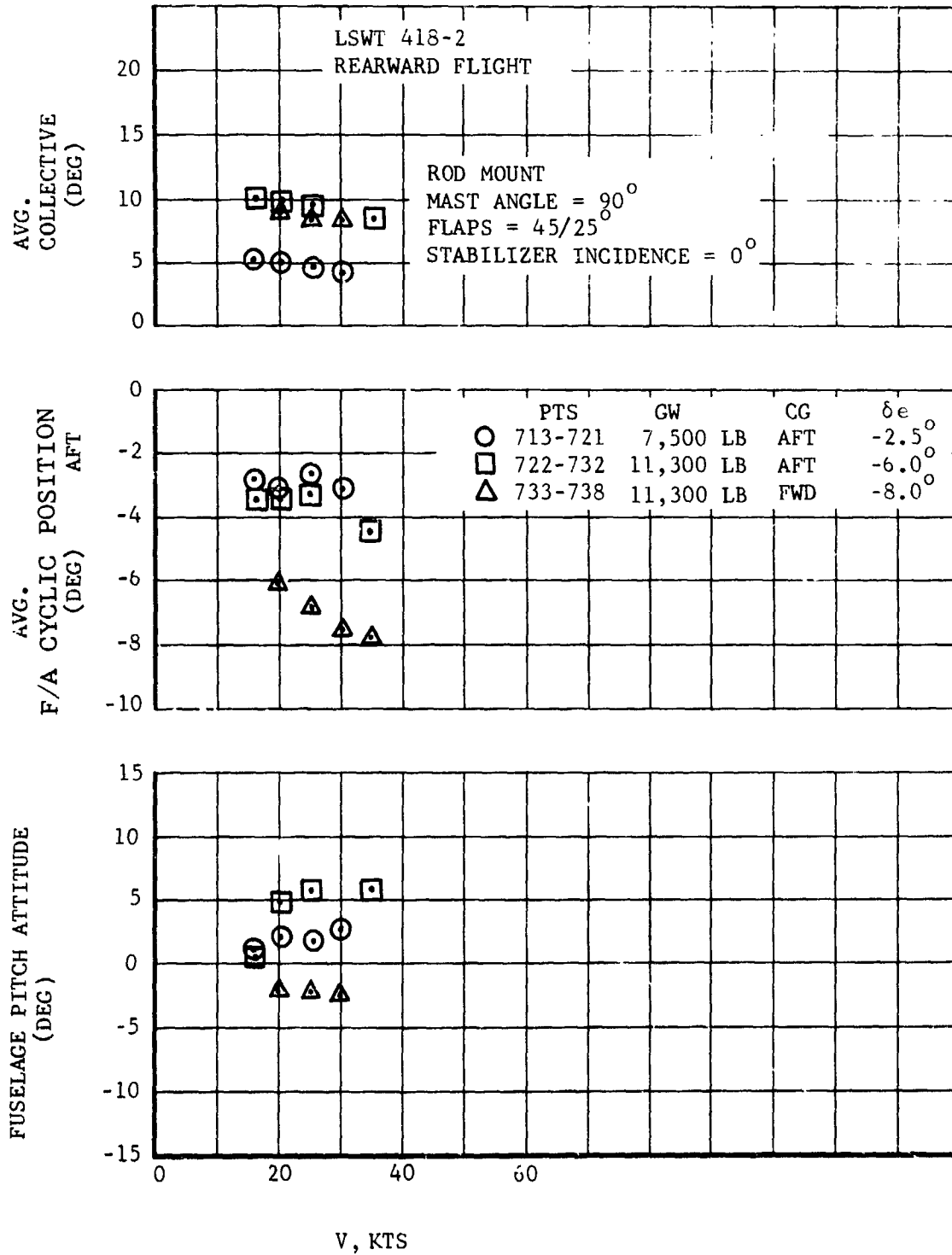


Figure V-19 Rearward Flight Trim Parameters

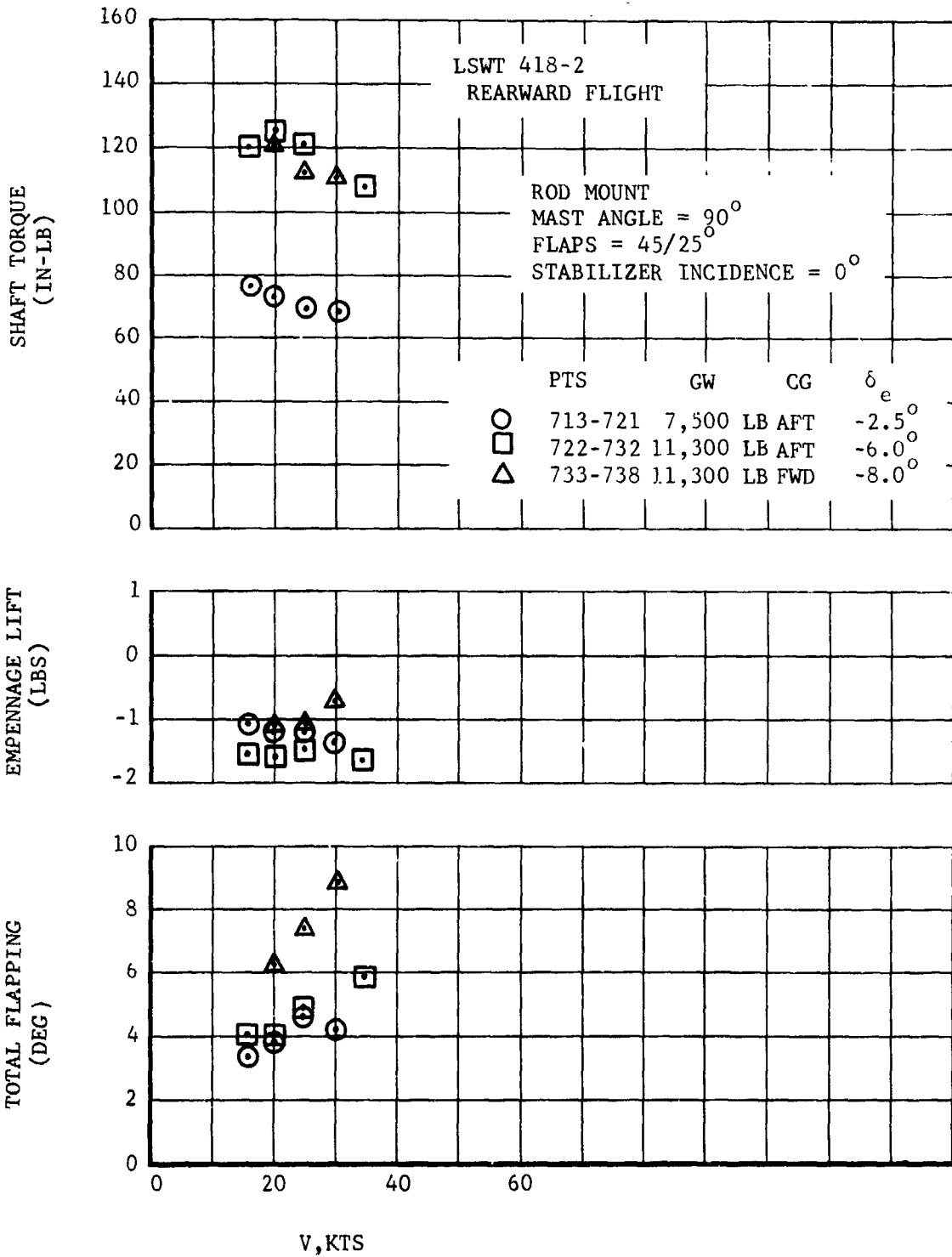


Figure V-19. Concluded

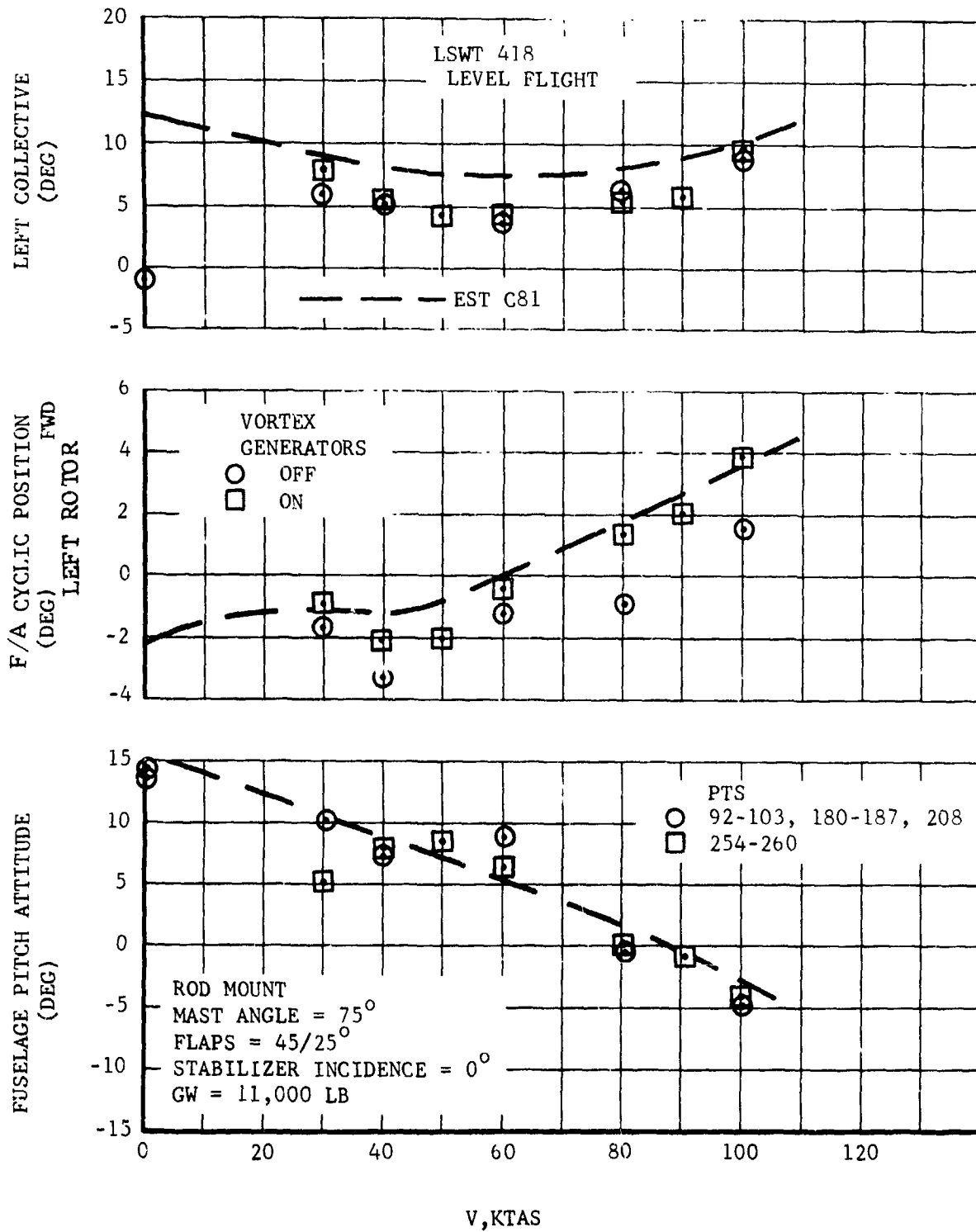


Figure V-20. Level Flight Trim Parameters, Mast Angle 75° .

Use of this information is limited to the specific aircraft and conditions for which it was developed.

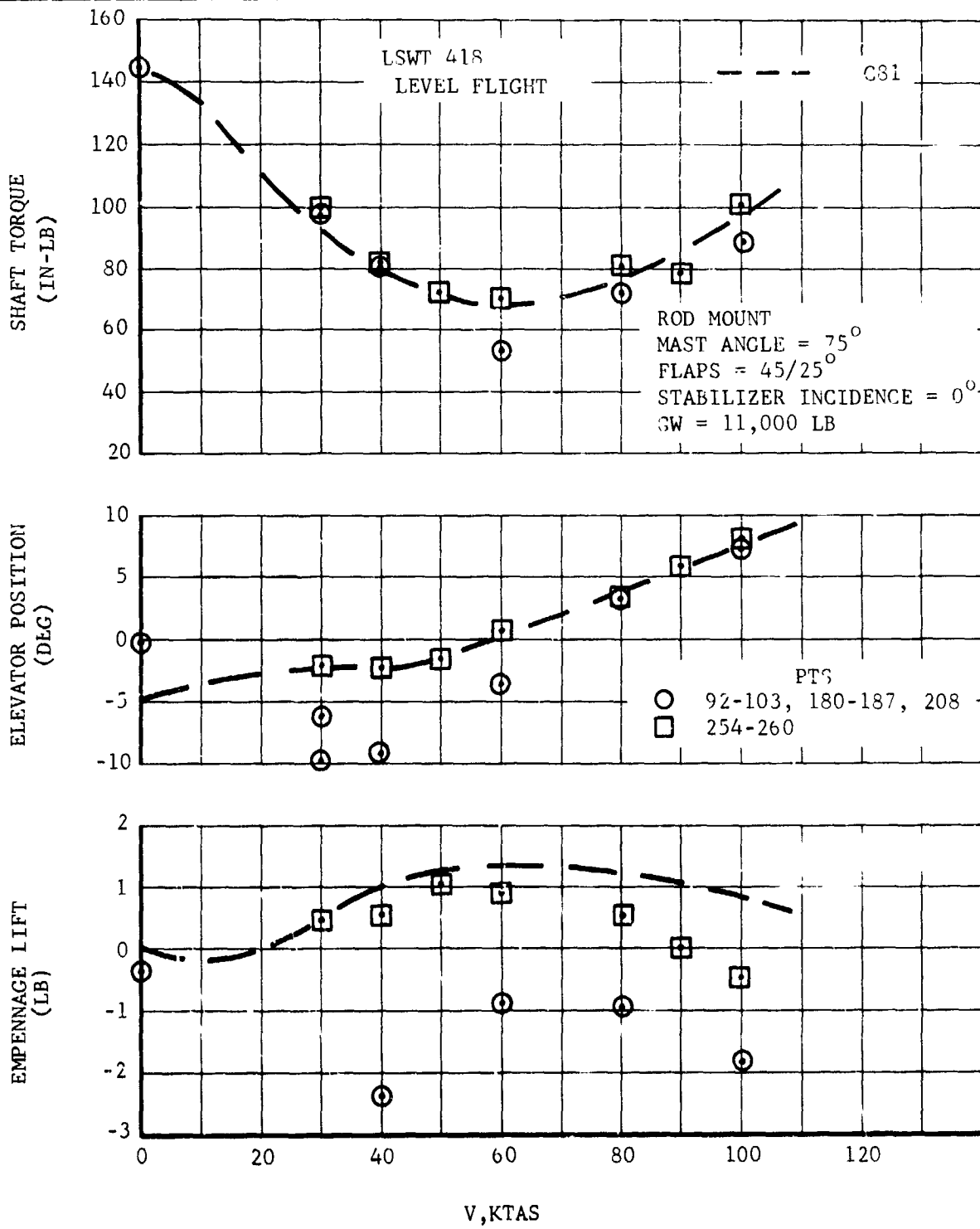


Figure V-20. Continued

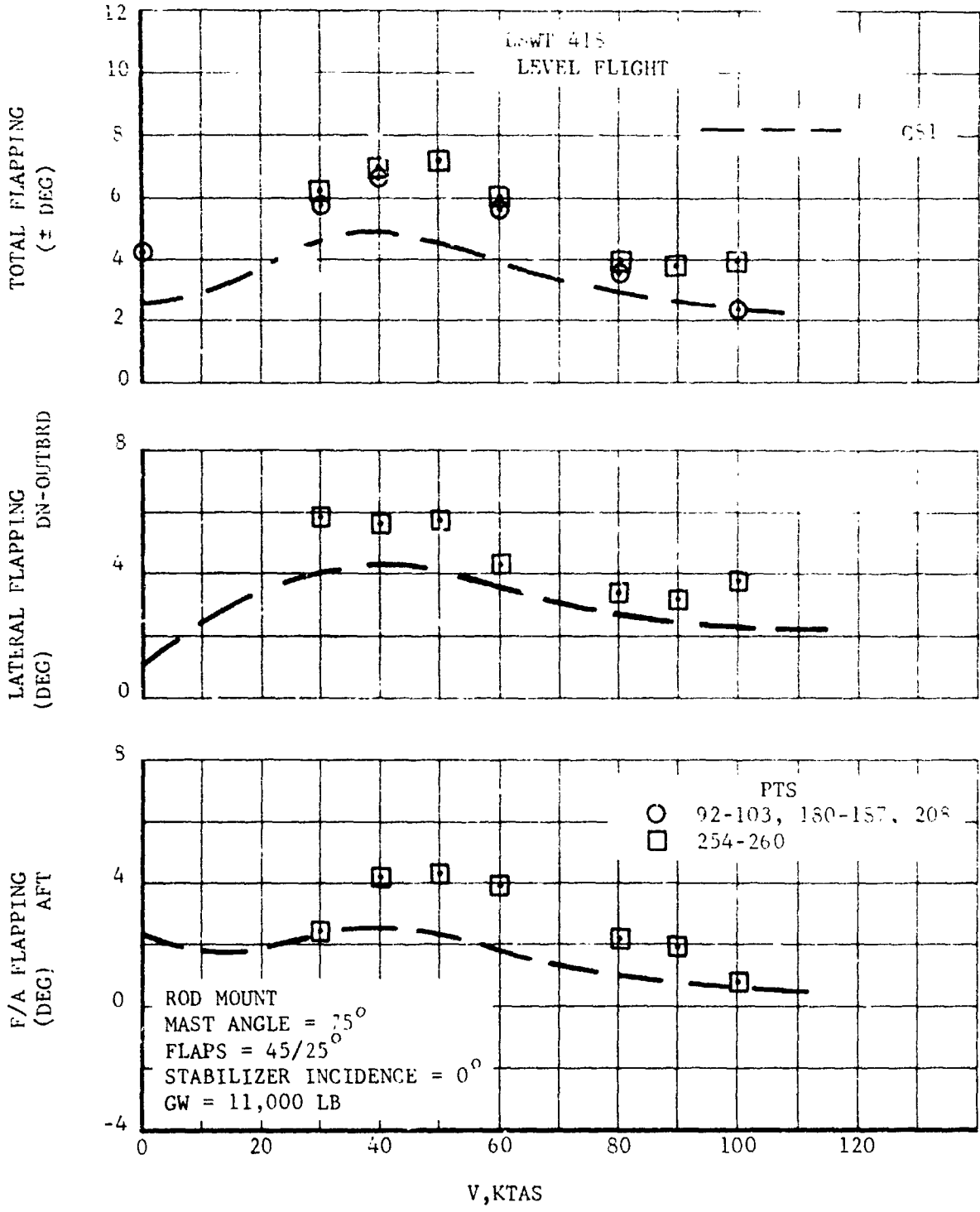


Figure V-20. Concluded

ROD MOUNT
 MAST ANGLE = 75°
 FLAPS = 45/25°
 STABILIZER INCIDENCE = 0°
 VORTEX GENERATORS OFF

CS1	GW
—○—	11,000 LB
—□—	12,900 LB
—◇—	15,500 LB
—x—	16,100 LB

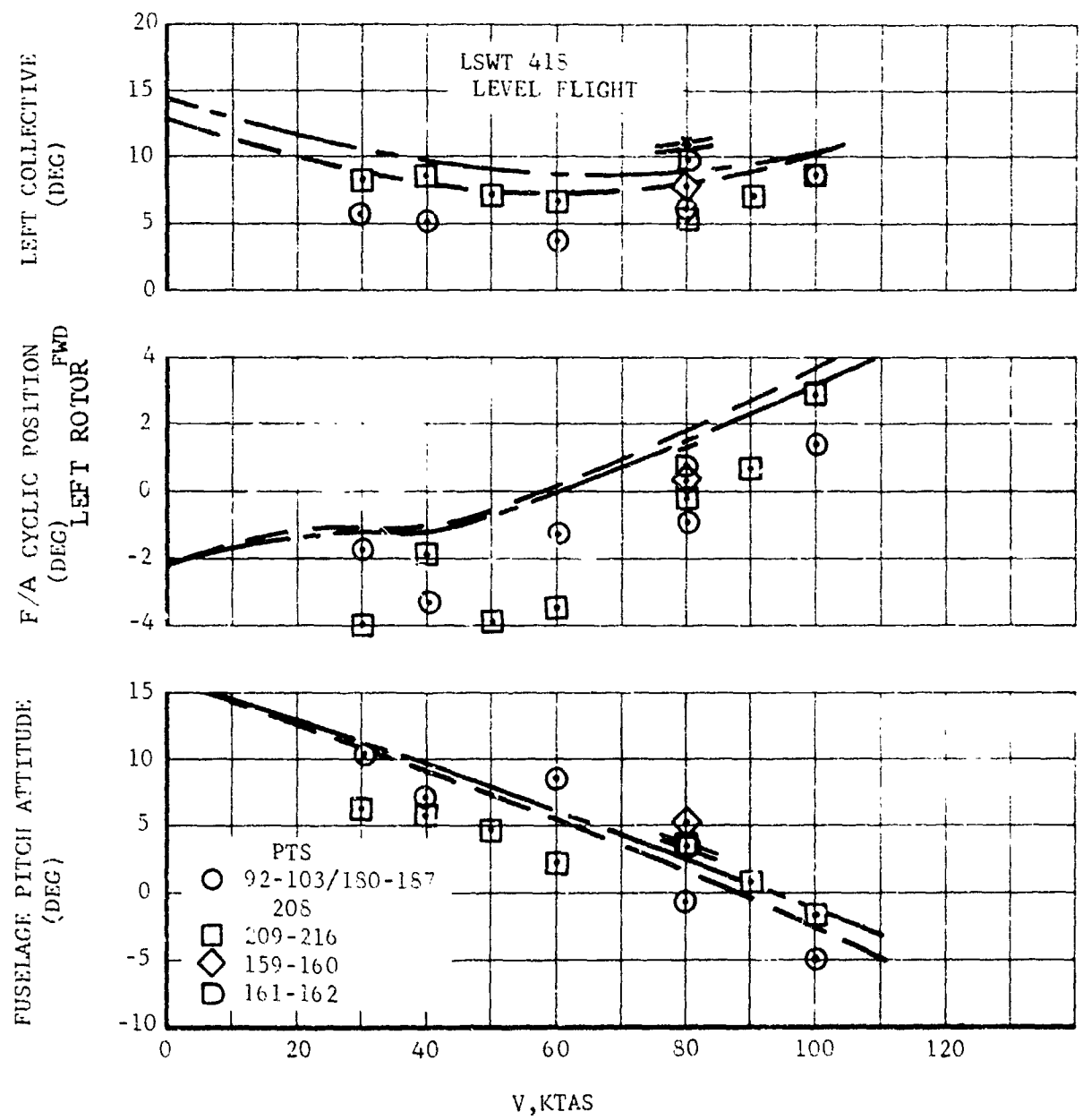


Figure V-21. Effect of Gross Weight on Level Flight Trim Parameters, Mast Angle 75°.

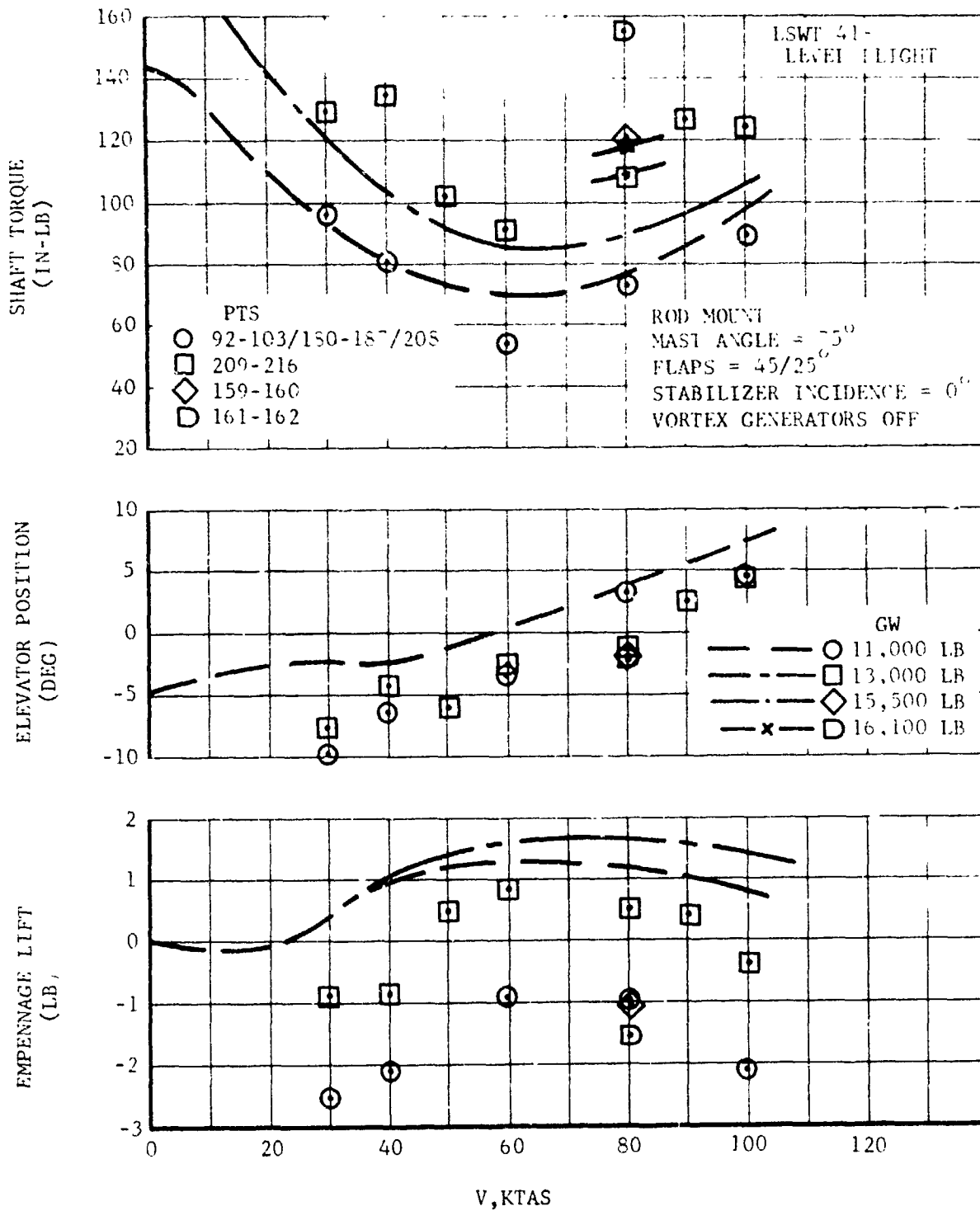


Figure V-21. Continued

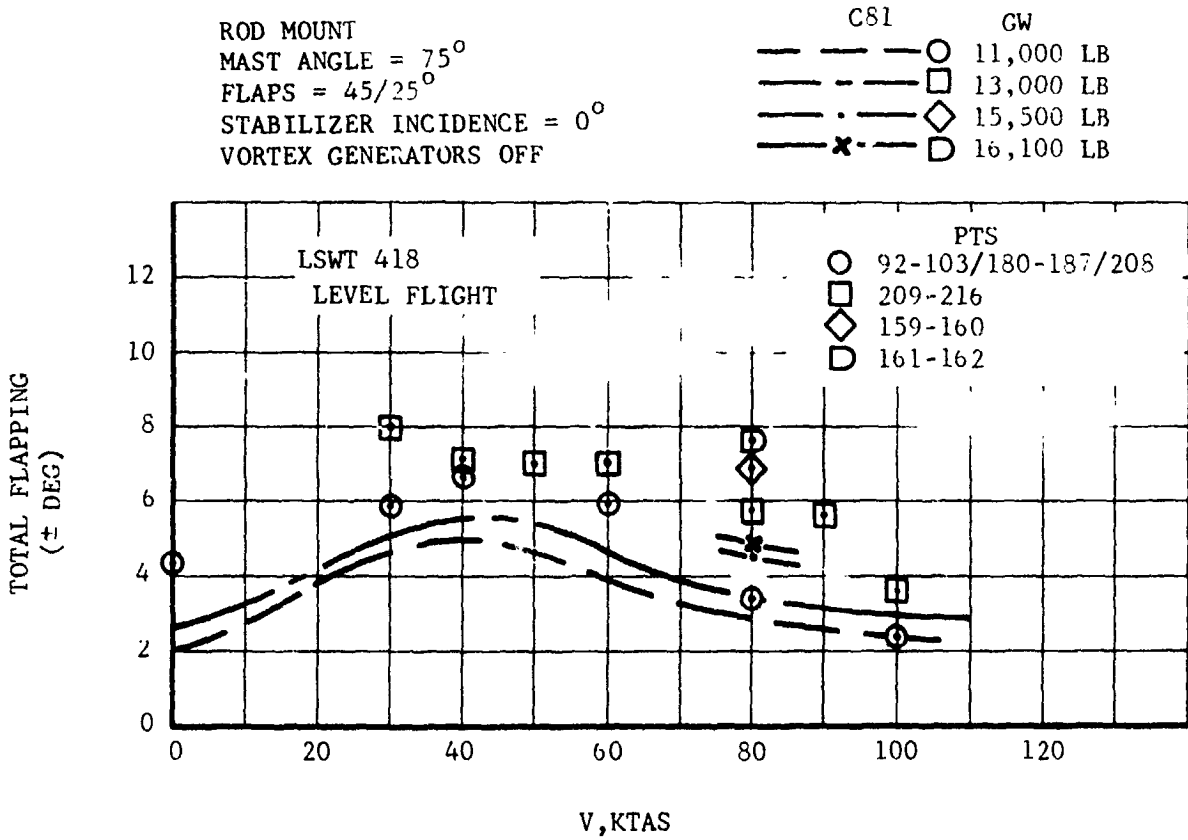


Figure V-21. Concluded

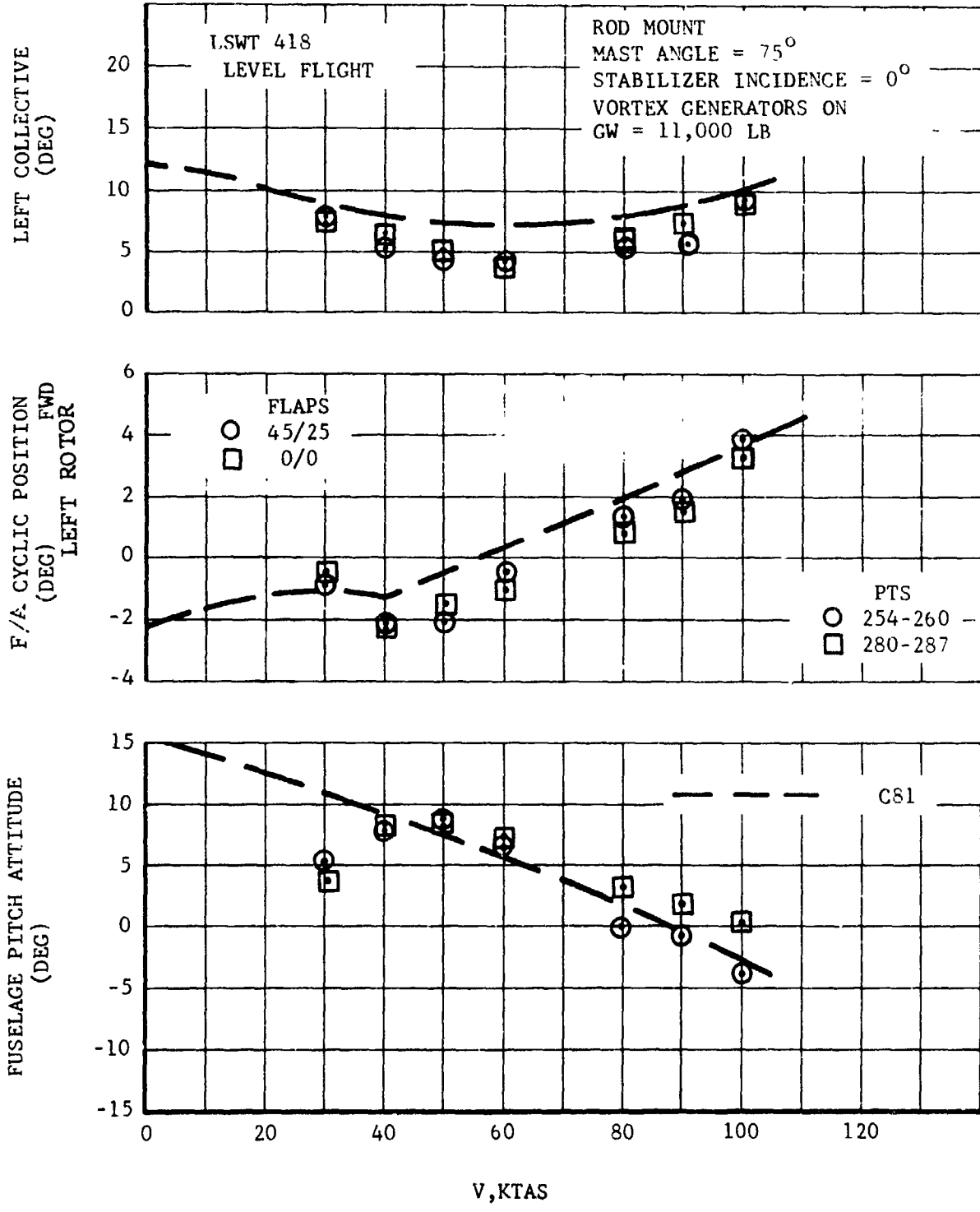


Figure V-22. Effect of Flaps on Level Flight Trim Parameters, Mast Angle 75°.

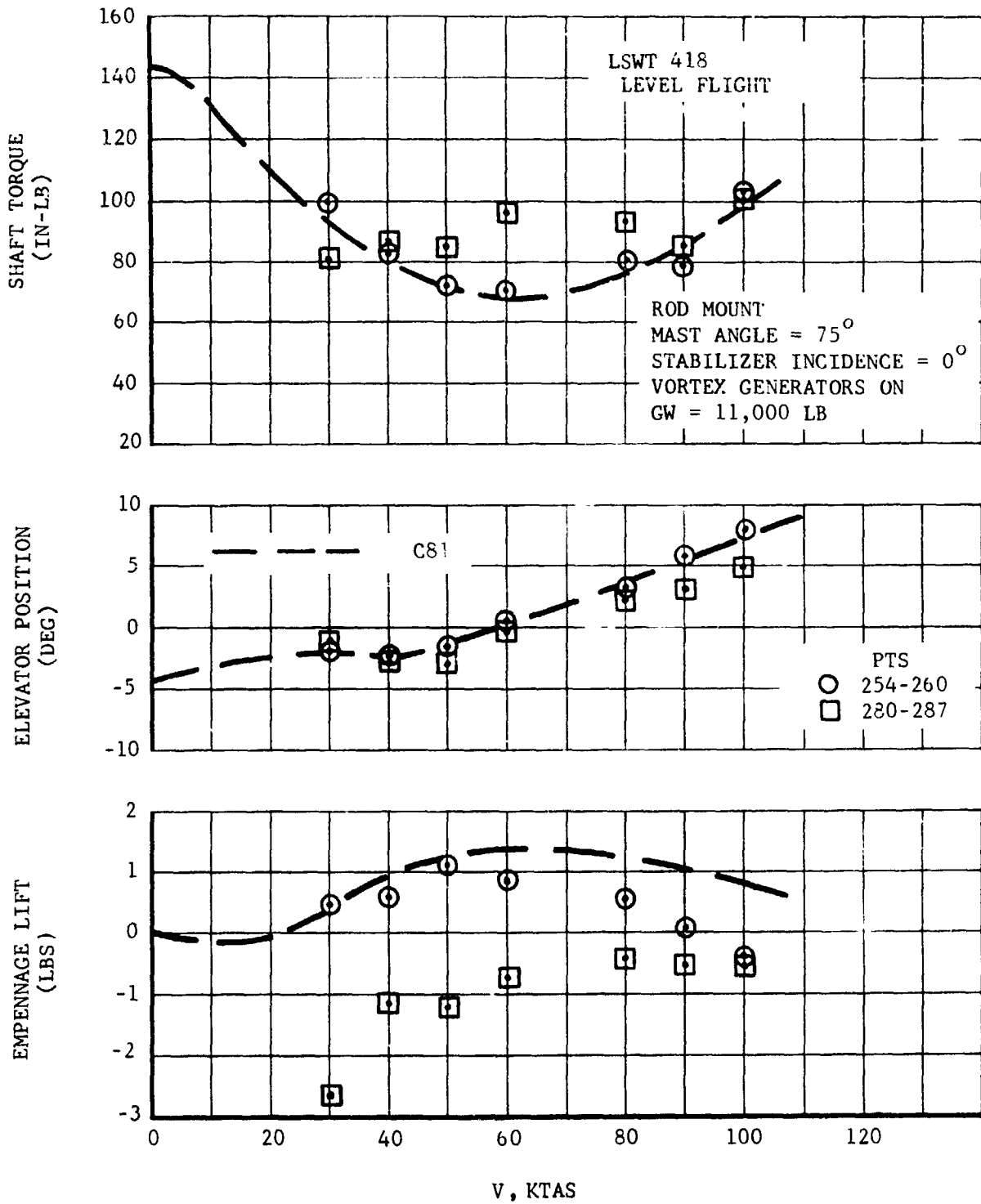


Figure V-22. Continued

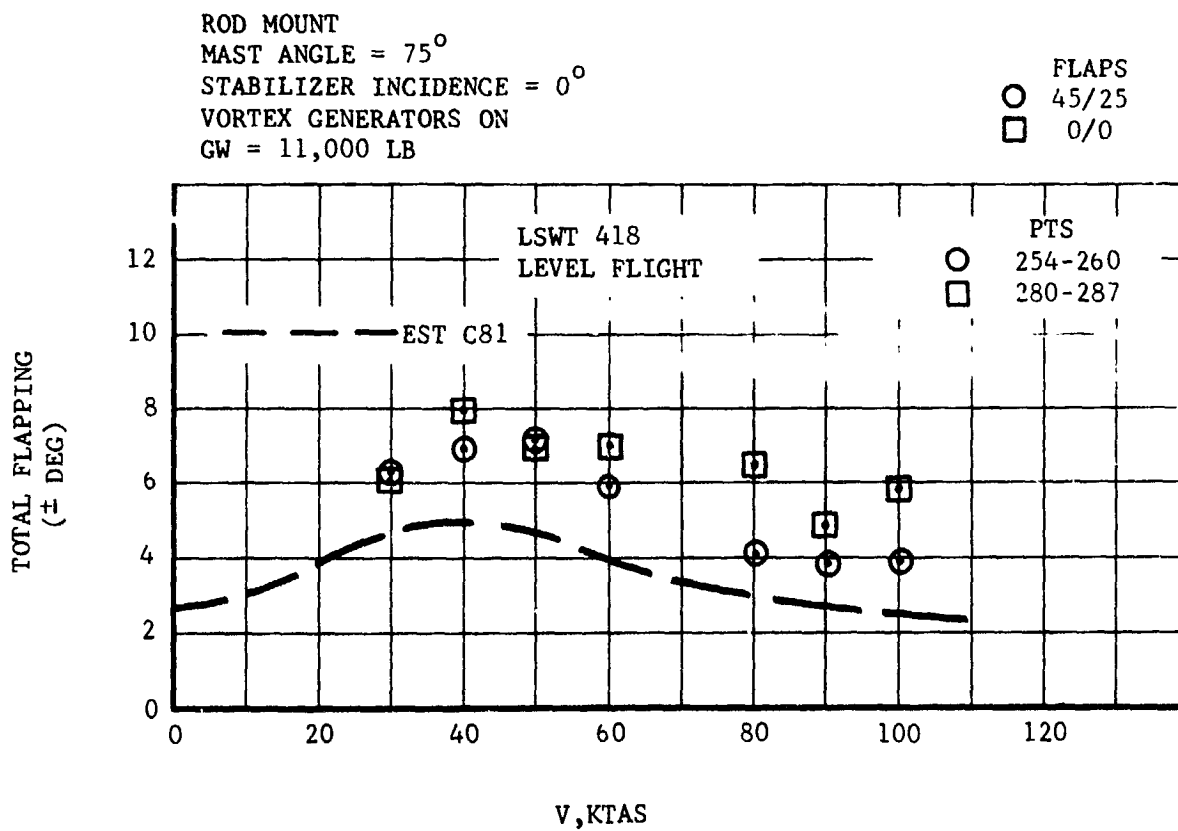


Figure V-22. Concluded

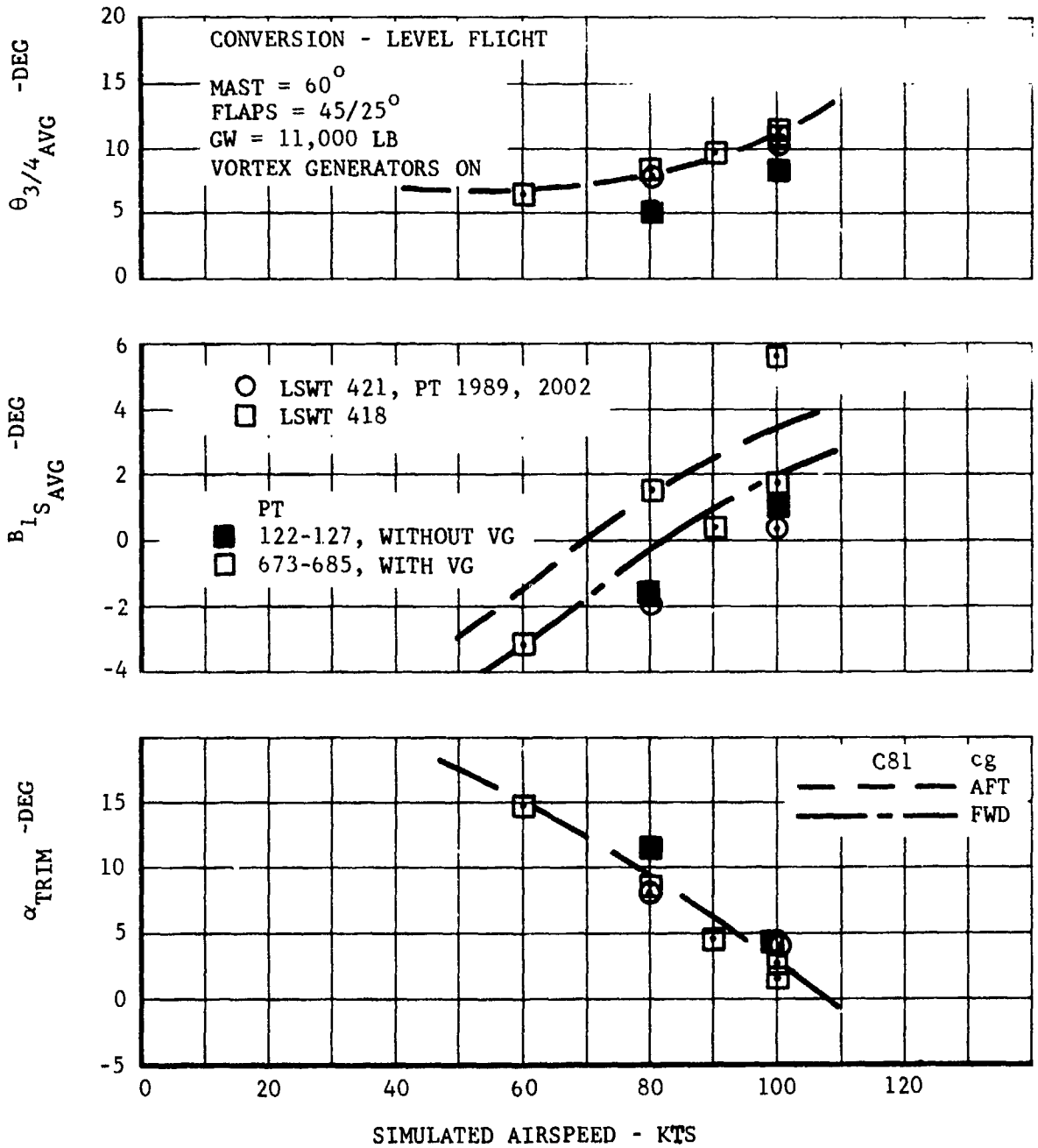


Figure V-23. Level Flight Trim Parameters, Mast Angle 60°.

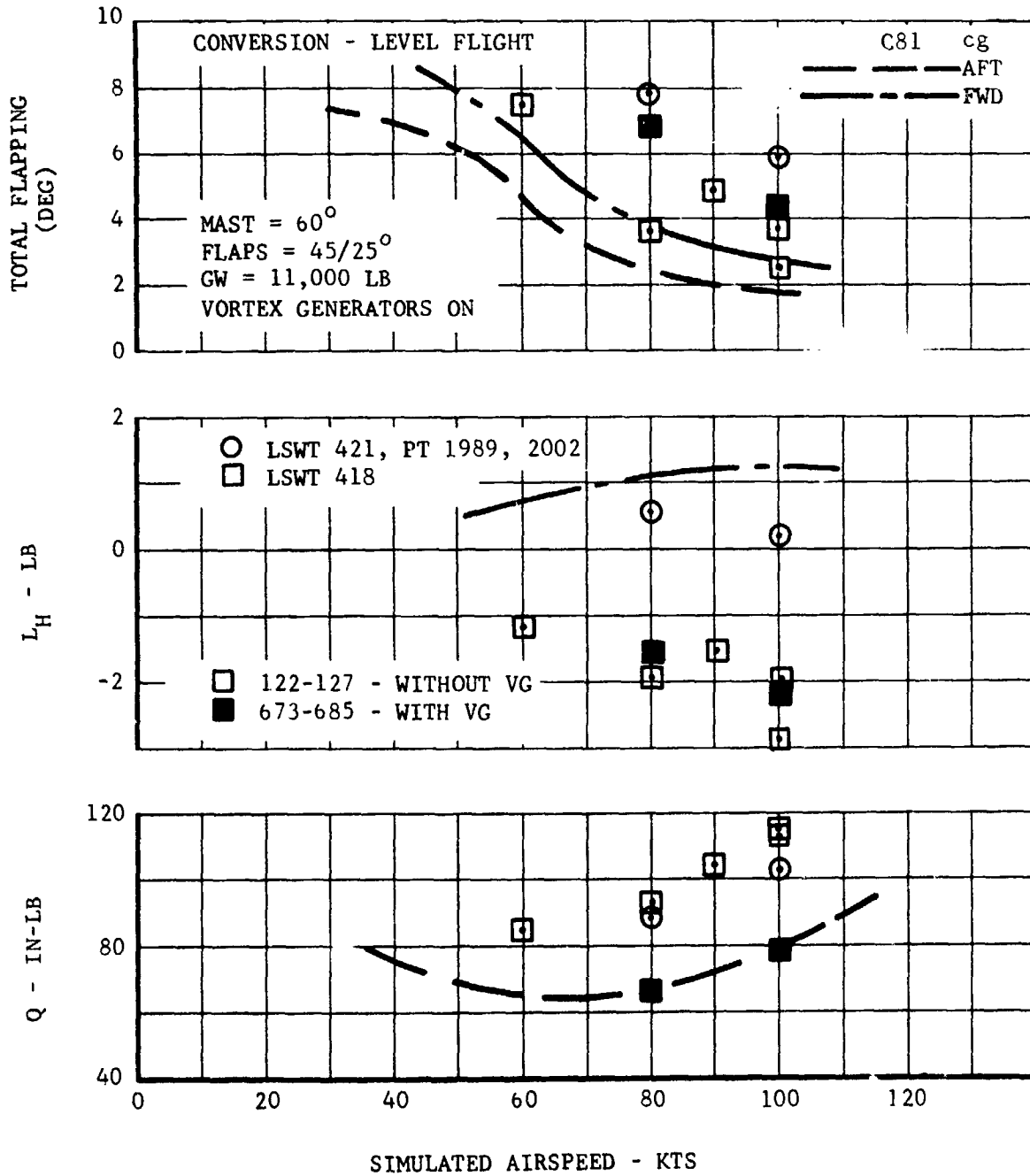


Figure V-23. Continued

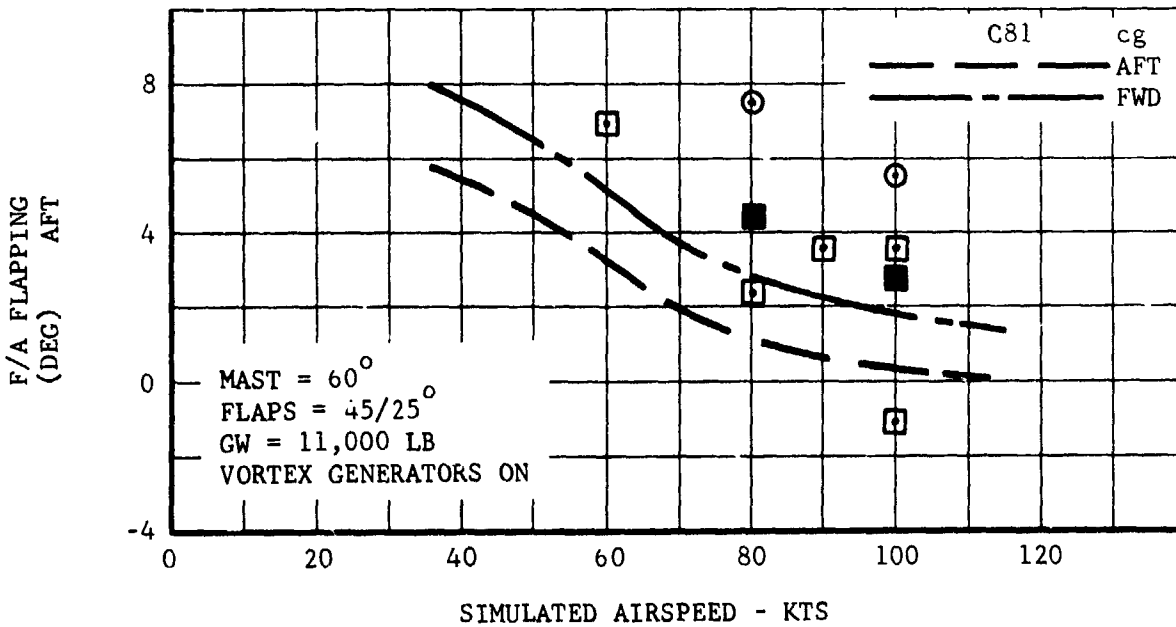
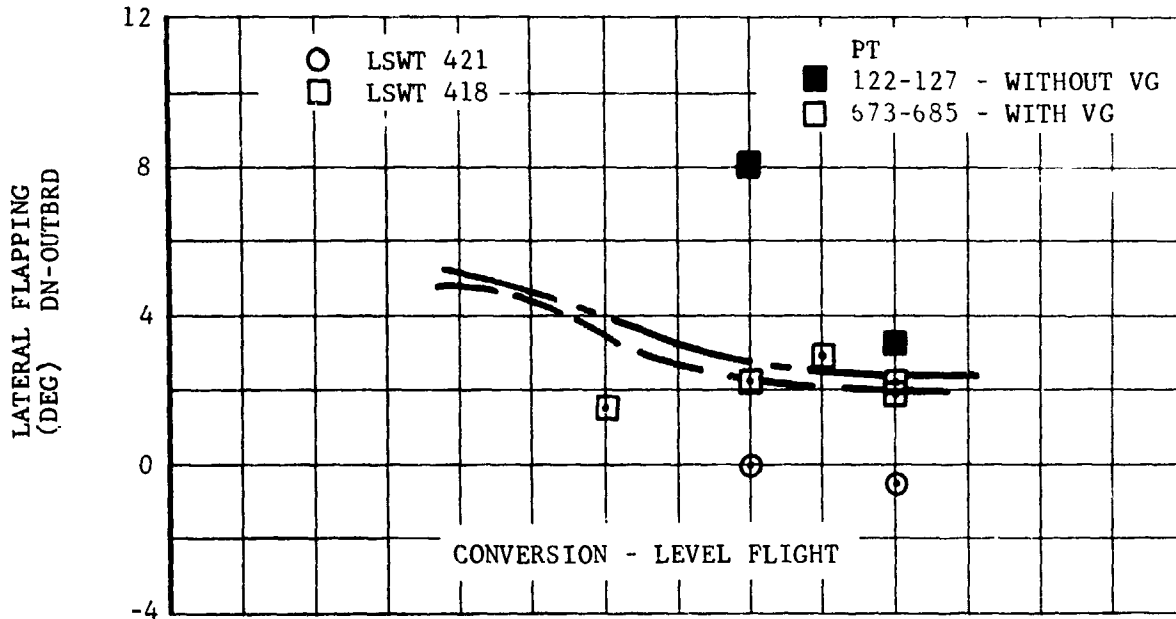


Figure V-23. Concluded

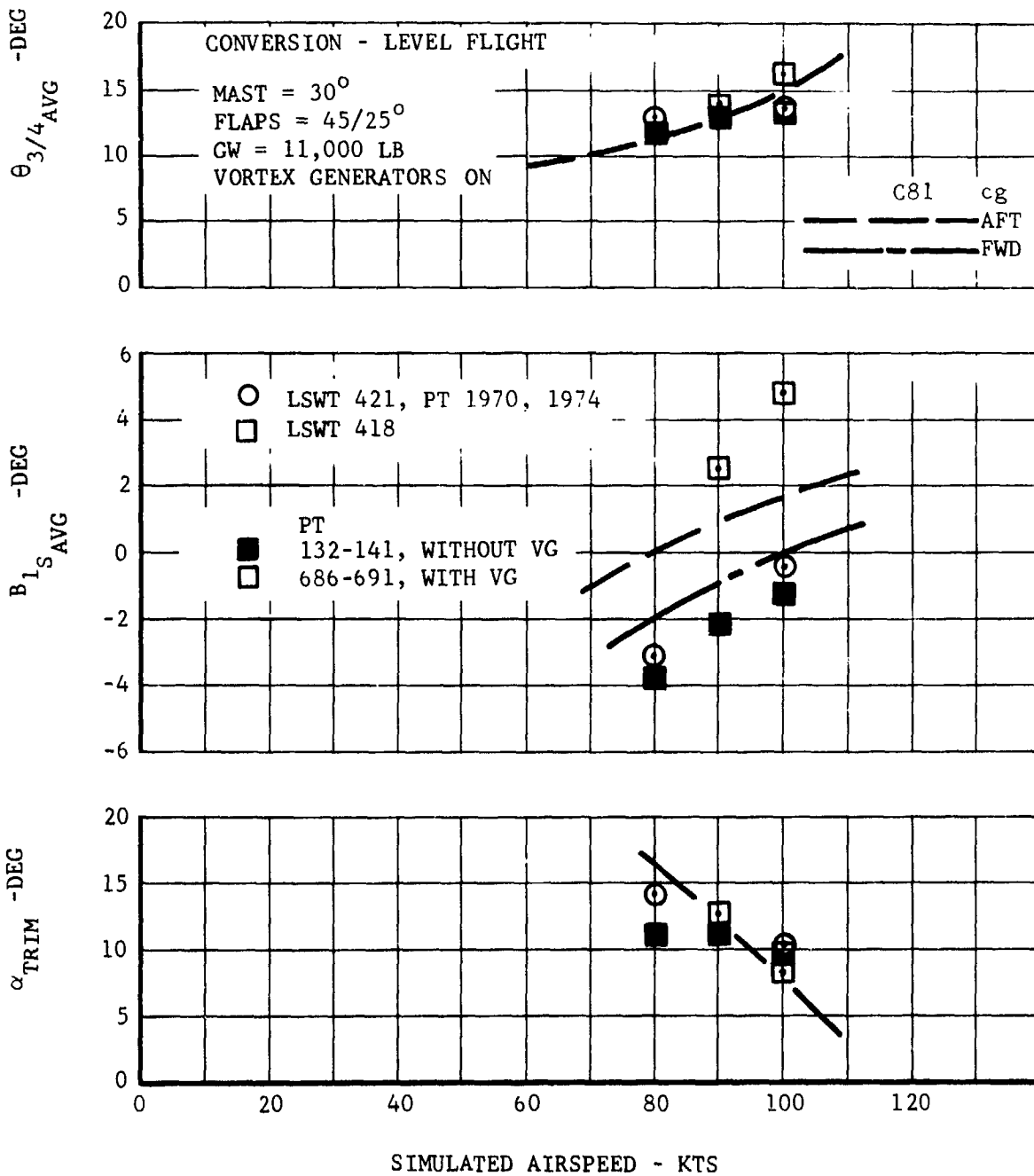


Figure V-24. Level Flight Trim Parameters, Mast Angle 30°.

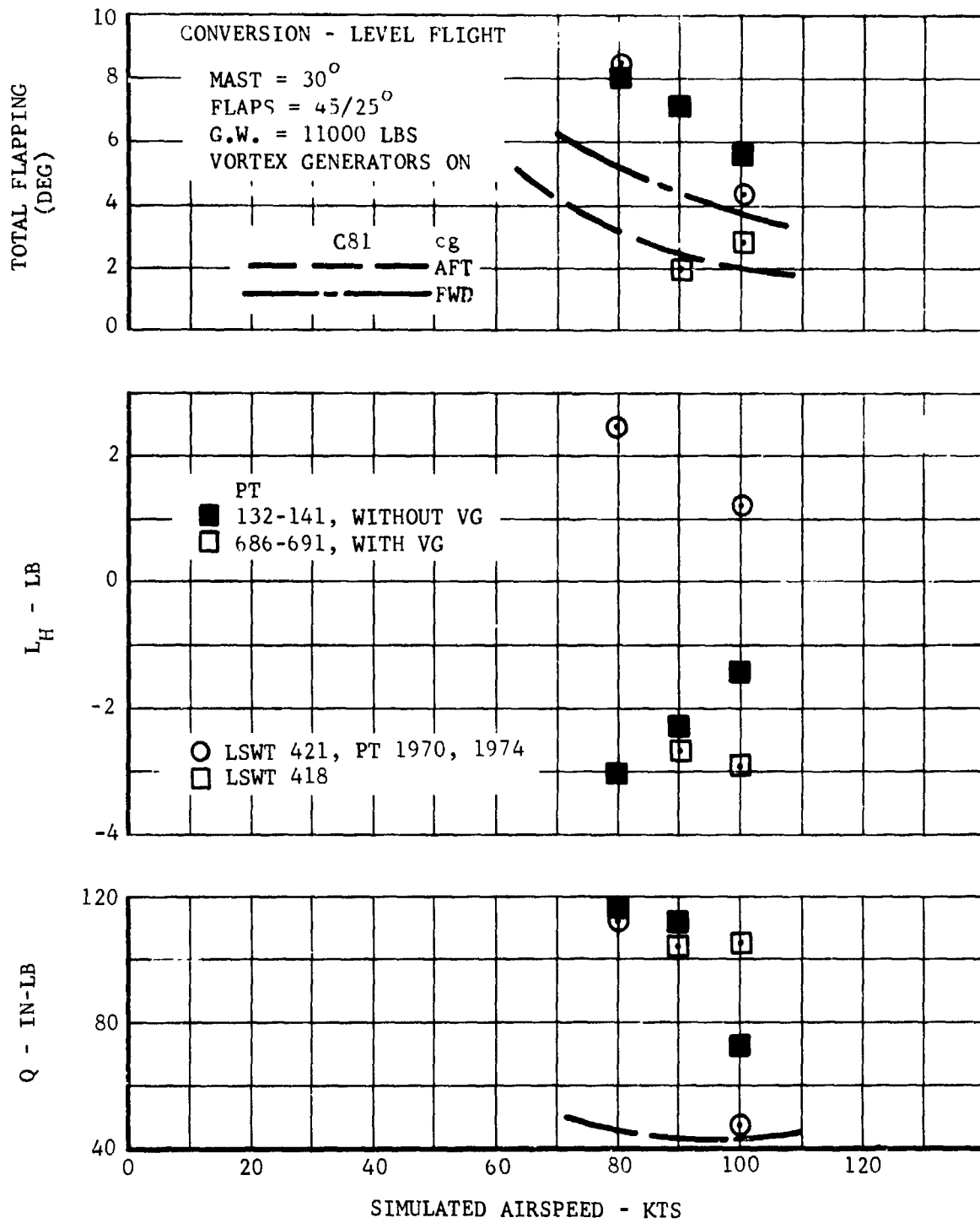


Figure V-24. Continued

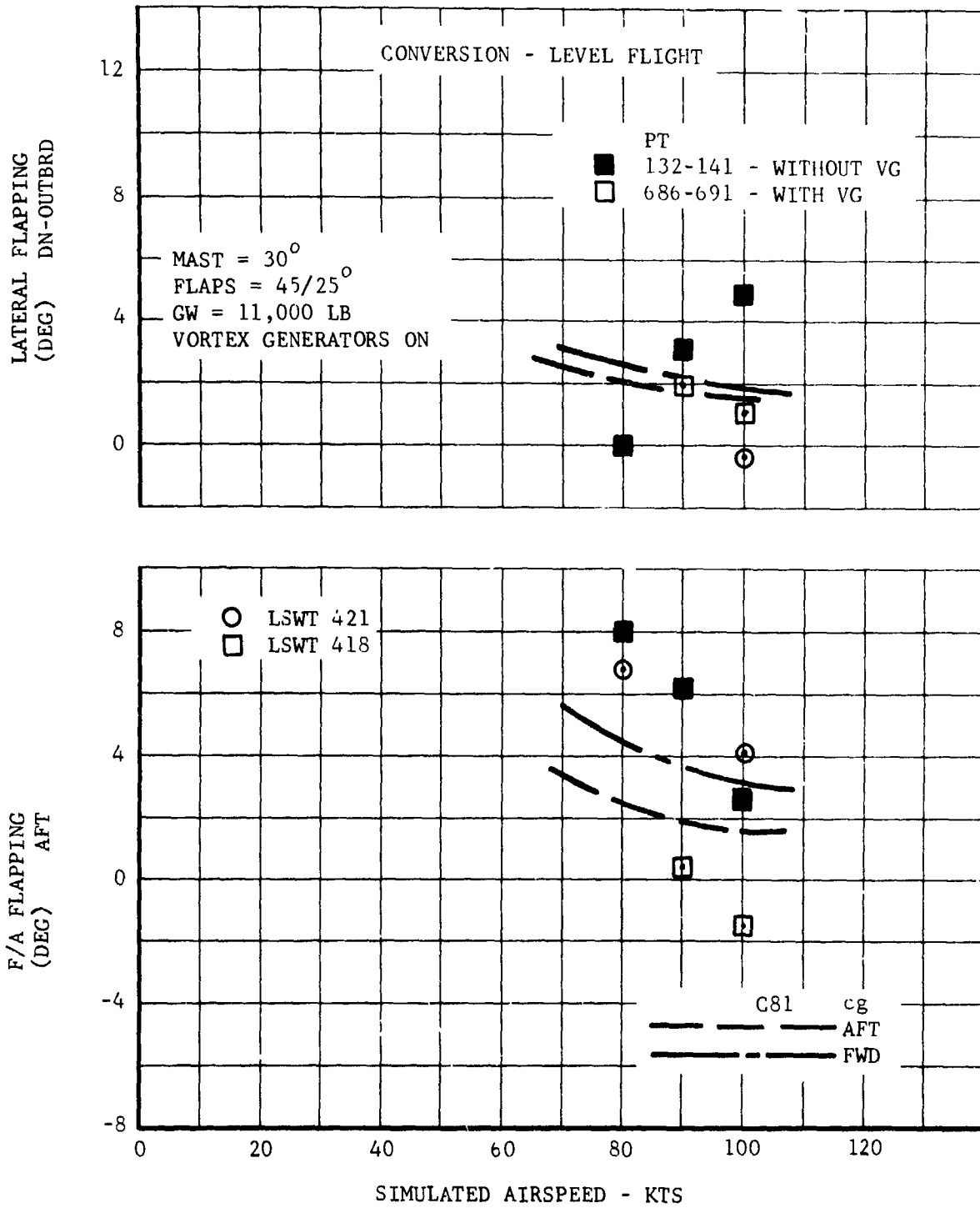


Figure V-24. Concluded

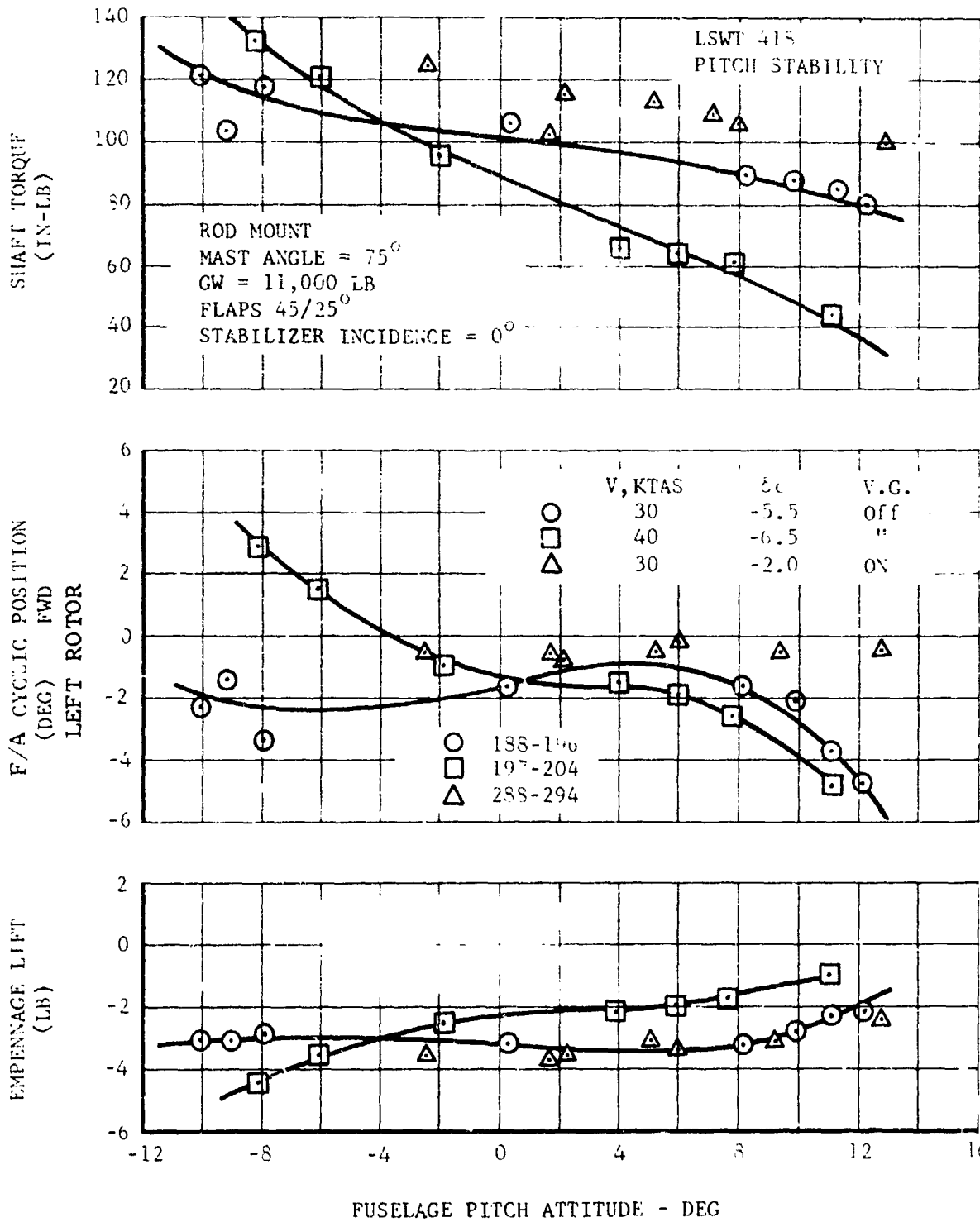


Figure V-26. Variation of Trim Parameters With Fuselage Angle of Attack, Mast Angle 75°.

ROD MOUNT
 MAST ANGLE = 90°
 FLAPS = $+5/25^\circ$
 STABILIZER INCIDENCE = 0°
 VORTEX GENERATORS ON
 GW = 11,000 LB
 ROLL LOCKED

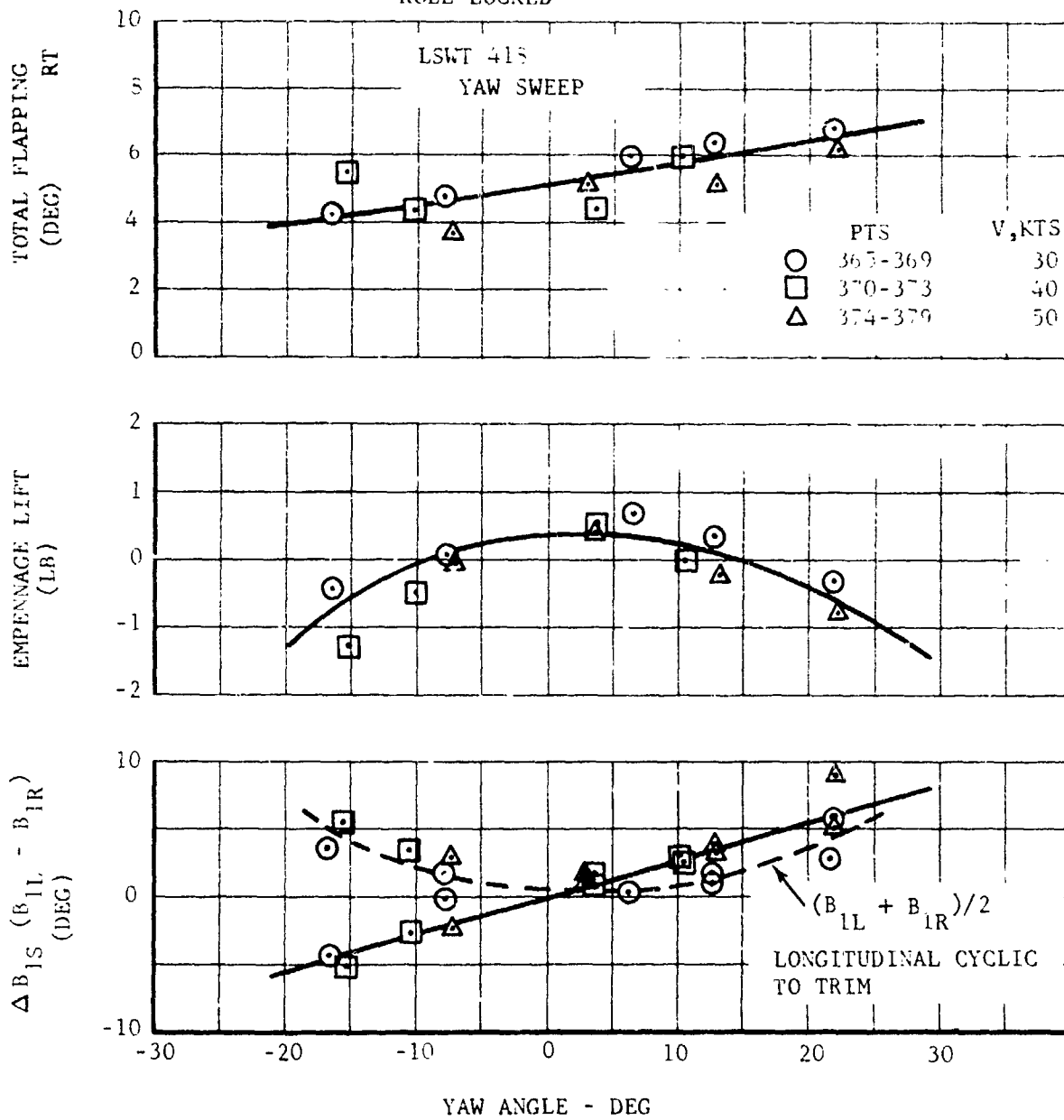


Figure V-27. Variation of Trim Parameters With Fuselage Yaw Angle, Mast Angle 90° .

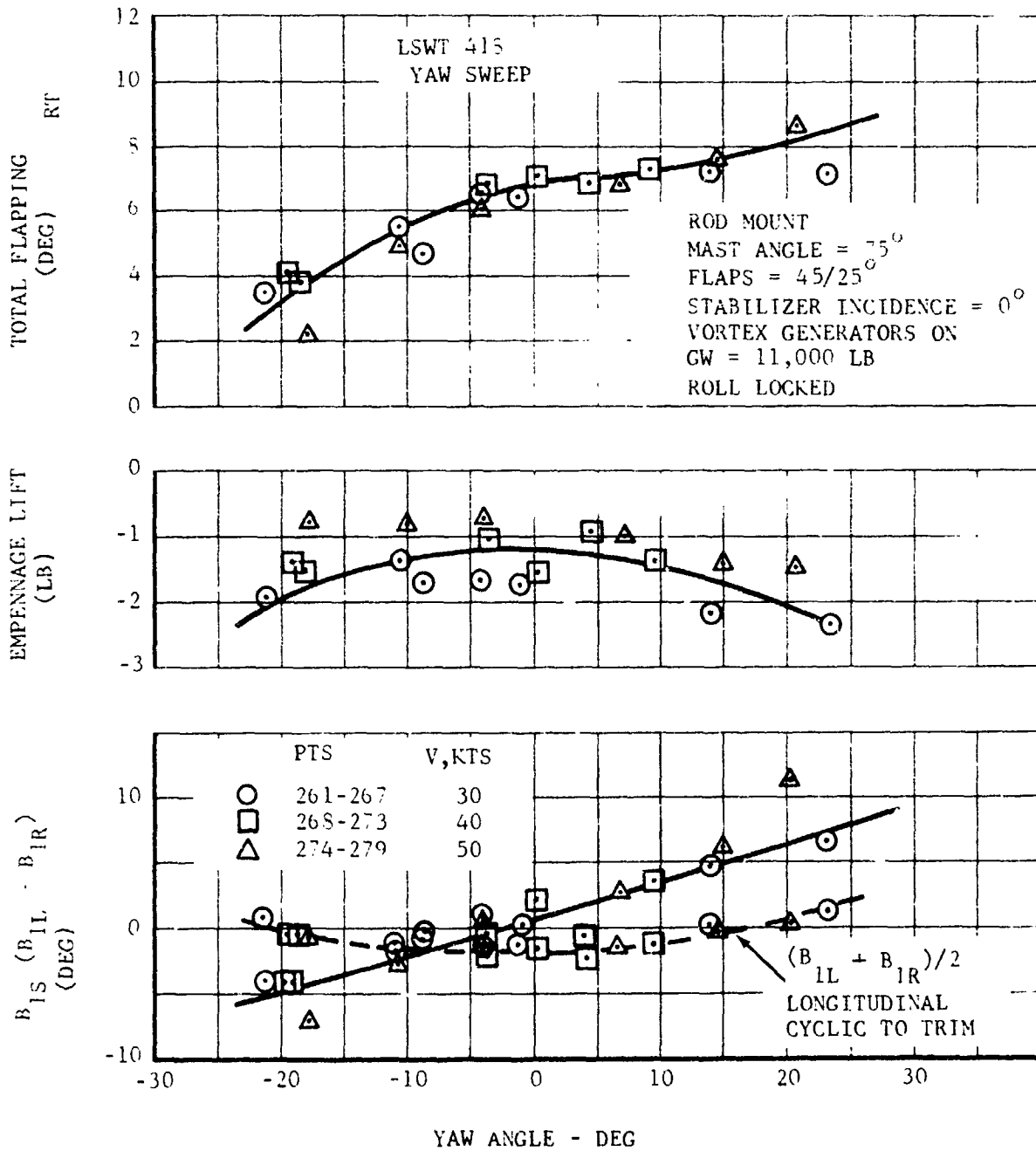


Figure V-28. Variation of Trim Parameters With Fuselage Yaw Angle, Mast Angle 75°.

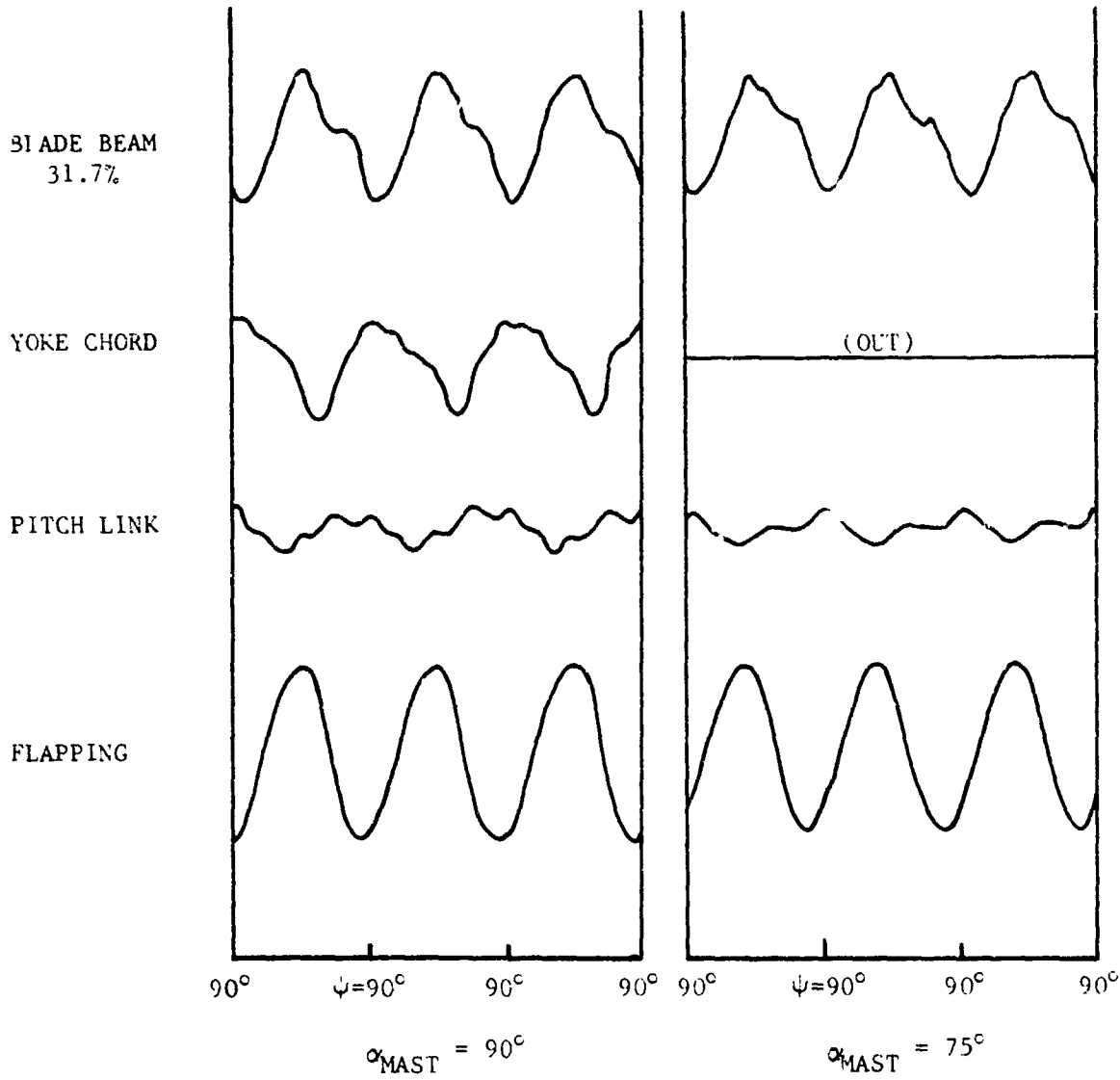


Figure V-29. Blade and Control System Load Waveforms at Mast Angles 90° and 75° .

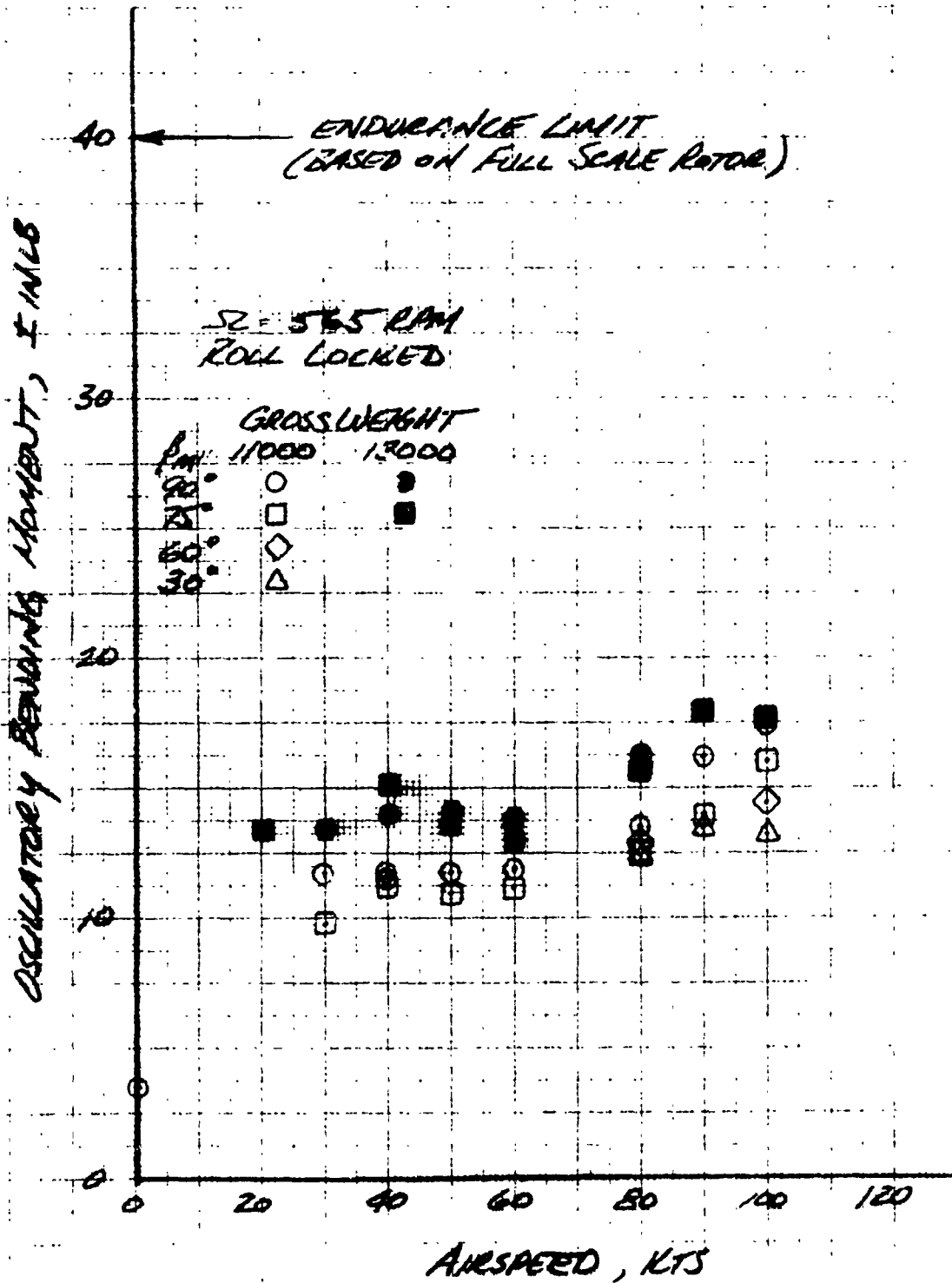


Figure V-30. Blade Station 52.5 Beamwise Oscillatory Bending Moment versus Airspeed.

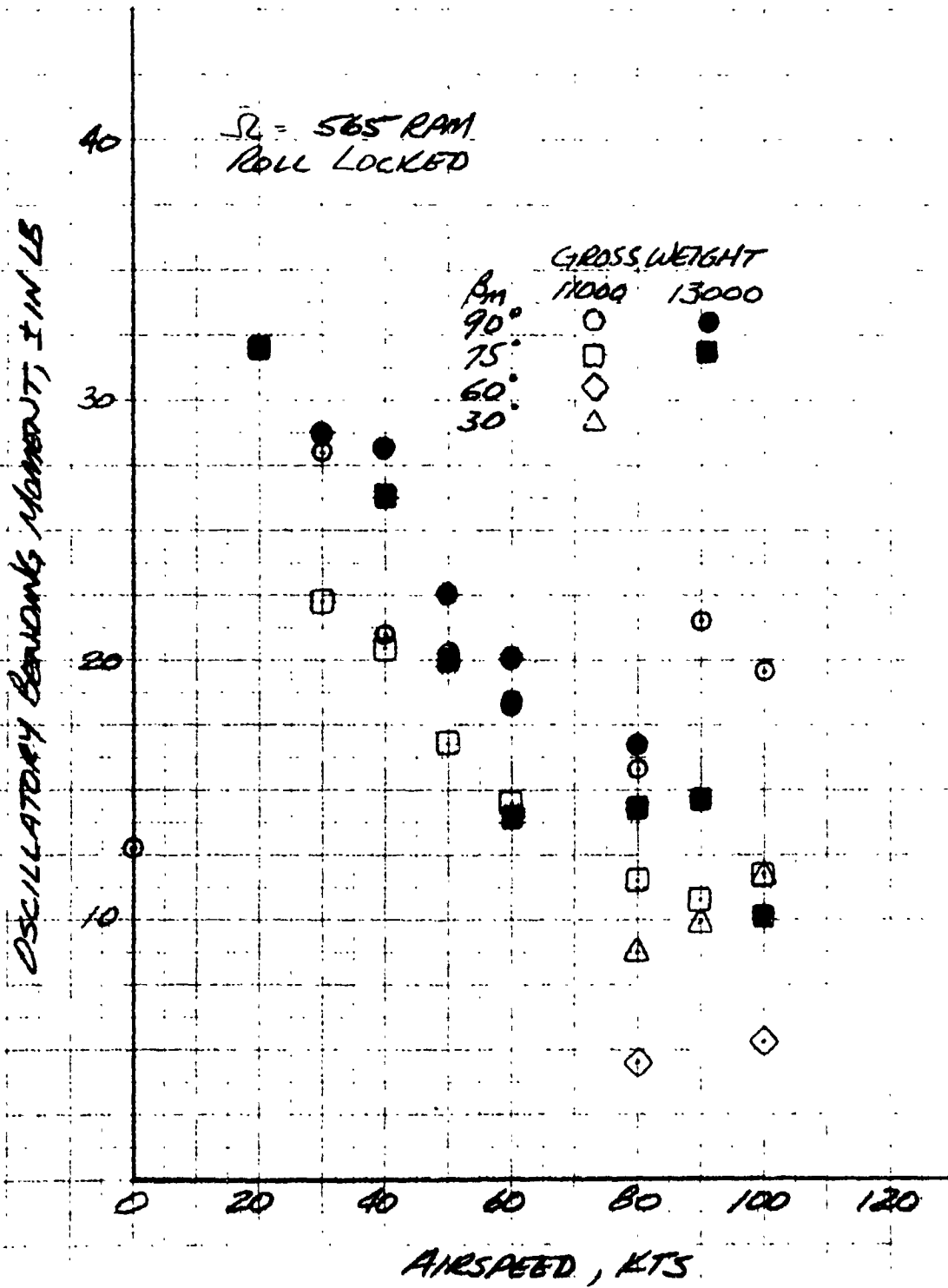


Figure V-31. Blade Station 52.5 Chordwise Oscillatory Bending Moment versus Airspeed.

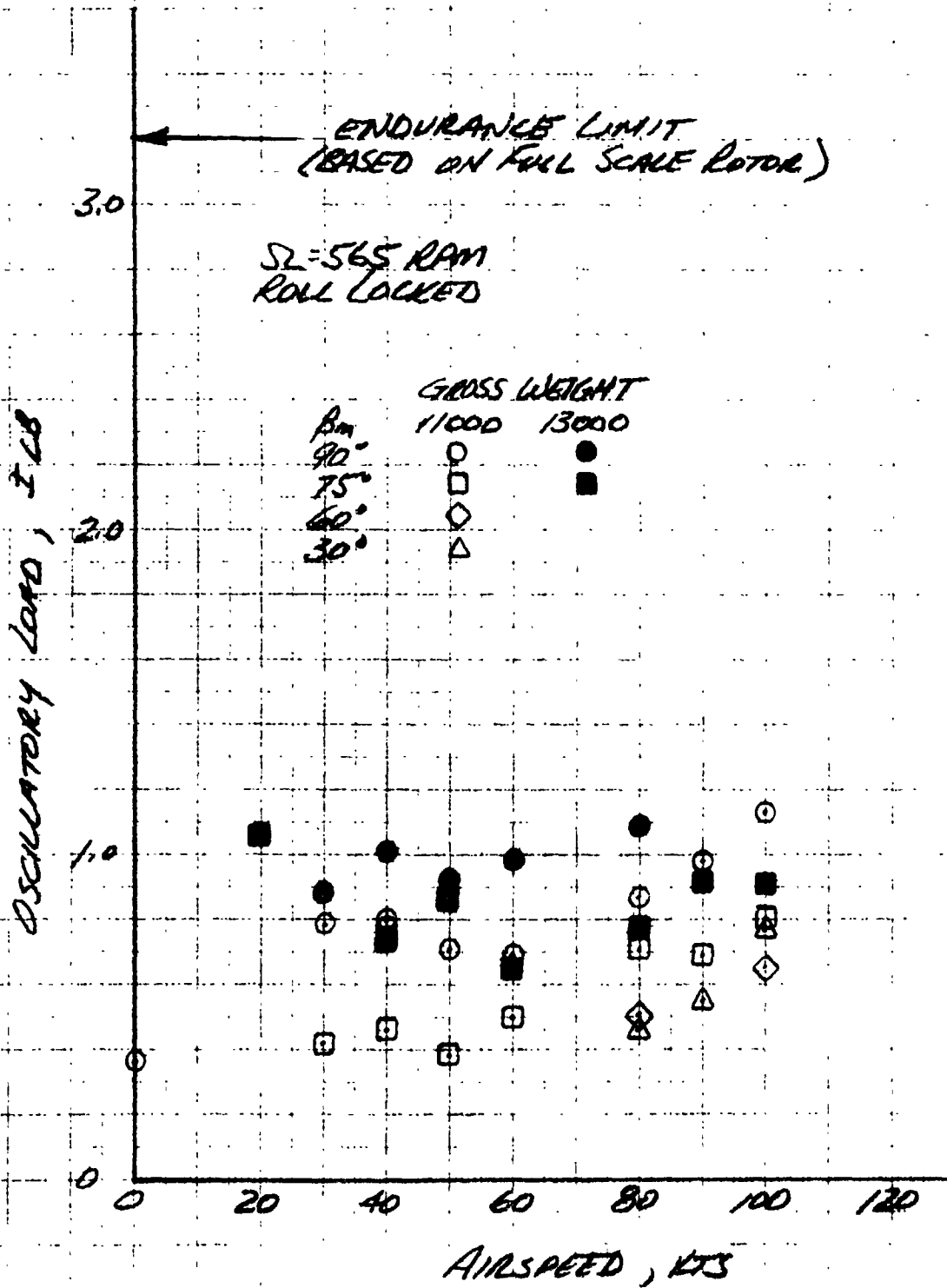


Figure V-32. Pitch Link Oscillatory Load versus Airspeed.

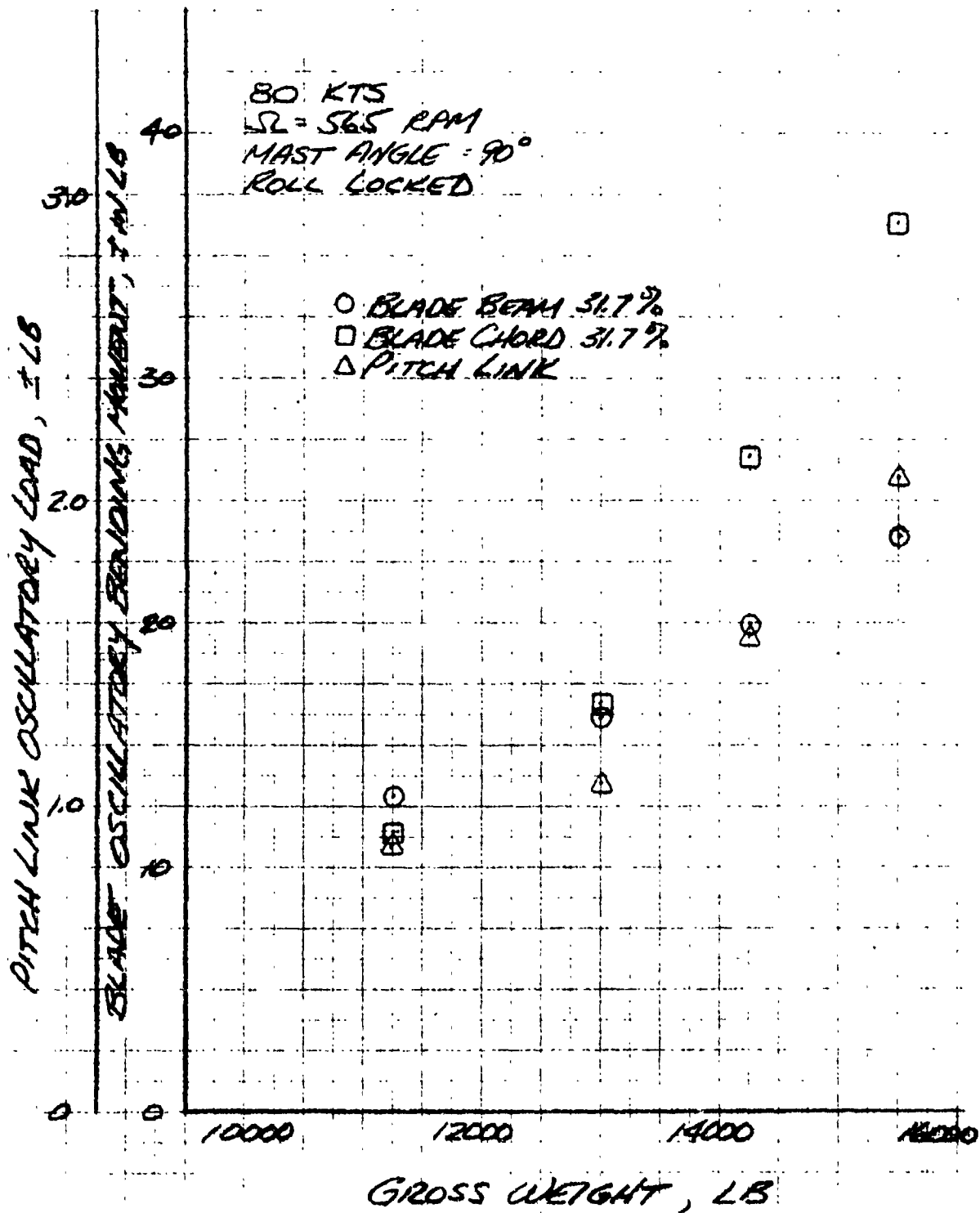
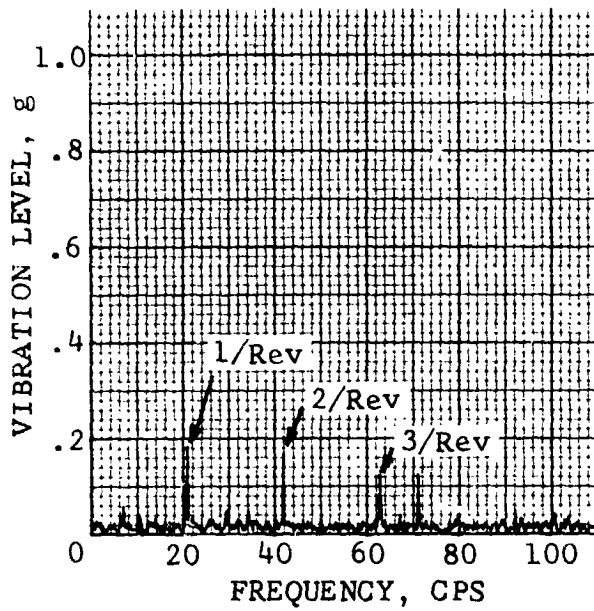
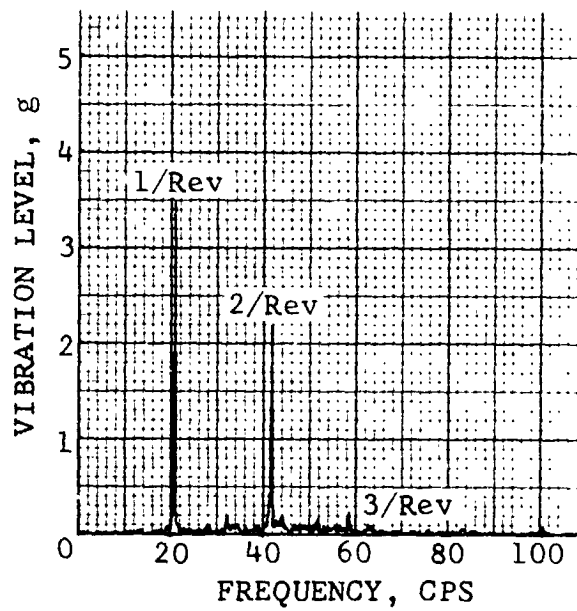


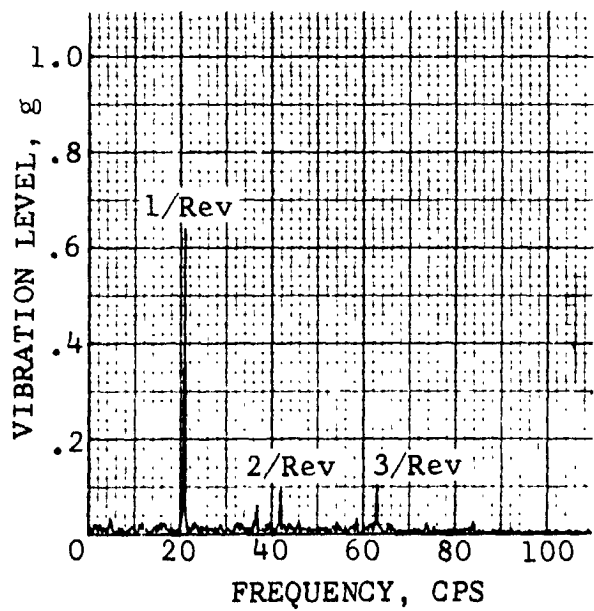
Figure V-33. Blade and Control System Loads versus Gross Weight.



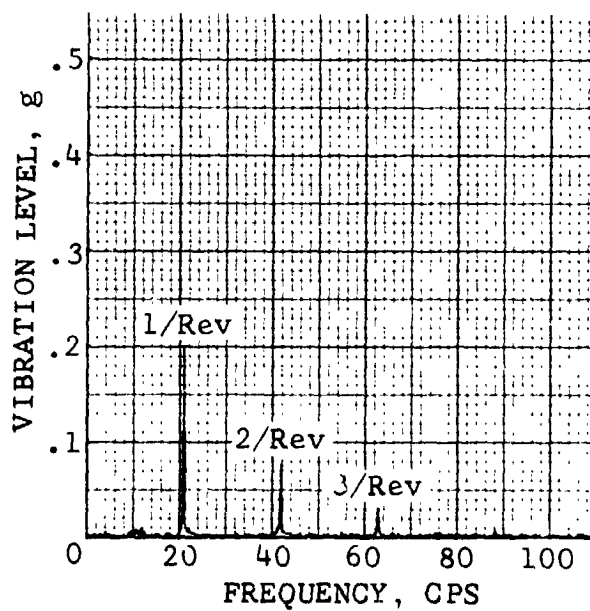
(a) AIRCRAFT CG
VERTICAL



(b) RH VERTICAL
STABILIZER F/A



(c) RH POD LATERAL
(XMSN CASE)



(d) LH POD LONGITUDINAL
(XMSN CASE)

Figure V-34. Frequency Spectrum of Airframe
Vibration for Several Accelerometer
Locations.

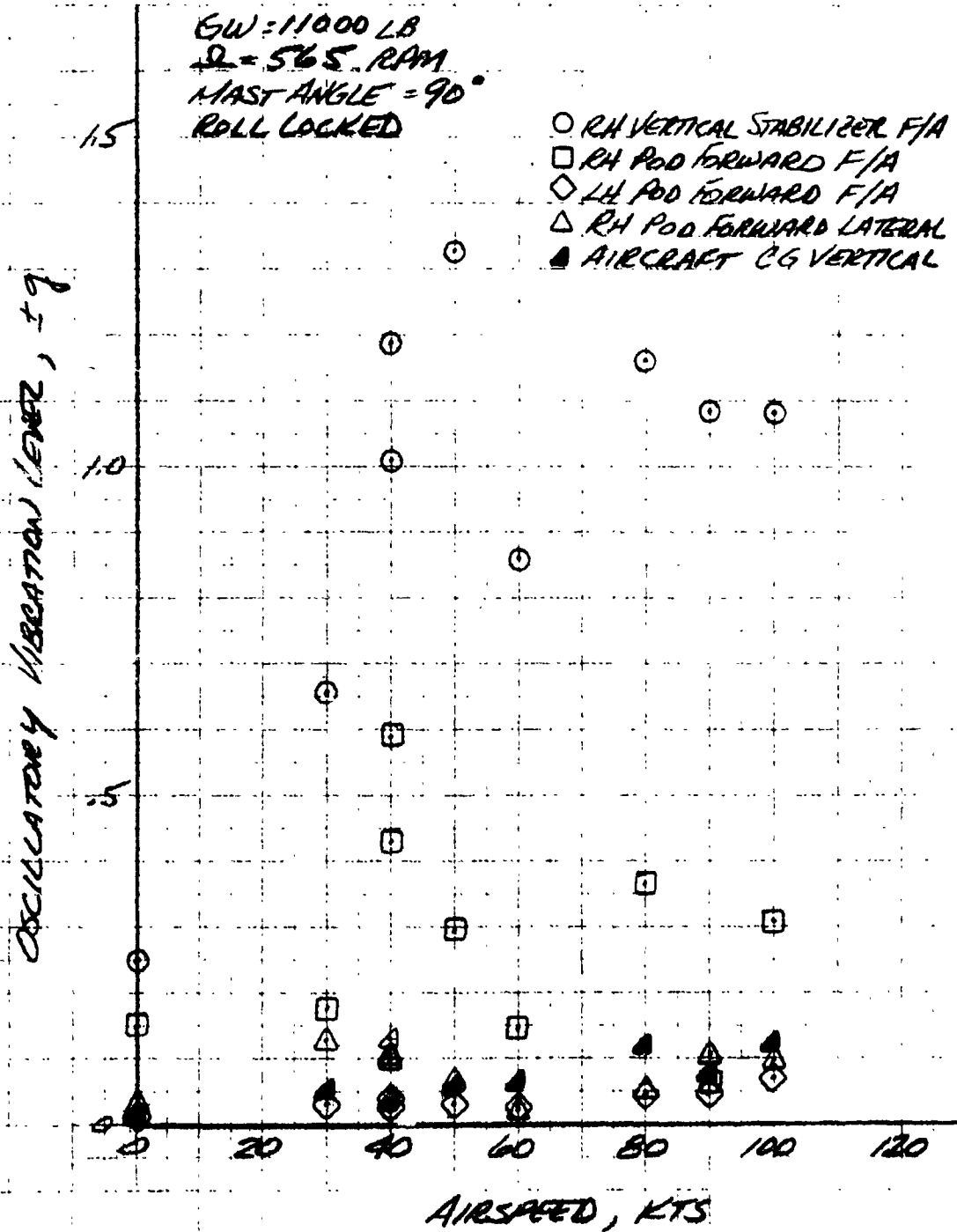


Figure V-35. Two-Per-Rev Vibration Level versus Airspeed.

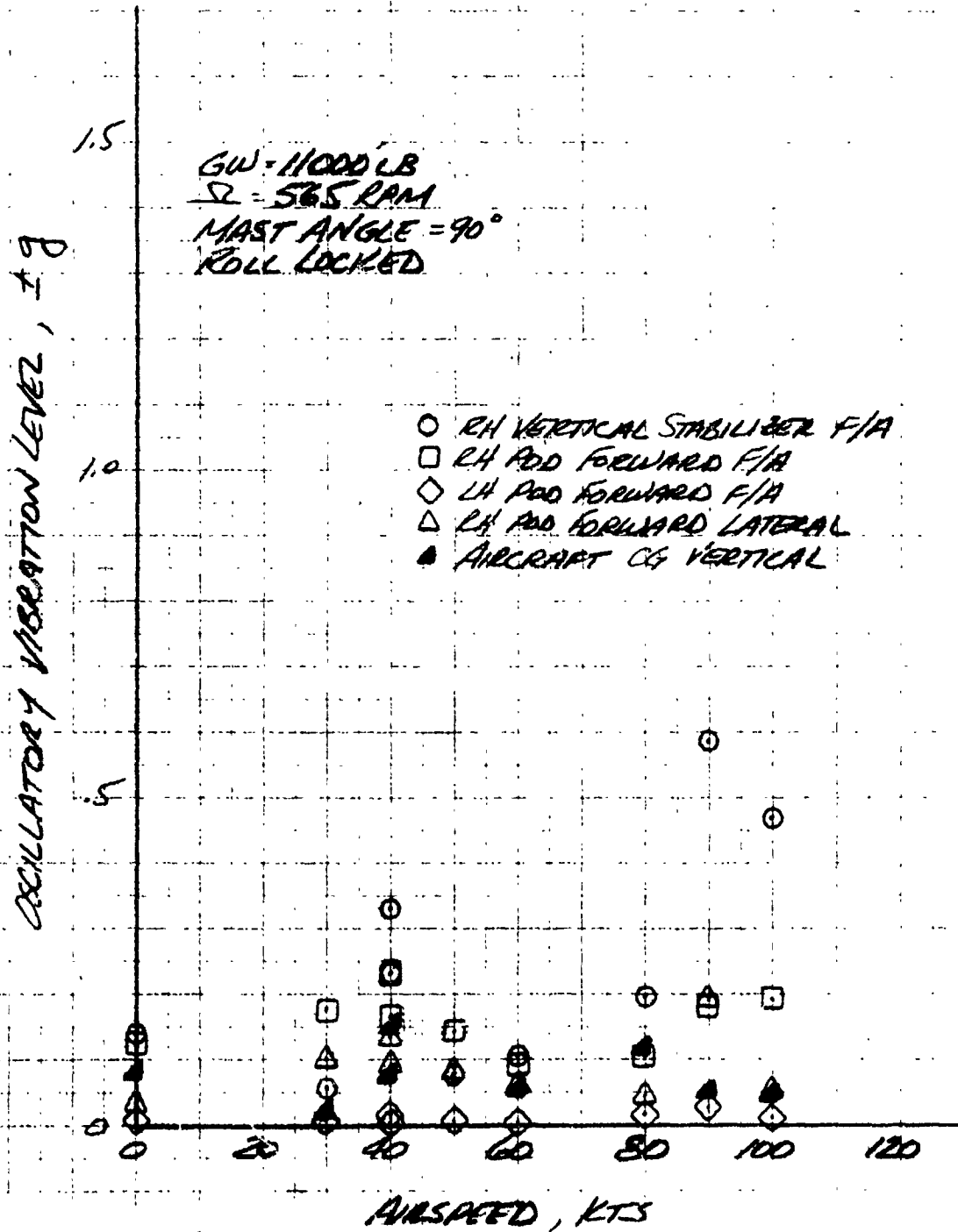


Figure V-36. Three-Per-Rev Vibration Level versus Airspeed.

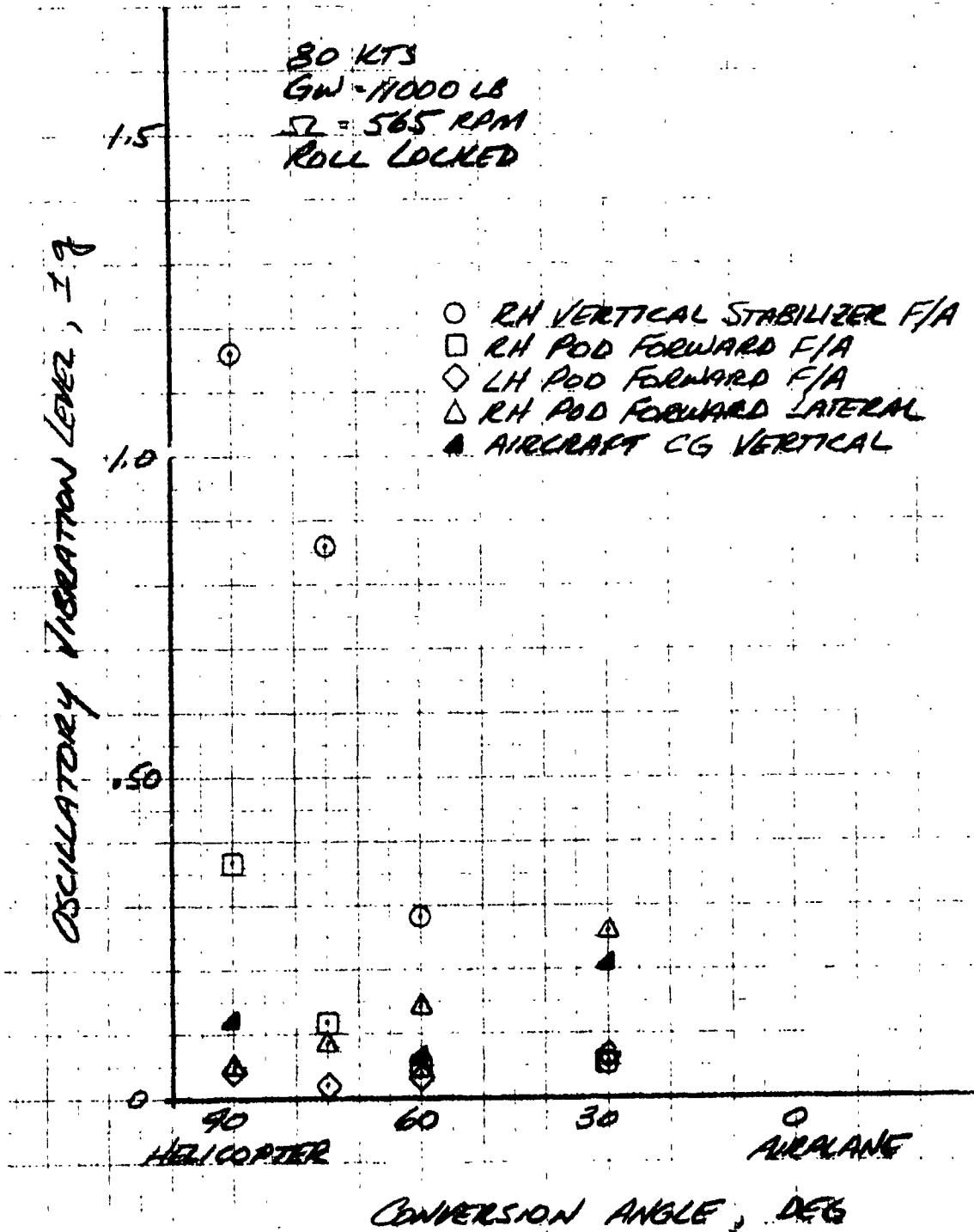


Figure V-37. Two-Per-Rev Vibration Level versus Conversion Angle.

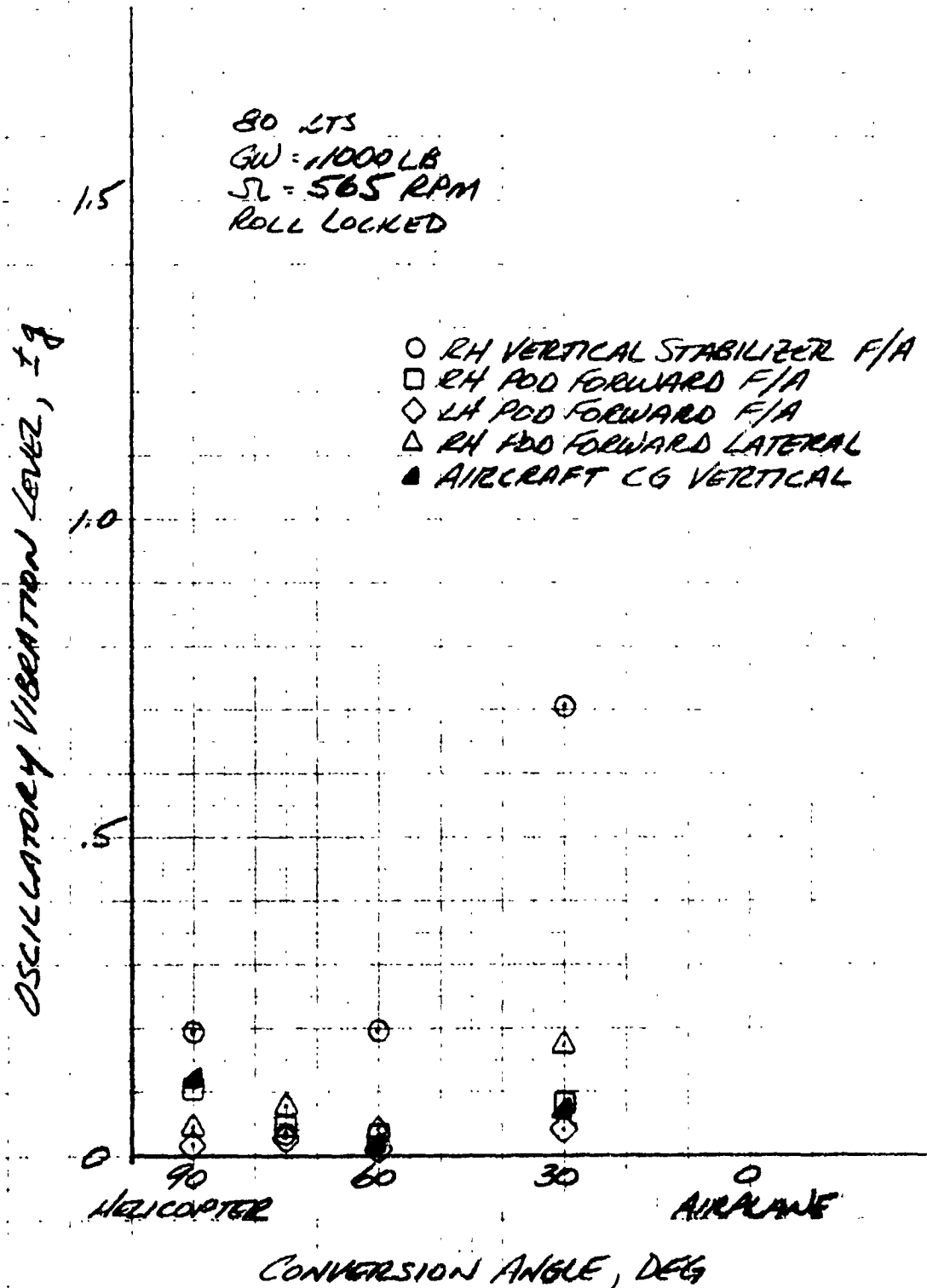


Figure V-38. Three-Per-Rev Vibration Level versus Conversion Angle.

AIRFRAME LIFT AND PITCHING MOMENT

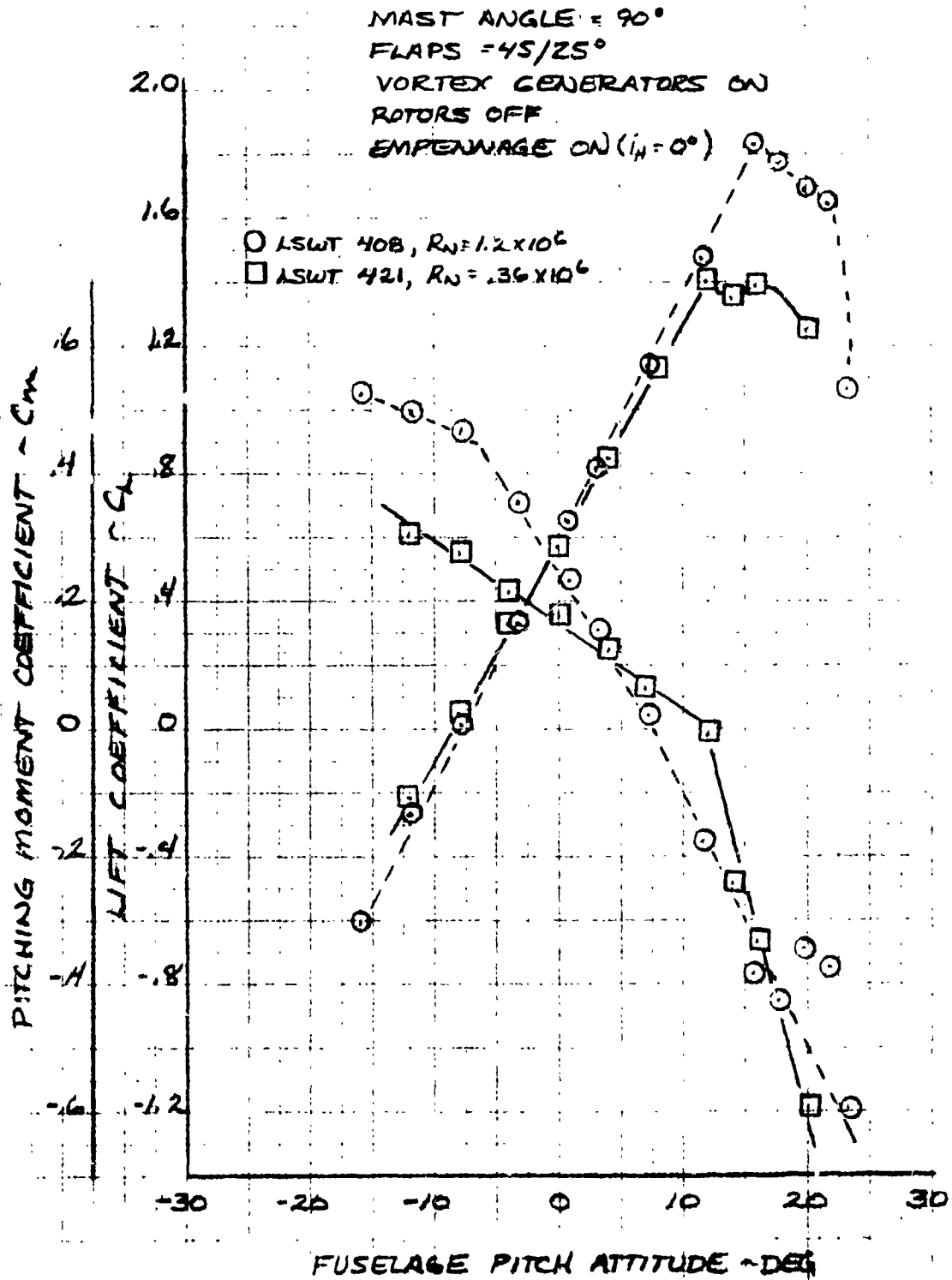


Figure V-39. Airframe Lift and Pitching Moment versus Angle of Attack, Rotors Removed.

AIRFRAME YAWING MOMENT

MAST ANGLE = 90°
FLAPS = 45/25°

ROTOR OFF
EMPENNAGE ON

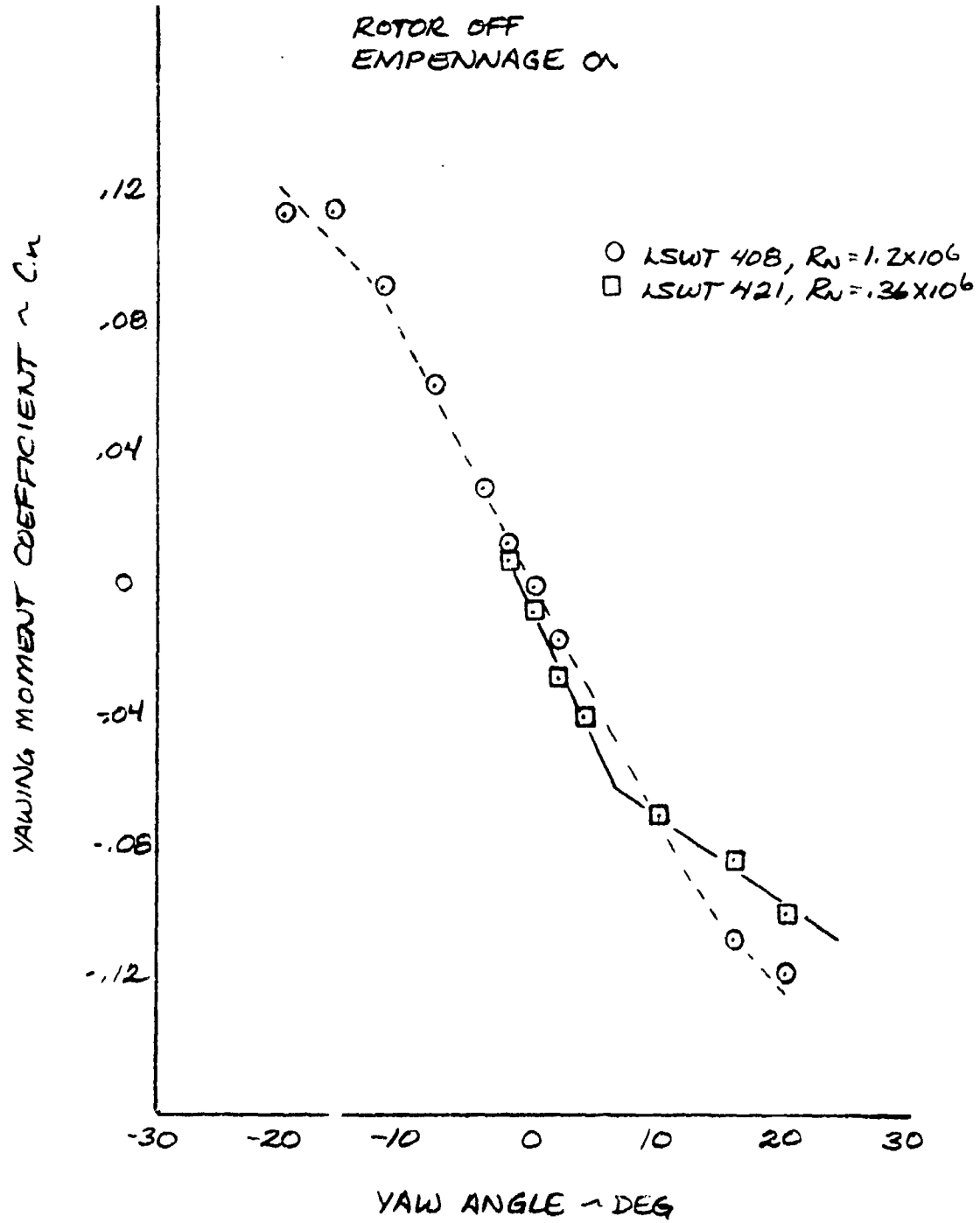


Figure V-40. Airframe Yaw Moment versus Yaw Angle, Rotors Removed.

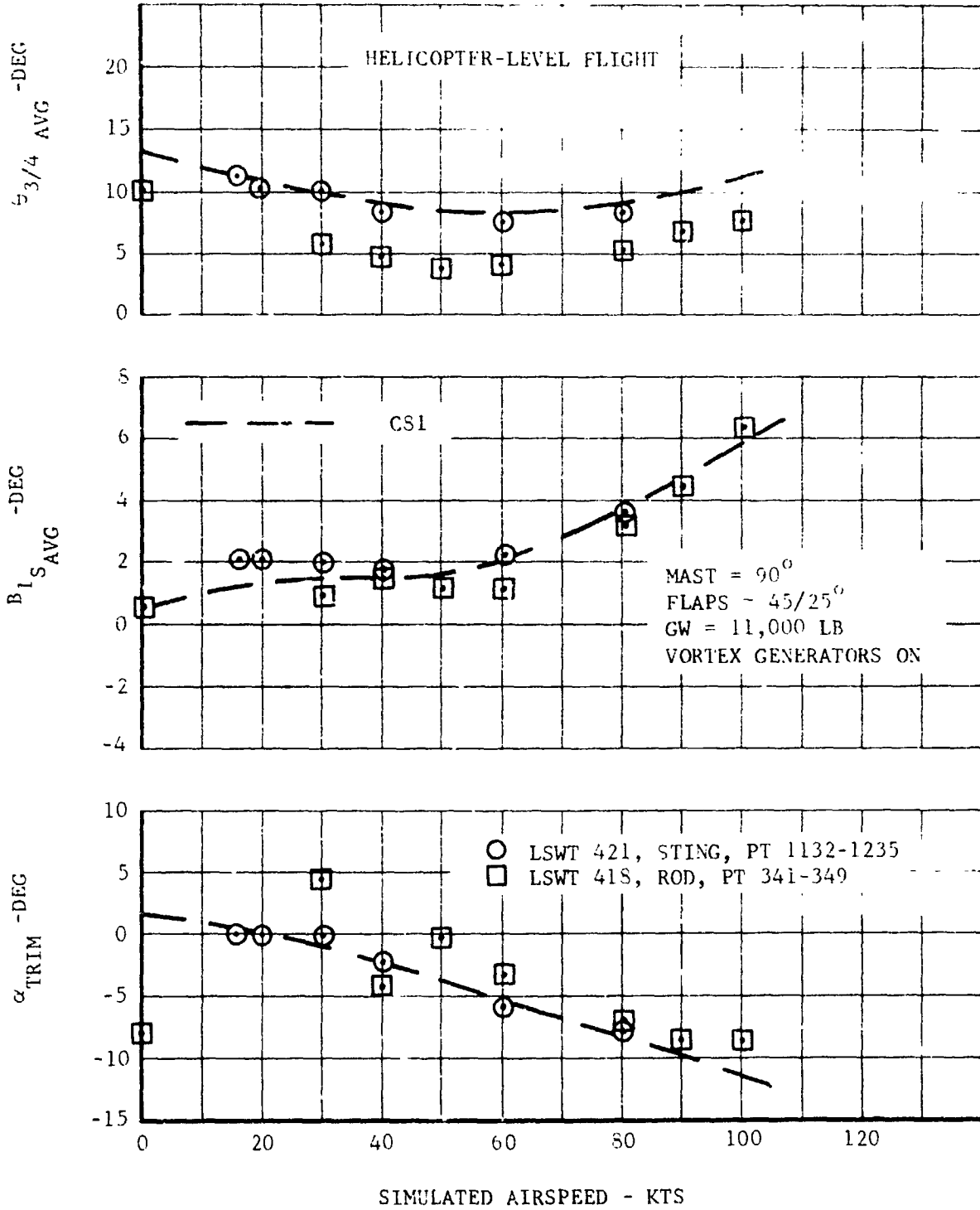


Figure V-41. Comparison of Rod Test with Sting Test Level Flight Trim Parameters, Mast 90°.

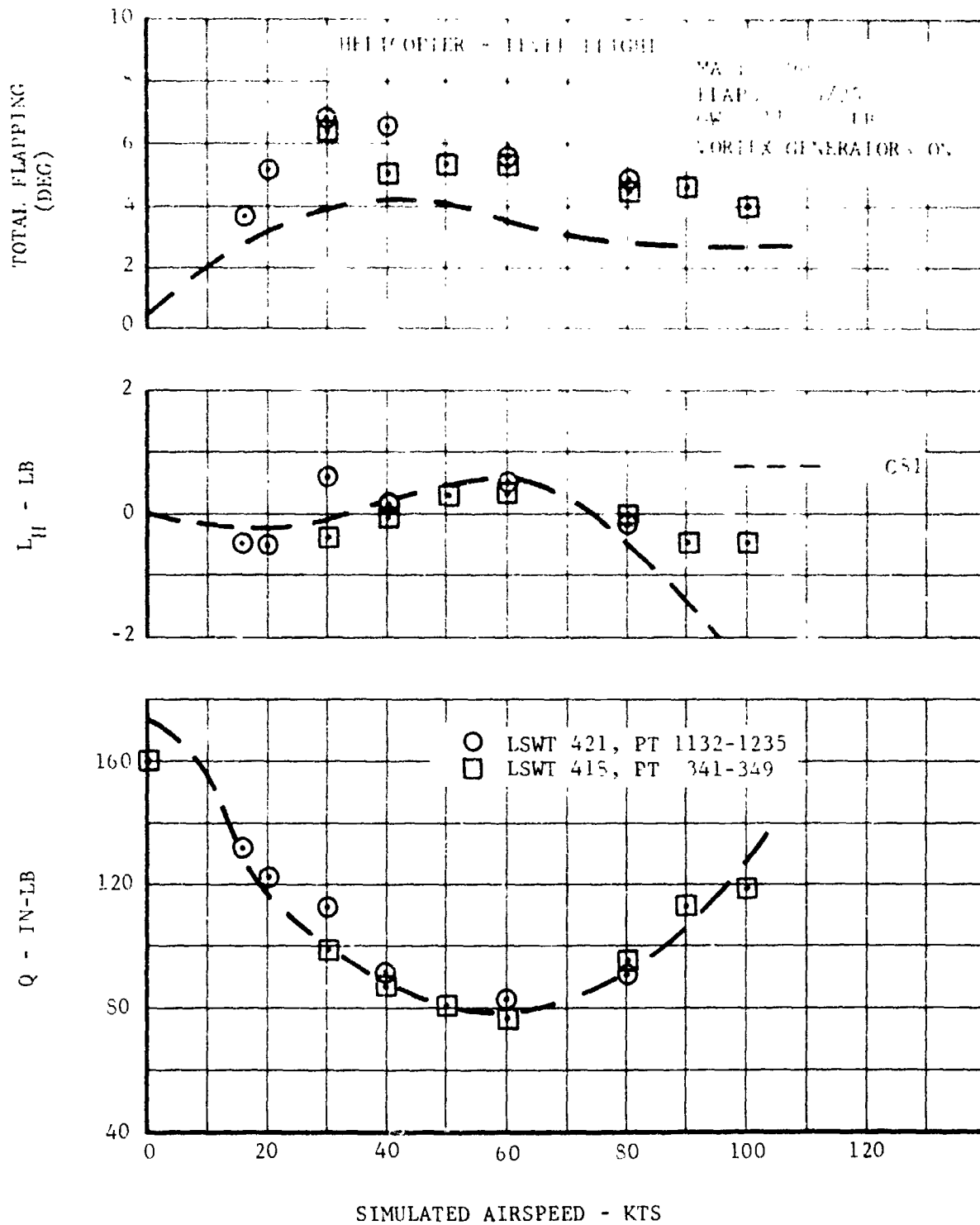


Figure V-41. Concluded

ROTOR AND AIRFRAME LIFT

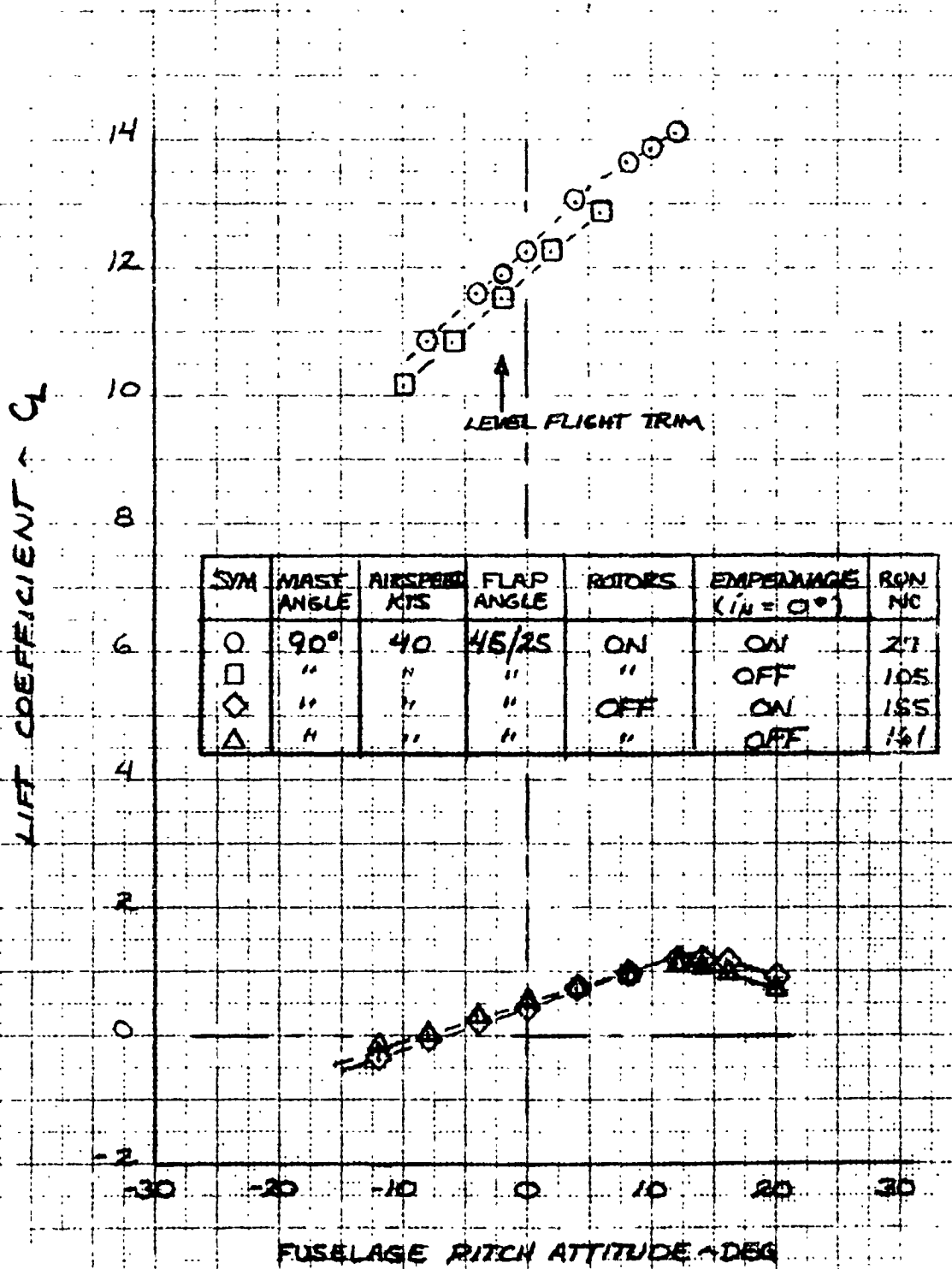


Figure V-42. Lift Coefficient versus Fuselage Angle of Attack, Mast Angle 90°, Airspeed 40 knots.

ROTOR AND AIRFRAME LIFT

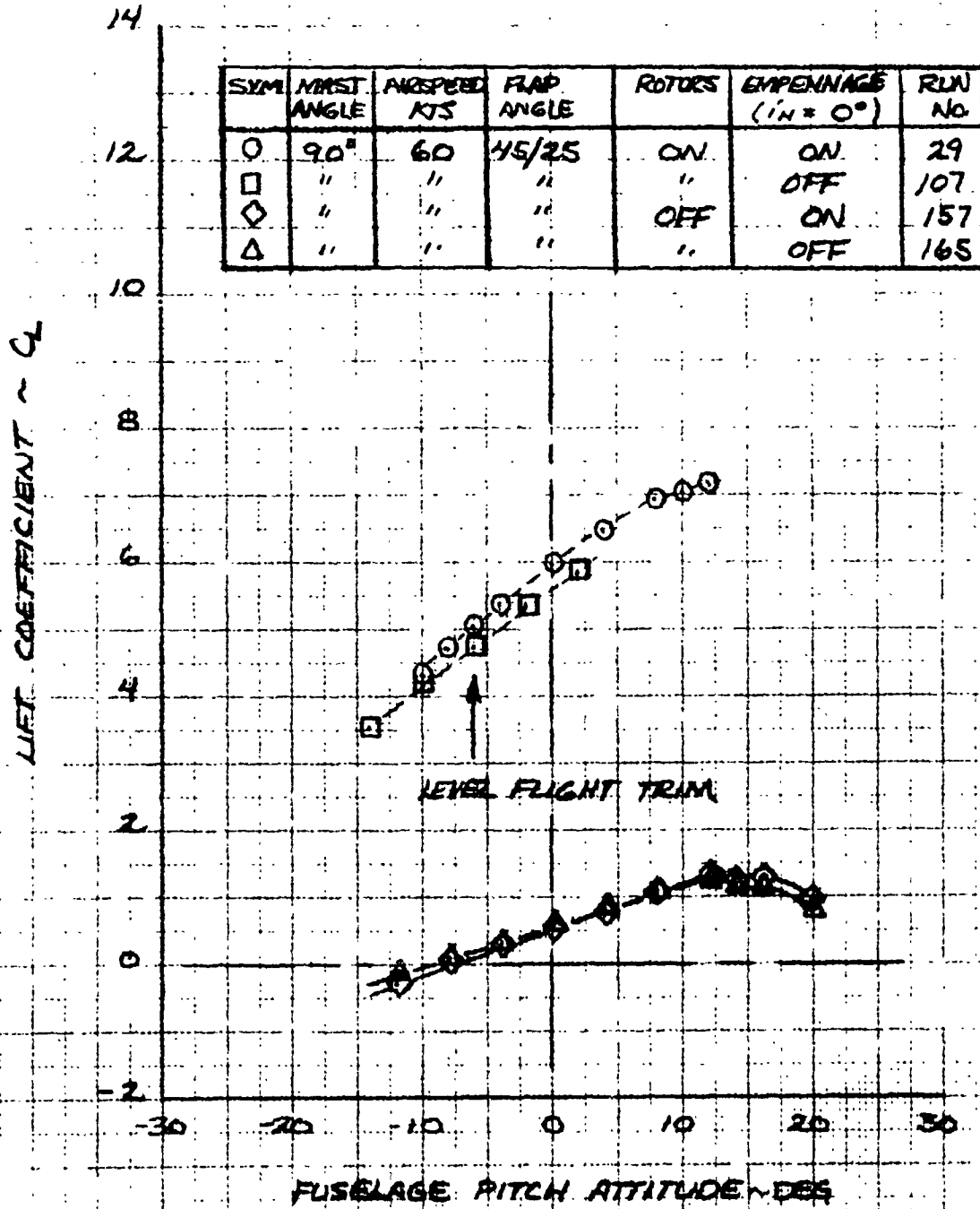


Figure V-43. Lift Coefficient versus Fuselage Angle of Attack, Mast Angle 90°, Airspeed 60 knots.

ROTOR AND AIRFRAME LIFT

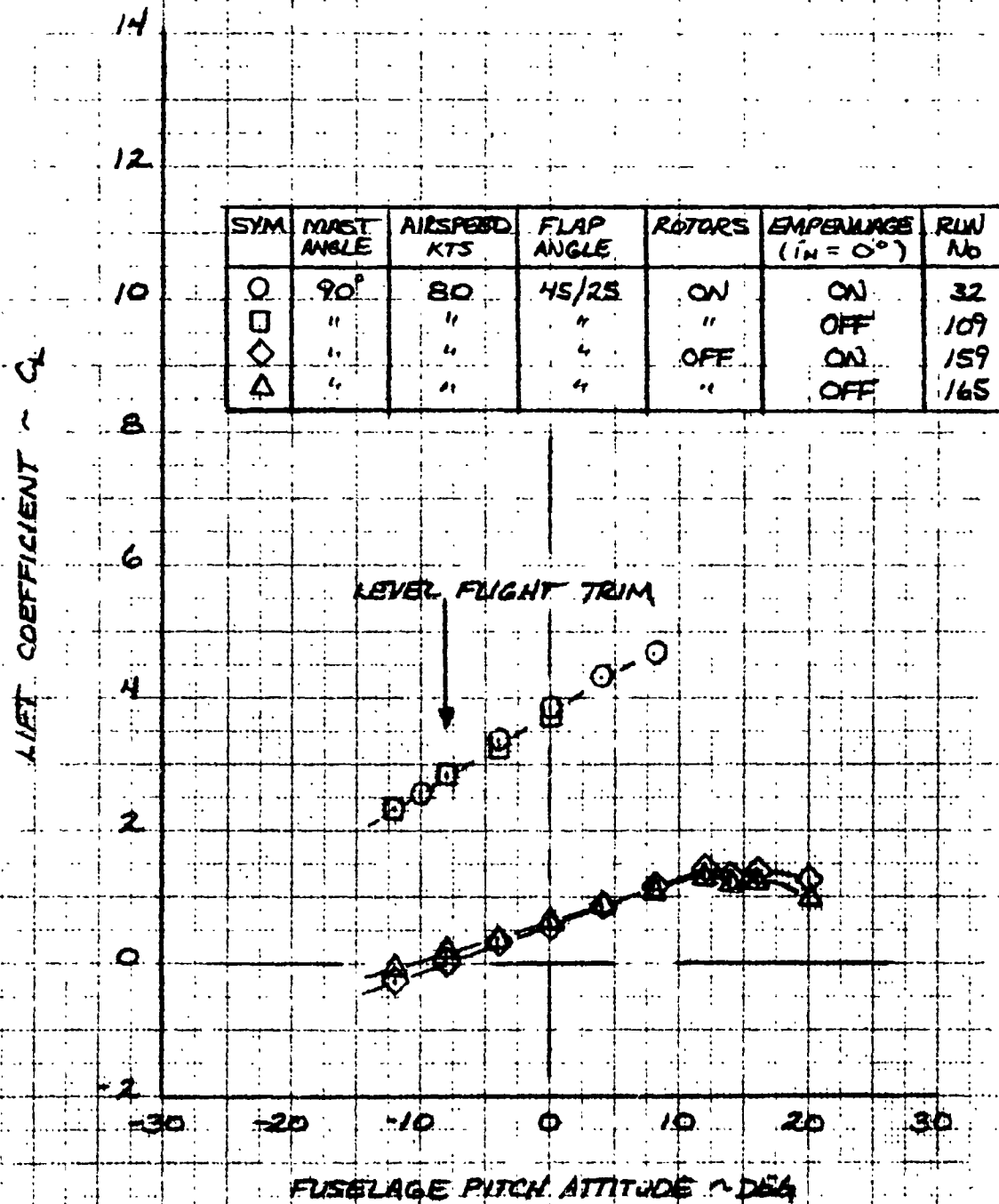


Figure V-44. Lift Coefficient versus Fuselage Angle of Attack, Mast Angle 90°, Airspeed 80 knots.

ROTOR AND AIRFRAME PITCHING MOMENT

40 KN

(SEE FIG V-42 FOR SYMBOLS)

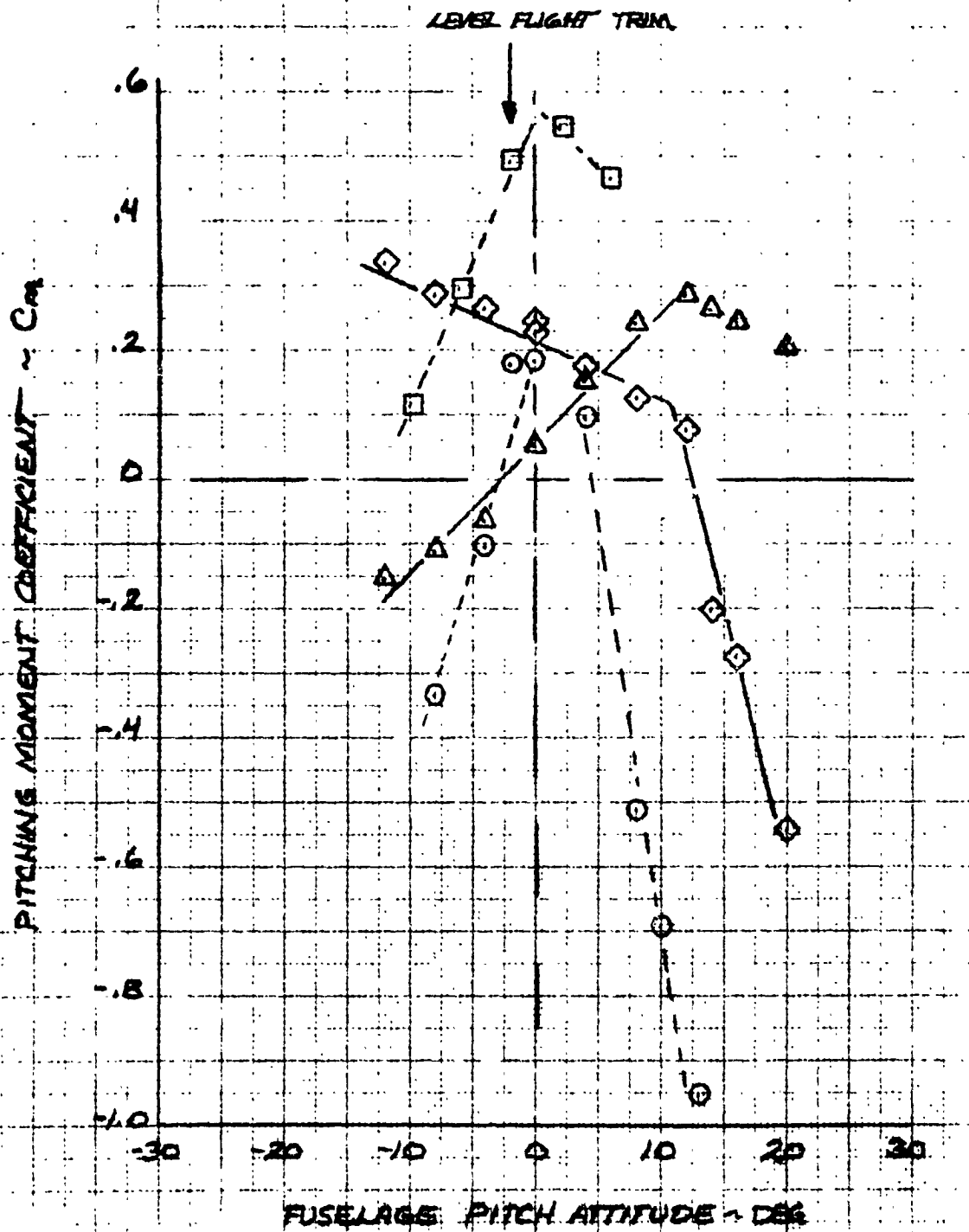


Figure V-45. Pitching Moment versus Fuselage Angle of Attack, Mast Angle 90°, Airspeed 40 knots.

ROTOR AND AIRFRAME PITCHING MOMENT
60 KN
(SEE FIG V-43 FOR SYMBOLS)

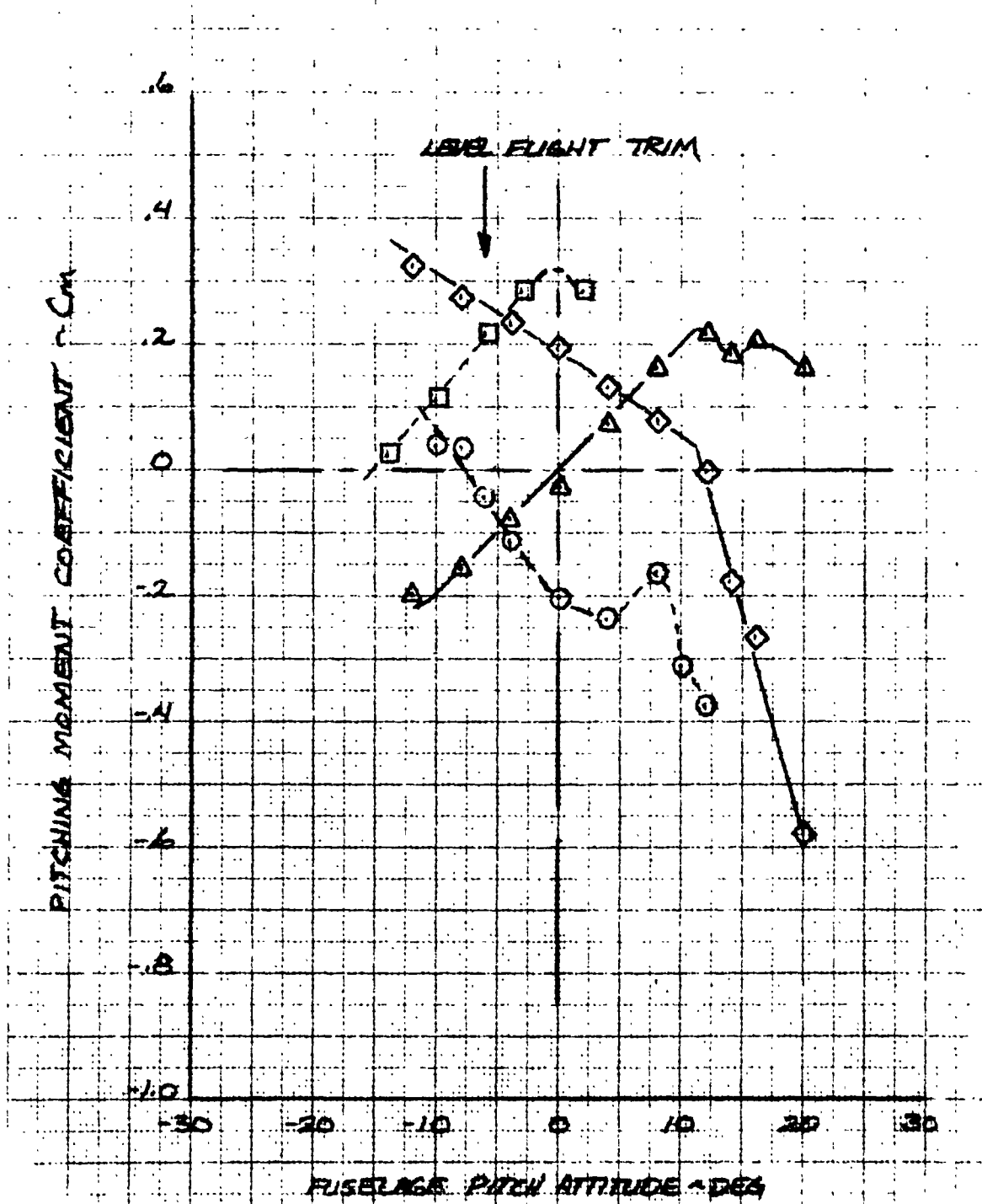


Figure V-46. Pitching Moment versus Fuselage Angle of Attack, Mast Angle 90°, Airspeed 60 knots.

ROTOR AND AIRFRAME PITCHING MOMENT
80 KN
(SEE FIG. V-44 FOR SYMBOLS)

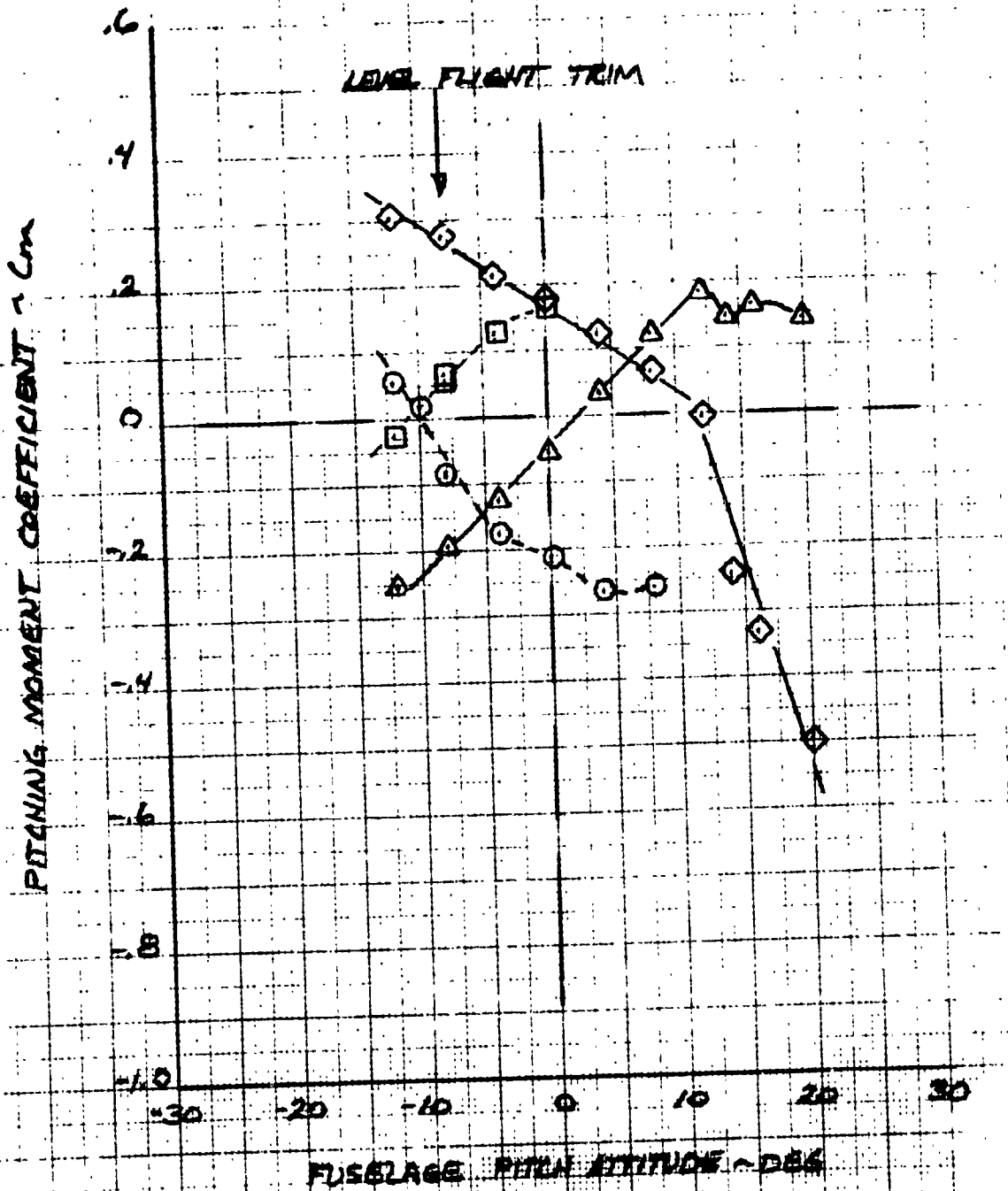


Figure V-47. Pitching Moment versus Fuselage Angle of Attack, Mast Angle 90°, Airspeed 80 knots.

ROTOR AND AIRFRAME YAWING MOMENT

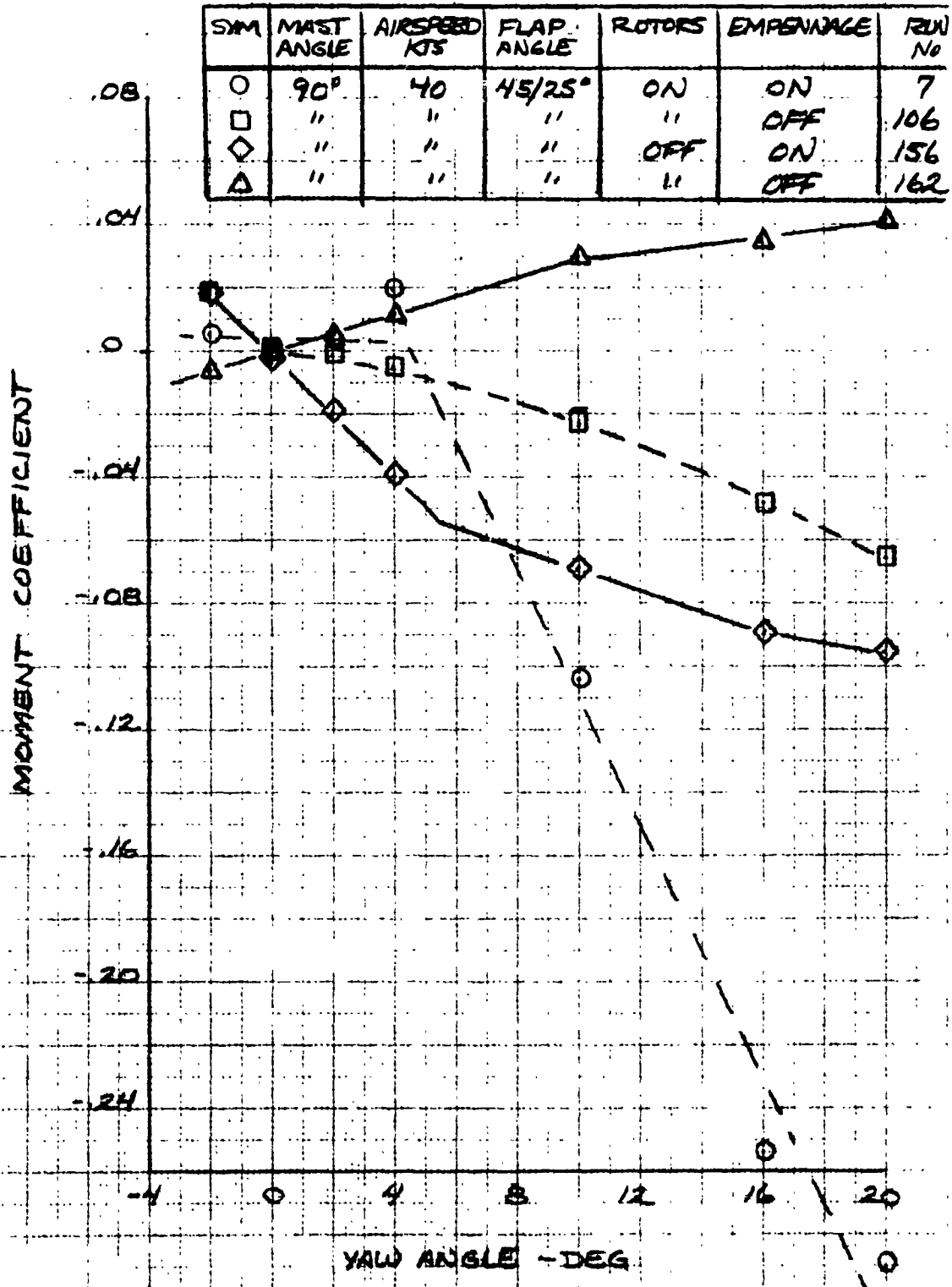


Figure V-48. Yaw Moment Coefficient versus Yaw Angle, Mast Angle 90°, Airspeed 40 knots.

ROTOR AND AIRFRAME YAWING MOMENT

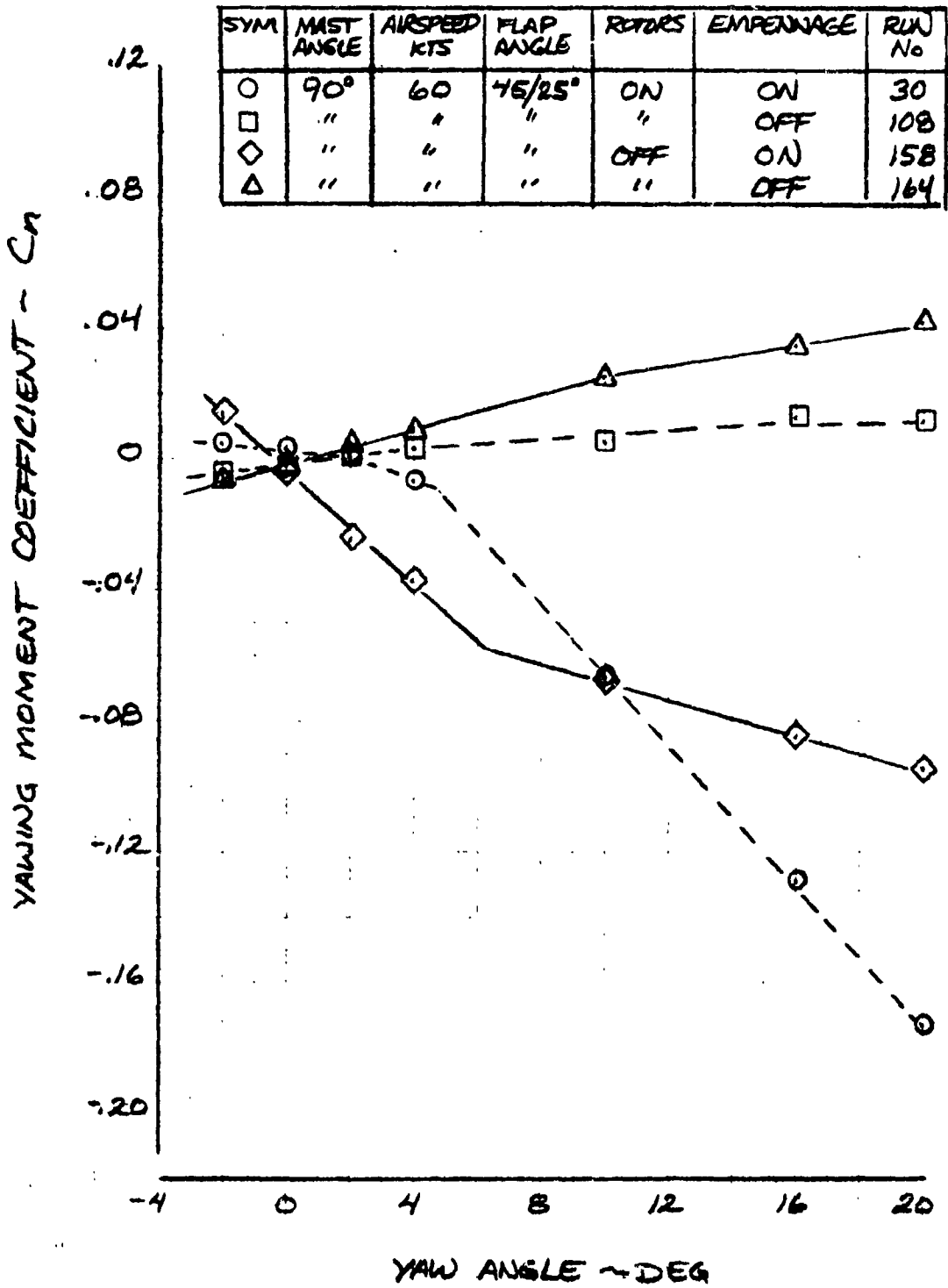


Figure V-49. Yaw Moment Coefficient versus Yaw Angle, Mast Angle 90°, Airspeed 60 knots.

ROTOR AND AIRFRAME YAWING MOMENT

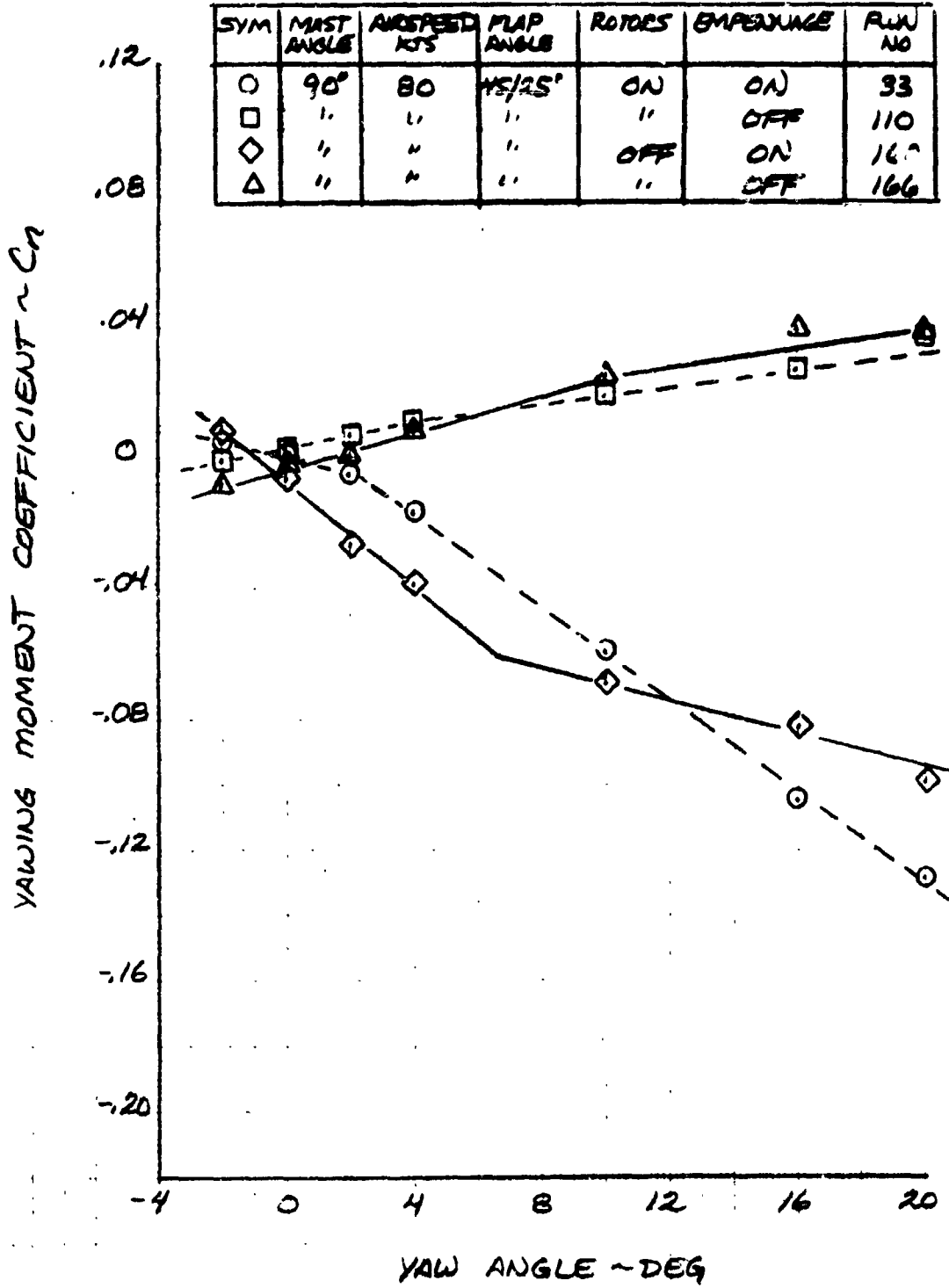


Figure V-50. Yaw Moment Coefficient versus Yaw Angle, Mast Angle 90°, Airspeed 80 knots.

ROTOR AND AIRFRAME LIFT

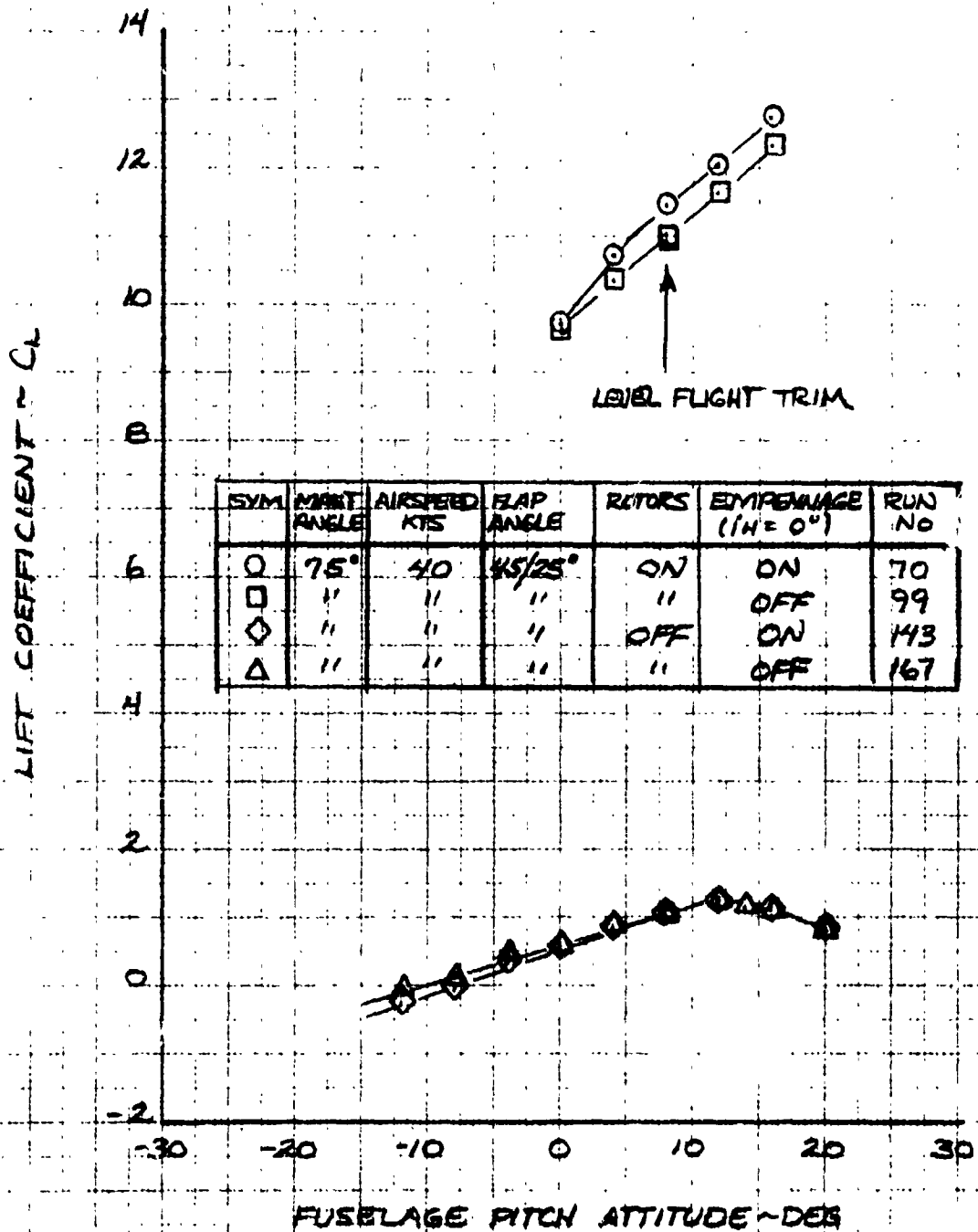


Figure V-51. Lift Coefficient versus Fuselage Angle of Attack, Mast Angle 75°, Airspeed 40 knots.

ROTOR AND AIRFRAME LIFT

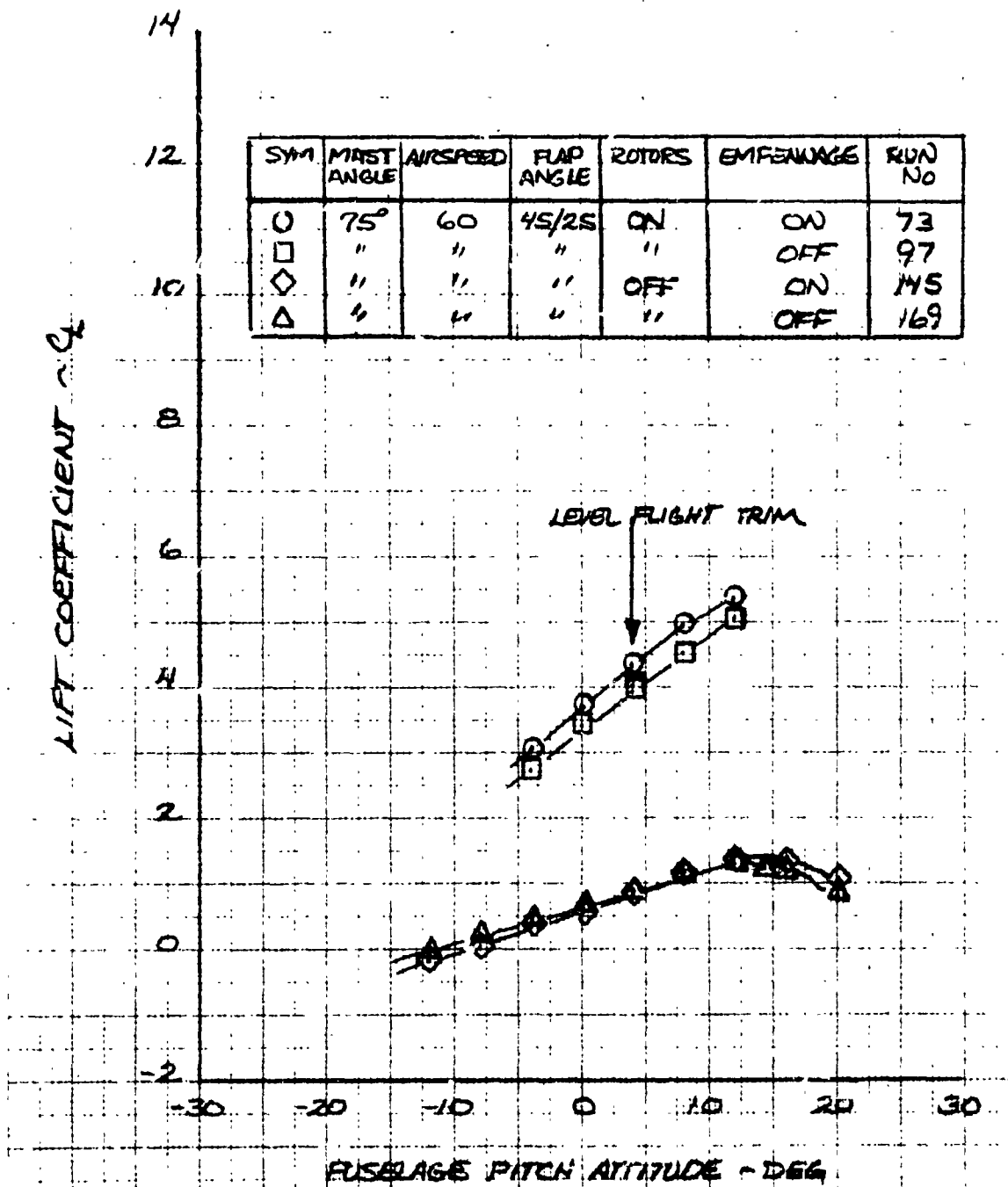


Figure V-52. Lift Coefficient versus Fuselage Angle of Attack, Mast Angle 75°, Airspeed 60 knots.

ROTOR AND AIRFRAME LIFT

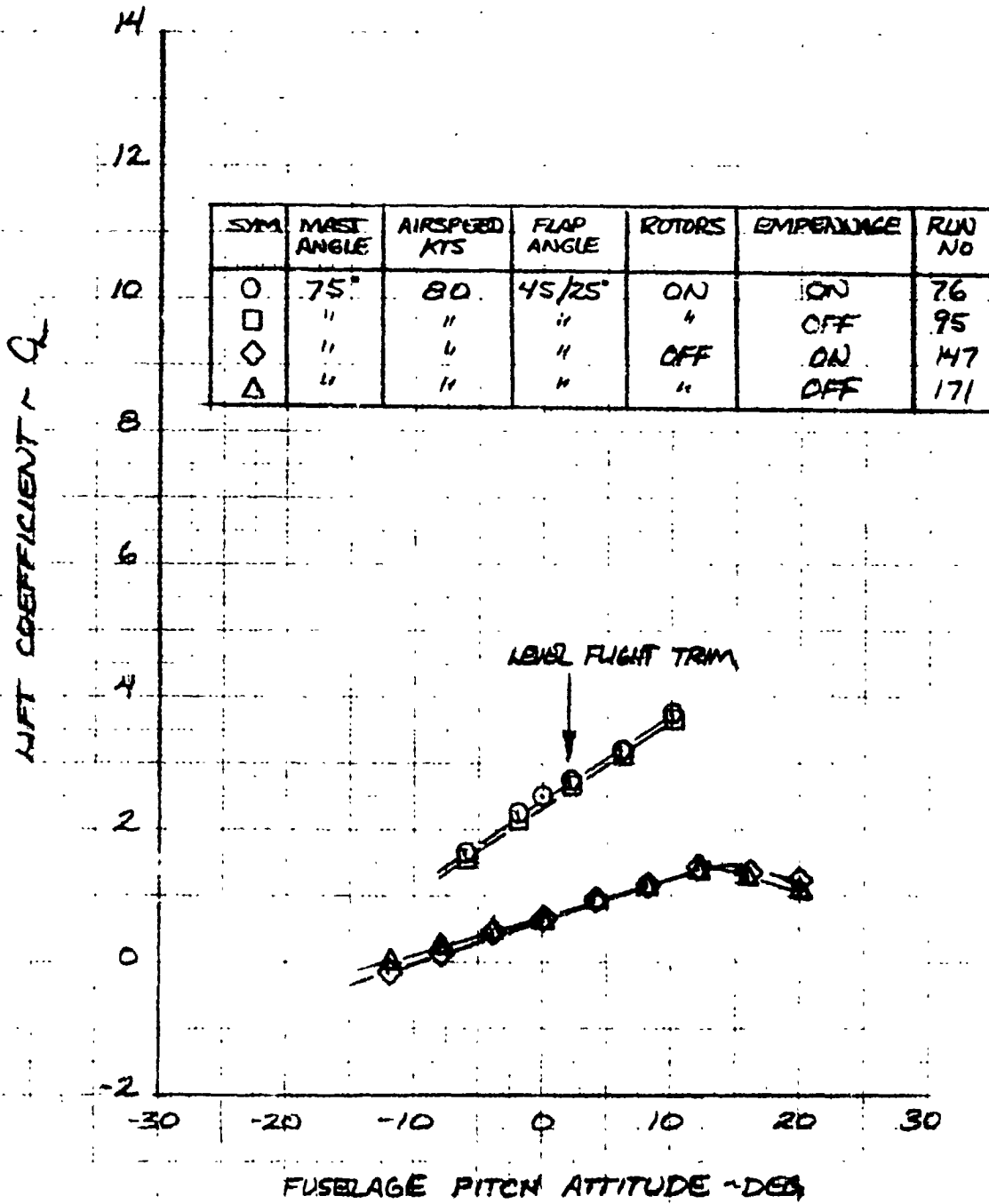


Figure V-53. Lift Coefficient versus Angle of Attack, Mast Angle 75°, Airspeed 80 knots.

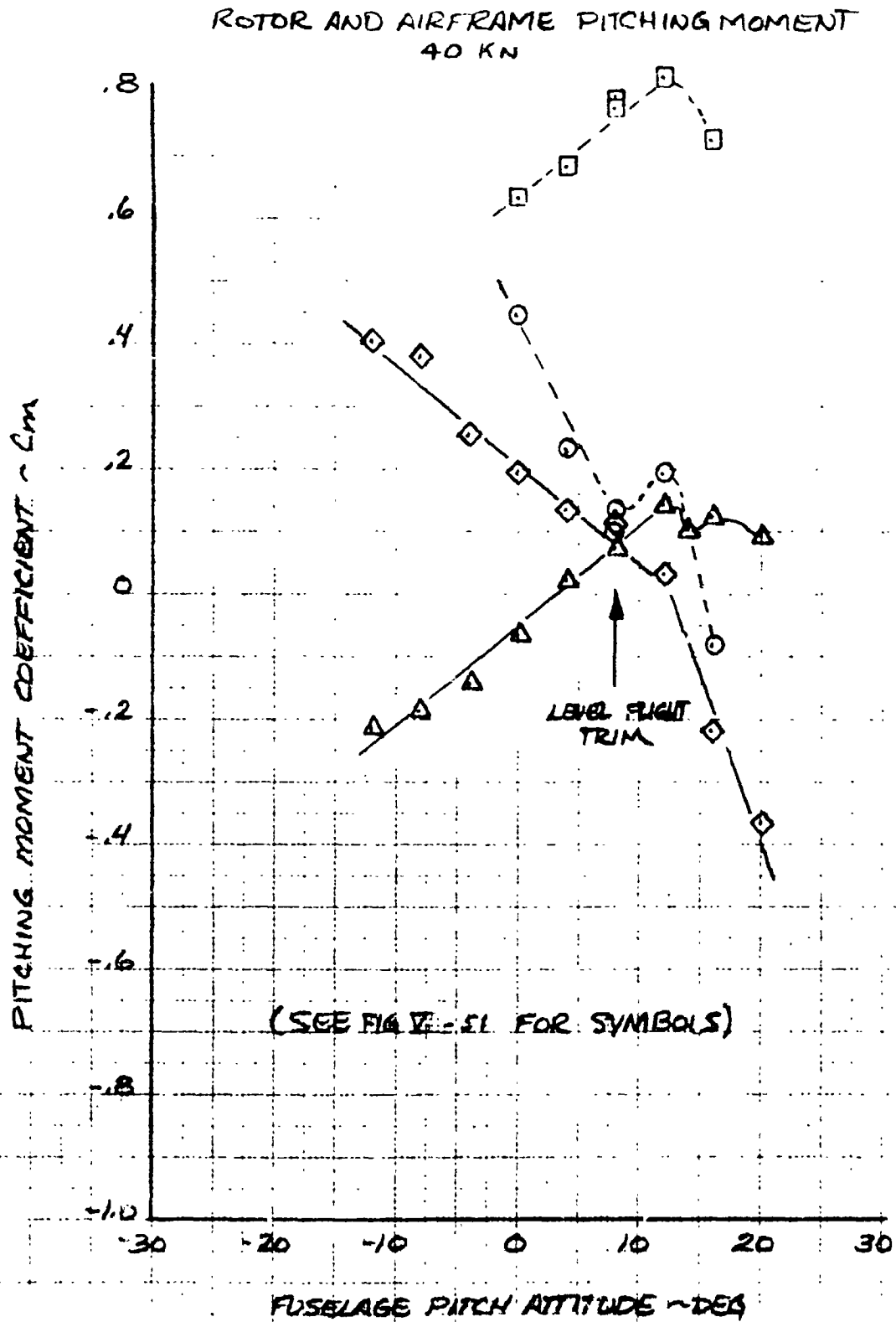


Figure V-54. Pitching Moment versus Fuselage Angle of Attack, Mast Angle 75°, Airspeed 40 knots.

ROTOR AND AIRFRAME PITCHING MOMENT
(SEE FIG I -5.2 FOR SYMBOLS)

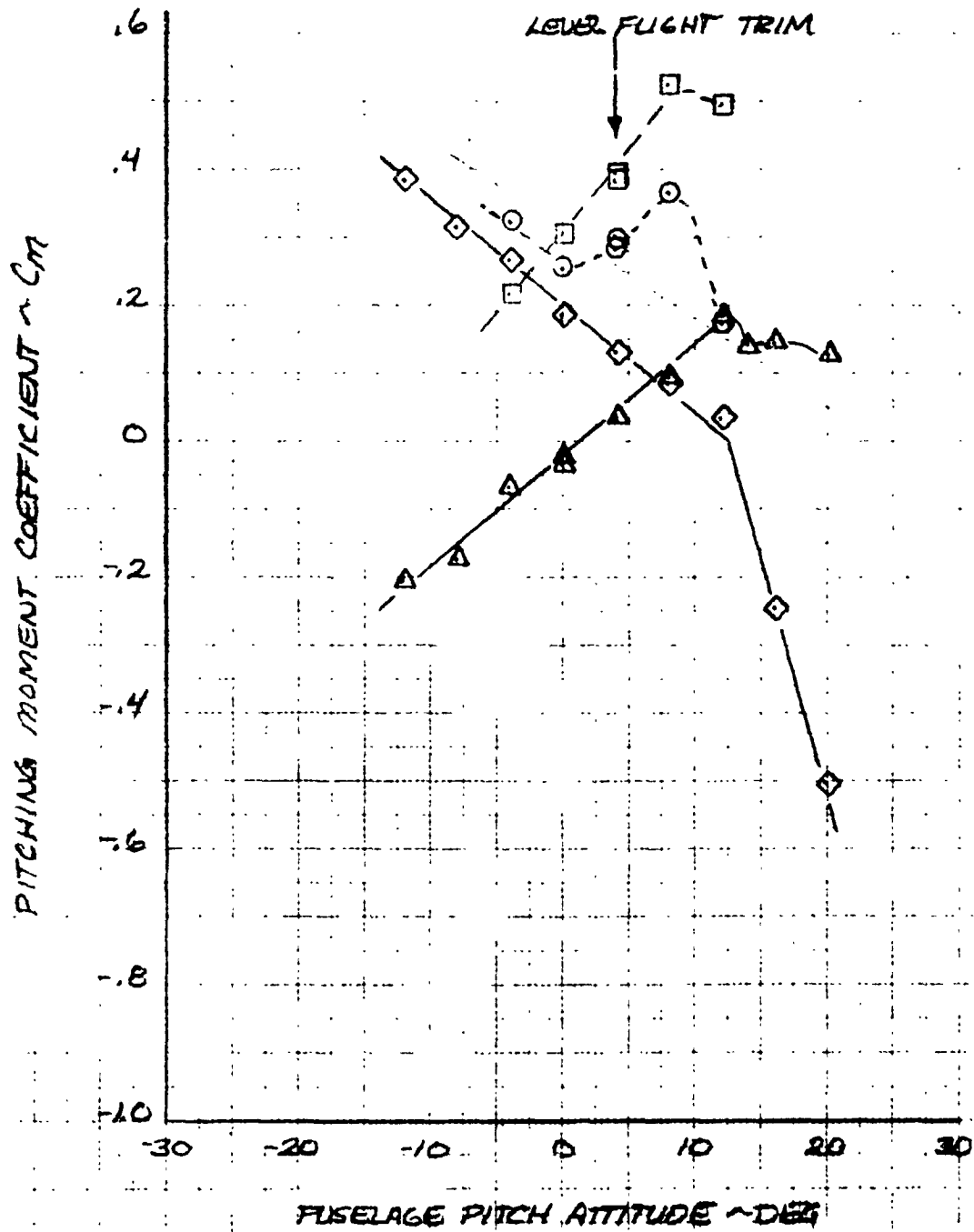


Figure V-55. Pitching Moment versus Fuselage Angle of Attack, Mast Angle 75°, Airspeed 60 knots.

ROTOR AND AIRFRAME PITCHING MOMENT (SEE FIG V-53 FOR SYMBOLS)

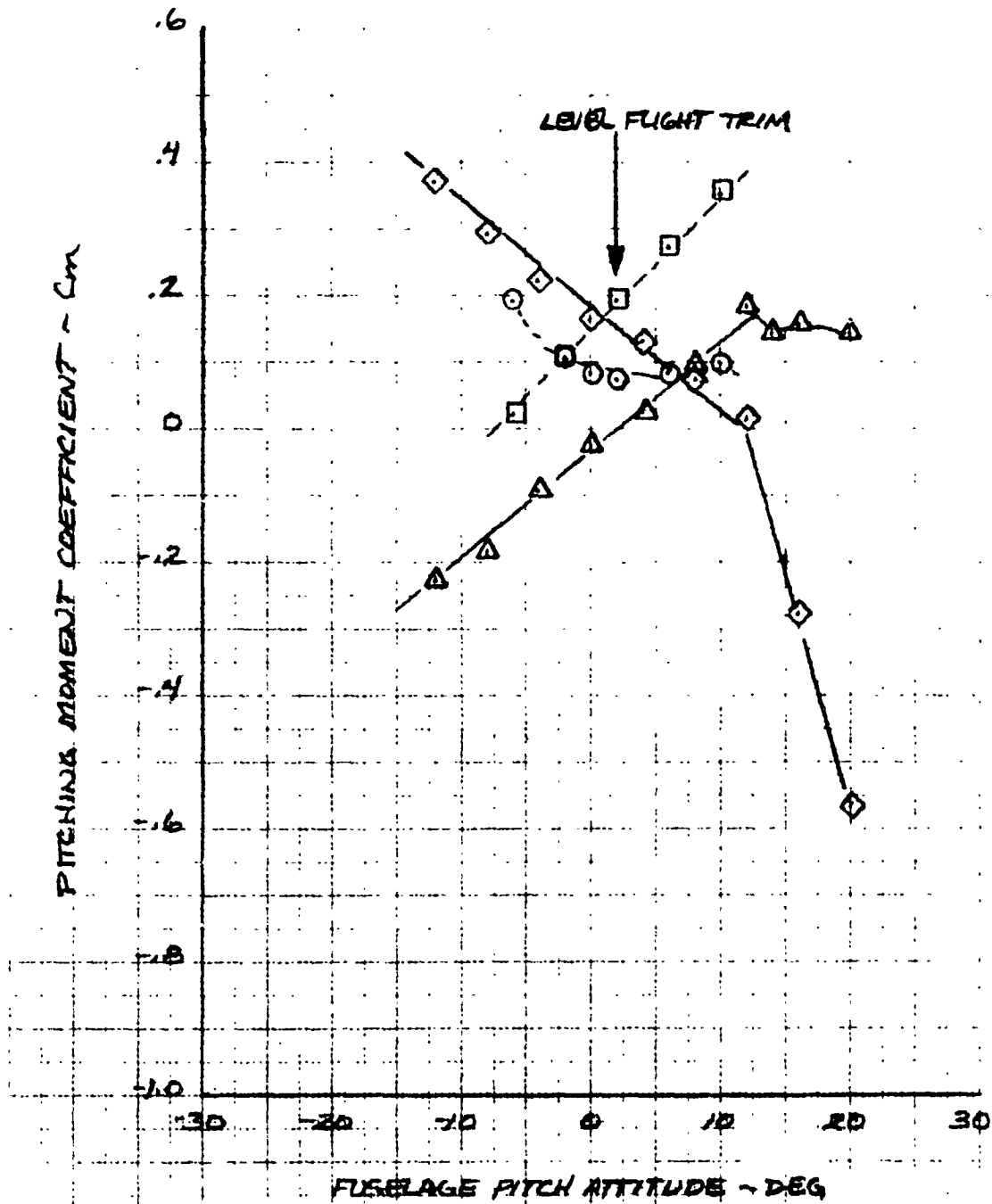


Figure V-56. Pitching Moment versus Fuselage Angle of Attack, Mast Angle 75°, Airspeed 80 knots.

ROTOR AND AIRFRAME YAWING MOMENT

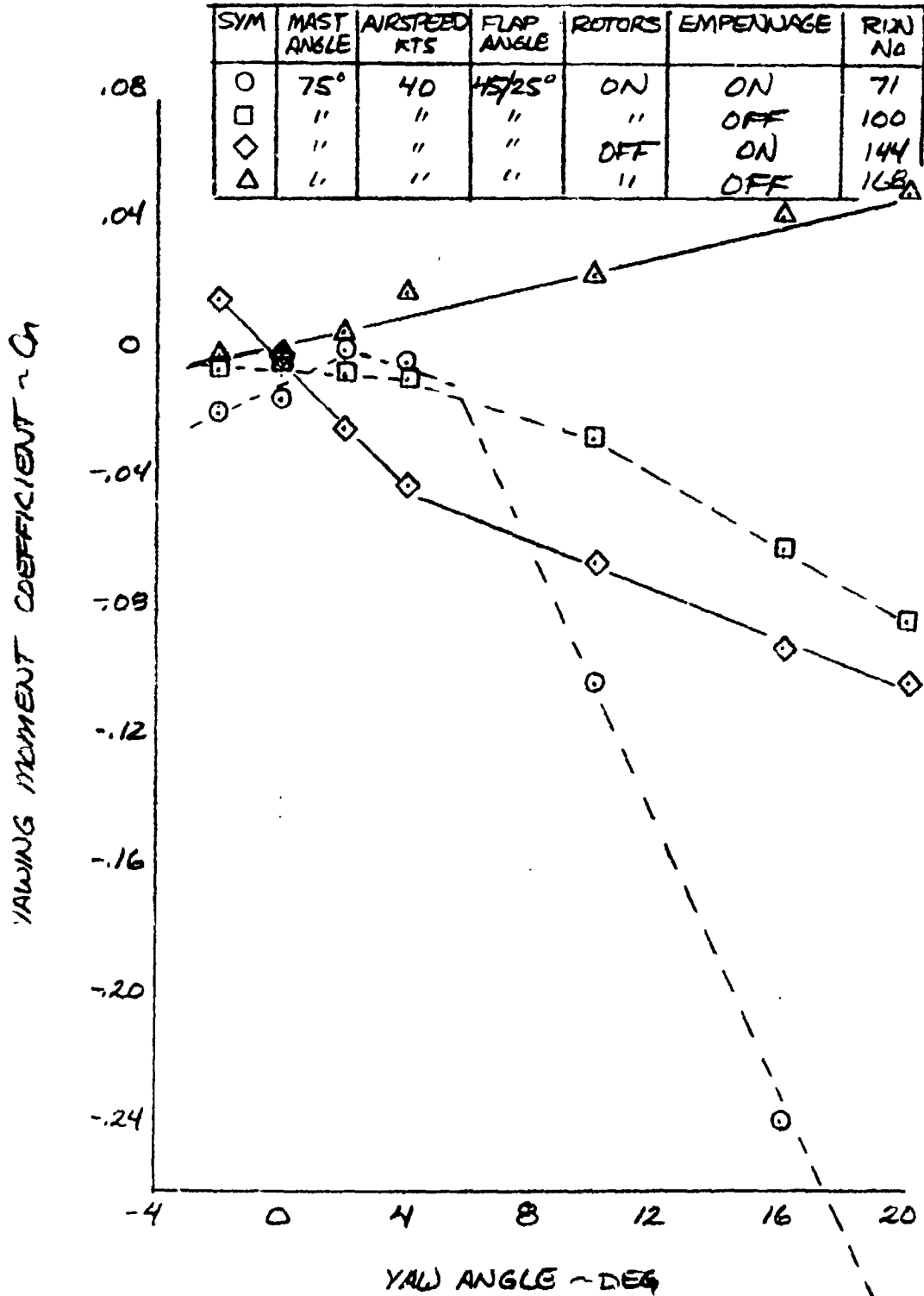


Figure V-57. Yawing Moment Coefficient versus Yaw Angle, Mast Angle 75°, Airspeed 40 knots.

ROTOR AND AIRFRAME YAWING MOMENT

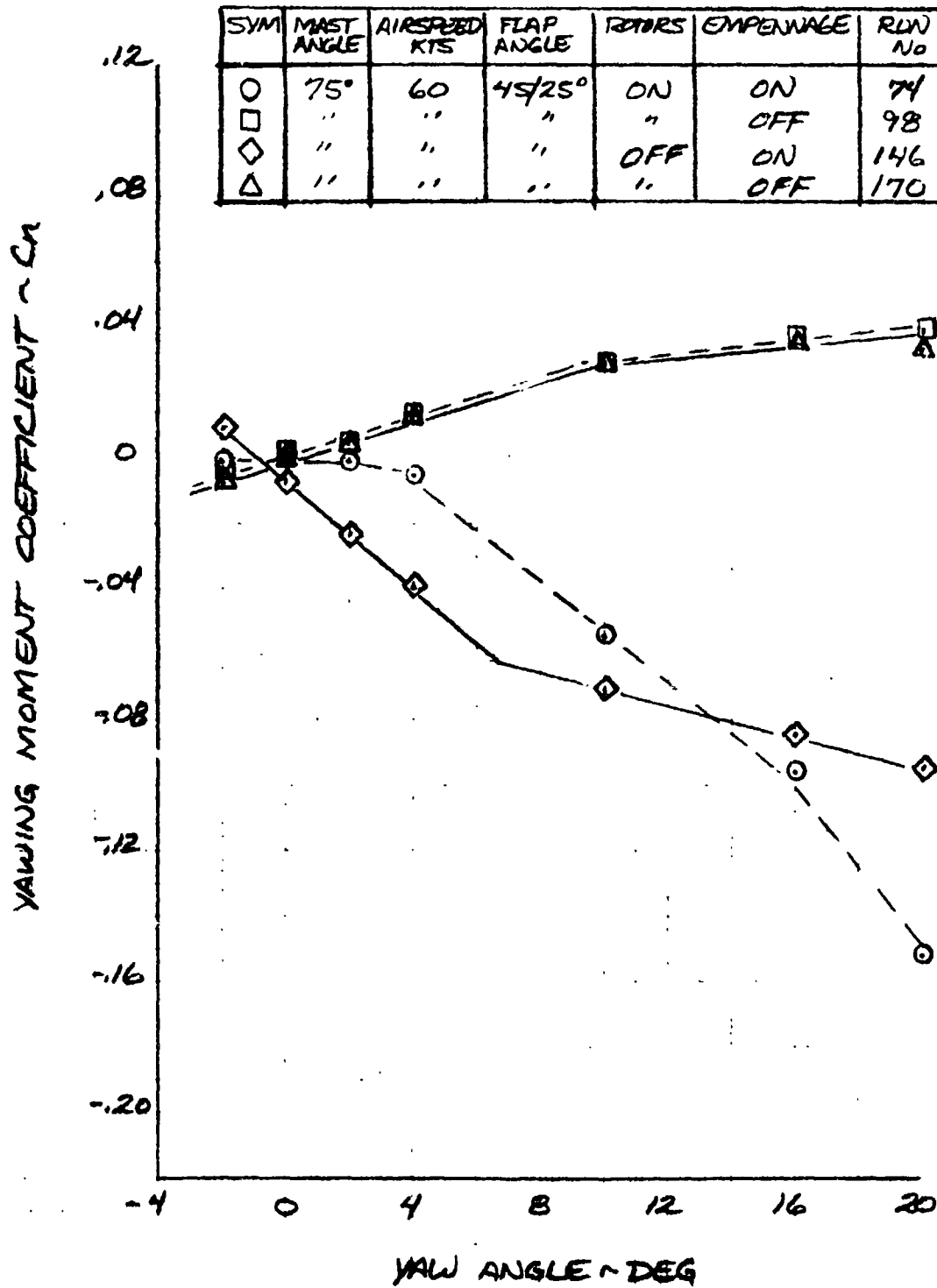


Figure V-58. Yawing Moment versus Yaw Angle, Mast Angle 75°
Airspeed 60 knots.

ROTOR AND AIRFRAME YAWING MOMENT

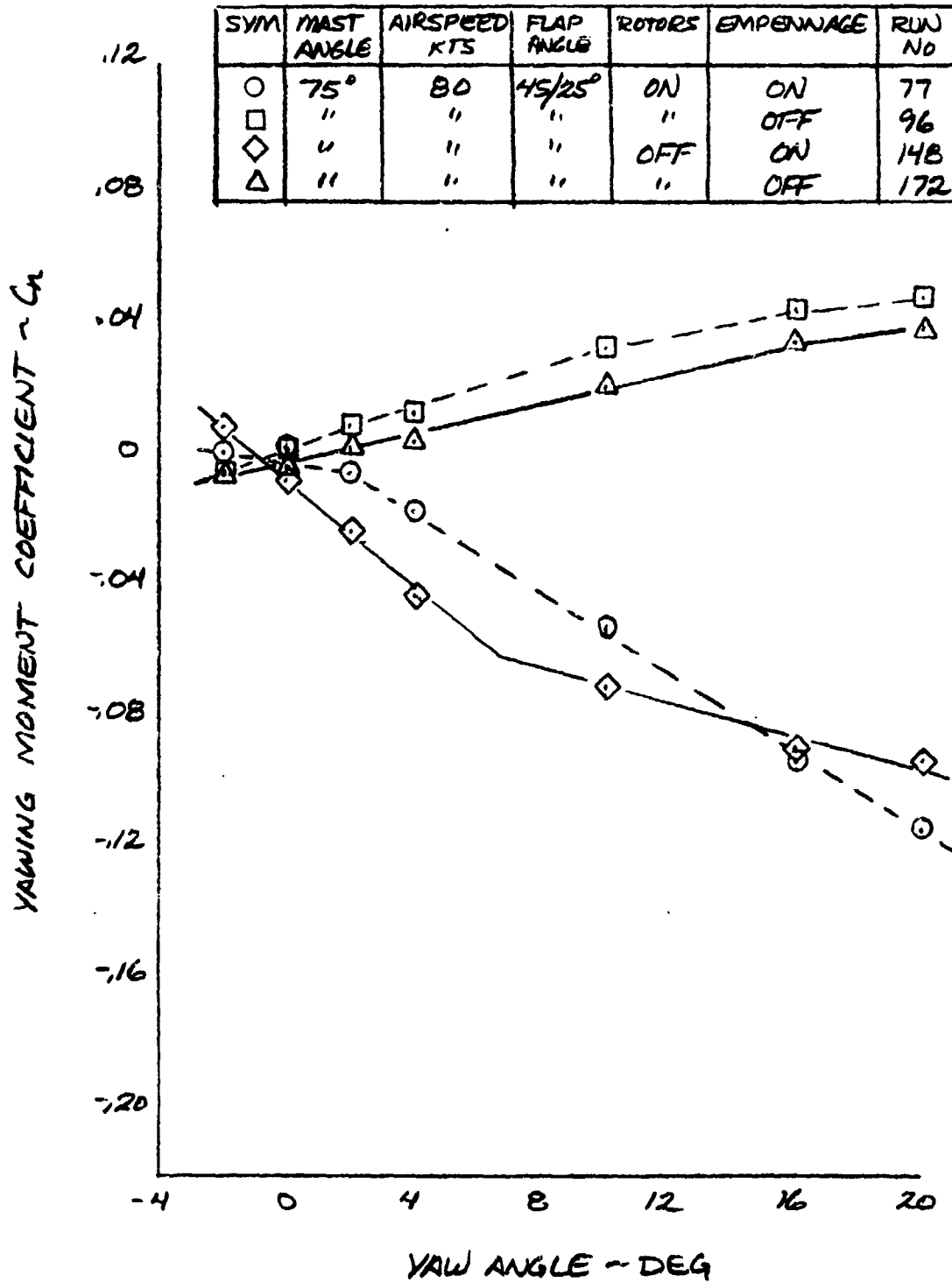


Figure V-59. Yawing Moment Coefficient versus Yaw Angle, Mast Angle 75°, Airspeed 80 knots.

ROTOR AND AIRFRAME LIFT

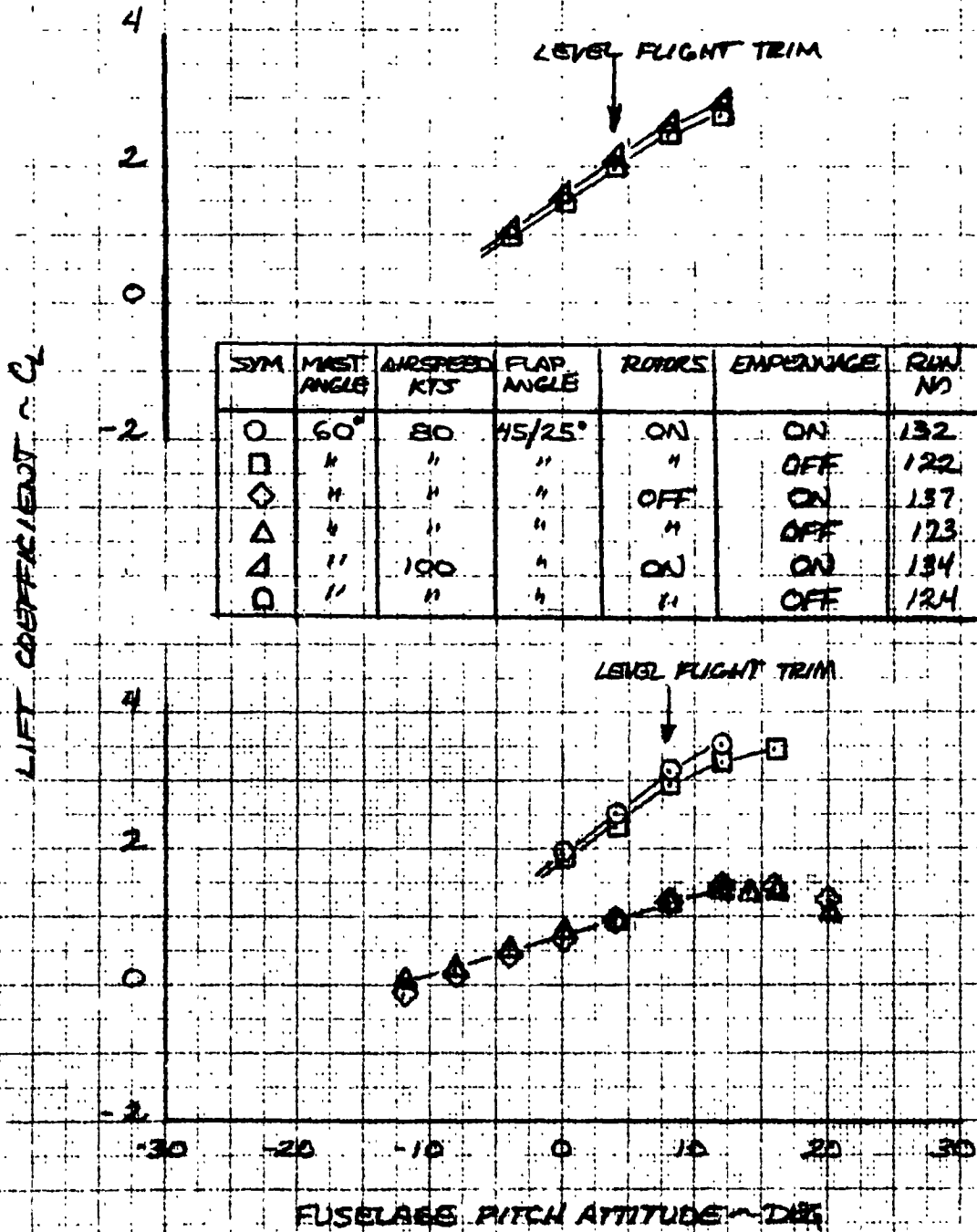


Figure V-60. Lift Coefficient versus Fuselage Angle of Attack, Mast Angle 60°.

ROTOR AND AIRFRAME LIFT

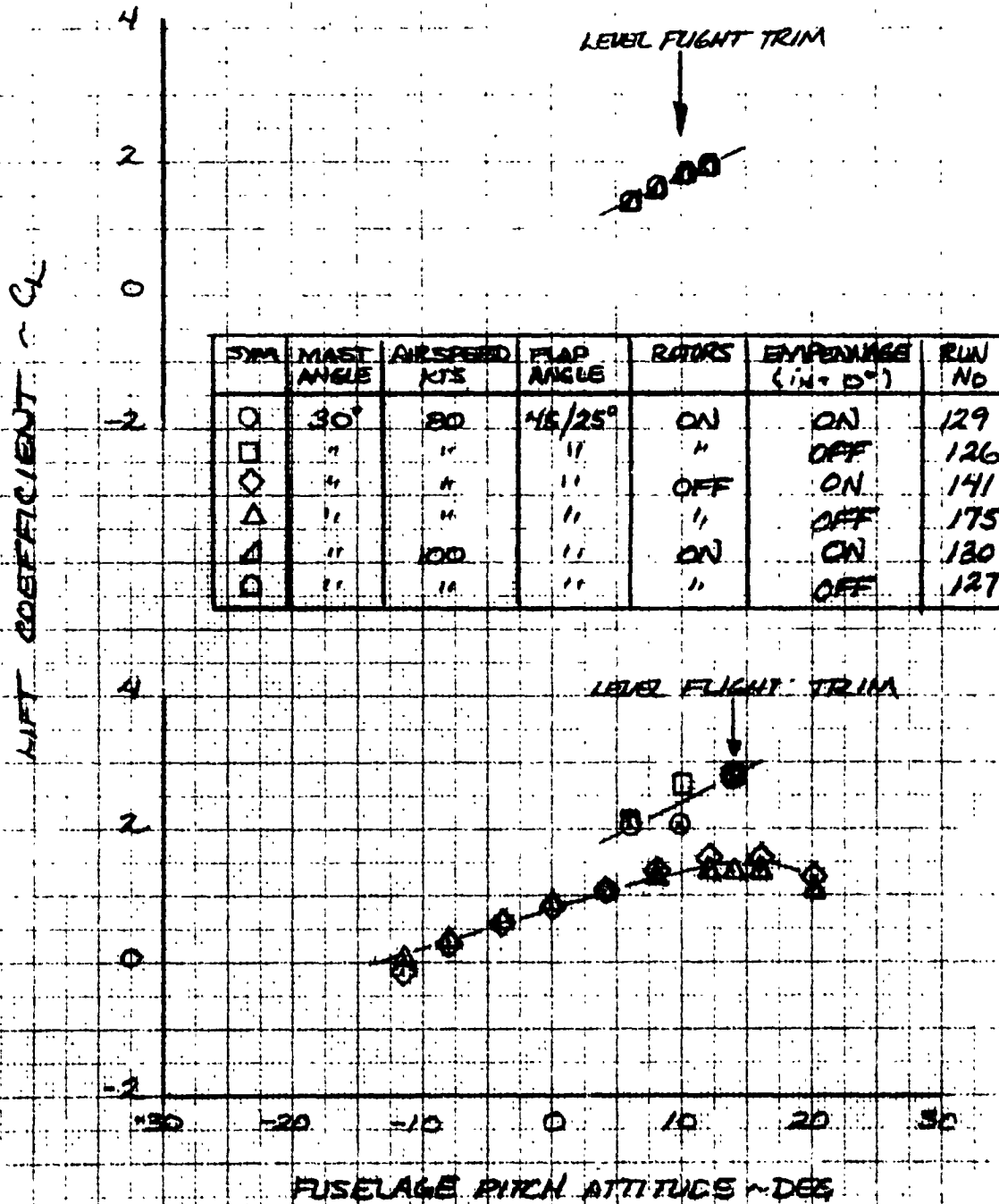


Figure V-61. Lift Coefficient versus Fuselage Angle of Attack, Mast Angle 30°.

ROTOR AND AIRFRAME PITCHING MOMENT

(SEE FIG. -60 FOR SYMBOLS)

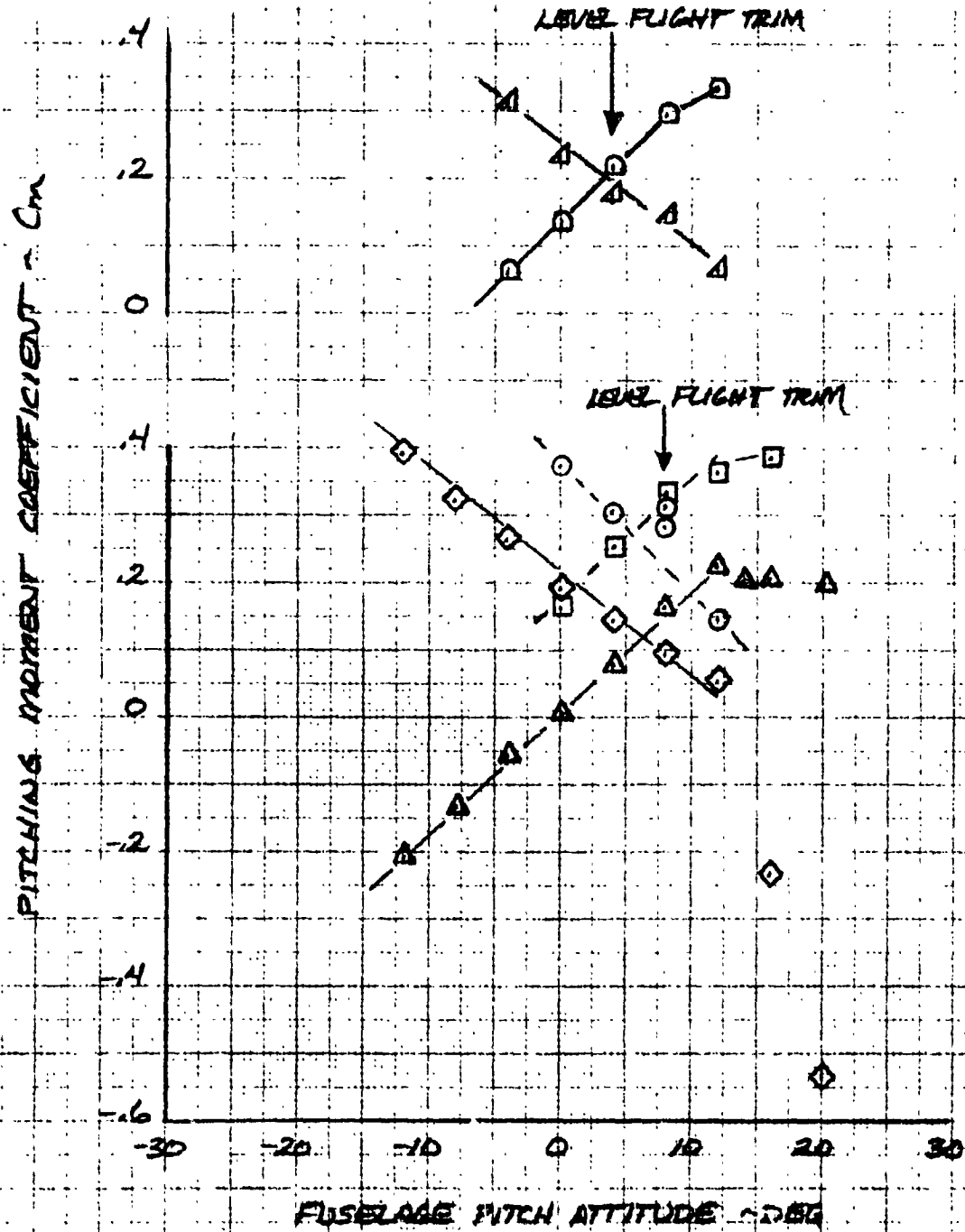


Figure V-62. Pitching Moment versus Fuselage Angle of Attack, Mast Angle 60°.

ROTOR AND AIRFRAME PITCHING MOMENT

(SEE FIG V-61 FOR SYMBOLS)

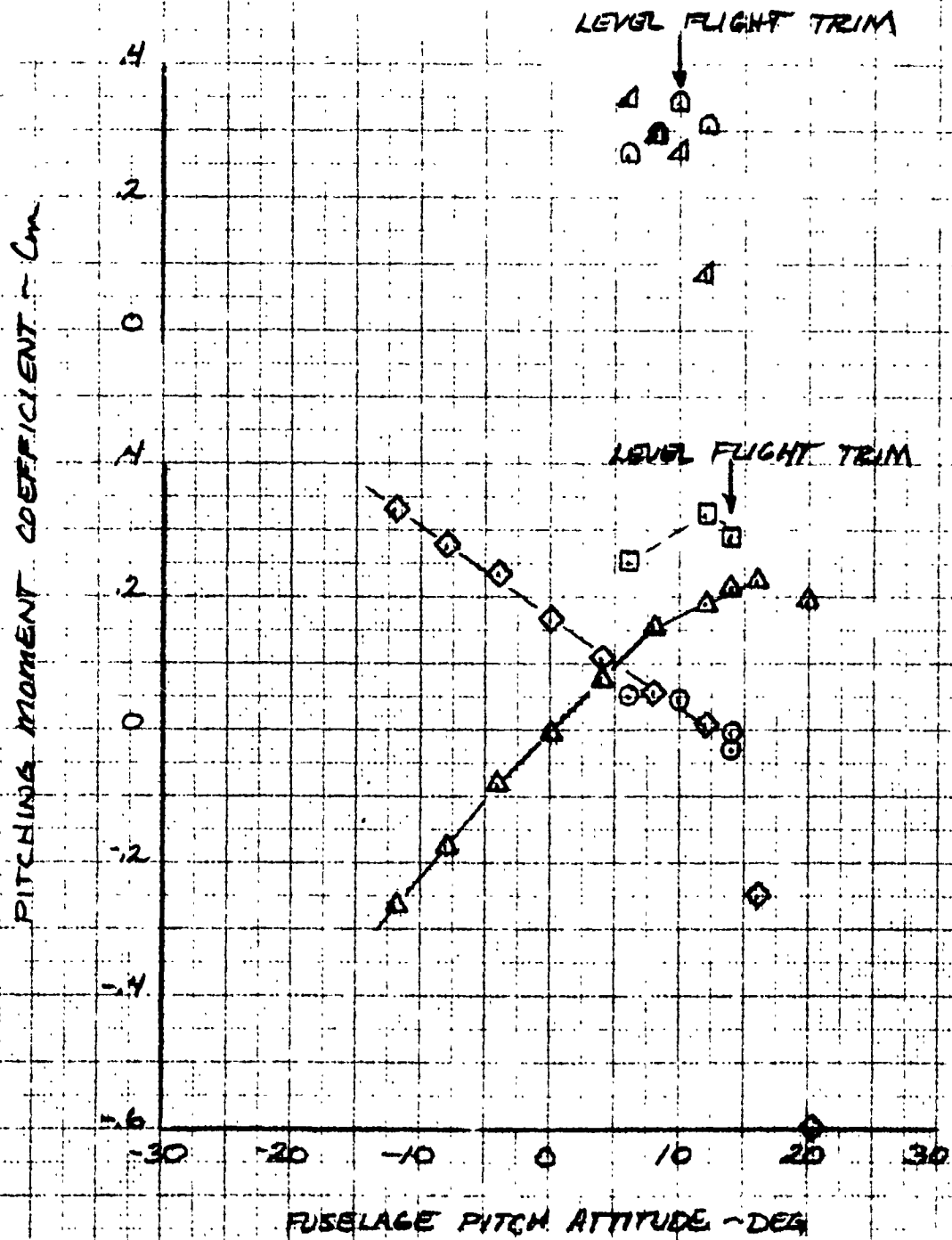


Figure V-63. Pitching Moment versus Fuselage Angle of Attack, Mast Angle 30°.

ROTOR AND AIRFRAME YAWING MOMENT

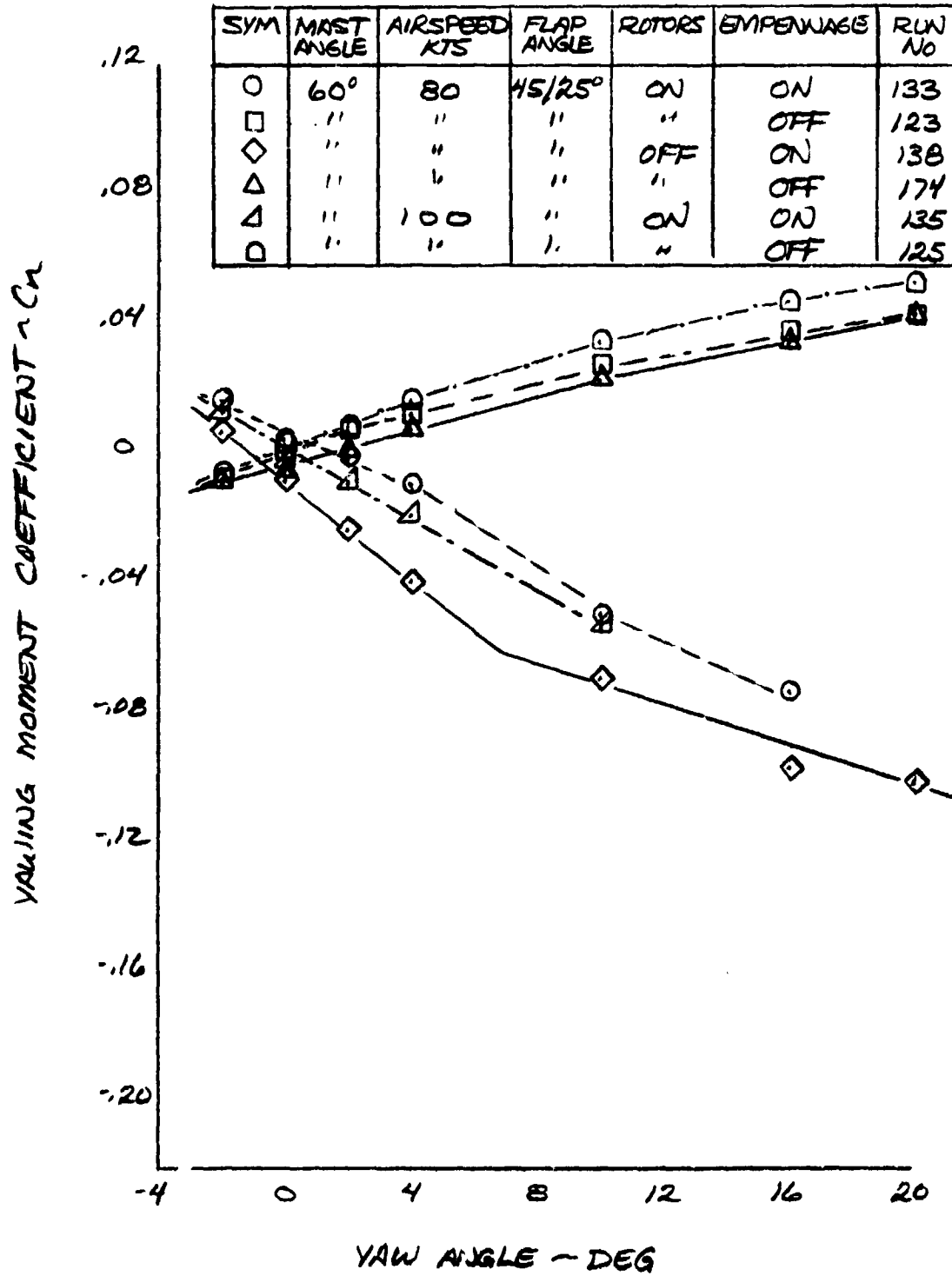


Figure V-64. Yawing Moment Coefficient versus Yaw Angle, Mast Angle 60°.

ROTOR AND AIRFRAME YAWING MOMENT

SYM	MAST ANGLE	AIRSPEED KTS	FLAP ANGLE	ROTBRS	EMPENNAGE	RUN NO
◇	30°	80	45/RS'	OFF	ON	142
△	"	"	"	"	OFF	176
△	"	100	"	ON	ON	131
□	"	"	"	"	OFF	128

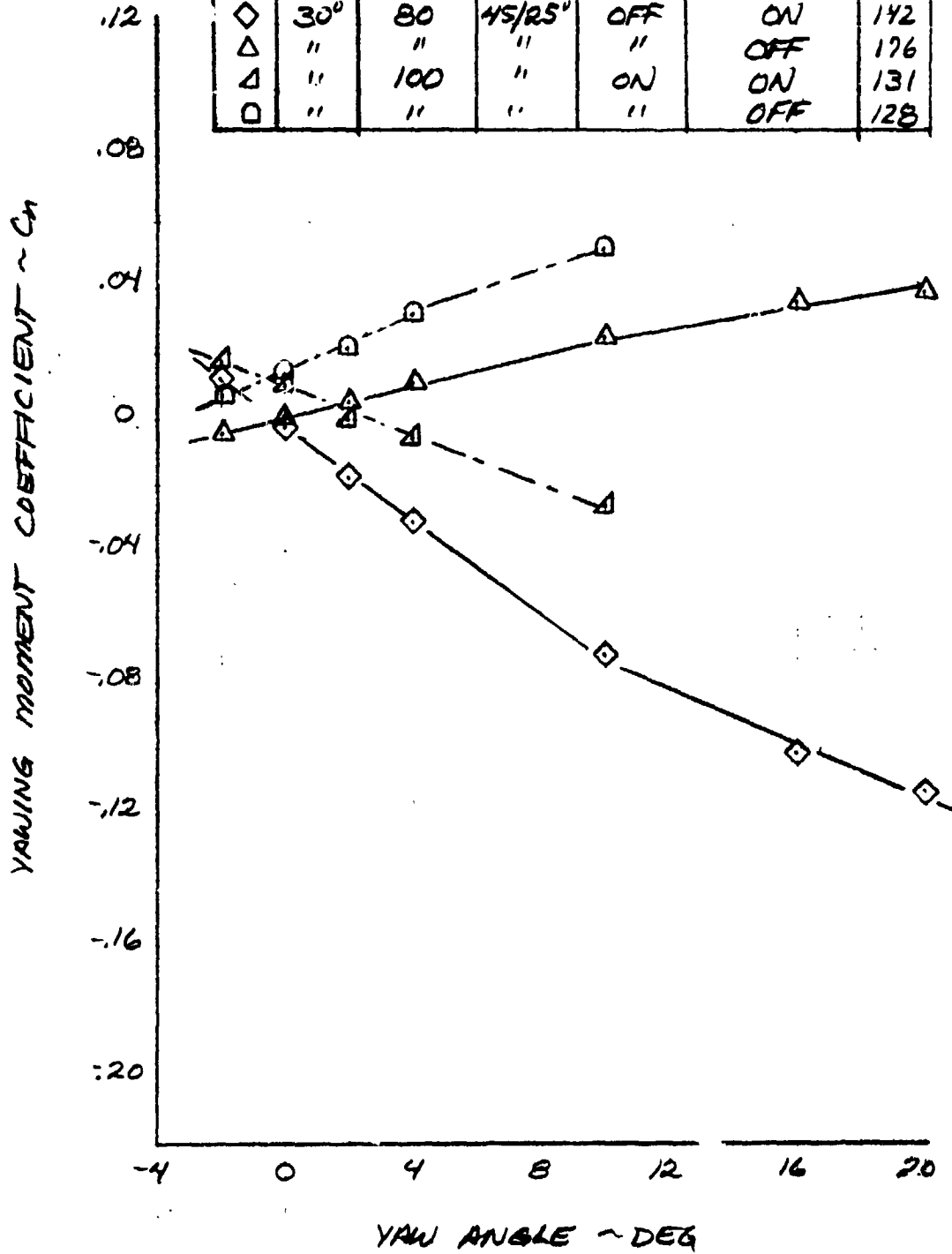


Figure V-65. Yawing Moment versus Yaw Angle, Mast Angle 30°.

VI. ANALYSIS OF RESULTS

The test data have been analyzed to determine qualitatively and quantitatively the effects of the rotor wake on the empennage. The results of this analysis will be used to update the Model 301 flight simulation mathematical model.

An analysis of the discrepancy with regard to predicted and measured flapping was also made and is discussed below.

A. Analysis of Rotor Wake Tuft Grid Patterns and Smoke Observations

A tuft grid measuring 3 by 4 feet and located 6 inches aft of the horizontal stabilizer trailing edge was used to visually observe the rotor wake in the vicinity of the empennage. A camera located downstream of the grid was used to record the tuft patterns. The tuft grid installation was shown in Figure IV-14.

Figures VI-1 and VI-2 have been sketched from photographs of the tuft grid patterns at several airspeeds and attitude conditions. The photographs are presented in Appendix C. The camera was laterally displaced from the center of the grid creating a skewed image of the tufts in the photographs. The sketches in Figures VI-1 and VI-2 have been drawn without the distortion of the patterns as shown in the photographs. In the sketches the flow streamlines represent the direction of flow only and do not indicate magnitude.

The flow at the horizontal stabilizer for 16 and 20 knots, Figure VI-1(a) and (b), was not well defined as the tufts fluctuated considerably. The photographs and sketches at these speeds represent one instant in the fluctuations; hence care must be taken in interpreting them. The net effect of the rotor wake at these speeds appears to be a downwash on the horizontal stabilizer (this was also indicated during smoke studies of the rotor wake). However, the strain gage balance data indicates a net upwash effect on the stabilizer at these speeds.

At speeds above 20 knots the flow became more distinct. The flow patterns at 30 and 40 knots, presented in Figure VI-1(c) and (d), shows the rotors vortices rolled up directly above the horizontal stabilizer. At these speeds the rotor wake has the characteristic of the wake of a low aspect ratio wing with the net effect of an upwash at the horizontal stabilizer. The upwash is probably due more to vortex induced lift than to a physical upwash at the horizontal

A. (Continued)

stabilizer. Analysis of balance data also shows that the effective dynamic pressure at the horizontal stabilizer is up to twice the freestream dynamic pressure.

The tuft grid was not used at speeds higher than 40 knots. Smoke patterns at higher speeds show rotor vortices move downward and outward as speed increases. At 50 knots the vortices were slightly outboard and below the horizontal stabilizer - vertical fin junctions. A net upwash over the span of the horizontal stabilizer, induced by the vortices, was clearly visible. The upwash was evident at speeds up to 100 knots.

Flow patterns at an airspeed of 40 knots and yaw angles of 0 and 10 degrees are compared in Figure VI-2. At 10 degrees right yaw the right rotor vortex core is clear of the empennage while the left rotor vortex core is nearly centered on the horizontal stabilizer. This shift in the position of the vortices with respect to the empennage has two effects:

- (1) The strength of the vortex lift on the horizontal stabilizer is reduced, reducing the upload and producing a nose up pitching moment, and
- (2) for yaw angles between 0 and 12 degrees, directional stability is reduced by the right fin being immersed in the right rotor vortex. At yaw angles greater than 12 degrees the vortex from the left rotor increases the effectiveness of the fins and the directional stability is increased over that of the basic airframe.

Smoke studies showed that the rotor induces a strong upwash on the wing inboard panel even at speeds as low as 20 knots. This is clearly evident in the balance pitching moment data presented in Section V, where wing stall occurs at several degrees lower angle of attack rotors-on than for rotors-off.

B. Determination of Net Effect of Rotor Wake at Empennage

1. Downwash at Horizontal Stabilizer - Rotors Off

The downwash at the horizontal stabilizer was determined using pitching moment data from tail-off, tail-on and incidence ($i_N = 0^\circ$ and $i_H = -4^\circ$) runs to obtain the wake angle. Rotors-off, the wake is the wing downwash ($\epsilon_{W/H}$). The method of obtaining the wing downwash is as follows:

1. (Continued)

Knowing,

$$C_{m_H} = C_{m_{TAIL-ON}} - C_{m_{TAIL-OFF}} \quad (1)$$

$$= -a_H \eta_{H_{WB}} \bar{V}_H \alpha_H \quad (2)$$

$$C_{m_{i_H}} = (C_{m_{i_H} = -4^\circ} - C_{m_{i_H} = 0^\circ}) / -4^\circ \quad (3)$$

$$= -a_H \eta_{H_{WB}} \bar{V}_H \quad (4)$$

$$\text{then, } \alpha_H = C_{m_H} / C_{m_{i_H}} \quad (5)$$

$$= \alpha_F - \epsilon_{W/H} + i_{/H}^{c^\circ} + \tau_e / \delta_e^{o^\circ} \quad (6)$$

$$\text{giving } \epsilon_{W/H} = \alpha_F - \alpha_H \quad (7)$$

The horizontal stabilizer lift curve slope was estimated using the method of USAF Datcom¹⁸ corrected to the model's Reynolds number. The horizontal tail volume (V_H) was obtained from model geometry. Knowing these two parameters the dynamic pressure ratio at the horizontal stabilizer was determined as follows:

$$a_H = .054/\text{degree}$$

$$\bar{V}_H = \frac{S_H l_H}{S_W C_W} = \frac{7.01(4.33)}{7.25(1.05)} = 1.14$$

$$\eta_{H_{WB}} = C_{m_{i_H}} / a_H \bar{V}_H \quad (8)$$

The horizontal stabilizer characteristics (C_{m_H} , $C_{m_{i_H}}$, α_H and $\eta_{H_{WB}}$) and wing downwash ($\epsilon_{W/H}$) for rotors-off, mast angles 90, 75, 60, and 30 degrees are shown in

1. (Continued)

Figures VI-3 through VI-6. The large amount of scatter in $\eta_{H_{WB}}$ is due to the very low test dynamic pressures.

Force model data at higher dynamic pressures do not show as much scatter. Also, the force model data show higher values of $\eta_{H_{WB}}$, indicating the horizontal stabilizer

lift curve slope for the aeroelastic model to be estimated too high. The values shown for $\eta_{H_{WB}}$ should only be

used in conjunction with the lift curve slope noted in the figures.

The rotors-off downwash is used in the current flight simulation mathematical model in computing the total wake. The wing downwash is assumed not to change due to the induced flow of the rotor other than by how the average wing angle of attack changes due to the induced flow of the rotor.

Rotors-off runs were made at the same equivalent airspeeds as for the rotors-on tests. This was to eliminate any differences due to Reynolds number effects.

2. Downwash at Horizontal Stabilizer - Rotors On

The horizontal stabilizer characteristics, rotors-on, are computed similarly to rotors-off except the total wake (ϵ_T) includes the elevator settings for trim.

Elevator effectiveness (τ_e) was obtained from an elevator sweep enabling the total wake angle (ϵ_T) due to the wing and rotor to be determined as follows:

$$C_{m_{H_{ROTOR\text{-ON}}}} = -a_H \eta_{H_T} \bar{V}_H \alpha_H \quad (9)$$

$$C_{m_{i_{H_{ROTOR\text{-ON}}}}} = -a_H \eta_{H_T} \bar{V}_H \quad (10)$$

$$C_{m_{\delta_e_{ROTOR\text{-ON}}}} = -a_H \eta_{H_T} \bar{V}_H \tau_e \quad (11)$$

2. (Continued)

$$\text{therefore, } \tau_e = C_{m_{\delta_e}} / C_{m_{i_H}} \quad (12)$$

$$\alpha_H = C_{m_H} / C_{m_{i_H}} \quad (13)$$

and $\alpha_H = \alpha_F - \epsilon_T + i_H + \tau_e \delta_e$ (14)

giving $\epsilon_T = \alpha_F - \alpha_H + \tau_e \delta_e$ (15)

$$\eta_{H_T} = -C_{m_{i_H}} / a_H \bar{V}_H \quad (16)$$

ROTOR-ON

These values for level flight mast angles 90, 75, 60, and 30 degrees are shown in Figures VI-7 through VI-10. A comparison with the rotors-off values for 80 knots is also shown. The total wake (ϵ_T) indicates an upwash occurring for all mast angles and pitch attitudes tested except for mast angle 30 degrees. Most noticeable is the large increase in dynamic pressure ratio at the tail (η_{H_T}) at low speeds for mast angles of 90 and 75 degrees. (This term was omitted for mast angles of 60 and 30 degrees since incidence sweeps were not made at these mast angles.)

The slope of the total wake with angle of attack ($\partial \epsilon_T / \partial \alpha_F$) is an indication of the level of aircraft static stability. The steeper the slope the less stable the aircraft. This is obtained from the following equation.

$$C_{m_\alpha} = C_{m_\alpha \text{TAIL-OFF}} + C_{m_\alpha H} \quad (17)$$

Since static stability (C_{m_α}) is proportional to the horizontal stabilizer $C_{m_\alpha H}$, and

$$C_{m_\alpha H} = -c_H \eta_{H_T} \bar{V}_H \left(1 - \frac{\partial \epsilon_T}{\partial \alpha_F} \right) \quad (18)$$

2. (Continued)

Therefore, the greater $\partial \epsilon_T / \partial \alpha_F$ the smaller the contribution of the horizontal stabilizer to static stability. As shown in Figure VI-7 for 40 knots this slope is greater than 1.0 at negative pitch attitudes and almost 0.0 at positive attitudes, i.e., the model is unstable at negative attitudes and stable at positive attitudes. At 60 and 80 knots the slope of the wake about trim pitch attitude is less than for rotors-off showing the model to be more stable rotors-on than for rotors-off.

The total wake angle (ϵ_T) at the horizontal stabilizer is made up of the wing downwash ($\epsilon_{W/H}$) and rotor wake ($\epsilon_{R/H}$). The rotor wake angle was computed using the following equations:

$$\epsilon_T = \epsilon_{W/H} + \epsilon_{R/H} \quad (19)$$

therefore,

$$\epsilon_{R/H} = \epsilon_{W/H} - \epsilon_T \quad (20)$$

The magnitude of the rotor upwash contribution was determined as follows:

$$K_{R/H} V_{iR} = V_\infty \tan \epsilon_{R/H} \quad (21)$$

Where the term V_{iR} is the rotor induced velocity at the rotor disk. The $K_{R/H}$ term is that used in the current math model to include the rotor wake at the horizontal. This parameter is given in Figures VI-11 through VI-15 for the various mast angles, airspeeds, and flight conditions tested.

It should be noted that the term $K_{R/H} V_{iR}$ is merely a convenient way to represent the rotor wake effects on the horizontal stabilizer and does not represent the actual upwash or downwash from the rotor. This is illustrated by the fact that by taking the vector sum of the freestream velocity and the rotor induced velocity factor ($K_{R/H} V_{iR}$) does not give the total velocity indicated by the measured horizontal stabilizer efficiency (Figures VI-7 and -8). Furthermore the variation of $K_{R/H} V_{iR}$ with airspeed shown in Figures VI-11 through -15 implies the rotor induced velocity increases with airspeed which is opposite to the momentum theory of rotor induced velocity. These differences are believed to be the result of vortex induced lift. However, combining the η_H and $K_{R/H} V_{iR}$ in the math model does give the correct empennage lift.

2. (Continued)

The rotor wake at the horizontal stabilizer measured in this test is compared to that used in the Phase I flight simulation in Figure VI-16. It should be noted that in the Phase I simulation η_T was assumed equal to 1.0 and the downwash/upwash was assumed invariant with angle of attack.

3. Effect of Yaw on Downwash at Horizontal Stabilizer

As the aircraft yaws the net rotor wake effect on the horizontal changes from an upwash to downwash causing a pitch-up with yaw. The rotor wake velocity is shown in Figure VI-17 through VI-19 to illustrate the change in the magnitude of the rotor wake with yaw angle. This effect was evaluated during the rod test and found to require only a small amount of longitudinal cyclic to maintain pitch attitude with yaw.

4. Effect of Rotor Wake on Vertical Stabilizer Characteristics

Rotor wake effects on the vertical stabilizer were evaluated in terms of a parameter defined as the rotor side-wash factor (K_β). This is the ratio of the vertical stabilizer yawing moment rotors-on to rotors-off and is determined as follows:

$$\text{Knowing, } C_{n_V} = C_{n_{\text{TAIL-ON}}} - C_{n_{\text{TAIL-OFF}}} \quad (22)$$

$$C_{n_V \text{ ROTORS-OFF}} = a_V \bar{V} \eta_{WB} (1 - \partial\sigma/\partial\beta)_{\text{OFF}} \beta \quad (23)$$

$$C_{n_V \text{ ROTORS-ON}} = a_V \bar{V}_V \eta_T (1 - \partial\sigma/\partial\beta)_{\text{ON}} \beta \quad (24)$$

therefore,

$$K_\beta = \frac{C_{n_V \text{ ROTORS-ON}}}{C_{n_V \text{ ROTORS-OFF}}} \quad (25)$$

$$\frac{\eta_T (1 - \partial\sigma/\partial\beta)_{\text{ON}}}{\eta_{WB} (1 - \partial\sigma/\partial\beta)_{\text{OFF}}} \quad (26)$$

4. (Continued)

This term is shown in Figure VI-20 through VI-22 for the various airspeeds and mast angles tested. The rotor wake is destabilizing for yaw angles of ± 4 degrees at low speeds for mast angles 90 and 75 degrees. Above twelve degrees yaw the rotors-on yawing moment exceeds that of the rotors-off. This effect also exists at mast angles of 60 and 30 degrees, although to a lesser degree. The directional stability is decreased for up to about four degrees of yaw and then increases as yaw angle increases. However, the yawing moment coefficient rotors-on did not exceed that of rotors-off.

5. Empennage Lift Characteristics

Empennage lift, rotors-on, is compared with lift rotors-off in Figures VI-23 through VI-26. Empennage lift is in general higher than that for rotors-off, reflecting; the net upwash effect of the rotors on the horizontal stabilizer. The decreasing difference between the rotors on and off lift with increasing speed reflects the fact that the rotor wake effects become less significant at the higher speeds.

C. Analysis of Discrepancy Between Measured and Calculated lateral Flapping

At mast angles 90 and 75 degrees the measured lateral flapping was found to be approximately 40 percent greater than that predicted prior to the test. Figure VI-27 compares the measured and predicted flapping. Several possible reasons for this discrepancy were theorized including aerodynamic interference between the wing and the rotor. (This was resolved by removing the wing fairings and flying the model at the same trim condition. Flapping was not changed.) However, smoke studies of the rotor induced flow indicated that the longitudinal distribution of induced velocity was considerably different than that used in the theory. It was therefore concluded that the theory used to predict lateral flapping was deficient with regard to the math model of the rotor induced velocity.

1. Induced Velocity Representation Used in Pretest Predictions

Program C81 was used to predict blade flapping prior to the test. In hover C81 uses a triangular distribution of induced velocity such that

$$v_i = \frac{4}{3} \times \bar{v}$$

1. (Continued)

where \bar{V}_i is the local spanwise induced velocity, χ is the nondimensional blade radius, r/R , and \bar{V} is the average induced velocity. For forward flight the triangular distribution is modified to increase the induced velocity at the rear of the disc ($\psi = 0^\circ$) and reduce it at the front of the disc ($\psi = 180^\circ$) as suggested in Reference 19. The downwash distribution is then assumed equal to

$$V_i = \frac{4}{3} \chi (1 + K \cos \psi) \bar{V}$$

where K has the following values

μ	K
$0 < \mu < .1067$	11.25μ
$.1067 < \mu < .5733$	$1.36-1.5 \mu$
$\mu \geq .5733$	0.5

These values for K were derived for low disc loading, low twist rotors²⁰ and have provided reasonable correlation with such rotors. By modifying the value of K arbitrarily to reflect the higher disc loading, high twist, tilt rotor, good correlation with the test data can be achieved. Figure VI-28 compares the original longitudinal distribution of induced velocity with one obtained by modifying the value of K to achieve correlation. Also shown is the approximate shape of the longitudinal distribution observed during smoke studies of the rotor wake. The very high value of induced velocity at the trailing edge of the disc is probably due to roll up of the rotor wake.

2. Investigation of More Advanced Methods of Predicting Lateral Flapping

The significant difference between the computed and observed distribution of induced velocity indicated a better method of predicting the distribution is needed. Therefore, an investigation into more advanced means of predicting the distribution was made.

A recent study of Harris, Reference 21, indicates the problem of predicting lateral flapping accurately is not confined to high disk loading tilt rotors. In Reference 21 a comparison is made between the lateral flapping

2. (Continued)

predicted by several induced velocity theories with that measured with a low disc loading model rotor. The trend of the measured flapping with advance ratio was similar to that measured in this test and the maximum lateral flapping occurred at nearly the same advance ratio ($\mu = .08$ compared to $.091$). Harris compared downwash theories ranging from uniform downwash to prescribed helical wakes. In no case did the predicted flapping exceed 70 percent of the measured flapping. Several theories, specifically that of Castles and DeLeeuw, Reference 22, and Heyson and Katzoff, Reference 23, predicted the correct trend with advance ratio but were off in magnitude by as much as 50 percent.

A comparison between lateral flapping predicted using various induced velocity theories, including those investigated by Harris is given in Table VI-I for mast angle 90 degrees, airspeed 40 knots (the speed for maximum lateral flapping). Castles and DeLeeuw's and Heyson and Katzoff's theories predict 57 percent and 67 percent of the measured lateral flapping respectively. Both are based on a prescribed wake geometry with Castles theory being for a uniform disc loading and Heyson's accounting for the nonuniformity of the loading. The distribution of induced velocity predicted using Heyson and Katzoff's method is very close to that observed in the test but the magnitude is too low. Also shown in Table VI-I is the flapping predicted by Bell computer program BRAM, Reference 24, which has a free trailing tip vortex. This accounts to some extent for the roll up of the wake but neglects the nonuniformity of the blade loading. BRAM comes closest to predicting the measured lateral flapping.

3. Prediction of Lateral Flapping For Design Purposes

Although none of the more advanced induced velocity theories satisfactorily predicts the lateral flapping, a method is available for design purposes. As noted earlier, by arbitrarily modifying the factor K used in the present C81 induced velocity representation to distribute the induced velocity longitudinally, good correlation with the measured flapping can be achieved. Figures VI-29 through VI-32 compare the flapping predicted using the modified value of K with the measured values. Correlation is good at all mast angles.

While this approach is not sophisticated it does achieve the basic objective of predicting the lateral flapping and is felt to be acceptable for design purposes. This method has the advantage of using a minimum of computer time whereas a free wake analysis such as BRAM requires a large computer run time.

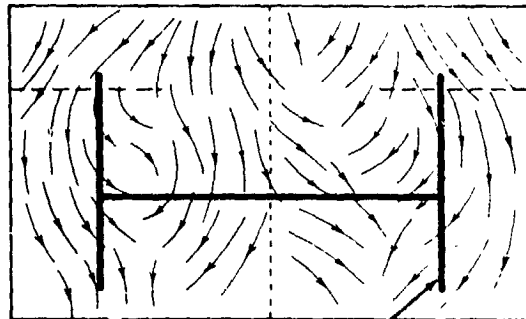
TABLE VI-1. COMPARISON OF LATERAL FLAPPING CALCULATED USING
SEVERAL THEORIES WITH MEASURED LATERAL FLAPPING

Flight Condition $\alpha_m = 90^\circ$, GW = 11,000 LB, 40 Knots
Measured b_1 Flapping = 6 Degrees¹

Theory	b_1 Flapping	% Of Measured
Pretest (Drees)	4.1°	68%
Post Test (Drees) ²	6.0°	100%
Castles and DeLeeuw	3.3°	57%
Heyson and Katzoff	4.0°	67%
BRAM (Free Vortex)	5.0°	83%

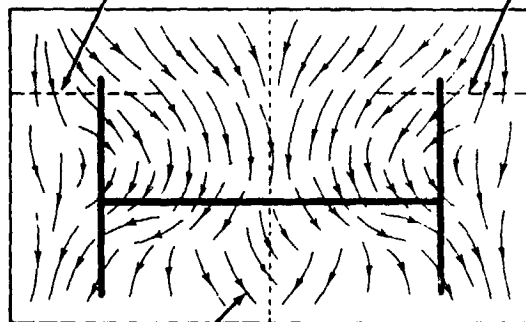
1. Based on line faired through test data.
2. Longitudinal distribution factor adjusted to achieve correlation.

VIEW LOOKING FORWARD FROM
AFT OF EMPENNAGE



(a) AIRSPEED = 16 KNOTS
 $\alpha = \gamma = 0^\circ$
RPM = 1260

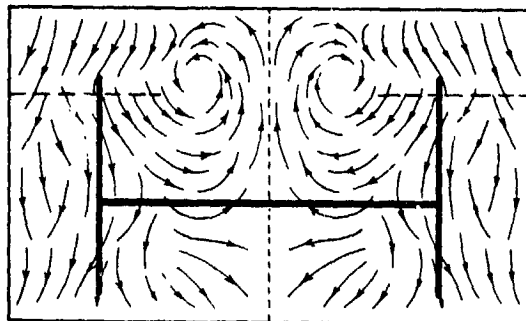
LEFT ROTOR EMPENNAGE RIGHT ROTOR



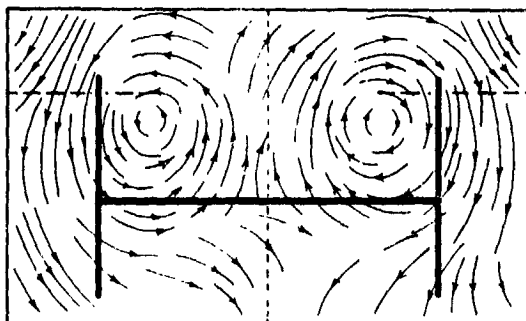
(b) AIRSPEED = 20 KNOTS
 $\alpha = \gamma = 0^\circ$
RPM = 1260

FLOW STREAMLINES

TUFT GRID



(c) AIRSPEED = 30 KNOTS
 $\alpha = \gamma = 0^\circ$
RPM = 1260



(d) AIRSPEED = 40 KNOTS
 $\alpha = -2^\circ, \gamma = 0^\circ$
RPM = 1260

Figure VI-1. Flow Patterns in the Vicinity of the Empennage
in Level Flight, Mast Angle 90° .

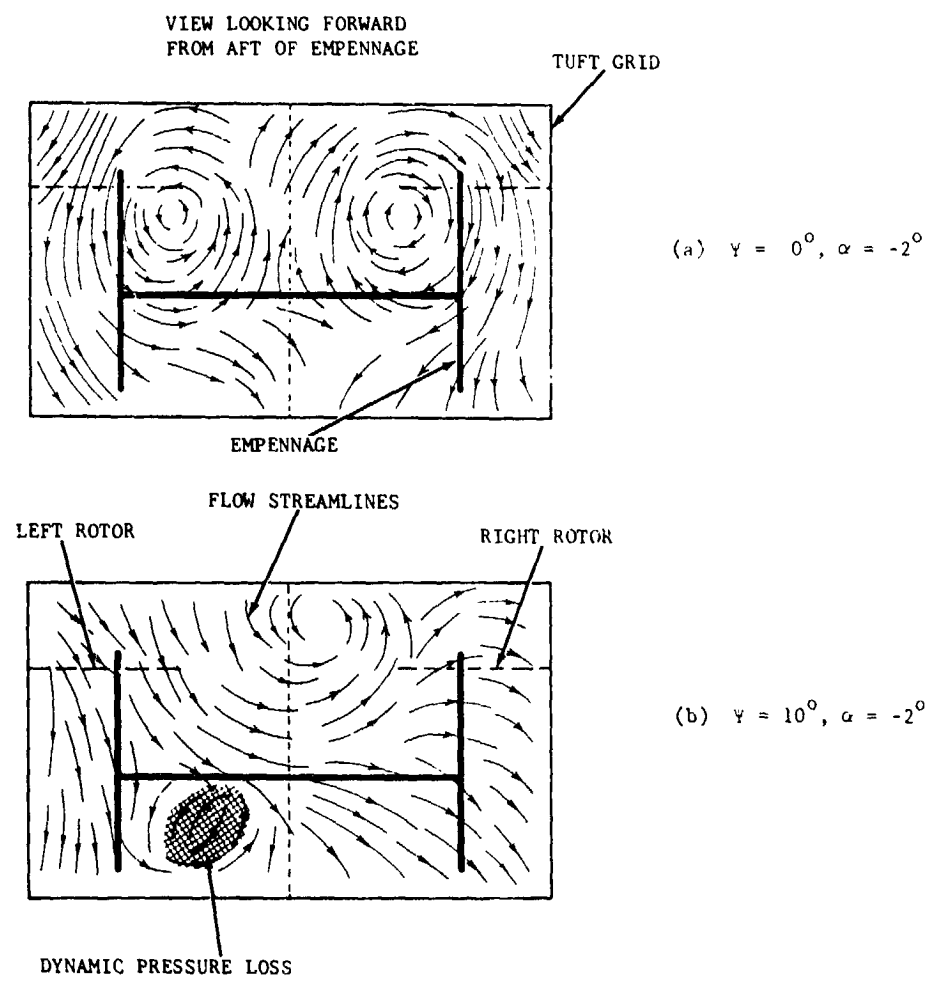


Figure VI-2. Effect of Yaw Angle on Flow Pattern,
Mast Angle 90° , Airspeed 40 Knots.

HORIZONTAL STABILIZER CHARACTERISTICS

- 40 KTS
- 60 KTS
- ◇ 80 KTS

MAST = 90°
FLAPS = 45/25°

ROTORS OFF

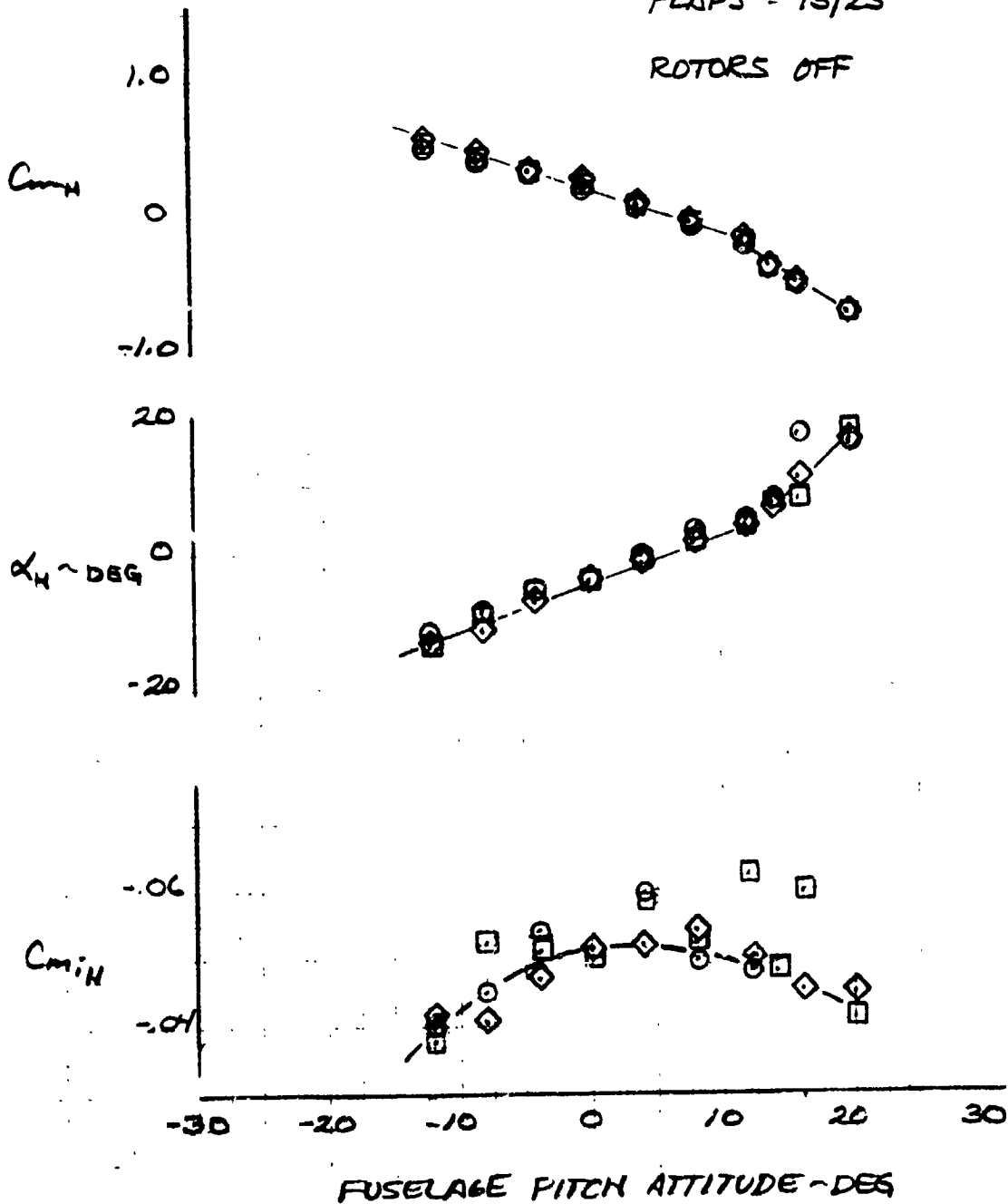


Figure VI-3. Horizontal Stabilizer Aerodynamic Characteristics, Mast Angle 90°, Rotors off.

HORIZONTAL STABILIZER DOWNWASH

- 40 KTS
- 60 KTS
- △ 80 KTS

MAST = 90°
FLAPS = 45/25°

ROTORS OFF

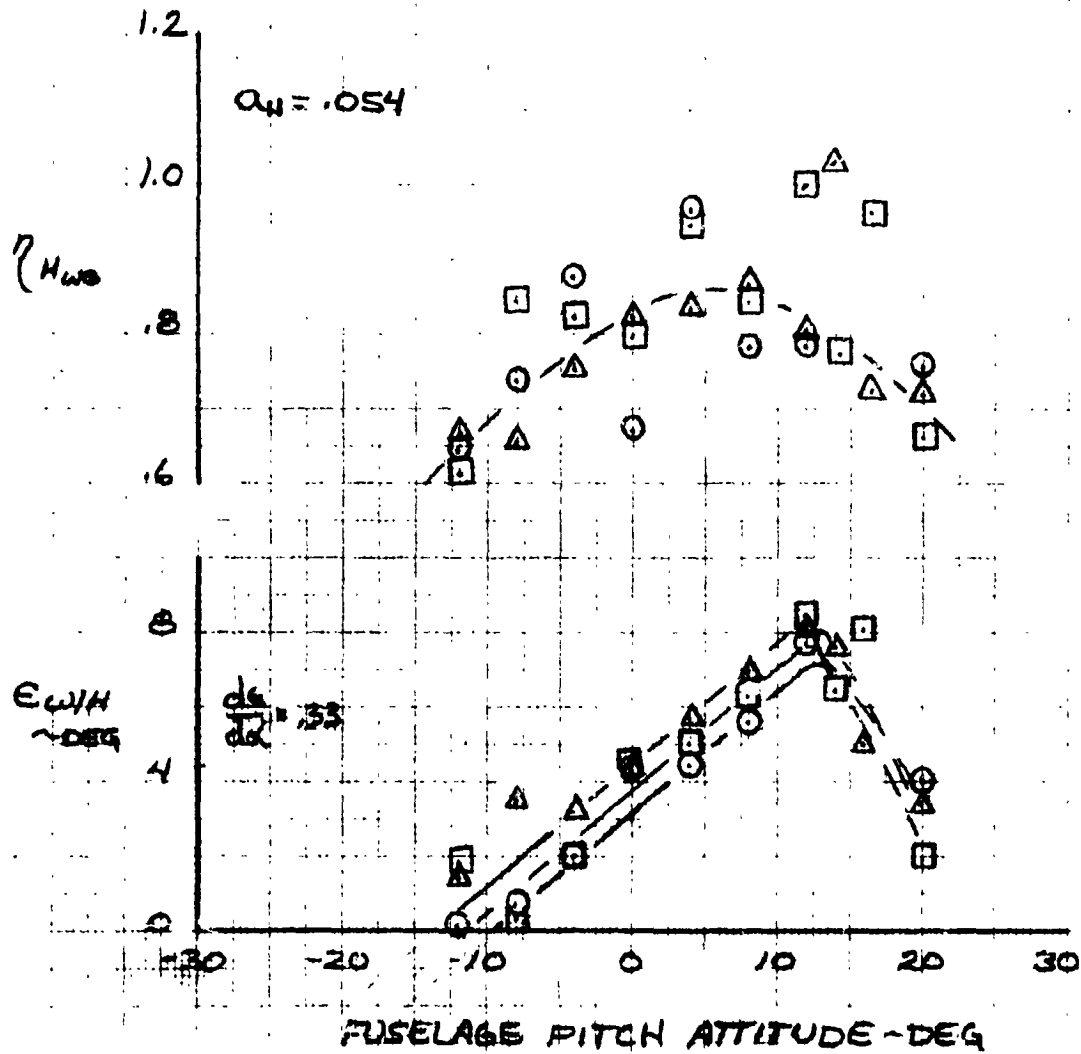


Figure VI-3. Concluded

HORIZONTAL STABILIZER CHARACTERISTICS

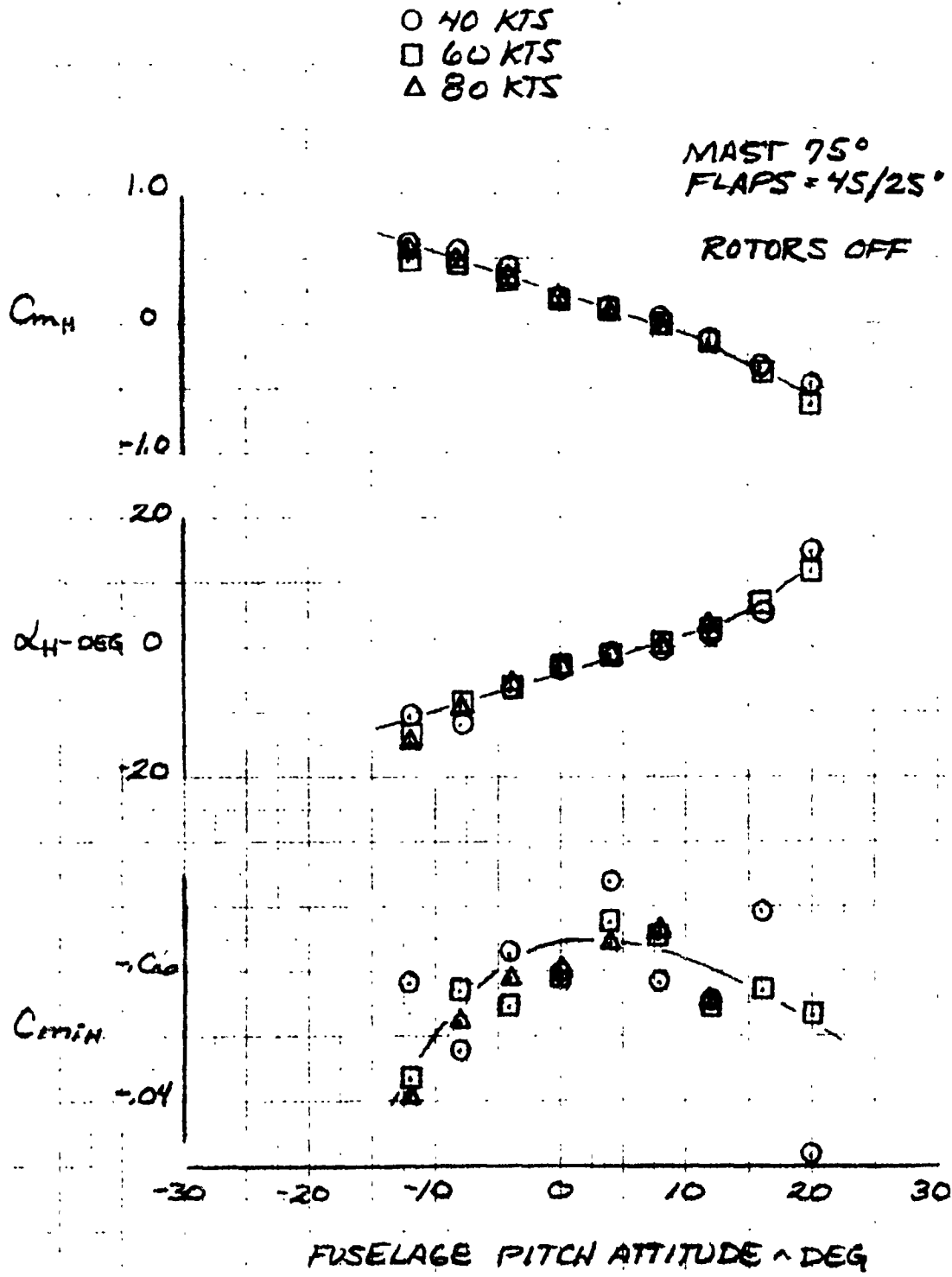


Figure VI-4. Horizontal Stabilizer Aerodynamic Characteristics, Mast Angle 75°, Rotors off.

HORIZONTAL STABILIZER DOWNWASH

- 40 KTS
- 60 KTS
- △ 80 KTS

MAST = 75°
FLAPS = 45/25°

ROTORS OFF

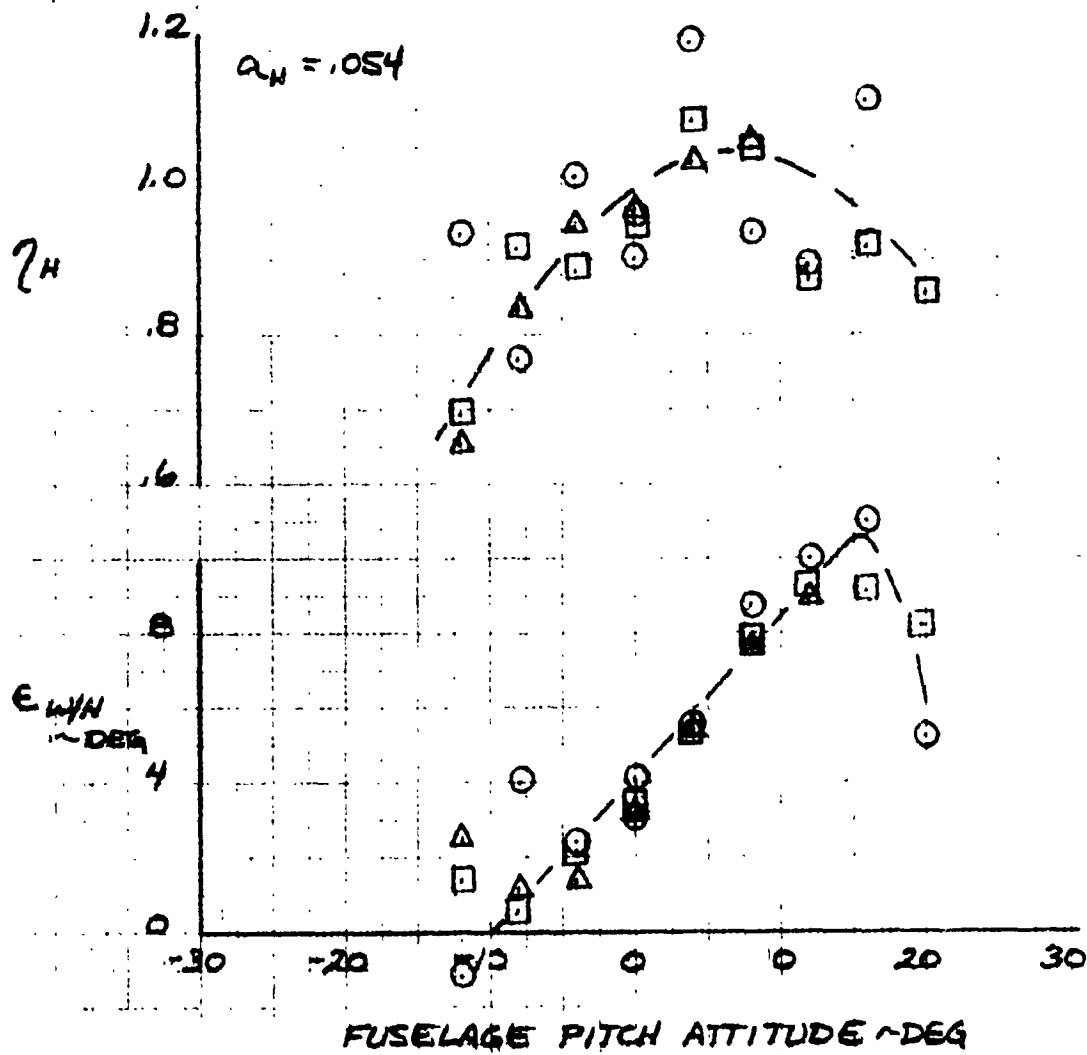


Figure VI-4. Concluded

HORIZONTAL STABILIZER CHARACTERISTICS

MAST = 60°
 FLAPS = 45/25°

ROTORS OFF
 V = 80 KTS

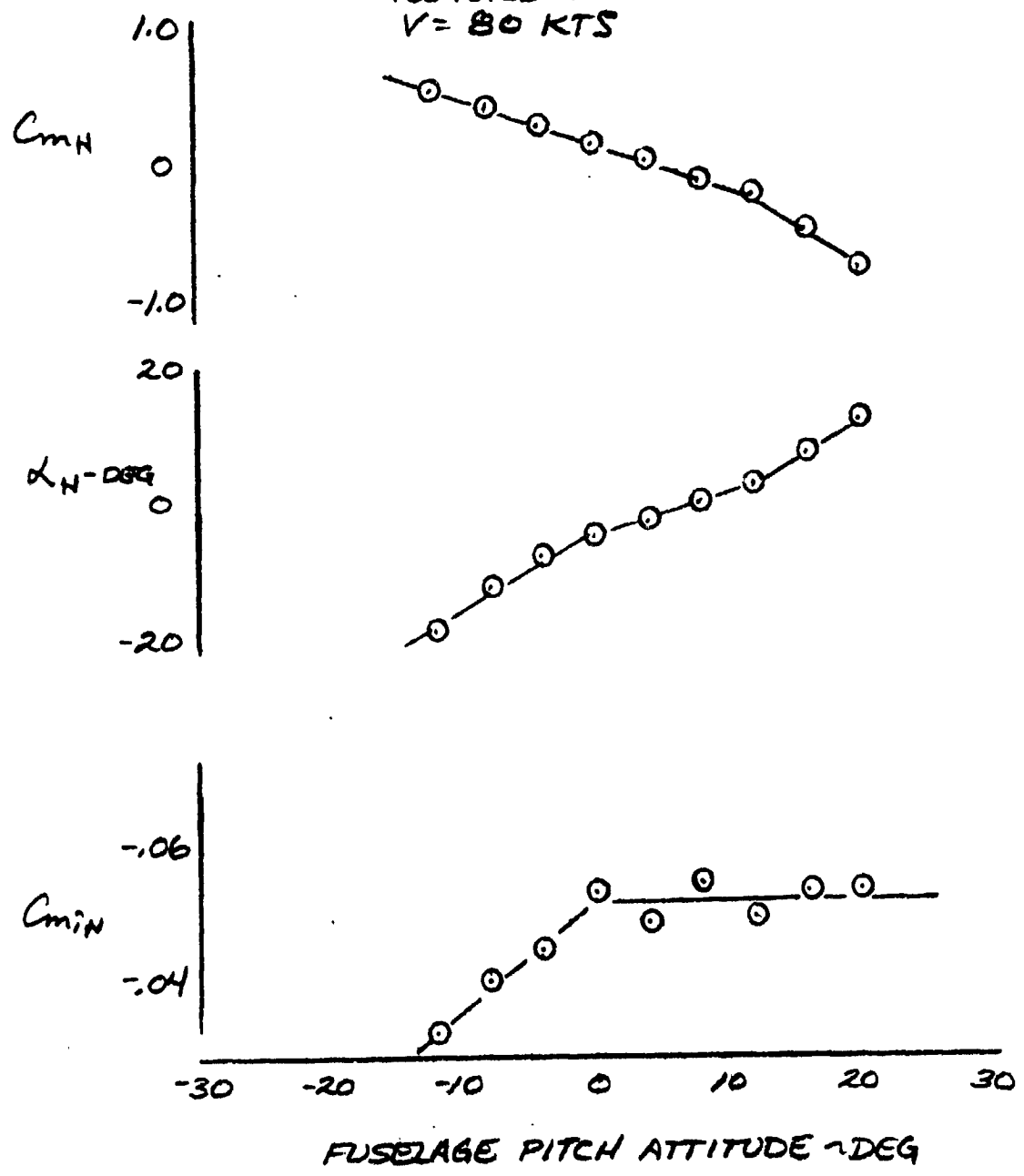


Figure VI-5. Horizontal Stabilizer Aerodynamic Characteristics, Mast Angle 60°, Rotors off.

HORIZONTAL STABILIZER DOWNWASH

MAST = 60°
FLAPS = 45/25°

ROTORS OFF
V = 80 KTS

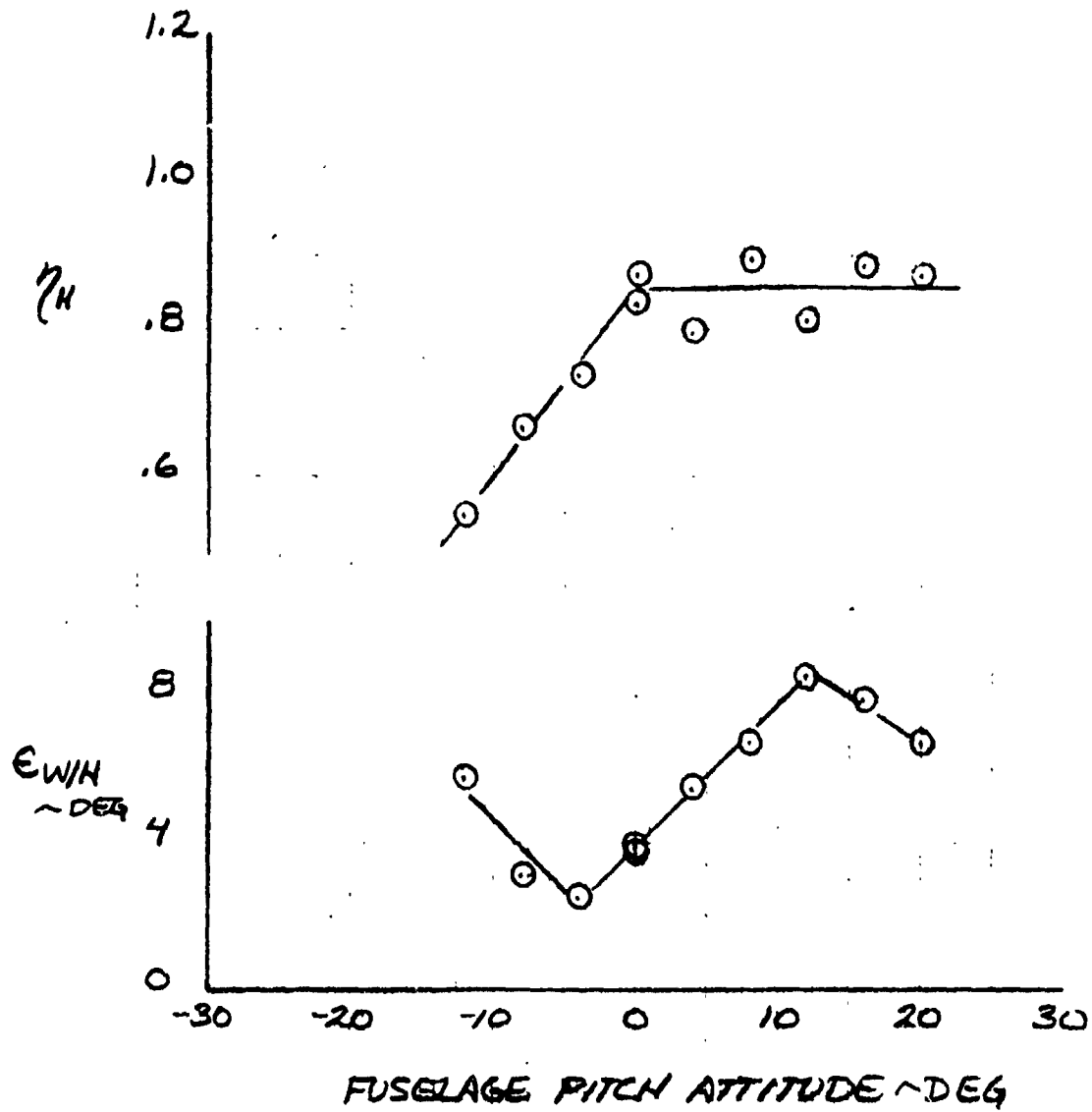


Figure VI-5. Concluded

HORIZONTAL STABILIZER CHARACTERISTICS

MAST = 30°
FLAPS = 45/25°

ROTORS OFF
V = 80 KTS

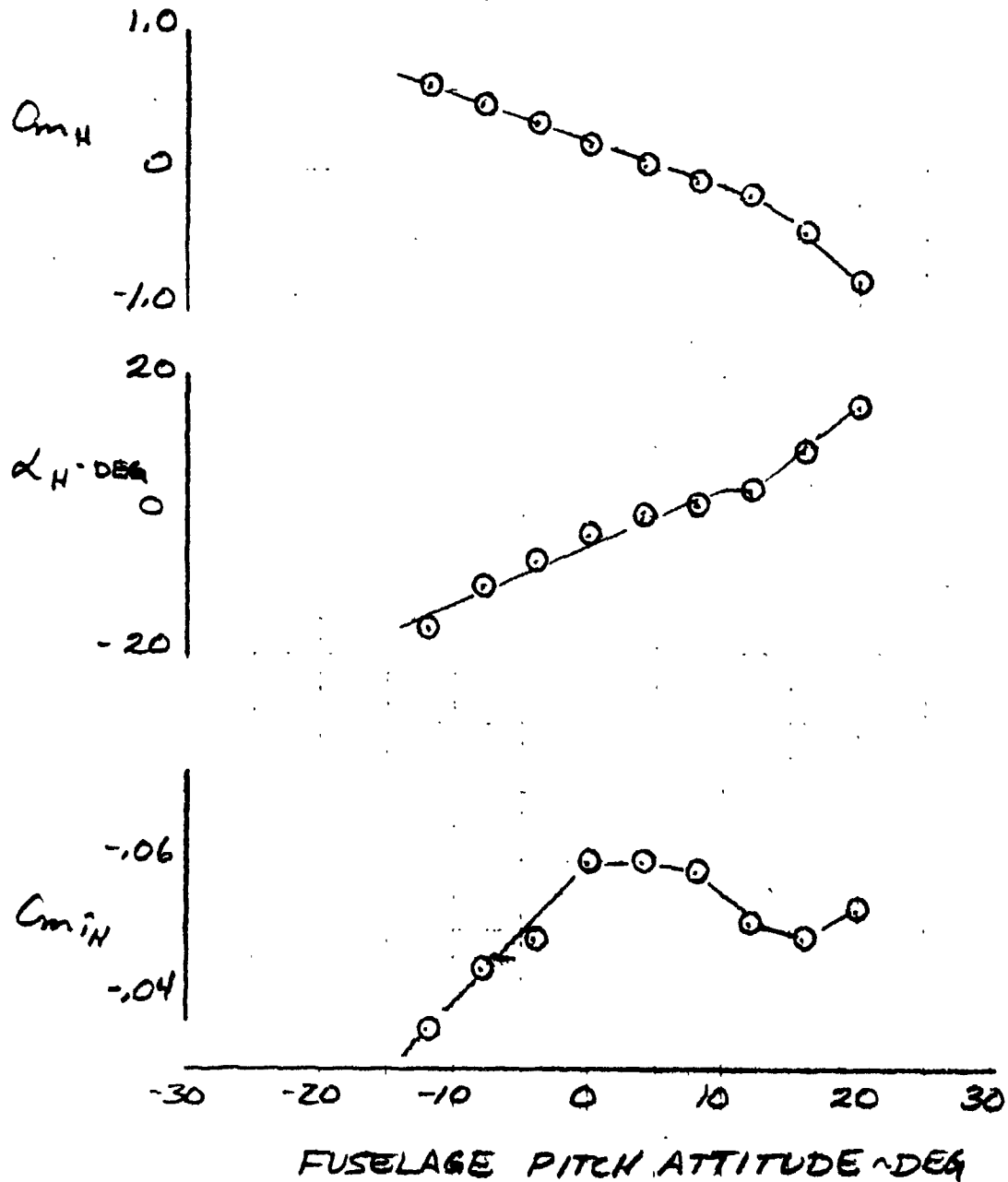


Figure VI-6. Horizontal Stabilizer Aerodynamic Characteristics, Mast Angle 30°, Rotors off.

HORIZONTAL STABILIZER DOWNWASH

MAST = 30°
FLAPS = 45/25°

ROTORS OFF
V = 80 KTS

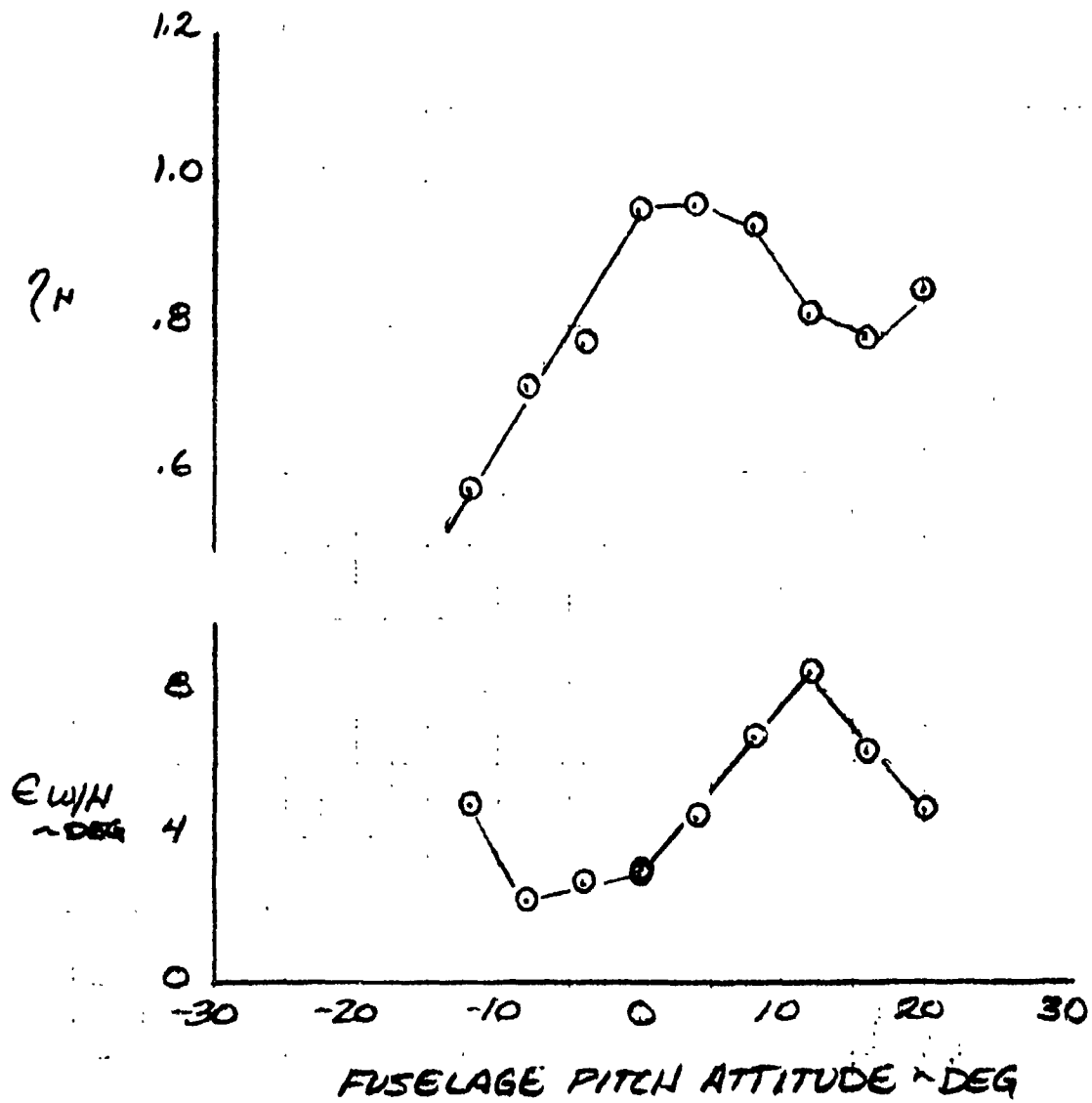


Figure VI-6. Concluded

HORIZONTAL STABILIZER CHARACTERISTICS

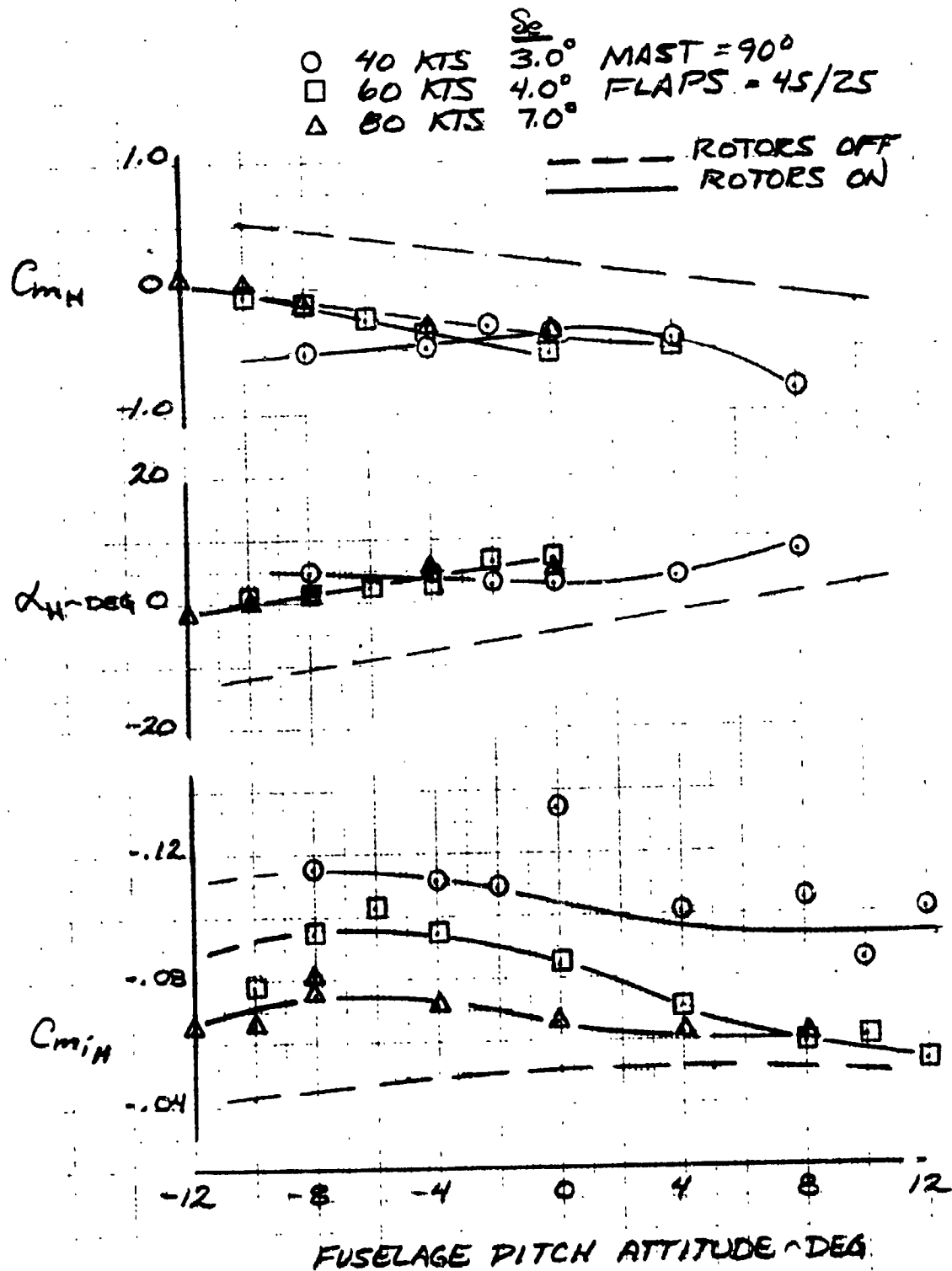


Figure VI-7. Horizontal Stabilizer Aerodynamic Characteristics, Mast Angle 90° , Rotors on.

HORIZONTAL STABILIZER DOWNWASH

- 40 KTS
- 60 KTS
- △ 80 KTS

MAST = 90°
FLAPS = 45/25°

ROTOR ON

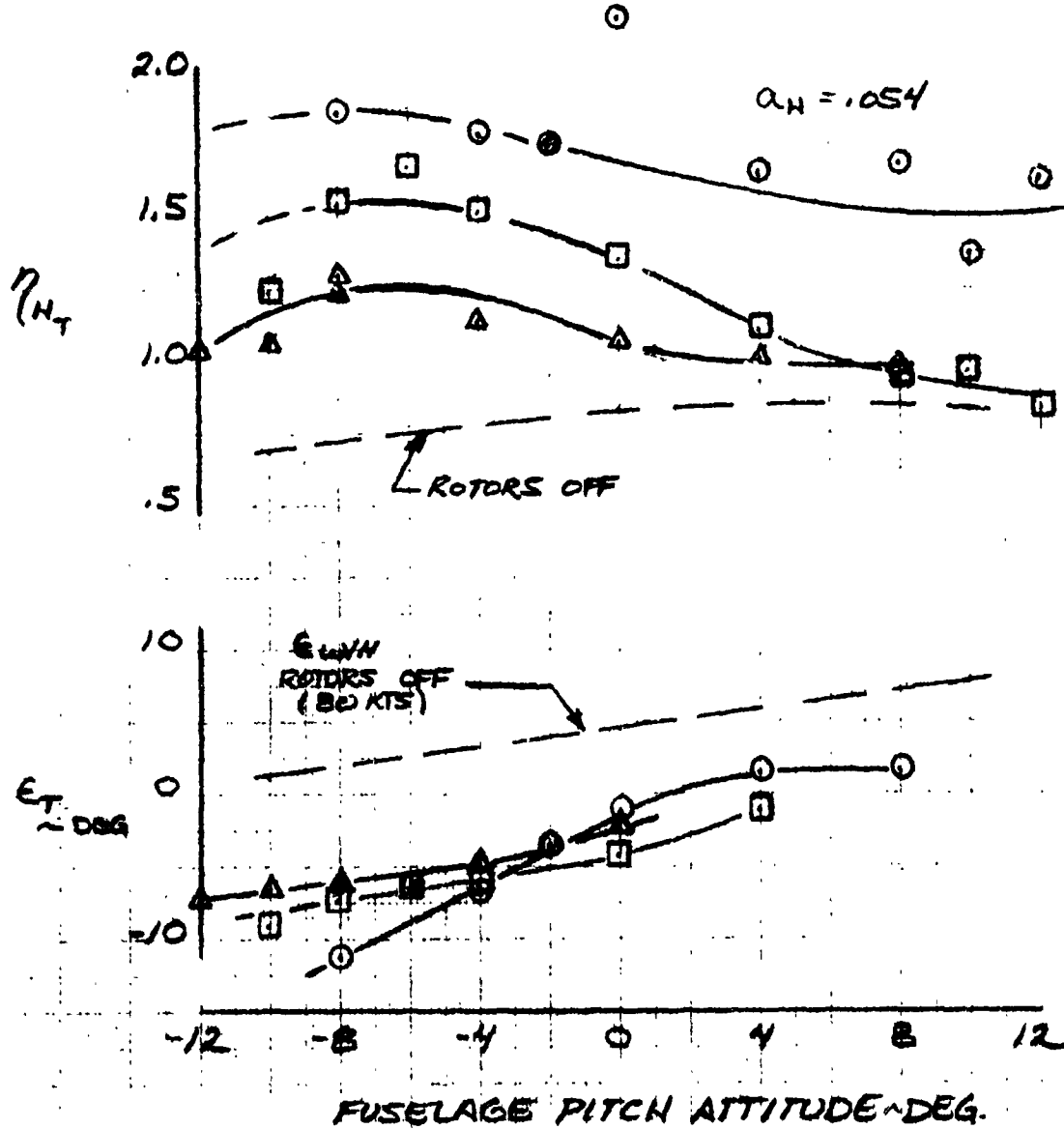


Figure VI-7. Concluded

HORIZONTAL STABILIZER CHARACTERISTICS

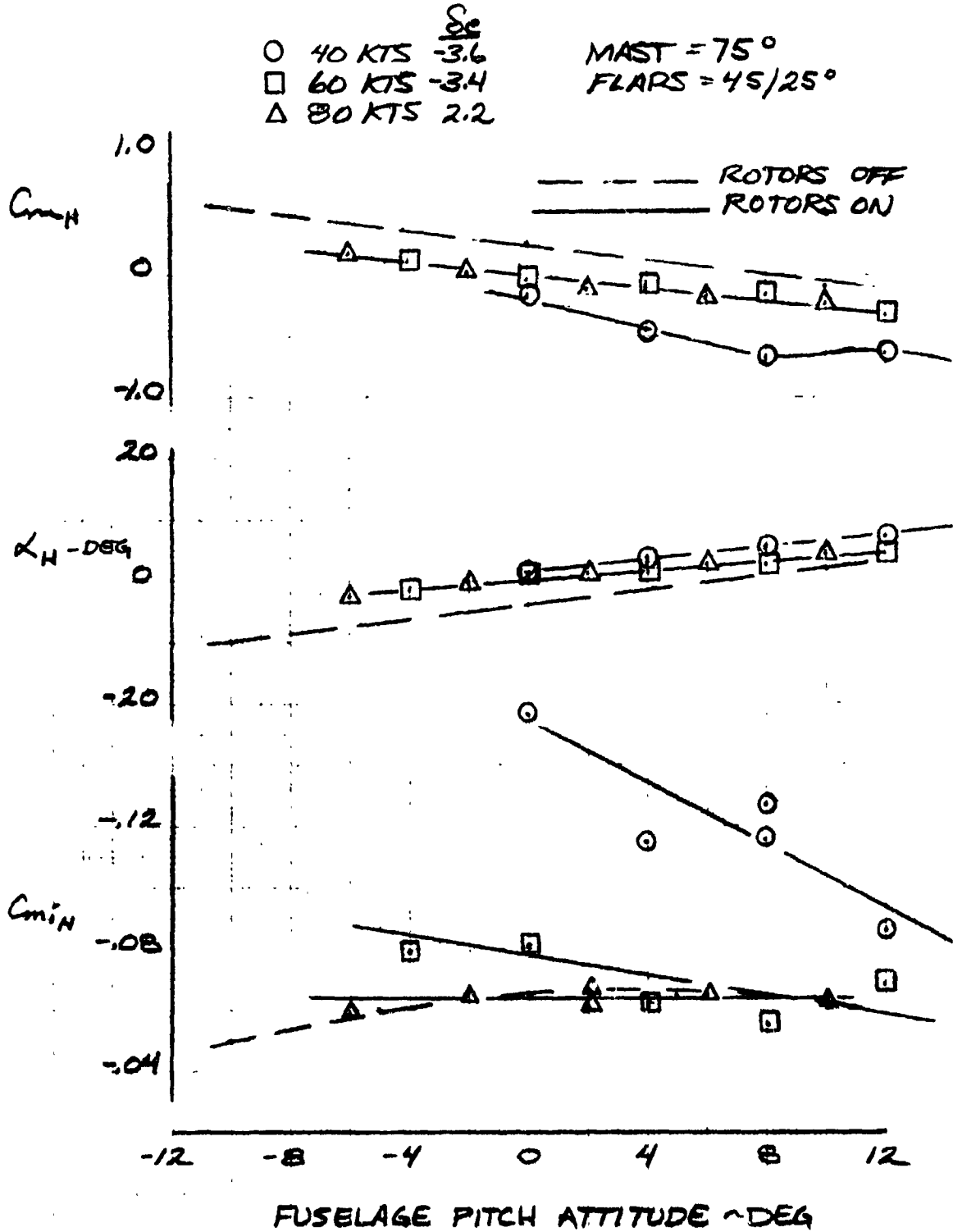


Figure VI-8. Horizontal Stabilizer Aerodynamic Characteristics, Mast Angle 75°, Rotors on.

HORIZONTAL STABILIZER DOWNWASH

- 40 KTS
- 60 KTS
- △ 80 KTS

MAST = 75°
FLAPS = 45/25°

--- ROTORS OFF
— ROTORS ON

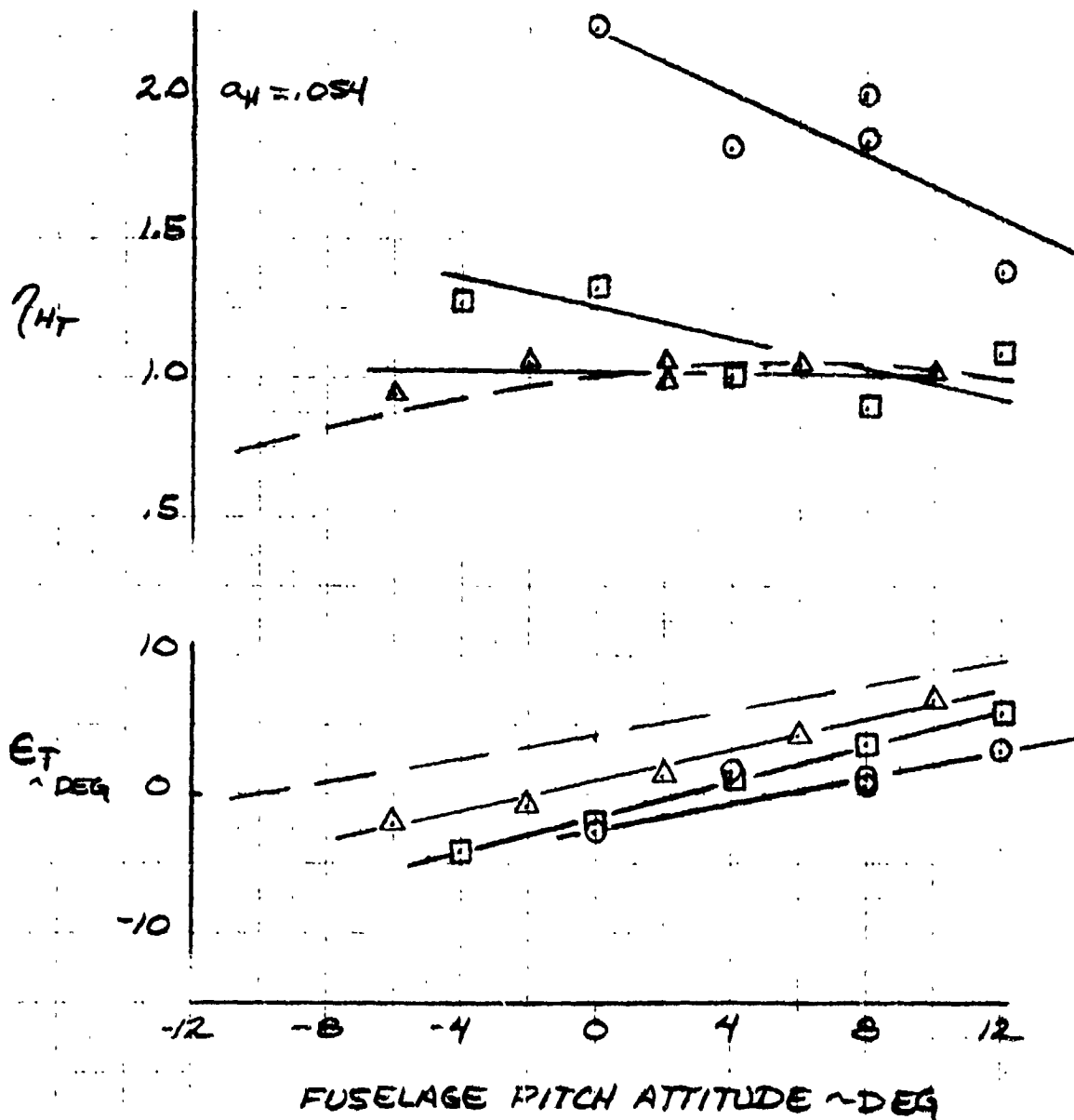


Figure VI-8. Concluded

HORIZONTAL STABILIZER CHARACTERISTICS
 ‡ DOWNWASH

○ 80 KTS $\frac{S_e}{V}$ -4°
 □ 100 KTS $.7^\circ$

MAST = 60°
 FLAPS = $4S/25^\circ$

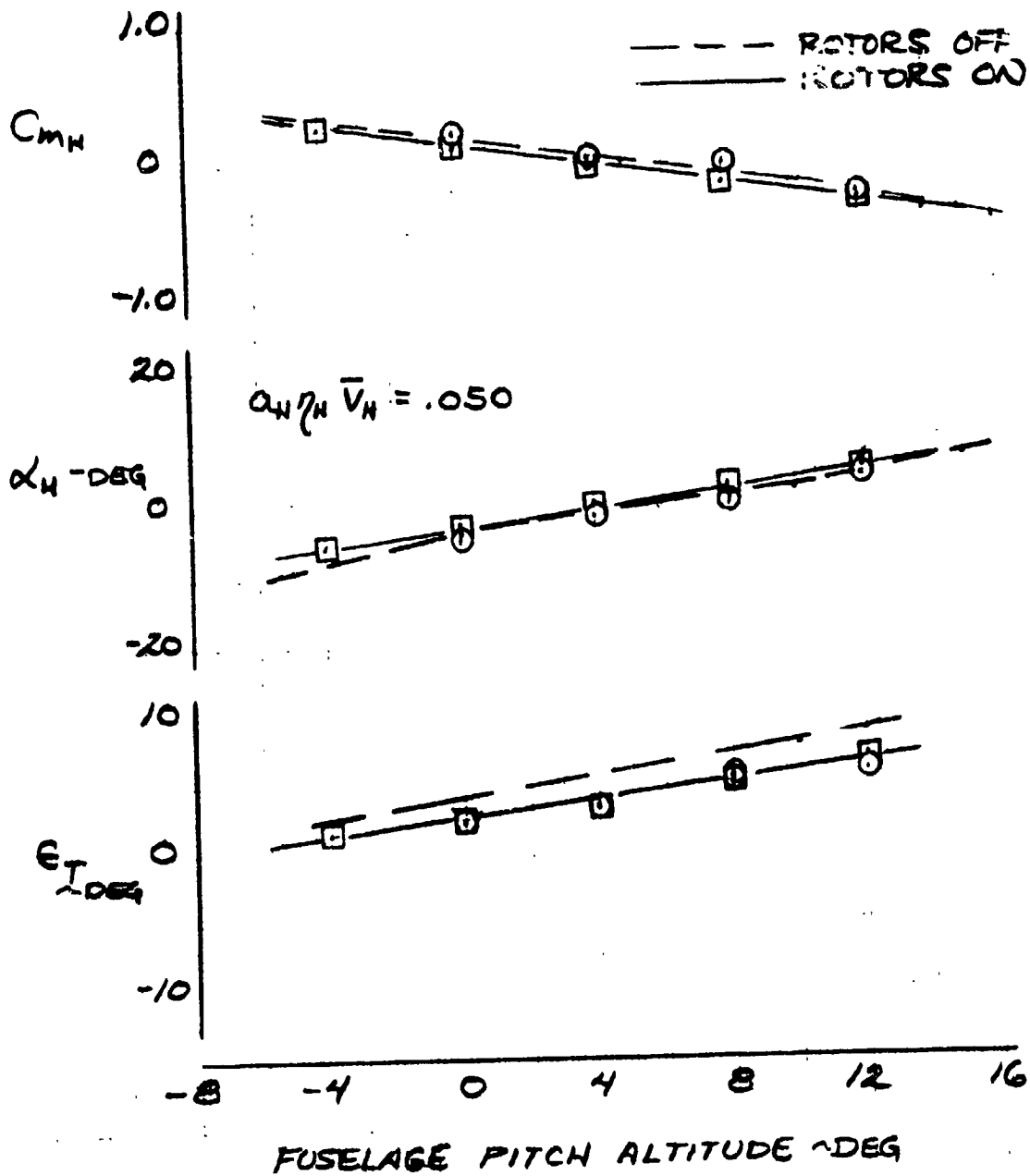


Figure VI-9. Horizontal Stabilizer Aerodynamic Characteristics, Mast Angle 60° , Rotors on.

HORIZONTAL STABILIZER CHARACTERISTICS

↓ DOWNWASH

○ 80 KTS $\frac{S_c}{S_r} = -9^\circ$
 □ 100 KTS -4°

MAST = 30°
 FLAPS = $45/25^\circ$

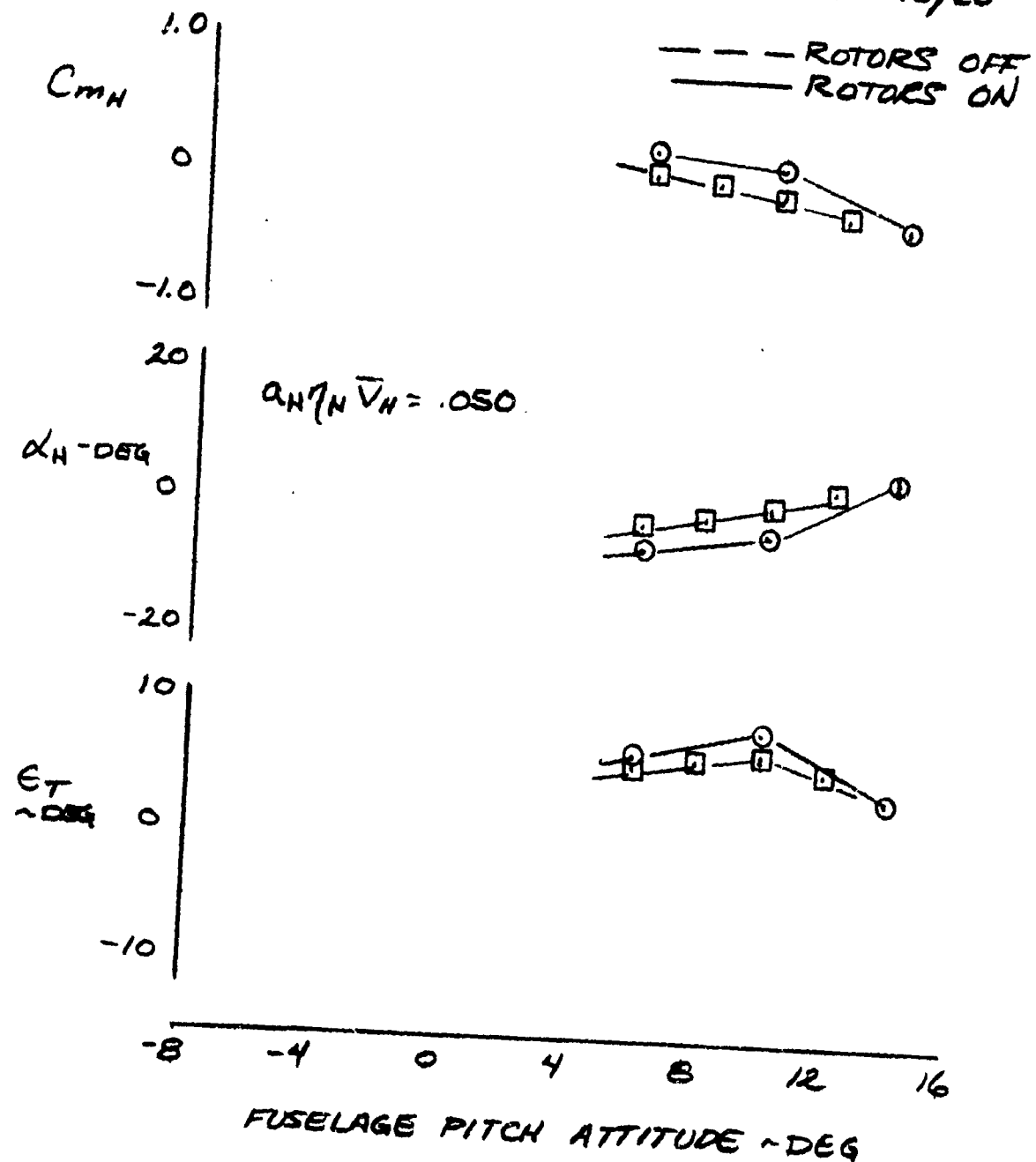


Figure VI-10. Horizontal Stabilizer Aerodynamic Characteristics, Mast Angle 30° , Rotors on.

ROTOR WAKE AT HORIZONTAL TAIL

- 20 KTS
- 40 KTS
- 60 KTS
- △ 80 KTS

MAST = 90°
FLAPS = 45/25°

LEVEL FLIGHT PITCH SWEEP

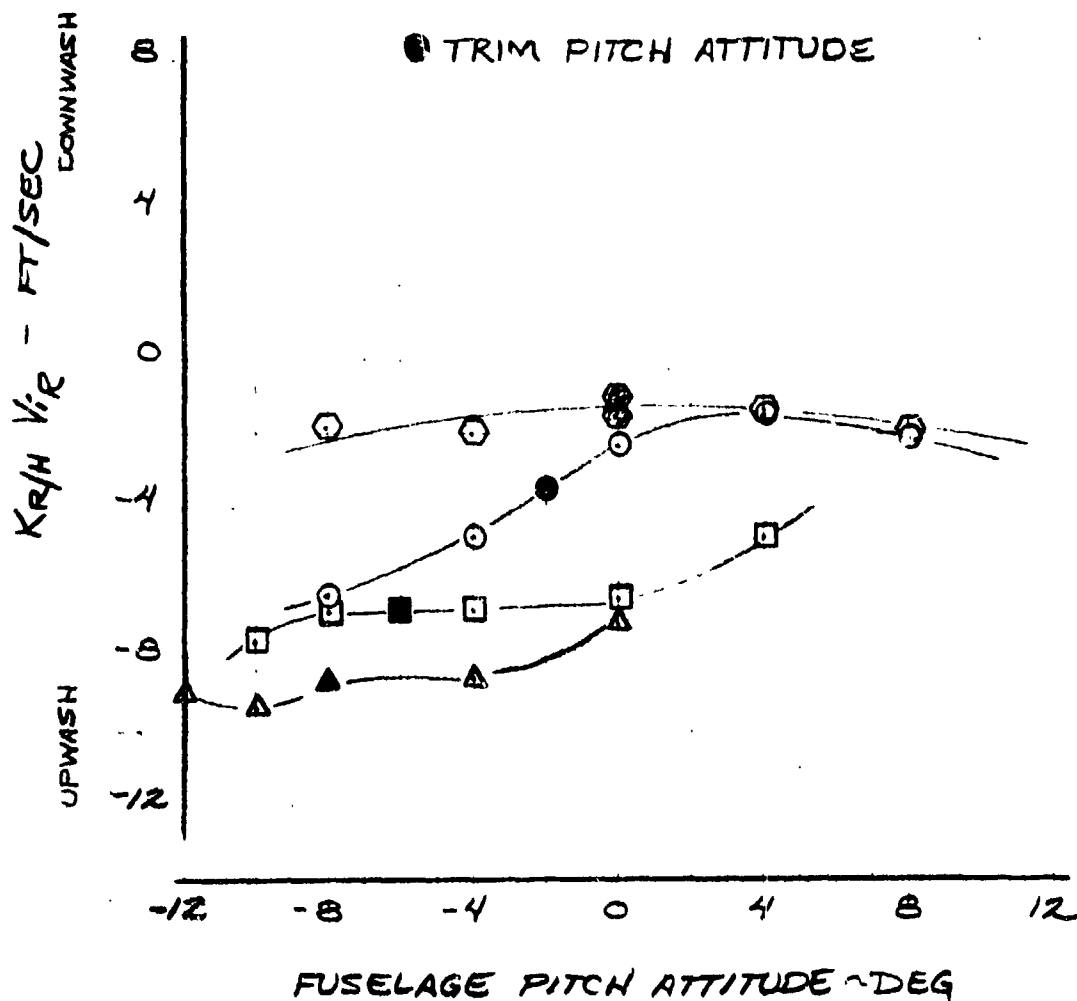


Figure VI-11. Rotor Upwash at the Horizontal Stabilizer versus Angle of Attack for Several Airspeeds, Mast Angle 90°.

ROTOR WAKE AT HORIZONTAL TAIL

- 40KTS
- 60 KTS
- △ 80KTS

MAST = 90°
FLAPS = 45/25°

- POWER**
- CLIMB ($\eta_H = 1.0$)
 - LEVEL
 - ⊙ DESCENT ($\eta_H = 1.0$)

PITCH SWEEP

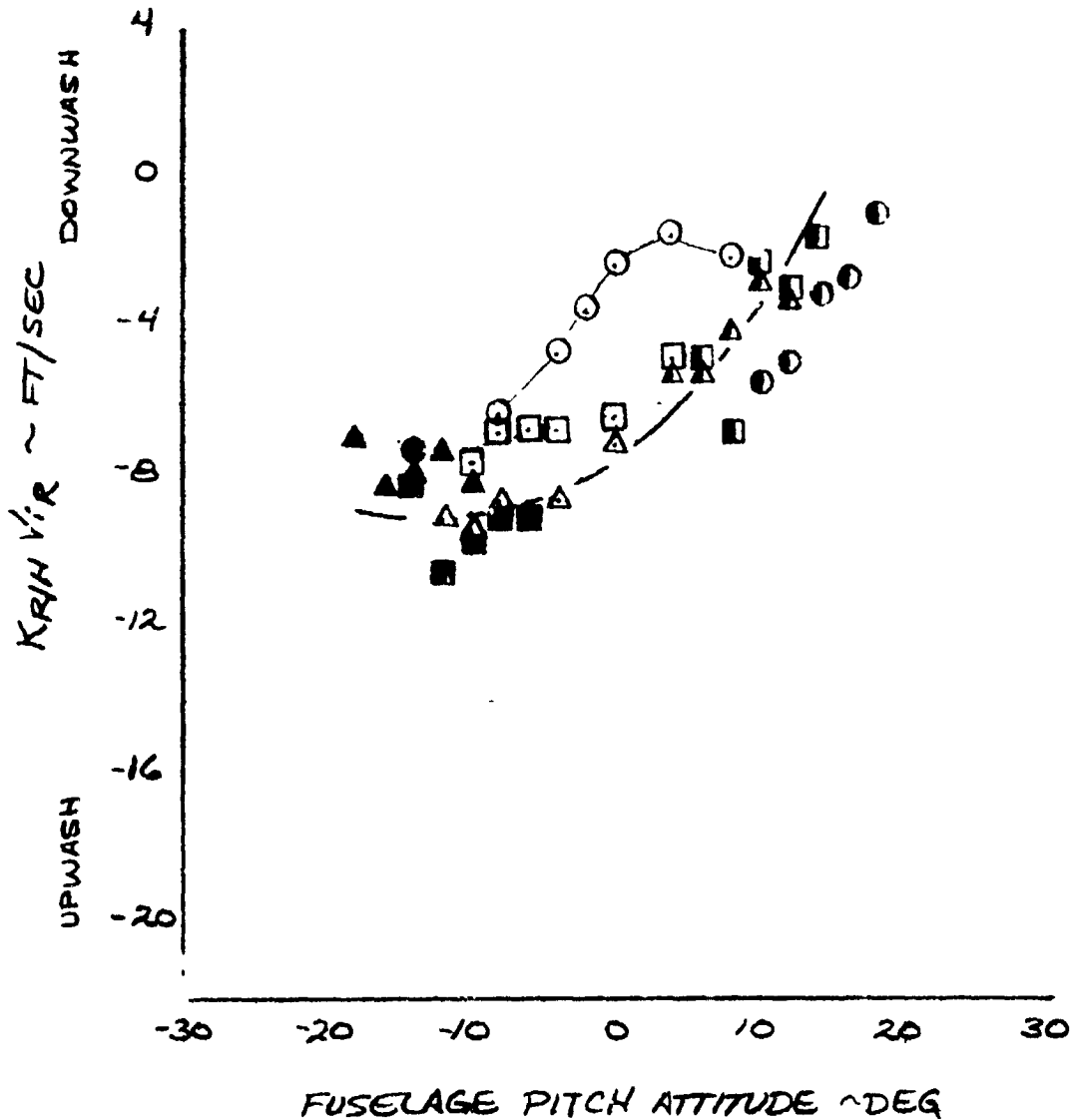


Figure VI-12. Rotor Upwash at Horizontal Stabilizer in Climb and Descent Compared to Level Flight, Mast Angle 90°.

ROTOR WAKE AT HORIZONTAL TAIL

- 30 KTS
- 40 KTS
- 60 KTS
- △ 80 KTS

MAST = 75°
FLAPS = 45/25°

LEVEL FLIGHT PITCH SWEEP

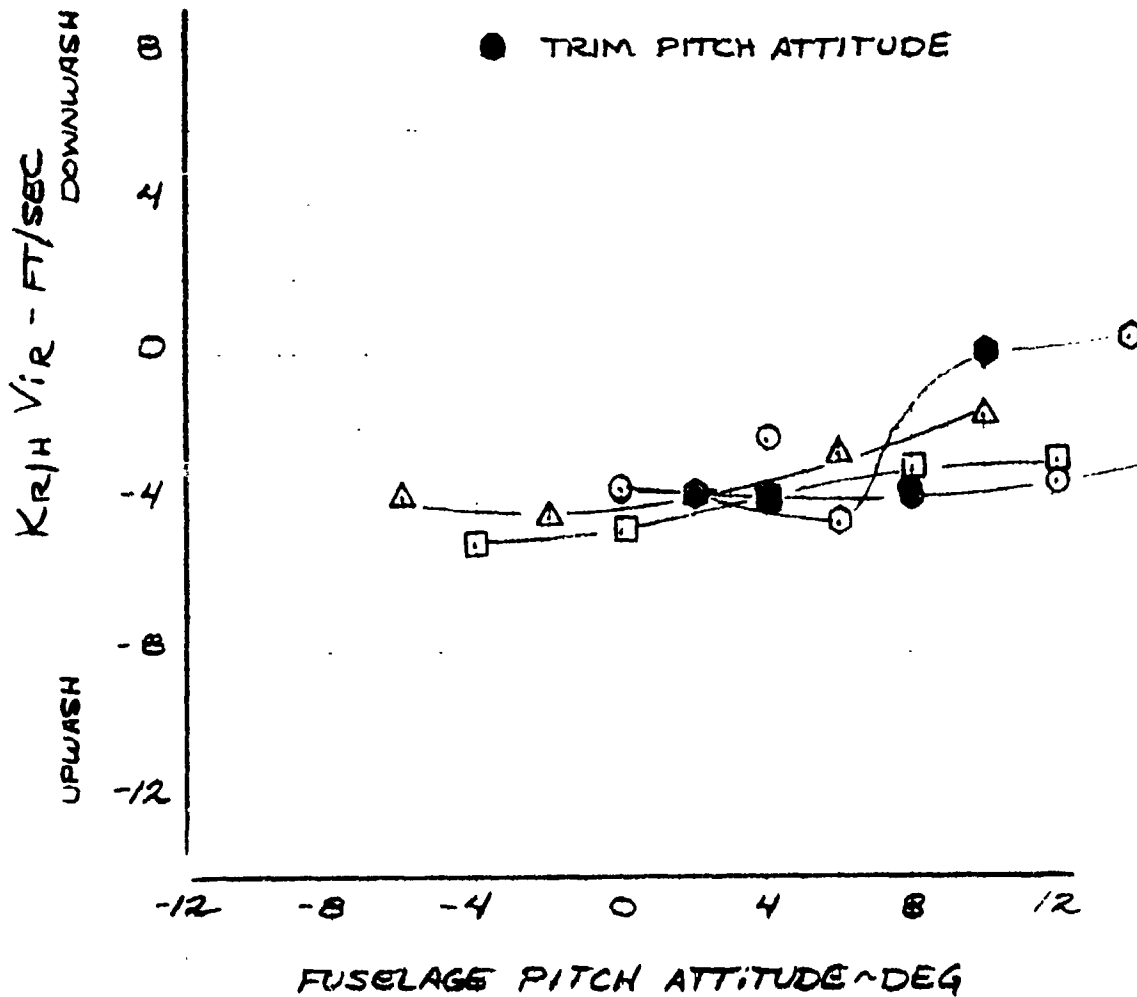


Figure VI-13. Rotor Upwash at Horizontal Stabilizer versus Fuselage Angle of Attack, Mast Angle 75°.

ROTOR WAKE AT HORIZONTAL TAIL

○ 80 KTS
□ 100 KTS

MAST = 60°
FLAPS = 45/25°

LEVEL FLIGHT PITCH SWEEP

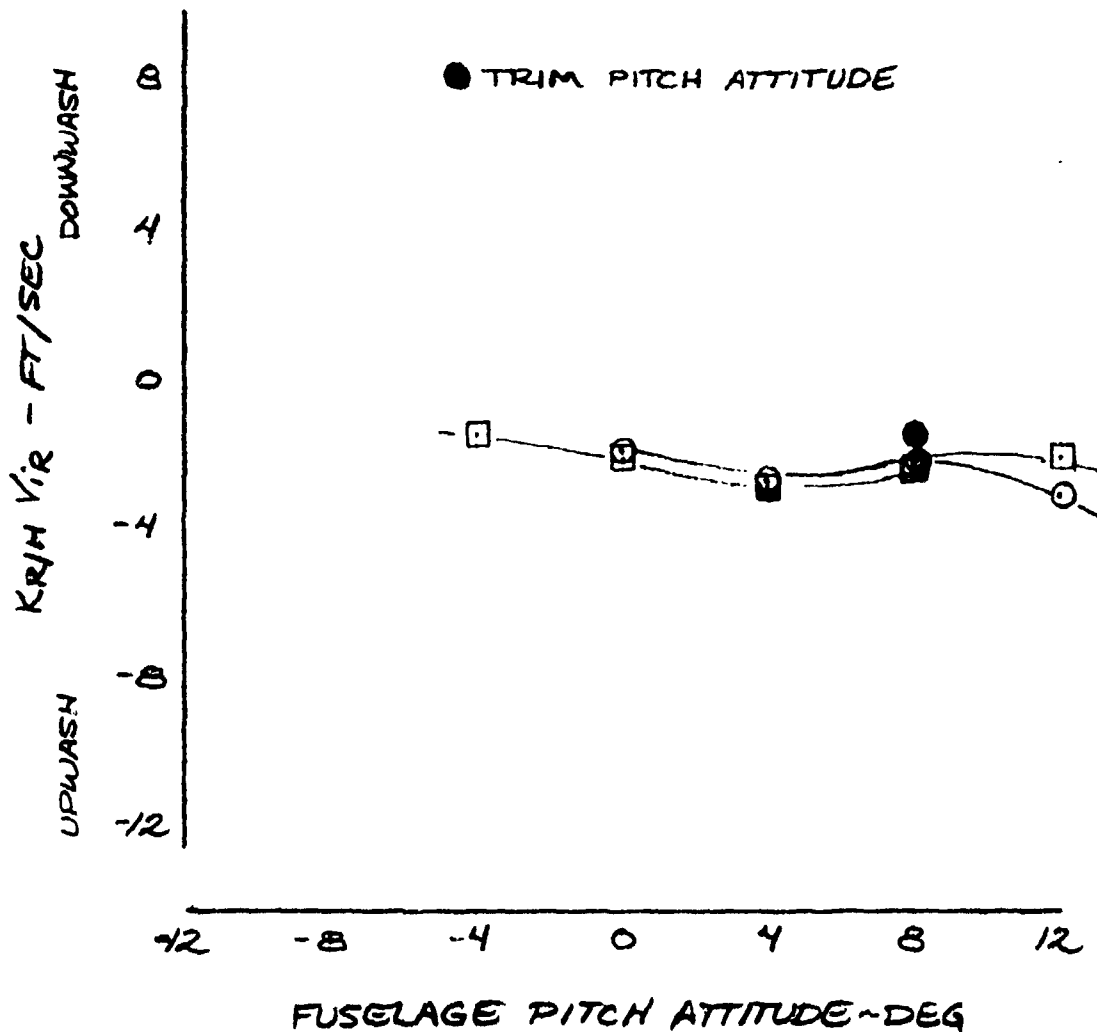


Figure VI-14. Rotor Upwash at Horizontal Stabilizer
versus Fuselage Angle of Attack,
Mast Angle 60°.

ROTOR WAKE AT HORIZONTAL TAIL

○ 80 KTS
□ 100 KTS

MAST = 30°
FLAPS = 45/25°

LEVEL FLIGHT PITCH SWEEP

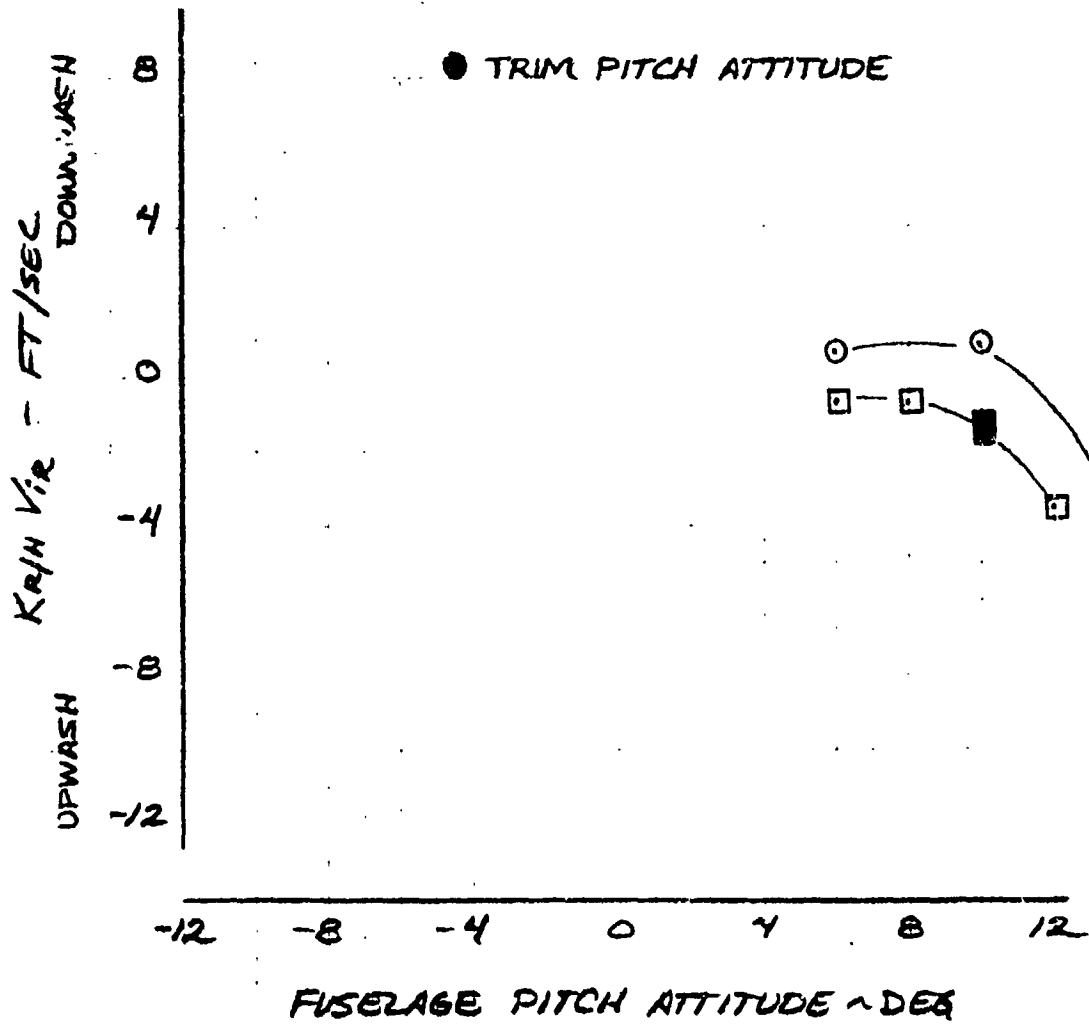


Figure VI-15. Rotor Upwash at Horizontal Stabilizer versus Fuselage Angle of Attack, Mast Angle 30°.

ROTOR WAKE AT HORIZONTAL TAIL

		η_{HT}	
○	40 KTS	1.75	MAST = 90°
□	60 KTS	1.54	FLAPS = 45/25°
△	80 KTS	1.22	

YAW SWEEP LEVEL FLIGHT

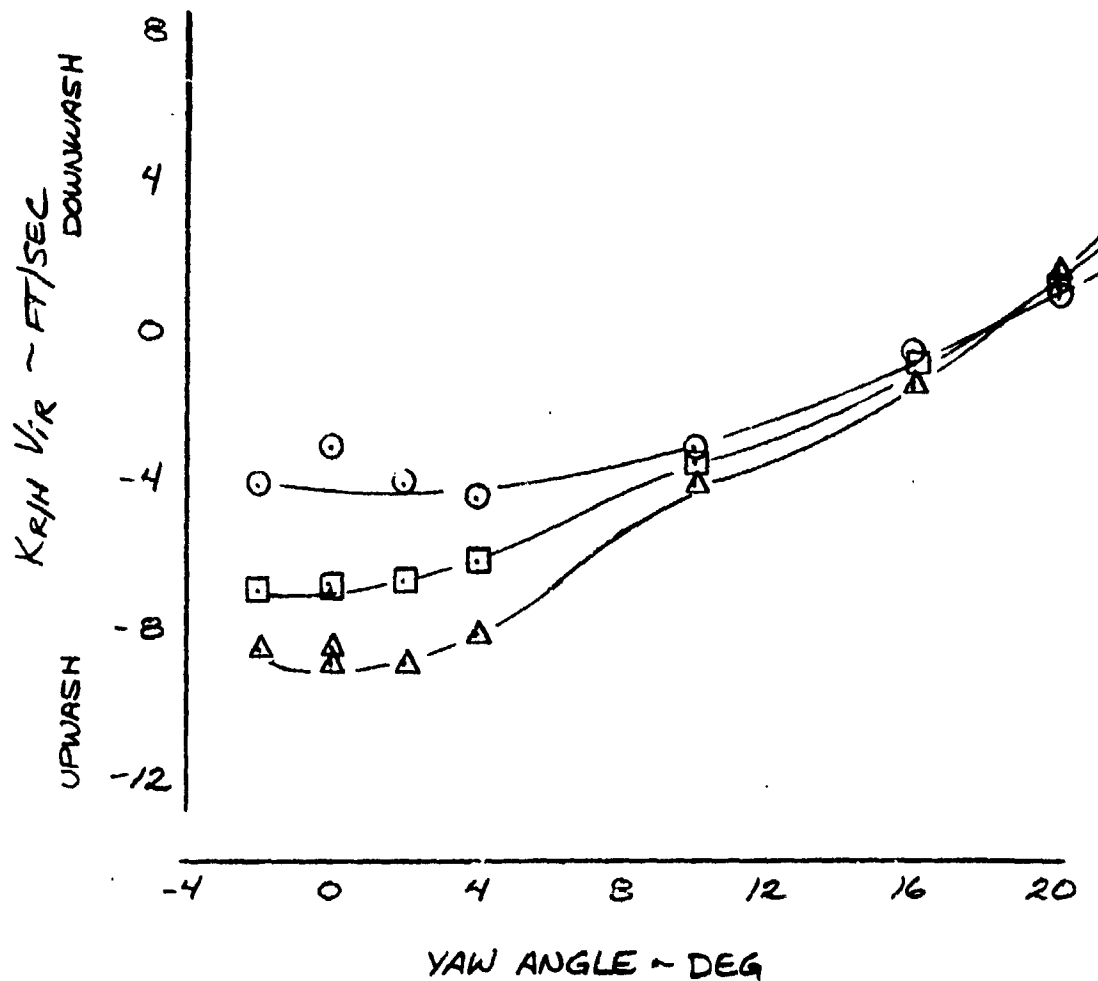


Figure VI-17. Effect of Yaw Angle on Rotor Wake Upwash at Horizontal Stabilizer, Mast Angle 90°.

ROTOR WAKE AT HORIZONTAL TAIL

○	40 KTS	η_{HT} 1.85	MAST = 75°
□	60 KTS	1.10	FLAPS = 45/25°
△	80 KTS	1.07	

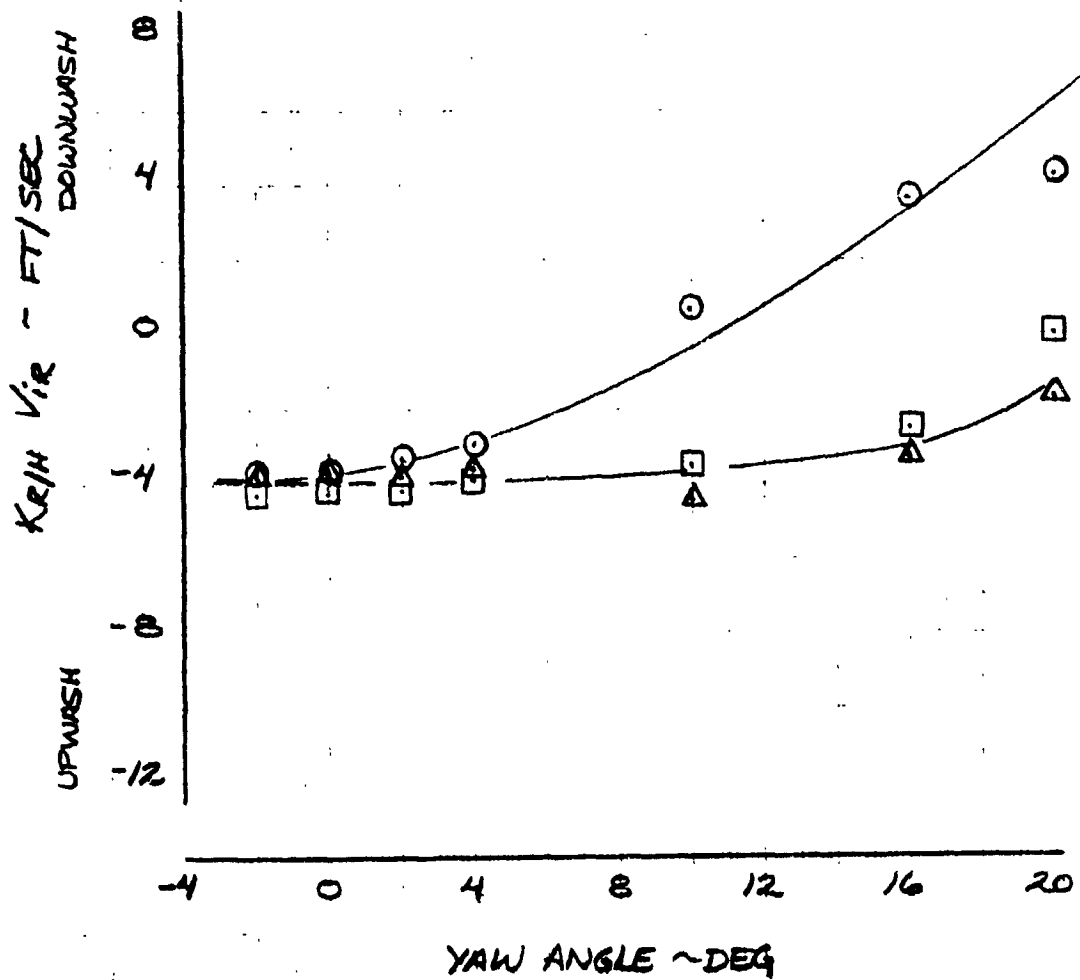


Figure VI-18. Effect of Yaw Angle on Rotor Wake Upwash at Horizontal Stabilizer, Mast Angle 75°.

ROTOR WAKE AT HORIZONTAL TAIL

MAST 60° η_{HT}
 ○ 80 KTS .81 FLAPS = 45/25°
 □ 100 KTS .81

MAST 30°
 ○ 100 KTS .81

YAW SWEEP LEVEL FLIGHT

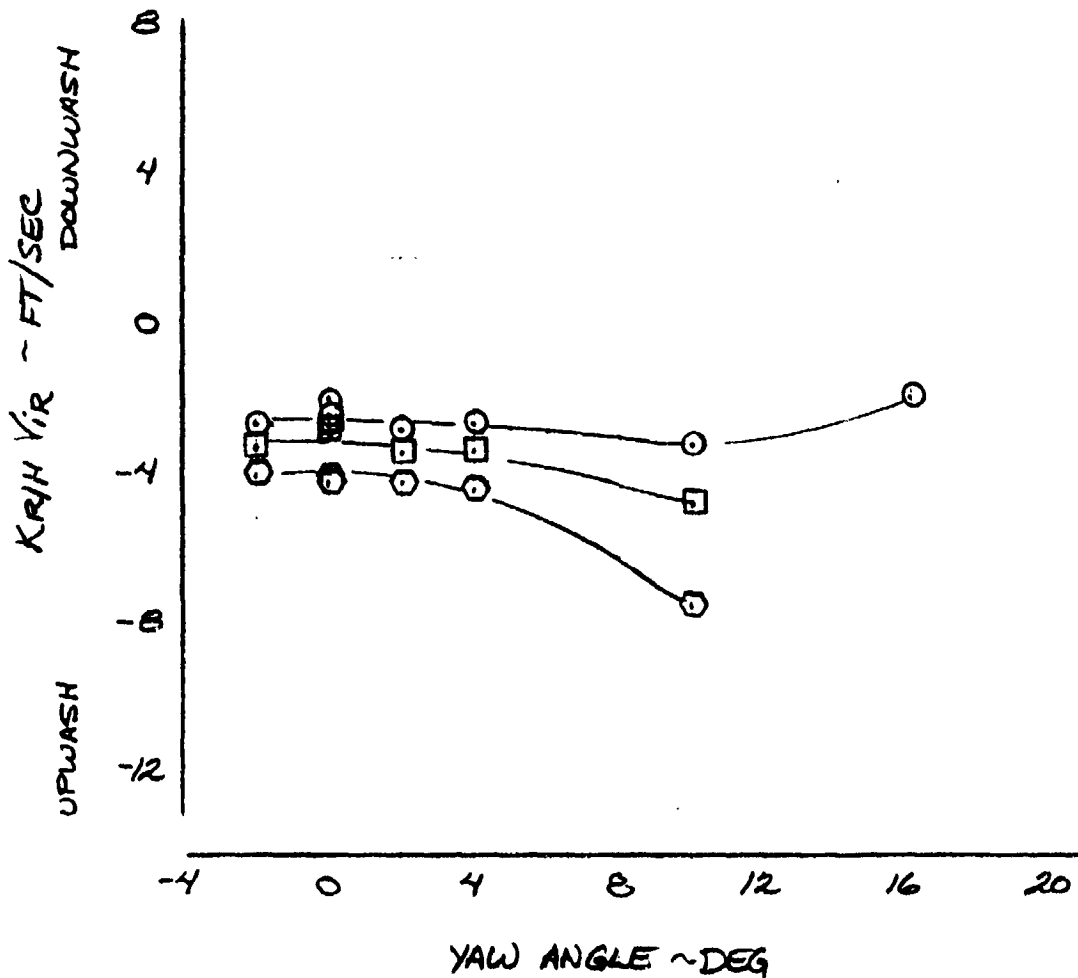


Figure VI-19. Effect of Yaw Angle on Rotor Wake Upwash at Horizontal Stabilizer, Mast Angles 60° and 30°.

ROTOR EFFECT ON DIRECTIONAL STABILITY

- 40 KTS
 - 60 KTS
 - △ 80 KTS
- MAST = 90°
FLAPS = 45/25°

$$K_{\beta} = \frac{\text{FIN YAWING MOMENT, ROTORS-ON}}{\text{FIN YAWING MOMENT, ROTORS-OFF}}$$

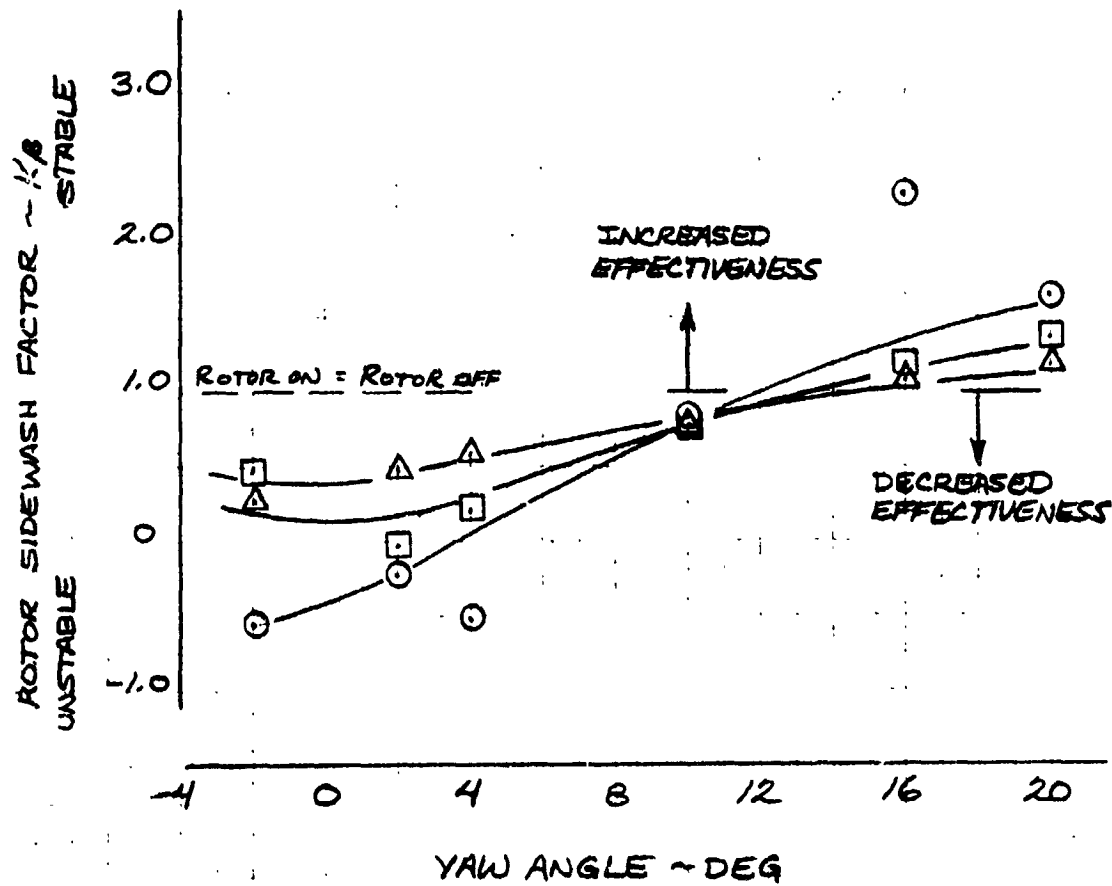


Figure VI-20. Effect of Rotor Wake on Directional Stability, Mast Angle 90°.

ROTOR EFFECT ON DIRECTIONAL STABILITY

- 40 KTS
 - 60 KTS
 - △ 80 KTS
- MAST = 75°
FLAPS = 45/25°

$$K_B = \frac{\text{FIN YAWING MOMENT, ROTORS-ON}}{\text{FIN YAWING MOMENT, ROTORS-OFF}}$$

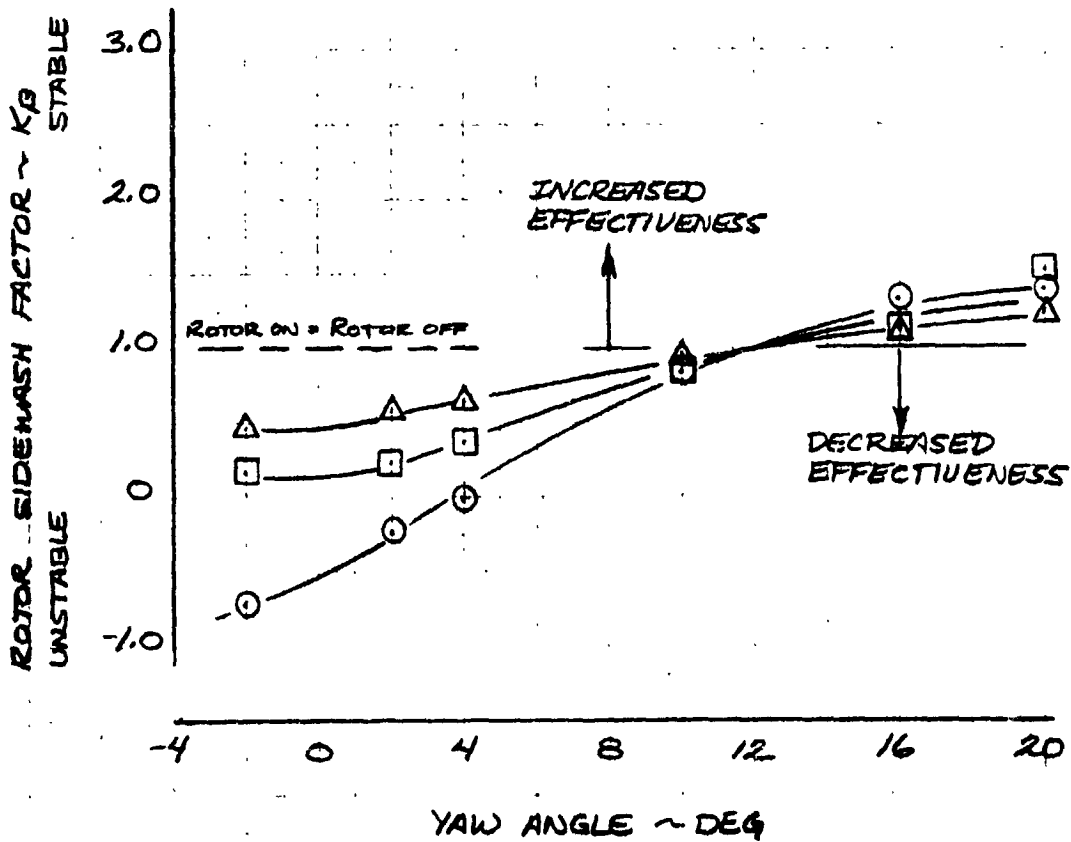


Figure VI-21. Effect of Rotor Wake on Directional Stability, Mast Angle 75°.

ROTOR EFFECT ON DIRECTIONAL STABILITY

MAST 60°

○ 80 KTS

FLAPS = 45/25°

MAST 30°

□ 100 KTS

$$K_B = \frac{\text{FIN YAWING MOMENT, ROTORS-ON}}{\text{FIN YAWING MOMENT, ROTORS-OFF}}$$

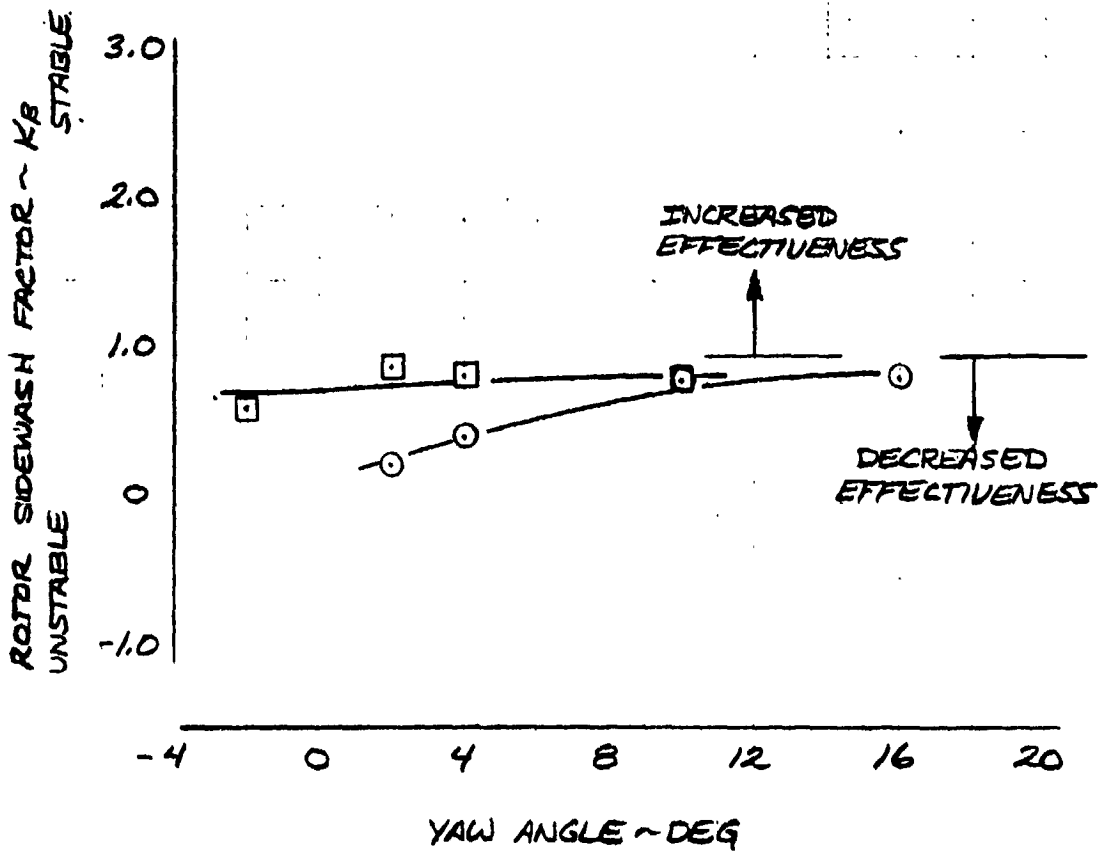


Figure VI-22. Effect of Rotor Wake on Directional Stability, Mast Angles 60° and 30°.

EMPENNAGE LIFT

MAST = 90°
FLAPS = 45/25°

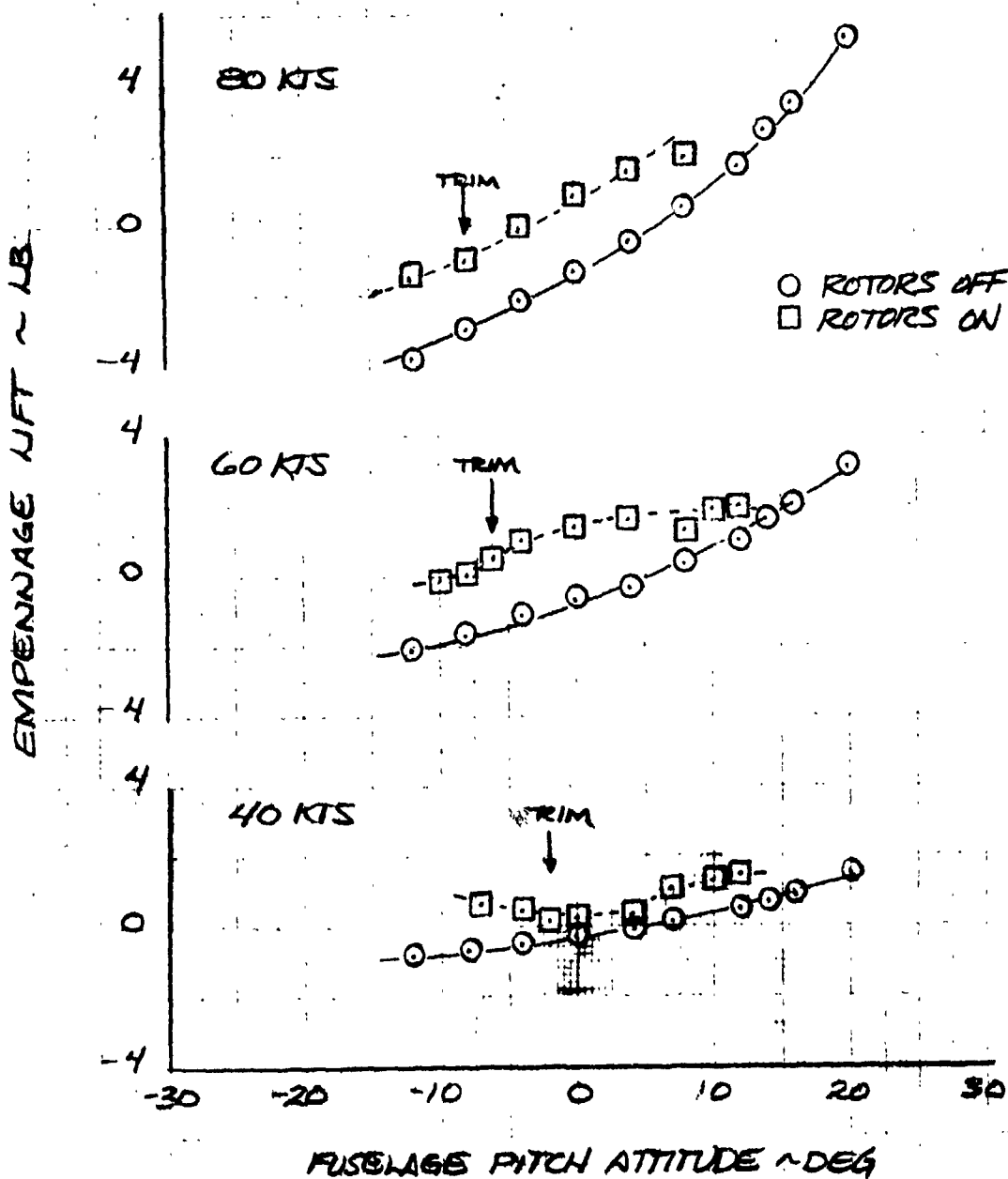


Figure VI-23. Comparison of Empennage Lift Rotors On and Rotors Off. Mast Angle 90°.

EMPENNAGE LIFT

MAST = 75°
FLAPS = 45/25°

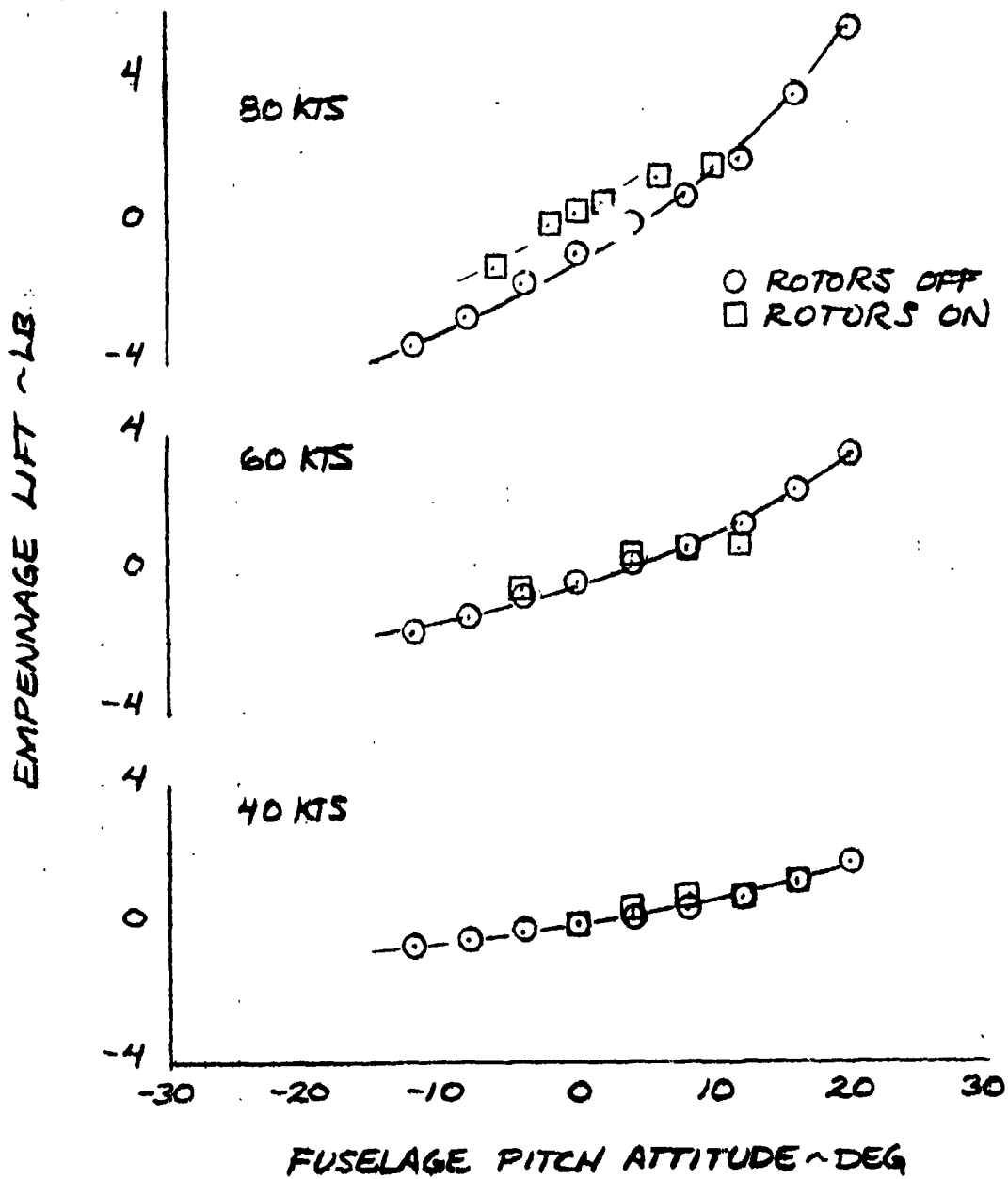


Figure VI-24. Comparison of Rotor Lift Rotors On and Rotors Off, Mast Angle 75°.

EMPENNAGE LIFT

MAST 60°
FLAPS = 45/25°

○ ROTORS OFF
□ ROTORS ON

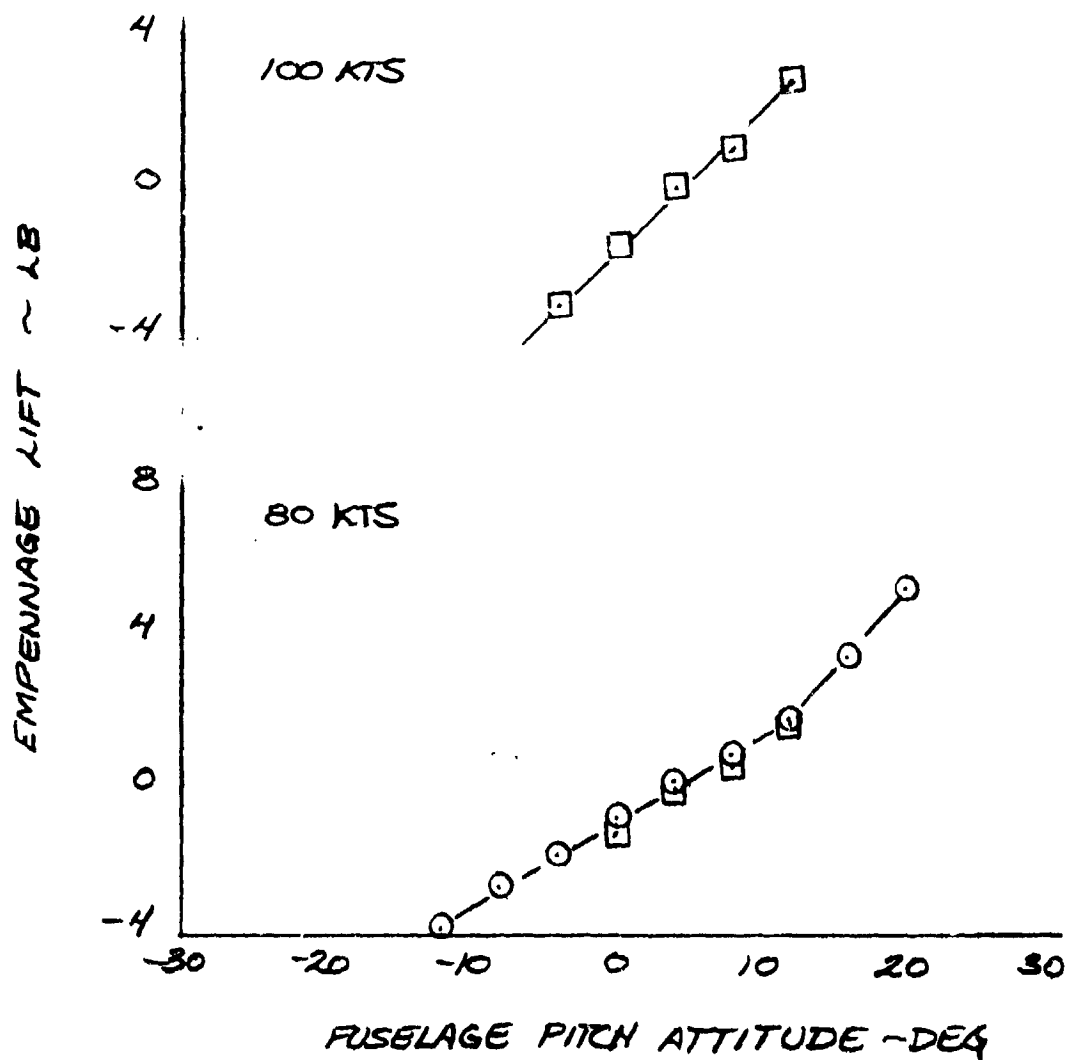


Figure VI-25. Comparison of Empennage Lift Rotors On and Rotors Off, Mast Angle 60°.

EMPENNAGE LIFT

MAST 30°
FLAPS = 45/25°

○ ROTORS OFF
□ ROTORS ON

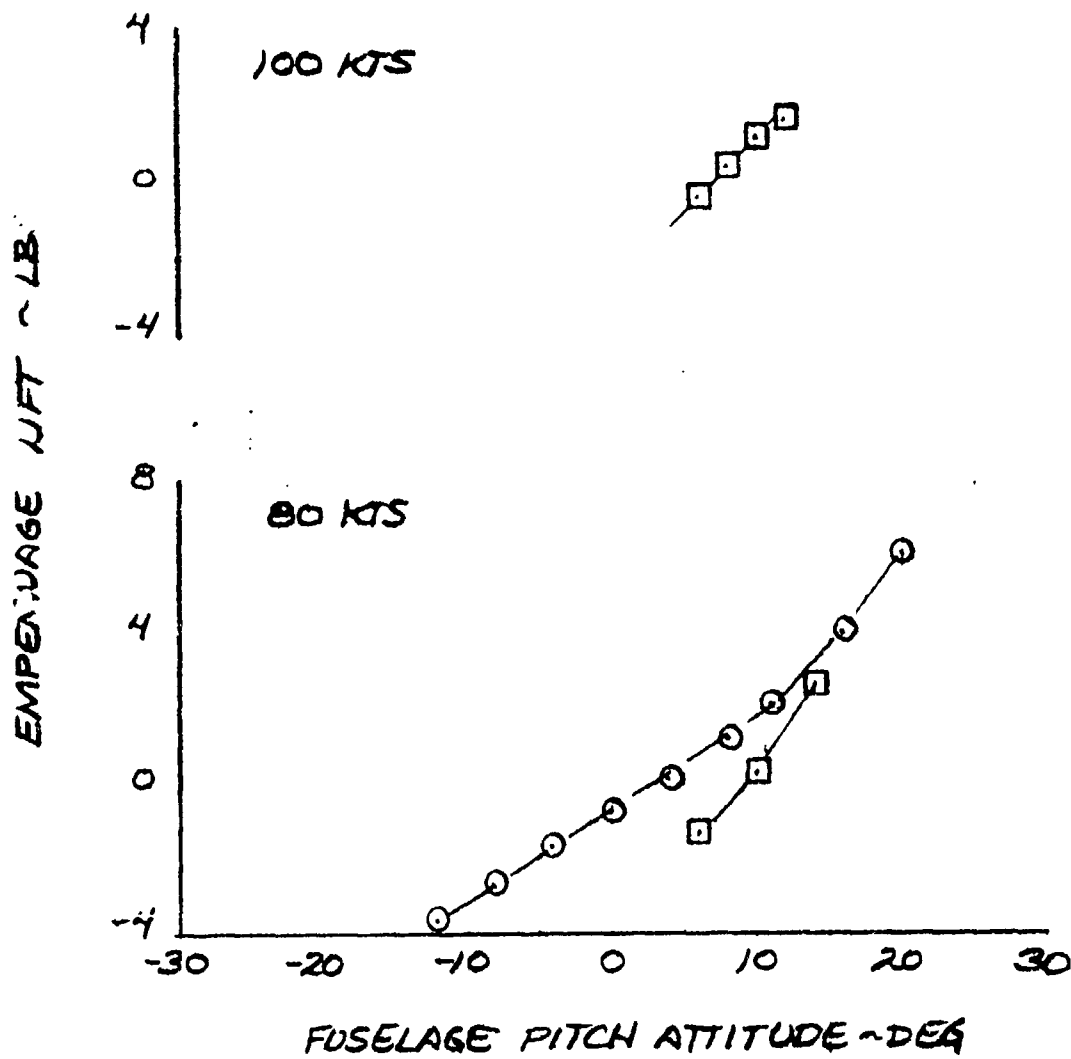


Figure VI-26. Comparison of Empennage Lift Rotors On and Rotors Off, Mast Angle 30°.

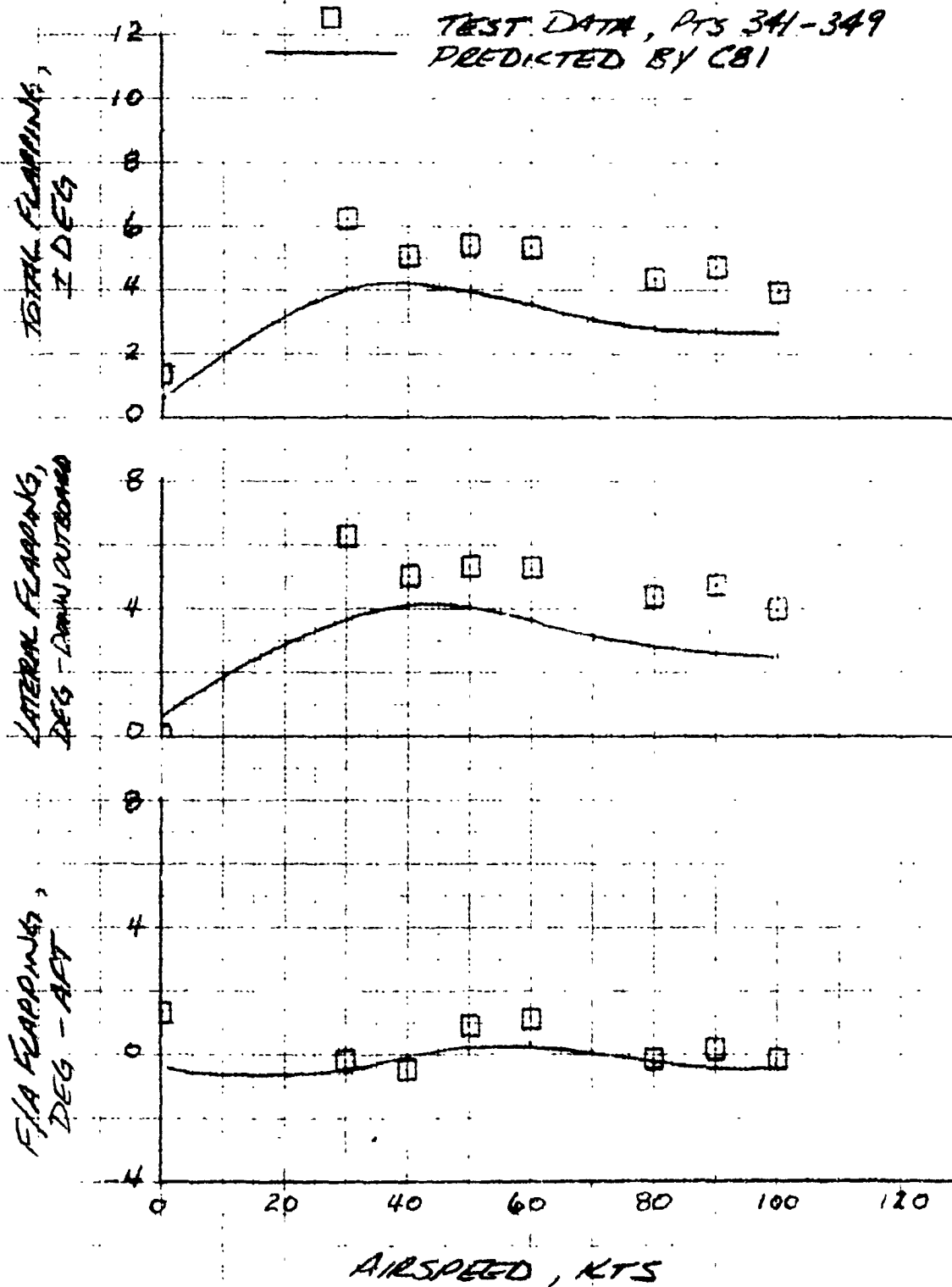


Figure VI-27. Comparison of Pretest Predicted Flapping With Measured Flapping, Mast Angle 90°.

AIRSPEED 40 KNOTS
GROSS WEIGHT - 11,000 LB

- CBI WITH $K = 1.20$ (PRETEST)
- - - CBI WITH $K = 1.62$ (REQ'D TO CORRELATE)
- OBSERVED DISTRIBUTION (APPROXIMATE)

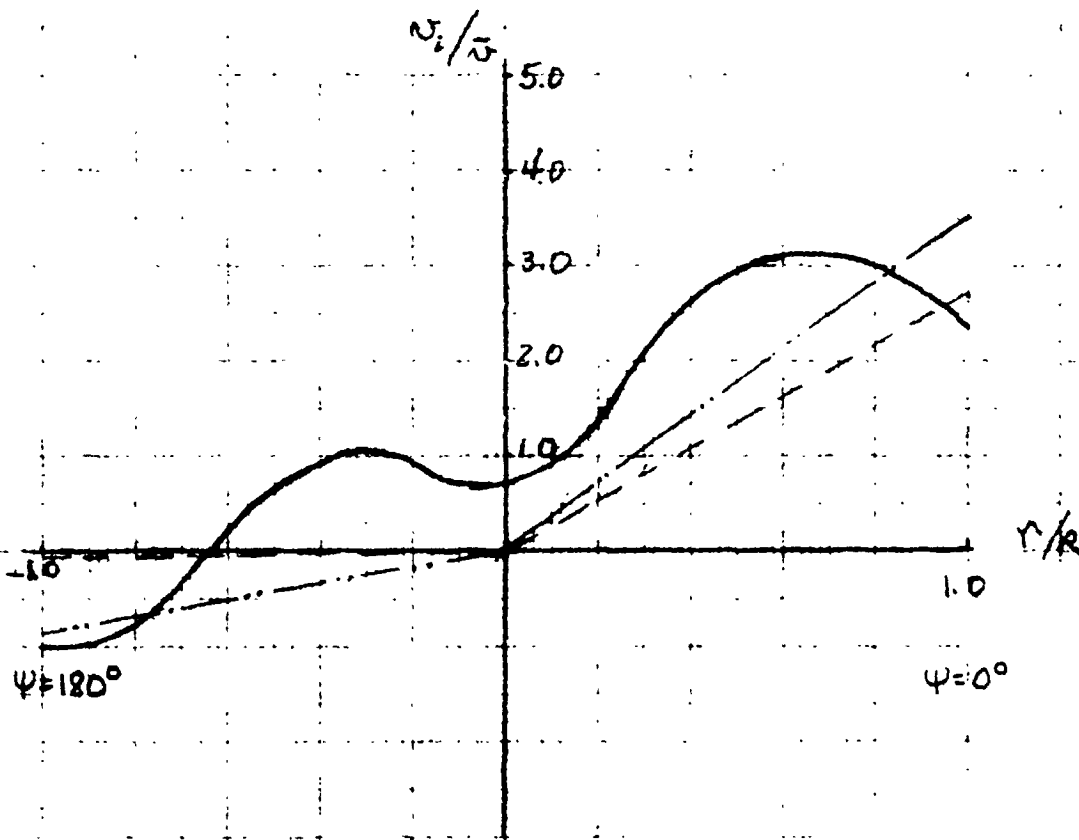


Figure VI-28. Comparison of Computer Program and Observed Longitudinal Distribution of Rotor Induced Velocity.

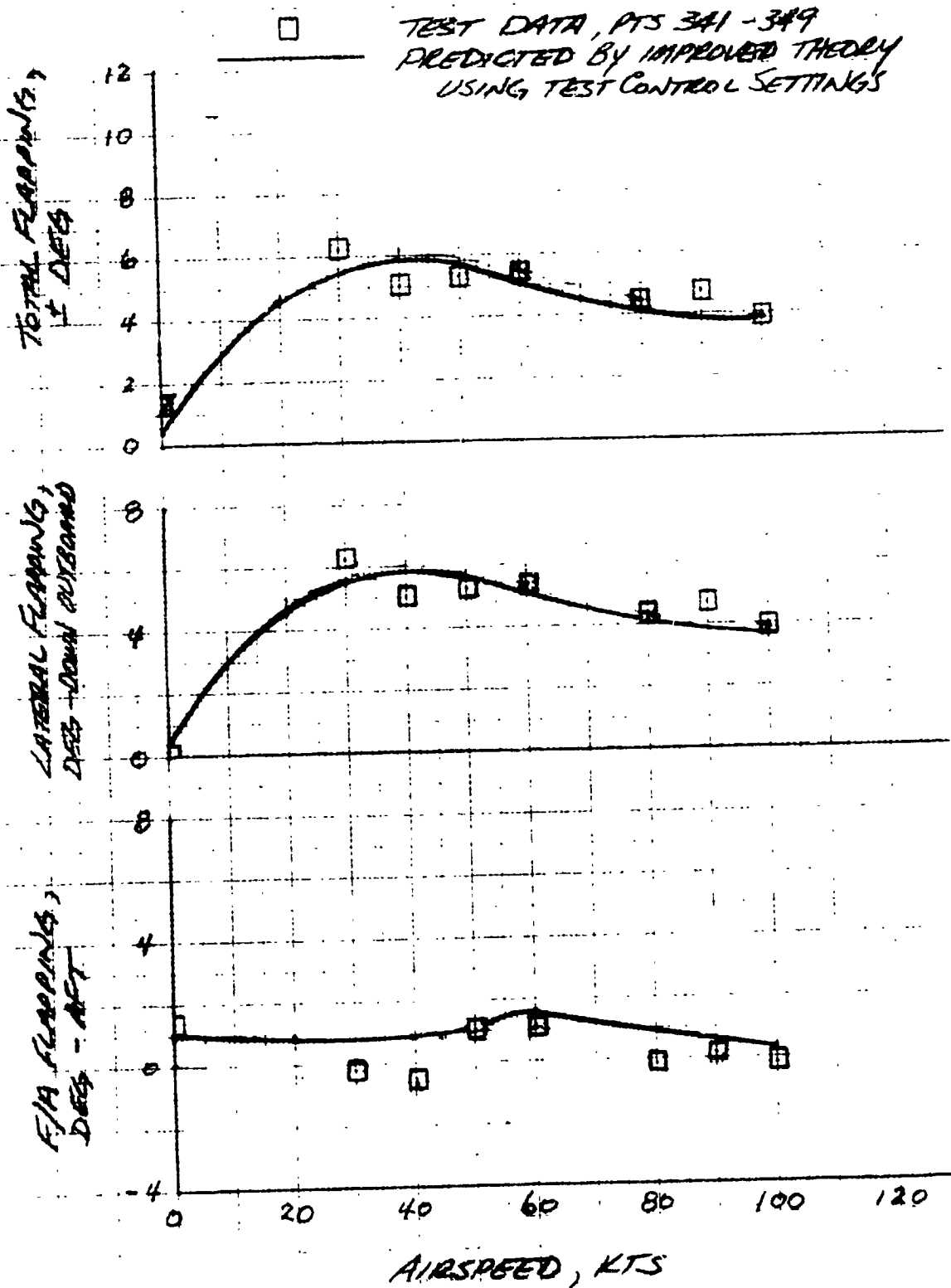


Figure VI-29. Comparison of Post Test Predicted Flapping With Measured Flapping, Mast Angle 90°.

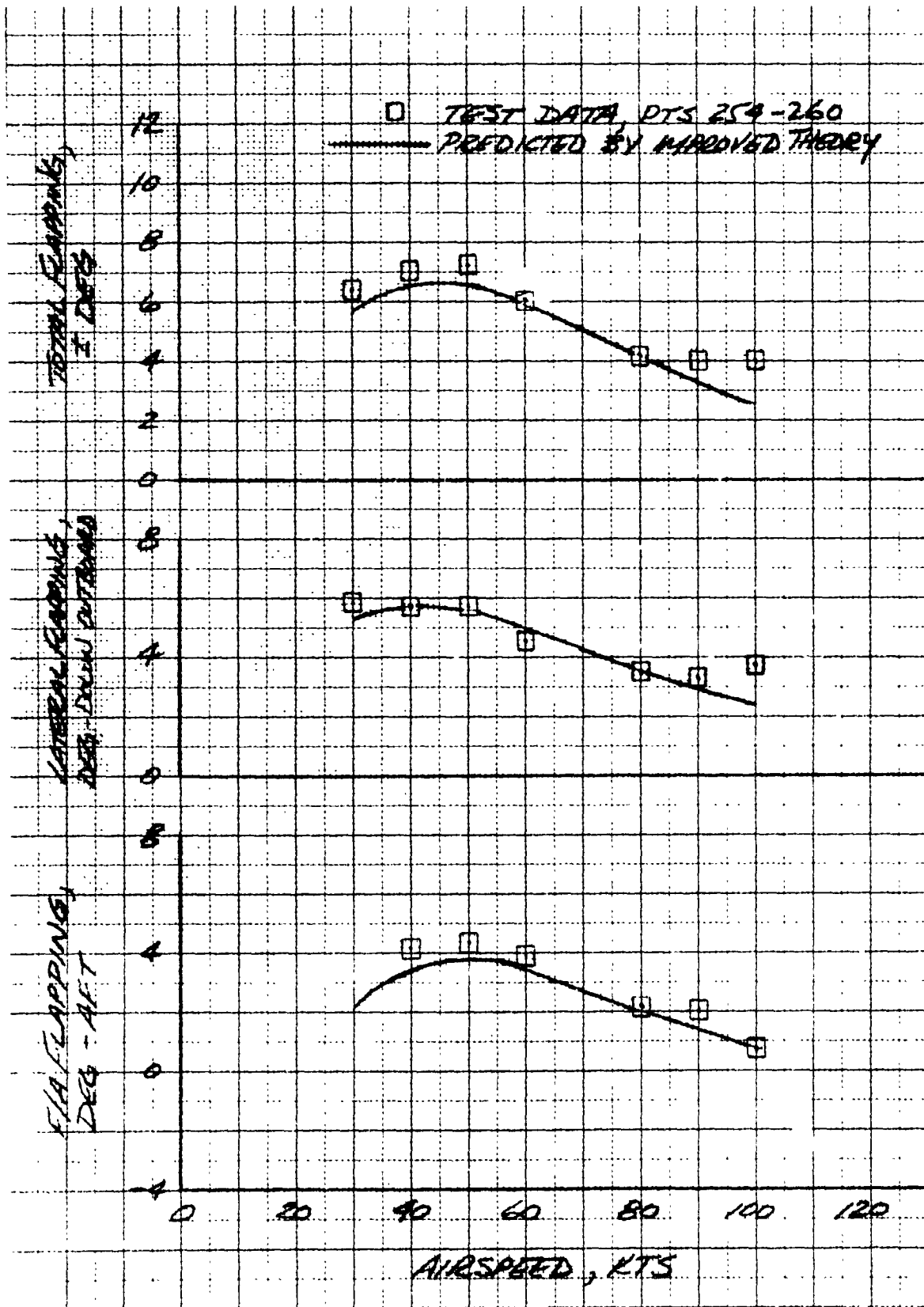


Figure VI-30. Correlation of Post Test Predicted Flapping with Measured Flapping, Mast Angle 75°.

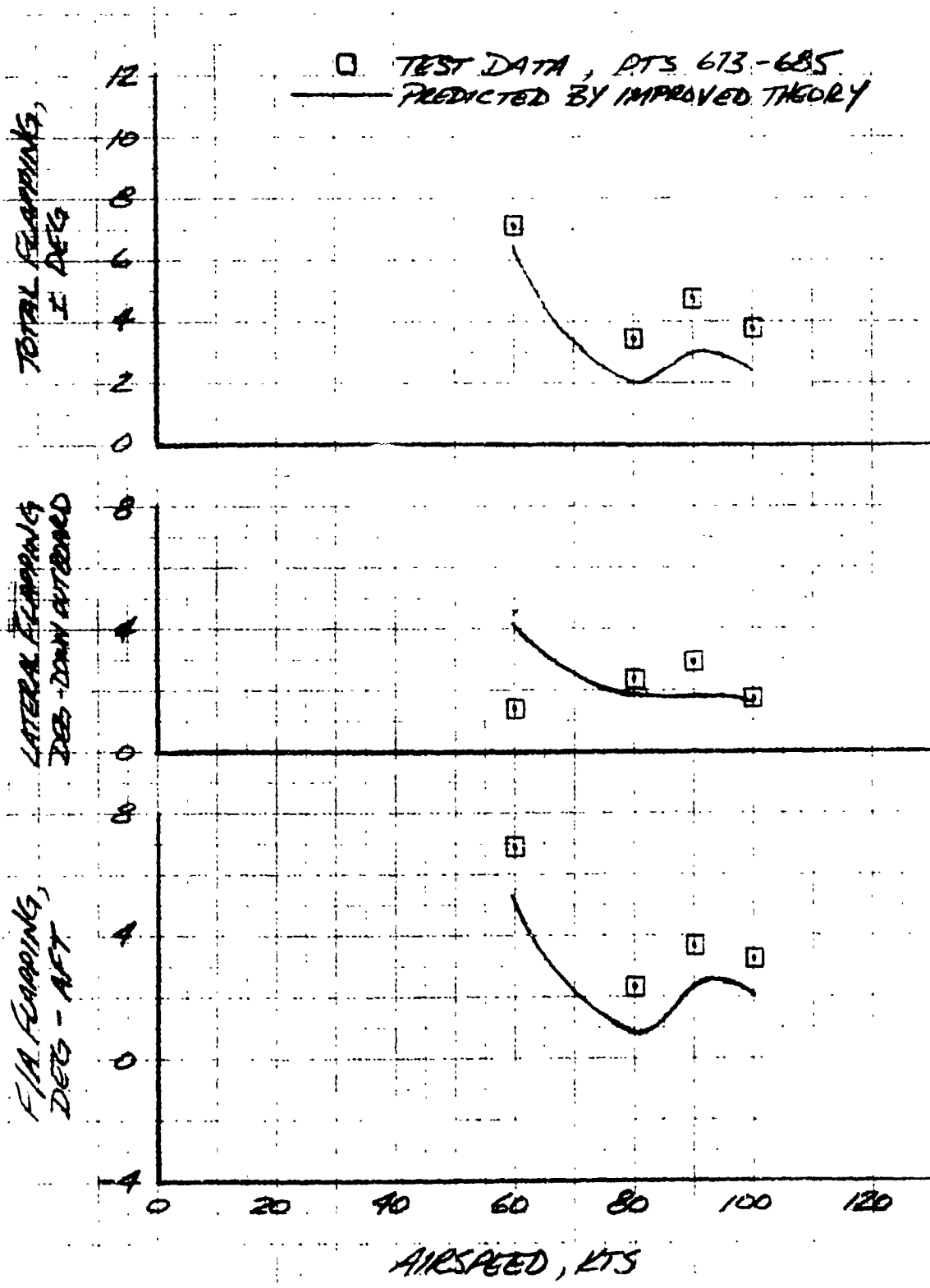


Figure VI-31. Comparison of Post Test Predicted Flapping with Measured Flapping, Mast Angle 60°.

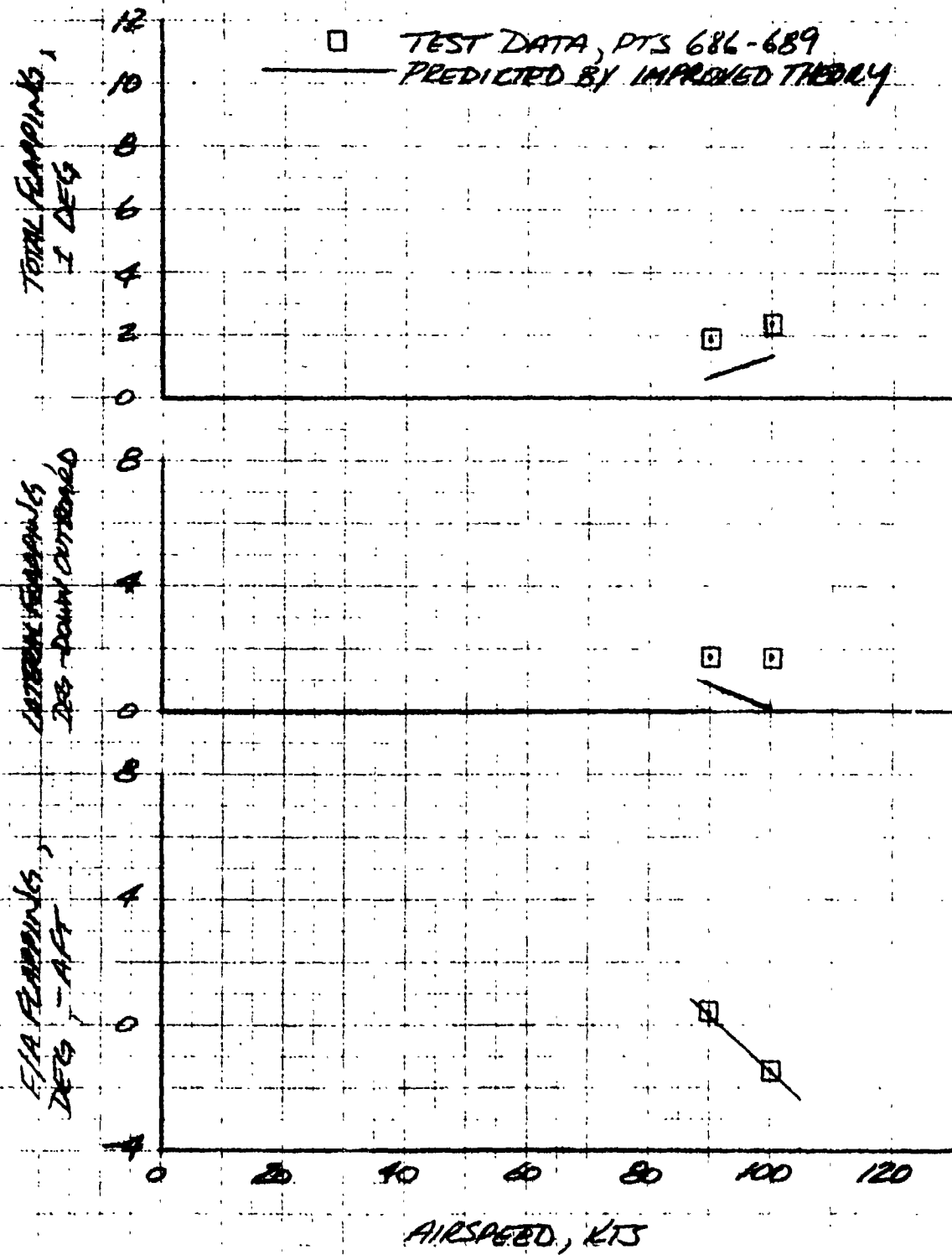


Figure VI-32. Comparison of Post Test Predicted Flapping with Measured Flapping, Mast Angle 30°.

VII. CONCLUSIONS

Observation of model behavior and analysis of measured data resulted in the following conclusions:

A. Hover

1. The hover test confirmed the presence of a static roll instability in an IGE hover. The magnitude of the instability was comparable to previous estimates and the instability vanishes at airspeeds above approximately 20 knots.
2. The wing download in hover was greater than that estimated from previous test results. The measured download was 11.4 percent compared to the 7 percent estimated for the full-scale aircraft. Analysis indicates this discrepancy may be the result of the model's very low Reynolds number.
3. Attempts to fly the model in a controlled hover on an essentially free-flight mount were not successful. Failure is attributed to the model's response being faster than full-scale by a factor of 2.24, and because the model pilots lacked many of the cues normally available in hover.

B. Low Speed Helicopter and Conversion Mode

1. Flow visualization techniques confirmed that the wakes from the two rotors do not merge and analysis of balance data indicate that the rotor wake has the effect of an upwash on the horizontal stabilizer.
2. At mast angles of 90 and 75 degrees, a shallow longitudinal stick gradient occurs between hover and 60 knots and a slight stick reversal occurs between 20 and 40 knots. The shallow gradient and reversal are caused by the rotor wake influence on the horizontal stabilizer.
3. The interaction between the rotor wake and the horizontal stabilizer causes a nose-up pitching moment when the aircraft is yawed. The longitudinal cyclic required to compensate for the pitching moment is easily within a pilot's ability. With the SCAS on, the altitude-hold loop will make the required cyclic input.
4. The rotor wake acts on the vertical fins in such a manner as to reduce directional stability for sideslip angles

4. (Continued)

less than about 12 degrees and to increase it for larger sideslip angles.

5. In autorotation, at the speeds tested (80 and 90 knots), the model was very stable but had a rate of descent in excess of 4000 fpm, compared to the 2200 fpm predicted for the Model 301. Analysis indicates that the model's low Reynolds number is responsible for its higher rates of descent and that the rate of descent predicted for the Model 301 is considered a reasonable estimate.
6. On the rod, the model was difficult to fly at speeds below 30 knots but was controllable. Above 30 knots, the model was relatively easy to fly. Controllability was adequate for rearward and sideward flight at speeds up to 35 knots.
7. Lateral flapping in helicopter mode was approximately 40 percent higher than predicted, but was within flapping limits for all conditions tested. Analysis shows that the theory used for the pretest predictions employed a representation of the longitudinal distribution of induced velocity which was not representative of the observed induced velocity distribution. By modifying the distribution good correlation with the measured flapping is achieved.

C. Dynamic Stability, Loads, and Vibration

1. There was no evidence of rotor or rotor-pylon-wing instability during the tests.
2. Scaled rotor and control system loads were significantly lower than those predicted for the full-scale aircraft.
3. Airframe vibration levels were higher than predicted but within design limits. The magnitude of the two-per-rev vibration indicates care will have to be taken to avoid resonance of airframe modes with two-per-rev.

D. Correlation of Theory With Measured Data

1. When Reynolds number effects are properly accounted for, theory adequately predicts model trim parameters and stability characteristics. (Extrapolation of model flight characteristics directly to full scale is not recommended because of Reynolds number effects.)
2. Theory predicts the measured lateral flapping when the rotor longitudinal distribution of induced velocity is correctly represented.

VIII. LIST OF REFERENCES

1. Contract NAS2-6599, Modification Number 2, Powered Aeroelastic Model Tests.
2. Bird, B. J.; Livingston, C. L.; and McLarty, T. T.: A Stability and Control Prediction Method for Helicopters and Stoppable Rotor Aircraft. AFFDL-TR-69-124, 4 Volumes, February 1970.
3. Lindsey, L.: A Low-Speed Wind-Tunnel Force Test of the 0.20 Scale Bell Helicopter Model 300. LTV Report LSWT 408, September 1972.
4. Hammond, G.: NASA-Langley Research Center Transonic Dynamics Tunnel Test of a Force Model of the Bell Helicopter Model 300. NASA-Langley TDT Report 195, to be published.
5. Hammond, G.: NASA-Langley Research Center Transonic Dynamics Tunnel Test of an Aeroelastic Bell Helicopter Model 300. NASA-Langley TDT Report 205 and 174, to be published.
6. Holbrook, J. W.: A Low-Speed Wind-Tunnel Test of the 0.20-Scale Bell Helicopter Model 300. LTV LSWT 311, January 1970.
7. Vaughn, J. B.: A Low-Speed Wind-Tunnel Force Test of the 0.20-Scale Bell Helicopter Model 300. LTV LSWT 333, May 1970.
8. Oldenbittel, R. H.: A Low-Speed Wind-Tunnel Test of the Bell Helicopter 0.20-Scale C-300-R/H Prop-Rotor Model to Obtain Rotor Normal and Side Force Data. LTV LSWT 360, January 1971.
9. Vaughn, J. B.: A Low-Speed Wind-Tunnel Test of the Aeroelastic 0.20-Scale Bell Helicopter Model 300. LTV Report LSWT 361, April 1971.
10. Holbrook, J. W.: A Low-Speed Wind-Tunnel Force Test of the 0.20-Scale Bell Helicopter Model 300. LTV Report LSWT 366, May 1971.
11. Vaughn, J. B.: A Low-Speed Wind-Tunnel Test of the Bell C300 A2A Model Investigating Flutter of Twin Vertical Tails, LTV Report LSWT 383, February 1972.

12. Marr, R. L.; and Neal, G. T.: Assessment of Model Testing of a Tilt Rotor VTOL Aircraft. Paper presented at AHS Symposium on Status of Testing and Modeling Techniques for V/STOL Aircraft, October 1972.
13. Deckert, W. H.; and Ferry, R. G.: Limited Flight Evaluation of the XV-3 Aircraft. Air Force Flight Test Center Report TR-60-4, May 1960.
14. Wilson, J. C.: Powered-Force Wind Tunnel Test of the Bell Helicopter Model C100-F/B Tilt Rotor Aircraft. NASA-Langley V/STOL Report 31, to be published.
15. Holbrook, J. W.: Low Speed Wind Tunnel Handbook, LTV Publication No. AER-EOR-12995-B, May 1968.
16. BHC Report 300-099-004, "Advancement of Proprotor Technology, Task II - Wind Tunnel Test Results, NASA CR 114363," September 1971.
17. BHC Report 301-199-003, "Volume 3 - Structural Loads and Dynamics, V/STOL Tilt Rotor Research Aircraft," January 1973.
18. Anon: USAF Stability and Control Datcom, Air Force Flight Dynamics Laboratory. Wright-Patterson Air Force Base, October 1960 (Rev. September 1970).
19. Wheatley, J. B.; and Bioletti, C.: Wind Tunnel Tests of a 10-Foot-Diameter Gyroplane Rotor. NACA TR 536, 1935.
20. Drees, M. J.: A Theory of Air Flow Through Rotors and Its Application to Some Helicopter Problems. The Journal of the Helicopter Society of Great Britain, 3(2), 1949.
21. Harris, F. D.: Articulated Rotor Blade Flapping Motion at Low Advance Ratio. Journal of the American Helicopter Society, January 1972.
22. Castles, W. Jr.; and DeLeeuw, J. H.: The Normal Component of the Induced Velocity in the Vicinity of a Lifting Rotor and Some Examples of Its Application. NACA TN 2912, March 1953.
23. Heyson, H. H.; and Katzoff, S.: Normal Component of Induced Velocity in the Vicinity of a Lifting Rotor With a Nonuniform Disk Loading. NACA TN 3690, April 1956.
24. Charles, B. D.: "Bell Rotor Aerodynamic Method," Bell Helicopter Report 599-102-900, July 1972.

APPENDIX A

Run Schedule Summary

Run Schedule Summary
Model C300-ARB Aeroplastic Model - Hover Test ($\alpha = 90^\circ$)

RUN No.	FLAP ANGLE (DEG)	Model Weight (LBS)	h/D	WING Panel	Comments
1	0/0	100	.5 to 1.0	ON	Hover Performance
2	"	90	"	"	"
3	"	75	"	"	"
4	"	50	"	"	"
5	"	75	1.0	"	"
6	45/25	79.5	"	"	"
7	75/75	78.5	"	"	"
8	75/45	79.5	"	"	"
9	60/45	"	"	"	"
10	75/45	90	.5 to 1.0	"	"
11	"	100	.5	"	"
12	"	75	.5 to 1.0	"	"
13	"	50	"	"	"
14	"	75	1.0	"	"
15-26	"	66	"	"	Roll Stability, $\phi = \pm 8^\circ$
28-37	"	"	.75	"	"
38	"	"	.50	"	Power-off calibration
39	"	"	"	"	Roll Stability, $\phi = \pm 8^\circ$
40	"	47	"	OFF	Hover Performance
41-42	"	66	"	"	"
43	"	"	"	"	Roll Stability, $\phi = \pm 8^\circ$
44	"	"	.75	"	Hover Performance
45	"	"	"	"	Roll Stability, $\phi = \pm 8^\circ$
46	"	"	1.0	"	Hover Performance
47	"	80	"	"	"
48	"	"	"	"	Roll Stability, $\phi = \pm 8^\circ$
50	"	50	"	"	TRANG, 2000 RPM
51	"	"	"	"	" Hover
52	"	"	"	"	" 2000 RPM
53	"	70	"	"	" Hover
54 ^a	"	"	"	"	Roll calibration
55-56	"	66	"	"	Hover Performance
57	"	"	"	"	Roll Stability, $\phi = \pm 6^\circ - 4^\circ$
58	"	"	.75	"	Hover Performance
59	"	"	"	"	Roll Stability, $\phi = \pm 6^\circ$
60	"	"	"	"	Roll Calibration
61	"	66	"	"	Hover Performance
62	"	"	"	"	Roll Stability, $\phi = \pm 6^\circ$
63	"	"	.50	"	Hover Performance
64	"	"	"	"	Roll Calibration
65	"	66	"	"	Roll Stability, $\phi = \pm 6^\circ$
66	"	"	"	"	Hover Performance
67	"	50	.5 to 1.0	"	"
68	"	60	"	"	"
69	"	70	"	"	"
70	"	80	"	"	"
71	"	"	"	"	"
72	75/45	66	.5	ON	"
73	"	"	"	"	Roll Calibration
74	"	66	"	"	Roll Stability, $\phi = \pm 6^\circ$
75	"	"	.75	"	Hover Performance
76	"	"	"	"	Roll Calibration
77	"	66	"	"	Roll Stability, $\phi = \pm 6^\circ$
78	"	"	1.0	"	Hover Perf, Roll Stab, $\phi = \pm 6^\circ$

LSWT 418
 Run Schedule Summary
 Model C300-A2B Aerodynamic Model - Rod Test*

Run No	Point No	MAST ANGLE (DEG)	AIRPEED (KT-FT)	INCIDENCE IN (DEG)	Model WEIGHT (LBS)	VERTEX Generator	Comments
1	5	90	30	0	88.5	OFF	Trim -level Fit
2	6-10	"	"	"	"	"	Stability - "
	11	"	40	"	"	"	Trim - "
	12-15	"	"	"	"	"	Stability - "
	16	"	60	"	"	"	Trim - "
3	17-23	"	"	"	"	"	Stability - "
	24-25	"	80	"	"	"	Trim - "
	26-29	"	"	"	"	"	Stability - "
	30	"	"	"	"	"	Trim - "
4	31-32	"	"	"	"	"	Stability - "
	33	"	90	"	"	"	Trim - "
	34-37	"	"	"	"	"	Stability - "
	38	"	100	"	"	"	Trim - "
5	39-42	"	"	"	"	"	Stability - "
	43	"	16	"	"	"	Trim - "
	44-47	"	"	"	"	"	Stability - "
	48	"	20	"	"	"	Trim - "
6	49-52	"	"	"	"	"	Stability - "
	53	"	40	"	"	"	Trim - "
	54	"	16	"	"	"	Stability - "
	55-60	"	"	"	"	"	Trim - "
7	61	"	20	"	"	"	Stability - "
	62-65	"	"	"	"	"	Trim - "
	66	"	60	"	"	"	Stability - "
	67-72	"	80	"	"	"	Trim - "
8	73	"	90	"	"	"	Trim - "
	74-75	"	100	"	"	"	Stability - "
	80	"	30	"	"	"	Trim - "
	81	"	40	"	"	"	Stability - "
9	82-84	"	60	"	"	"	Trim - "
	85	"	80	"	"	"	Trim - "
	86	"	70	"	"	"	Stability - "
	87-89	"	100	"	"	"	Trim - "
10	90	"	40	+10	"	"	Trim - B ₁
	91	"	60	"	"	"	Stability - "
11	92	75	60	0	"	"	Trim - "
	93-96	"	"	"	"	"	Stability - "
	97	"	80	"	"	"	Trim - "
	98-101	"	"	"	"	"	Stability - "
12	102	"	100	"	"	"	Trim - "
	103	"	"	"	"	"	Stability - "
	104-107	"	"	"	"	"	Trim - "
	108	"	40	-10	"	"	Stability - "
13	109-113	"	"	"	"	"	Trim - "
	114	"	60	"	"	"	Stability - "
	115-118	"	"	"	"	"	Trim - "
	119	"	"	"	"	"	Stability - "
14	120	"	40	+10	"	"	Trim - Climb
	121	"	60	"	"	"	Stability - Level Fit
15	122	60	80	0	"	"	Trim - "
	123-126	"	100	"	"	"	Stability - "
	127	"	"	"	"	"	Trim - "

* SF = 45/25 unless noted, $\Omega = 1260$ RPM

LSWT 418
Run Schedule Summary
Model C300 Aeroblastic Model - Rod Test

Run No	Point No	MAST ANGLE (DEG)	AIR SPEED (KTS-FS)	INCIDENCE IN (DEG)	Model Height (LBS)	VORTEX Sensors	Comments
14	132	30	80	0	88.5	OFF	Trim - Level Flt
	133	"	90	"	"	"	" - "
	134	"	100	"	"	"	" - "
	135-134	"	"	"	"	"	Stability - "
15	147	90	30	"	104.0	"	Trim - "
	148	"	40	"	"	"	" - "
	149	"	50	"	"	"	" - "
	151	"	60	"	"	"	" - "
	152	"	80	"	"	"	" - "
16	153	"	100	"	"	"	" - "
	155-156	"	60	"	114.0	"	" - "
	157	"	80	"	"	"	" - "
17	158	"	"	"	124.0	"	" - "
	159-160	75	"	"	124.0	"	" - "
18	161-162	"	"	"	129.0	"	" - "
	163-167	90	60	"	82.5	"	Trim - Descent
19	168-169	"	80	"	"	"	" - "
	171-172	"	60	"	"	"	" - Sr. 25° - "
20	173-175	"	80	"	"	"	" - "
	176	75	60	"	"	"	Trim - Climb
21	177-179	"	80	"	"	"	" - "
	180-181	"	30	"	"	"	Trim - Level Flt
22	182-186	"	"	"	"	"	Stability - "
	187	"	40	"	"	"	Trim - "
23	188-196	"	30	"	"	"	Pitch sweep
	197-204	"	60	"	"	"	" - "
24	205	"	Hover	"	"	"	Trim - Level Flt
	209	"	30	"	104.0	"	" - "
	210	"	40	"	"	"	" - "
	211	"	50	"	"	"	" - "
	212	"	60	"	"	"	" - "
	214	"	80	"	"	"	" - "
	215	"	90	"	"	"	" - "
216	"	100	"	"	"	" - "	
25	217-219	"	80	"	89.5	"	" - Climb
	220-221	"	30	"	104.0	"	" - Level Flt
26	224	"	30	"	"	ON	" - "
	225	"	40	"	"	"	" - "
	226	"	50	"	"	"	" - "
27	227-233	"	Hover	"	"	"	Trim - B ₁ - "
	234-240	"	30	"	89.5	"	Trim - B ₁ - "
28	241-244	"	40	"	"	"	Trim - B ₁ - "
	245-253	"	"	"	"	"	Trim - B ₁ - "
29	254	"	30	"	"	"	Trim - Level Flt
	255	"	40	"	"	"	" - "
	256	"	50	"	"	"	" - "
	257	"	60	"	"	"	" - "
	258	"	80	"	"	"	" - "
	259	"	90	"	"	"	" - "
260	"	100	"	"	"	" - "	

LSWT 418
 Run Schedule Summary
 Model C300 AZB Aerelastic Model - Rod Test

Run No	Point No	Mast Angle (DEG)	Airspeed (KTS - IAS)	Incl. Inc (DEG)	Metal Weight (LBS)	Vertex Generator	Comments
29	261-267	75	30	0	89.5	ON	Yaw Sweep
	268-273	"	40	"	"	"	"
	274-279	"	50	"	"	"	"
30	280	"	30	"	"	"	Trim - 2° - Level FL
	281	"	40	"	"	"	"
	282	"	50	"	"	"	"
	283	"	60	"	"	"	"
	284	"	80	"	"	"	"
	285-286	"	90	"	"	"	"
31	287-294	"	30	"	"	"	Pitch Sweep - 0°
	295-306	90	80	"	"	"	Trim - 0° - 1100 RPM
32	307-312	"	60	"	"	"	"
33	313-317	"	80	"	"	"	Trim - Descend
34/35	318-320	95	"	"	"	"	"
36	321-323	"	"	"	"	"	1100 RPM - "
	324	"	"	"	"	"	900 - "
	325	"	"	"	"	"	950 - "
	326	"	70	"	"	"	1100 - "
	327	"	"	"	"	"	"
37	328	"	60	"	"	"	"
	329-330	"	50	"	"	"	"
38	331-332	"	90	"	"	"	"
	333-336	"	"	"	"	"	1100 - "
39	337	90	80	"	1040	"	"
	338	"	"	"	"	"	1100 - "
	339	"	"	"	"	"	950 - "
	340	"	"	"	"	"	900 - "
	341	"	"	"	"	"	"
41	342	"	Hover	"	89.5	"	Trim - Level Flt
	343-344	"	30	"	"	"	"
	345	"	40	"	"	"	"
	346	"	50	"	"	"	"
	347	"	60	"	"	"	"
	348	"	80	"	"	"	"
	349	"	90	"	"	"	"
42	350-351	"	30	-4	"	"	"
	352	"	40	"	"	"	"
	353	"	50	"	"	"	"
	354	"	60	"	"	"	"
	355	"	80	"	"	"	"
	356	"	90	"	"	"	"
	357	"	100	"	"	"	"
43	361	"	40	74	"	"	"
	362	"	50	"	"	"	"
	363	"	60	"	"	"	"
	364	"	80	"	"	"	"
44	365-369	"	30	0	"	"	Yaw Sweep
	370-373	"	40	"	"	"	"
	374-379	"	50	"	"	"	"

Note: Run 1-44 Roll locked out, Roll Free Run 45 ON

LSWT 418
Run Schedule Summary
Model C300 A2B Aerelastic Model - Rod Test

Run No	Point No	Mast Angle (DEG)	Average Incidence (KTS-FS) (DEG)	Model Weight (LBS)	Vortex Generator	Comments
45	383	90	50	89.5	ON	Trim - level fit
	384-397	"	60	"	"	Roll Sweep
46	398-403	"	80	"	"	"
48	406-419	"	50	90.5	"	Pitch Sweep
49	420-429	"	40	"	"	"
	430-437	"	30	"	"	"
	438-439	"	40	"	"	"
50	442-453	"	40	"	"	Pitch Sweep, $\delta\alpha = 75^\circ$
51	455-471	"	30	"	"	"
52	473-486	"	50	"	"	"
	489-501	"	60	"	"	"
53	504-512	"	60	"	"	"
54	517	"	30	"	"	Trim, wing-off, level fit
	519	"	40	"	"	"
55	523-528	"	16	"	"	"
	530-536	"	20	"	"	"
	537-543	"	30	"	"	"
	546-550	"	40	"	"	"
	552-556	"	50	"	"	"
56	558	"	16	"	"	"
	559	"	20	"	"	"
	560	"	30	"	"	"
	561	"	40	"	"	"
57	562-569	"	60	"	"	"
	571-572	"	80	"	"	"
	573	"	"	105.5	"	"
	574	"	"	103.5	"	"
58	577-578	"	16	90.5	ON	Trim - level fit
	579-580	"	20	"	"	"
	581-582	"	30	"	"	"
59	583-585	"	40	"	"	"
60	586-575	"	"	"	"	"
61	596	"	20	"	"	"
	597	"	40	"	"	"
62	598	"	20	"	"	"
	599-600	"	40	"	"	"
	601-602	"	50	"	"	"
63	603-604	"	20	"	"	Trim, $\delta\alpha = 75^\circ$ - level fit
	605-607	"	30	"	"	"
	608-615	"	40	"	"	"
	616-617	"	50	"	"	"
64	618-619	"	16	"	"	" $\delta\alpha = 0^\circ$
	620-624	"	20	"	"	"
	626-631	"	30	"	"	"
65	633-636	"	40	"	"	"
	637-641	"	50	"	"	"
66	646	"	80	"	"	"
	647	"	"	105.5	"	"
	648	"	"	120.5	"	"
	649	"	"	117.0	"	"

LSWIT 418
Run Schedule Summary
Model C300 AZB Aeroclastic Model - Rod Test

Run No	Point No	Mast Angle (DEG)	Air Speed (KTS-F.S)	Inclination (DEG)	Model Weight (LBS)	Vortex Generators	Comments
67	650	90	30	0	90.5	ON	Trim, Roll free, level fit
	651	"	40	"	"	"	"
	652	"	50	"	"	"	"
	653	"	60	"	"	"	"
	654	"	80	"	"	"	"
	657	"	90	"	"	"	"
68	658	"	100	"	"	"	"
	659	"	110	"	"	"	"
	663	"	Hover	"	75	"	Trim, Sr: 35
	664	"	"	"	"	"	" = 45
	665	"	"	"	"	"	" = 60
	666	"	"	"	"	"	" = 75
69	667	"	"	"	"	"	" = 45
	668	"	16	"	29	"	Trim - Level fit
	669	"	20	"	"	"	"
70-74	670	"	30	"	"	"	"
	673	60	60	"	"	"	"
	675-680	"	80	"	"	"	"
	681-682	"	90	"	"	"	"
75	683-685	"	100	"	"	"	"
	686-689	30	90	"	"	"	"
	690-692	"	100	"	"	"	"
77-78	693	90	16	"	60	"	Trim - Sideward fit
	696	"	Hover	"	"	"	"
	697	"	16	"	"	"	"
	695	"	20	"	"	"	"
	699	"	25	"	"	"	"
79	700	"	30	"	"	"	"
	702	"	Hover	"	90	"	"
	703	"	16	"	"	"	"
	704	"	20	"	"	"	"
	705	"	25	"	"	"	"
	706	"	30	"	"	"	"
80	707-711	"	30	"	63	"	"
	713	"	16	"	60	"	Keenward fit
	714-717	"	20	"	"	"	"
	718	"	25	"	"	"	"
	719-721	"	30	"	"	"	"
81	722	"	16	"	90	"	"
	723-724	"	20	"	"	"	"
	725-728	"	25	"	"	"	"
	731-732	"	35	"	"	"	"
82	733	"	20	"	"	"	Engg, Remmed
	731-736	"	25	"	"	"	"
	737	"	30	"	"	"	"
	738	"	35	"	"	"	"
83	740-741	"	Hover	"	"	"	Trim, LGE, MID: 75
	742-743	"	16	"	"	"	"
	744	"	20	"	"	"	"
	745-751	"	25	"	"	"	"
	752-757	"	30	"	"	"	"

LSWT 418
Run Schedule Summary
Model C370 AZB Aeroelastic Model - Rod Test

Run No	Point No	Mast Angle (DEG)	Airspeed (KTS IAS)	Inertia I _H (LBS)	Mass Weight (LBS)	Vortex Generator	Comments
83	758	90	16	0	90	ON	Trim, IGE, h/D = .75
	760-761	"	20	"	"	"	" " " "
	762-763	"	25	"	"	"	" " " "
	764-765	"	30	"	"	"	" " " "
84	770-772	"	16	"	"	"	" " " h/D = .6
	773-774	"	20	"	"	"	" " " "
	779-781	"	25	"	"	"	" " " "
	782-783	"	30	"	"	"	" " " "
	789-790	"	20	"	"	"	" " " "
	791-793	"	40	"	"	"	" " " "
85	794-796	"	40	"	"	"	" " " h/D = .75
	797-799	"	60	"	"	"	" " " "
86	800-802	"	60	"	"	"	" " " h/D = .6
87	805	75	40	"	"	"	" " " "
	806	"	"	"	"	"	" " " h/D = .75
	807-809	"	"	"	"	"	" " " h/D = .6
	810-812	"	"	"	"	"	" " " h/D = .75
	813-817	"	"	"	"	"	" " " h/D = .6
	818-820	"	60	"	"	"	" " " h/D = .75
	821-823	"	16	"	"	"	" " " h/D = .6
	824-826	"	"	"	"	"	" " " h/D = .75
	827-829	"	20	"	"	"	" " " = .6
	830-832	"	"	"	"	"	" " " = .75
	833-838	"	25	"	"	"	" " " = .75
88	839-845	"	"	"	"	"	" " " = .75
	846-852	"	30	"	"	"	" " " = .6
	853-858	"	"	"	"	"	" " " = .75
	859-860	"	80	"	"	"	" " " "
	864	90	30	"	"	"	" " " h/D = .75
89	865	"	40	"	"	"	" " " "
	866	"	50	"	"	"	" " " "
	867-868	"	30	"	"	"	" " " "
90,91	869-875	"	30,40	"	"	"	Smoke studies
End of Rod Test							

LSWT 421
Run Schedule Summary
Model C300-A2B Aeroclastic Model - Sting test*

Run No	Point No	MAST Angle (DEG)	Airspeed (KTS-FS)	Inclination IN (DEG)	TRIM (DEG)	Rotors	Comments
1	1003-1004	90	40	0	-2	ON	Elevator Sweep
2	1005-1009	"	"	"	"	"	"
3	1010-1015	"	"	"	"	"	"
4	1017-1025	"	"	"	"	"	Pitch Sweep - Level
5	1026-1034	"	"	"	"	"	YAW SWEEP d = -2
6	1035-1043	"	"	"	"	"	"
7	1047-1055	"	"	"	"	"	"
8	1056-1064	"	"	"	"	"	"
9	1065-1073	"	"	"	"	"	"
10	1074-1081	"	"	"	-	"	Pitch Sweep - Descent
11	1082-1088	"	"	"	-	"	"
12	1089-1095	"	"	"	-	"	"
13	1096-1103	"	"	"	-	"	" - Climb
14	1104-1110	"	"	"	-	"	"
15	1111-1114	"	"	"	-	"	"
16	1116-1119	"	16-40	"	0 to -2	"	Smoke Judice - cycle
17	1120-1123	"	"	"	"	"	" - Top
18	1126-1131	"	30	"	0	"	Elevator Sweep
19	1132-1137	"	"	"	"	"	Pitch Sweep - Level
20	1138-1146	"	"	"	"	"	Yaw Sweep - "
21	1147-1154	"	20	"	"	"	Elevator Sweep
22	1155-1161	"	"	"	"	"	Pitch Sweep - Level
23	1162-1170	"	"	"	"	"	Yaw Sweep - "
24	1171-1177	"	16	"	"	"	Pitch Sweep - "
25	1178-1185	"	"	"	"	"	Yaw Sweep - "
26	1188-1194	"	40	"	-2	"	Pitch Sweep - "
27	1195-1202	"	"	"	"	"	Yaw Sweep - "
28	1203-1208	"	60	"	-6	"	Elevator Sweep - "
29	1209-1212	"	"	"	"	"	Pitch Sweep - "
30	1218-1225	"	"	"	"	"	Yaw Sweep - "
31	1228-1234	"	80	"	-8	"	Elevator Sweep - "
32	1235-1243	"	"	"	"	"	Pitch Sweep - "
33	1244-1254	"	"	"	"	"	Yaw Sweep - "
34	1255-1264	"	"	"	"	"	Pitch Sweep - Descent
35	1265-1267	"	"	"	"	"	" - Arbitrary
36	1268-1273	"	"	"	"	"	" - Climb
37	1276-1283	"	40	-4	-2	"	Pitch Sweep - Level
38	1284-1292	"	60	"	-6	"	"
39	1293-1300	"	80	"	-8	"	"
40	1301-1306	"	20	"	0	"	"
41	1307-1312	"	30	"	0	"	"
42	1319-1321	"	16-40	0	0 to -2	"	Test grid - Level
43	1323-1341	"	40	"	"	"	Pitch Sweep - Descent
44	1342-1349	"	"	"	"	"	" - Climb
45	1350-1356	"	30	"	"	"	Pitch Sweep - Descent
46	1357-1365	"	"	"	"	"	Yaw Sweep - "
47	1366-1372	"	"	"	"	"	Pitch Sweep - Climb
48	1373-1380	"	"	"	"	"	Yaw Sweep - "
49	1382-1388	"	25	"	"	"	Pitch Sweep - Descent
50	1389-1396	"	"	"	"	"	Yaw Sweep - "
51	1397-1403	"	"	"	"	"	Pitch Sweep - Climb

* Sr-45/25, Model 101: 90 LBS, JL-1260 RPM, VORTEX Generators ON unless noted

LSWT 421
Run Schedule Summary
Model C300-A2B Acroelastic Model - Sting Test

Run No	Point No.	MAST Angle (DEG)	Airspeed (KTS-FS)	Incidence IN (DEG)	TRIM (DEG)	Rotors	Comments
52	1405-1411	90	60	0	-	ON	Pitch Sweep - Descent
53	1412-1420	"	"	"	-	"	Yaw Sweep - "
54	1421-1427	"	"	"	-	"	Pitch Sweep - Climb
55	1428-1435	"	"	"	-	"	Yaw Sweep - "
56	1436-1441	"	80	"	-	"	" " - Descent
57	1442-1451	"	"	"	-	"	" " - Climb
58	1452-1461	"	"	"	-	"	Pitch Sweep, & Descent
59	1462-1470	"	"	"	-	"	" " - "
60	1471-1478	75	16	"	12	"	Elevator Sweep - Level
61	1479-1484	"	"	"	"	"	Pitch Sweep - "
62	1485-1492	"	"	"	"	"	Yaw Sweep - "
63	1493-1498	"	20	"	"	"	Elevator Sweep - "
64	1499-1503	"	"	"	"	"	Pitch Sweep - "
65	1504-1511	"	"	"	"	"	Yaw Sweep - "
66	1512-1520	"	30	"	10	"	Elevator Sweep - "
67	1521-1526	"	"	"	"	"	Pitch Sweep - "
68	1527-1534	"	"	"	"	"	Yaw Sweep - "
69	1535-1540	"	40	"	8	"	Elevator Sweep - "
70	1541-1546	"	"	"	"	"	Pitch Sweep - "
71	1547-1551	"	"	"	"	"	Yaw Sweep - "
72	1552-1562	"	60	"	4	"	Elevator Sweep - "
73	1563-1569	"	"	"	"	"	Pitch Sweep - "
74	1570-1577	"	"	"	"	"	Yaw Sweep - "
75	1578-1584	"	80	"	2	"	Elevator Sweep - "
76	1585-1591	"	"	"	"	"	Pitch Sweep - "
77	1592-1600	"	"	"	"	"	Yaw Sweep - "
78	1601-1608	"	20	-4	12	"	Pitch Sweep - "
79	1609-1614	"	30	"	10	"	" " - "
80	1615-1620	"	40	"	8	"	" " - "
81	1621-1626	"	60	"	4	"	" " - "
82	1627-1633	"	80	"	2	"	" " - "
83	1634-1639	"	40	0	-	"	Pitch Sweep - Descent
84	1640-1648	"	"	"	-	"	Yaw Sweep - "
85	1649-1657	"	"	"	-	"	Pitch Sweep - Climb
86	1658-1665	"	"	"	-	"	Yaw Sweep - "
87	1666-1671	"	60	"	-	"	Pitch Sweep - Descent
88	1672-1679	"	"	"	-	"	Yaw Sweep - "
89	1680-1685	"	"	"	-	"	Pitch Sweep - Climb
90	1686-1693	"	"	"	-	"	Yaw Sweep - "
91	1694-1699	"	80	"	-	"	Pitch Sweep - Descent
92	1700-1701	"	"	"	-	"	Yaw Sweep - "
93	1702-1713	"	"	"	-	"	Pitch Sweep - Climb
94	1714-1721	"	"	"	-	"	Yaw Sweep - "
RUN 1-94 tail on Run 95-128 tail off							
95	1722-1732	75	80	-	2	ON	Pitch Sweep - Level
96	1733-1740	"	"	-	"	"	Yaw Sweep - "
97	1741-1746	"	60	-	4	"	Pitch Sweep - "
98	1747-1754	"	"	-	"	"	Yaw Sweep - "
99	1755-1760	"	40	-	8	"	Pitch Sweep - "
100	1761-1765	"	"	-	"	"	Yaw Sweep - "
101	1766-1774	"	30	-	10	"	Pitch Sweep - "
102	1775-1783	"	"	-	"	"	Yaw Sweep - "

Use or disclosure of data on this page is subject to the restriction on the title page

LSWT 421
Run Schedule Summary
Model C300-A2B Aeroelastic Model - Stung Test

Run No	Point No	Mast Angle (D.G)	Airspeed (KTS - F.S)	Inclination (DEG)	Trim (DEG)	Rotors	Comments
103	1785-1790	90	30	-	0	ON	Pitch Sweep - Level
104	1791-1799	"	"	-	"	"	Yaw Sweep - "
105	1800-1805	"	40	-	-2	"	Pitch Sweep - "
106	1806-1814	"	"	-	"	"	Yaw Sweep - "
107	1815-1823	"	60	-	-6	"	Pitch Sweep - "
108	1824-1832	"	"	-	"	"	Yaw Sweep - "
109	1833-1837	"	80	-	-8	"	Pitch Sweep - "
110	1838-1846	"	"	-	"	"	Yaw Sweep - "
111	1847-1852	"	80	-	-	"	Pitch Sweep - Descent
112	1853-1858	"	"	-	-	"	" - Climb
113	1859-1864	"	60	-	-	"	" - Descent
114	1865-1872	"	20	-	0	"	" - Level
115	1873-1880	"	"	-	"	"	Yaw Sweep - "
116	1881-1886	"	"	-	"	"	Pitch Sweep - Descent
117	1887-1892	"	30	-	-	"	" - Climb
118	1893-1898	"	"	-	-	"	" - Descent
119	1900-1905	"	40	-	-	"	" - Climb
120	1906-1911	"	"	-	-	"	" - "
121	1912-1917	"	60	-	-	"	" - "
122	1920-1925	60	80	-	8	"	Pitch Sweep - Level
123	1926-1933	"	"	-	"	"	Yaw Sweep - "
124	1934-1940	"	100	-	4	"	Pitch Sweep - "
125	1941-1948	"	"	-	"	"	Yaw Sweep - "
126	1951-1957	30	80	-	14	"	Pitch Sweep - "
127	1955-1959	"	100	-	10	"	" - "
128	1960-1967	"	"	-	"	"	Yaw Sweep - "
Run 129-136 Tail-on							
129	1970-1973	30	80	0	14	ON	Pitch Sweep - Level
130	1974-1978	"	100	"	10	"	" - "
131	1979-1985	"	"	"	"	"	Yaw Sweep - "
132	1986-1993	60	80	"	8	"	Pitch Sweep - "
133	1994-2001	"	"	"	"	"	Yaw Sweep - "
134	2002-2007	"	100	"	4	"	Pitch Sweep - "
135	2008-2013	"	"	"	"	"	Yaw Sweep - "
136	2014-2018	"	"	"	"	"	Yaw Sweep - "
END OF ROTOR-ON TESTING							
137	2021-2030	60	80	0	-	OFF	Pitch Sweep
138	2031-2039	"	"	-4	-	"	Yaw Sweep
139	2040-2049	"	"	"	-	"	Pitch Sweep
140	2051-2061	30	"	"	-	"	" - "
141	2063-2072	"	"	0	-	"	" - "
142	2073-2080	"	"	"	-	"	Yaw Sweep
143	2083-2092	75	40	0	-	"	Pitch Sweep
144	2093-2100	"	"	"	-	"	Yaw Sweep
145	2101-2110	"	60	"	-	"	Pitch Sweep
146	2111-2118	"	"	"	-	"	Yaw Sweep
147	2120-2129	"	80	"	-	"	Pitch Sweep
148	2130-2138	"	"	"	-	"	Yaw Sweep
149	2139-2146	"	40	-4	-	"	Pitch Sweep
150	2149-2158	"	60	"	-	"	" - "
151	2159-2166	"	80	"	-	"	" - "

LSWT 421
Run Schedule Summary
Model C300-A2B Aeroelastic Model - Sting Test

Run No	Point No	Mast Angle (DEG)	Axised Incidence (K/S-F/S)	Incidence IN (DEG)	TRIM (DEG)	Rotors	Comments
152	2172-2181	90	40	-4	-	OFF	Pitch Sweep
153	2182-2192	"	60	"	-	"	"
154	2193-2204	"	80	"	-	"	"
155	2207-2217	"	40	0	-	"	Pitch Sweep
156	2218-2225	"	"	"	-	"	Yaw Sweep
157	2226-2236	"	60	"	-	"	Pitch Sweep
158	2237-2244	"	"	"	-	"	Yaw Sweep
159	2245-2255	"	80	"	-	"	Pitch Sweep
160	2256-2264	"	"	"	-	"	Yaw Sweep
Run 137-160 tail-on Run 161-176 tail-off							
161	-	90	40	-	-	OFF	Pitch Sweep
162	-	"	"	-	-	"	Yaw Sweep
163	-	"	60	-	-	"	Pitch Sweep
164	-	"	"	-	-	"	Yaw Sweep
165	-	"	80	-	-	"	Pitch Sweep
166	-	"	"	-	-	"	Yaw Sweep
167	-	75	40	-	-	"	Pitch Sweep
168	-	"	"	-	-	"	Yaw Sweep
169	-	"	60	-	-	"	Pitch Sweep
170	-	"	"	-	-	"	Yaw Sweep
171	-	"	80	-	-	"	Pitch Sweep
172	-	"	"	-	-	"	Yaw Sweep
173	-	60	80	-	-	"	Pitch Sweep
174	-	"	"	-	-	"	Yaw Sweep
175	-	30	30	-	-	"	Pitch Sweep
176	-	"	"	-	-	"	Yaw Sweep
End of Sting Test							

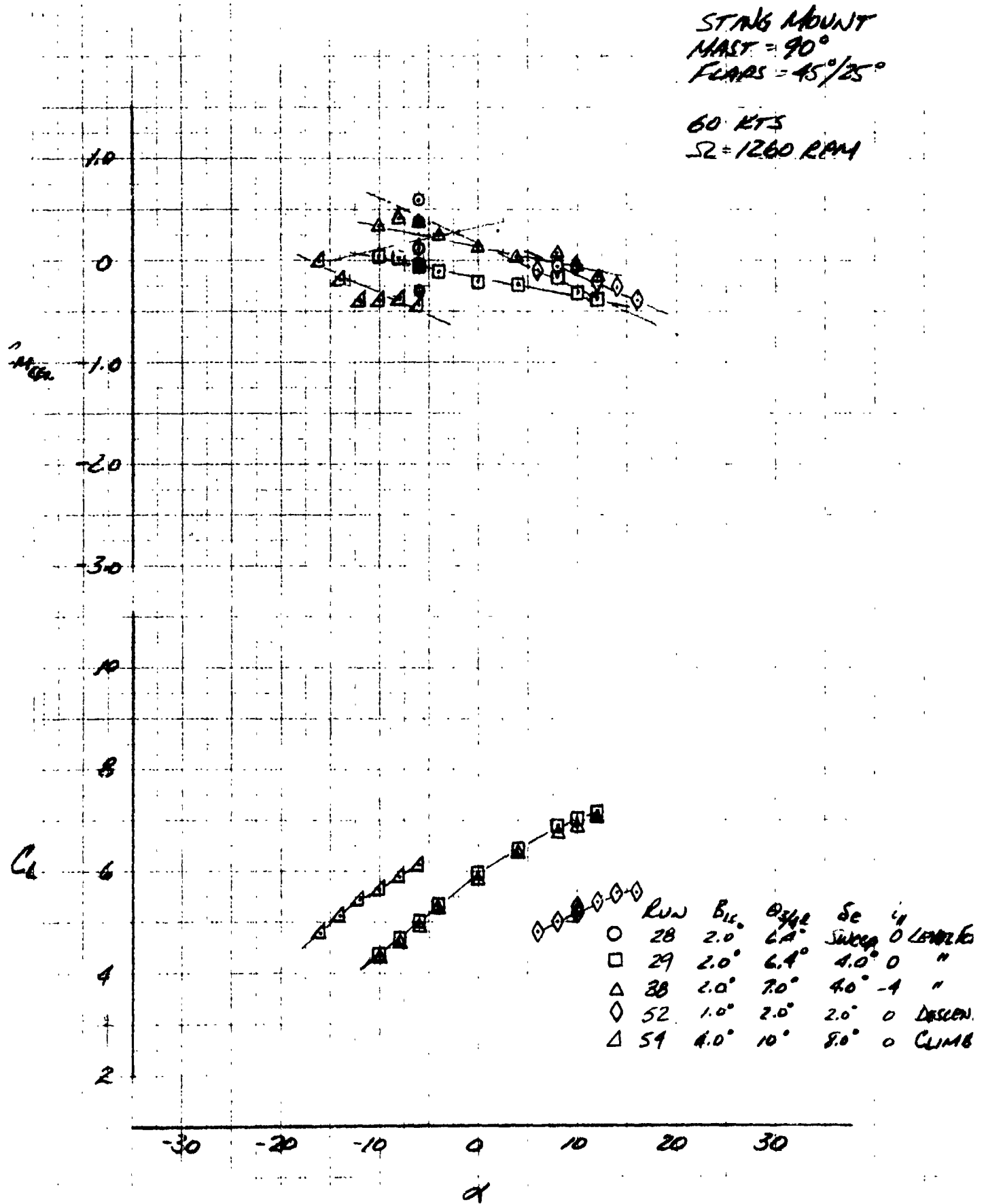
APPENDIX B

Sting Test Balance Data

LSWT 421

STING MOUNT
 MAST = 90°
 FCARS = 45°/25°

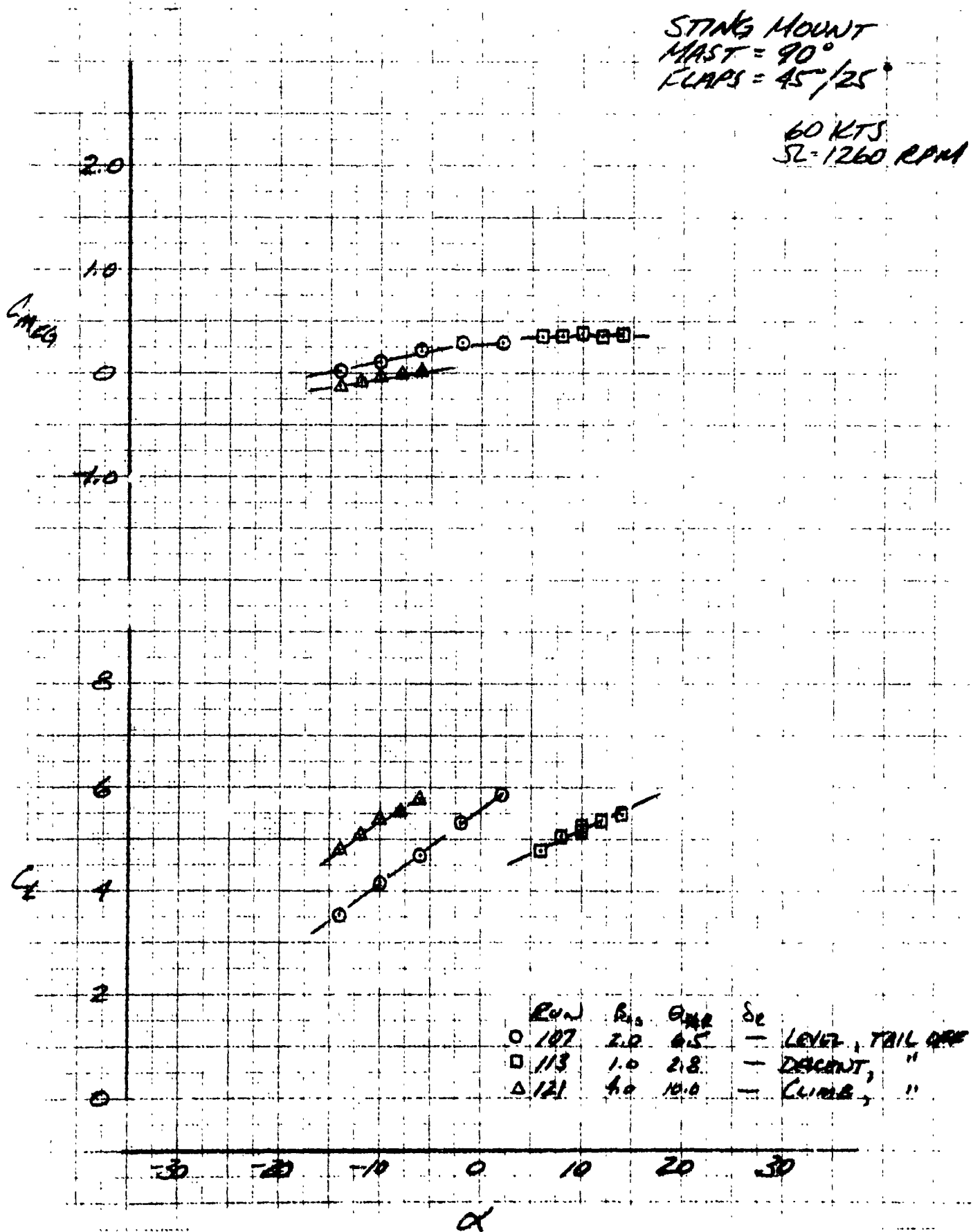
60 KTS
 Ω = 1260 RPM



LSWT 421

STING MOUNT
MAST = 90°
FLAPS = 45°/25°

60 KTS
SL-1260 RPM

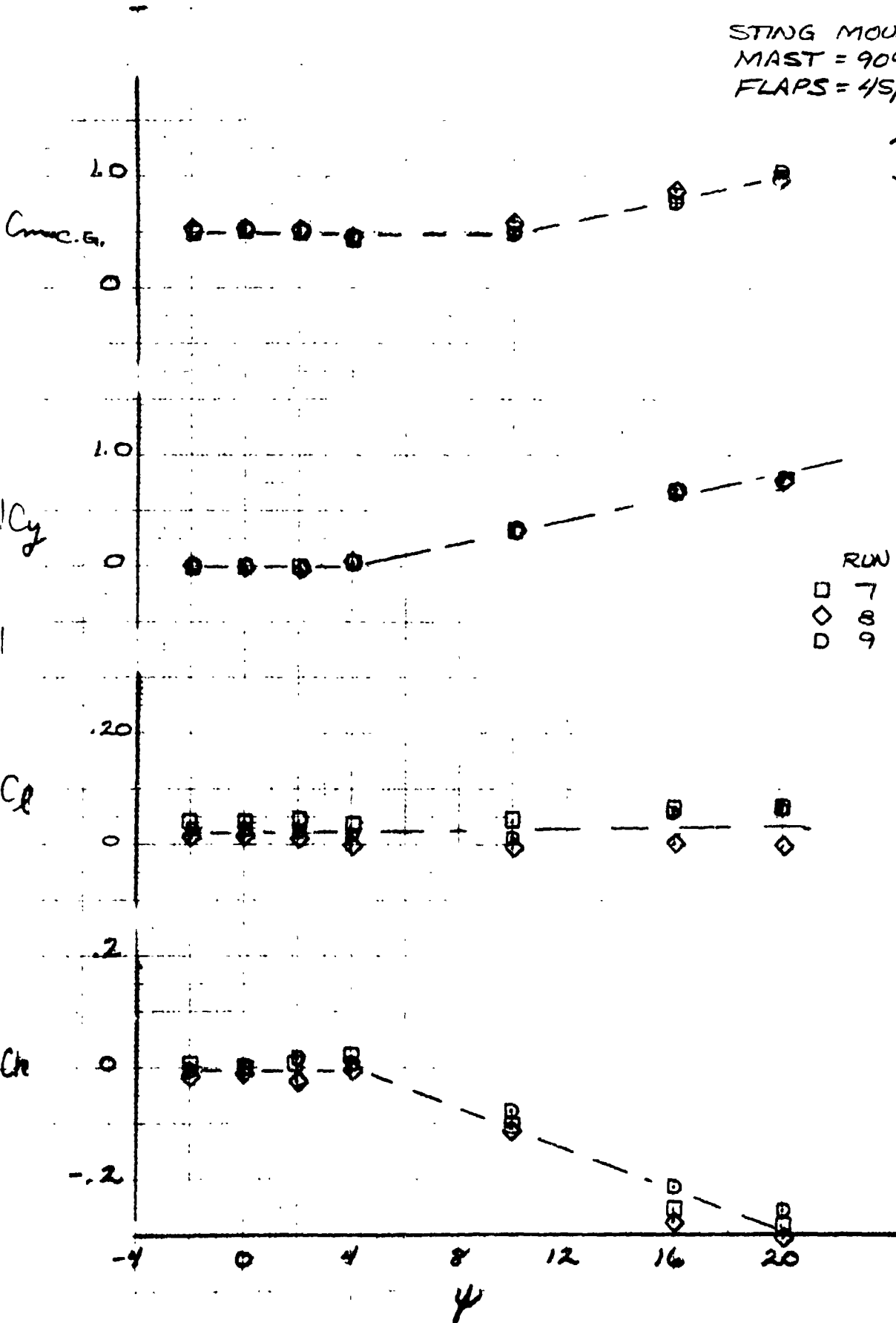


LSWT 421

STING MOUNT
MAST = 90°
FLAPS = 45/25°

40 KTS
SL = 1260 RPM

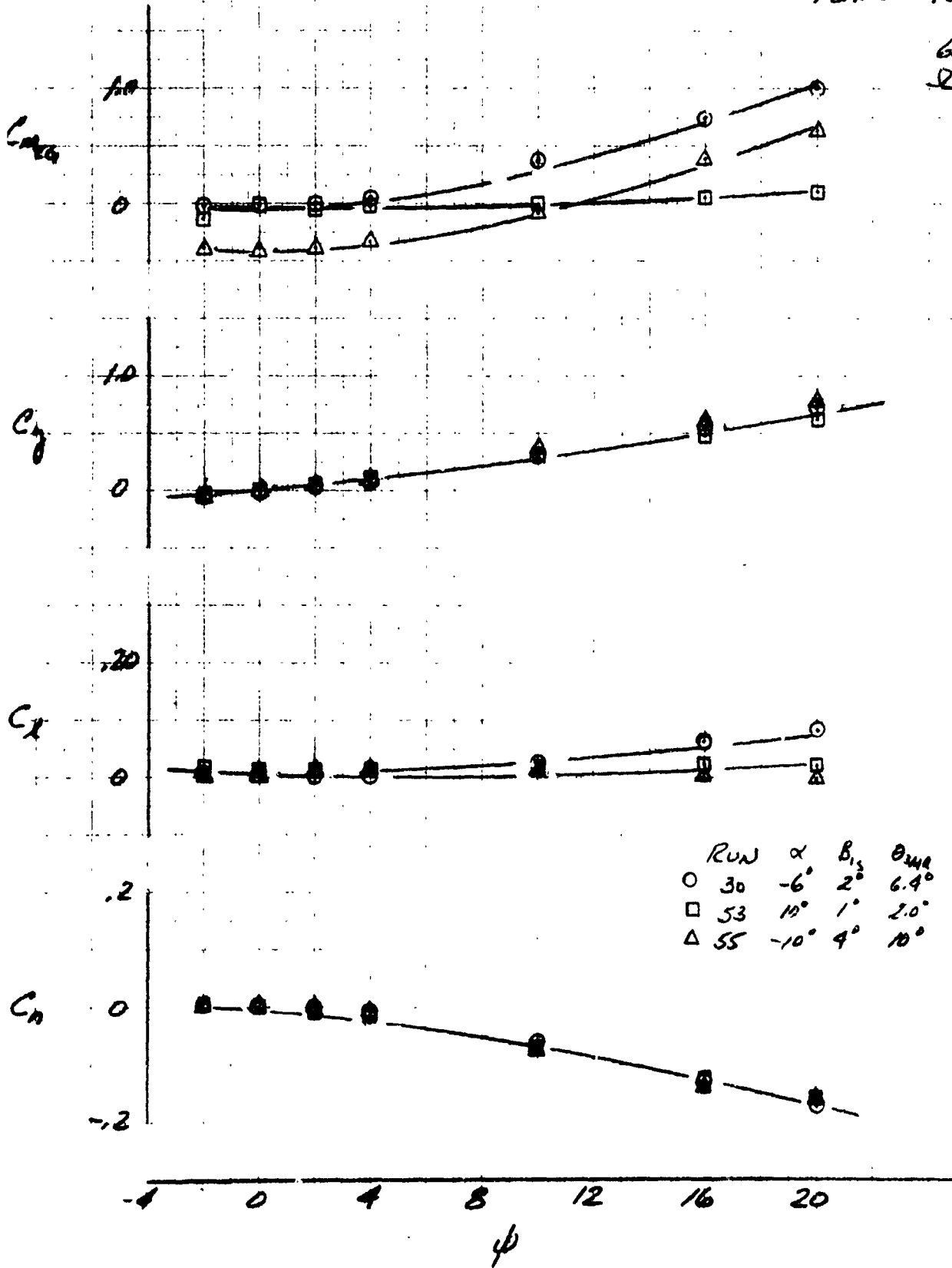
$B_1 = 16^\circ$
 $\Theta_{3/4r} = 7.0$
 $Se = 3.0^\circ$



LSWT 421

STING MOUNT
MAST = 90°
FLAPS = 45°/25°

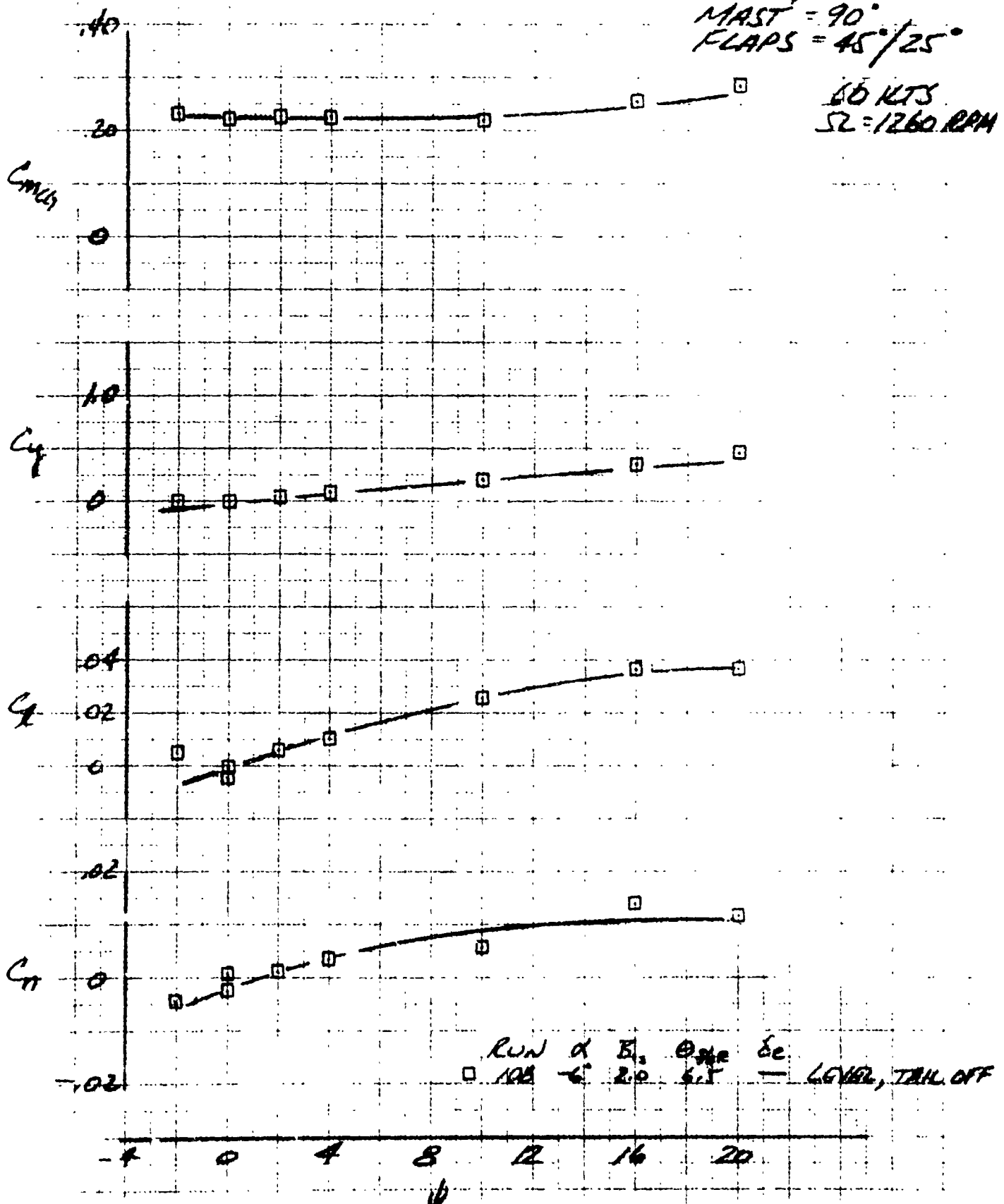
60 KTS
 $\rho = 1260$



LSWT 421

STING MOUNT
 MAST = 90°
 FLAPS = 45°/25°

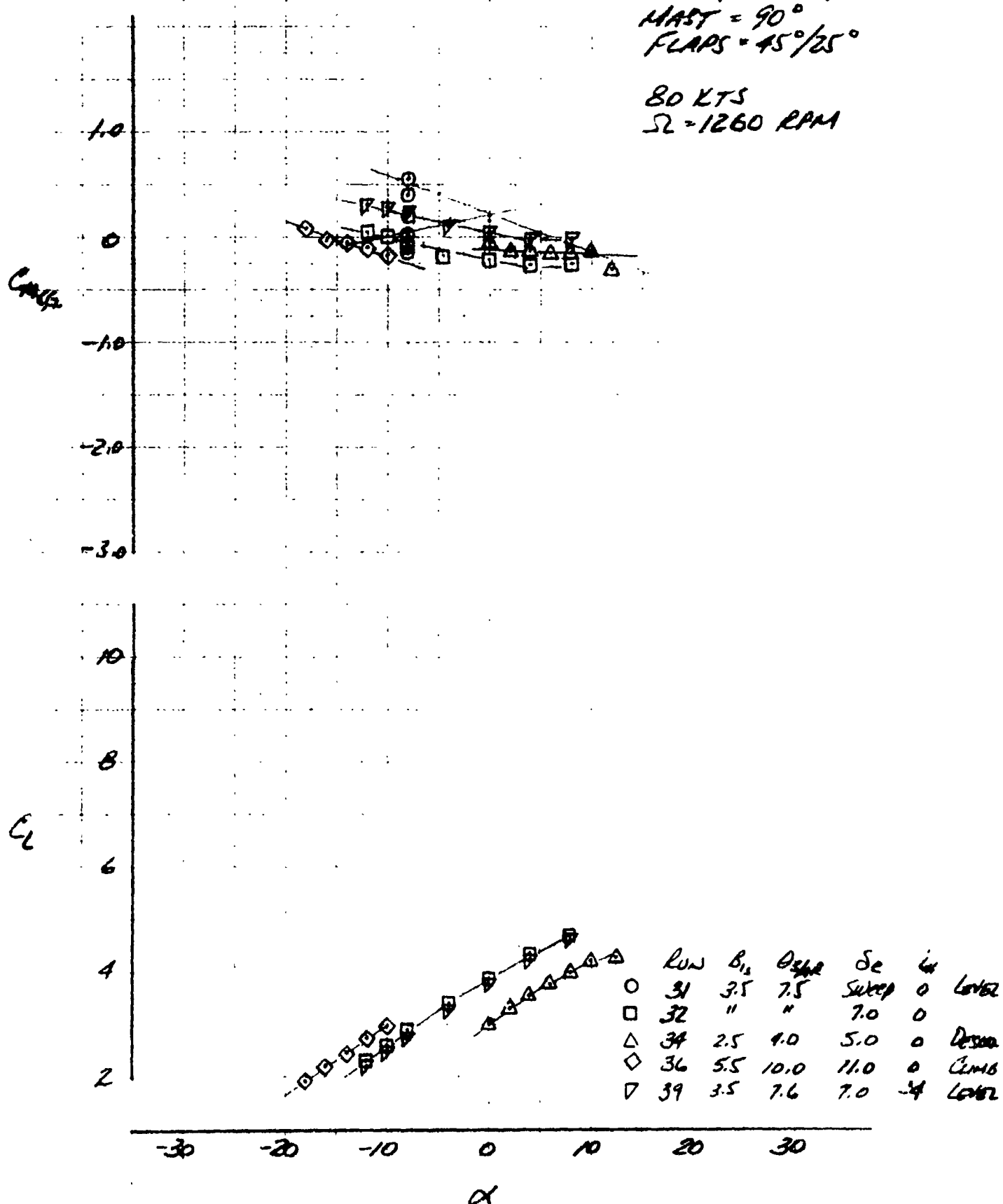
60 KTS
 SZ = 1260 RPM



LSWT 421

STING MOUNT
 MAST = 90°
 FLAPS = 45°/25°

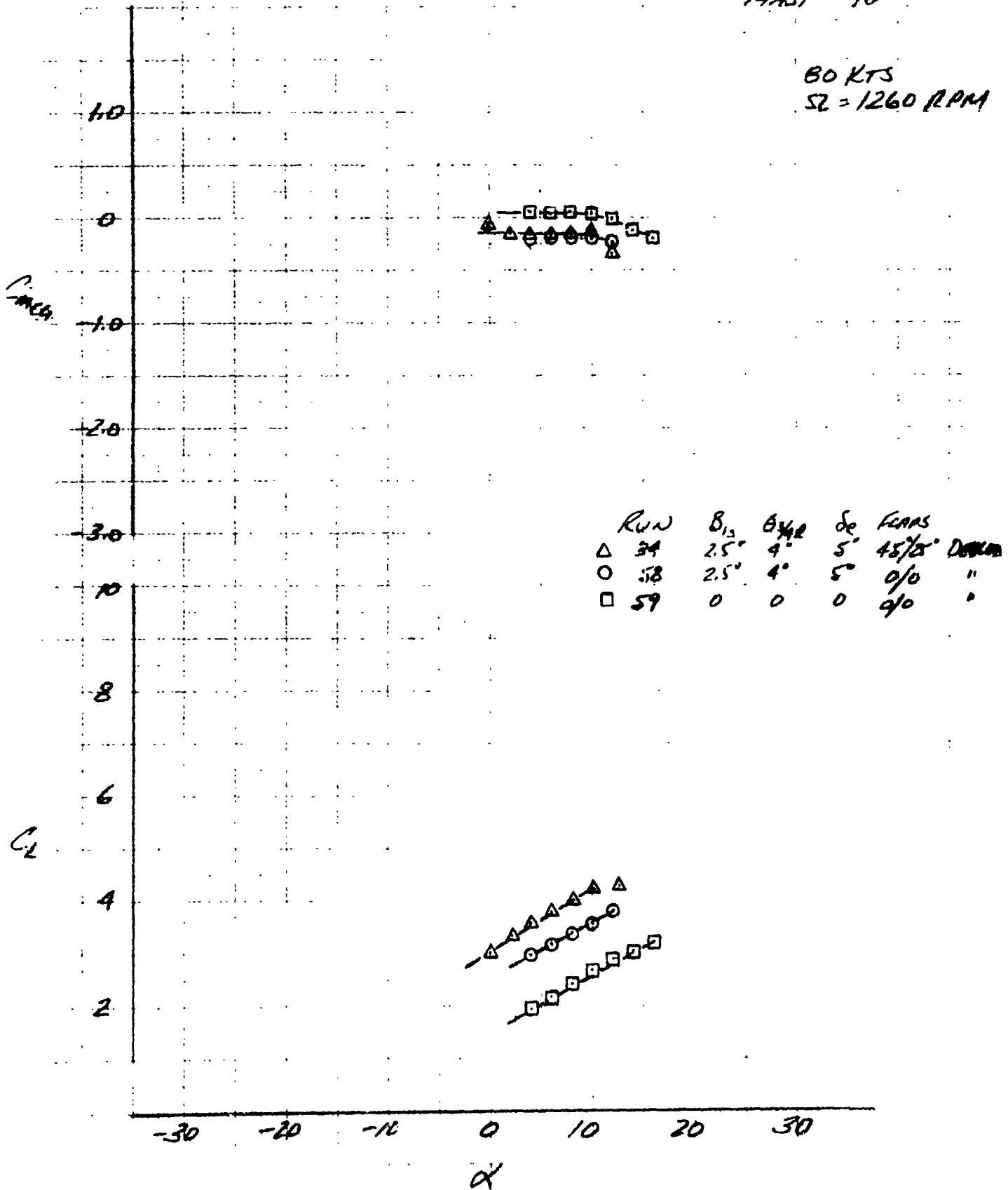
80 KTS
 Ω = 1260 RPM



LSWT 421

STING MOUNT
MAST = 90°

80 KTS
SL = 1260 RPM

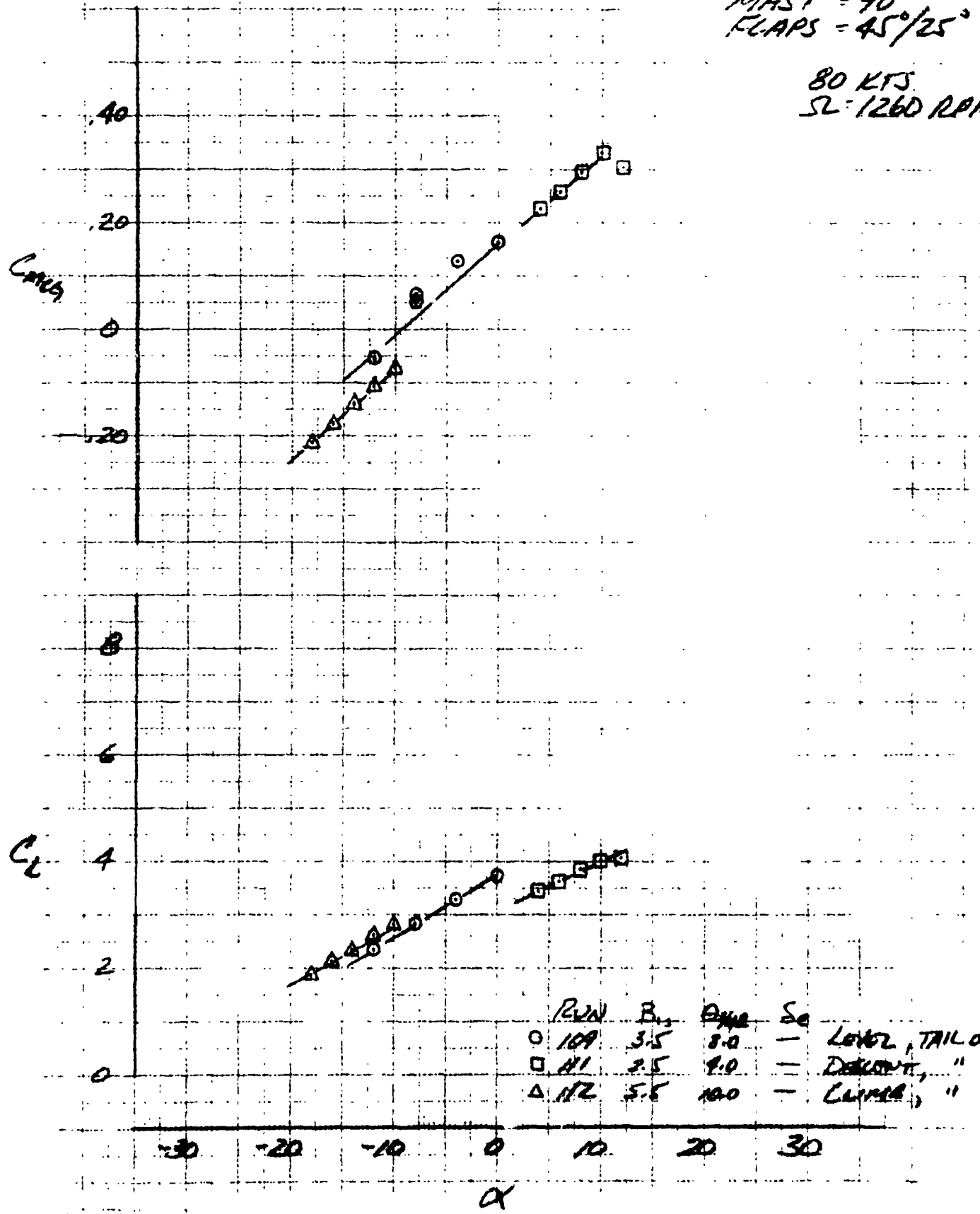


Use of this figure of data in this figure is subject to the restrictions on the title page.

LSWT 421

STING MOUNT
MAST = 90°
FLAPS = 45°/25°

80 KTS
SL = 1260 RPM

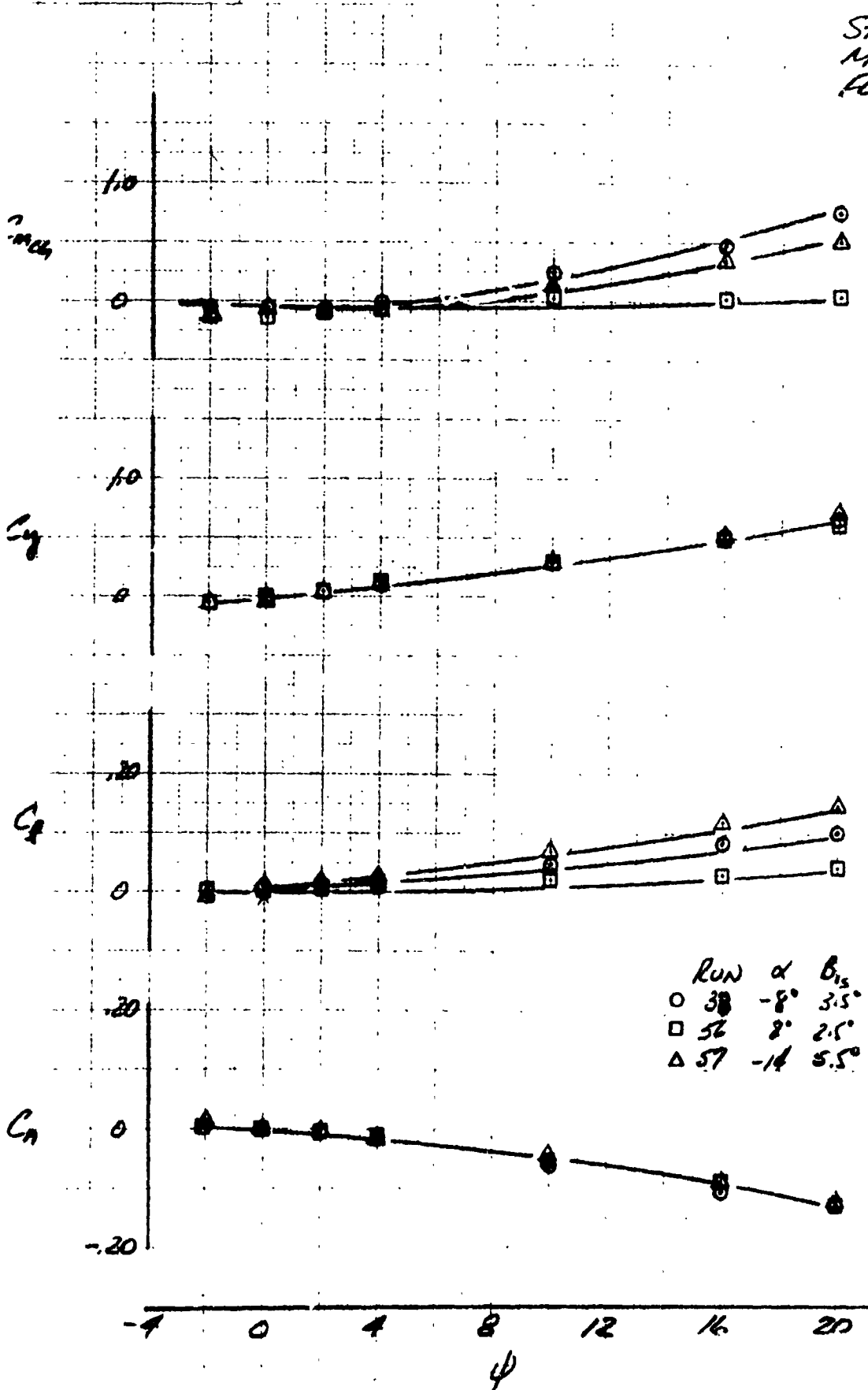


LSWT 421

STING MOUNT
MAST = 90°
FLAPS = 45°/25°

80 KTS
Q = 1260

δ_{15} = 3.5°
 δ_{25} = 7.5°
 δ_e = 7.0°

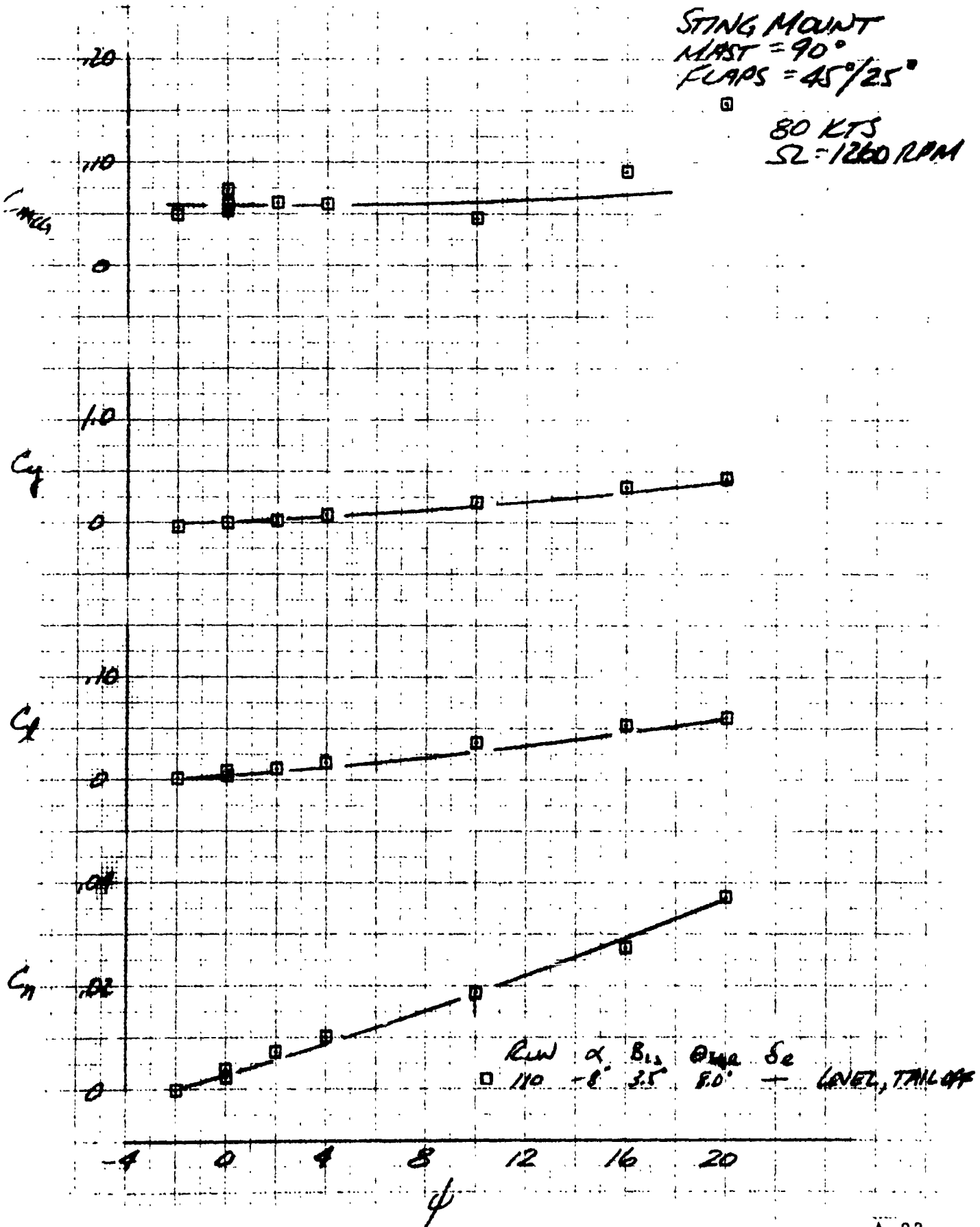


RUN	α	δ_{15}	δ_{25}	δ_e	LEVEL
○ 38	-8°	3.5°	7.5°	7.0°	LEVEL
□ 52	8°	2.5°	4.0°	5.0°	DESCENT
△ 57	-14°	5.5°	10°	11°	CLIMB

LSWT 421

STING MOUNT
MAST = 90°
FLAPS = 45°/25°

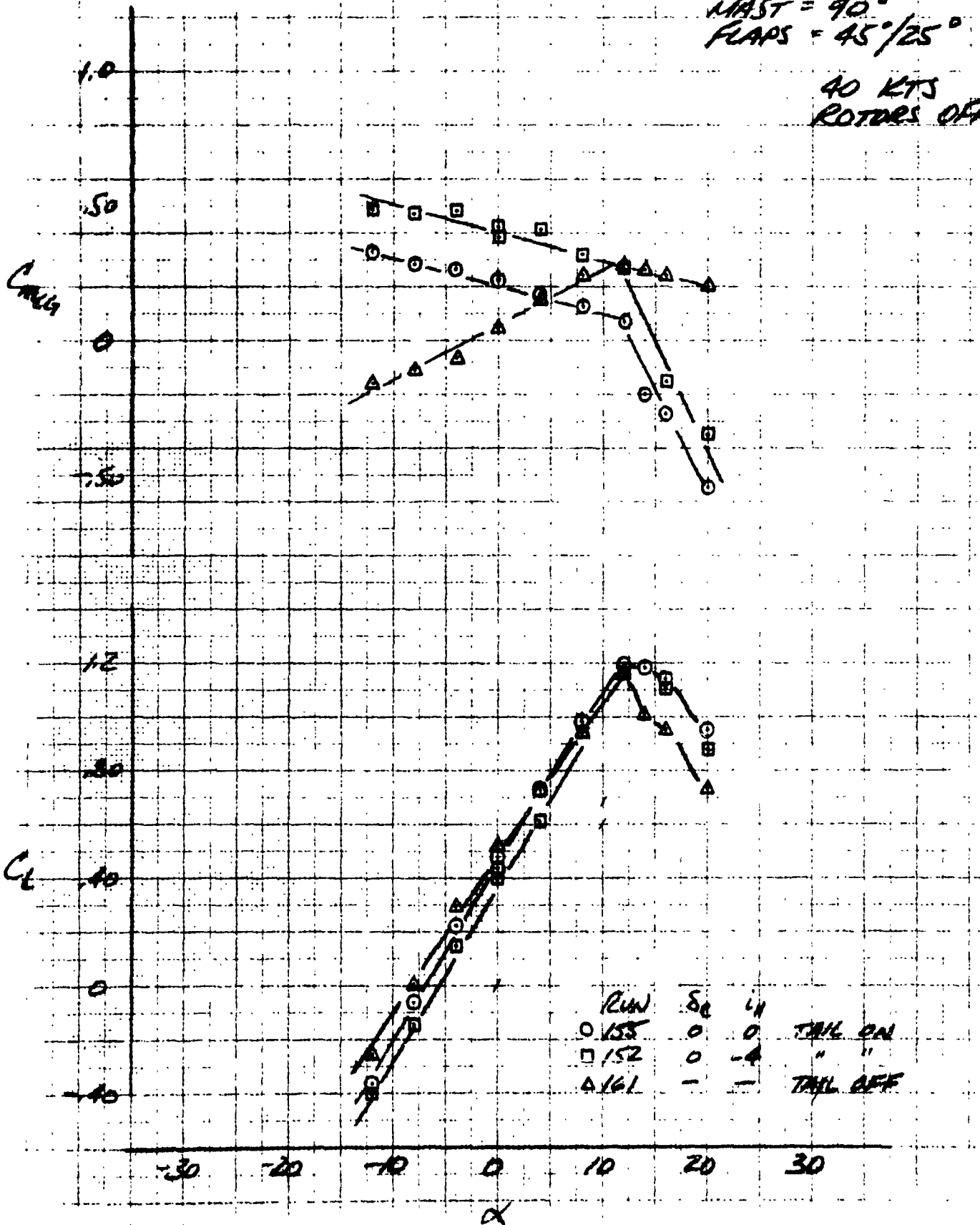
80 KTS
SL = 1260 RPM



LSWT 421

STAND MOUNT
MAST = 90°
FLAPS = 45°/25°

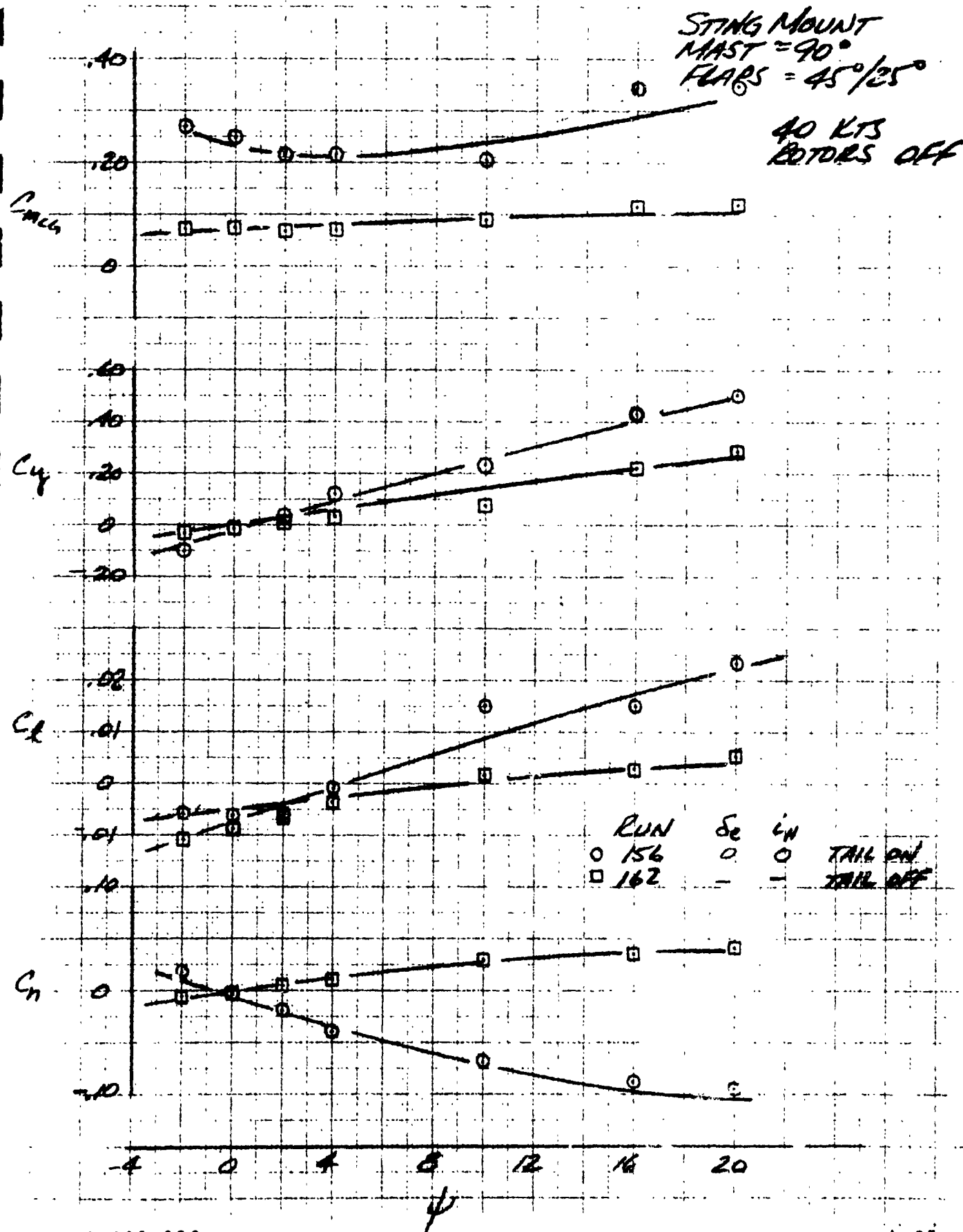
40 KTS
ROTOR OFF



LSWT 421

STING MOUNT
MAST = 90°
FLARS = 45°/25°

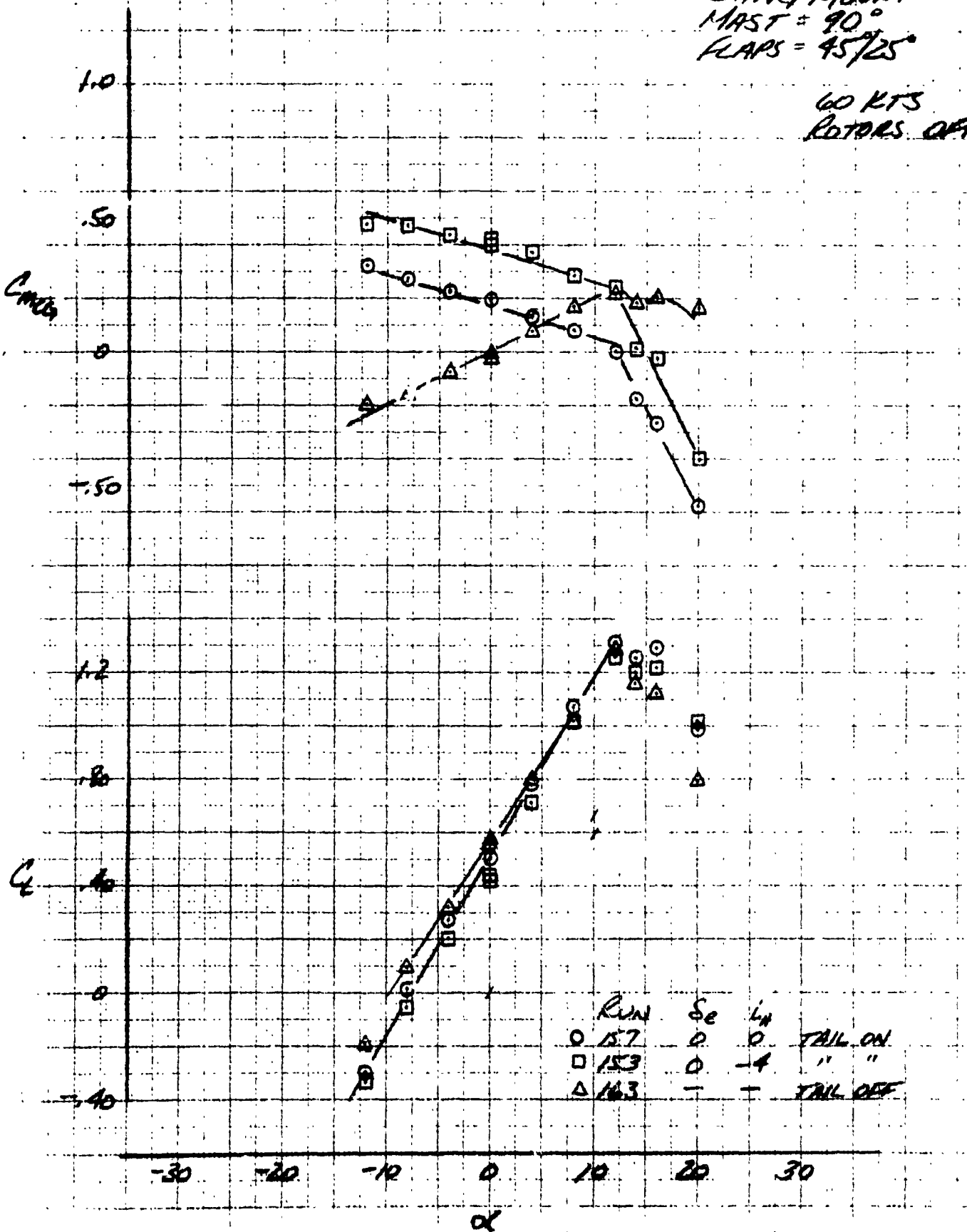
40 KTS
ROTORS OFF



LSWT 421

STING MOUNT
MAST = 90°
FLAPS = 45/25°

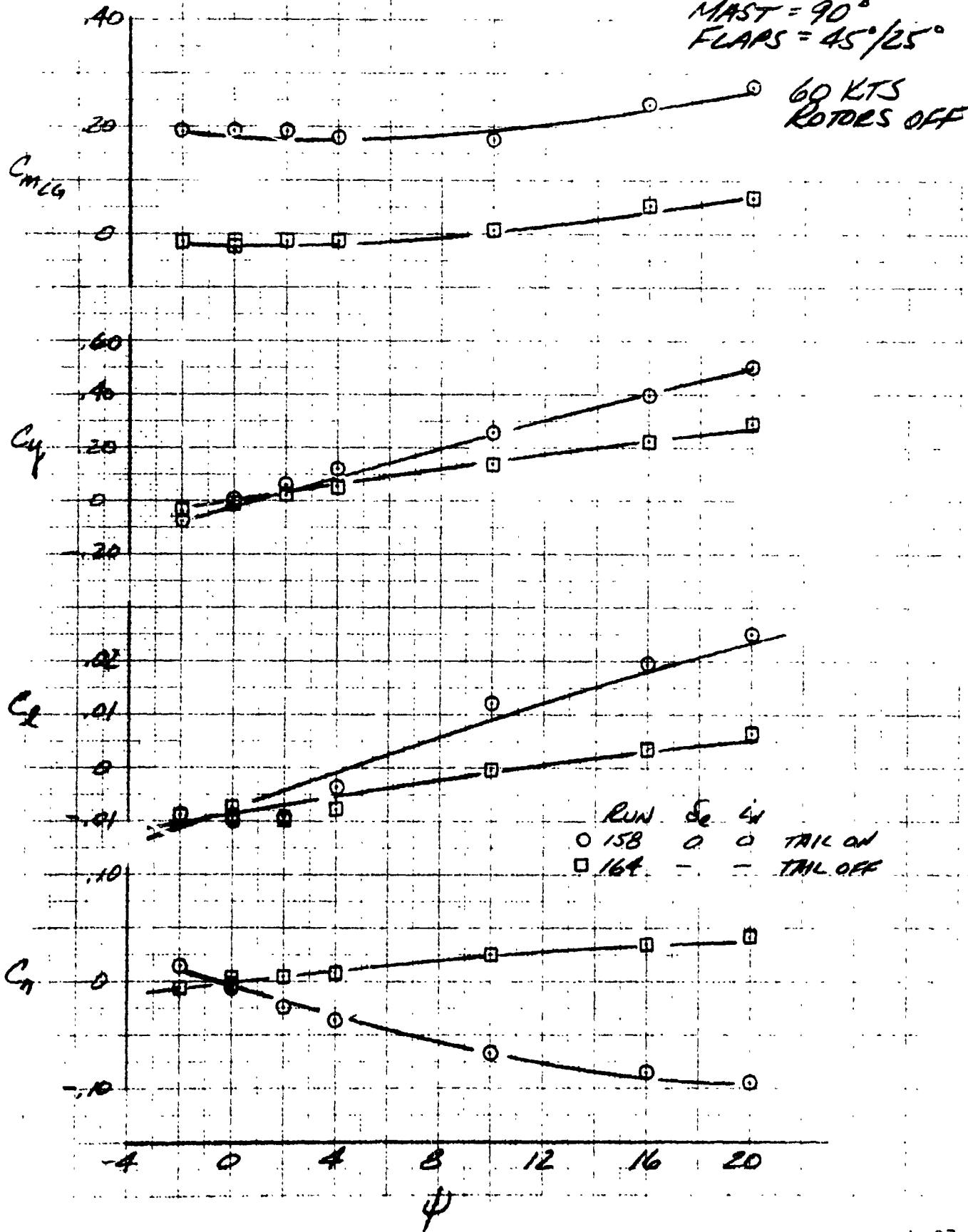
60 KTS
ROTORS OFF



LSWT 421

STING MOUNT
MAST = 90°
FLAPS = 45°/25°

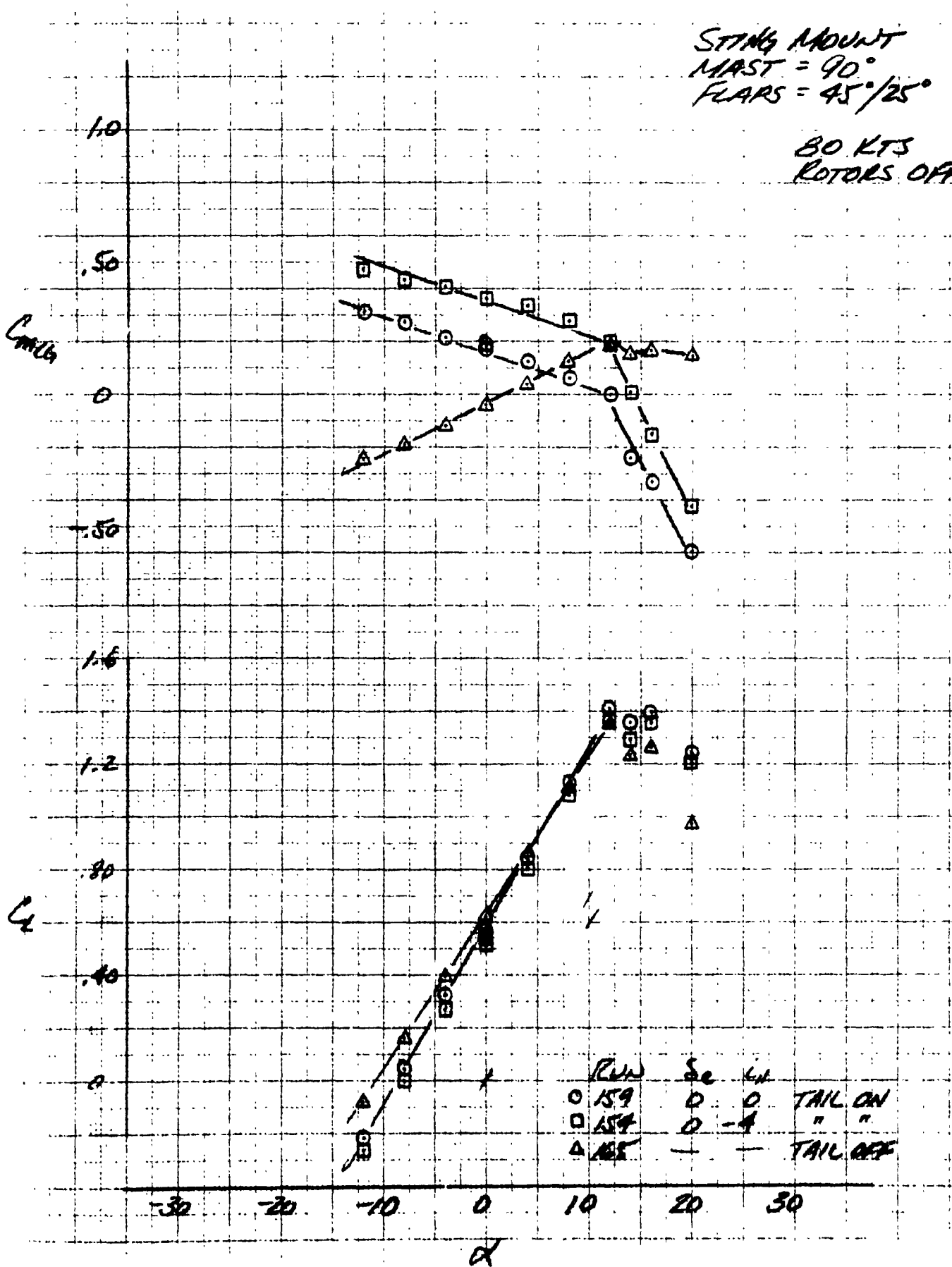
60 KTS
ROTOR OFF



LSWT 421

STING MOUNT
MAST = 90°
FLAPS = 45°/25°

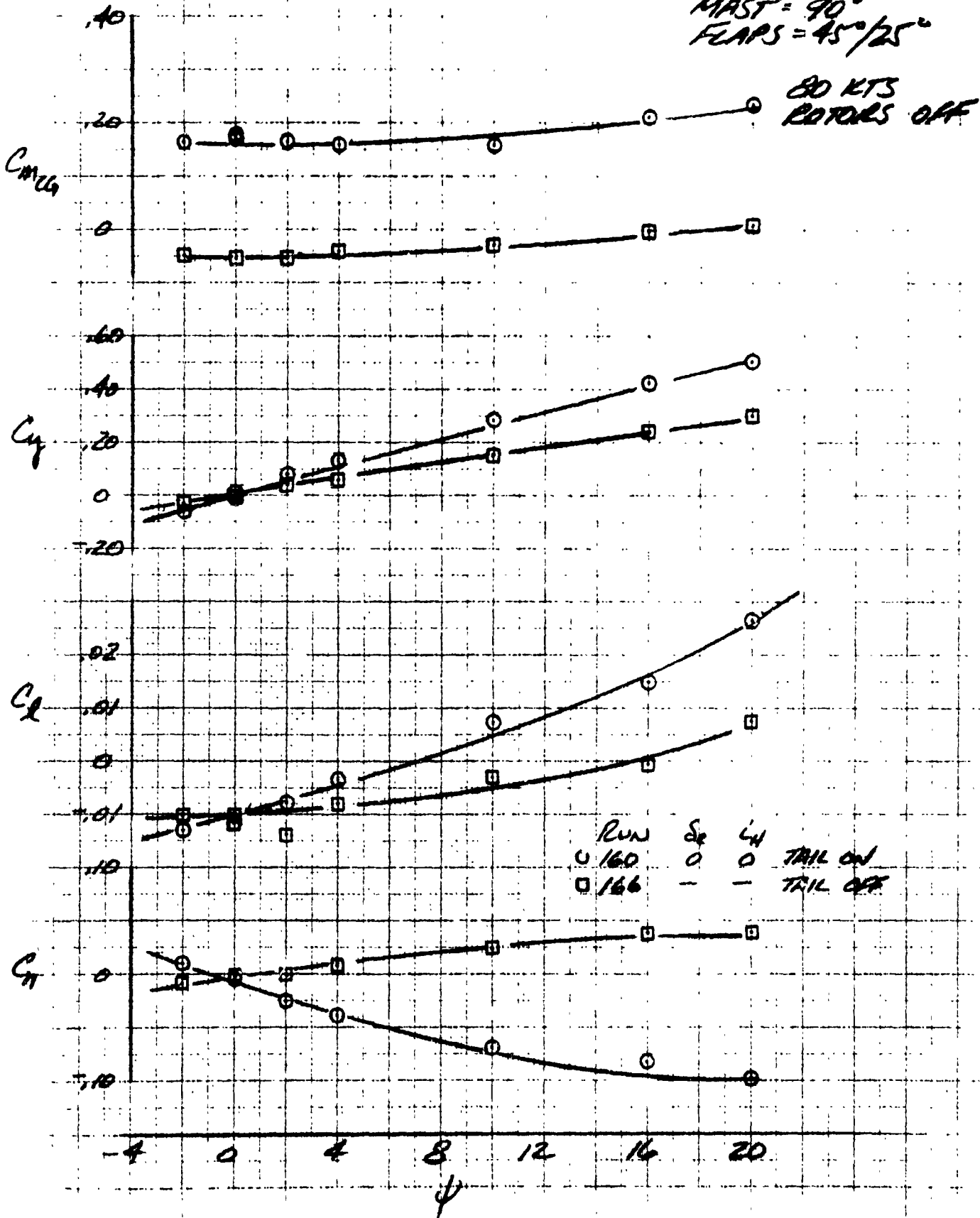
80 KTS
ROTORS OFF



LSWT 421

STING MOUNT
MAST = 90°
FLAPS = 45°/25°

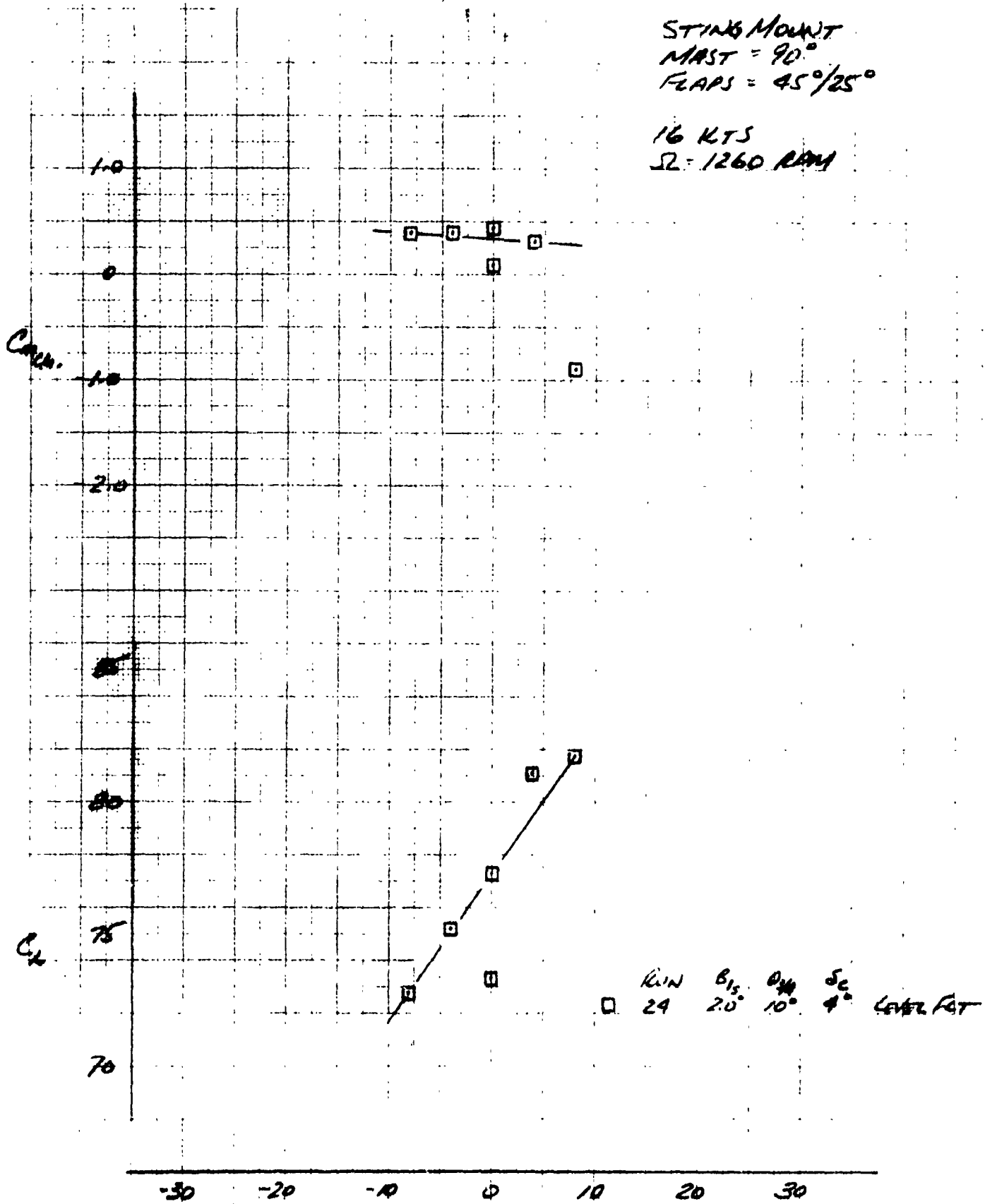
80 KTS
ROTORS OFF



LSWT 421

STING MOUNT
 MAST = 90°
 FLAPS = 45°/25°

16 KTS
 SL = 1260 RPM



R_{in} 24 B_{15} 2.0° θ_{14} 10° S_c 4° LEVEL FAT

LSWT 421

STING MOUNT
MAST = 9°
FLARS = 45°/25°

16 KTS
 $\Omega = 1260$

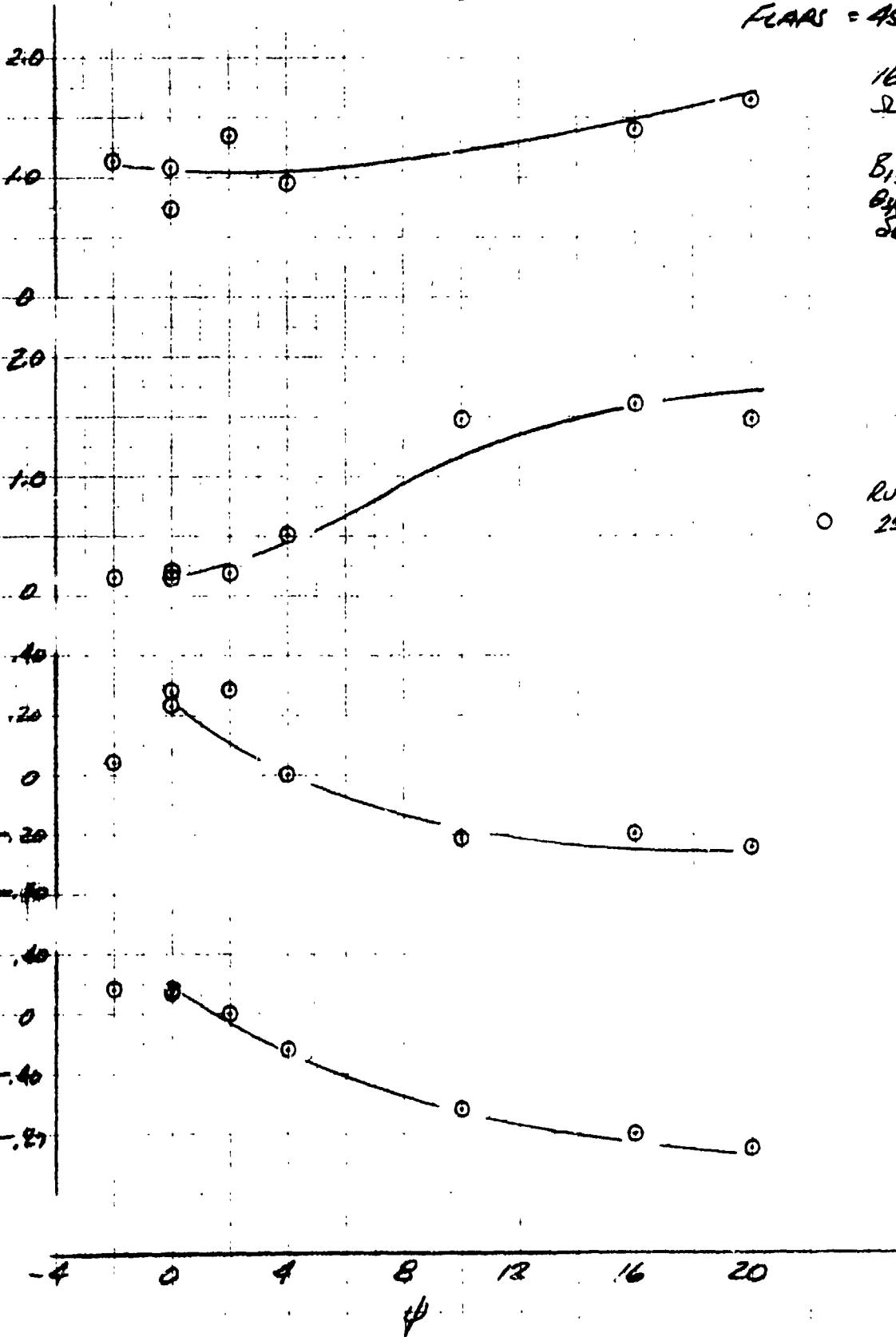
$B_{13} = 2.0$
 $B_{14} = 10°$
 $S_e = 4.0$

C_{mCA}

$C_{y\dot{\psi}}$

C_x

C_n

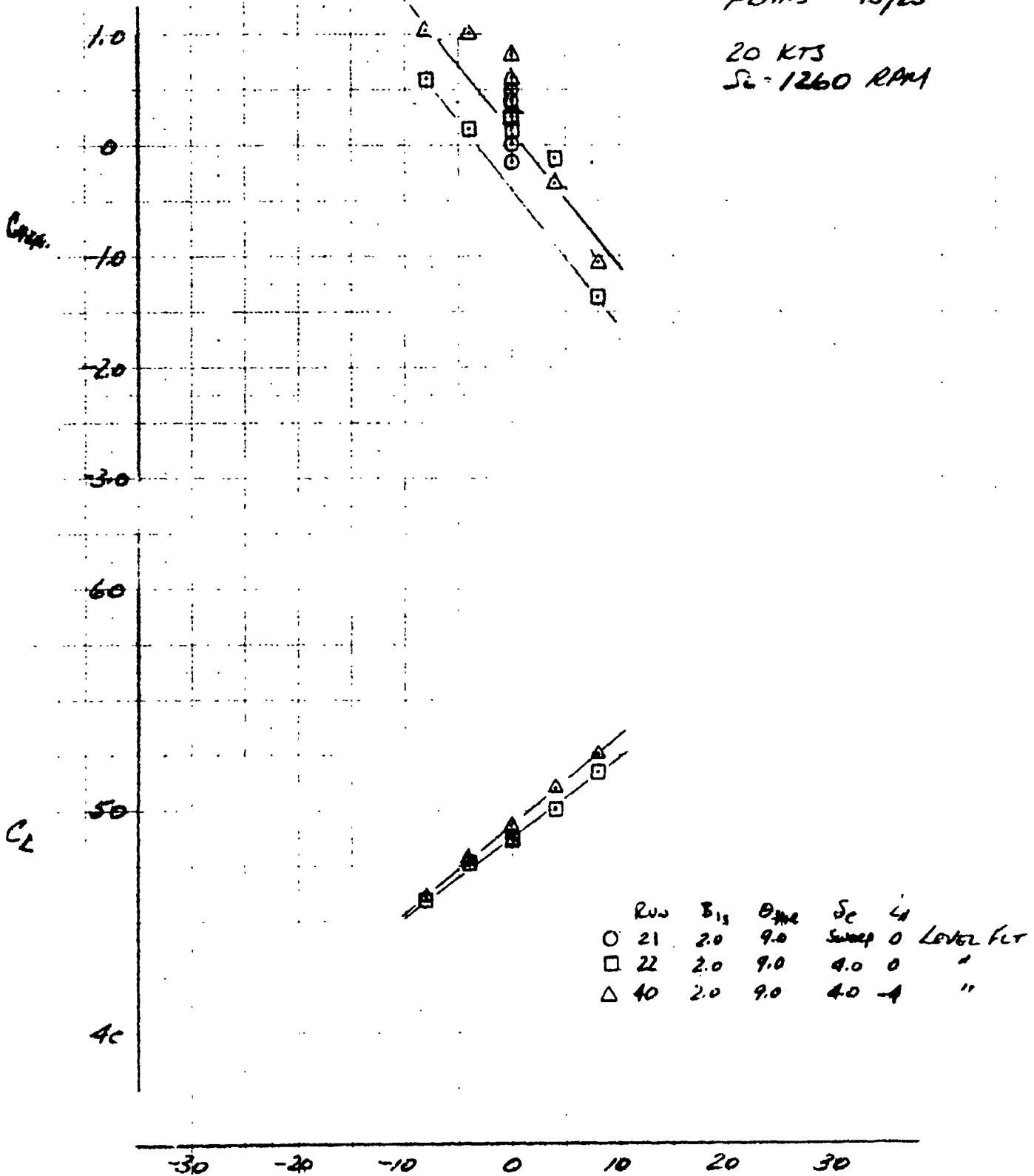


$R_{W\dot{\psi}} = 25$

LSWT 421

STING MOUNT
MAST = 90°
FLAPS = 45/25

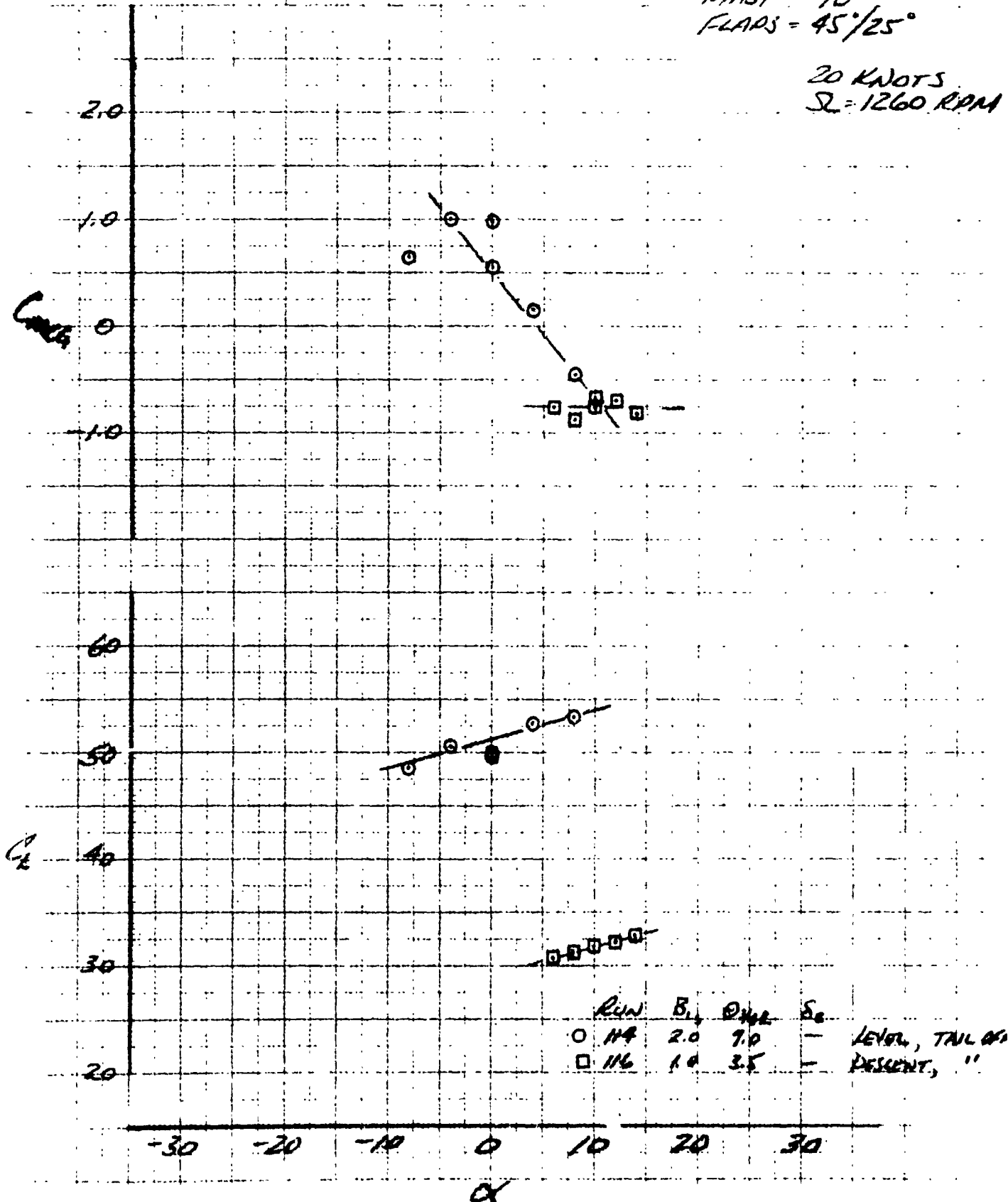
20 KTS
S_c = 1260 RPM



LSWT 421

STING MOUNT
 MAST = 90°
 FLAPS = 45°/25°

20 KNOTS
 $\Omega = 1260$ RPM

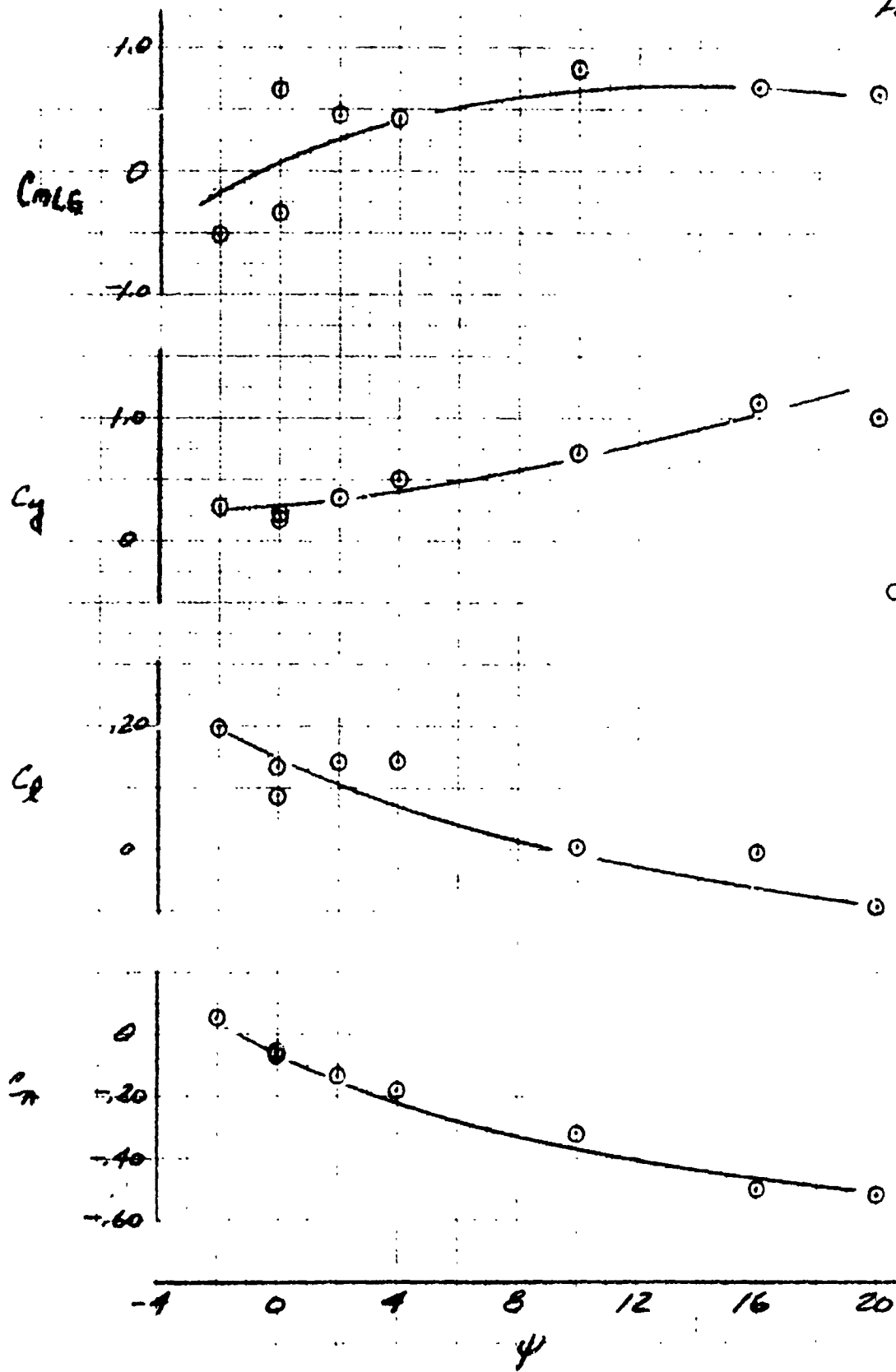


LSWT 421

STING MOUNT
MAST = 90°
FLAPS = 45°/25°

20 KTS
 $\Omega = 1260$

$B_{15} = 2.0^\circ$
 $\theta_{4R} = 9.0^\circ$
 $\delta_c = 4.0^\circ$

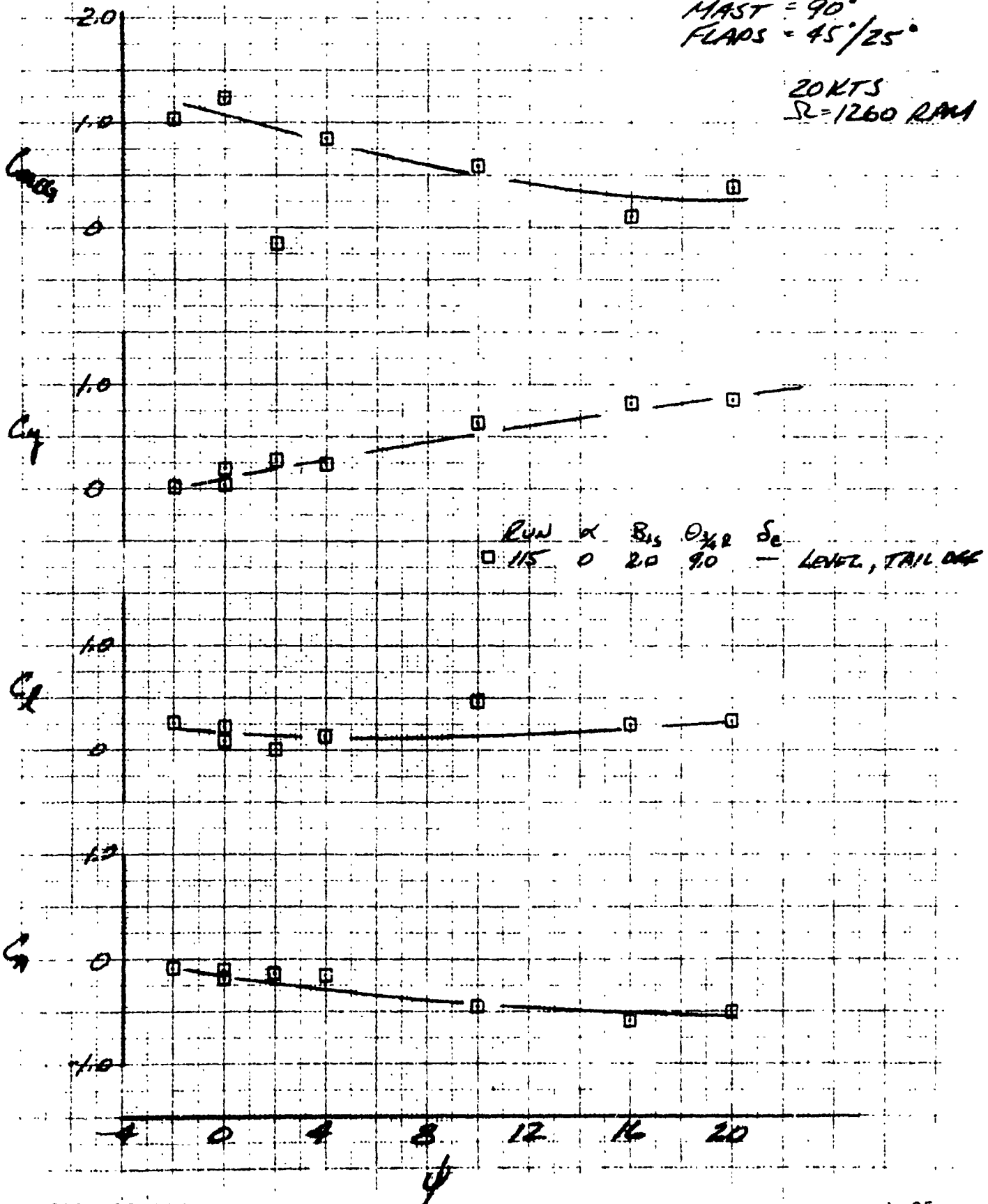


$R_{0.5}$ α
○ 23 0°

LSWT 421

STING MOUNT
MAST = 90°
FLAPS = 45°/25°

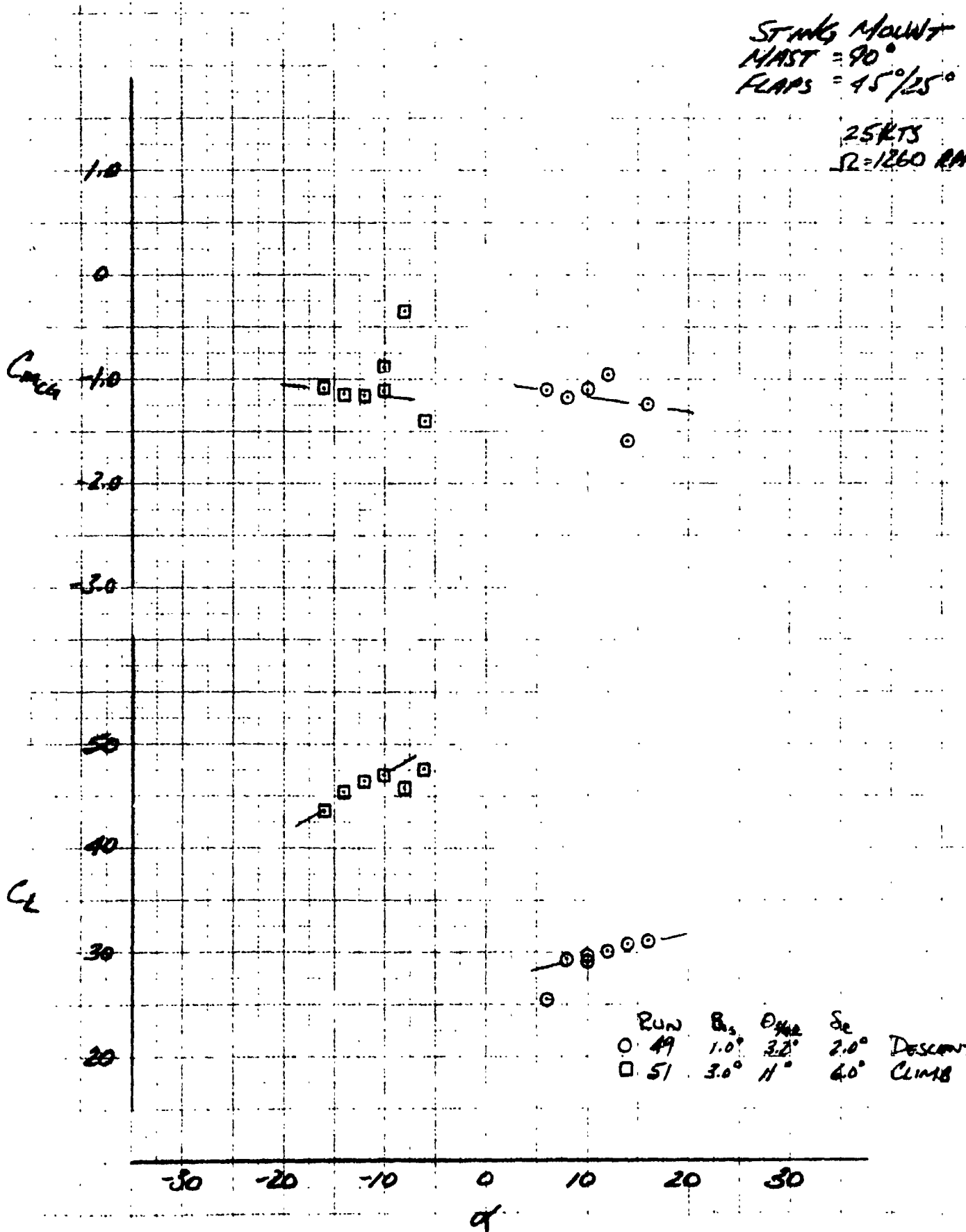
20 KTS
R = 1260 RPM



LSWT 421

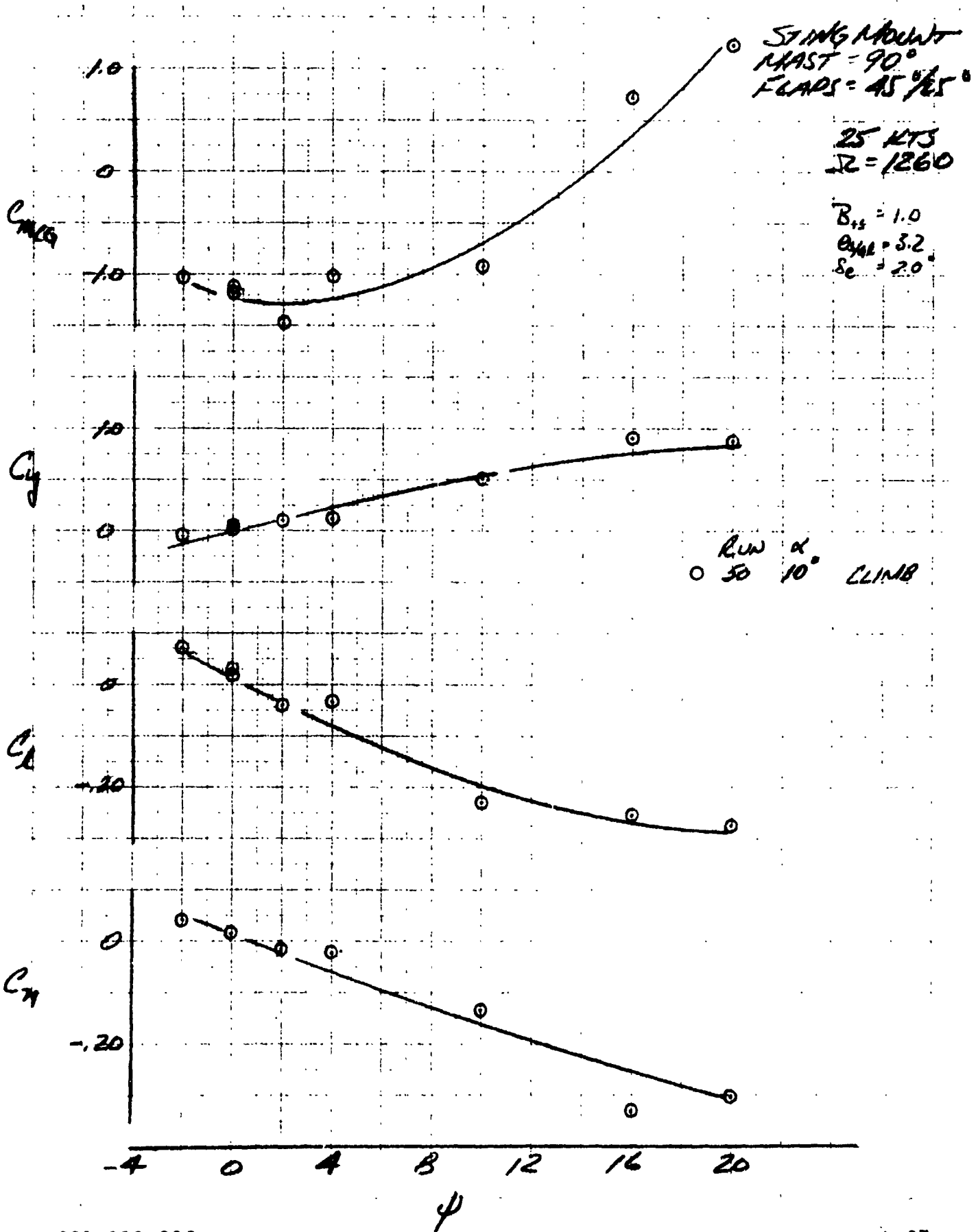
STING MOUNT
MAST = 90°
FLAPS = 45°/25°

25KTS
Ω = 1260 RPM



○	RUN 49	δ_s 1.0°	θ_{Hub} 3.2°	δ_c 2.0°	DESCENT
□	RUN 51	δ_s 3.0°	θ_{Hub} 11°	δ_c 6.0°	CLIMB

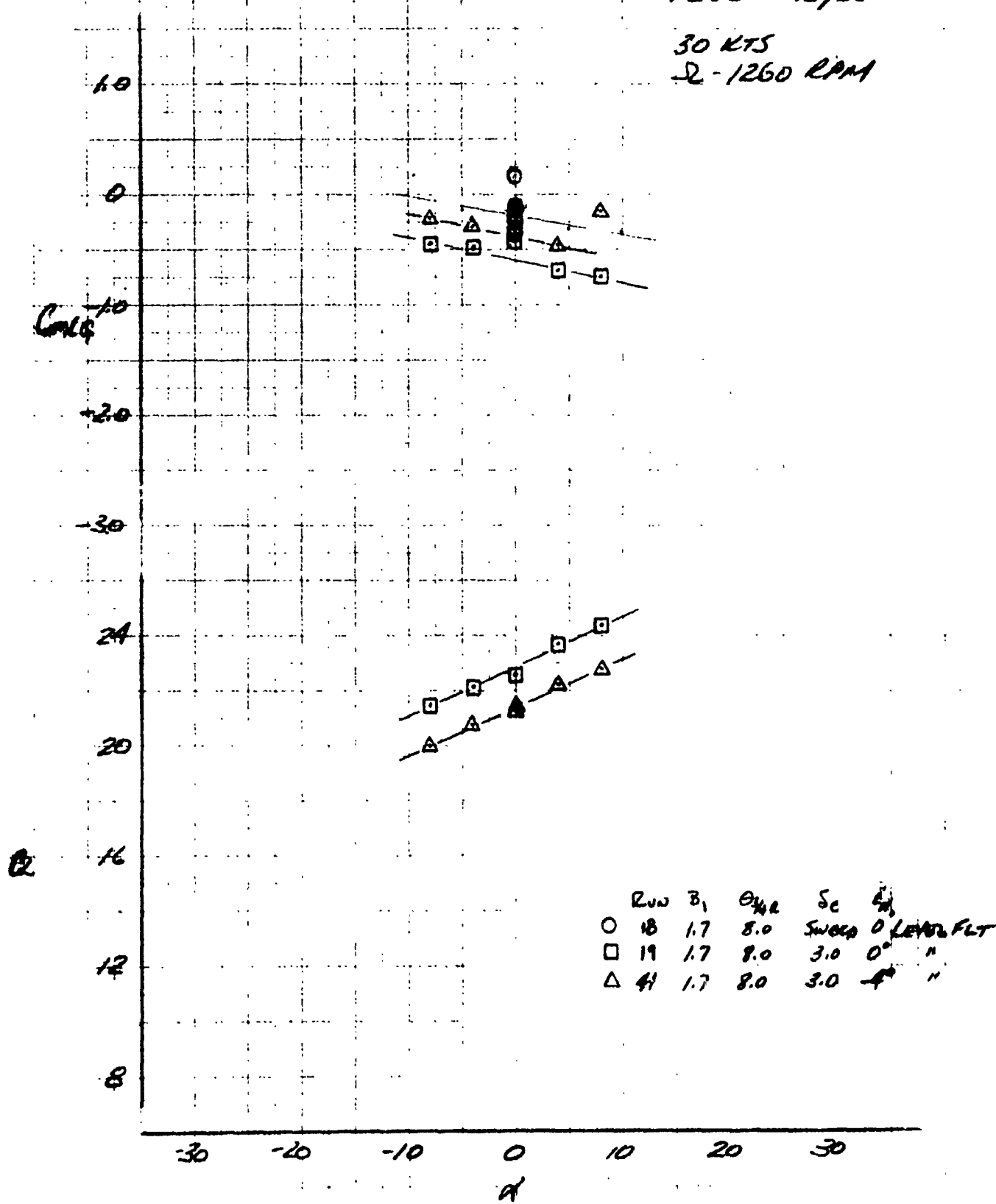
LSWT 421



LSWT 421

STING MOUNT
MAST = 90°
FLAPS - 45°/25°

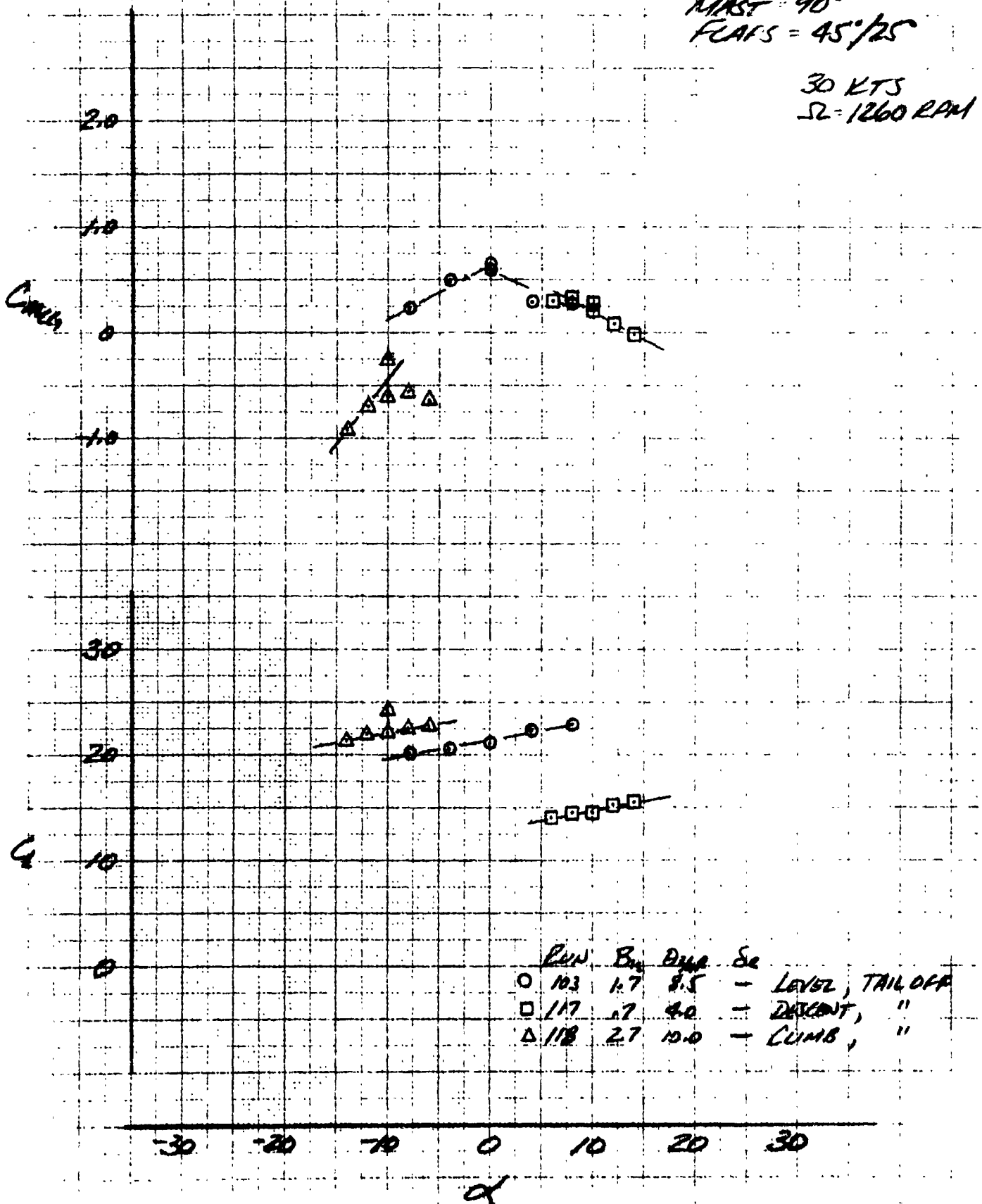
30 KTS
Ω - 1260 RPM



LSWT 421

STING MOUNT
 MAST = 90°
 FLAPS = 45°/25°

30 KTS
 SL = 1260 RPM

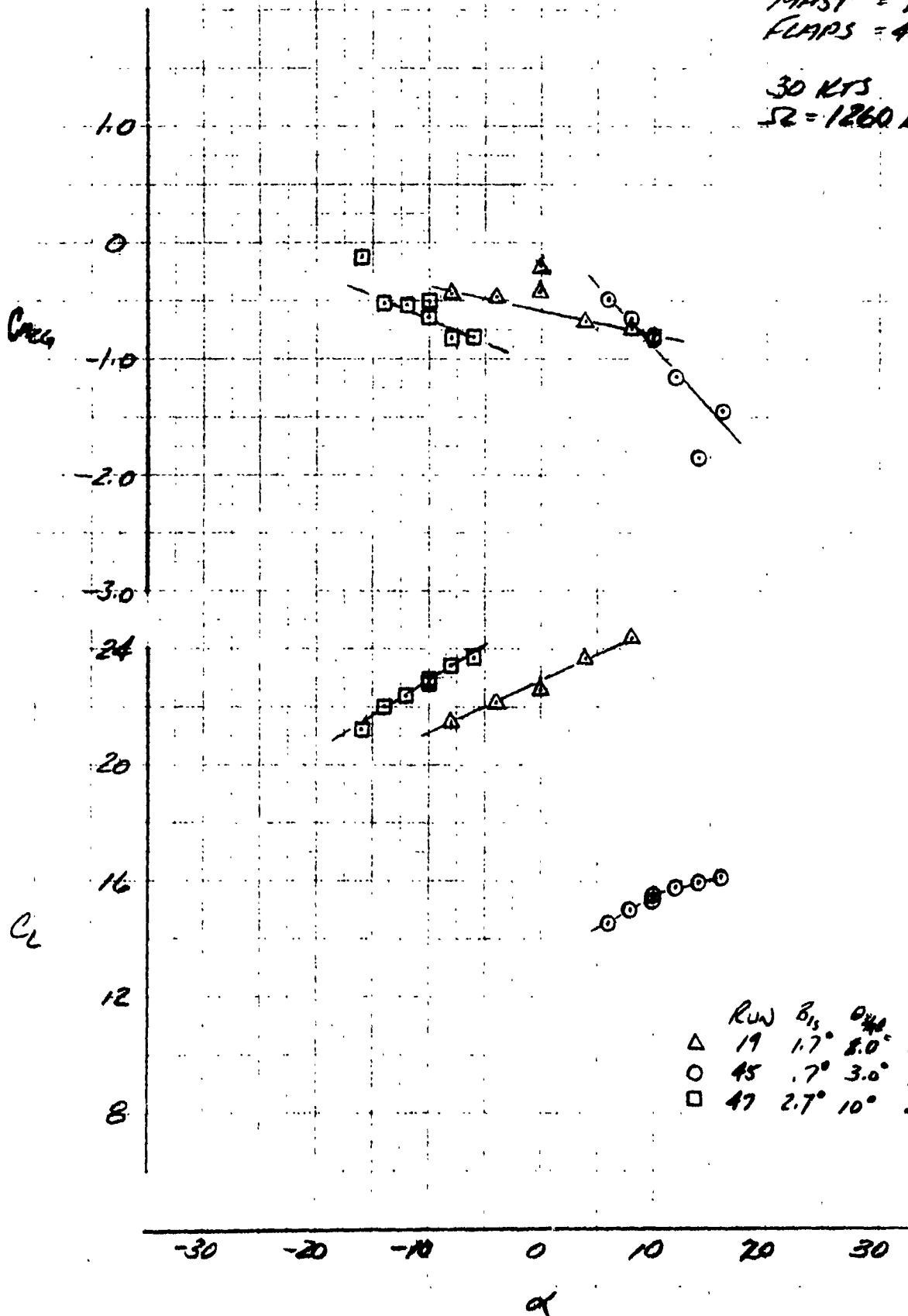


Run	B _y	B _z	S _e	
○ 103	1.7	8.5	-	LEVEL, TAIL OFF
□ 117	1.7	4.0	-	DESCENT, "
△ 118	2.7	10.0	-	CLIMB, "

LSWT 421

STING MOUNT
MAST = 90°
FLAPS = 45°/25°

30 KTS
SR = 1260 RPM

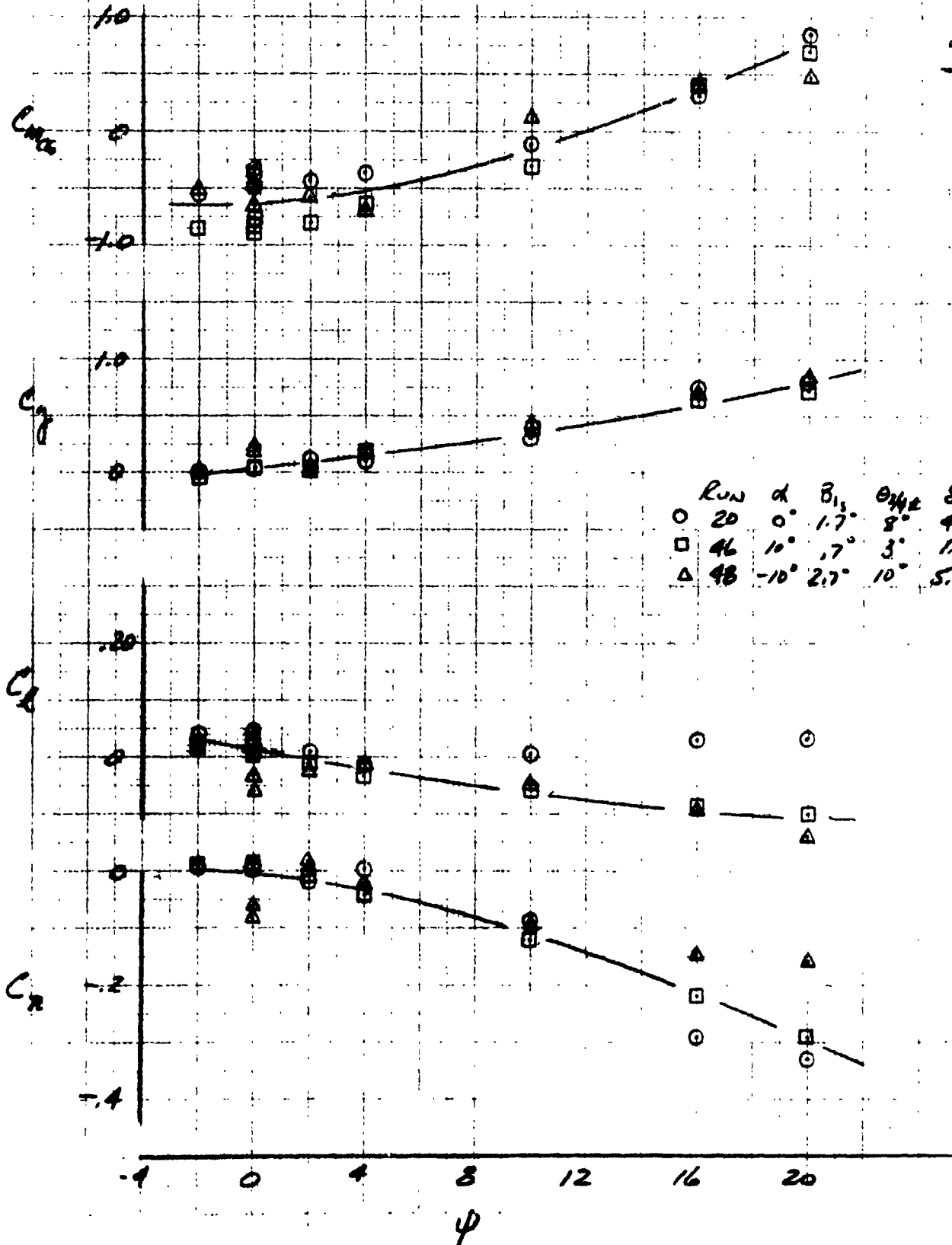


	RUN	β_{15}	θ_{45}	δ_2	
△	19	1.7°	8.0°	3.0°	LEVEL FLT
○	45	.7°	3.0°	1.0°	DESCENT
□	47	2.7°	10°	5.0°	CLIMB

LSWT 421

STING MOUNT
MAST = 90°
FLAPS 45/25

36 KTS
SL = 1280

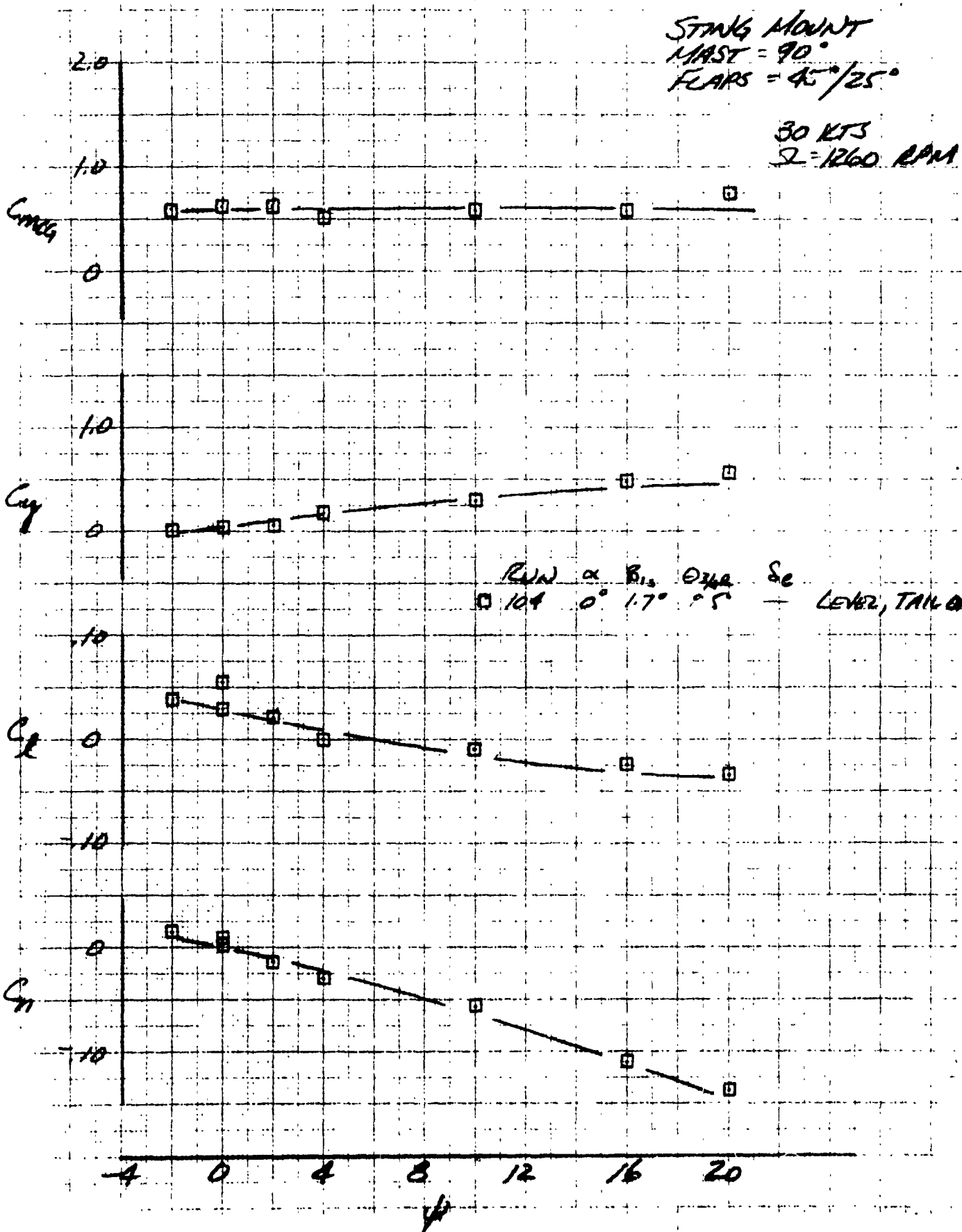


Run	α	$\beta_{1/2}$	$\theta_{1/2}$	S_e	Level
20	0°	1.7°	8°	4.0°	Level
46	10°	1.7°	3°	1.0°	Down
48	-10°	2.7°	10°	5.0°	Down

LSWT 421

STING MOUNT
MAST = 90°
FLAPS = 45°/25°

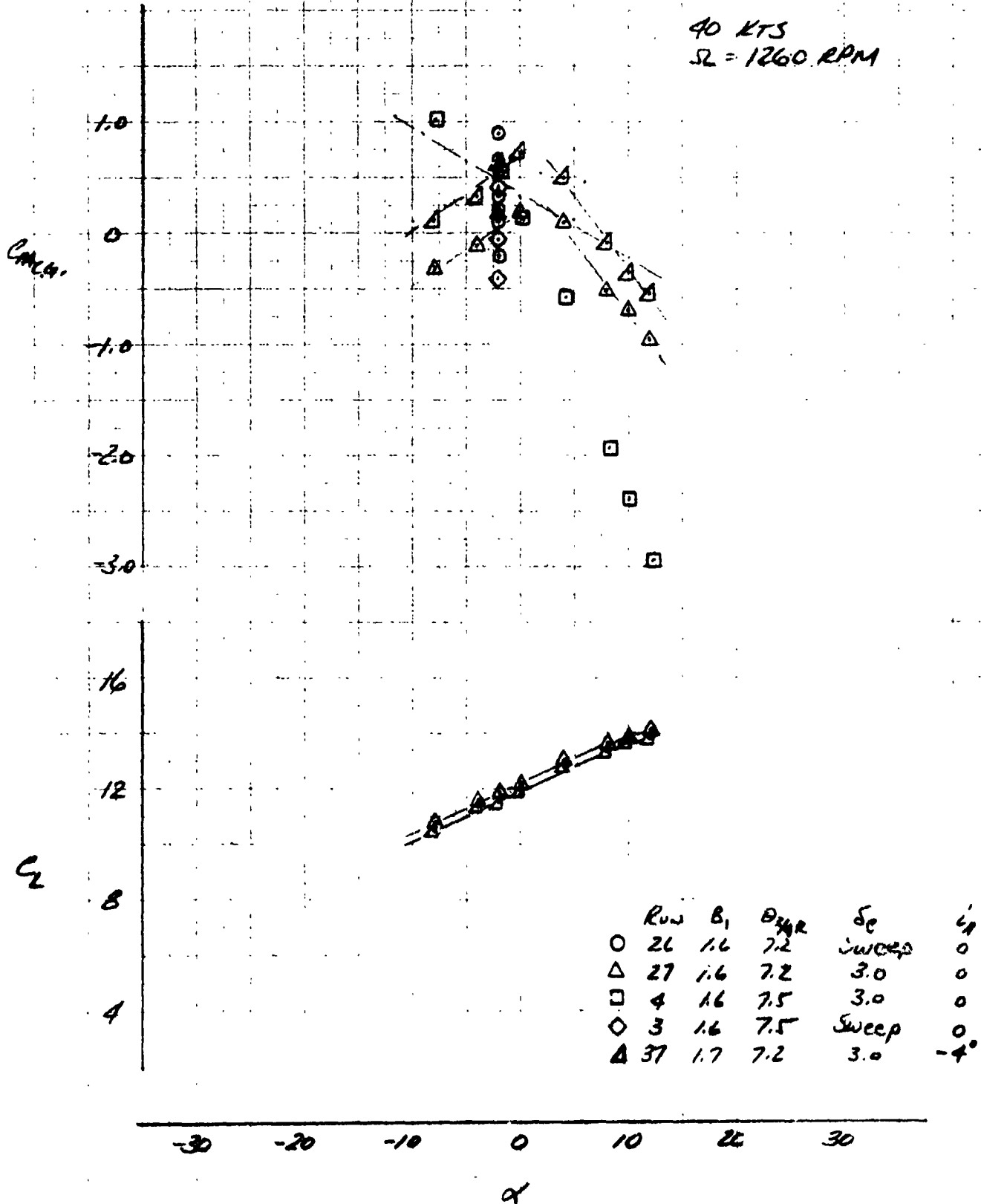
30 KTS
Ω = 1260 RPM



LSWT 421

STING MOUNT
MAST = 90°
FLAPS - 45°/25°

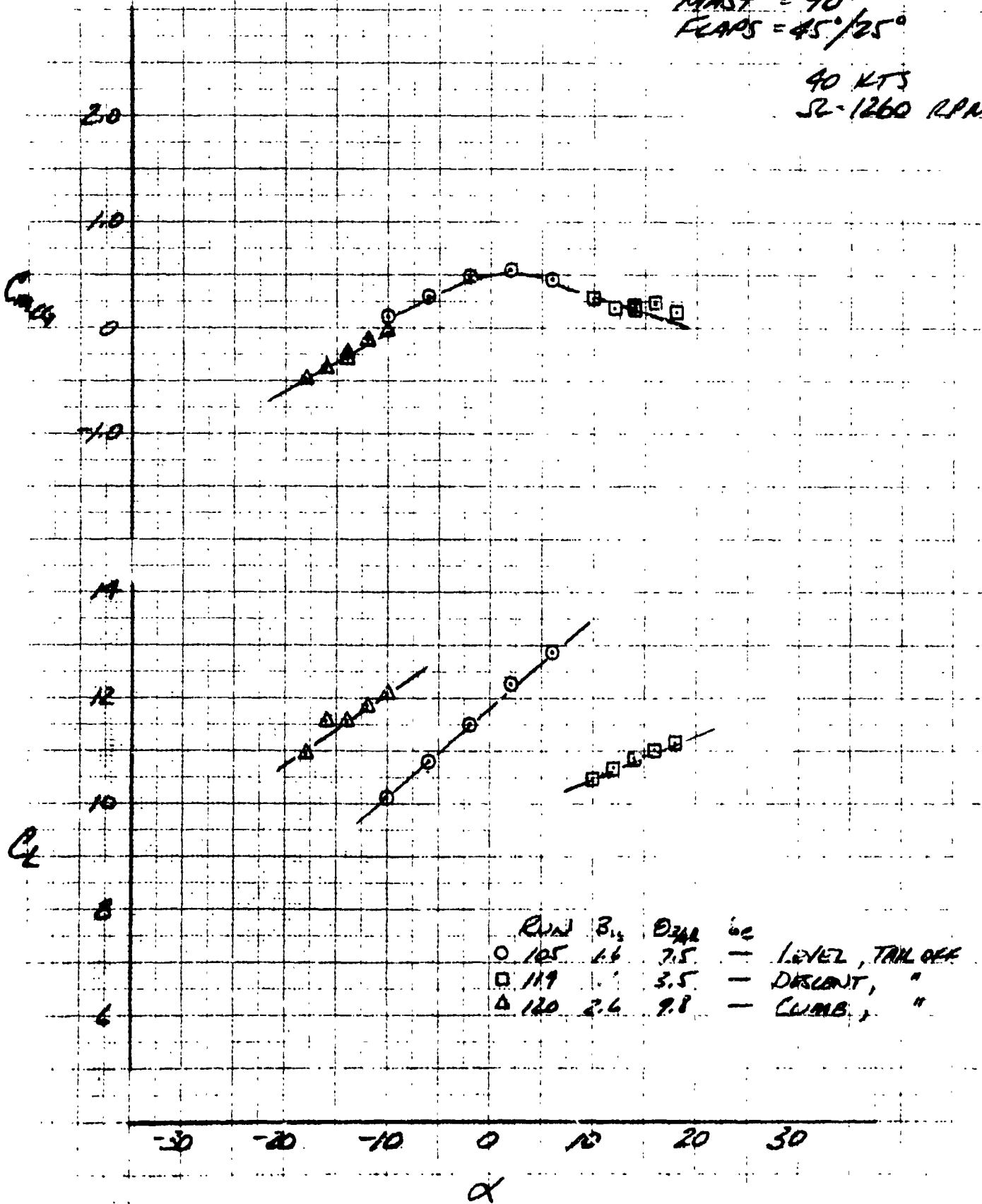
40 KTS
SL = 1260 RPM



LSWT 421

STING MOUNT
MAST = 90°
FLAPS = 45°/25°

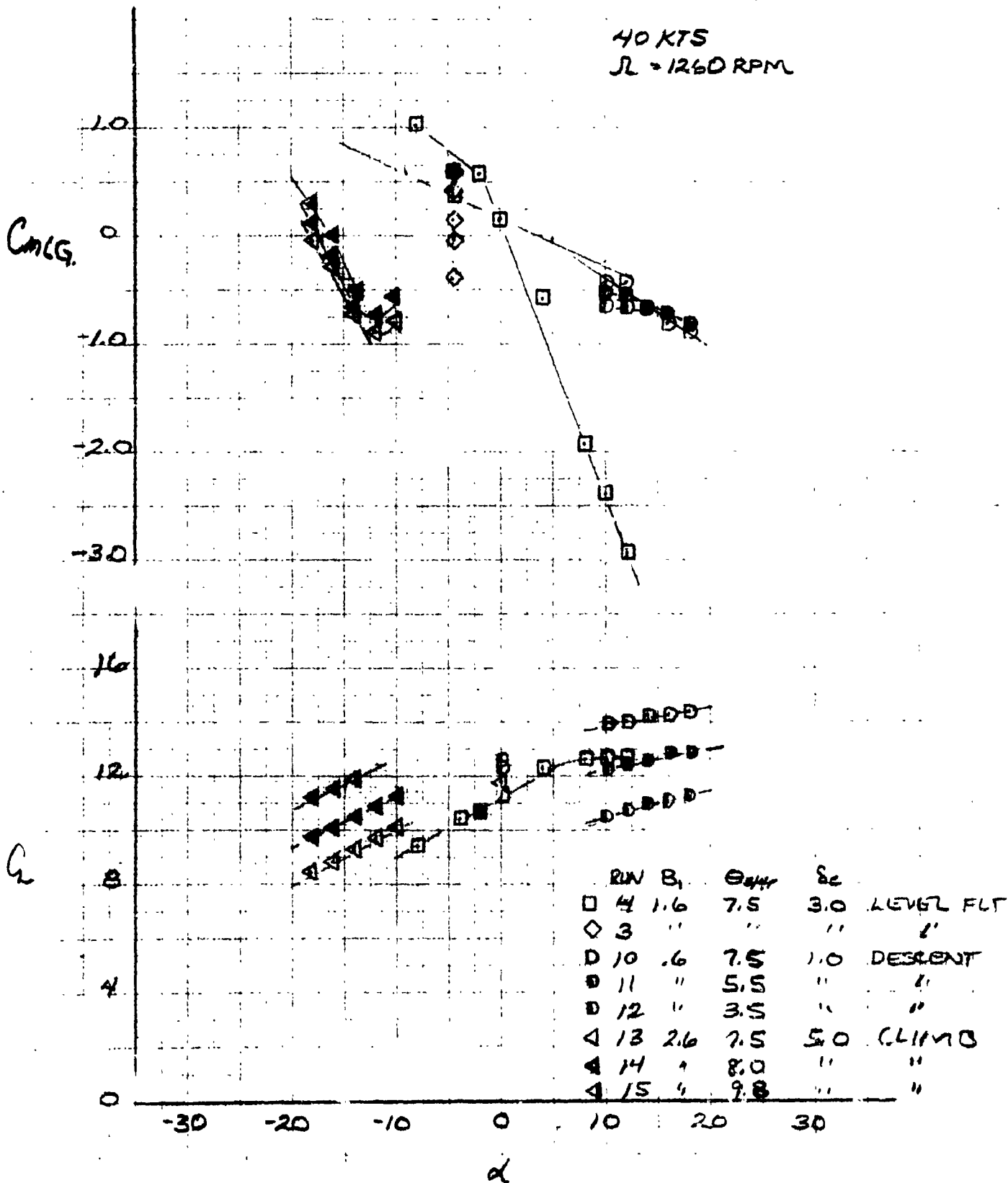
40 KTS
SC-1260 RPM



LSWT 421

STING MOUNT
MAST = 90°
FLAPS = 40/25°

40 KTS
R = 1260 RPM



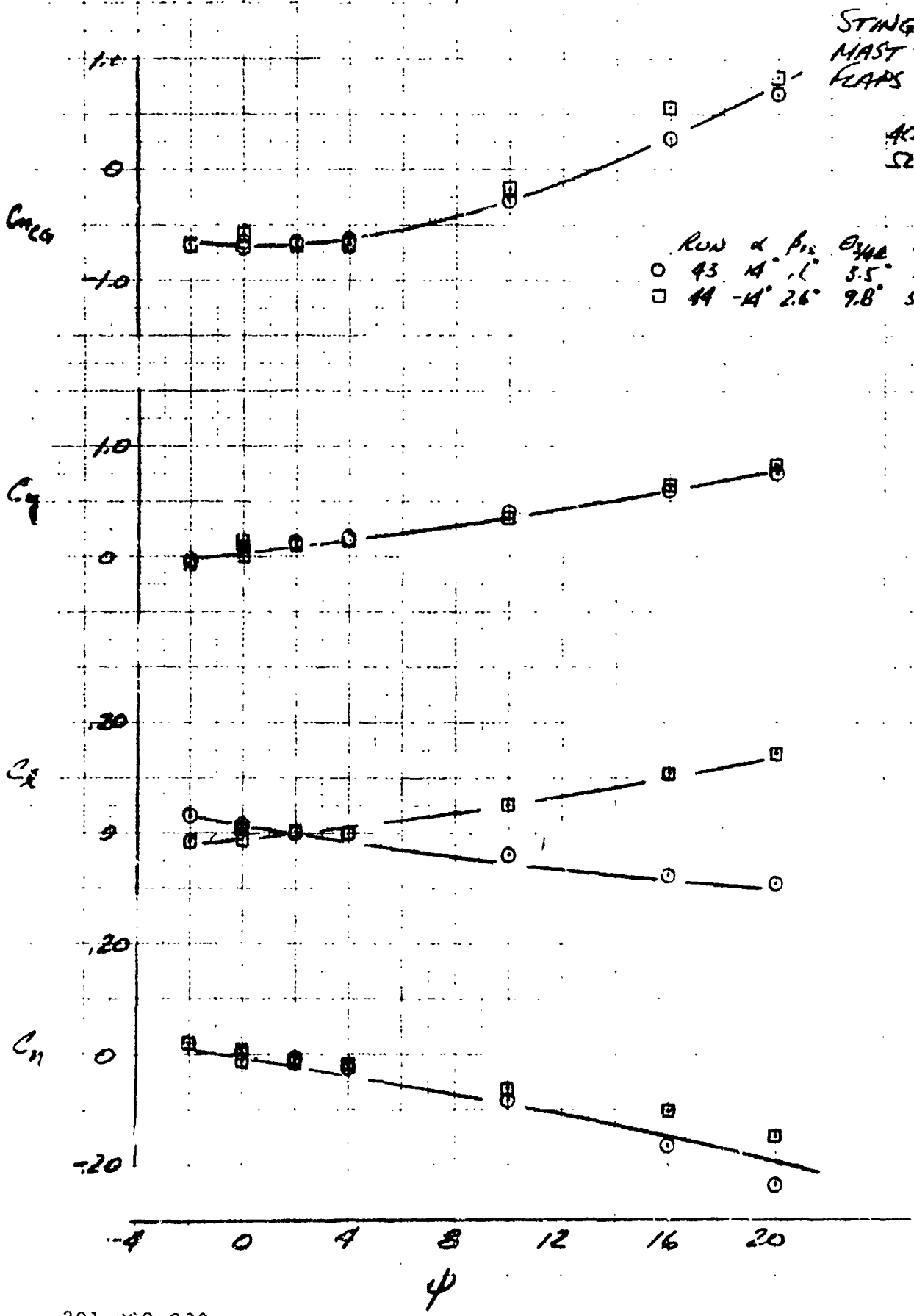
LSWT 421

STING MOUNT
 MAST = 90°
 FLAPS = 45°/25°

40 KTS
 SR = 1260

RUN	α	P_{10}	θ_{44}	δ_c	
○	43	14	1.1	3.5	1.0
□	44	-14	2.6	9.8	5.0

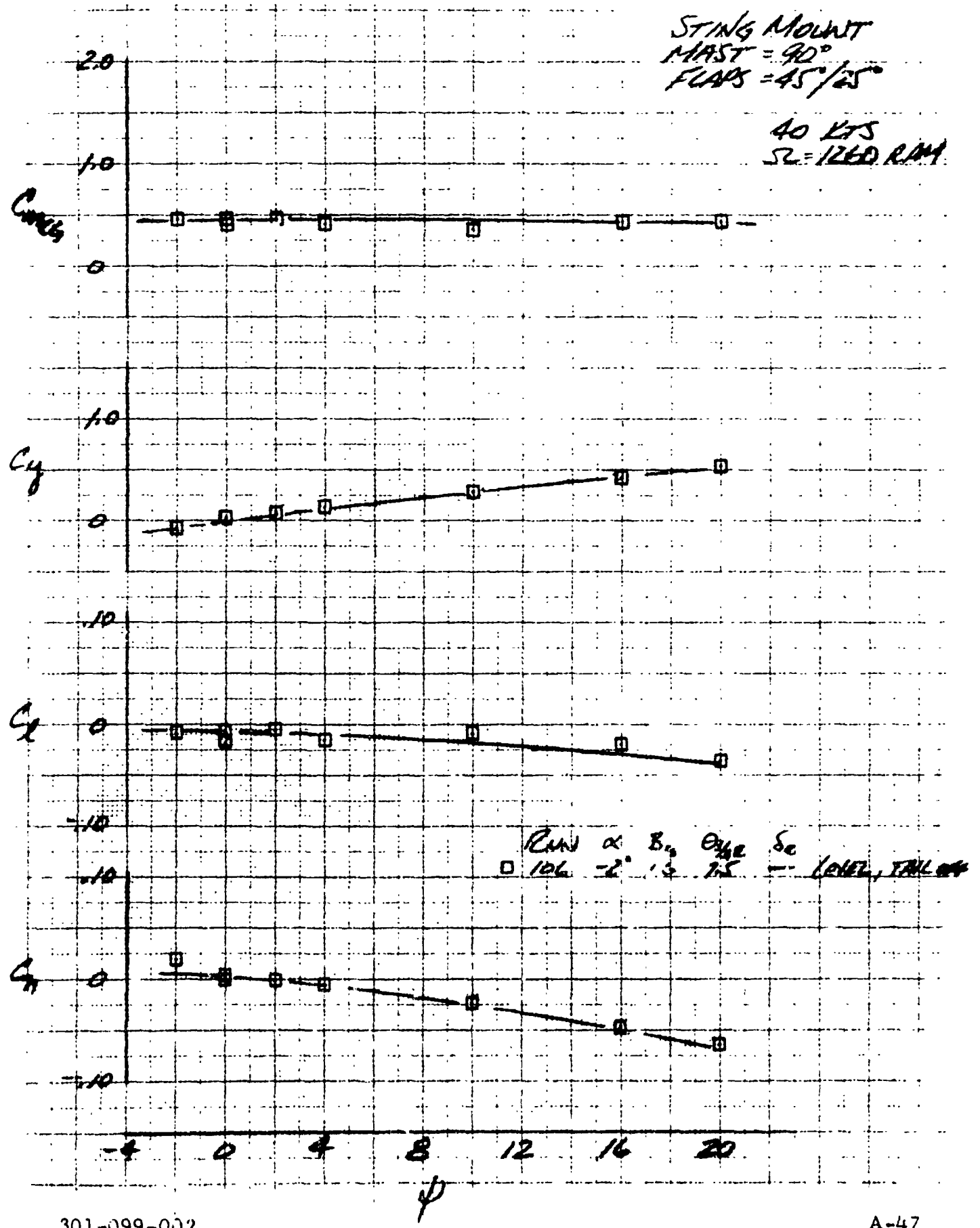
DESCEND CLIMB



LSWT 421

STING MOUNT
MAST = 90°
FLAPS = 45°/25°

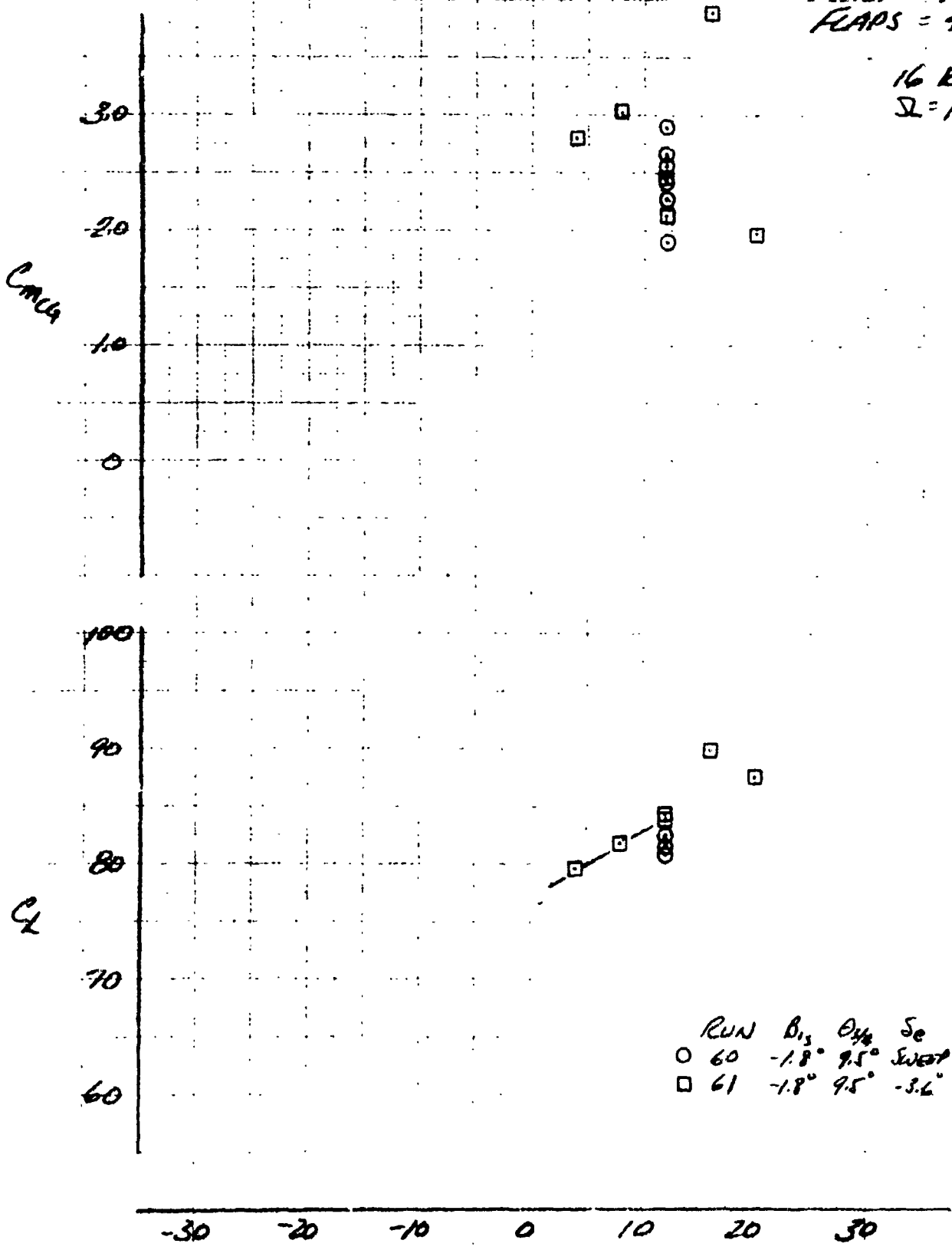
40 KTS
SL = 1260 RPM



LSWT 421

STING MOUNT
MAST = 75°
FLAPS = 45°/25°

16 KTS
SL = 1260 RPM

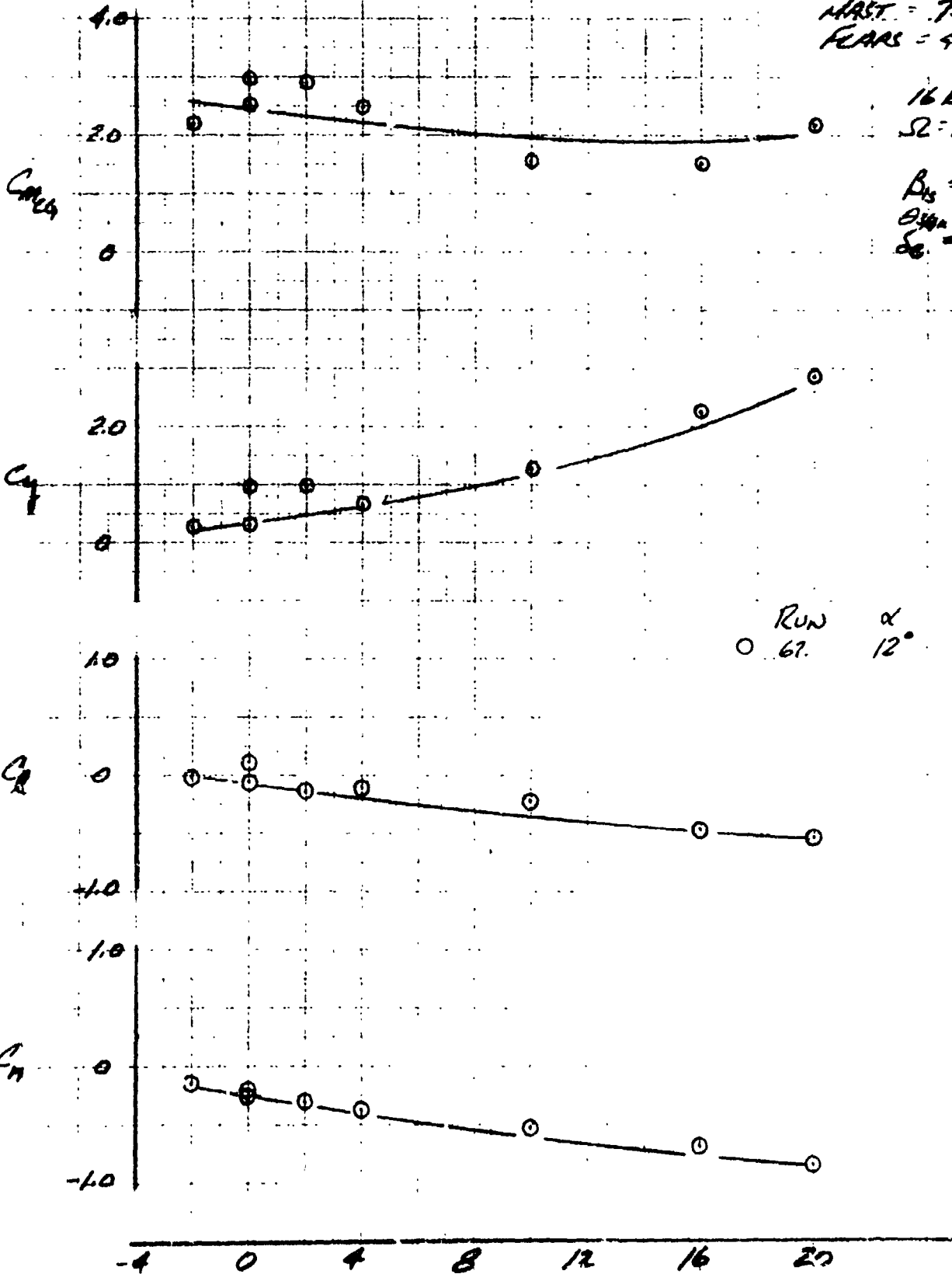


LSWT 421

STING MOUNT
 HAST. = 75°
 FEARS = 45°/25°

16 KTS
 Ω = 1260 RPM

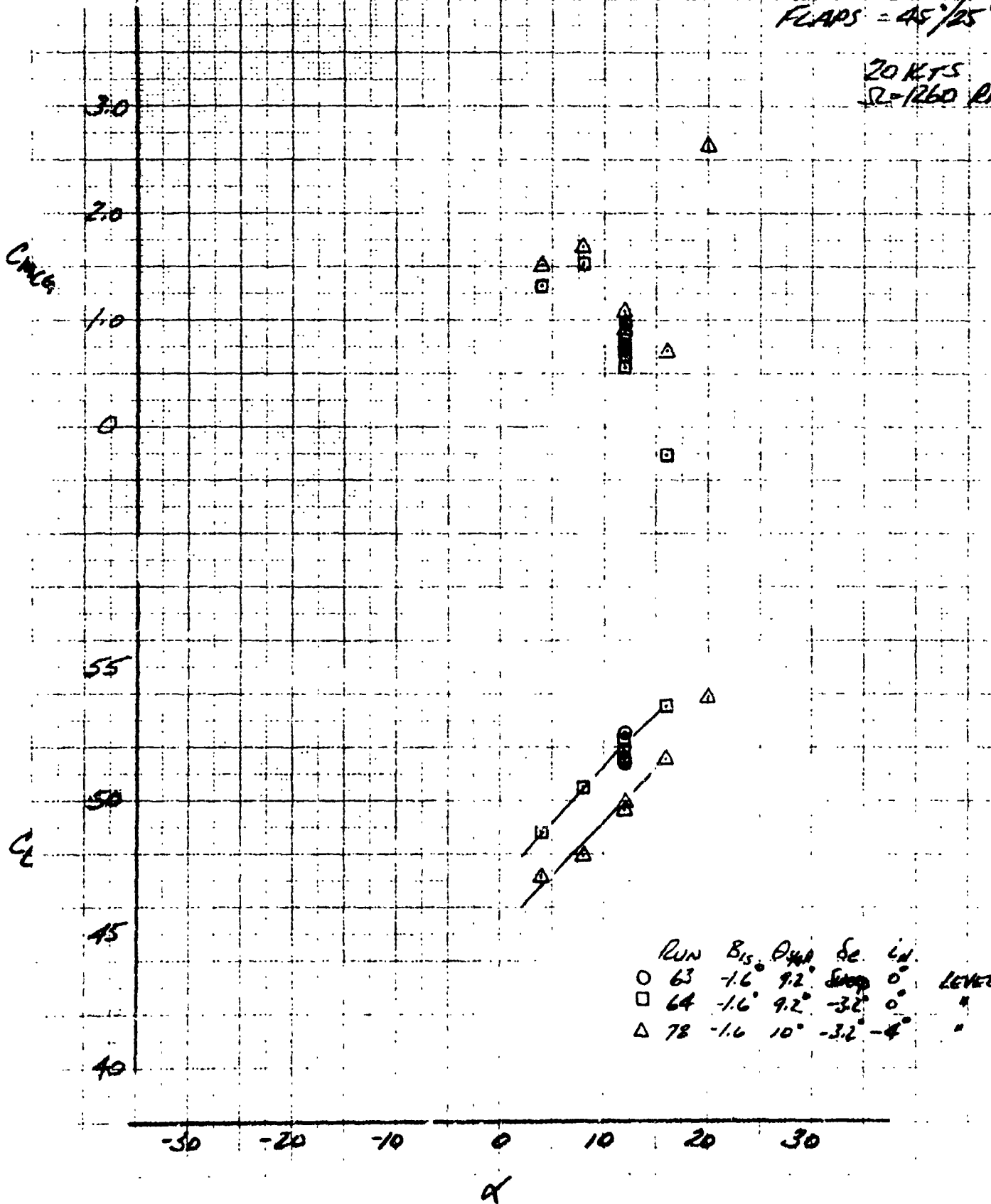
$\beta_{15} = -1.8^\circ$
 $\theta_{15} = 9.5^\circ$
 $\delta_{15} = -5.6^\circ$



LSWT 421

STING MOUNT
MAST = 75°
FLAPS = 45°/25°

20 KTS
SL-1260 RAM

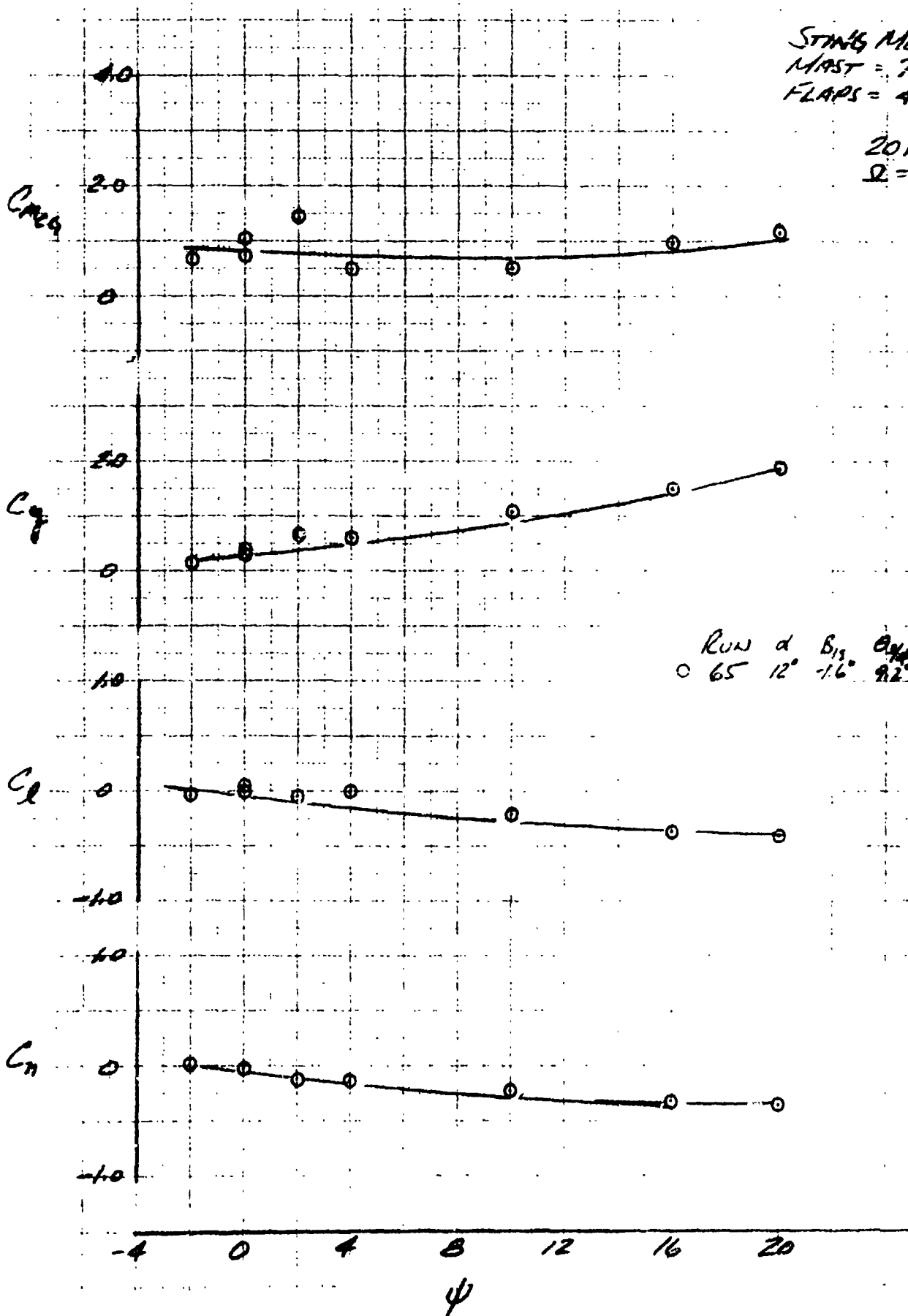


Run	Bis.	Q ₄₀	Se.	id.	
○ 63	-1.6	9.2	Swop	0°	LEVEL
□ 64	-1.6	9.2	-3.2	0°	"
△ 78	-1.6	10°	-3.2	-4°	"

LSWT 421

STING MOUNT
 MAST = 75°
 FLAPS = 45°/25°

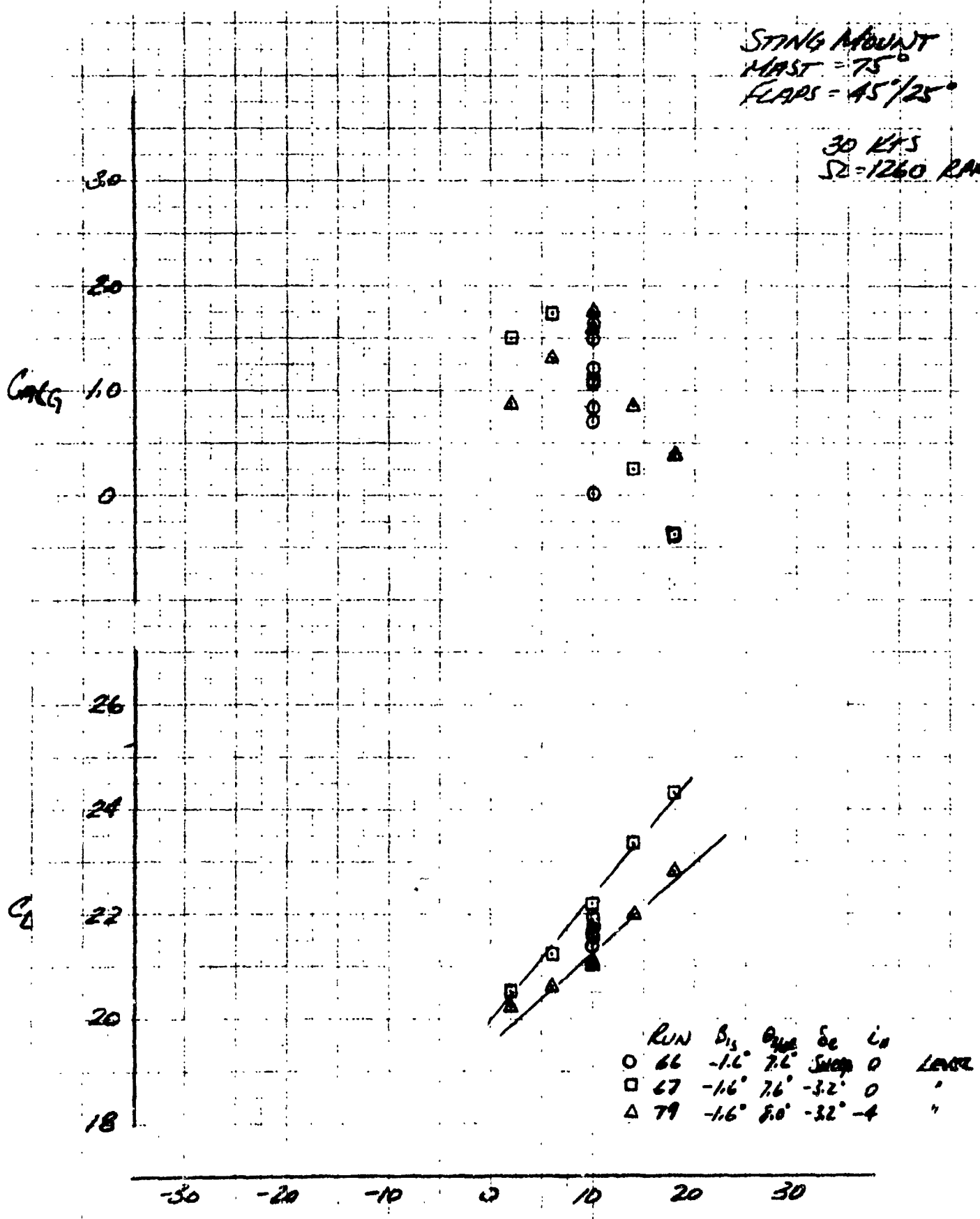
20 KTS
 $\Omega = 1260 \text{ RPM}$



LSWT 421

STING MOUNT
MAST = 75°
FLAPS = 45°/25°

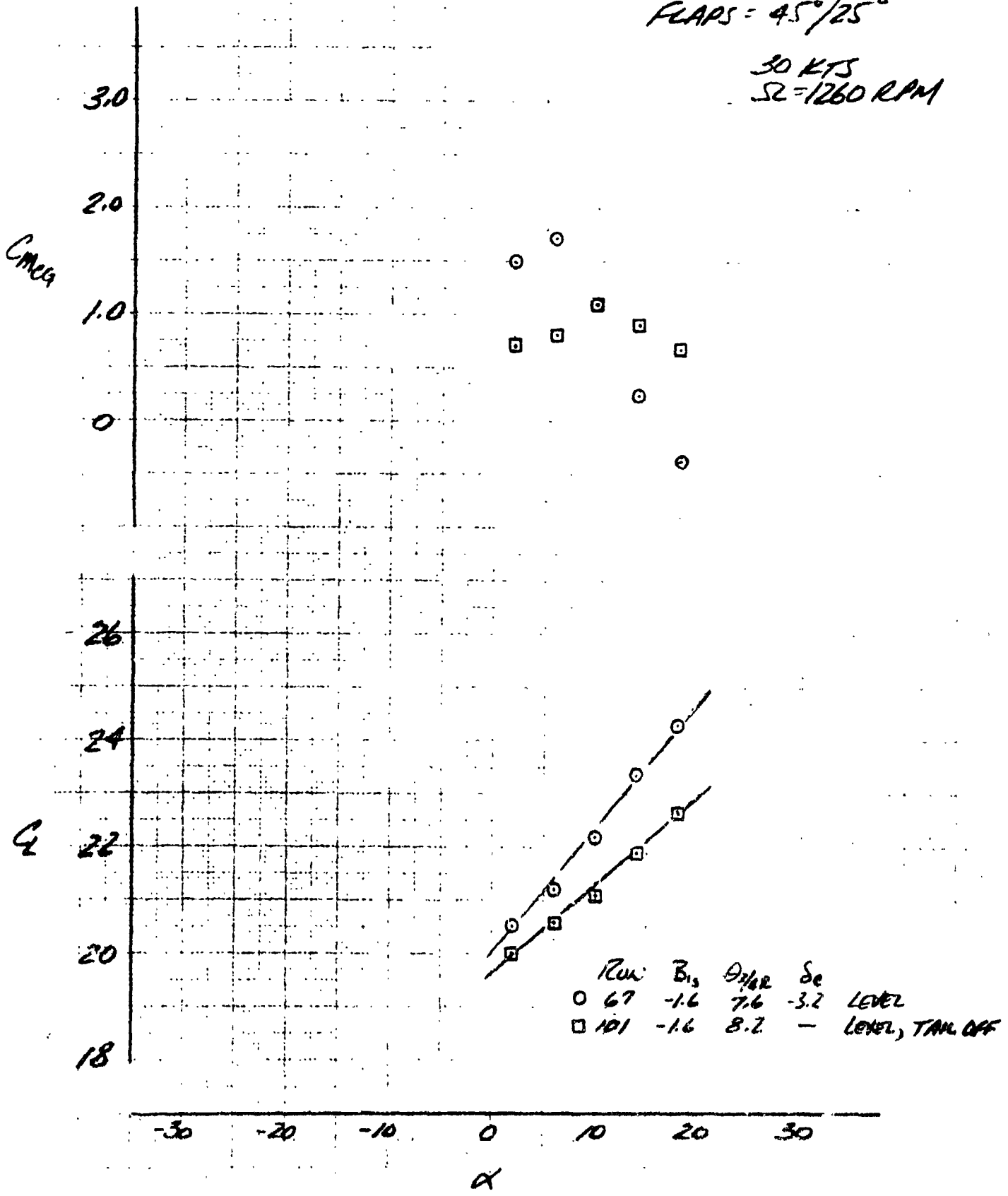
30 KTS
S2-1260 RAM



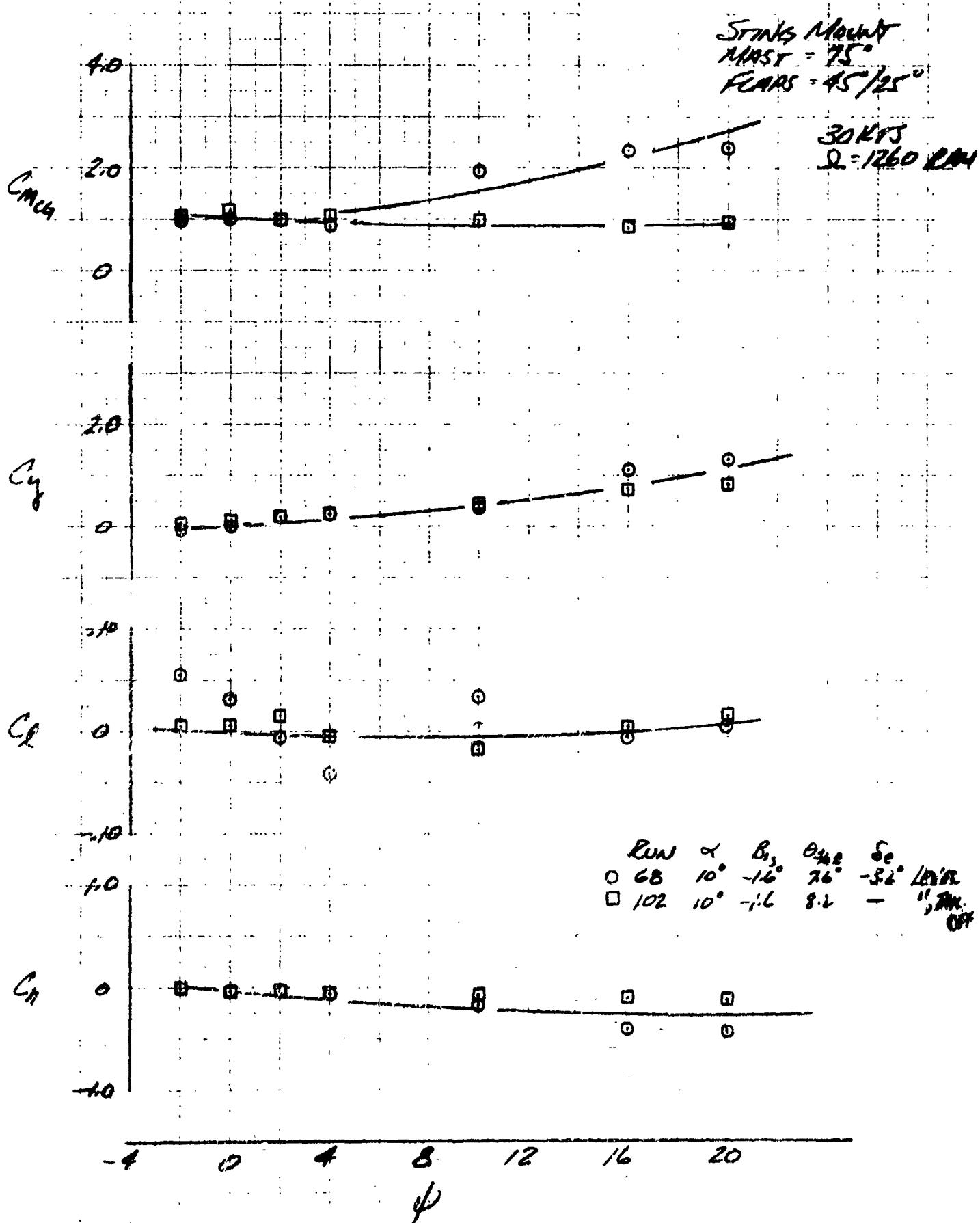
LSWT 421

STING MOUNT
 NMAST = 75°
 FLAPS = 4.5°/25°

30 KTS
 Ω = 1260 RPM



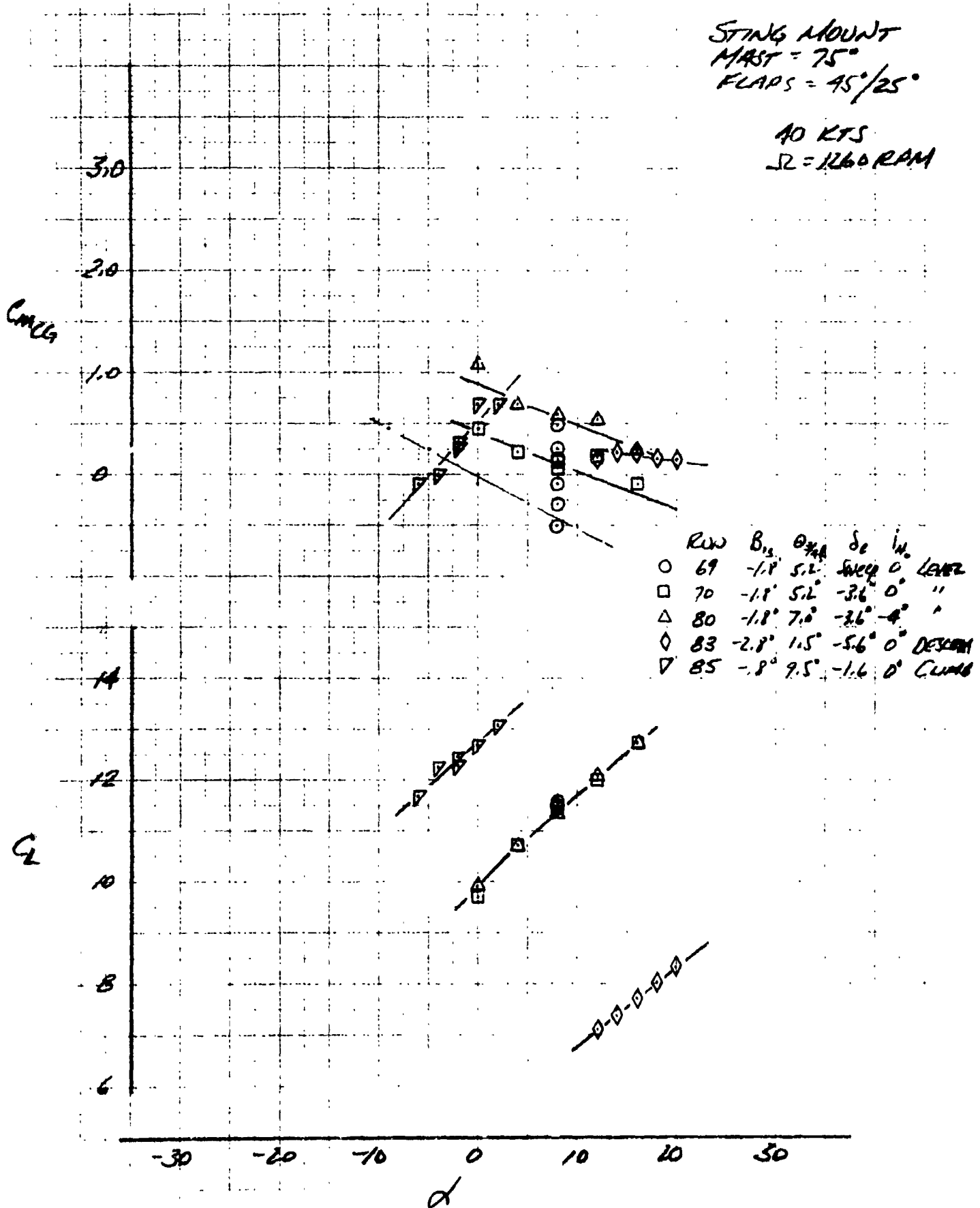
LSWT 421



LSWT 421

STING MOUNT
 MAST = 75°
 FLAPS = 45°/25°

40 KTS
 SL = 1260 RPM



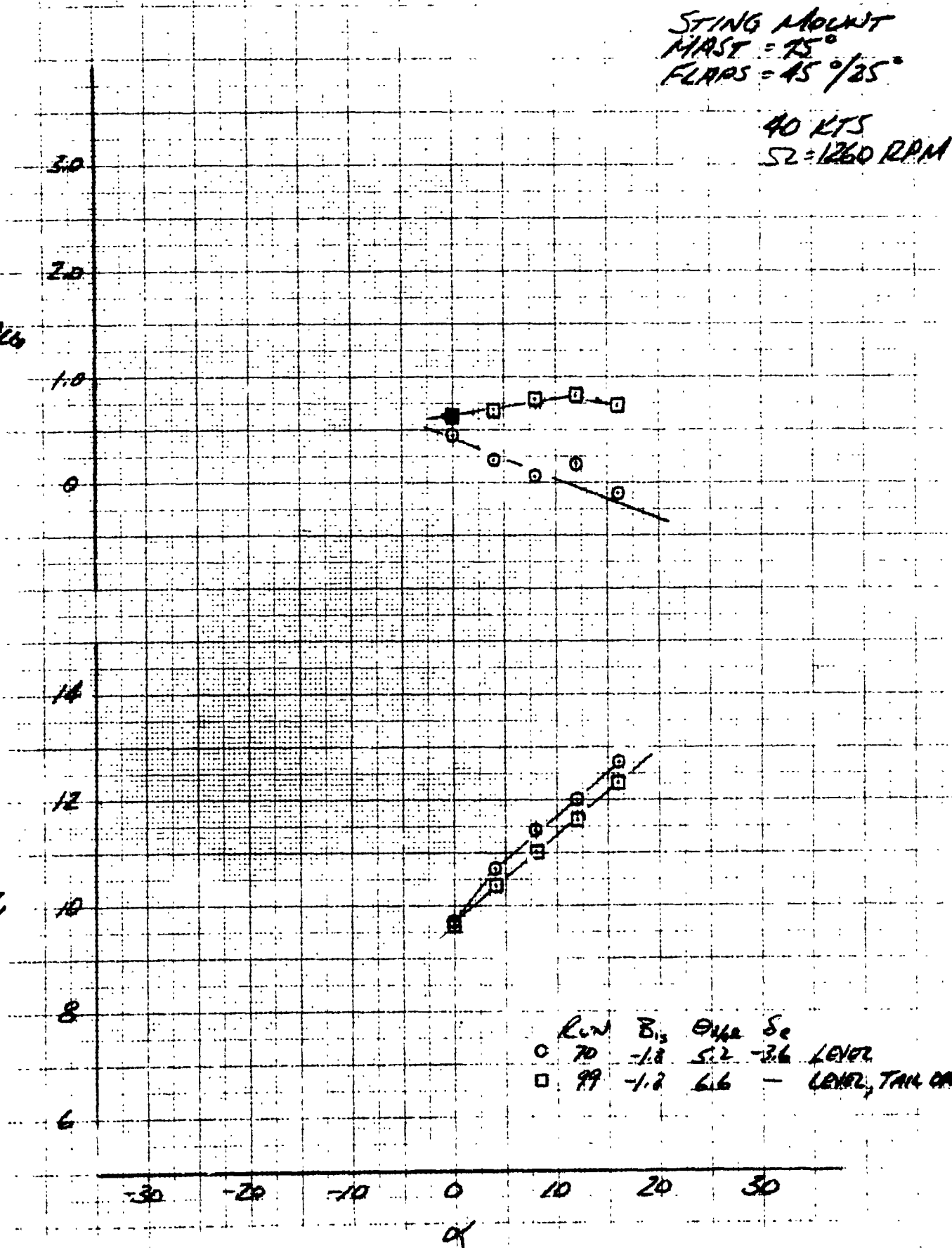
LSWT 421

STING MOUNT
 HAST = 75°
 FLAPS = 45°/25°

40 KTS
 SZ = 1260 RPM

$C_{m/c}$

C_L

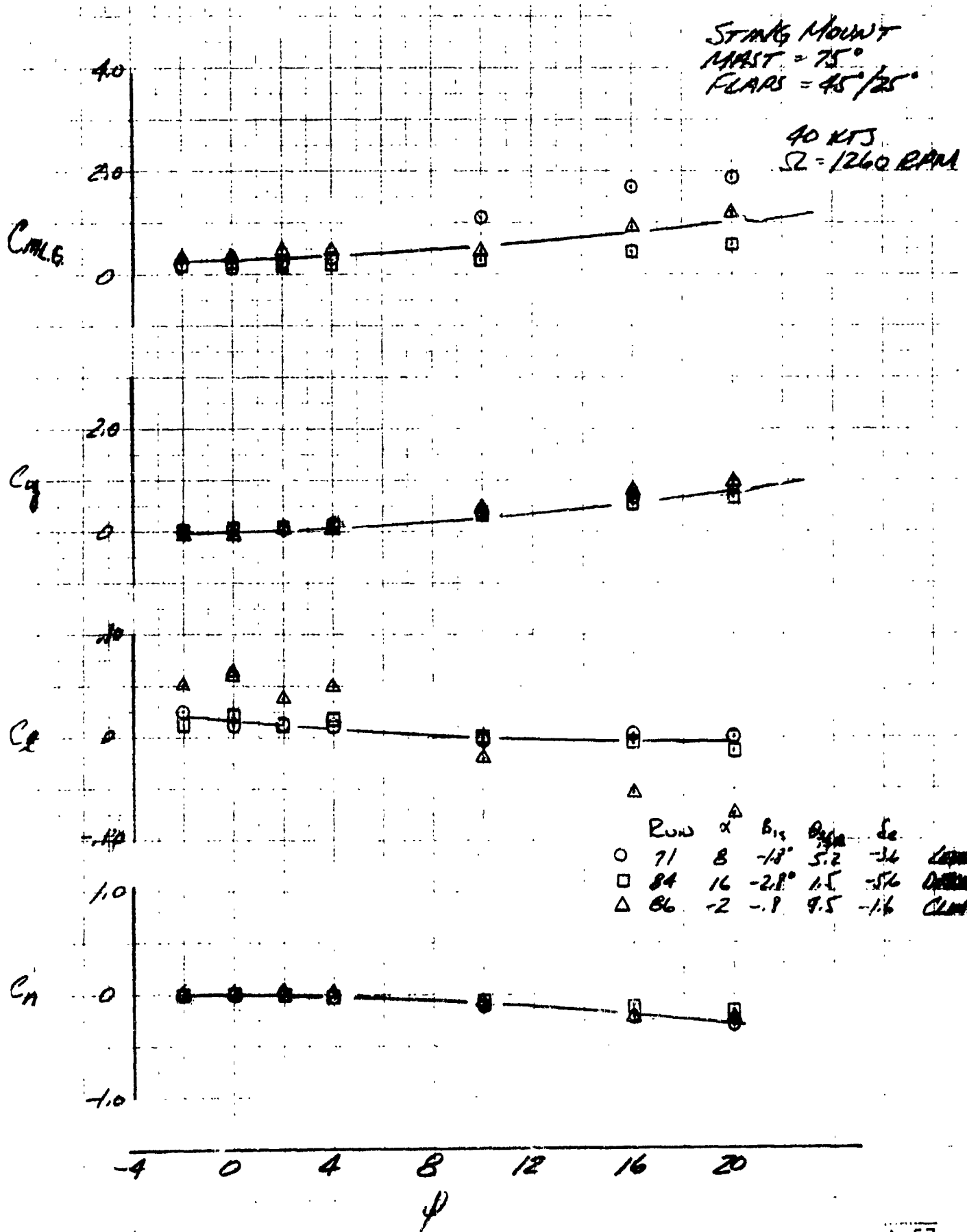


Row B_{12} $\Theta_{1/2}$ S_e
 ○ 70 -1.8 5.2 -3.6 LEVEL
 □ 99 -1.8 6.6 - LEVEL, TAIL OFF

LSWT 421

STING MOUNT
MAST = 75°
FLAPS = 45/25°

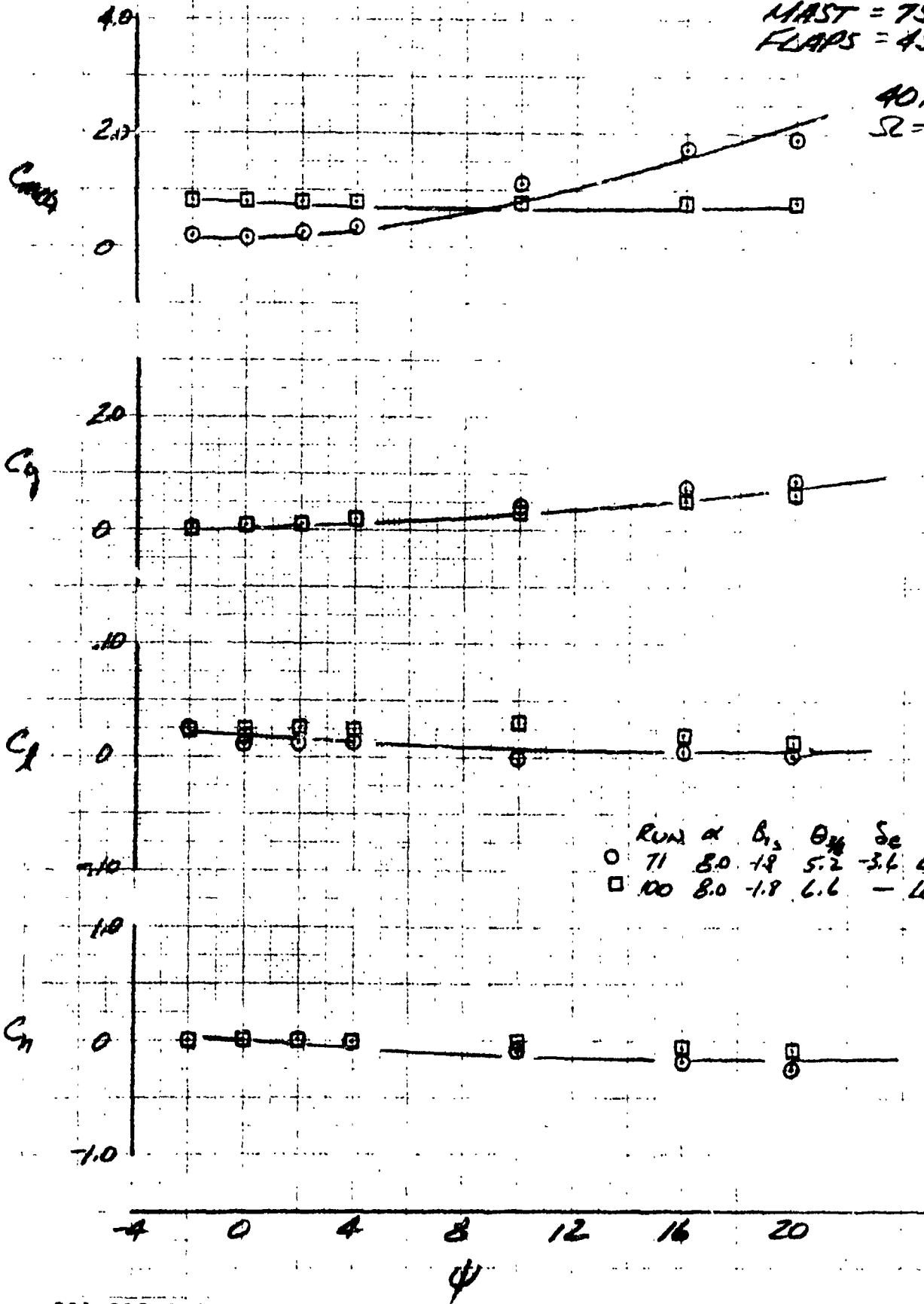
40 KTS
 $\Omega = 1260$ RPM



LSWT 421

STING MOUNT
MAST = 75°
FLAPS = 45°/25°

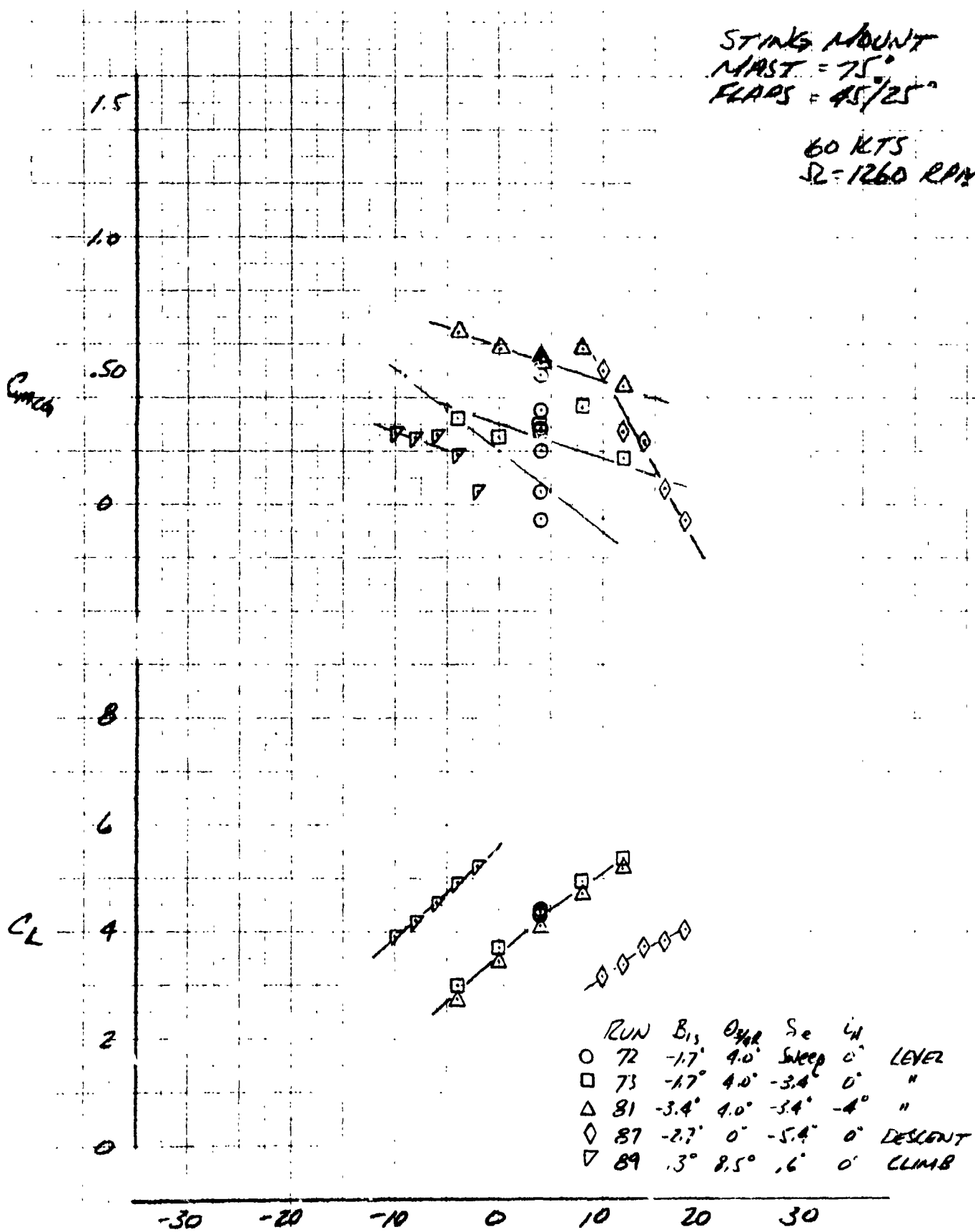
40 KTS
R = 1260 RPM



LSWT 421

STING MOUNT
MAST = 75°
FLAPS = 45/25°

60 KTS
R = 1260 RPM

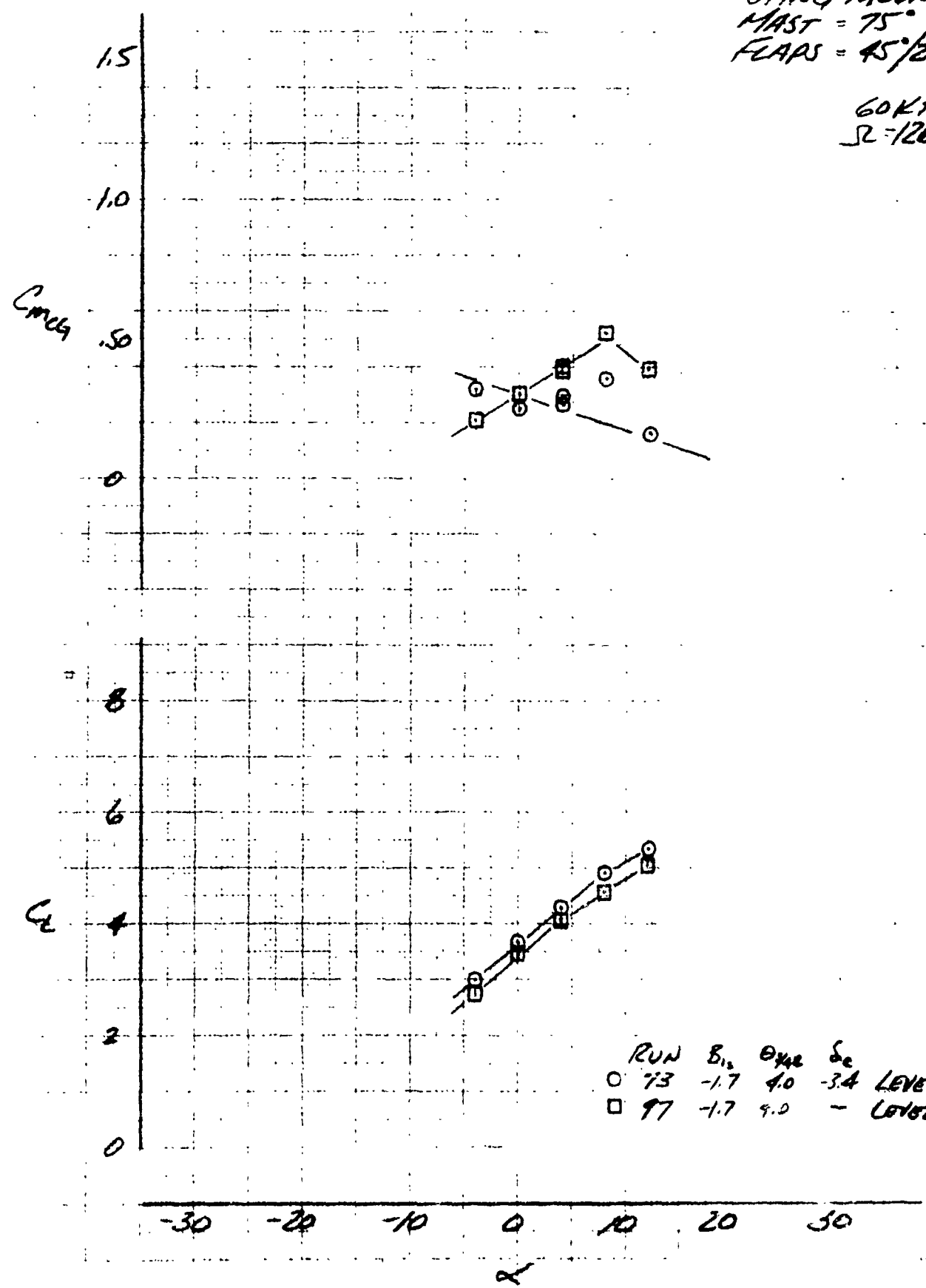


RUN	B ₁₅	O _{1/2}	S _e	LH	LEVEL
○ 72	-1.7°	4.0°	Sweep	0°	LEVEL
□ 73	-1.7°	4.0°	-3.4°	0°	"
△ 81	-3.4°	4.0°	-3.4°	-4°	"
◇ 87	-2.7°	0°	-5.4°	0°	DESCENT
▽ 89	.3°	8.5°	.6°	0°	CLIMB

LSWT 421

STING MOUNT
 MAST = 75°
 FLAPS = 45°/25°

60 KTS
 SL = 1260 RPM

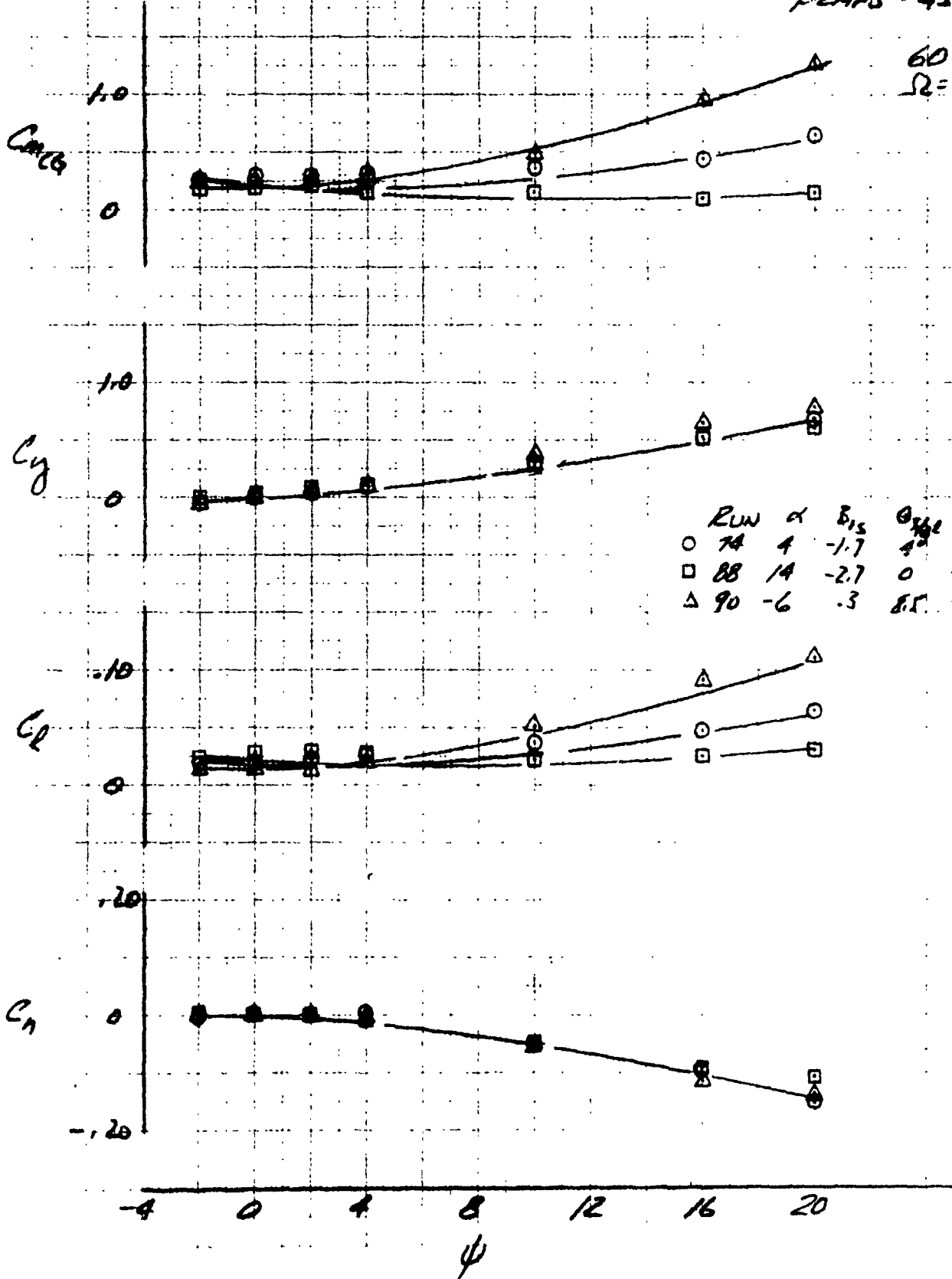


RUN	B_{12}	θ_{42}	S_c	LEVEL
○ 73	-1.7	4.0	-3.4	LEVEL
□ 97	-1.7	9.0	-	LEVEL 2, TAN DAY

LSWT 421

STING MOUNT
MAST = 75°
FLAPS = 45°/25°

60 KTS
 $\Omega = 1260 \text{ RPM}$

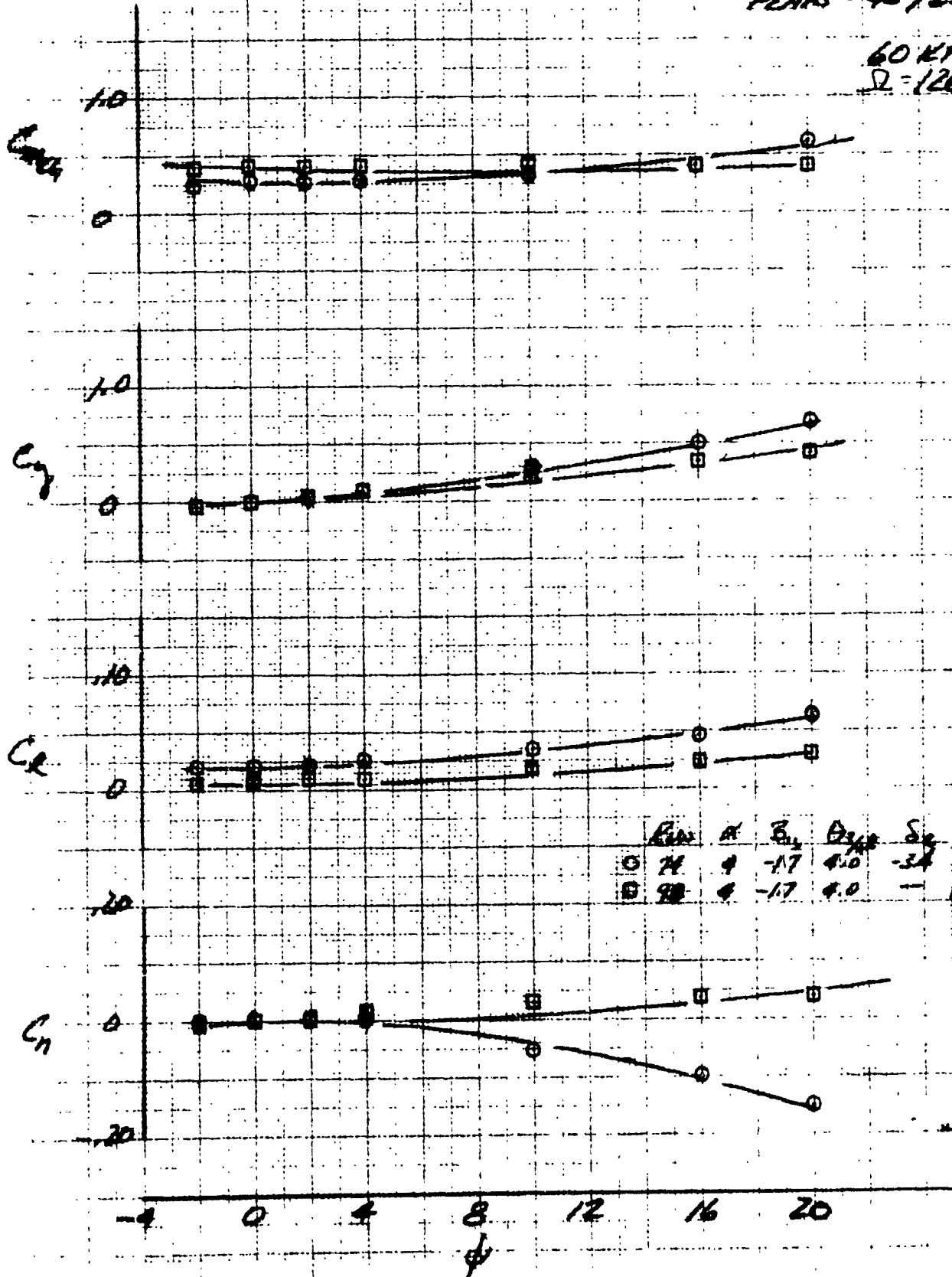


ROW	α	β_{15}	θ_{15}	δ	CLIMB
○	74	4	-1.7	4°	-3.4° LEVEL
□	88	14	-2.7	0	-5.4° DESCENT
△	90	-6	.3	8.5°	-6° CLIMB

LSWT 421

STING MOUNT
 HAST = 75°
 FLARE = 45°/25°

60 KTS
 Ω = 1260 RPM

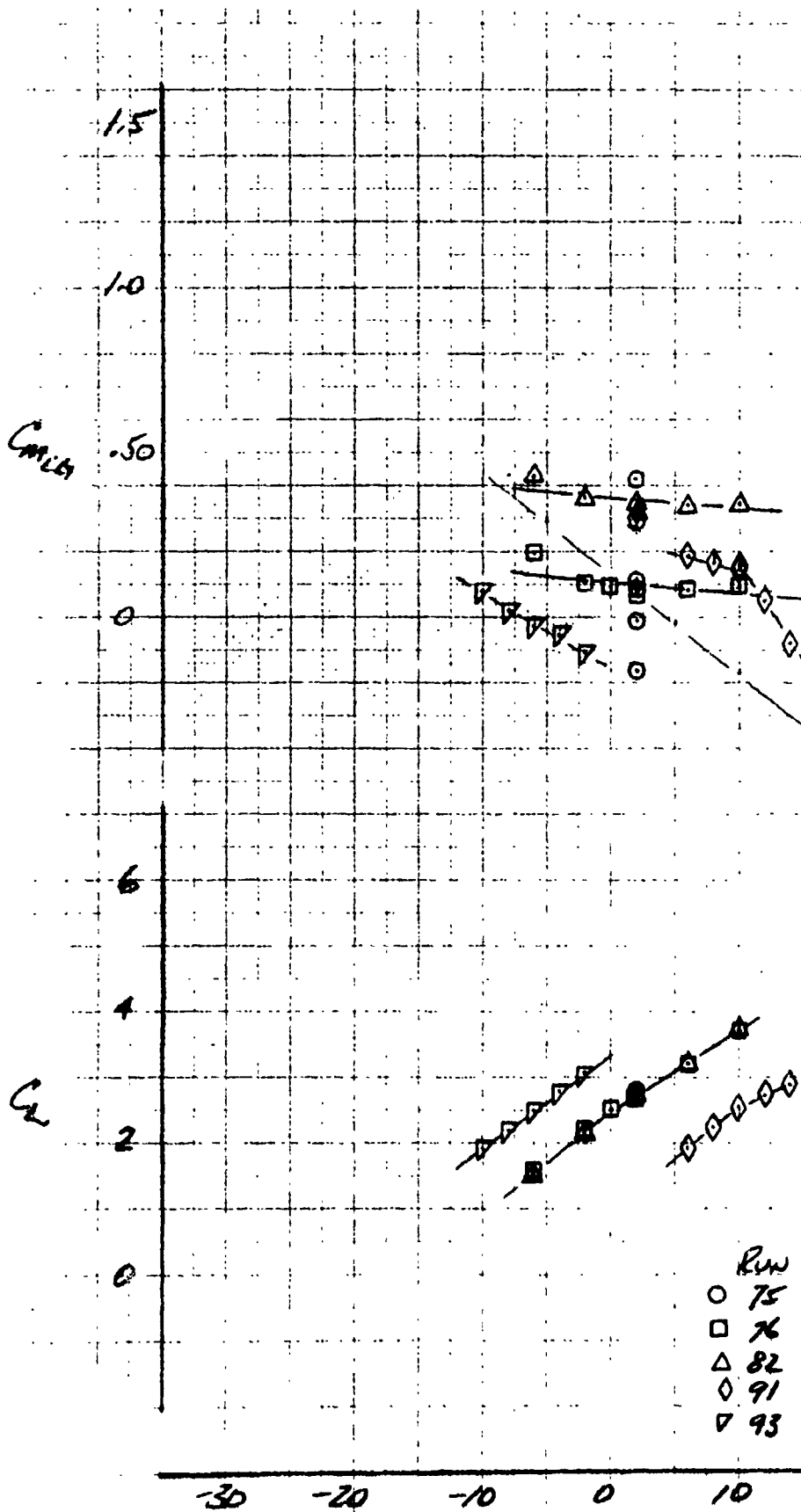


Series	Re	α	β	θ_{tip}	S_{tip}	Notes
○	74	4	-17	4.0	-34	LOAD
□	98	4	-17	4.0	-	LOAD, TOWER

LSWT 421

STING MOUNT
MAST = 75°
FLAPS = 45°/25°

80 KTS
R = 1260 RPM

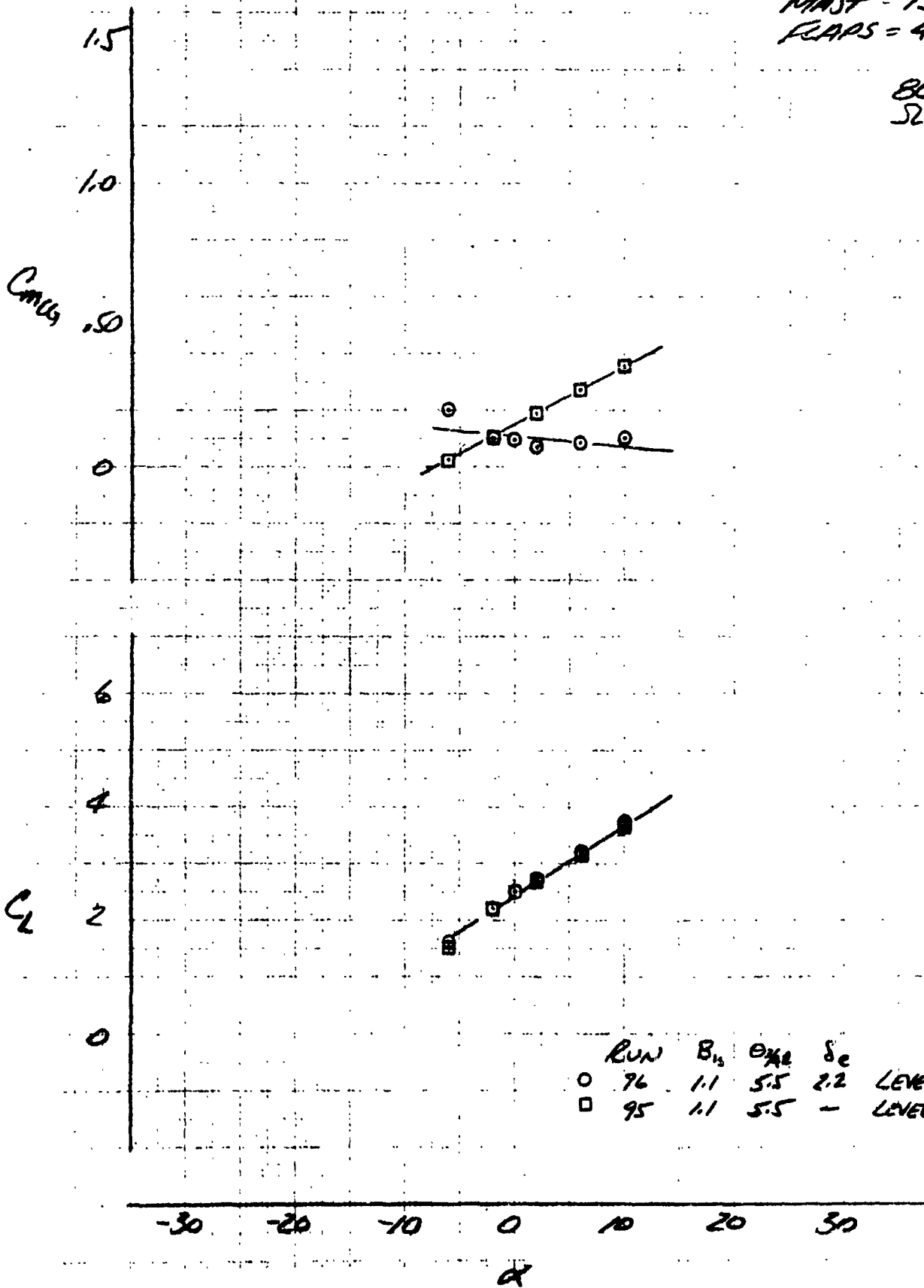


Run	B ₁₅	B ₂₅	S ₂	L ₁	
○ 75	1.1°	5.5°	Sweep	0°	LEVEL
□ 76	1.1°	5.5°	2.2	0°	"
△ 82	1.1°	6.0°	2.2°	-4°	"
◇ 91	.2	1.0	4.0	0	DESCENT
▽ 93	3.2	10	6.4	0	CLIMB

LSWT 421

STING MOUNT
MAST = 75°
FLAPS = 45°/25°

80 KTS
SL = 1260 RPM

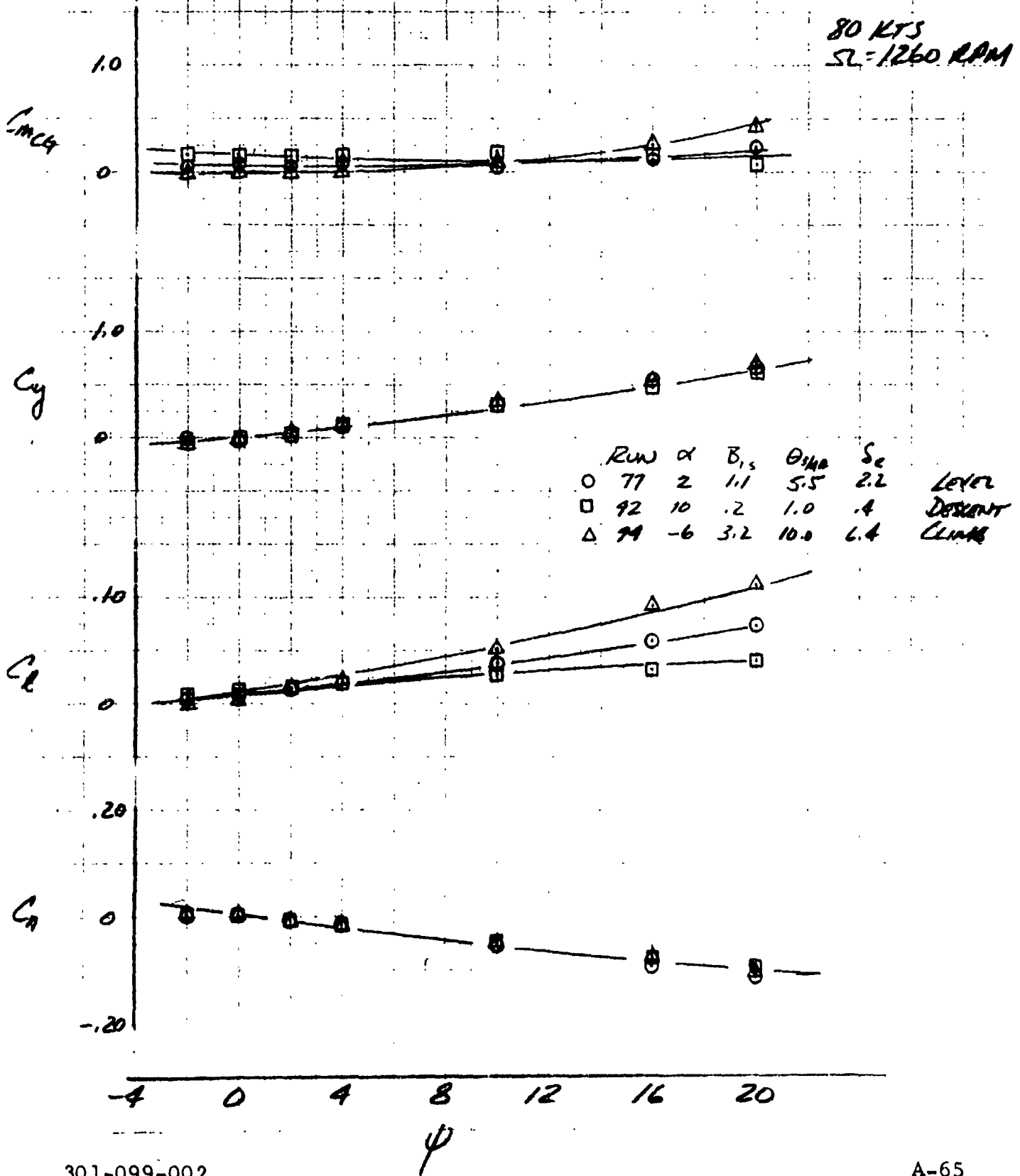


Run	B_{11}	θ_{12}	δ_c	
○ 96	1.1	5.5	2.2	LEVEL
□ 95	1.1	5.5	-	LEVEL, TAIL OFF

LSWT 421

STING MOUNT
MAST = 75°
FLAPS = 45°/25°

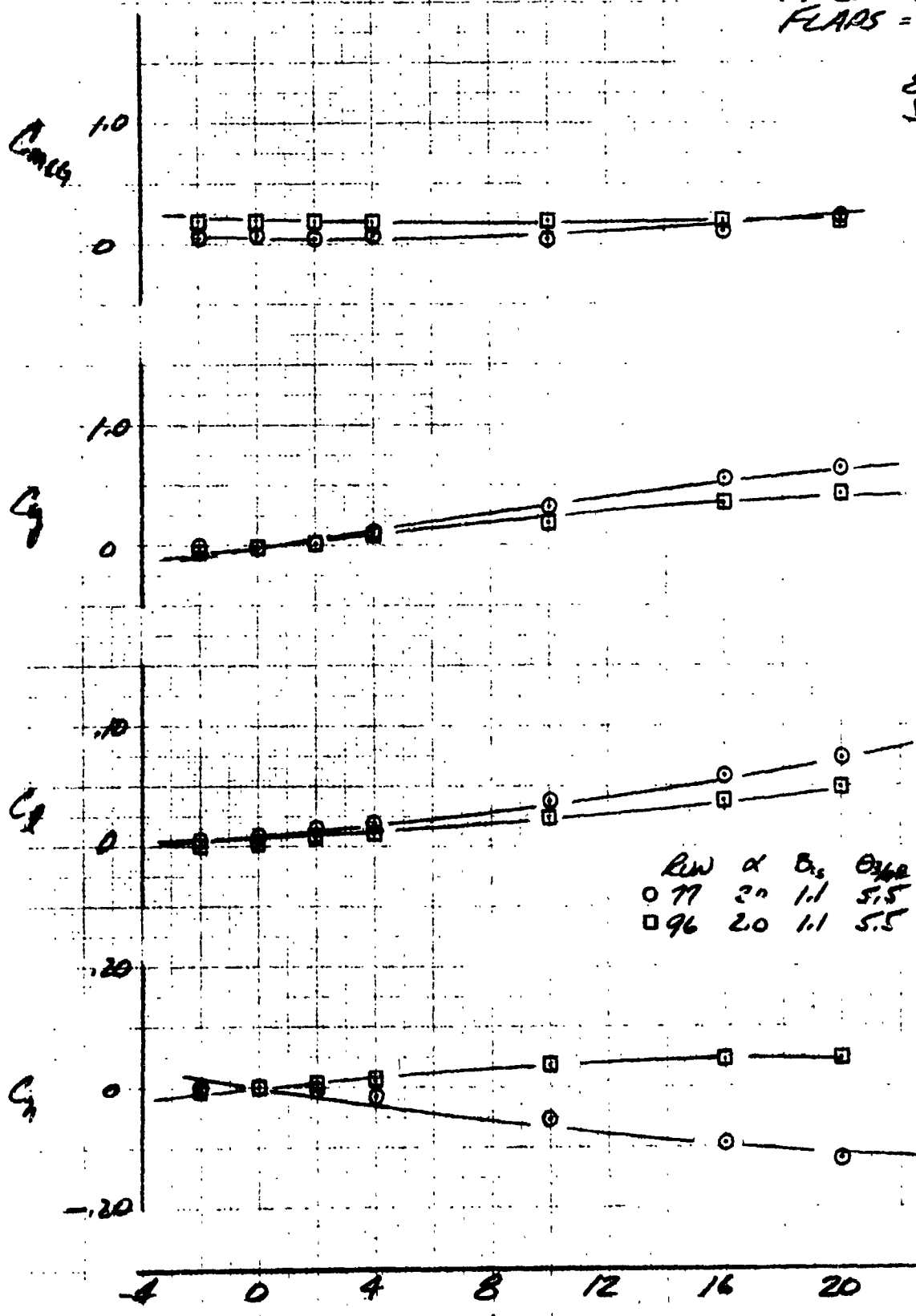
80 KTS
SL = 1260 RPM



LSUIT 421

STING MOUNT
MAST = 75°
FLAPS = 45°/25°

80 KTS
SL-1260 RAM

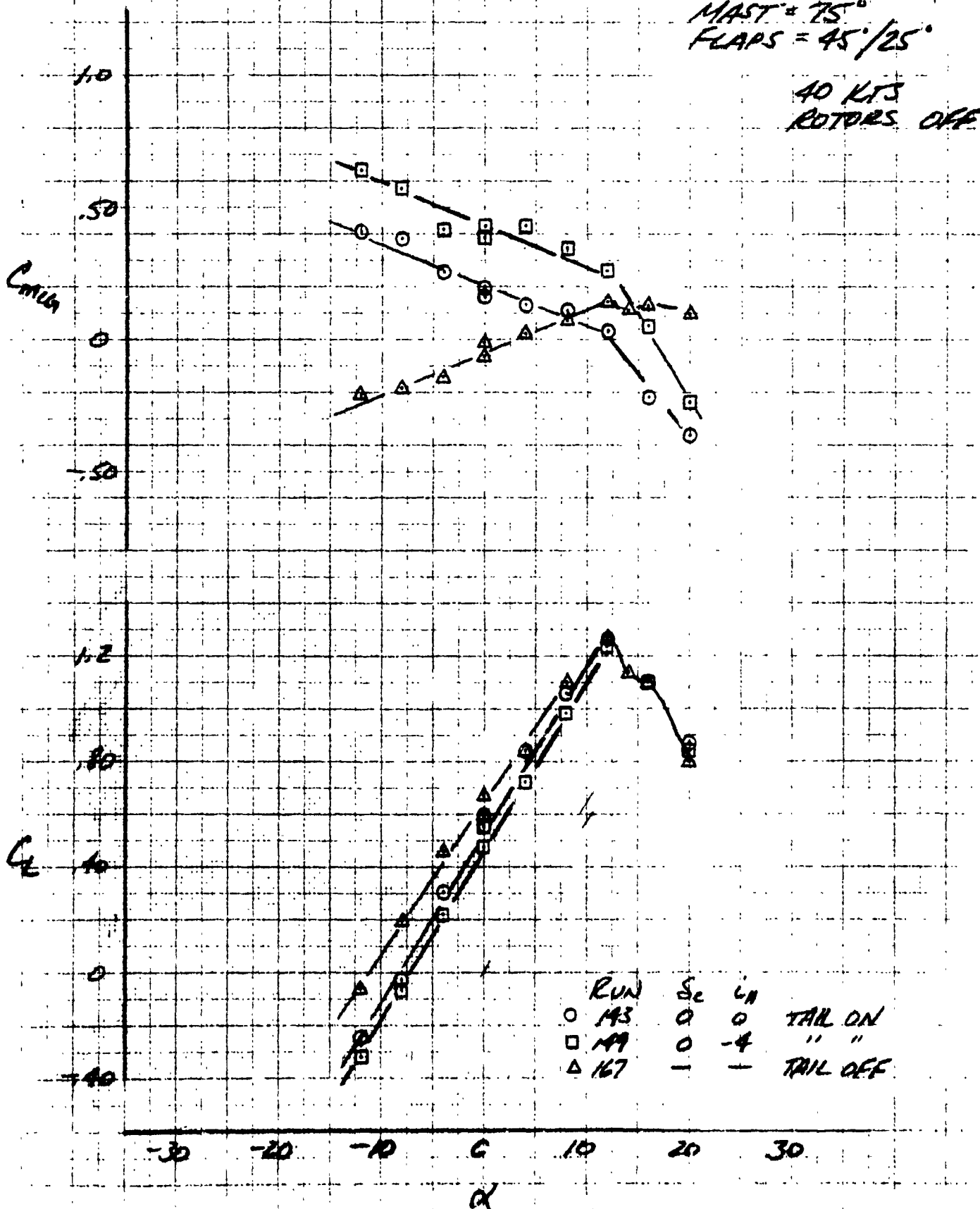


Row	α	B_{15}	B_{16}	S_c
○ 77	20	1.1	5.5	LEVEL
□ 96	20	1.1	5.5	LEVEL, TAIL ROTOR

LSWT 421

STING MOUNT
MAST = 75°
FLAPS = 45°/25°

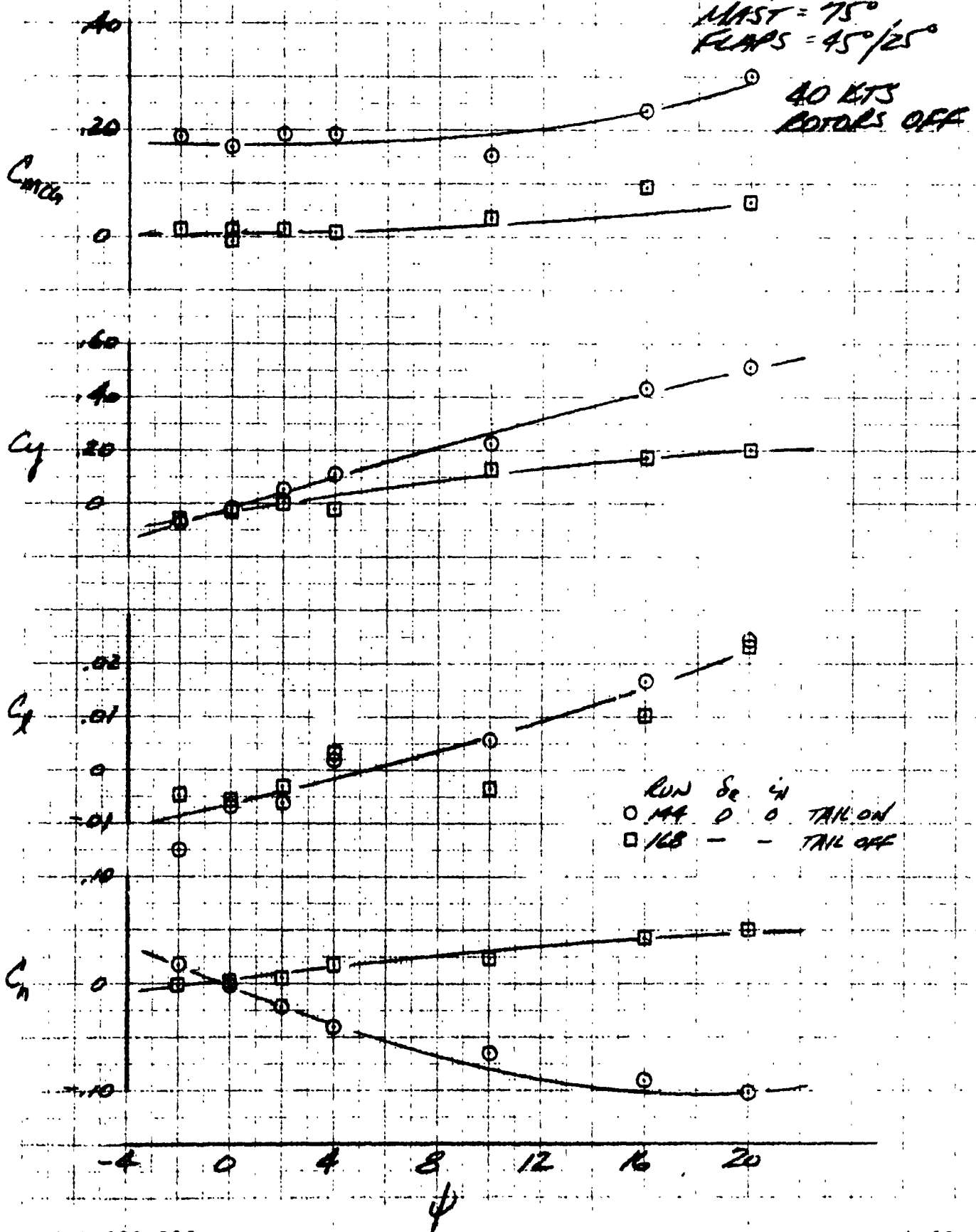
40 KTS
ROTOR OFF



LSUT 421

STING MOUNT
MAST = 75°
FLAPS = 45°/25°

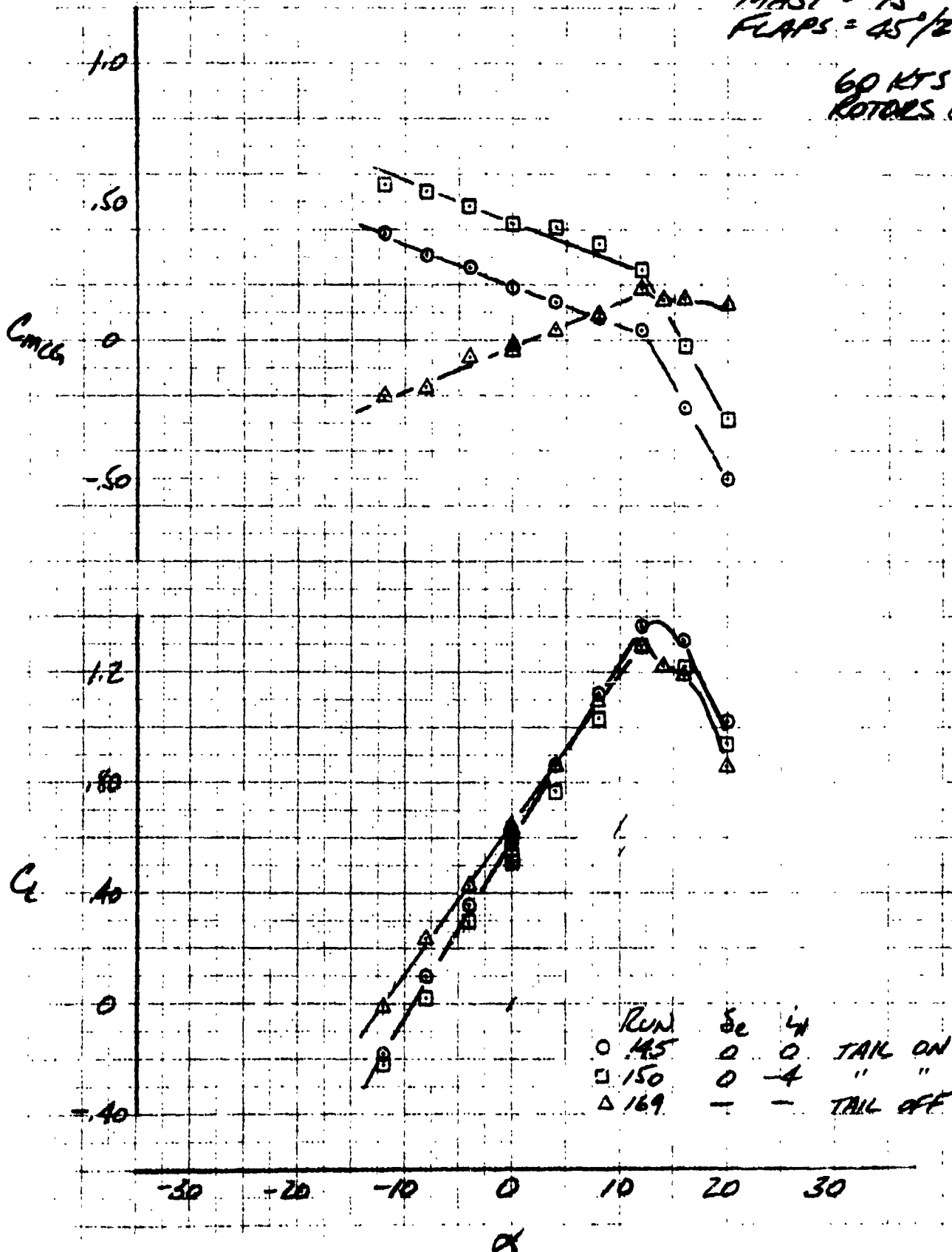
40 KTS
ROTORS OFF



LSWT 421

STING MOUNT
MAST = 75°
FLAPS = 45°/25°

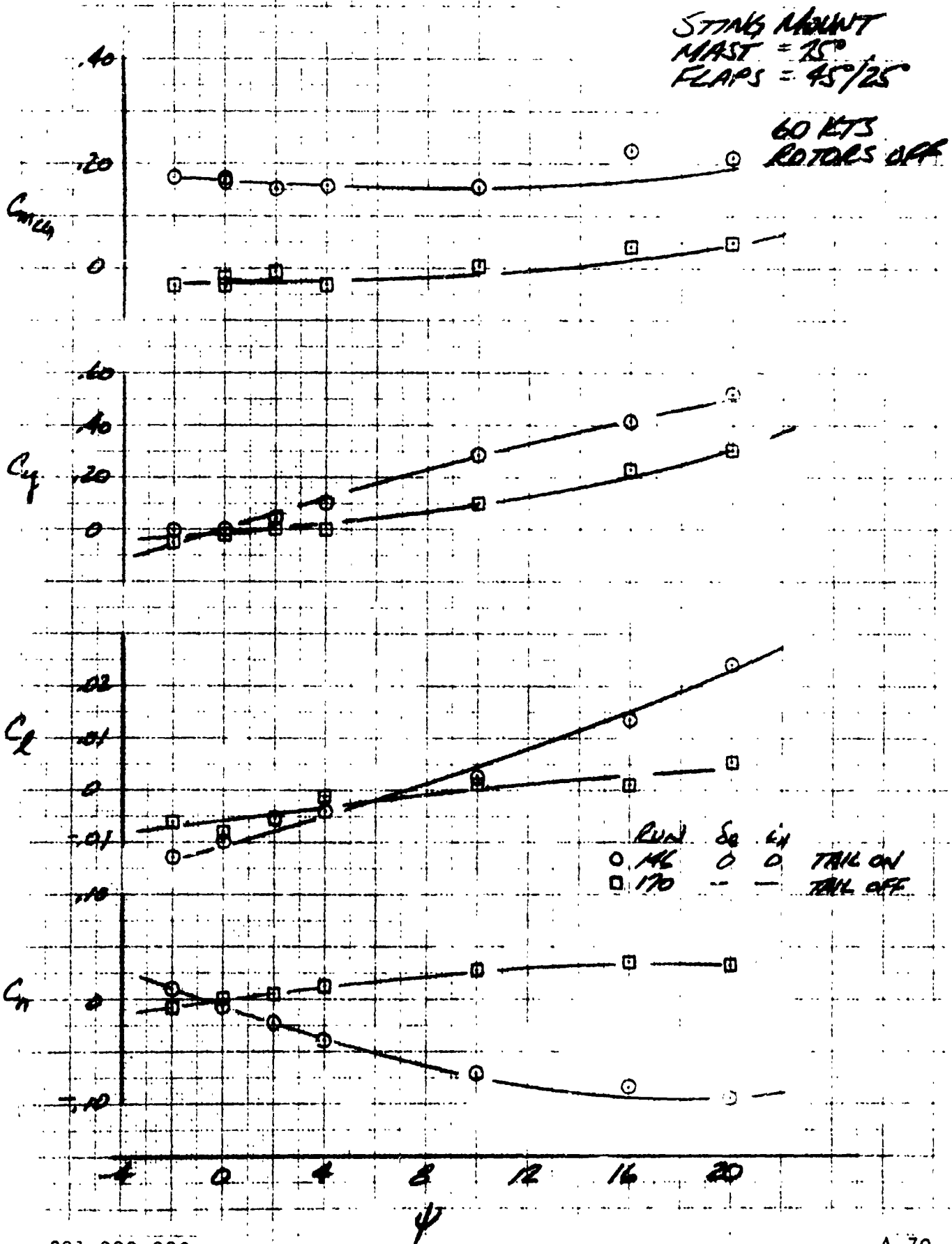
60 KTS
ROTOR OFF



LSWT 421

STING MOUNT
MAST = 15°
FLAPS = 45/25

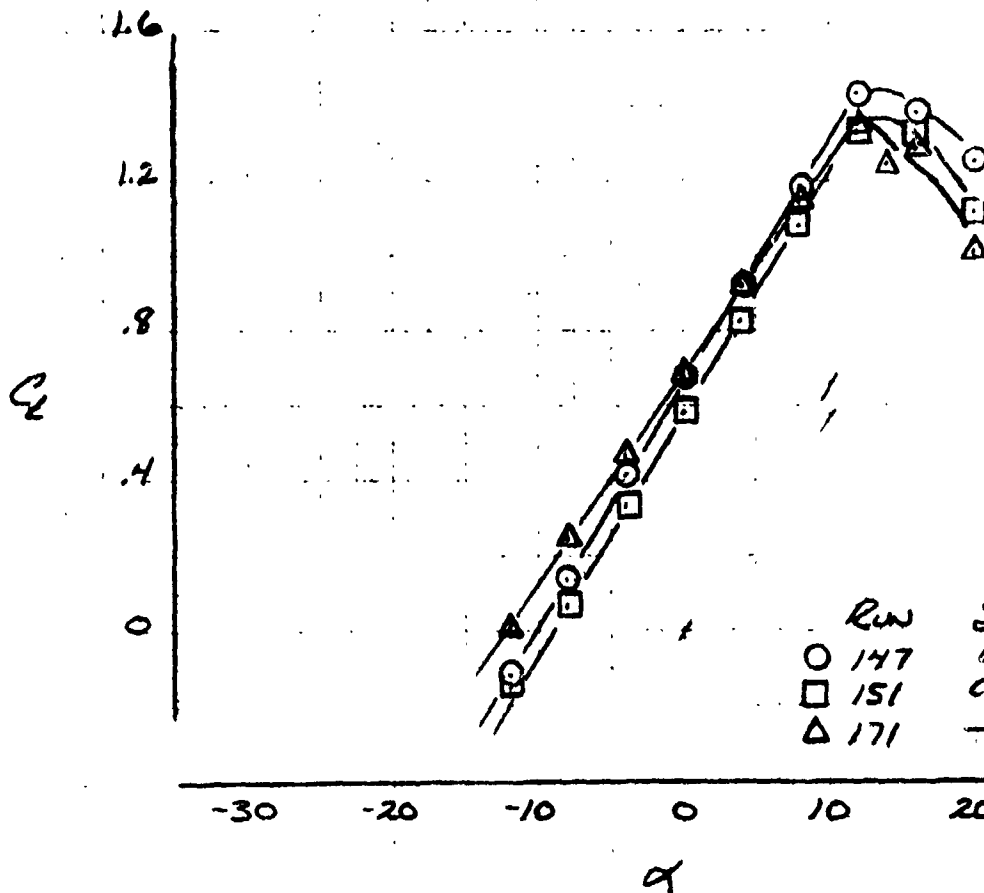
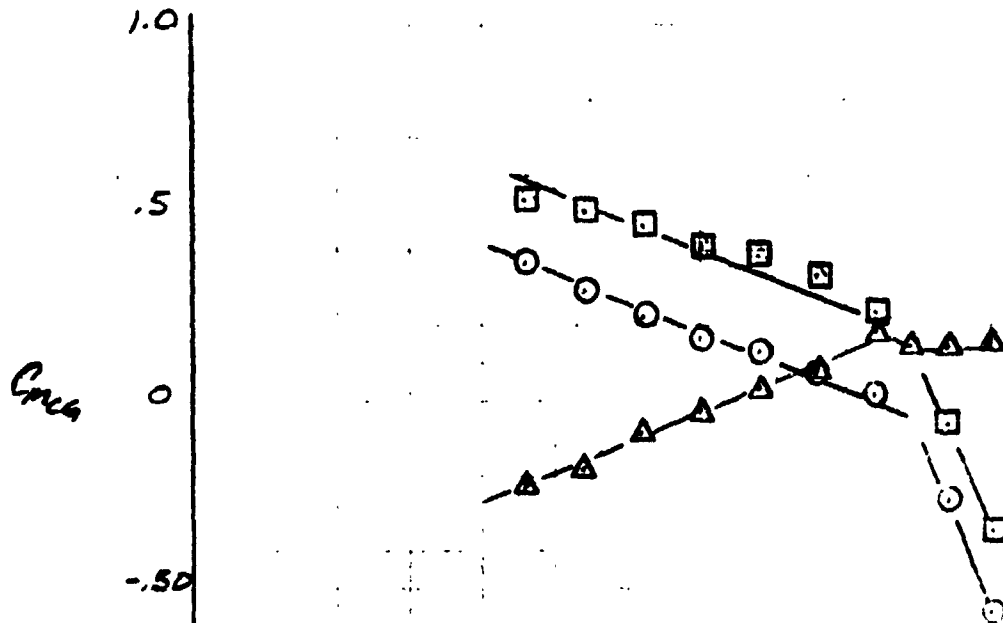
60 KTS
ROTOR OFF



LSWT 421

STING MOUNT
MAST = 75°
FLAPS = 45°/25°

80 KTS
ROTOR OFF

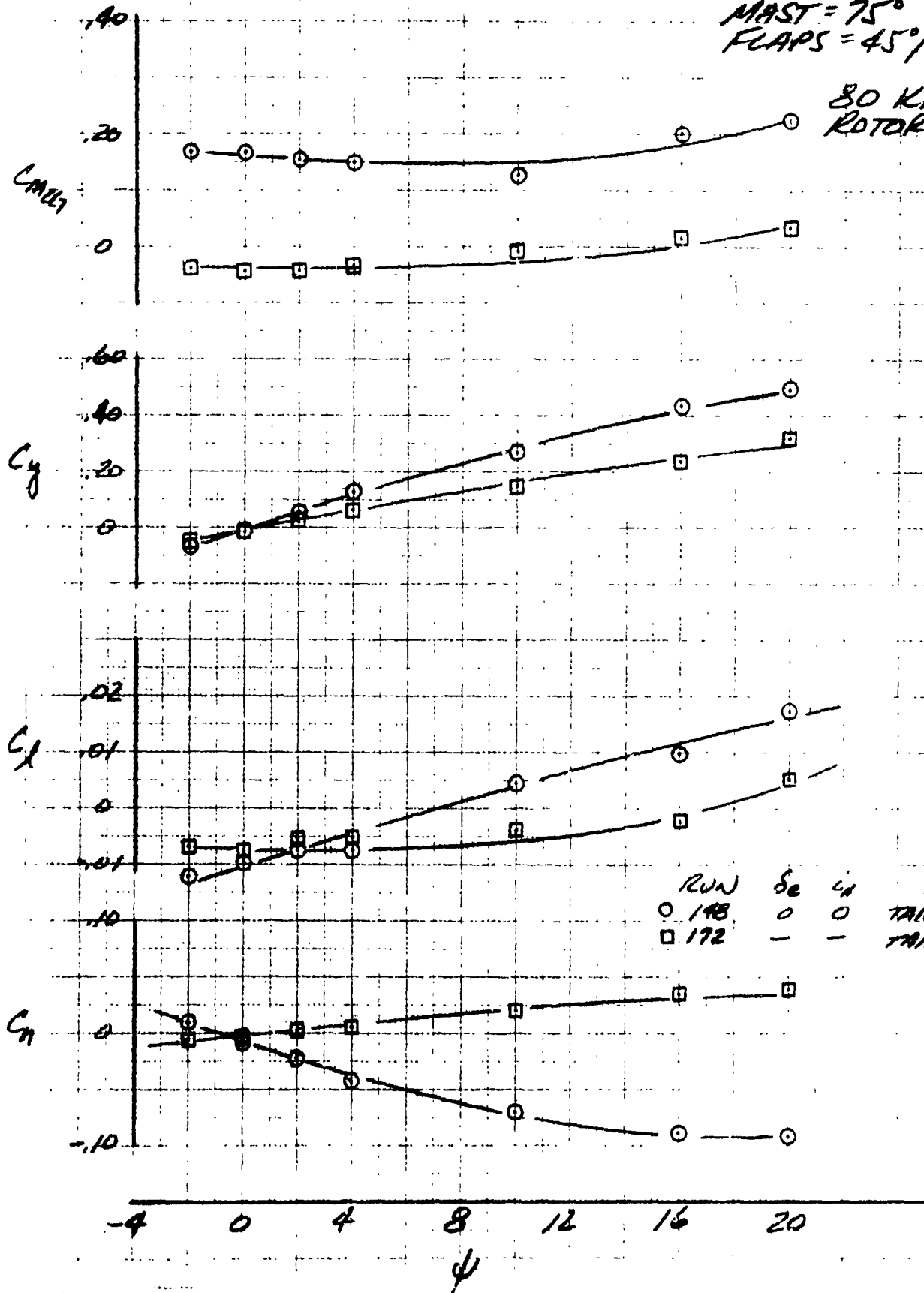


Row	Se	LH	
○ 147	0	0	TAIL ON
□ 151	0	4	" "
△ 171	-	-	TAIL OFF

LSWT 421

STING MOUNT
MAST = 75°
FLAPS = 45°/25°

80 KTS
ROTORS OFF



RUN	δe	C_H	TAIL
○ 198	0	0	TAIL ON
□ 192	-	-	TAIL OFF

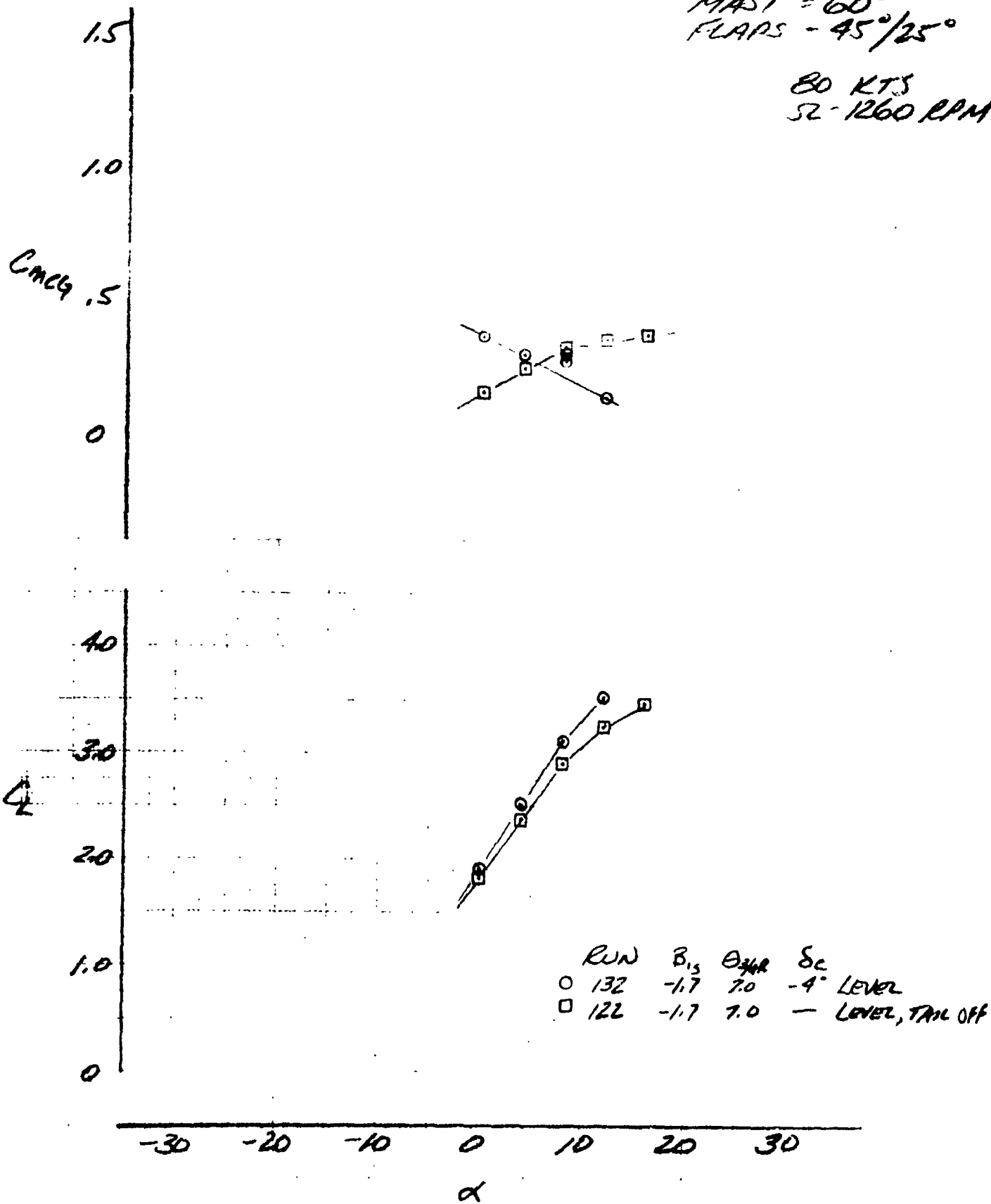
REPRODUCIBILITY OF THE ORIGINAL PAGE IS POOR.

BELL HELICOPTER COMPANY

LSWT 421

STRING MOUNT
 MAST = 60°
 FLAPS - 45°/25°

80 KTS
 52-1260 RPM



REPRODUCIBILITY OF THE ORIGINAL PAGE IS POOR.

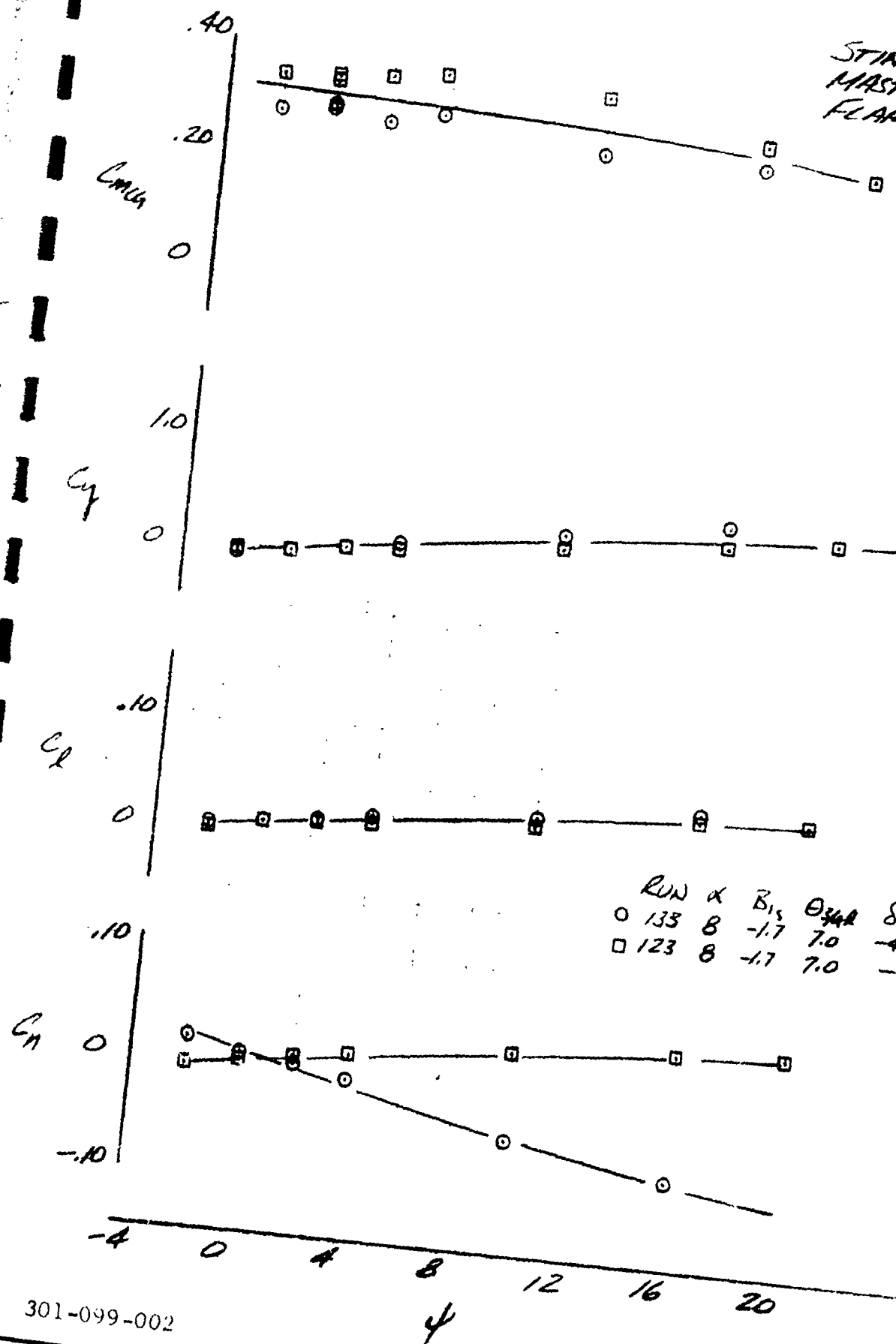
BELL HELICOPTER COMPANY

LSWT 421

For disclosure information, subject to the restriction on the title page.

STING MOUNT
MAST = 60°
FLAPS = 45°/25°

80 KTS
Q = 1260 RPM



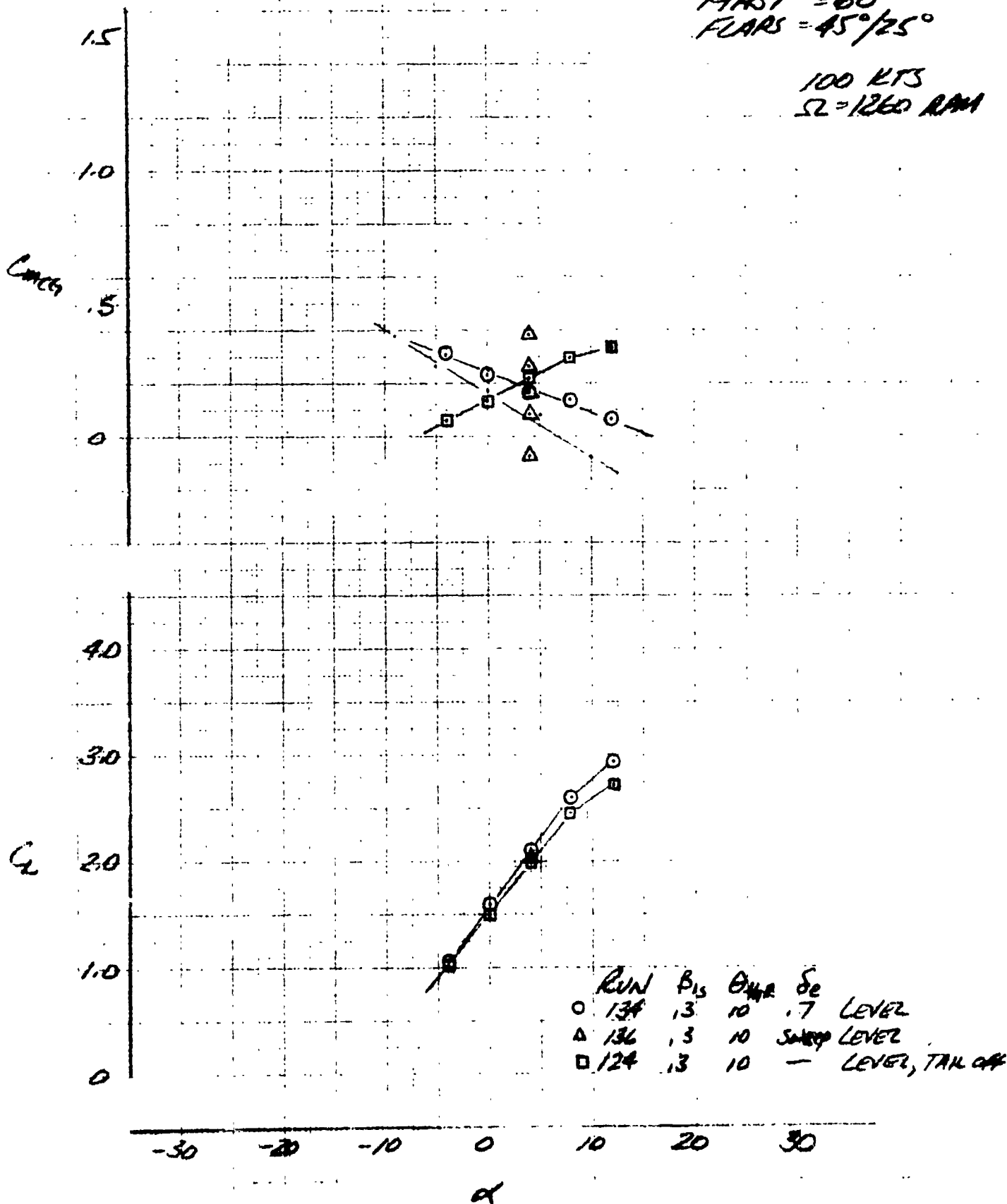
Run	α	B_{15}	θ_{34A}	S_e
○ 133	8	-1.7	7.0	-4 Level
□ 123	8	-1.7	7.0	- Level, TAN OFF

301-099-002

LSWT 421

STING MOUNT
MAST = 60°
FLAPS = 45°/25°

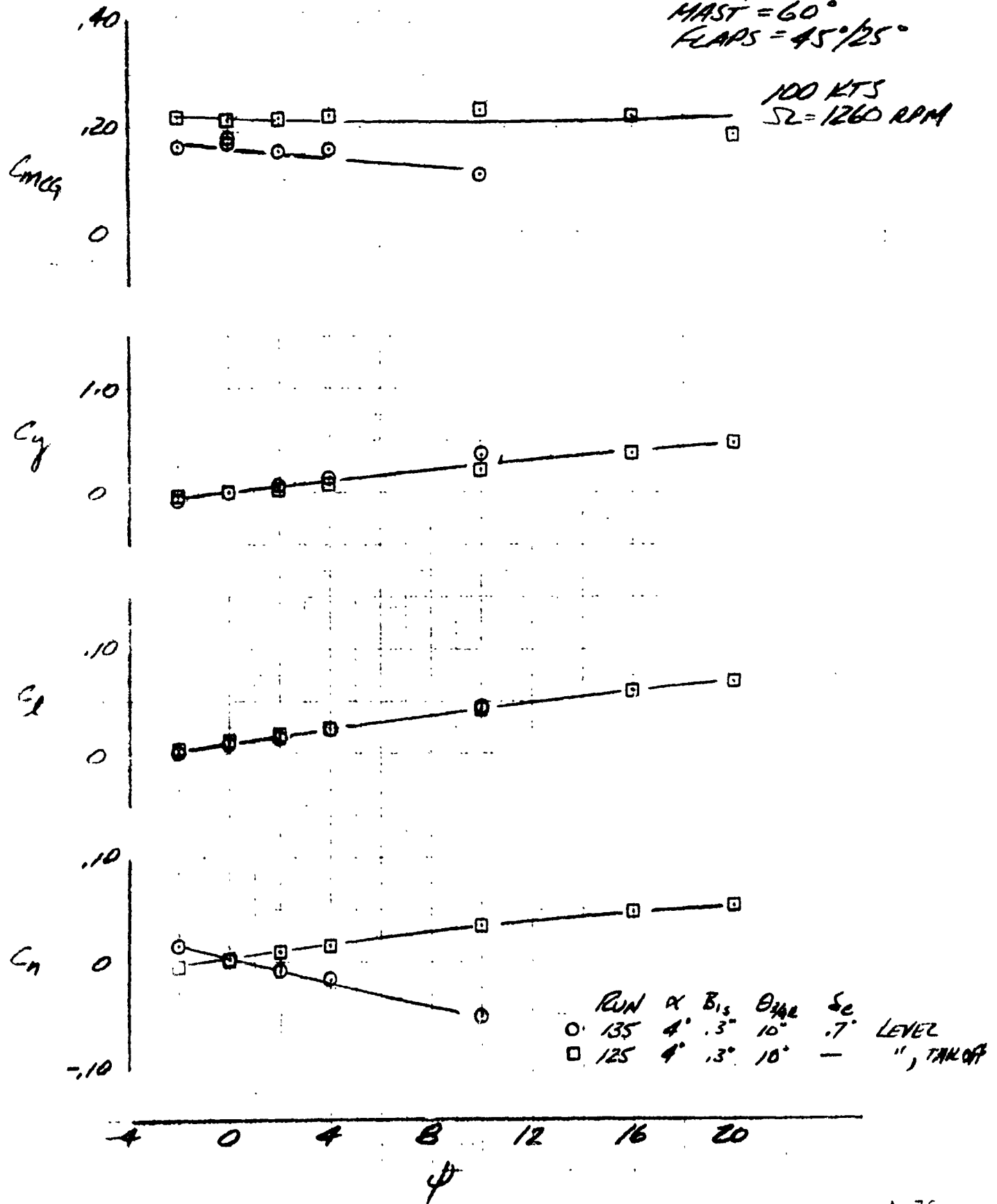
100 KTS
Ω = 1260 RPM



LSWT 421

STING MOUNT
MAST = 60°
FLAPS = 45°/25°

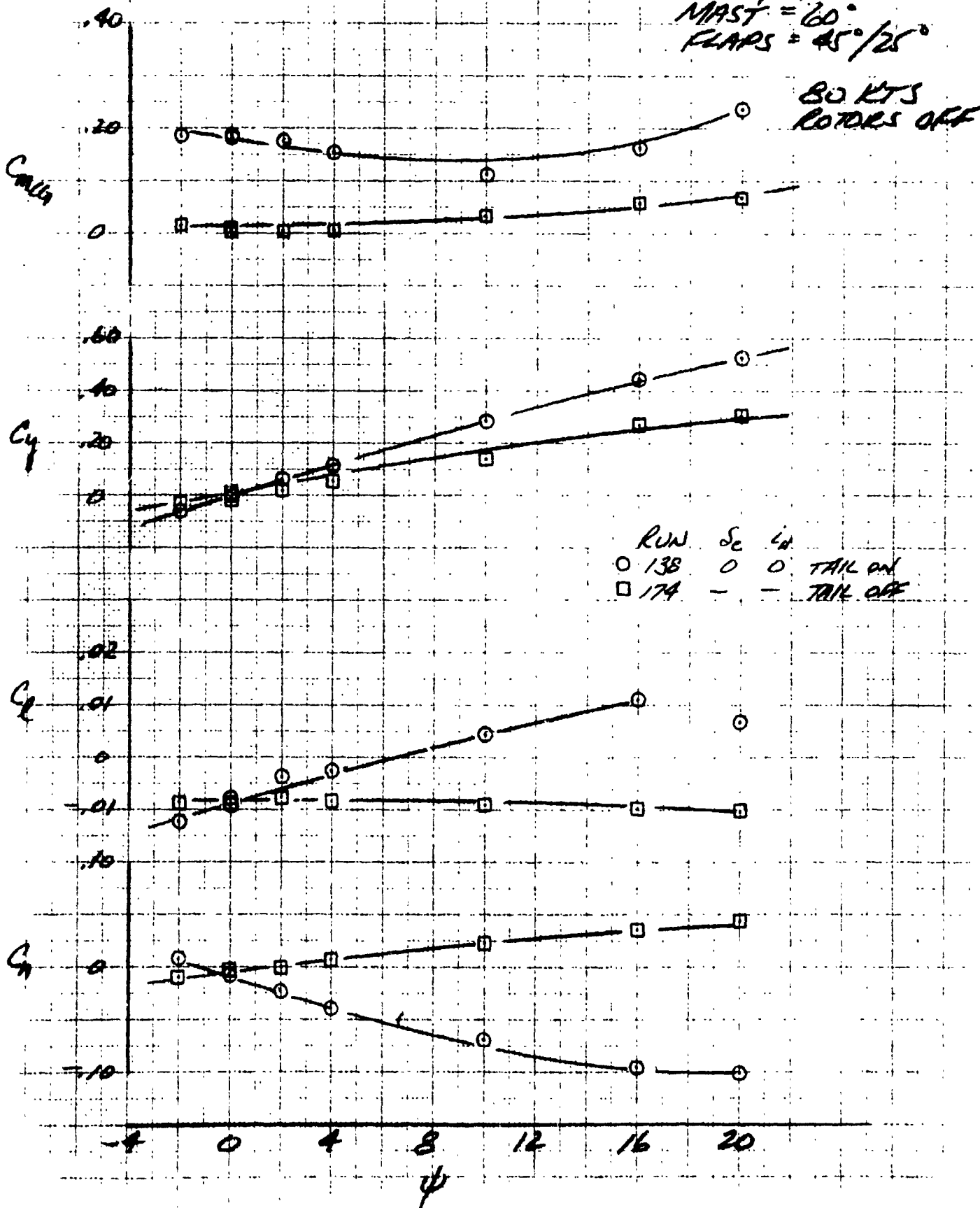
100 KTS
SL = 1260 RPM



LSWT 421

STING MOUNT
MAST = 60°
FLAPS = 45°/25°

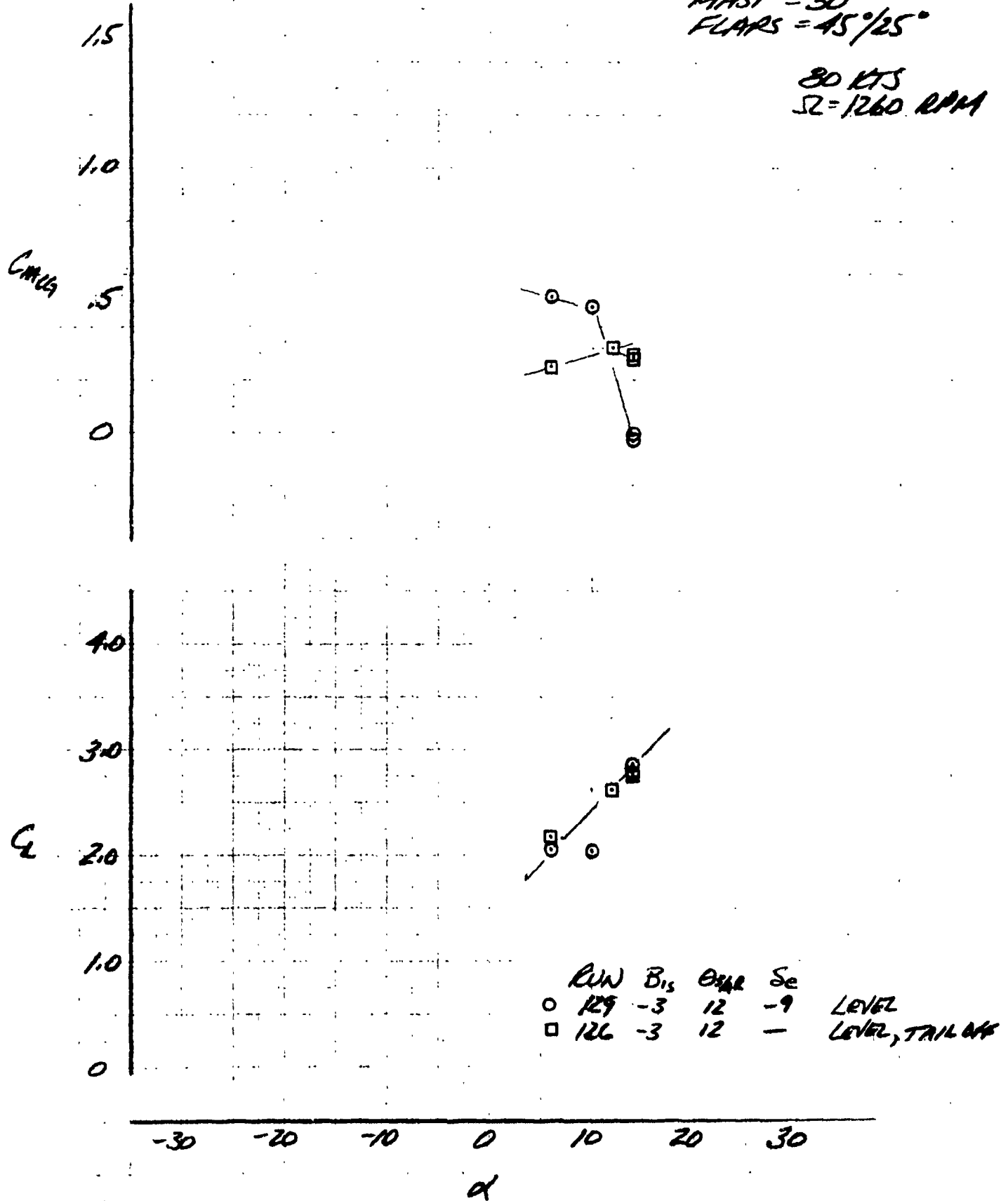
80 KTS
ROTORS OFF



LSWT 421

STING MOUNT
MAST = 30°
FLAPS = 45°/25°

80 KTS
Ω = 1260 RPM



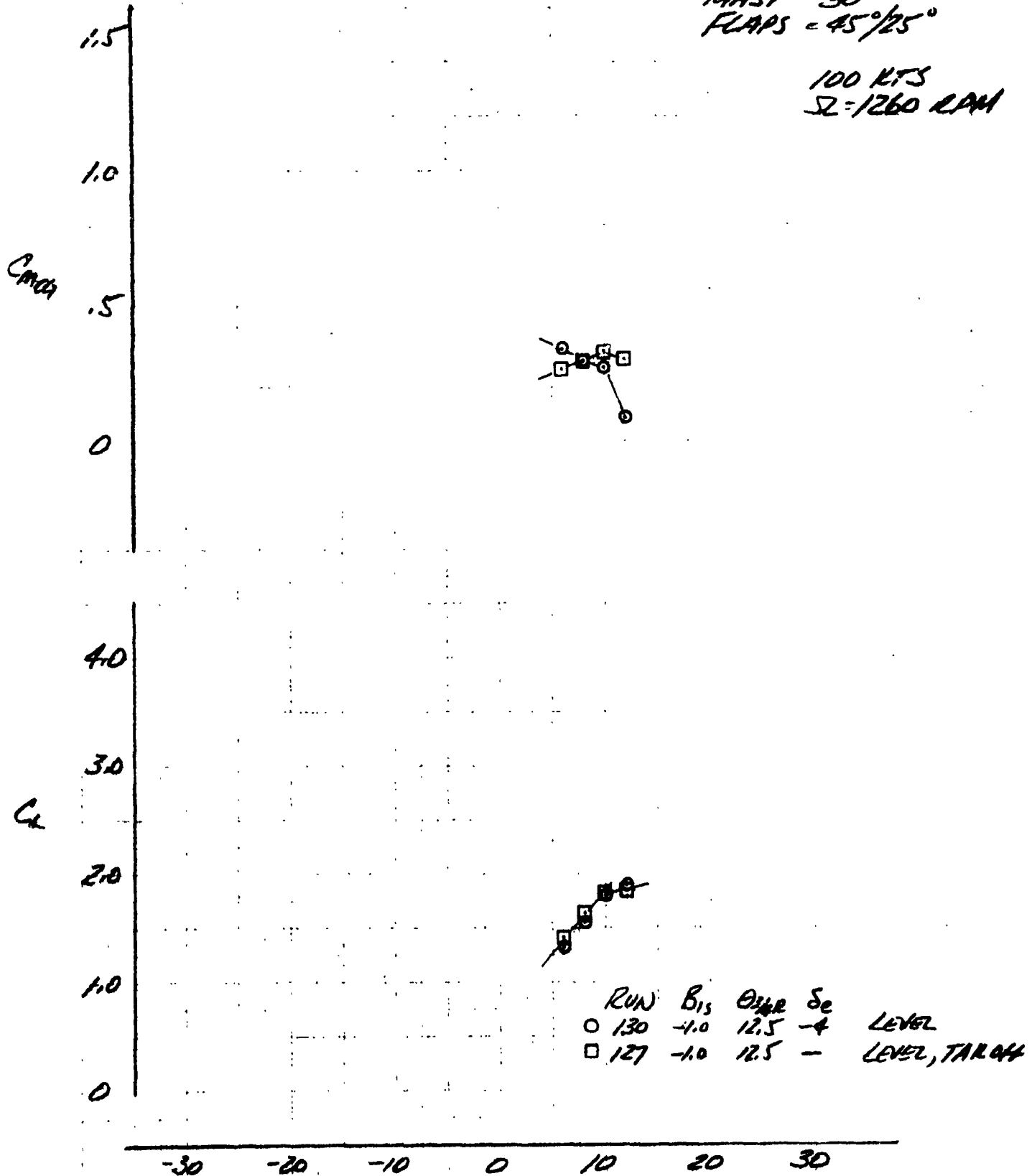
BH BELL
HELICOPTER COMPANY

Use or disclosure of data on this page is
subject to the restriction on the title page

LSWT 421

STING MOUNT
MAST = 30°
FLAPS = 45°/25°

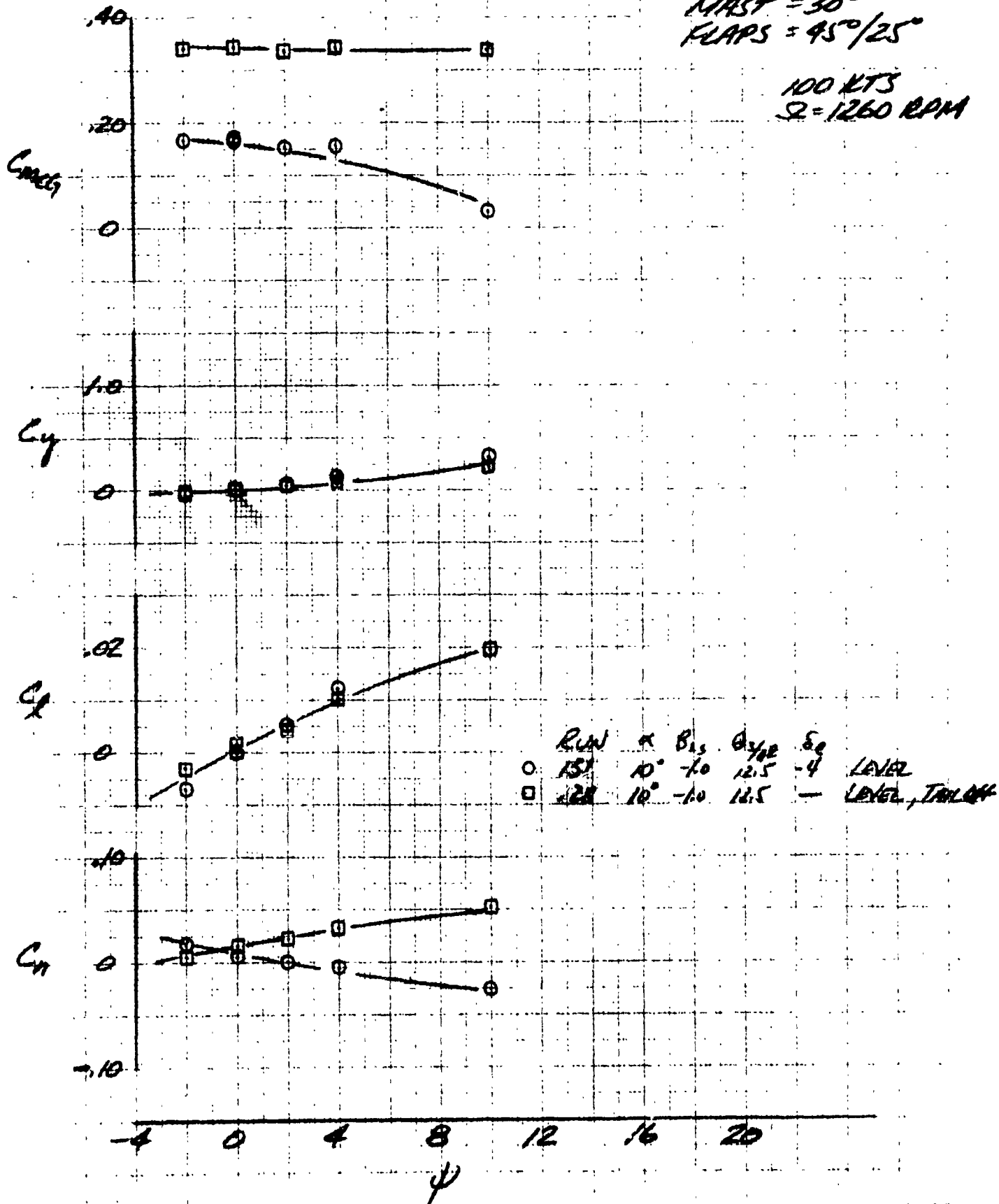
100 KTS
Ω = 1260 RPM



LSWT 421

STING MOUNT
MAST = 30°
FLAPS = 45°/25°

100 KTS
 $\Omega = 1260$ RPM



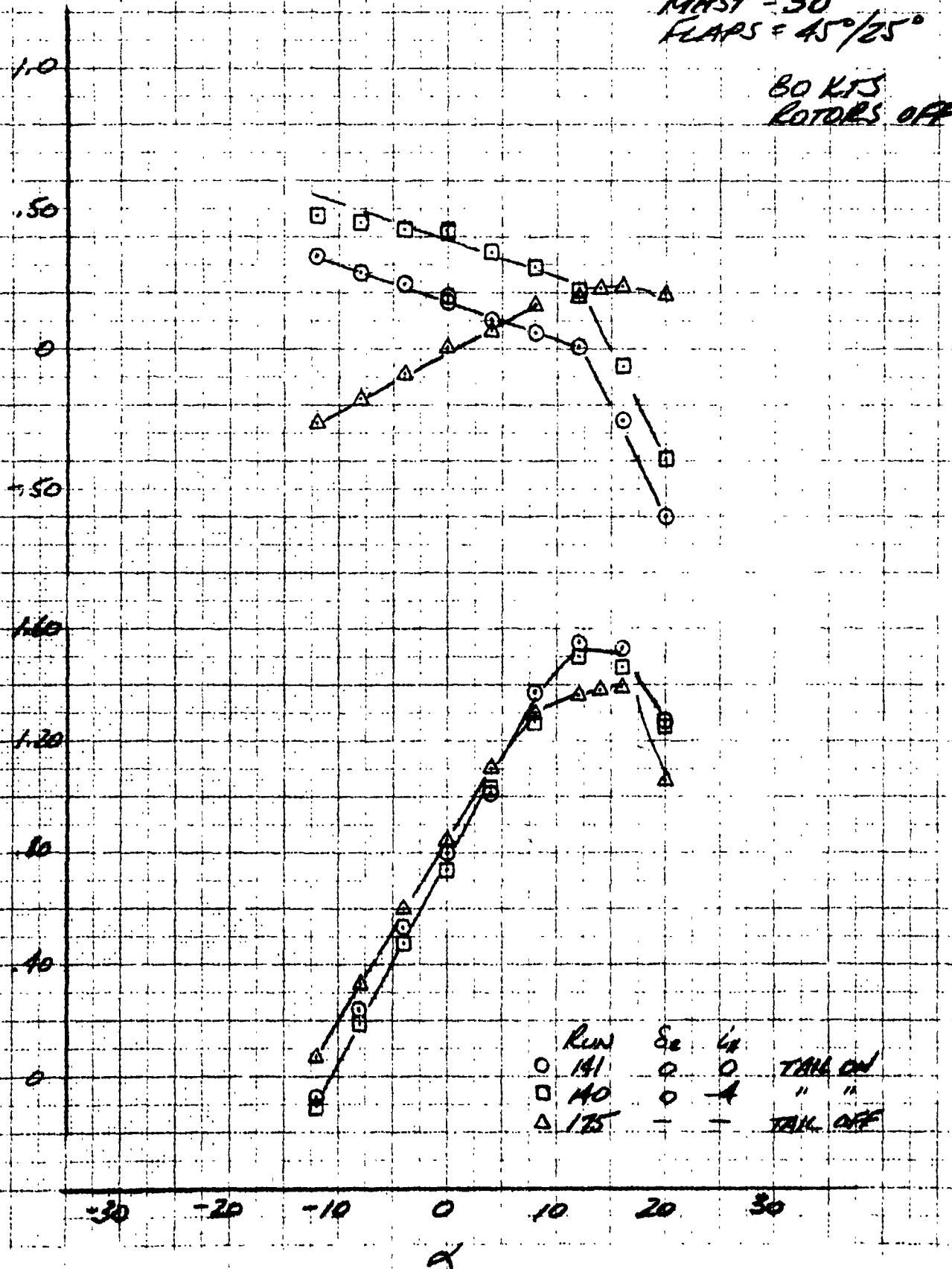
LSWT 421

STING MOUNT
MAST = 30°
FLAPS = 45°/25°

80 KTS
ROTORS OFF

C_{mi}

C_L

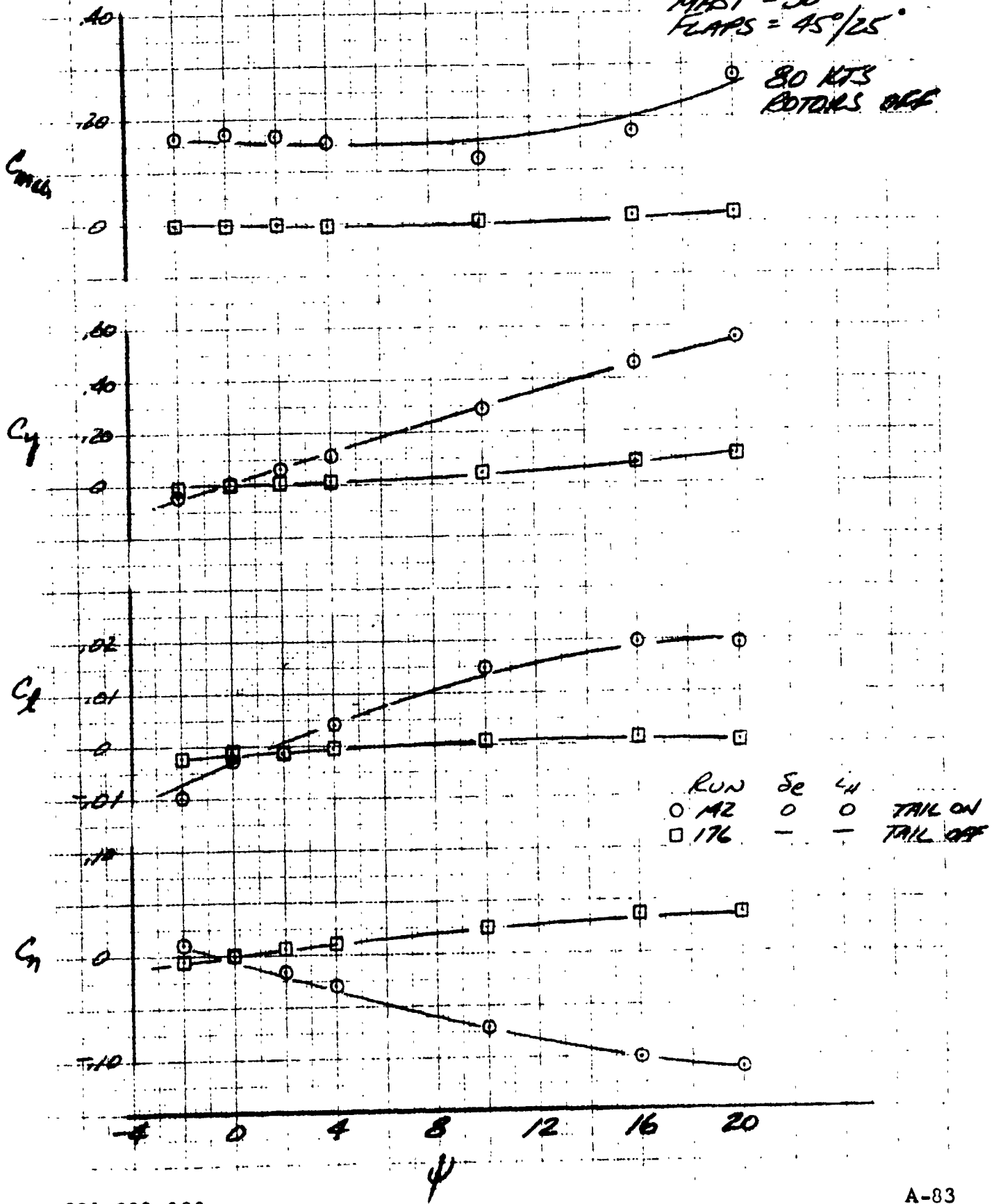


Run	Se	Vt	Tail
○ 141	○	○	TAIL ON
□ 140	○	△	" "
△ 175	-	-	TAIL OFF

LSUT 421

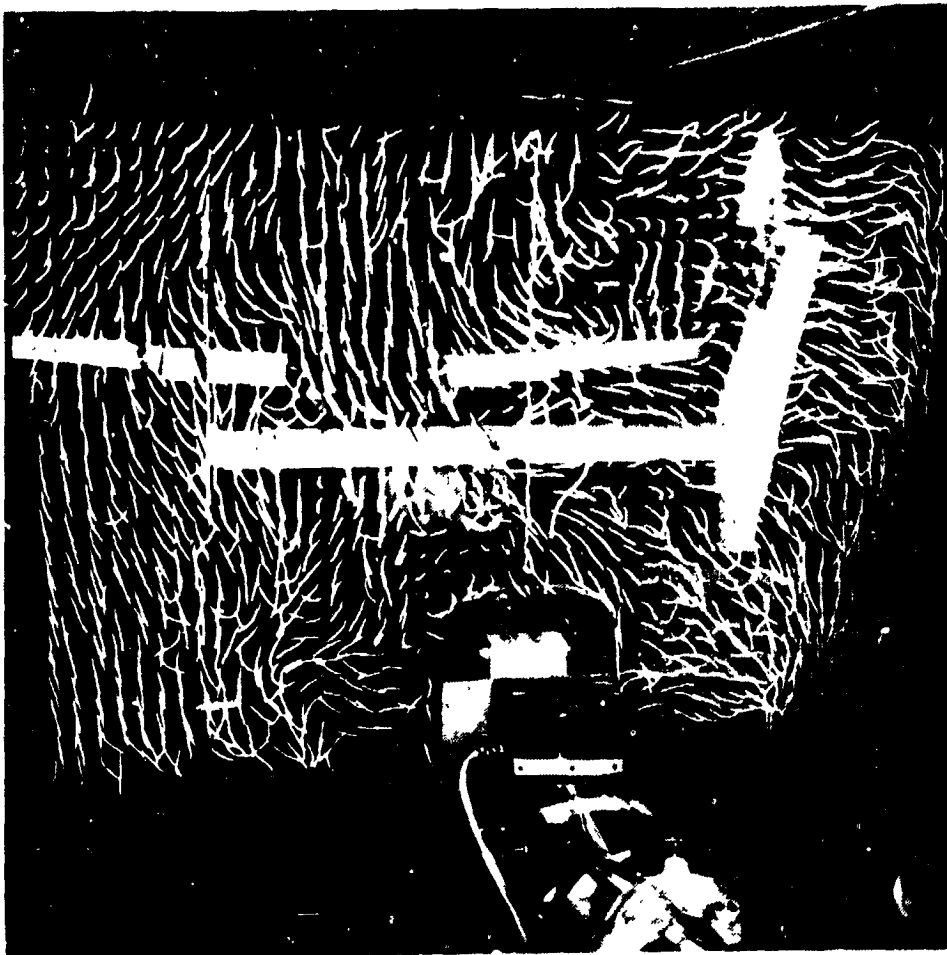
STING MOUNT
MAST = 30°
FLAPS = 45°/25°

80 KTS
ROTORS OFF

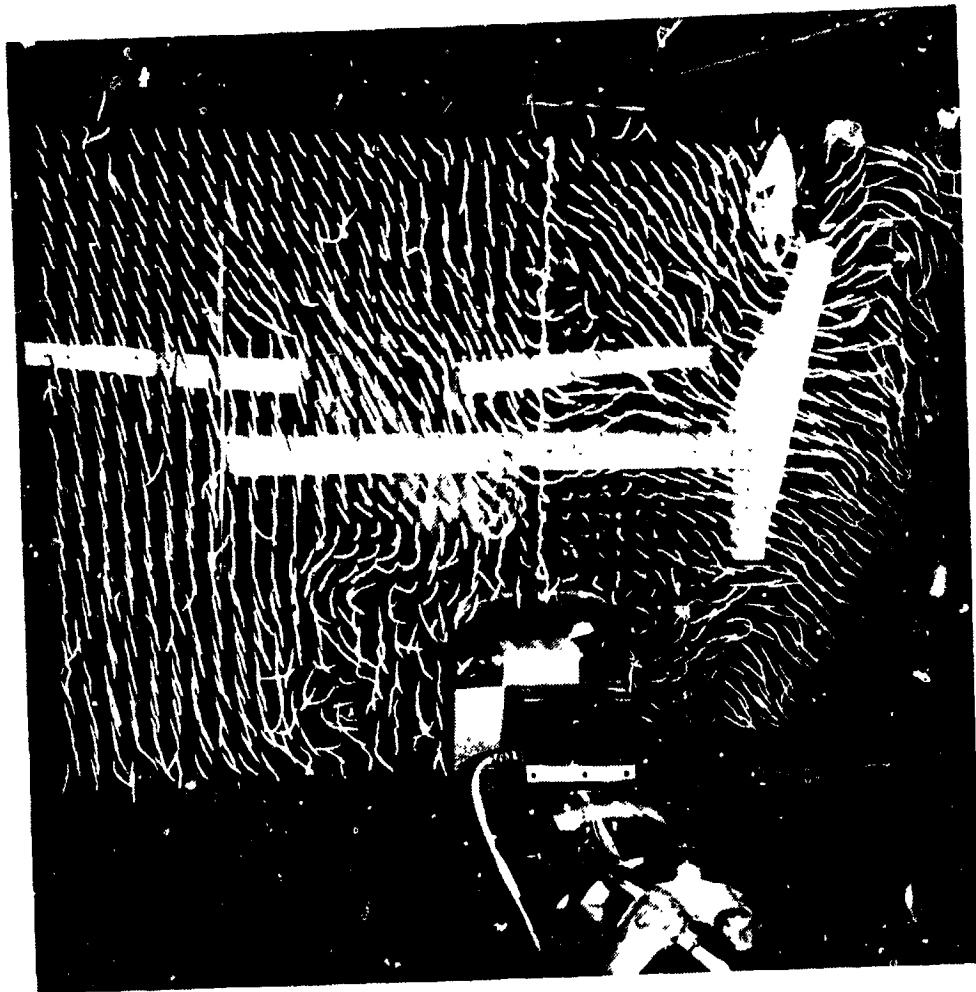


APPENDIX C

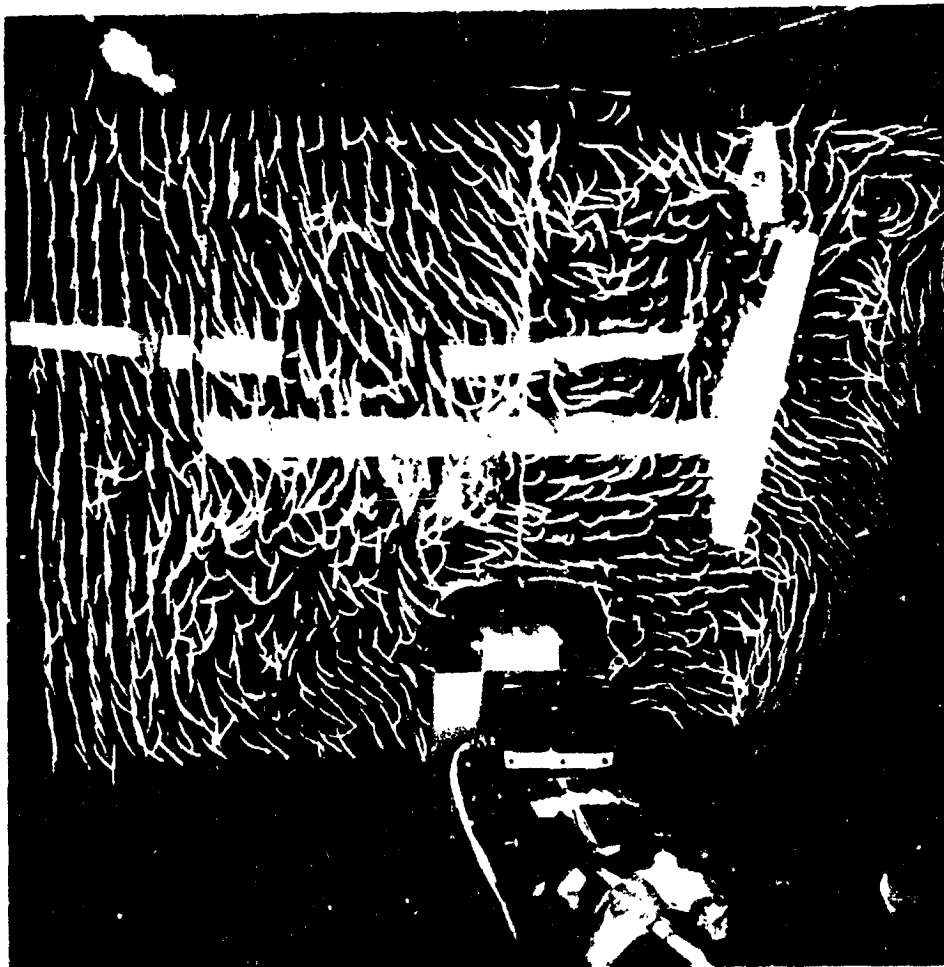
Tuft Grid Photographs



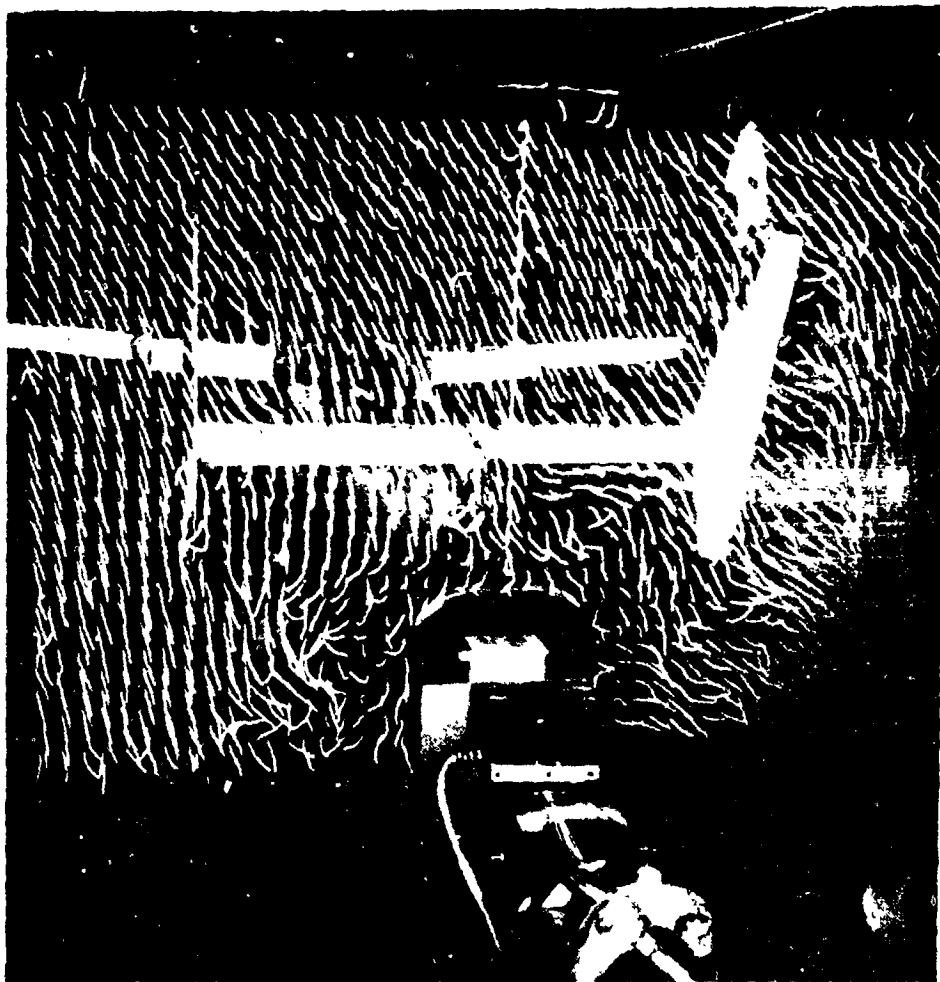
16 KTS, $\Omega = 1260$ RPM, $\alpha = 0$, $\psi = 0$, $\rho = 130$ in lb



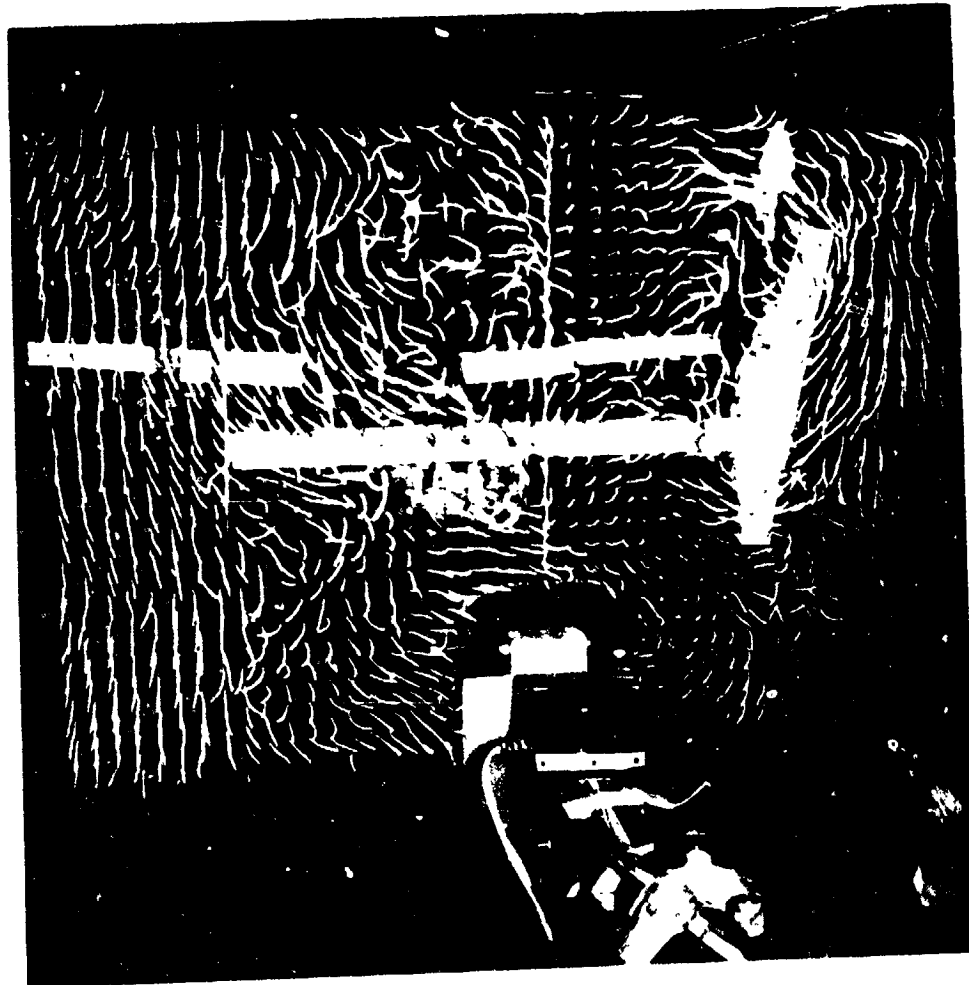
16 KTS, $\Omega = 1260$ RPM, $\alpha = 0$, $\psi = 10$



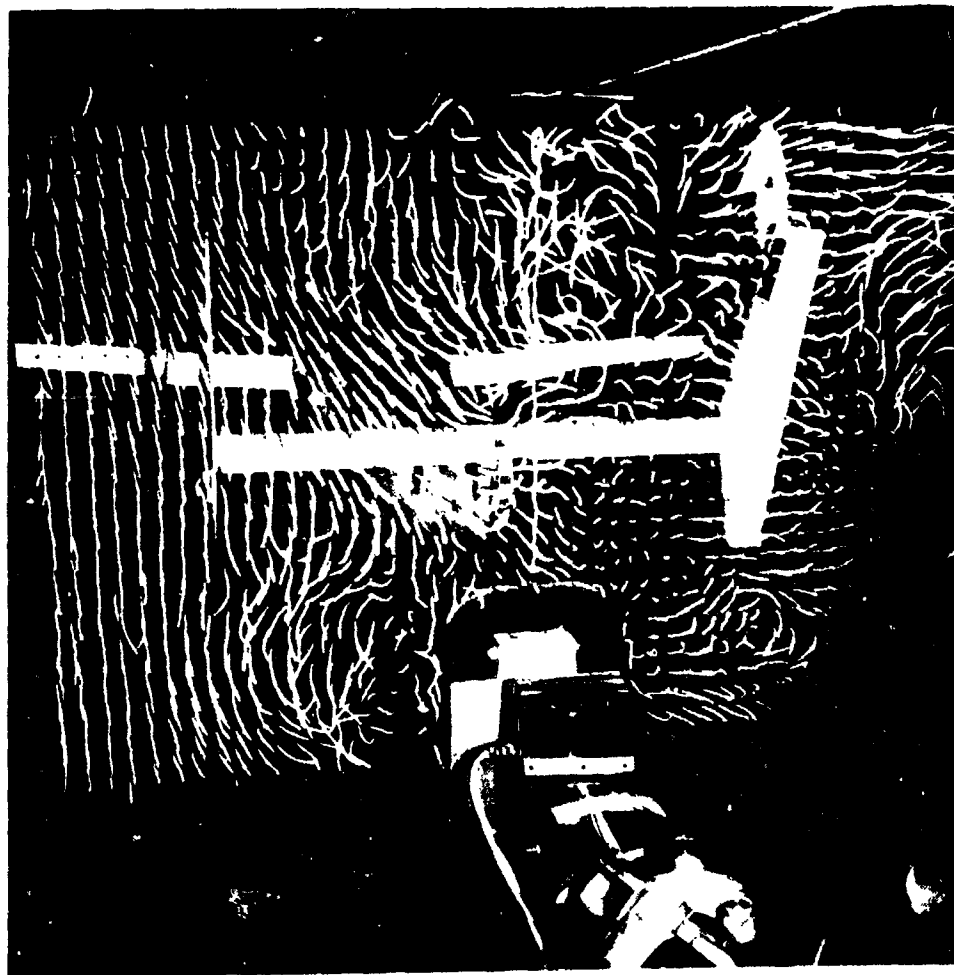
20 KTS, $\Omega = 1260$ RPM, $\alpha = 0$, $\psi = 0$, $Q = 120$ in lb



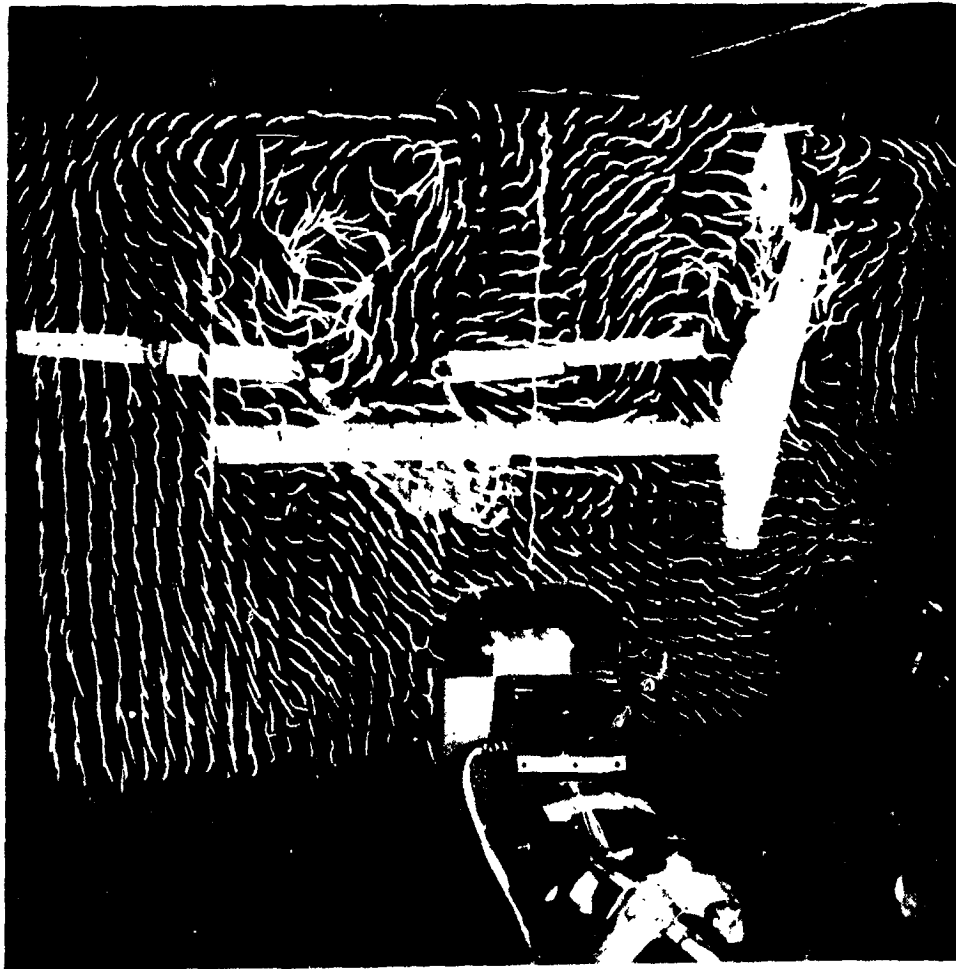
20 KTS, $\Omega = 1260$ RPM, $\alpha = 0$, $\psi = 10$



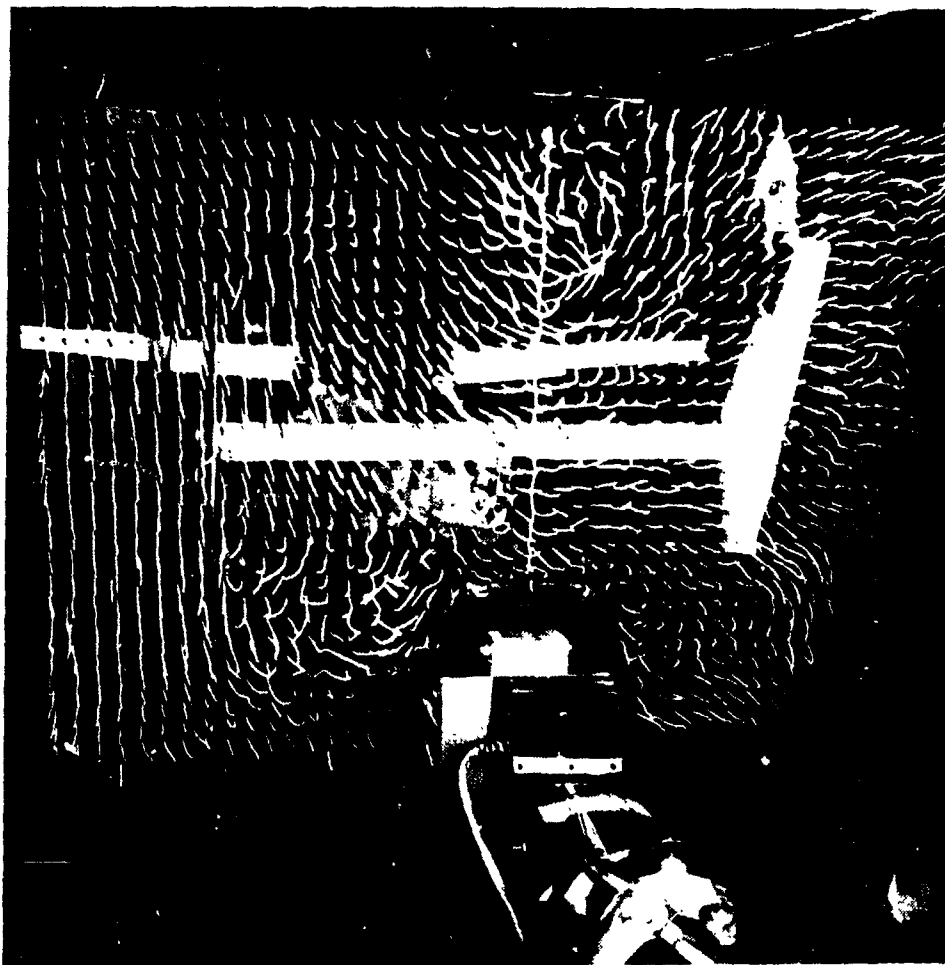
30 KTS, $\Omega = 1260$ RPM, $\alpha = 0$, $\psi = 0$, $Q = 103$ in lb



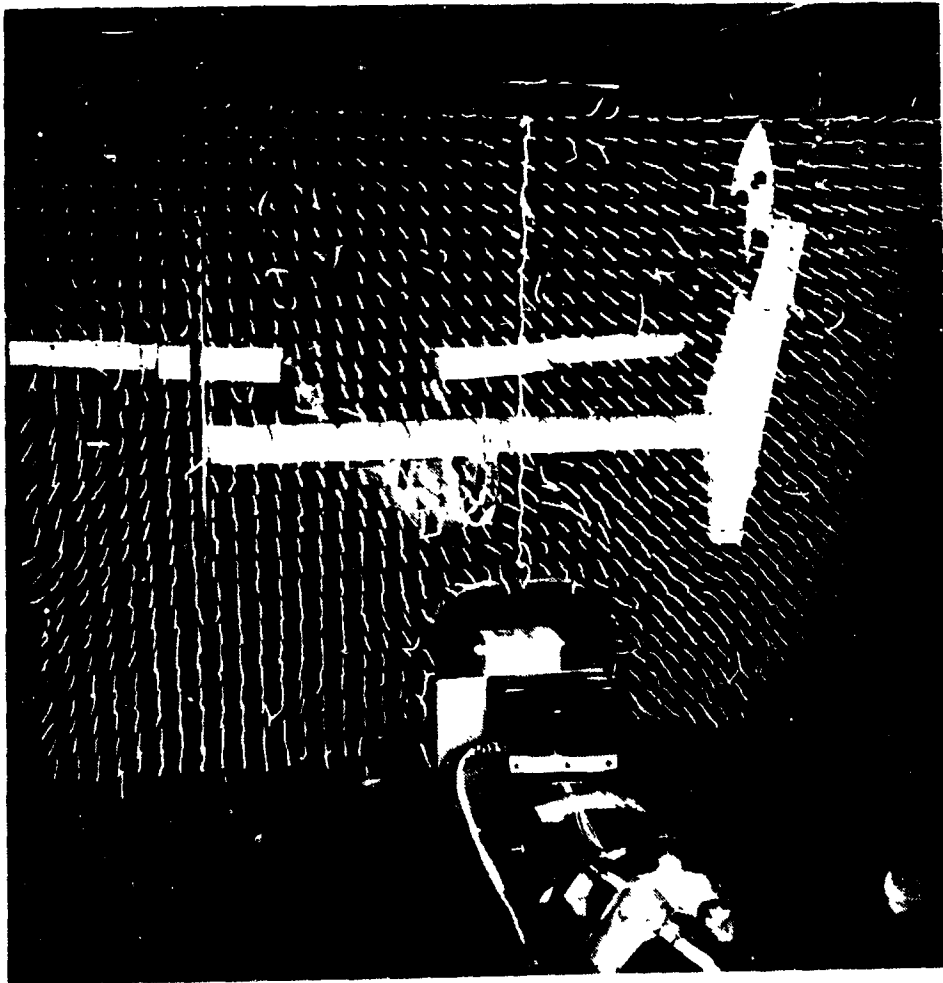
30 KTS, $\Omega = 1260$ RPM, $\alpha = 0$, $\psi = 10^\circ$



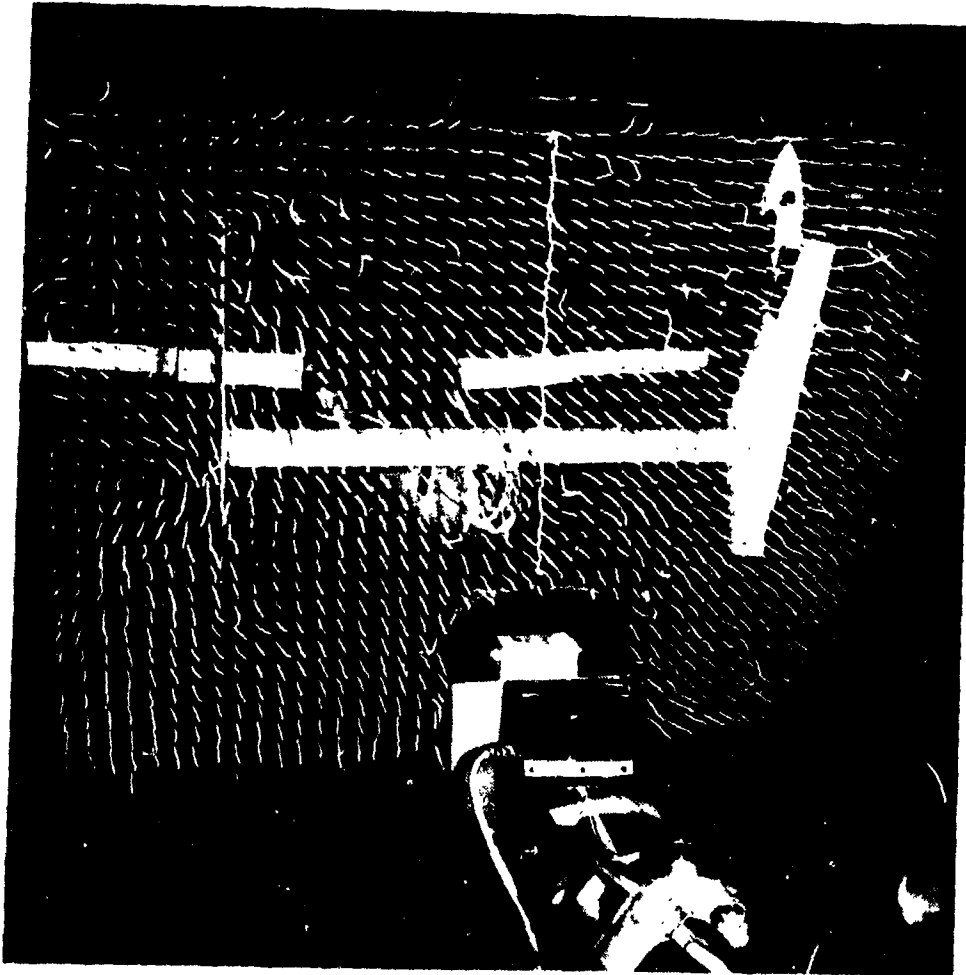
40 KTS, $\Omega = 1260$ RPM, $\alpha = -2$, $\psi = 0$, $Q = 90$ in lb



40 KTS, $\Omega = 1260$ RPM, $\alpha = -2$, $\psi = 10$



40 KTS, $\Omega = 0$ RPM, $\alpha = -2$, $\psi = 0$



40 KTS, $\Omega = 0$ RPM, $\alpha = -2$, $\psi = 10$